IEEE Press Series on Power and Energy Systems
Ganesh Kumar Venayagamoorthy, Series Editor

Fourth Edition

Analysis of Electric Machinery and Drive Systems

Paul C. Krause, Oleg Wasynczuk,
Scott D. Sudhoff, Steven D. Pekarek

Analysis of Electric Machinery and Drive Systems

IEEE Press
445 Hoes Lane
Piscataway, NJ 08854

Analysis of Electric Machinery and Drive Systems

Fourth Edition

Paul C. Krause
PC Krause and Associates, Inc
West Lafayette, Indiana, United States

Oleg Wasynczuk
Purdue University
West Lafayette, Indiana, United States

Scott D. Sudhoff
Purdue University
West Lafayette, Indiana, United States

Steven D. Pekarek
Purdue University
West Lafayette, Indiana, United States

IEEE Press Series on Power and Energy Systems
Ganesh Kumar Venayagamoorthy, Series Editor

IEEE*Press*
WILEY

Published by John Wiley & Sons, Inc., Hoboken, New Jersey.
Published simultaneously in Canada.

The manufacturer's authorized representative according to the EU General Product Safety Regulation is Wiley-VCH GmbH, Boschstr. 12, 69469 Weinheim, Germany, e-mail: Product_Safety@wiley.com.

Library of Congress Cataloging-in-Publication Data Applied for:

Hardback ISBN: 9781394293865

Cover Design & Image: Wiley

Set in 9.5/12.5pt STIXTwoText by Straive, Chennai, India

Contents

About the Authors

Paul C. Krause is a former professor in the School of Electrical and Computer Engineering at Purdue University. He is the founder of PC Krause and Associates, Inc., and the recipient of the 2010 IEEE Nikola Tesla Award.

Oleg Wasynczuk is a professor emeritus of Electrical and Computer Engineering at Purdue University. He also served as Chief Technical Officer of PC Krause and Associates, Inc., and is the recipient of the 2008 IEEE PES Cyril Veinott Electromechanical Energy Conversion Award.

Scott D. Sudhoff is the Michael and Katherine Birck Distinguished Professor of Electrical and Computer Engineering at Purdue University. He is former Editor-in-Chief of the IEEE Transactions on Energy Conversion and the recipient of the 2025 IEEE Nikola Tesla Award.

Steven D. Pekarek is the Edmund O. Schweitzer, III, Professor of Electrical and Computer Engineering at Purdue University. He has served as an editor of the IEEE Transactions on Energy Conversion and the IEEE Transactions on Power Electronics, and is the recipient of the 2018 IEEE PES Cyril Veinott Electromechanical Energy Conversion Award.

Preface

This book is written for graduate students and engineers interested in machines and drives analysis. Chapter 1 covers some basic concepts that are common to books in this area. This fourth edition differs from previous editions in several ways. For example, the transformation for both the q and d variables is obtained from the expression of the rotating magnetomotive force or mmf. This is a very straightforward approach that provides an analytic origin of the transformation. Also, the analysis of each machine is focused on motor action to set the stage for electric drives, although generator action is considered in the case of the synchronous machine. Also, since for analysis purposes the stators of the AC machines considered in this text are the same, the stators are considered once in Chapter 2 rather than repeating the analysis for each machine. However, the rotors are different and are treated separately for each machine. This reduces the work considerably.

The induction machine is considered in Chapter 3. Most induction motors have squirrel-cage rotors. However, if the stator has sinusoidally distributed windings, the rotor may also be considered as having sinusoidally distributed windings even though the rotor may consist of solid bars. The transformation of the rotor variables to the q and d axes differs only in that the rotor windings are rotating relative to the stator. The permanent-magnet AC machine and the synchronous generator are considered in Chapters 4 and 5, respectively. In Chapter 4, we treat the brushless DC machine with $L_d = L_q$. Three different values of angle between $\tilde{V}_{as}$ and $\tilde{E}_a$, or ϕ_v, are considered. These are: $\phi_v = 0$, which is the most common operating mode, $\phi_v = \phi_{v,MT/V}$ or maximum torque per volt, and $\phi_v = \phi_{v,MT/A}$ or maximum torque per ampere. In this case, the permanent-magnet rotor is considered to be magnetized sinusoidally.

The first part of Chapter 5 is devoted to motor action of a synchronous machine. The second part is devoted to generator action with positive current assumed out of the machine. This latter mode of operation was treated by Park in his classic paper written in 1929. The basic analysis of AC machines covered in this text ends

with Chapter 5. Power systems engineers could continue with Chapters 6, 7, and 8. The drives engineer would not cover these chapters, but would skip to Chapters 10 through 14, and would likely omit some of the material in Chapter 5.

In Chapter 6, the concept of neglecting stator transients is treated. This chapter would be of most interest to the power systems engineer since it deals with the basis of transient stability programs used in stability studies for power systems. Both power systems and drives engineers could find Chapter 9 interesting. Drives engineers would want to study Chapter 10, as it describes the most commonly used modulation strategies. Chapter 11 deals with DC drives. This chapter is brief but relevant to electric drive engineering.

In Chapter 12, the torque control of permanent-magnet AC and synchronous reluctance machines are considered. The analysis of the permanent-magnet machine is similar to the material in Chapter 4. The difference is that $L_d \neq L_q$ and a reluctance torque exists. The parameters of the machine considered are representative of electric drive motors used in hybrid and electric vehicles. The synchronous reluctance machine is considered with the permanent magnets removed, whereby only a reluctance torque exists. Synchronous reluctance machines are also considered as viable candidates as electric drive motors in hybrid and electric vehicles. It is shown that with power-electronic-based current control, the electric transients are so fast that they may be neglected when considering the mechanical dynamics.

Induction motor control is considered in Chapter 13, including the volt-per-hertz, constant-slip, and field-oriented control methods. Each is considered in substantial detail. Finally, the control of permanent-magnet AC machines is considered in Chapter 14.

Although this is a graduate text, the first six or seven chapters could be used at the senior-level with the remaining chapters used as a graduate text.

February 2025

Paul C. Krause
Oleg Wasynczuk
Scott D. Sudhoff
Steven D. Pekarek
West Lafayette, Indiana

Acknowledgments

To Our Families

About the Companion Website

This book is accompanied by a companion website:

www.wiley.com/go/krause_aem4e

The website includes Solution Manuals.

1

Introductory Concepts

1.1 Introduction

This chapter is a review for most since the material is covered in undergraduate courses in the analysis of electromechanical devices [1]. The material is presented to start everyone with the same background. The chapter begins with coupled circuits (transformers) where the phasor equivalent circuit is established. Since phasors are not always taught the same, they are covered briefly in Appendix B to make sure everyone understands the concept of phasors as used in this text. Although we will give several approaches for the calculation of torque of electric machines; Section 1.1-3 sets forth a method of calculating force and torque that is generally taught at the undergraduate level.

Some instructors may choose to skip some material and/or select topics that were not covered in undergraduate courses at their school. As mentioned, the material will be a review for most and can be covered rather fast. On the other hand, Chapter 2 dives into machine analysis that contains new material and can be taught at a much slower pace.

1.2 Stationary Magnetically Coupled Circuits

Magnetically coupled electric circuits are central to the operation of transformers and electromechanical motion devices. In the case of transformers, stationary circuits are magnetically coupled for the purpose of changing the ac voltage and current levels. The two windings shown in Fig. 1.2-1 consist of turns N_1 and N_2, and they are wound on a common core, which is a ferromagnetic material with a permeability large relative to that of air. The magnetic core is illustrated in two dimensions.

Analysis of Electric Machinery and Drive Systems, Fourth Edition.
Paul C. Krause, Oleg Wasynczuk, Scott D. Sudhoff, and Steven D. Pekarek.

Companion website: www.wiley.com/go/krause_aem4e

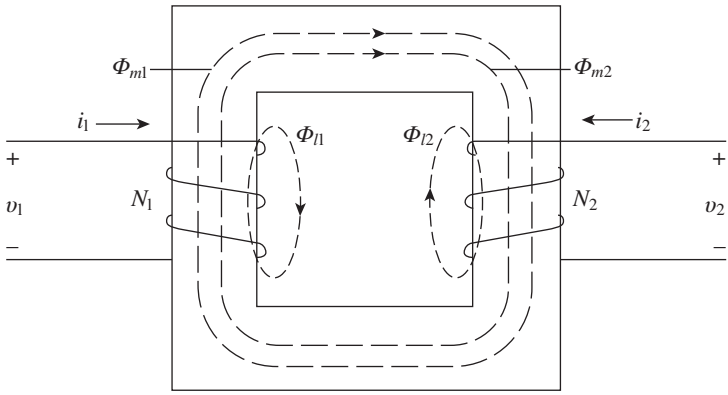

Figure 1.2-1 Magnetically coupled circuits.

The flux produced by each winding can be separated into two components: a leakage component denoted by the subscript l and a magnetizing component denoted by the subscript m. Each of these components is depicted by a single streamline with the positive direction determined by applying the right-hand rule to the directions of current flow in the winding. The leakage flux associated with a given winding links only that winding, whereas the magnetizing flux, whether it is due to current in winding 1 or winding 2, links both windings.

The flux linking of each winding may be expressed as

$$\boldsymbol{\Phi}_1 = \boldsymbol{\Phi}_{l1} + \boldsymbol{\Phi}_{m1} + \boldsymbol{\Phi}_{m2} \tag{1.2-1}$$

$$\boldsymbol{\Phi}_2 = \boldsymbol{\Phi}_{l2} + \boldsymbol{\Phi}_{m2} + \boldsymbol{\Phi}_{m1} \tag{1.2-2}$$

The leakage flux $\boldsymbol{\Phi}_{l1}$ is produced by current flowing in winding 1, and it links only the turns of winding 1. Likewise, the leakage flux $\boldsymbol{\Phi}_{l2}$ is produced by current flowing in winding 2, and it links only the turns of winding 2. The flux $\boldsymbol{\Phi}_{m1}$ is produced by current flowing in winding 1, and it links all turns of windings 1 and 2. Similarly, the magnetizing flux $\boldsymbol{\Phi}_{m2}$ is produced by current flowing in winding 2, and it also links all turns of windings 1 and 2. Both $\boldsymbol{\Phi}_{m1}$ and $\boldsymbol{\Phi}_{m2}$ are called *magnetizing fluxes*. With the selected positive directions of current flow and the manner in which the windings are wound, the magnetizing flux produced by positive current flowing in one winding can add to or subtract from the magnetizing flux produced by positive current flowing in the other winding. Thus, the mutual inductance can be positive or negative. In Fig. 1.2-1, it is positive.

It is appropriate to point out that this is an idealization of the actual magnetic system. It seems logical that all of the leakage flux will not link all the turns of the winding producing it; hence, $\boldsymbol{\Phi}_{l1}$ and $\boldsymbol{\Phi}_{l2}$ are "equivalent" leakage fluxes.

Similarly, all of the magnetizing fluxes of one winding may not link all of the turns of the other winding.

The voltage equations may be expressed as

$$v_1 = r_1 i_1 + \frac{d\lambda_1}{dt} \tag{1.2-3}$$

$$v_2 = r_2 i_2 + \frac{d\lambda_2}{dt} \tag{1.2-4}$$

In matrix form,

$$\begin{bmatrix} v_1 \\ v_2 \end{bmatrix} = \begin{bmatrix} r_1 & 0 \\ 0 & r_2 \end{bmatrix} \begin{bmatrix} i_1 \\ i_2 \end{bmatrix} + \frac{d}{dt} \begin{bmatrix} \lambda_1 \\ \lambda_2 \end{bmatrix} \tag{1.2-5}$$

The resistances r_1 and r_2 and the flux linkages λ_1 and λ_2 are related to windings 1 and 2, respectively. Since it is assumed that $\boldsymbol{\Phi}_1$ links the equivalent turns of winding 1 (N_1) and $\boldsymbol{\Phi}_2$ links the equivalent turns of winding 2 (N_2), the flux linkages may be written as

$$\lambda_1 = N_1 \boldsymbol{\Phi}_1 \tag{1.2-6}$$

$$\lambda_2 = N_2 \boldsymbol{\Phi}_2 \tag{1.2-7}$$

where $\boldsymbol{\Phi}_1$ and $\boldsymbol{\Phi}_2$ are given by (1.2-1) and (1.2-2), respectively.

If we assume that the magnetic system is magnetically linear (i.e., core losses and saturation are neglected), we may apply Ohm's law for magnetic circuits to express the fluxes. Thus, the fluxes may be written as

$$\boldsymbol{\Phi}_{lk} = \frac{N_k i_k}{\mathfrak{R}_{\mathrm{lk}}} \tag{1.2-8}$$

$$\boldsymbol{\Phi}_{mk} = \frac{N_k i_k}{\mathfrak{R}_m} \tag{1.2-9}$$

where $k = 1$ or 2 and $\mathfrak{R}_{l1}$ and $\mathfrak{R}_{l2}$ are the reluctances of the leakage paths, and $\mathfrak{R}_m$ is the reluctance of the path of magnetizing fluxes. Typically, the reluctances associated with leakage paths are much larger than the reluctance of the magnetizing path. The reluctance associated with an individual leakage path is difficult to determine exactly, and it is usually approximated from test data or by using the computer to solve the field equations numerically. On the other hand, the reluctance of the magnetizing path of the core shown in Fig. 1.2-1 may be computed with sufficient accuracy.

For the iron

$$\mathfrak{R}_i = \frac{l_i}{\mu_r \mu_0 A_i} \tag{1.2-10}$$

where l_i is the length of the path in iron, μ_r is the relative permeability of iron, μ_0 is the permeability of free space, and A_i is the cross-sectional area of the flux

in the iron. In electromechanical devices, we will find that the magnetizing flux must transverse air gaps and

$$\mathfrak{R}_m = \mathfrak{R}_i + \mathfrak{R}_g \tag{1.2-11}$$

Substituting (1.2-8) and (1.2-9) into (1.2-1) and (1.2-2) yields

$$\Phi_1 = \frac{N_1 i_1}{\mathfrak{R}_{l1}} + \frac{N_1 i_1}{\mathfrak{R}_m} + \frac{N_2 i_2}{\mathfrak{R}_m} \tag{1.2-12}$$

$$\Phi_2 = \frac{N_2 i_2}{\mathfrak{R}_{l2}} + \frac{N_2 i_2}{\mathfrak{R}_m} + \frac{N_1 i_1}{\mathfrak{R}_m} \tag{1.2-13}$$

Substituting (1.2-12) and (1.2-13) into (1.2-6) and (1.2-7) yields

$$\lambda_1 = \frac{N_1^2}{\mathfrak{R}_{l1}} i_1 + \frac{N_1^2}{\mathfrak{R}_m} i_1 + \frac{N_1 N_2}{\mathfrak{R}_m} i_2 \tag{1.2-14}$$

$$\lambda_2 = \frac{N_2^2}{\mathfrak{R}_{l2}} i_2 + \frac{N_2^2}{\mathfrak{R}_m} i_2 + \frac{N_2 N_1}{\mathfrak{R}_m} i_1 \tag{1.2-15}$$

When the magnetic system is linear, the flux linkages are generally expressed in terms of inductances and currents. We see that the coefficients of the first two terms on the right-hand side of (1.2-14) depend on N_1 and the reluctance of the magnetic system, independent of the existence of winding 2. An analogous statement may be made regarding (1.2-15) with the roles of winding 1 and winding 2 reversed. Hence, the self-inductances are defined as

$$L_{11} = \frac{N_1^2}{\mathfrak{R}_{l1}} + \frac{N_1^2}{\mathfrak{R}_m} = L_{l1} + L_{m1} \tag{1.2-16}$$

$$L_{22} = \frac{N_2^2}{\mathfrak{R}_{l2}} + \frac{N_2^2}{\mathfrak{R}_m} = L_{l2} + L_{m2} \tag{1.2-17}$$

where L_{l1} and L_{l2} are the leakage inductances and L_{m1} and L_{m2} are the magnetizing inductances of windings 1 and 2, respectively. From (1.2-16) and (1.2-17), it follows that the magnetizing inductances may be related as

$$\frac{L_{m2}}{N_2^2} = \frac{L_{m1}}{N_1^2} \tag{1.2-18}$$

which is $1/\mathfrak{R}_m$.

The mutual inductances are defined as the coefficient of the third term on the right-hand side of (1.2-14) and (1.2-15). In particular,

$$L_{12} = \frac{N_1 N_2}{\mathfrak{R}_m} \tag{1.2-19}$$

$$L_{21} = \frac{N_2 N_1}{\mathfrak{R}_m} \tag{1.2-20}$$

We see that $L_{12} = L_{21}$ and, with the assumed positive direction of current flow and the manner in which the windings are wound as shown in Fig. 1.2-1, the mutual inductances are positive. If, however, the assumed positive directions of the current or the direction of the windings were such that $\boldsymbol{\Phi}_{m1}$ opposed $\boldsymbol{\Phi}_{m2}$, then the mutual inductances would be negative.

The mutual inductances may be related to the magnetizing inductances. Comparing (1.2-16) and (1.2-17) with (1.2-19) and (1.2-20), we see that

$$L_{12} = \frac{N_2}{N_1} L_{m1} = \frac{N_1}{N_2} L_{m2} \tag{1.2-21}$$

The flux linkages may now be written as

$$\lambda_1 = L_{11} i_1 + L_{12} i_2 \tag{1.2-22}$$

$$\lambda_2 = L_{21} i_1 + L_{22} i_2 \tag{1.2-23}$$

where L_{11} and L_{22} are defined by (1.2-16) and (1.2-17), respectively, and L_{12} and L_{21} by (1.2-19) and (1.2-20), respectively. The self-inductances L_{11} and L_{22} are always positive; however, the mutual inductances $L_{12}(L_{21})$ may be positive or negative, as previously mentioned.

Although the voltage equations given by (1.2-3) and (1.2-4) may be used for purposes of analysis, it is customary to perform a change of variables that yields the well-known equivalent T circuit of two windings coupled by a linear magnetic circuit. To set the stage for this derivation, let us express the flux linkages from (1.2-22) and (1.2-23) as

$$\lambda_1 = L_{l1} i_1 + L_{m1} \left(i_1 + \frac{N_2}{N_1} i_2 \right) \tag{1.2-24}$$

$$\lambda_2 = L_{l2} i_2 + L_{m2} \left(\frac{N_1}{N_2} i_1 + i_2 \right) \tag{1.2-25}$$

With λ_1 in terms of L_{m1} and λ_2 in terms of L_{m2}, we see two logical candidates for substitute variables, in particular, $(N_2/N_1)i_2$ or $(N_1/N_2)i_1$. If we let

$$i_2' = \frac{N_2}{N_1} i_2 \tag{1.2-26}$$

then we are using the substitute variable i_2', which, when flowing through winding 1, produces the same mmf as the actual i_2 flowing through winding 2; $N_1 i_2' = N_2 i_2$. This is said to be referring the current in winding 2 to winding 1 or to a winding with N_1 turns, whereupon winding 1 becomes the reference or primary winding and winding 2 is the secondary winding and i_2' is negative. On the other hand, if we let

$$i_1' = \frac{N_1}{N_2} i_1 \tag{1.2-27}$$

then i_1' is the substitute variable that produces the same mmf when flowing through winding 2 as i_1 does when flowing in winding 1; $N_2 i_1' = N_1 i_1$. This change of variables is said to refer to the current of winding 1 to winding 2 or to a winding with N_2 turns, whereupon winding 2 becomes the reference or primary winding and winding 1 the secondary with i_1'.

We will demonstrate the derivation of the equivalent T circuit by referring the current of winding 2 to a winding with N_1 turns; thus, i_2' is expressed by (1.2-26). We want the instantaneous power to be unchanged by this substitution of variables. Therefore,

$$v_2' i_2' = v_2 i_2 \tag{1.2-28}$$

Hence,

$$v_2' = \frac{N_1}{N_2} v_2 \tag{1.2-29}$$

Flux linkages, which have the units of V · s, are related to the substitute flux linkages in the same way as voltages. In particular,

$$\lambda_2' = \frac{N_1}{N_2} \lambda_2 \tag{1.2-30}$$

Now, replace $(N_2/N_1)i_2$ with i_2' in the expression for λ_1, given by (1.2-24). Next, solve (1.2-26) for i_2 and substitute it into λ_2 given by (1.2-25). Now, multiply this result by N_1/N_2 to obtain λ_2' and then substitute $(N_2/N_1)^2 L_{m1}$ for L_{m2} in λ_2'. If we do all this, we will obtain

$$\lambda_1 = L_{l1} i_1 + L_{m1} \left(i_1 + i_2' \right) \tag{1.2-31}$$

$$\lambda_2' = L_{l2}' i_2' + L_{m1} \left(i_1 + i_2' \right) \tag{1.2-32}$$

where

$$L_{l2}' = \left(\frac{N_1}{N_2} \right)^2 L_{l2} \tag{1.2-33}$$

The flux linkage equations given by (1.2-31) and (1.2-32) may also be written as

$$\lambda_1 = L_{11} i_1 + L_{m1} i_2' \tag{1.2-34}$$

$$\lambda_2' = L_{m1} i_1 + L_{22}' i_2' \tag{1.2-35}$$

where

$$L_{22}' = \left(\frac{N_1}{N_2} \right)^2 L_{22} = L_{l2}' + L_{m1} \tag{1.2-36}$$

and L_{22} is defined by (1.2-17).

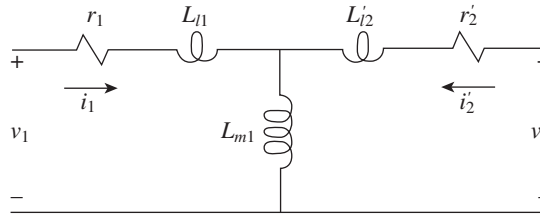

Figure 1.2-2 Equivalent *T* circuit with winding 1 selected as reference winding.

If we multiply (1.2-4) by N_1/N_2 to obtain v'_2, the voltage equations become

$$\begin{bmatrix} v_1 \\ v'_2 \end{bmatrix} = \begin{bmatrix} r_1 & 0 \\ 0 & r'_2 \end{bmatrix} \begin{bmatrix} i_1 \\ i_2 \end{bmatrix} + \frac{d}{dt} \begin{bmatrix} \lambda_1 \\ \lambda'_2 \end{bmatrix} \tag{1.2-37}$$

where

$$r'_2 = \left(\frac{N_1}{N_2}\right)^2 r_2 \tag{1.2-38}$$

The previous voltage equations, (1.2-37), together with the flux linkage equations, (1.2-34) and (1.2-35), suggest the equivalent *T* circuit shown in Fig. 1.2-2. This method may be extended to include any number of windings wound on the same core.

Example 1A ***The equivalent* T *circuit.***

It is instructive to illustrate the method of deriving an equivalent *T* circuit from open- and short-circuit measurements. When winding 2 of the two-winding transformer shown in Fig. 1.2-2 is open circuited and a 60 Hz voltage of 110 V (rms) is applied to winding 1, the average power supplied to winding 1 is 6.66 W. The measured current in winding 1 is 1.05 A (rms). Next, with winding 2 short-circuited, the current flowing in winding 1 is 2 A (rms) when the applied voltage is 30 V at 60 Hz. The average input power is 44 W. If we assume $L_{l1} = L'_{l2}$, an approximate equivalent *T* circuit can be determined from these measurements with winding 1 selected as the reference winding.

With $\tilde{V}_1 = |\tilde{V}_1| \angle\theta_{ev}(0)$ and $\tilde{I}_1 = |\tilde{I}_1| \angle\theta_{ei}(0)$ then the average power supplied to winding 1 may be expressed as

$$P_1 = |\tilde{V}_1||\tilde{I}_1| \cos \phi_{pf} \tag{1A-1}$$

where

$$\phi_{pf} = \theta_{ev}(0) - \theta_{ei}(0) \tag{1A-2}$$

Here, $\tilde{V}_1$ and $\tilde{I}_1$ are phasors with the positive direction of $\tilde{I}_1$ taken in the direction of the voltage drop, and $\theta_{ev}(0)$ and $\theta_{ei}(0)$ are the phase angles of $\tilde{V}_1$ and $\tilde{I}_1$,

respectively. Phasors are covered in Appendix B. Solving for ϕ_{pf} during the open-circuit test, we have

$$\phi_{pf} = \cos^{-1} \frac{P_1}{|\tilde{V}_1||\tilde{I}_1|} = \cos^{-1} \frac{6.66}{(110)(1.05)} = 86.7^\circ \tag{1A-3}$$

Although $\phi_{pf} = -86.7^\circ$ is also a legitimate solution of (1A-3), the positive value is taken since $\tilde{V}_1$ leads $\tilde{I}_1$ in an inductive circuit. With winding 2 open-circuited, the input impedance of winding 1 is

$$Z = \frac{\tilde{V}_1}{\tilde{I}_1} = r_1 + j(X_{l1} + X_{m1}) \tag{1A-4}$$

With $\tilde{V}_1$ as the reference phasor, $\tilde{V}_1 = 110\underline{/0^\circ}$, $\tilde{I}_1 = 1.05\underline{/-86.7^\circ}$. Thus,

$$r_1 + j(X_{l1} + X_{m1}) = \frac{110\underline{/0^\circ}}{1.05\underline{/-86.7^\circ}} = 6 + j104.6\ \Omega \tag{1A-5}$$

If we neglect core losses, then, from (1A-5), $r_1 = 6\ \Omega$. We also see from (1A-5) that $X_{l1} + X_{m1} = 104.6\ \Omega$. For the short-circuit test, we will assume that $\tilde{I}_1 = -\tilde{I}_2'$ since transformers are designed so that at rated frequency $X_{m1} >> |r_2' + jX_{l2}'|$. Hence, using (1A-1) again,

$$\phi_{pf} = \cos^{-1} \frac{44}{(30)(2)} = 42.8^\circ \tag{1A-6}$$

In this case, the input impedance is $Z = \left(r_1 + r_2'\right) + j\left(X_{l1} + X_{l2}'\right)$. This may be determined as

$$Z = \frac{30\underline{/0^o}}{2\underline{/-42.8^o}} = 11 + j10.2\ \Omega \tag{1A-7}$$

Hence, $r_2' = 11 - r_1 = 5\ \Omega$ and, since it is assumed that $X_{l1} = X_{l2}'$, both are $10.2/2 = 5.1\ \Omega$. Therefore, $X_{m1} = 104.6 - 5.1 = 99.5\ \Omega$. In summary, $r_1 = 6\ \Omega$, $L_{l1} = 13.5$ mH, $L_{m1} = 263.9$ mH, $r_2' = 5\ \Omega$, $L_{l2}' = 13.5$ mH. Make sure we converted from X's to L's correctly.

1.2.1 Nonlinear Magnetic System

Although the analysis of transformers and electric machines is often performed assuming a magnetically linear system, economics and physics dictate that in the practical design of many of these devices, some saturation occurs and that heating of the magnetic material exists due to hysteresis loss [2]. The magnetization characteristics of transformer or machine materials are typically given in the form of

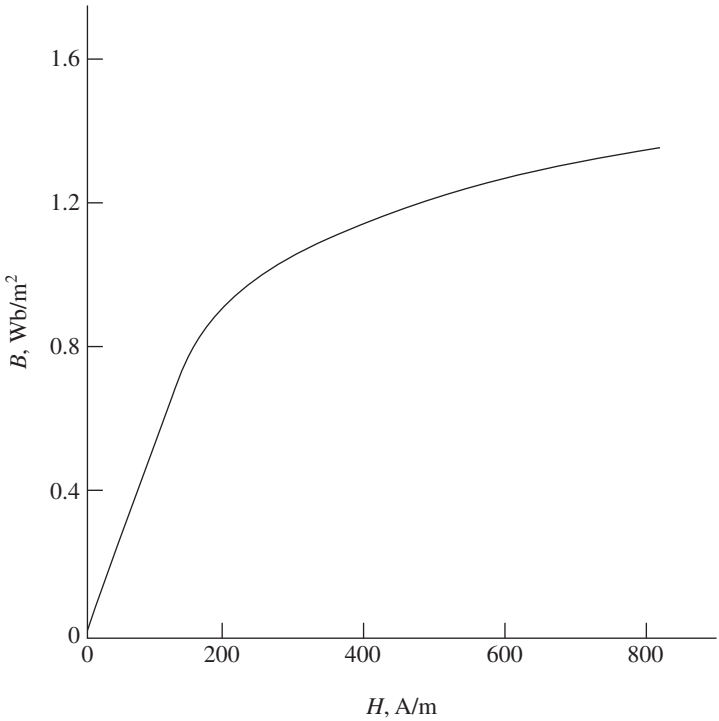

Figure 1.2-3 Typical *B–H* curve for silicon steel used in transformers.

the magnitude of flux density versus magnitude of field strength (*B–H* curve) as shown in Fig. 1.2-3.

If it is assumed that the magnetic flux is uniform through most of the core, then B is proportional to Φ and H is proportional to magnetomotive force (mmf). Hence, a plot of flux versus current is of the same shape as the *B–H* curve. A transformer is generally designed so that some saturation occurs during normal operation. During transients, saturation may occur resulting in large currents during startup transients. Electric machines are also designed similarly in that a machine generally operates slightly in the saturated region during normal, rated operating conditions. Since saturation causes coefficients of the differential equations describing the behavior of an electromagnetic device to be functions of the coil currents, transient analysis is difficult without the aid of a computer. Our purpose here is not to set forth methods of analyzing nonlinear magnetic systems. A method of incorporating the effects of saturation into a computer representation is of interest.

Formulating the voltage equations of stationary coupled windings appropriate for computer simulation is straightforward and yet this technique is fundamental

to the computer simulation of ac machines. Therefore, it is to our advantage to consider this method here. For this purpose, let us first write (1.2-31) and (1.2-32) as

$$\lambda_1 = L_{l1} i_1 + \lambda_m \tag{1.2-39}$$

$$\lambda'_2 = L'_{l2} i'_2 + \lambda_m \tag{1.2-40}$$

where

$$\lambda_m = L_{m1} \left(i_1 + i'_2 \right) \tag{1.2-41}$$

Solving (1.2-39) and (1.2-40) for the currents yields

$$i_1 = \frac{1}{L_{l1}} (\lambda_1 - \lambda_m) \tag{1.2-42}$$

$$i'_2 = \frac{1}{L'_{l2}} \left(\lambda'_2 - \lambda_m \right) \tag{1.2-43}$$

If (1.2-42) and (1.2-43) are substituted into (1.2-37), and if we solve the resulting equations for flux linkages, the following equations are obtained:

$$\lambda_1 = \int \left[v_1 + \frac{r_1}{L_{l1}} (\lambda_m - \lambda_1) \right] dt \tag{1.2-44}$$

$$\lambda'_2 = \int \left[v'_2 + \frac{r'_2}{L'_{l2}} \left(\lambda_m - \lambda'_2 \right) \right] dt \tag{1.2-45}$$

Substituting (1.2-42) and (1.2-43) into (1.2-41) yields

$$\lambda_m = L_a \left(\frac{\lambda_1}{L_{l1}} + \frac{\lambda'_2}{L'_{l2}} \right) \tag{1.2-46}$$

where

$$L_a = \left(\frac{1}{L_{m1}} + \frac{1}{L_{l1}} + \frac{1}{L'_{l2}} \right)^{-1} \tag{1.2-47}$$

We now have the equations expressed with λ_1 and λ'_2 as state variables. In the computer simulation, (1.2-44) and (1.2-45) are used to solve for λ_1 and λ'_2 and (1.2-46) is used to solve for λ_m. The currents can then be obtained from (1.2-42) and (1.2-43).

If the magnetization characteristics (magnetization curve) of the coupled winding are known, the effects of saturation of the mutual flux path may be incorporated into the computer simulation. Generally, the magnetization curve can be adequately determined from a test wherein one of the windings is open-circuited (winding 2, for example) and the input impedance of the other winding (winding 1) is determined from measurements as the applied

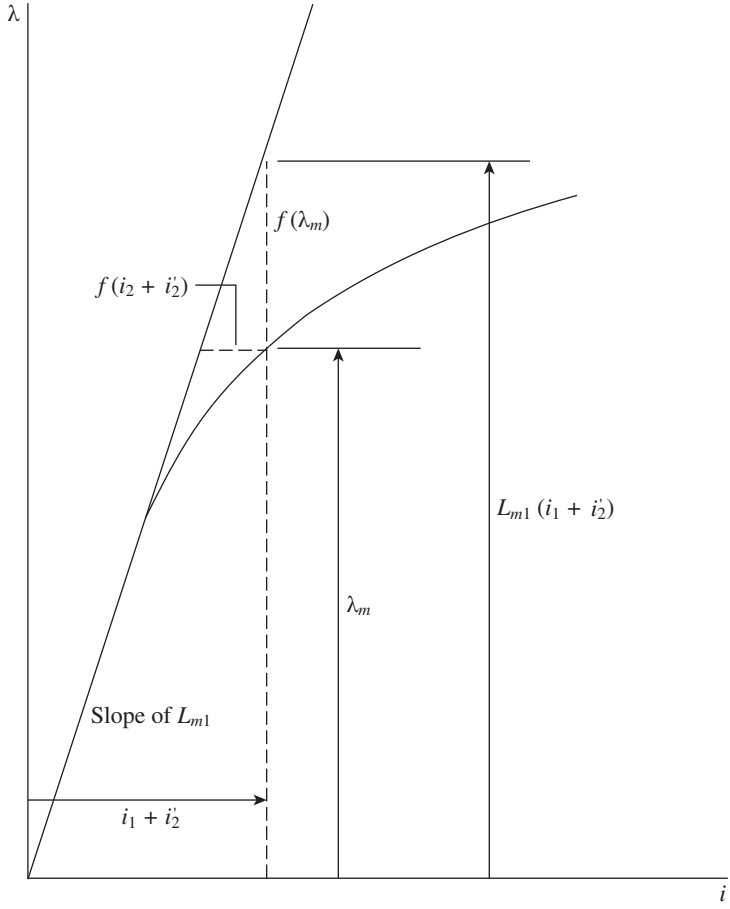

Figure 1.2-4 Magnetization curve.

voltage is increased in magnitude from zero to say 150% of the rated value. With information obtained from this type of test, we can plot λ_m versus $\left(i_1 + i_2'\right)$ as shown in Fig. 1.2-4 wherein the slope of the linear portion of the curve is L_{m1}. From Fig. 1.2-4, it is clear that in the region of saturation we have

$$\lambda_m = L_{m1}\left(i_1 + i_2'\right) - f(\lambda_m) \tag{1.2-48}$$

where $f(\lambda_m)$ may be determined from the magnetization curve for each value of λ_m. In particular, $f(\lambda_m)$ is a function of λ_m given by (1.2-48) and shown in Fig. 1.2-5. Therefore, the effects of saturation of the mutual flux path may be taken into account by replacing (1.2-41) with (1.2-48) for λ_m. Substituting (1.2-42) and (1.2-43) for i_1 and i_2', respectively, into (1.2-48) yields the following equation

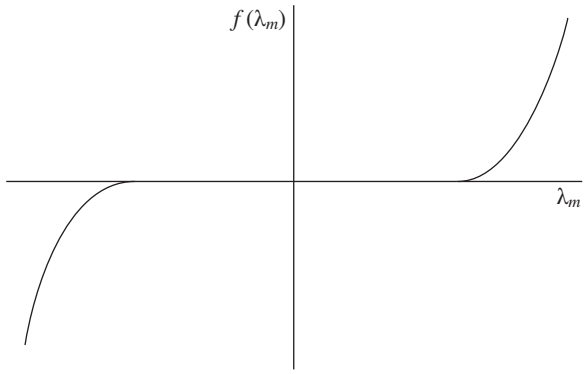

Figure 1.2-5 $f(\lambda_m)$ versus λ_m from Figure 1.2-4.

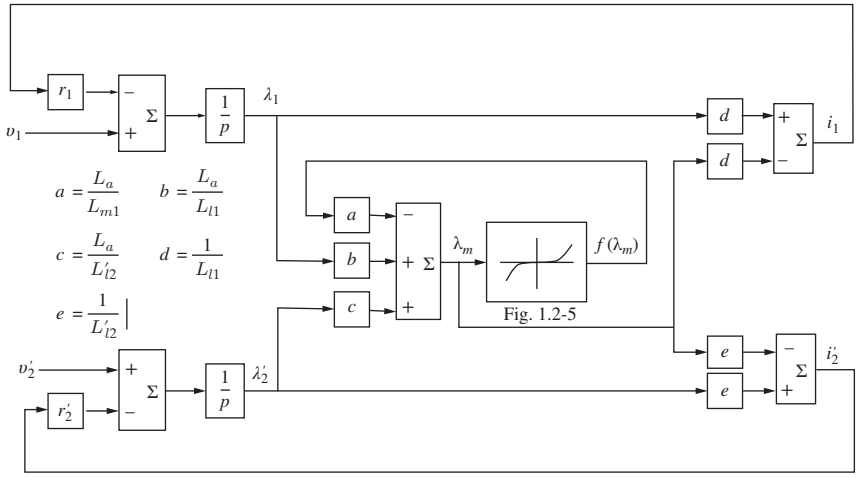

Figure 1.2-6 Time-domain block diagram of a two-winding transformer with saturation.

for λ_m

$$\lambda_m = L_a\left(\frac{\lambda_1}{L_{l1}} + \frac{\lambda'_2}{L'_{l2}}\right) - \frac{L_a}{L_{m1}}f(\lambda_m) \tag{1.2-49}$$

Hence, the computer simulation for including saturation involves replacing λ_m given by (1.2-46) with (1.2-49) where $f(\lambda_m)$ is a generated function of λ_m determined from the plot shown in Fig. 1.2-5. The time-domain block diagram of a two-winding transformer with saturation is shown in Fig. 1.2-6.

1.3 Energy Balance Relationships

Electromechanical systems consist of an electric system, a mechanical system, and a means whereby the electric and mechanical systems can interact. Interactions can take place through any and all electromagnetic and electrostatic fields that are common to both systems, and energy is transferred from one system to the other as a result of this interaction [3]. We will focus on the electromagnetic system, and the electrostatic system is treated in [2]. An electromechanical system with one electric subsystem, one mechanical subsystem, and one coupling field is depicted in Fig. 1.3-1. Electromagnetic radiation is neglected, and it is assumed that the electric system operates at a frequency sufficiently low so that the electric system may be considered a lumped-parameter system.

Heat loss will occur in the mechanical system due to friction, and the electric system will dissipate heat due to the resistance of the current-carrying conductors. Eddy current and hysteresis losses occur in the ferromagnetic materials. If W_E is the total energy supplied by the electric source and W_M the total energy supplied by the mechanical source, then the energy distribution could be expressed as

$$W_E = W_e + W_{eL} + W_{eS} \tag{1.3-1}$$

$$W_M = W_m + W_{mL} + W_{mS} \tag{1.3-2}$$

In (1.3-1), W_{eS} is the energy stored in the magnetic fields, which are not coupled with the mechanical system. The energy W_{eL} is the heat loss associated with the electric system excluding the coupling field losses. This loss occurs due to the resistance of the current-carrying conductors as well as the energy dissipated in the form of heat owing to hysteresis and eddy current losses external to the coupling field. W_e is the energy transferred to the coupling field by the electric system. The energies common to the mechanical system may be defined in a similar manner. In (1.3-2), W_{mS} is the energy stored in the moving member and compliances of the mechanical system, W_{mL} is the energy loss in the mechanical system in the form of heat, and W_m is the energy transferred to the coupling field. It is important to note that, with the convention adopted, the energy transferred to the coupling field by either source is considered positive. Also, W_E (W_M) is negative when energy is supplied to the electric source (mechanical source).

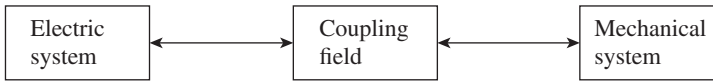

Figure 1.3-1 Block diagram of an elementary electromechanical system.

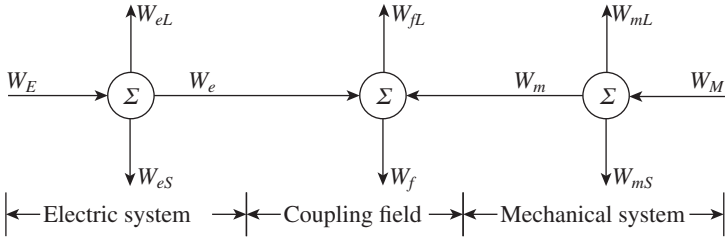

Figure 1.3-2 Energy balance.

If W_F is defined as the total energy transferred to the coupling field, then

$$W_F = W_f + W_{fL} \tag{1.3-3}$$

where W_f is energy stored in the coupling field and W_{fL} is the energy dissipated in the form of heat due to losses within the coupling field (eddy current or hysteresis losses). In order to comply with convention, we will use W_f to denote the energy stored in the coupling field rather than W_{fS}. The electromechanical system must obey the law of conservation of energy, thus,

$$W_f + W_{fL} = (W_E - W_{eL} - W_{eS}) + (W_M - W_{mL} - W_{mS}) \tag{1.3-4}$$

which may be written as

$$W_f + W_{fL} = W_e + W_m \tag{1.3-5}$$

This energy balance is shown schematically in Fig. 1.3-2.

The actual process of converting electric energy into mechanical energy (or vice versa) is independent of (1) the loss of energy in either the electric or the mechanical systems (W_{eL} and W_{mL}), (2) the energies stored in the electric or magnetic fields that are not common to both systems (W_{eS}), or (3) the energies stored in the mechanical system (W_{mS}). If the losses of the coupling field are neglected, then the field is conservative and (1.3-5) becomes

$$W_f = W_e + W_m \tag{1.3-6}$$

An example of an elementary electromechanical system is shown in Fig. 1.3-3. It has a magnetic coupling field with the space between the movable and stationary members exaggerated for clarity. The voltage of the electric source is denoted v, and f is an externally applied mechanical force. The electromagnetic force is denoted f_e. The resistance of the current-carrying conductor is denoted by r, with l denoting the inductance of a linear (conservative) electromagnetic system that does not couple with the mechanical system. In the mechanical system, M is the mass of the movable member, and the linear compliance and damper are represented by a spring constant K and a damping coefficient D. The displacement x_0

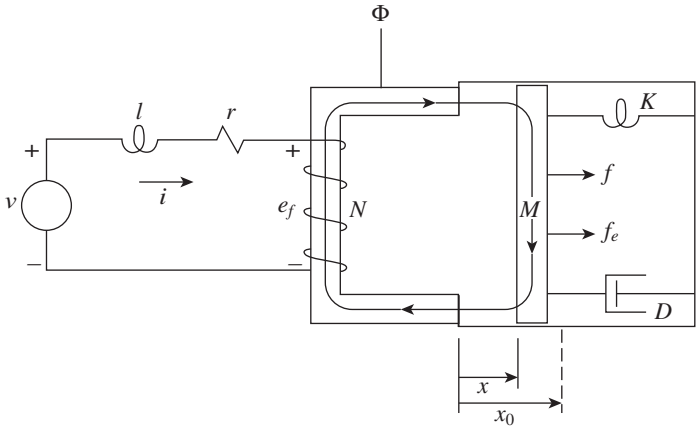

Figure 1.3-3 Electromechanical system with magnetic field.

is the zero force or equilibrium position of the mechanical system, which is the steady-state position of the mass with f_e and f equal to zero.

The voltage equation that describes the electric systems shown in Fig. 1.3-3 may be written as

$$v = ri + l\frac{di}{dt} + e_f \tag{1.3-7}$$

where e_f is the voltage drop due to the coupling field. The dynamic behavior of the translational mechanical systems may be expressed by employing Newton's law of motion. Thus,

$$f = M\frac{d^2x}{dt^2} + D\frac{dx}{dt} + K(x - x_0) - f_e \tag{1.3-8}$$

Since power is the time rate of energy transfer, the total energy supplied by the electric source is

$$W_E = \int vidt \tag{1.3-9}$$

The total energy supplied by the mechanical source is

$$W_M = \int fdx \tag{1.3-10}$$

which may also be expressed as

$$W_M = \int f\frac{dx}{dt}dt \tag{1.3-11}$$

Substituting (1.3-7) into (1.3-9) yields

$$W_E = r\int i^2dt + l\int i\frac{di}{dt}dt + \int e_f idt \tag{1.3-12}$$

The first term on the right-hand side of (1.3-12) represents the energy loss due to the resistance of the conductors (W_{eL}). The second term represents the energy stored in the linear electromagnetic field external to the coupling field (W_{eS}). Therefore, the total energy transferred to the coupling field from the electric system is

$$W_e = \int e_f i dt \tag{1.3-13}$$

Similarly, for the mechanical system

$$W_M = M \int \frac{d^2x}{dt^2} dx + D \int \left(\frac{dx}{dt}\right)^2 dt + K \int (x - x_0) dx - \int f_e dx \tag{1.3-14}$$

Here, the first and third terms on the right-hand side of (1.3-14) represent the kinetic energy stored in the mass and the potential energy stored in the spring, respectively. The sum of these two stored energies is W_{mS}. You should take a moment to look at the first term on the right-hand side of (1.3-14) and recognize that it can be written as $\frac{1}{2}M(dx/dt)^2$. The second term is the heat loss due to friction (W_{mL}). Thus, the total energy transferred to the coupling field from the mechanical system is

$$W_m = -\int f_e dx \tag{1.3-15}$$

It is important to note from Fig. 1.3-3 that a positive force f_e is assumed to be in the same direction as a positive displacement dx. Substituting (1.3-13) and (1.3-15) into the energy balance relation, (1.3-6), yields

$$W_f = \int e_f i dt - \int f_e dx \tag{1.3-16}$$

The equations set forth may be readily extended to include an electromechanical system with any number of electric and mechanical inputs. Whereupon the field may be expressed as

$$W_f = \sum_{j=1}^{J} W_{ej} + \sum_{k=1}^{K} W_{mk} \tag{1.3-17}$$

wherein J electric and K mechanical inputs exist. The total energy supplied to the coupling field from the electric inputs is

$$\sum_{j=1}^{J} W_{ej} = \int \sum_{j=1}^{J} e_{fj} i_j dt \tag{1.3-18}$$

The total energy supplied to the coupling field from the mechanical inputs is

$$\sum_{k=1}^{K} W_{mk} = -\int \sum_{k=1}^{K} f_{ek} dx_k \tag{1.3-19}$$

In our analysis of electromechanical systems, we will consider devices with only one mechanical input, for example, the shaft of the electric machine or the moving arm of a magnetic solenoid. On the other hand, since machines may have more than one electric terminal, it is necessary to consider systems with multiple electric inputs. In all cases, however, the multiple electric inputs have a common coupling field. Therefore, we need not become too ambitious in the following derivations. More specifically, hereafter we will restrict our analysis to electromechanical devices with only one mechanical input. Thus, the k subscript will be dropped from f_e, x, and W_m. This reduces our work considerably without restricting the practical application of our results. With one mechanical input, the energy balance equation becomes

$$W_f = \int \sum_{j=1}^{J} e_{fj} i_j dt - \int f_e dx \tag{1.3-20}$$

In differential form, which will be the form we will use extensively,

$$dW_f = \sum_{j=1}^{J} e_{fj} i_j dt - f_e dx \tag{1.3-21}$$

Example 1B ***Calculation of inductance.***
We will consider the electromechanical system shown in Fig. 1B-1. The system is at x_0 when v and f are both zero. The value of x_0 is 3 mm, which is very much exaggerated in Fig. 1B-1. The distance from c to d is 20 cm and 10 cm from a to b. The cross-sectional area of the iron and air gap is $A_i = A_g = 0.01$ m^2. The relative permeability of the iron is 4000, and the permeability of air is $4\pi \times 10^{-7}$ H · m.

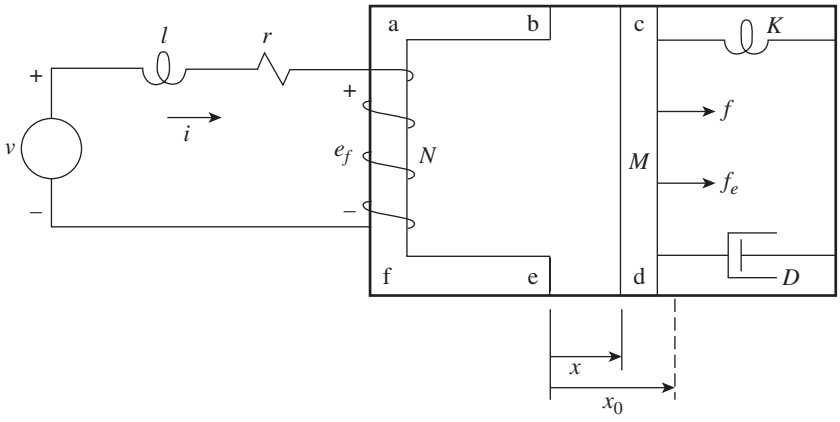

Figure 1B-1 Electromechanical system.

In Section 1.6, we let

$$L_m = \frac{k}{x} \tag{1B-1}$$

Determine N (turns) for $k = 6.283 \times 10^{-5}$ H · m.

The reluctance to the magnetizing flux with $x = x_0$

$$\begin{aligned}\mathfrak{R}_m = \mathfrak{R}_i + \mathfrak{R}_g &= \frac{l_i}{\mu_r \mu_0 A_i} + \frac{2l_g}{\mu_0 A_g} \\ &= \frac{60 \times 10^{-2}}{4 \times 10^3 \times 4\pi \times 10^{-7} \times 1 \times 10^{-3}} + \frac{2 \times 3 \times 10^{-3}}{4\pi \times 10^{-7} \times 10^{-3}} \\ &= 1.19 \times 10^5 + 47.8 \times 10^5 \end{aligned} \tag{1B-2}$$

Clearly, the reluctance is dominated by the reluctance of the two air gaps.

Now, if we neglect the reluctance of the iron, then

$$L_m = \frac{N^2 \mu_0 A_g}{2x} \tag{1B-3}$$

Comparing (1B-1) and (1B-3) we see that

$$k = \frac{1}{2} N^2 \mu_0 A_g \tag{1B-4}$$

Solving for N yields

$$\begin{aligned} N &= \left(\frac{2k}{\mu_0 A_g} \right)^{\frac{1}{2}} = \left(\frac{2 \times 6.283 \times 10^{-5}}{4\pi \times 10^{-7}\, 1 \times 10^{-2}} \right)^{\frac{1}{2}} \\ &= 100 \text{ turns} \end{aligned} \tag{1B-5}$$

1.4 Energy in Coupling Field

Before using (1.3-21) to obtain an expression for the electromagnetic force f_e, it is necessary to derive an expression for the energy stored in the coupling field. Once we have an expression for W_f, we can take the total derivative to obtain dW_f, which can then be substituted into (1.3-21). When expressing the energy in the coupling field, it is convenient to neglect all losses associated with the magnetic coupling field, whereupon the field is assumed to be conservative and the energy stored therein is a function of the state of the electrical and mechanical variables. Although the effects of the core losses of the coupling field may be functionally accounted for by appropriately introducing resistance in the electric circuit, this refinement is generally not necessary since the ferromagnetic material is selected and arranged in laminations so as to minimize the hysteresis and eddy current losses. Moreover, most of the energy stored in the coupling field is stored in the

air gap of the electromechanical device. Since air is a conservative medium, all of the energy stored therein can be returned to the electric or mechanical systems. Therefore, the assumption of a lossless coupling field is not as restrictive as it might first appear.

The energy stored in a conservative field is a function of the state of the system variables and not the manner in which the variables reached that state. It is convenient to take advantage of this feature when developing a mathematical expression for the field energy. In particular, it is convenient to fix mathematically the position of the mechanical system associated with the coupling field and then excite the electric system with the displacement of the mechanical system held fixed. During the excitation of the electric inputs, $dx = 0$, hence, W_m is zero even though electromagnetic forces may occur. Therefore, with the displacement held fixed, the energy stored in the coupling field during the excitation of the electric inputs is equal to the energy supplied to the coupling field by the electric inputs. Thus, with $dx = 0$, the energy supplied from the electric system may be expressed from (1.3-20) as

$$W_f = \int \sum_{j=1}^{J} e_{fj} i_j \, dt \quad \text{with } dx = 0 \tag{1.4-1}$$

Let us consider a singly excited electromagnetic system similar to that shown in Fig. 1.3-3. In this case, $e_f = d\lambda/dt$, whereupon (1.4-1) becomes

$$W_f = \int i d\lambda \quad \text{with } dx = 0 \tag{1.4-2}$$

Here, $j = 1$; however, the subscript is omitted for the sake of brevity. The area to the left of the λi relationship, shown in Fig. 1.4-1 for a singly excited electromagnetic system, is the area described by (1.4-2). In Fig. 1.4-1, this area represents the energy stored in the field at the instant when $\lambda = \lambda_a$ and $i = i_a$. The λi relationship need not be linear; it need only be single-valued, a property that is characteristic of a conservative or lossless field. Moreover, since the coupling field is conservative, the energy stored in the field with $\lambda = \lambda_a$ and $i = i_a$ is independent of the excursion of the electrical and mechanical variables before reaching this state.

The area to the right of the λi curve is called the *coenergy* and can be expressed as

$$W_c = \int \lambda di \quad \text{with } dx = 0 \tag{1.4-3}$$

Although the coenergy has little or no physical significance, we will find it a convenient quantity for expressing the electromagnetic force. From Fig. 1.4-1, we see that the sum of W_f and W_c is λ times i, that is,

$$\lambda i = W_c + W_f \tag{1.4-4}$$

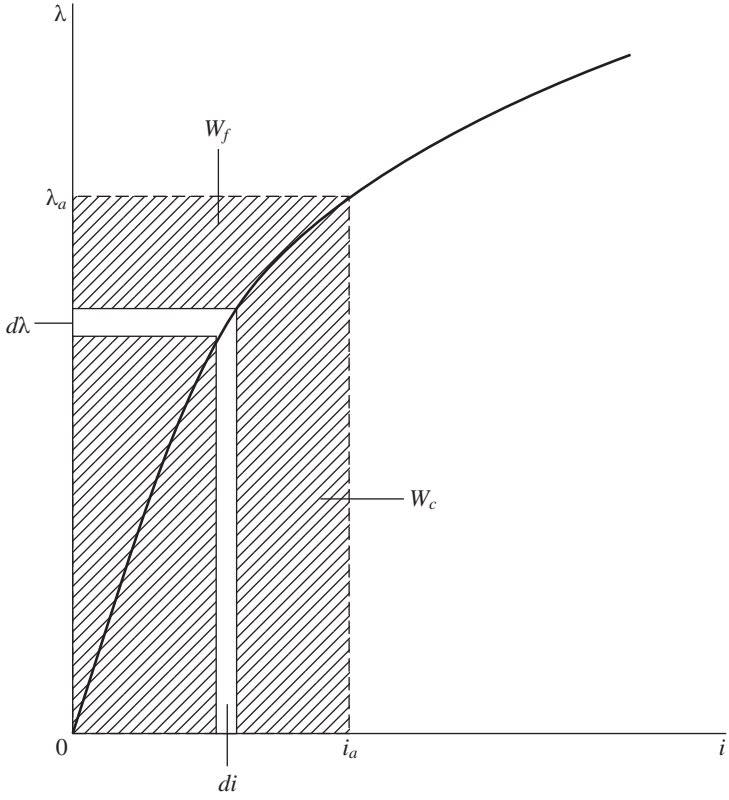

Figure 1.4-1 Stored energy and coenergy in a magnetic field of a singly excited electromagnetic device.

which is also valid for multiple electric inputs, where λi in (1.4-4) is replaced by $\sum_{j=1}^{J} \lambda_j i_j$. It should be clear that, for a linear magnetic system where the λi plots are straight-line relationships, $W_f = W_c = \frac{1}{2}\lambda i$.

The displacement x defines completely the influence of the mechanical system upon the coupling field; however, since λ and i are related, only one is needed in addition to x in order to describe the state of the electromechanical system. Therefore, we can select either λ and x as independent variables or i and x. If i and x are selected as the independent variables, it is convenient to express the field energy and the flux linkages as

$$W_f = W_f(i,\ x) \tag{1.4-5}$$

$$\lambda = \lambda(i,\ x) \tag{1.4-6}$$

With i and x as independent variables, we must express $d\lambda$ in terms of di before substituting into (1.4-2). Thus, from 1.4-6,

$$d\lambda = \frac{\partial \lambda(i,x)}{\partial i} di + \frac{\partial \lambda(i,x)}{\partial x} dx \tag{1.4-7}$$

In the derivation of an expression for the energy stored in the field, dx is set equal to zero. Hence, in the evaluation of field energy where $dx = 0$, $d\lambda$ is equal to the first term on the right-hand side of (1.4-7). Substituting into (1.4-2) yields

$$\begin{aligned} W_f(i,x) &= \int i \frac{\partial \lambda(i,x)}{\partial i} di \\ &= \int_0^i \xi \frac{\partial \lambda(\xi,x)}{\partial \xi} d\xi \text{ with } dx = 0 \end{aligned} \tag{1.4-8}$$

where ξ is a substitute variable of integration. Evaluation of (1.4-8) gives the energy stored in the field of the singly excited system. The coenergy in terms of i and x may be evaluated from (1.4-3) as

$$\begin{aligned} W_c(i,x) &= \int \lambda(i,x) di \\ &= \int_0^i \lambda(\xi,x) d\xi \end{aligned} \tag{1.4-9}$$

With λ and x as independent variables

$$W_f = W_f(\lambda, x) \tag{1.4-10}$$

$$i = i(\lambda, x) \tag{1.4-11}$$

The field energy may be evaluated from (1.4-2) as

$$\begin{aligned} W_f(\lambda,x) &= \int i(\lambda,x) d\lambda \\ &= \int_0^\lambda i(\xi,x) d\xi \end{aligned} \tag{1.4-12}$$

To evaluate the coenergy with λ and x as independent variables, we need to express di in terms of $d\lambda$. Thus, from (1.4-11),

$$di = \frac{\partial i(\lambda,x)}{\partial \lambda} d\lambda + \frac{\partial i(\lambda,x)}{\partial x} dx \tag{1.4-13}$$

Since $dx = 0$ in this evaluation, (1.4-13) becomes

$$\begin{aligned} W_c(\lambda,x) &= \int \lambda \frac{\partial i(\lambda,x)}{d\lambda} d\lambda \\ &= \int_0^\lambda \xi \frac{\partial i(\xi,x)}{\partial \xi} d\xi \text{ with } dx = 0 \end{aligned} \tag{1.4-14}$$

For a linear electromagnetic system, the λi plots are straight-line relationships. Thus, for the singly excited magnetically linear system,

$$\lambda(i,x) = L(x)i \tag{1.4-15}$$

or

$$i(\lambda,x) = \frac{\lambda}{L(x)} \tag{1.4-16}$$

where $L(x)$ is the inductance. Let us evaluate $W_f(i, x)$. With $dx = 0$ and, since $\frac{\partial\lambda(i,x)}{\partial i} = L(x)$, (1.4-7) becomes

$$d\lambda = L(x)di \tag{1.4-17}$$

Hence, from (1.4-8),

$$W_f(i,x) = \int_0^i \xi L(x)d\xi = \frac{1}{2}L(x)i^2 \tag{1.4-18}$$

It is left to the reader to show that by a similar procedure $W_f(\lambda, x)$, $W_c(i, x)$, and $W_c(\lambda, x)$ are equivalent to (1.4-18) for this magnetically linear system.

The field energy is a state function and the expression describing the field energy in terms of system variables is valid regardless of the variations in the system variables. For example, (1.4-18) expresses the field energy regardless of the variations in $L(x)$ and i. The fixing of the mechanical system so as to obtain an expression for the field energy is a mathematical convenience and not a restriction upon the result.

In the case of a multi-excited electromagnetic system, an expression for the field energy may be obtained by evaluating the following relation with $dx = 0$:

$$\int \sum_{j=1}^{J} i_j d\lambda_j \text{ with } dx = 0 \tag{1.4-19}$$

Since the coupling field is considered conservative, (1.4-19) may be evaluated independent of the order in which the flux linkages or currents are brought to their final values. To illustrate the evaluation of (1.4-19) for a multi-excited system, we will allow the currents to establish their final states one at a time while all other currents are mathematically fixed in their either unexcited or final states. This procedure may be illustrated by considering a doubly excited electric system with one mechanical input. An electromechanical system of this type could be constructed by placing a second winding, supplied from a second electric system, on either the stationary or movable member of the system shown in Fig. 1.3-3. In this evaluation, it is convenient to use currents and displacement as the independent variables. Hence, for a doubly excited electric system,

$$W_f(i_1,i_2,x) = \int \left[i_1 d\lambda_1(i_1,i_2,x) + i_2 d\lambda_2\left(i_1,i_2,x\right)\right] \quad \text{with } dx = 0 \tag{1.4-20}$$

In this determination of an expression for W_f, the mechanical displacement is held constant ($dx = 0$); thus, (1.4-20) becomes

$$W_f(i_1, i_2, x) = \int i_1 \left[\frac{\partial \lambda_1(i_1, i_2, x)}{\partial i_1} di_1 + \frac{\partial \lambda_1(i_1, i_2, x)}{\partial i_2} di_2 \right] + i_2 \left[\frac{\partial \lambda_2(i_1, i_2, x)}{\partial i_1} di_1 + \frac{\partial \lambda_2(i_1, i_2, x)}{\partial i_2} di_2 \right] \text{ with } dx = 0 \tag{1.4-21}$$

We will evaluate the energy stored in the field by employing (1.4-21) twice. First, we will mathematically increase the current i_1 from zero to its desired final value while holding i_2 at zero. Thus, i_1 is the variable of integration and $di_2 = 0$. Energy is supplied to the coupling field from the source connected to winding 1. As the second evaluation of (1.4-21), i_2 is increased from zero to its desired final value while maintaining i_1 at the value attained in the preceding step. Hence, i_2 is the variable of integration and $di_1 = 0$. During this time, energy is supplied from both sources to the coupling field since $d\lambda_1$ is, in general, nonzero. The total energy stored in the coupling field is the sum of the two evaluations. Following this two-step procedure, the evaluation of (1.4-21) for the total field energy becomes

$$W_f(i_1, i_2, x) = \int i_1 \frac{\partial \lambda_1(i_1, 0, x)}{\partial i_1} di_1 + \int \left[i_1 \frac{\partial \lambda_1(i_1, i_2, x)}{\partial i_2} di_2 + i_2 \frac{\partial \lambda_2(i_1, i_2, x)}{\partial i_2} di_2 \right] \tag{1.4-22}$$

which should be written

$$W_f(i_1, i_2, x) = \int_0^{i_1} \xi \frac{\partial \lambda_1(\xi, 0, x)}{\partial \xi} d\xi + \int_0^{i_2} \left[i_1 \frac{\partial \lambda_1(i_1, \xi, x)}{\partial \xi} + \xi \frac{\partial \lambda_2(i_1, \xi, x)}{\partial \xi} d\xi \right] \tag{1.4-23}$$

The first integral on the right-hand side of (1.4-22) or (1.4-23) results from the first step of the evaluation with i_1 as the variable of integration and with $i_2 = 0$ and $di_2 = 0$. The second integral comes from the second step of the evaluation with i_1 equal to its final value ($di_i = 0$) and i_2 as the variable of integration. The order of allowing the currents to reach their final state is irrelevant; that is, as our first step, we could have made i_2 the variable of integration while holding i_1 at zero ($di_1 = 0$) and then let i_1 become the variable of integration while holding i_2 at its final value. The results would be the same. For three electric inputs, the evaluation procedure would require three steps, one for each current to be brought mathematically to its final state.

Let us now evaluate the energy stored in a magnetically linear system with two electric inputs and one mechanical input. For this, let

$$\lambda_1(i_1, i_2, x) = L_{11}(x)i_1 + L_{12}(x)i_2 \tag{1.4-24}$$

$$\lambda_2(i_1, i_2, x) = L_{21}(x)i_1 + L_{22}(x)i_2 \tag{1.4-25}$$

where the self-inductances $L_{11}(x)$ and $L_{22}(x)$ include the leakage inductances. With the mechanical displacement held constant ($dx = 0$),

$$d\lambda_1(i_1, i_2, x) = L_{11}(x)di_1 + L_{12}(x)di_2 \tag{1.4-26}$$

$$d\lambda_2(i_I, i_2, x) = L_{21}(x)di_1 + L_{22}(x)di_2 \tag{1.4-27}$$

The coefficients on the right-hand side of (1.4-26) and (1.4-27) are the partial derivatives. For example, $L_{11}(x)$ is the partial derivative of $\lambda_1(i_1, i_2, x)$ with respect to i_1. Appropriate substitution into (1.4-23) gives

$$W_f(i_1, i_2, x) = \int_0^{i_1} \xi L_{11}(x)d\xi + \int_0^{i_2} [i_1 L_{12}(x) + \xi L_{22}(x)]\, d\xi \tag{1.4-28}$$

which yields

$$W_f(i_1, i_2, x) = \frac{1}{2}L_{11}(x)i_1^2 + L_{12}(x)i_1 i_2 + \frac{1}{2}L_{22}(x)i_2^2 \tag{1.4-29}$$

It follows that the total field energy of a linear electromagnetic system with J electric inputs may be expressed as

$$W_f(i_1, \ldots, i_J, x) = \frac{1}{2}\sum_{p=1}^{J}\sum_{q=1}^{J} L_{pq}i_p i_q \tag{1.4-30}$$

1.5 Electromagnetic Forces

The stage is set for us to obtain expressions for the electromagnetic force in electromechanical devices. For this purpose, recall that e_{fj} in (1.3-21) may be expressed as

$$e_{fj} = \frac{d\lambda_j}{dt} \tag{1.5-1}$$

If we substitute (1.5-1) into (1.3-21) and if we solve for $f_e dx$, we obtain

$$f_e dx = \sum_{j=1}^{J} i_j\, d\lambda_j - dW_f \tag{1.5-2}$$

Although we will use (1.5-2), it is helpful to express it in an alternative form. For this purpose, let us first write (1.4-4) for multiple electrical inputs:

$$\sum_{j=1}^{J} \lambda_j i_j = W_c + W_f \tag{1.5-3}$$

If we take the total derivative of (1.5-3), we obtain

$$\sum_{j=1}^{J} \lambda_j \, di_j + \sum_{j=1}^{J} i_j \, d\lambda_j = dW_c + dW_f \tag{1.5-4}$$

We realize that when we evaluate the force f_e we must select the independent variables; that is, either the flux linkages and x or the currents and x. The flux linkages and the currents both cannot be considered independent variables when evaluating the force f_e. Nevertheless, (1.5-4), wherein both $d\lambda_j$ and di_j appear, is valid in general, before a selection of independent variables is made to evaluate f_e. If we solve (1.5-4) for the field energy dW_f and substitute the result into (1.5-2), we obtain

$$f_e dx = -\sum_{j=1}^{J} \lambda_j \, di_j + dW_c \tag{1.5-5}$$

Either (1.5-2) or (1.5-5) can be used to evaluate the electromagnetic force f_e. If flux linkages and x are selected as independent variables, (1.5-2) is the most direct, whereas (1.5-5) is the most direct if currents and x are selected.

With flux linkages and x as the independent variables, the currents are expressed functionally as

$$i_j(\lambda_1, \cdots, \lambda_j, x) \tag{1.5-6}$$

For the purpose of compactness, we will denote $(\lambda_1, \ldots, \lambda_j, x)$ as $(\boldsymbol{\lambda}, x)$, where $\boldsymbol{\lambda}$ is an abbreviation for the complete set of flux linkages associated with the J windings. Let us write (1.5-2) with flux linkages and x as independent variables:

$$f_e(\boldsymbol{\lambda}, x)dx = \sum_{j=1}^{J} i_j(\boldsymbol{\lambda}, x) \, d\lambda_j - dW_f(\boldsymbol{\lambda}, x) \tag{1.5-7}$$

If we take the total derivative of the field energy with respect to $\boldsymbol{\lambda}$ and x, and substitute that result into (1.5-7) we obtain

$$f_e(\boldsymbol{\lambda}, x)dx = \sum_{j=1}^{J} i_j(\boldsymbol{\lambda}, x) d\lambda_j - \sum_{j=1}^{J} \frac{\partial W_f(\boldsymbol{\lambda}, x)}{\partial \lambda_j} d\lambda_j - \frac{\partial W_f(\boldsymbol{\lambda}, x)}{\partial x} dx \tag{1.5-8}$$

Equating the coefficients of dx gives

$$f_e(\boldsymbol{\lambda}, x) = -\frac{\partial W_f(\boldsymbol{\lambda}, x)}{\partial x} \tag{1.5-9}$$

If we now select i and x as independent variables, where $(\mathbf{i}, x)$ is the abbreviated notation for $(i_1, \ldots, i_J, x)$, then (1.5-5) can be written as

$$f_e(\mathbf{i}, x)dx = -\sum_{j=1}^{J} \lambda_j(\mathbf{i}, x)di_j + dW_c(\mathbf{i}, x) \tag{1.5-10}$$

If we take the total derivative of $W_c(i, x)$ with i and x as independent variables and substitute the result into (1.5-11), we obtain

$$f_e(\mathbf{i}, x)dx = -\sum_{j=1}^{J} \lambda_j(\mathbf{i}, x)di_j + \sum_{j=1}^{J} \frac{\partial W_c(\mathbf{i}, x)}{\partial i_j}di_j + \frac{\partial W_c(\mathbf{i}, x)}{\partial x}dx \tag{1.5-11}$$

Equating coefficients of dx yields

$$f_e(\mathbf{i}, x) = \frac{\partial W_c(\mathbf{i}, x)}{\partial x} \tag{1.5-12}$$

We will make extensive use of (1.5-12).

Although only translational mechanical systems have been considered, all force relationships developed herein may be modified for the purpose of evaluating the torque in rotational systems. In particular, when considering a rotational system, f_e is replaced with the electromagnetic torque T_e and x with the angular displacement θ_r of the rotating member. These substitutions are justified since the change of mechanical energy in a rotational system is expressed as

$$dW_m = -T_e\, d\theta_r \tag{1.5-13}$$

When dealing with machines, we perform a transformation that allows torque to be calculated more directly from the voltage equations. Nevertheless, the equations that we have developed for f_e given by (1.5-12) can be used to calculate T_e, that is

$$T_e = \frac{\partial W_c(i, \theta_r)}{\partial \theta_r} \tag{1.5-14}$$

Example 1C ***Detailed calculation of electromagnetic force.***
One may prefer to determine the electromagnetic force or torque by starting with the relationship $dW_f = dW_e + dW_m$ rather than by selecting a formula from the text. To illustrate this procedure, let

$$\lambda = L(x)i \tag{1C-1}$$

First, we must evaluate the field energy. Since losses in the coupling field are neglected, W_f is a function of state. Hence, W_f may be evaluated by fixing the mechanical displacement. This is done by setting $dx = 0$, whereupon

$$dW_f = dW_e = id\lambda \quad \text{with } dx = 0 \tag{1C-2}$$

where dW_e is obtained from (1.3-13) with $e_f = d\lambda/dt$. From (1C-1) with $dx = 0$,

$$d\lambda = L(x)di \tag{1C-3}$$

Substituting (1C-3) into (1C-2) and solving for W_f yields

$$W_f = \int_0^i L(x)\xi d\xi = \frac{1}{2}L(x)i^2 \tag{1C-4}$$

To obtain an expression for f_e, we go back to the basic relationship that $dW_f = dW_e + dW_m$; however, now $dx \neq 0$. Thus, from (1C-4),

$$dW_f = \frac{1}{2}i^2\frac{dL(x)}{dx}dx + L(x)idi \tag{1C-5}$$

Now,

$$dW_e = id\lambda = i^2\frac{dL(x)}{dx} + L(x)idi \tag{1C-6}$$

and from (1.3-15),

$$dW_m = -f_e dx \tag{1C-7}$$

Substituting into $dW_f = dW_e + dW_m$ yields

$$\frac{1}{2}i^2\frac{dL(x)}{dx}dx + L(x)idi = i^2\frac{dL(x)}{dx}dx + L(x)idi - f_e dx \tag{1C-8}$$

Equating the coefficients of dx,

$$f_e = \frac{1}{2}i^2\frac{dL(x)}{dx} \tag{1C-9}$$

1.6 Steady-State and Dynamic Performance of an Electromechanical System

It is instructive to consider the steady-state and dynamic performance of the elementary electromagnetic system shown in Fig. 1.3-3. The differential equations that describe this system are given by (1.3-7) for the electrical system and (1.3-8) for the mechanical system. The electromagnetic force f_e is expressed by (1.5-12). If the applied voltage, v, and the applied mechanical force, f, are constant, all derivatives with respect to time are zero during steady-state operation and the behavior can be predicted by

$$v = ri \tag{1.6-1}$$

$$f = K(x - x_0) - f_e \tag{1.6-2}$$

Equation (1.6-2) may be written as

$$-f_e = f - K(x - x_0) \tag{1.6-3}$$

The magnetic core of the system in Fig. 1.3-3 is generally constructed of ferromagnetic material with a relative permeability in the order of 2000–4000 (see Example 1B). $L(x)$ can be adequately approximated by

$$L(x) = \frac{k}{x} \tag{1.6-4}$$

In the actual system, the inductance will be a large finite value rather than infinity, as predicted by (1.6-4), when $x = 0$. Nevertheless, (1.6-4) is quite sufficient to illustrate the action of the system for $x > 0$. Substituting (1.6-4) into (1.5-12) where $W_c(i, x) = \frac{1}{2}L(x)i^2$ yields

$$f_e(i, x) = -\frac{ki^2}{2x^2} \tag{1.6-5}$$

A plot of (1.6-3), with f_e replaced by (1.6-5), is shown in Fig. 1.6-1 for the following system parameters:

$$r = 10\ \Omega \qquad x_0 = 3\ \text{mm}$$
$$K = 2667\ \text{N/m} \qquad k = 6.283 \times 10^{-5}\ \text{H} \cdot \text{m}$$

In Fig. 1.6-1, the plot of the negative of the electromagnetic force is for an applied voltage of 5 V whereupon the steady-state current of 0.5 A. The straight lines represent the right-hand side of (1.6-3) with $f = 0$ (lower straight line) and $f = 4$ N (upper straight line). Both lines intersect the $-f_e$ curve at two points. In particular, the upper line intersects the $-f_e$ curve at 1 and 1′; the lower line intersects at 2 and 2′. Stable operation occurs at only points 1 and 2. The system will not operate stably at points 1′ and 2′. This can be explained by assuming the system is operating at one of these points (1′ and 2′) and then showing that any system disturbance will cause the system to move away from these points. If, for example, x increases slightly from its value corresponding to point 1′, the restraining force $f - K(x - x_0)$ is larger in magnitude than $-f_e$, and x will continue to increase until the system reaches operating point 1. If x increases beyond its value corresponding to operating point 1, the restraining force is less than the electromagnetic force. Therefore, the system will establish steady-state operation at 1. If, on the other hand, x decreases from point 1′ the electromagnetic force is larger than the restraining force and the movable member will move until it comes in contact with the stationary member ($x = 0$). It is clear that the restraining force that yields a straight line below the $-f_e$ curve will not permit stable operation with $x > 0$.

The dynamic behavior of the system during step changes in the source voltage is shown in Fig. 1.6-2, and in Figs. 1.6-3 and 1.6-4 for step changes in the applied

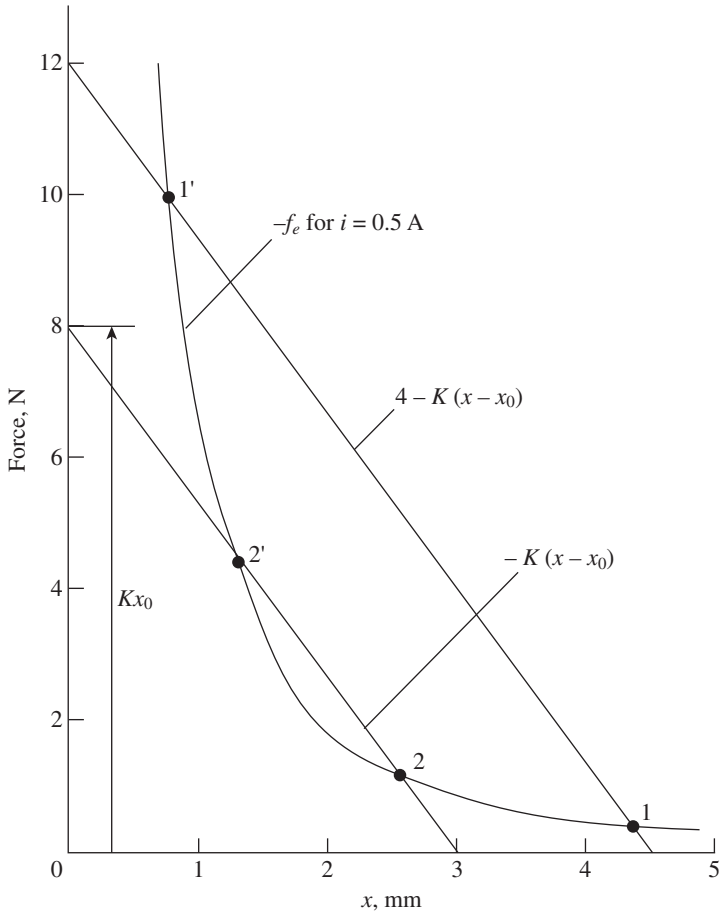

Figure 1.6-1 Steady-state operation of an electromechanical system in Fig. 1.3-1.

force f. The following system parameters were used in addition to those given previously:

$$l = 0 \quad M = 0.055\,\text{kg} \quad D = 4\,\text{N} \cdot \text{s/m}$$

The computer traces shown in Fig. 1.6-2 depict the dynamic performance of the example system when the applied voltage is stepped from zero to 5 V and then back to zero with the applied mechanical force held equal to zero. The following system variables are plotted: e_f, λ, i, f_e, x, W_e, W_f, and W_m. The energies are plotted in millijoules (mJ). Initially, the mechanical system is at rest with $x = x_0$ (3 mm). When the source voltage is applied, x decreases, and when steady-state operation is

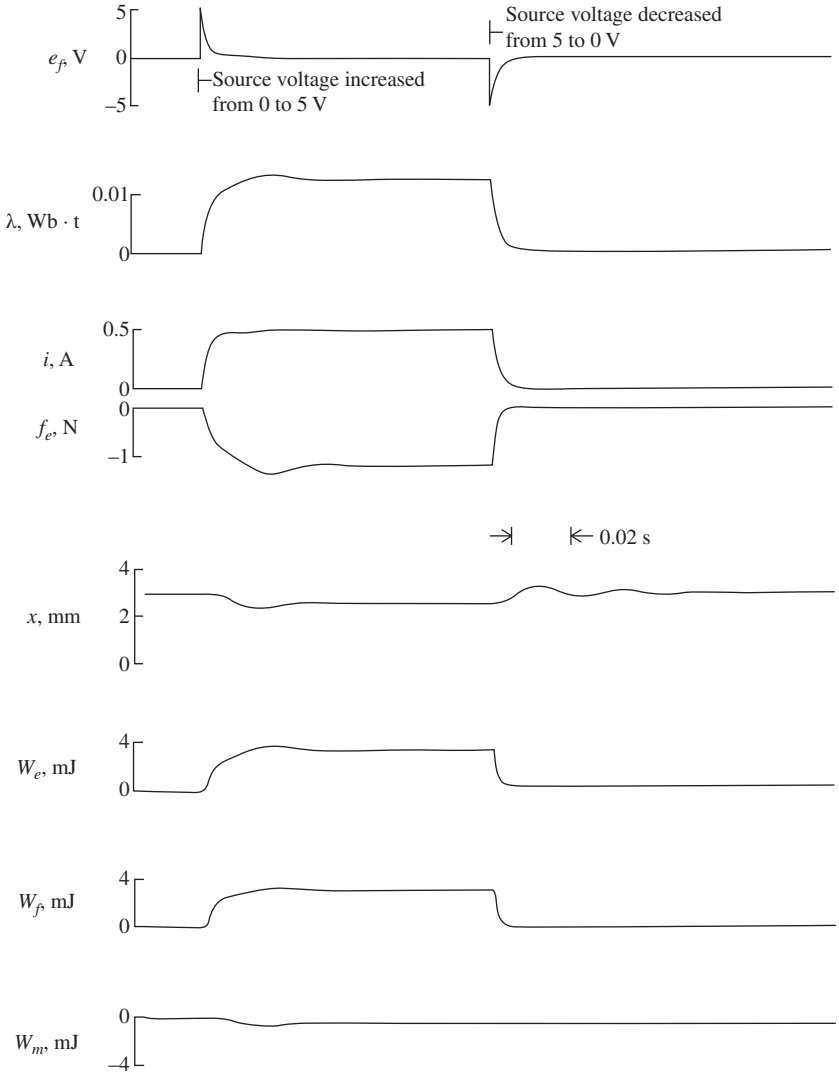

Figure 1.6-2 Dynamic performance of the electromechanical system shown in Fig. 1.3-3 during step changes in the source voltage.

reestablished, x is approximately 2.5 mm. Energy enters the coupling field via W_e. The bulk of this energy is stored in the field (W_f) with a smaller amount transferred to the mechanical system; some of that is dissipated in the damper during the transient period while the remainder is stored in the spring. When the applied

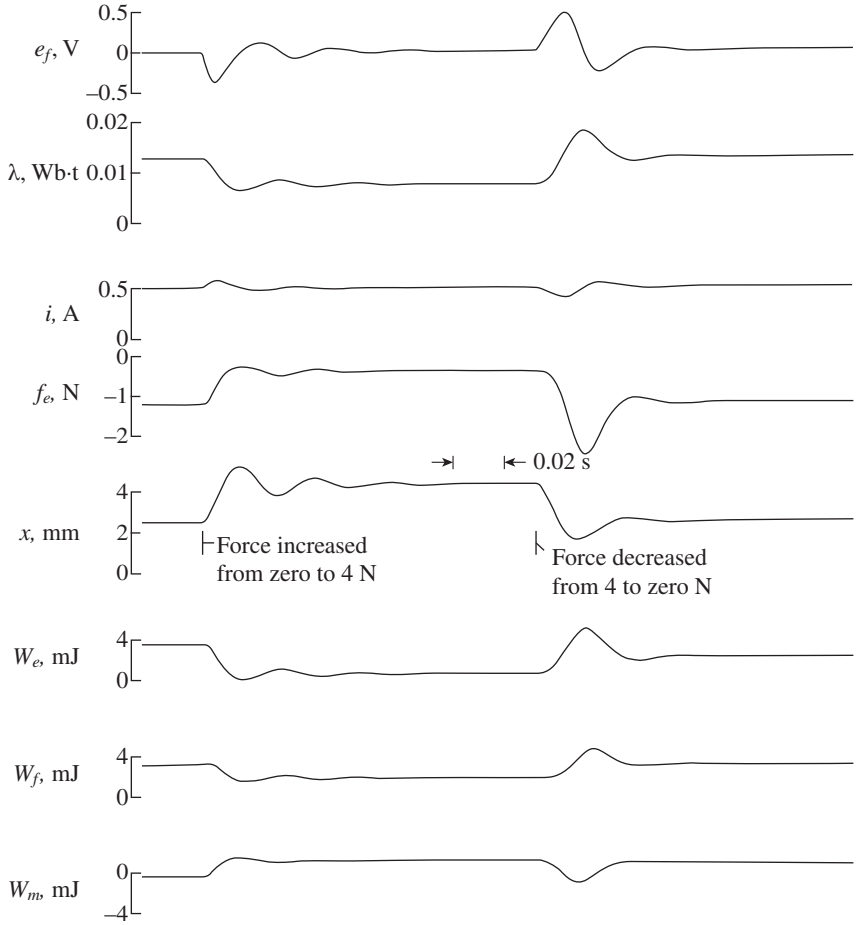

Figure 1.6-3 Dynamic performance of the electromechanical system shown in Fig. 1.3-3 during step changes in the applied force.

voltage is removed, the electrical and mechanical systems return to their original states. The change in W_m is small, increasing only slightly. Hence, during the transient period, there is an interchange of energy between the spring and mass that is finally dissipated in the damper. The net change in W_f during the application and removal of the applied voltage is zero; hence, the net change in W_e is positive and equal to the negative of the net change in W_m. The energy transferred to the mechanical system during this cycle is dissipated in the damper since f is fixed at zero, and the mechanical system returns to its initial rest position with zero energy stored in the spring.

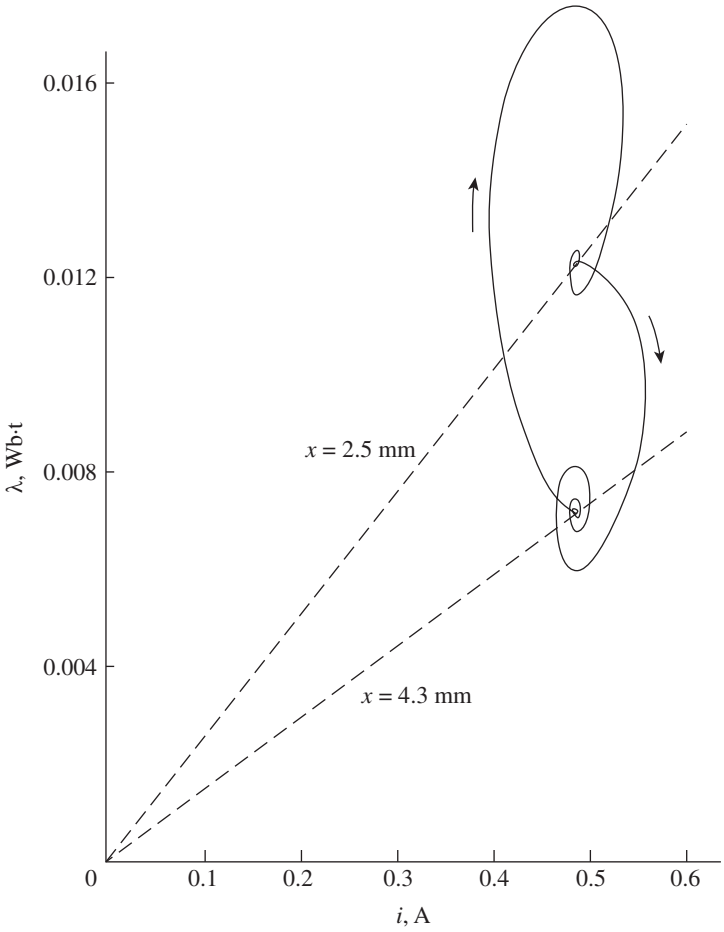

Figure 1.6-4 System response shown in Fig. 1.6-2.

In Fig. 1.6-3, the initial state is that shown in Fig. 1.6-2 with 5 V applied to the electrical system. The mechanical force f is increased from zero to 4 N, whereupon energy enters the coupling field from the mechanical system. Energy is transferred from the coupling field to the electrical system, some coming from the mechanical system and some from the energy originally stored in the magnetic field. Next, the force is stepped back to zero from 4 N. The electrical and mechanical systems return to their original states. During the cycle, a net energy has been transferred from the mechanical system to the electrical system that is dissipated in the resistance. This cycle is depicted on the λ versus i plot shown in Fig. 1.6-4.

References

1 P. C. Krause, O. Wasynczuk, S. D. Pekarek, and T. O'Connell, *Electromechanical Motion Devices*, Third Edition, Wiley and IEEE Press, 2020.

2 P. C. Krause, *Analysis of Electric Machinery,* McGraw-Hill, 1986.

3 D. C. White and H. H. Woodson, *Electromechanical Energy Conversion*, John Wiley and Sons, New York, 1959.

Problems

1.1 A two-winding, iron-core transformer is shown in Fig. 1P-1. $N_1 = 50$ turns, $N_2 = 100$ turns, and $\mu_r = 4000$. Calculate L_{m1} and L_{m2}.

1.2 Repeat Problem 1 if the iron core has an air gap of 0.2 cm in length and is cut through the complete cross section. Assume that fringing does not occur in the air gap, that is, the effective cross-sectional area of the air gap is 25 cm^2.

1.3 Two coupled coils have the following parameters:

$$L_{11} = 100\,\text{mH} \quad r_1 = 10$$
$$L_{22} = 25\,\text{mH} \quad r_2 = 2.5$$

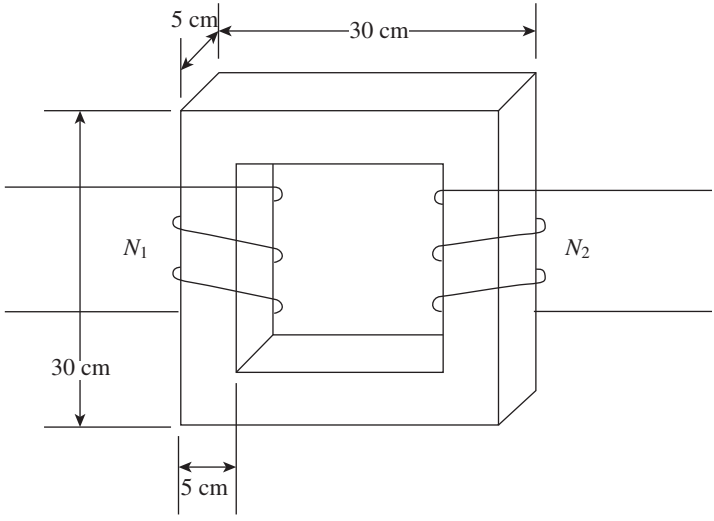

Figure 1P-1 Two-winding, iron-core transformer.

$$N_1 = 1000 \text{ turns} \quad N_2 = 500 \text{ turns}$$
$$L_{l1} = 0.1L_{11} \quad L_{L2} = 0.1L_{L2}$$

Develop a T equivalent circuit with coil 1 as the reference coil. Repeat with coil 2 as the reference coil.

1.4 A system with two windings has a flux linkage versus a current profile of

$$\lambda_1 = \left(0.1 + \frac{0.03}{x}\right) i_1 - \frac{0.01}{x} i_2$$
$$\lambda_2 = \left(0.0111 + \frac{0.03}{9x}\right) i_2 - \frac{0.01}{x} i_1$$

The resistance of the coils is $r_1 = 1\ \Omega$ and $r_2 = 0.3\ \Omega$. The winding voltage equations can be expressed in the form:

$$v_1 = r_1 i_1 + p\lambda_1$$

$$v_2 = r_2 i_2 + p\lambda_2$$

Derive the T equivalent circuit model for this system, assuming coil 1 as the reference. Show all component values. Label directions of all currents and voltages.

1.5 Obtain (1.2-47).

1.6 Determine the input impedance of the coupled circuits given in Problem 3 if the applied frequency to coil 1 is 60 Hz with coil 2 (*a*) open-circuited and (*b*) short-circuited. Repeat (*b*) with the current flowing in the magnetizing reactance neglected.

1.7 A third coil is wound on the ferromagnetic core shown in Fig. 1P-1. The resistance is r_3 and the leakage and magnetizing inductances are L_{l3} and L_{m3}, respectively. The coil is wound so that positive current (i_3) produces $\boldsymbol{\Phi}_{m3}$ in the same direction as $\boldsymbol{\Phi}_{m1}$ and $\boldsymbol{\Phi}_{m2}$. Derive the T equivalent circuit for this three-winding transformer. Actually, one should be able to develop the equivalent circuit without derivation.

1.8 A resistor and an inductor are connected as shown in Fig. 1P-2 with $R = 15\ \Omega$ and $L = 250$ mH. Determine the energy stored in the inductor W_{eS} and the energy dissipated by the resistor W_{eL} for $i > 0$ if $i(0) = 10$ A.

Figure 1P-2 *R-L* circuit.

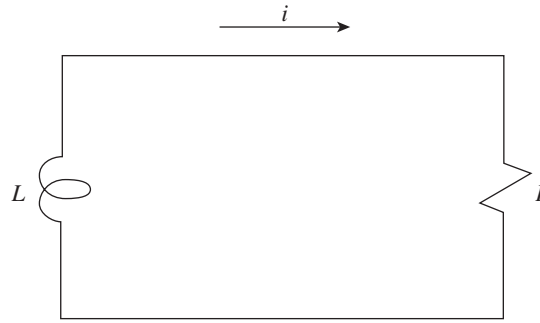

1.9 Consider the spring-mass-damper system shown in Fig. 1P-3. At $t = 0$, $x(0) = x_0$ (rest position) and $dx/dt = 1.5$ m/s. $M = 0.8$ kg, $D = 10$ N · s/m, and $K = 120$ N · m. For $t > 0$, determine the energy stored in the spring W_{ms1}, the kinetic energy of the mass W_{ms2}, and the energy dissipated by the damper W_{mL}.

Figure 1P-3
Spring-mass-damper system.

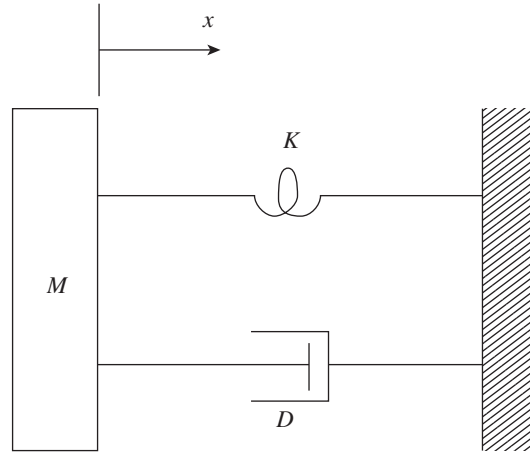

1.10 For the system shown in Fig. 1P-4, determine the winding inductance if the leakage inductance is one-tenth of the magnetizing inductance. If 10 V is applied to the winding at $t = 0$ *s*, determine W_f and the force of attraction that acts to attempt to reduce the gap at $t = 1$ *s*.

1.11 Express $W_f(i, x)$ and $W_c(i, x)$ for (a) $\lambda(i, x) = i^{2/3}x^2$ and (b) $\lambda(i, x) = ki \sin(x/a)\pi - xi$.

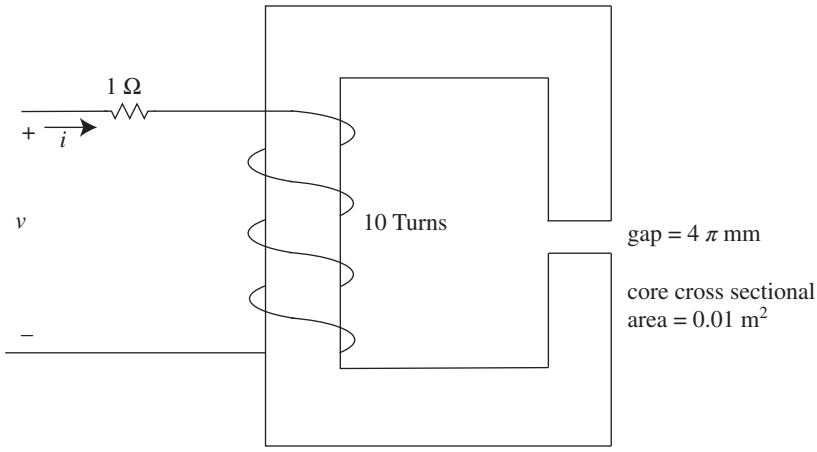

Figure 1P-4 Core configuration.

1.12 An electromechanical system has two electrical inputs. The flux linkages may be expressed as

$$\lambda_1(i_1, i_2, x) = x^2 i_1^2 + x i_2$$

$$\lambda_2(i_1, i_2, x) = x^2 i_2^2 + x i_1$$

Express $W_f(i_1, i_2, x)$ and $W_c(i_1, i_2, x)$.

1.13 Express $f_e(i, x)$ for the electromechanical systems described by the relations given in Problem 11.

1.14 Express $f_e(i_1, i_2, x)$ for the electromechanical system given in Problem 12.

1.15 Refer to Fig. 1.6-2. Following the system transients due to the application of the source voltage ($v = 5$ V), the system assumes steady-state operation. For this steady-state operation, calculate W_{eS}, W_f, and W_{mS}.

1.16 Refer to Fig. 1.6-3. Repeat Problem 15 for steady-state operation following the application of $f = 4$ N.

1.17 Refer to Fig. 1.6-4. Identify the area corresponding to ΔW_m when (*a*) x moves from 2.5 to 4.3 mm and (*b*) x moves from 4.3 to 2.5 mm.

2

Symmetrical Three-Phase Stator

2.1 Introduction

For analysis purposes, the stators of synchronous and induction machines are essentially the same. Therefore, in this chapter, we will treat the stator once for both types of machines. The rotors, however, are different and the modes of operation are different.

In this chapter, the rotor is assumed to be cylindrical thus a uniform air gap. The two-pole electric machines, synchronous or induction, have the same air-gap length every π radians for a two-pole device. We will analyze the two-pole stator using reference frame theory. In Chapter 3, we will show that all machines can be treated as two-pole devices. The extension to any number of pole pairs is straightforward, accomplished by a simple change of variables.

2.2 Stator Winding Configuration and Air-Gap mmf

The stationary member (stator) of the electric machine is an important part of the device. For analysis purposes, it is essentially the same for synchronous and induction machines. Therefore, we need to treat it only once. The windings of the stator are distributed to produce a space sinusoid of mmf. We find that in order to achieve this, we must have a sinusoidal distribution of the windings. In practice, we can only approximate a sinusoidal winding distribution. In the case of synchronous generators, the design of the stator mmf space harmonics is important since these harmonics cause harmonics in the output voltage. This is of less importance in the case of an induction motor. In the analysis of ac machines, we often consider only the fundamental component of the stator mmf.

The stator windings are shown in Fig. 2.2-1. As we can see, this multiphase stator is very involved. In this section, we are going to consider the stator windings as simply as possible. To form the stator of an electric machine, conductive wire is

Analysis of Electric Machinery and Drive Systems, Fourth Edition.
Paul C. Krause, Oleg Wasynczuk, Scott D. Sudhoff, and Steven D. Pekarek.

Companion website: www.wiley.com/go/krause_aem4e

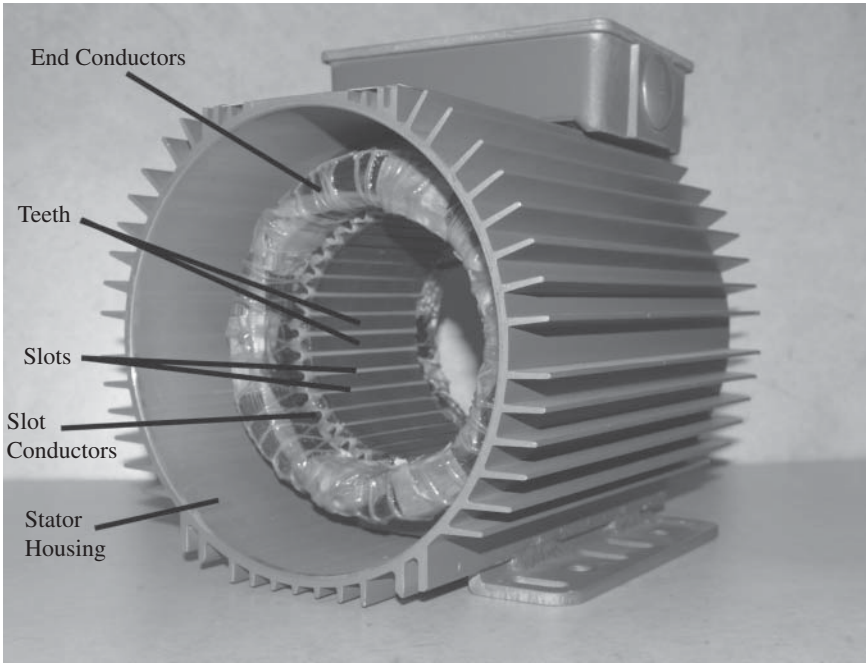

Figure 2.2-1 Stator windings of a multiphase machine.

wound in slots in an iron structure. The number of turns or coils of the stator windings of most ac machines is distributed to approximate a space sinusoid as shown in Fig. 2.2-2.

We will use *s* as a subscript or superscript for stator or stationary member. Also in Fig. 2.2-2, the "*as*" subscript denotes the variables associated with the *a* phase of the stator. In synchronous generators, great pains are taken to closely approximate a sinusoidal distribution of the stator windings to meet harmonic specifications. We attempt to distribute windings sinusoidally because sinusoidal currents through sinusoidally distributed windings create a constant-amplitude rotating air gap mmf. We will use the terms rotating air gap mmf and rotating magnetic field interchangeably.

In Fig. 2.2-2, each coil, $as_1 - as'_1$, $as_2 - as'_2$, …, $as_4 - as'_4$ has nc_s turns for each ⊗ or ⊙. Positive current is into the paper indicated by ⊗ and out of the paper at ⊙. The current through the windings is alternating so the cross, ⊗, and ⊙, will change; however, we are looking at an instant of time where the positive current is in at as_1, as_2, …, as_4.

The winding distribution is shown in Fig. 2.2-2(a), Ampere's law ($\oint H \cdot dL = i$) is shown in Fig. 2.2-2(b), and a developed plot of mmf_{as} is shown in Fig. 2.2-2(c). This

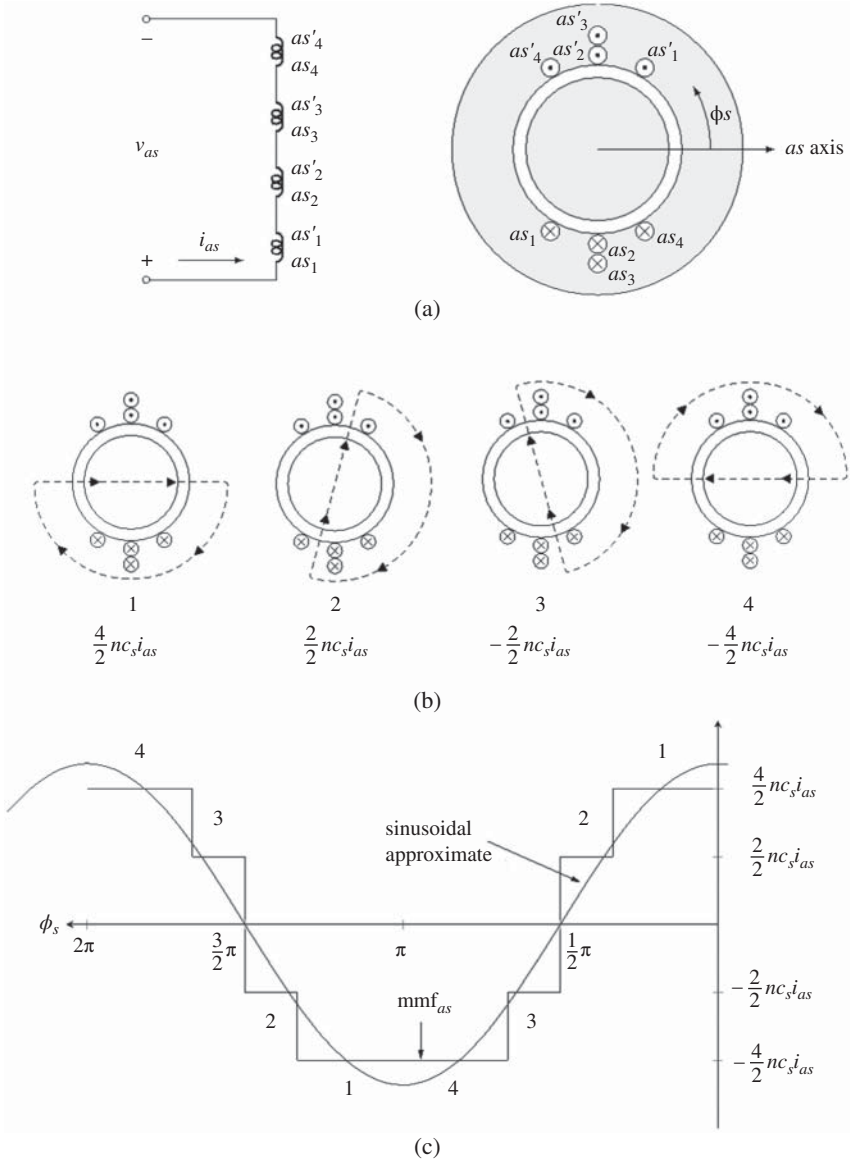

Figure 2.2-2 (a) The *as* winding. (b) Ampere's Law (c) mmf_{as}.

linear plot is possible since the radius is much larger than the length of the air gap. Each coil $as - as'$ spans π radians for the two-pole device and the positive as axis is determined by the current direction and the right-hand rule. Figures 2.2-2(a) and 2.2-2(b) are cross-sectional views of the stator.

If we follow the path of assumed positive current i_{as} flowing in the as winding, we see that current enters as_1, depicted by $\otimes$, to indicate that the assumed direction of positive current is down the length of the stator in an axial direction (into the paper). Current flows down the length of the stator, loops at the end, and flows back down the length of the stator and out at as'_1, depicted by $\odot$. Note that as_1 and as'_1 are placed in stator slots that span π radians. This is referred to as the *winding pitch* of π radians, which is characteristic of a two-pole machine. Now, as_1 around to as'_1 is referred to as a *coil* and as_1 or as'_1 is a *coil side*. In practice, a coil will contain more than one conductor. Current flows into as_1 in a conductor and out as'_1 via the same conductor. The conductor, which is insulated, may then be looped back to as_1 and the winding of the conductor around the $as_1 - as'_1$ path repeated, thereby forming a coil with numerous turns. The number of conductors in a coil side tells us the number of turns in the coil, which is denoted nc_s.

Once we have wound nc_s turns in the $as_1 - as'_1$ coil, we will take the same conductor and repeat this winding process to form the $as_2 - as'_2$ coil. We will assume that the same number of turns (nc_s) make up the $as_2 - as'_2$ coil as the $as_1 - as'_1$ coil and, similarly, for all stator coils. We could have wound a different number of turns in each coil but we will assume that this was not done. Once the winding is wound, we can use the right-hand rule to give a meaning to the as axis shown in Fig. 2.2-2(a). It is, by definition, the principal direction of the magnetic flux established by the assumed positive current flowing in the as winding. It is said to indicate the assumed positive direction of the magnetic axis of the as winding of this elementary sinusoidally distributed winding. The positive direction of the as axis reverses when i_{as} reverses.

Using Fourier analysis, the mmf_{as} waveform shown in Fig. 2.2-2 may be expressed as a Fourier series, e.g.,

$$\text{mmf}_{as} = 2.37\, nc_s\, i_{as}(\cos\phi_s + 0.179\cos 3\phi_s + \ldots) \tag{2.2-1}$$

If the windings are assumed to be distributed sinusoidally with a peak turns density of N_s turns/rad, it can be shown via Ampere's law that

$$\text{mmf}_{as} = \frac{N_s}{2} i_{as}\cos\phi_s \tag{2.2-2}$$

Although an exact sinusoidal winding distribution cannot be achieved in practice (it can only be approximated), it is typically reasonable to neglect the harmonic components in (2.2-1) and approximate mmf_{as} using (2.2-2). We are considering the mmf dropped across one air gap rather than the total mmf dropped. Here, we are considering a uniform air gap; however, as we have mentioned, in two-pole *ac* machines, the air gap is the same π radians of a nonuniform rotor.

For a two-phase stator, the *bs* winding is identical to the *as* winding but shifted $\pi/2$ radians either clockwise (cw) or counterclockwise (ccw) from the *as* winding. In a double-layer two-phase winding, each slot could contain *as* and/or *bs* coils. For a ccw shift, mmf_{bs} may be approximated as

$$\text{mmf}_{bs} = \frac{N_s}{2} i_{bs} \sin \phi_s \tag{2.2-3}$$

For a three-phase machine, the *as*, *bs*, and *cs* windings are identical and displaced $\frac{2\pi}{3}$ radians apart from one another. In this case, each slot in a double-layer winding distribution such as that shown in Fig. 2.2-2 would contain two *as*, two *bs*, two *cs*, an *as* and *bs*, or a *bs* and *cs* coil. The corresponding mmf_{bs} and mmf_{cs} may be approximated as

$$\text{mmf}_{bs} = \frac{N_s}{2} i_{bs} \cos\left(\phi_s - \frac{2\pi}{3}\right) \tag{2.2-4}$$

$$\text{mmf}_{cs} = \frac{N_s}{2} i_{cs} \cos\left(\phi_s + \frac{2\pi}{3}\right) \tag{2.2-5}$$

Tesla's rotating magnetic field is obtained by adding mmf_{as} and mmf_{bs} for a two-phase stator or mmf_{as}, mmf_{bs}, and mmf_{cs} for a three-phase stator. In particular, if we neglect, as Park did [1], the harmonic components of mmf_s we have for the two-phase stator.

$$\begin{aligned} \text{mmf}_s &= \text{mmf}_{as} + \text{mmf}_{bs} \\ &= \frac{N_s}{2}(i_{as} \cos \phi_s + i_{bs} \sin \phi_s) \end{aligned} \tag{2.2-6}$$

For a three-phase stator

$$\begin{aligned} \text{mmf}_s &= \text{mmf}_{as} + \text{mmf}_{bs} + \text{mmf}_{cs} \\ &= \frac{N_s}{2}\left[i_{as} \cos \phi_s + i_{bs} \cos\left(\phi_s - \frac{2\pi}{3}\right) + i_{cs} \cos\left(\phi_s + \frac{2\pi}{3}\right)\right] \end{aligned} \tag{2.2-7}$$

2.3 Transformation Equations

Park considered only sinusoidally distributed windings in his classic paper on the analysis of synchronous machines [1]. Thus, Tesla's rotating magnetic field would include only the fundamental component as given in (2.2-6) and (2.2-7). We are going to use these equations for Tesla's rotating magnetic field to determine the transformation equations, but first let us consider Fig. 2.3-1, which represents a three-phase stator.

In Fig. 2.3-1, the *as*, *bs*, and *cs* windings are each shown by two circles placed at the point of maximum winding density of sinusoidally distributed windings. The three windings are identical whereupon the stator is termed a symmetrical stator.

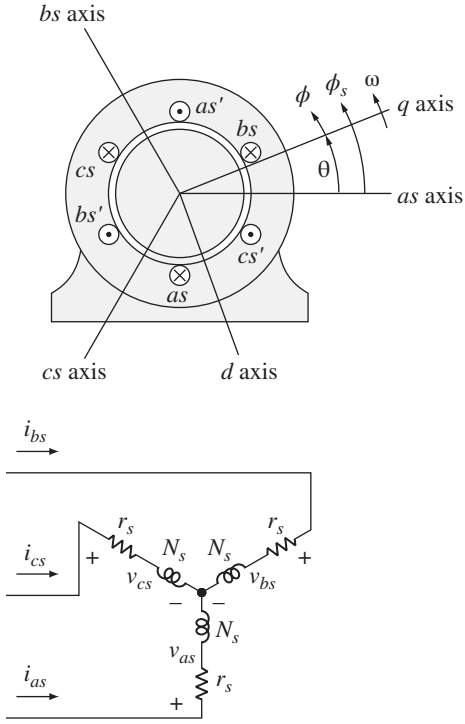

Figure 2.3-1 Elementary two-pole three-phase sinusoidally distributed stator windings.

Also, we have added q and d axes, which are displaced from the as axis by the angle θ and ϕ is the displacement from the q axis. We can express ϕ_s as

$$\phi_s = \theta + \phi \tag{2.3-1}$$

The angular velocity of the q and d axes, which we can select depending on which reference frame we wish to use, is

$$\omega(t) = \frac{d\theta(t)}{dt} \tag{2.3-2}$$

Here, ω is the speed of the reference frame, ω_r is the rotor angular velocity, and ω_e is the frequency of the stator applied voltages. For steady-state operating conditions, ω_r and ω_e are constant and ω is generally selected to be constant. We realize that we have introduced terms that may be new to many of us; however, these terms will be made clear as we go along.

Substituting (2.3-1) into (2.2-7) and after some work, we have

$$\begin{aligned}\text{mmf}_s = {} & \frac{N_s}{2}\cos\phi\left[i_{as}\cos\theta + i_{bs}\cos\left(\theta - \frac{2\pi}{3}\right) + i_{cs}\cos\left(\theta + \frac{2\pi}{3}\right)\right] \\ & -\frac{N_s}{2}\sin\phi\left[i_{as}\sin\theta + i_{bs}\sin\left(\theta - \frac{2\pi}{3}\right) + i_{cs}\sin\left(\theta + \frac{2\pi}{3}\right)\right]\end{aligned} \tag{2.3-3}$$

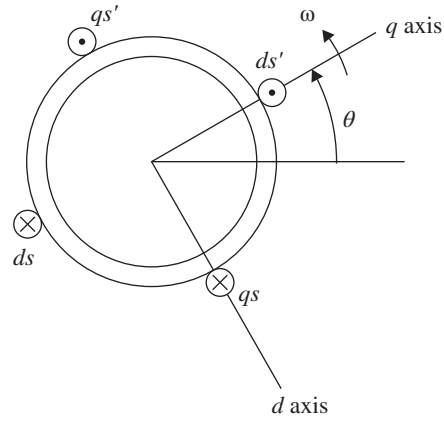

Figure 2.3-2 Fictitious *qs* and *ds* windings.

Equation (2.3-3) is the air gap mmf established by the three-phase stator. If we let $\phi = 0$, then we are looking at mmf_s along the q axis and the sum of currents inside the [ ] are i_{qs}, which we call a substitute current, that flows in a fictitious *qs* winding as shown in Fig. 2.3-2. Note that the *qs* winding is displaced $\frac{\pi}{2}$ degrees from the q axis. The second axis is the d axis and with $\phi = -\frac{\pi}{2}$, the sum of currents inside the [ ] are i_{ds}, which is assumed to flow in a fictitious *ds* winding. We now have two substitute currents (i_{qs} and i_{ds}) and two fictitious (*qs* and *ds*) windings. The substitute currents i_{qs} and i_{ds} flowing in the fictitious *qs* and *ds* windings produce the same mmf_s that is produced by the actual i_{as}, i_{bs}, and i_{cs} flowing in the physical *as*, *bs*, and *cs* windings [2].

Since we have two substitute currents, we need a third substitute variable since we are replacing three stator currents (i_{as}, i_{bs}, and i_{cs}). We will call the third substitute variable the zero current, which is defined as

$$i_{0s} = \frac{1}{3}(i_{as} + i_{bs} + i_{cs}) \tag{2.3-4}$$

The expression for zero current is independent of θ and, from (2.3-3), does not contribute to mmf_s.

We are now at a stage where we can define a transformation of *as*, *bs*, and *cs* variables into *qs*, *ds*, and 0*s* variables. In matrix form [3, 4]

$$\begin{bmatrix} f_{qs} \\ f_{ds} \\ f_{0s} \end{bmatrix} = \frac{2}{3} \begin{bmatrix} \cos\theta & \cos\left(\theta - \frac{2\pi}{3}\right) & \cos\left(\theta + \frac{2\pi}{3}\right) \\ \sin\theta & \sin\left(\theta - \frac{2\pi}{3}\right) & \sin\left(\theta + \frac{2\pi}{3}\right) \\ \frac{1}{2} & \frac{1}{2} & \frac{1}{2} \end{bmatrix} \begin{bmatrix} f_{as} \\ f_{bs} \\ f_{cs} \end{bmatrix} \tag{2.3-5}$$

The $\frac{2}{3}$ factor was introduced by Park [1] and we have replaced i with f, where f can be i, v, or λ. That is, we will use the same transformation equations for all electrical variables (currents, voltages, and flux linkages). Eq. (2.3-5) can be expressed

symbolically as

$$\mathbf{f}_{qd0s} = \mathbf{K}_s \mathbf{f}_{abcs} \tag{2.3-6}$$

where $\mathbf{K}_s$ is the transformation of stator variables to *qs*, *ds*, and 0*s* variables. The inverse of $\mathbf{K}_s$ is

$$(\mathbf{K}_s)^{-1} = \begin{bmatrix} \cos\theta & \sin\theta & 1 \\ \cos\left(\theta - \frac{2\pi}{3}\right) & \sin\left(\theta - \frac{2\pi}{3}\right) & 1 \\ \cos\left(\theta + \frac{2\pi}{3}\right) & \sin\left(\theta + \frac{2\pi}{3}\right) & 1 \end{bmatrix} \tag{2.3-7}$$

and the inverse transformation may be expressed as

$$\begin{bmatrix} f_{as} \\ f_{bs} \\ f_{cs} \end{bmatrix} = \begin{bmatrix} \cos\theta & \sin\theta & 1 \\ \cos\left(\theta - \frac{2\pi}{3}\right) & \sin\left(\theta - \frac{2\pi}{3}\right) & 1 \\ \cos\left(\theta + \frac{2\pi}{3}\right) & \sin\left(\theta + \frac{2\pi}{3}\right) & 1 \end{bmatrix} \begin{bmatrix} f_{qs} \\ f_{ds} \\ f_{0s} \end{bmatrix} \tag{2.3-8}$$

The transformations $\mathbf{K}_s$ and $(\mathbf{K}_s)^{-1}$ are for stator variables *as*, *bs*, and *cs* to and from the arbitrary reference frame variables *qs*, *ds*, and 0*s*. Expanding (2.3-8) into three scalar equations reveals that the zero-variable f_{0s} contributes equally to the *as*, *bs*, and *cs* variables. It will later be argued that in many cases the zero variables (i_{0s}, v_{0s}, and/or λ_{0s}) are identically equal to 0. Although the *as*, *bs*, and *cs* variables are associated with stationary (stator) windings, the *qs* and *ds* variables are substitute variables associated with fictitious windings that rotate at ω, which we can select. Each selection of ω establishes a reference frame. There are an infinite number of reference frames; however, we generally use $\omega = 0$ stationary or stator reference frame, $\omega = \omega_r$ a reference frame fixed at the rotor speed, or $\omega = \omega_e$ the synchronously rotating reference frame. Let us think about this for a minute. When we select a reference frame, we select where the fictitious circuits are placed. With $\omega = 0$, the circuits are stationary. The question to ask yourself is what would be the steady-state frequency of the balanced substitute variables to cause Tesla's rotating magnetic field to rotate at ω_e. The answer is the frequency of the substitute variables would be ω_e. We already knew this since the *as*, *bs*, and *cs* circuits are stationary and the frequency of the stator variables is ω_e.

If we select $\omega = \omega_e$ the fictitious circuits are rotating at ω_e. In this case, the steady-state frequency of the variables flowing in these circuits in order to have mmf_s rotate at ω_e is *dc*. Now, fixing the circuits at the rotor speed ω_r, which we will say varies from zero to ω_e, the circuits are changing speed from $\omega_r = 0$ to ω_e. The balanced substitute variables ω_r have a frequency of ω_e when $\omega = 0$ and *dc* when ω_r reaches ω_e. Actually, reference frame theory is nothing more than changing the frequency of the substitute variables to portray mmf_s from the selected reference frame.

The $\frac{2}{3}$ factor in (2.3-5) was introduced by Park, which makes the f_{qd0s} variables equal in magnitude to the f_{abcs} variables. This must be accounted for when we calculate power and torque. We are taking a three-phase system (*as*, *bs*, and *cs*) and considering it as a two-phase system (*qs* and *ds*), but we have reduced the three-phase system back to a two-phase system with the $\frac{2}{3}$ factor. Therefore, we must multiply the power by $\frac{3}{2}$ when using substitute variables to obtain the three-phase power. Now, f_{0s} is not a function of the angular velocity ω; therefore, the zero variables do not contribute to the torque, only the *qs* and *ds* variables do. We will see this when we calculate torque of machines.

The mmf_s given by (2.3-3) can be expressed in terms of *qs* and *ds* currents as

$$\text{mmf}_s = \frac{N_s}{2}(i_{qs}\cos\phi + i_{ds}\sin\phi). \tag{2.3-9}$$

We are starting to see that the *qs* and *ds* variables, associated with fictitious circuits rotating at ω angular velocity, will have the steady-state frequency that is necessary to portray the rotating mmf as viewed from the ω reference frame. We will talk more about this as we go along.

We should do one more thing before leaving this section. Let us assume that the steady-state three-phase stator variables are

$$F_{as} = \sqrt{2}F_s\cos[\omega_e t + \theta_{esf}(0)] \tag{2.3-10}$$

$$F_{bs} = \sqrt{2}F_s\cos\left[\omega_e t - \frac{2}{3}\pi + \theta_{\text{esf}}(0)\right] \tag{2.3-11}$$

$$F_{cs} = \sqrt{2}F_s\cos\left[\omega_e t + \frac{2}{3}\pi + \theta_{esf}(0)\right] \tag{2.3-12}$$

These variables form a balanced three-phase set of *abc* sequence and if these currents are flowing in *as*, *bs*, and *cs* two-pole windings shown in Fig. 2.3-1 they will produce a magnetic field rotating ccw at ω_e (synchronous speed). Substituting (2.3-10)–(2.3-12) for currents into (2.3-5) to obtain I_{qs} and I_{ds} and then substituting these currents into (2.3-9) and with (2.3-1) for ϕ_s and with $\theta(0) = 0$, we obtain

$$\text{mmf}_s = \frac{N_s}{2}\sqrt{2}I_s\frac{3}{2}\cos[(\omega_e - \omega)t + \theta_{esi}(0) - \phi] \tag{2.3-13}$$

If now we view this from the synchronously rotating reference frame, $\omega = \omega_e$, we have

$$\text{mmf}_s^e = \frac{N_s}{2}\sqrt{2}I_s\frac{3}{2}\cos[\theta_{esi}(0) - \phi_e] \tag{2.3-14}$$

where $\theta_{esi}(0)$ is the phase angle of the stator phase currents, I_s is the rms value of the stator currents, and ϕ_e is the displacement from the *q* axis in the synchronous reference frame. If $\theta_{esi}(0)$ is the negative value, we can plot mmf_s^e as shown in Fig. 2.3-3 [5]. We see that $\theta_{esi}(0)$ is the position at which mmf_s^e is a positive maximum, which is the location of the stator south pole S^s.

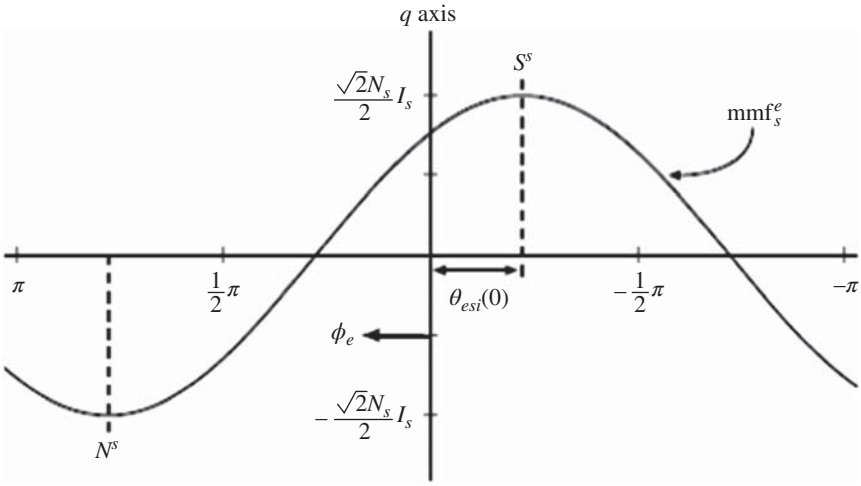

Figure 2.3-3 Tesla's balanced steady-state rotating magnetic field $\left(\text{mmf}_s^e\right)$ viewed from $-\pi$ to π by an observer rotating counterclockwise about the air gap at ω_e with $\theta(0) = 0$ and $\theta_{esi}(0)$ is negative. This is the synchronously rotating reference frame.

If we had 2π vision, Fig. 2.3-3 is what we would see if we ran at ω_e in the ccw direction. It is a constant for balanced steady-state conditions. Note that the stator poles N^s and S^S are located at maximum positive and negative currents $\left(\text{mmf}_s^e\right)$.

2.4 Voltage Equations in Arbitrary Reference Frame

The voltage equations in the arbitrary reference frame may be obtained by first expressing the phase voltages as

$$v_{as} = r_s i_{as} + \frac{d\lambda_{as}}{dt} \tag{2.4-1}$$

$$v_{bs} = r_s i_{bs} + \frac{d\lambda_{bs}}{dt} \tag{2.4-2}$$

$$v_{cs} = r_s i_{cs} + \frac{d\lambda_{cs}}{dt} \tag{2.4-3}$$

which may be written as

$$\mathbf{v}_{abcs} = \mathbf{r}_s \mathbf{i}_{abcs} + p\boldsymbol{\lambda}_{abcs} \tag{2.4-4}$$

where

$$\mathbf{r}_s = r_s \mathbf{I} \tag{2.4-5}$$

and p is the operator $\frac{d}{dt}$. From (2.3-6), (2.4-4) can be written as

$$(\mathbf{K}_s)^{-1}\mathbf{v}_{qd0s} = r_s(\mathbf{K}_s)^{-1}\mathbf{i}_{qd0s} + p(\mathbf{K}_s)^{-1}\boldsymbol{\lambda}_{qd0s} \tag{2.4-6}$$

Multiplying by $\mathbf{K}_s$ gives

$$\mathbf{v}_{qd0s} = r_s\mathbf{i}_{qd0s} + \mathbf{K}_s p(\mathbf{K}_s)^{-1}\boldsymbol{\lambda}_{qd0s} + \mathbf{K}_s(\mathbf{K}_s)^{-1}p\boldsymbol{\lambda}_{qd0s} \tag{2.4-7}$$

The second term on the right-hand side becomes

$$\begin{aligned}\mathbf{K}_s p(\mathbf{K}_s)^{-1}\boldsymbol{\lambda}_{qd0s} &= \frac{2}{3}\begin{bmatrix}\cos\theta & \cos\left(\theta-\frac{2\pi}{3}\right) & \cos\left(\theta+\frac{2\pi}{3}\right)\\ \sin\theta & \sin\left(\theta-\frac{2\pi}{3}\right) & \sin\left(\theta+\frac{2\pi}{3}\right)\\ \frac{1}{2} & \frac{1}{2} & \frac{1}{2}\end{bmatrix}\\ &\quad \omega\begin{bmatrix}-\sin\theta & \cos\theta & 0\\ -\sin\left(\theta-\frac{2\pi}{3}\right) & \cos\left(\theta-\frac{2\pi}{3}\right) & 0\\ -\sin\left(\theta+\frac{2\pi}{3}\right) & \cos\left(\theta+\frac{2\pi}{3}\right) & 0\end{bmatrix}\begin{bmatrix}\lambda_{qs}\\ \lambda_{ds}\\ \lambda_{0s}\end{bmatrix}\\ &= \omega\begin{bmatrix}0 & 1 & 0\\ -1 & 0 & 0\\ 0 & 0 & 0\end{bmatrix}\begin{bmatrix}\lambda_{qs}\\ \lambda_{ds}\\ \lambda_{0s}\end{bmatrix}\end{aligned} \tag{2.4-8}$$

The third term is

$$\mathbf{K}_s(\mathbf{K}_s)^{-1}p\boldsymbol{\lambda}_{qd0s} = p\boldsymbol{\lambda}_{qd0s} \tag{2.4-9}$$

From (2.4-7) through (2.4-9), the voltage equations are

$$\mathbf{v}_{qd0s} = r_s\mathbf{i}_{qd0s} + \omega\boldsymbol{\lambda}_{dqs} + p\boldsymbol{\lambda}_{qd0s} \tag{2.4-10}$$

where

$$\boldsymbol{\lambda}_{dqs} = \begin{bmatrix}\lambda_{ds}\\ -\lambda_{qs}\end{bmatrix} \tag{2.4-11}$$

In expanded form

$$v_{qs} = r_s i_{qs} + \omega\lambda_{ds} + p\lambda_{qs} \tag{2.4-12}$$

$$v_{ds} = r_s i_{ds} - \omega\lambda_{qs} + p\lambda_{ds} \tag{2.4-13}$$

$$v_{0s} = r_s i_{0s} + p\lambda_{0s} \tag{2.4-14}$$

These are the voltage equations for the three-phase stator in the arbitrary reference frame. We have the flux linkages to deal with now. In particular, we can express λ_{as}, λ_{bs}, and λ_{cs} as

$$\begin{bmatrix}\lambda_{as}\\ \lambda_{bs}\\ \lambda_{cs}\end{bmatrix} = \begin{bmatrix}L_{ls}+L_{ms} & -\frac{1}{2}L_{ms} & -\frac{1}{2}L_{ms}\\ -\frac{1}{2}L_{ms} & L_{ls}+L_{ms} & -\frac{1}{2}L_{ms}\\ -\frac{1}{2}L_{ms} & -\frac{1}{2}L_{ms} & L_{ls}+L_{ms}\end{bmatrix}\begin{bmatrix}i_{as}\\ i_{bs}\\ i_{cs}\end{bmatrix} \tag{2.4-15}$$

Let us consider Fig. 2.3-1 to define the inductances given in (2.4-15). In Chapter 1, we talked about leakage and magnetizing inductances (L_l and L_m) when considering the two-winding transformer. These inductances are L_{ls} and L_{ms} in (2.4-15). In particular, L_{ls} is the leakage inductances of each phase winding shown in Fig. 2.3-1. That is, due to the flux that does not cross the air gaps. The magnetizing flux (inductance) occurs due to the flux at each phase winding that crosses the air gap, travels through the rotor iron, and crosses the second air gap.

The mutual coupling between the phase given in (2.4-15) is the coupling between phases. If we take the *bs* winding and move it cw through the iron until it is atop the *as* winding the mutual inductance would be L_{ms}. Now as we move the *bs* winding back to its original position the mutual coupling would vary as a cosine of the angle between the axes of the *as* and *bs* winding. When it gets to its original position of 120°, the coupling is the cosine of 120°, or $-\frac{1}{2}L_{ms}$. Thus, the off-diagonal terms in (2.4-15) are $-\frac{1}{2}L_{ms}$.

Now if the stator windings are connected in wye without a neutral connection, the zero-current for balanced or unbalanced conditions is zero. That is

$$i_{os} = \frac{1}{3}\left(i_{as} + i_{bs} + i_{cs}\right) = 0 \tag{2.4-16}$$

whereupon (2.4-15) may be written

$$\begin{bmatrix} \lambda_{as} \\ \lambda_{bs} \\ \lambda_{cs} \end{bmatrix} = \begin{bmatrix} L_{ls} + L_{Ms} & 0 & 0 \\ 0 & L_{ls} + L_{Ms} & 0 \\ 0 & 0 & L_{ls} + L_{Ms} \end{bmatrix} \begin{bmatrix} i_{as} \\ i_{bs} \\ i_{cs} \end{bmatrix} \tag{2.4-17}$$

where

$$L_{Ms} = \frac{3}{2}L_{ms} \tag{2.4-18}$$

We can also write (2.4-15) as

$$\boldsymbol{\lambda}_{abcs} = \mathbf{L}_{ss}\mathbf{i}_{abcs} \tag{2.4-19}$$

In terms of substitute variables, (2.4-19) becomes

$$(\mathbf{K}_s)^{-1}\boldsymbol{\lambda}_{qd0s} = \mathbf{L}_{ss}(\mathbf{K}_s)^{-1}\mathbf{i}_{qd0s} \tag{2.4-20}$$

Multiplying by $\mathbf{K}_s$, (2.4-20) becomes

$$\boldsymbol{\lambda}_{qd0s} = \mathbf{L}_{ss}\mathbf{i}_{qd0s} \tag{2.4-21}$$

In expanded form

$$\lambda_{qs} = (L_{ls} + L_{Ms})i_{qs} \tag{2.4-22}$$

$$\lambda_{ds} = (L_{ls} + L_{Ms})i_{ds} \tag{2.4-23}$$

$$\lambda_{0s} = L_{ls}i_{0s} \tag{2.4-24}$$

In (2.4-24), $L_{Ms}i_{0s}$ is zero since the *as*, *bs*, and *cs* phases are mutually coupled and the zero-current i_{0s}, if nonzero, contributes equally to all three phases with the

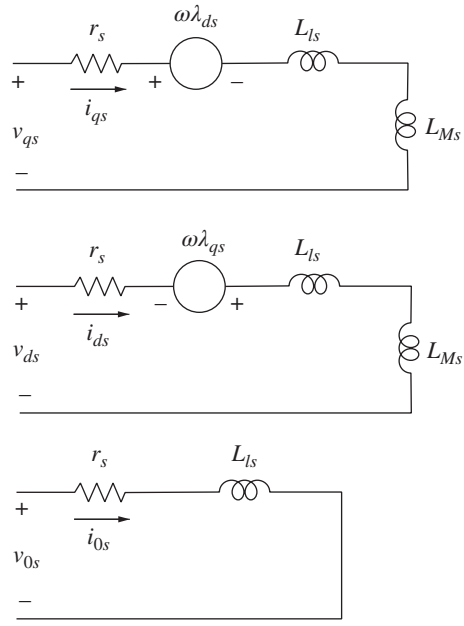

Figure 2.4-1 Arbitrary reference frame equivalent circuits for stator substitute variables.

corresponding mutual coupling terms canceling to zero. The equivalent circuits for the substitute variables in the arbitrary reference frame can be obtained from (2.4-12) through (2.4-14) and (2.4-22) through (2.4-24) as given in Fig. 2.4-1.

2.4.1 Electric Power

The instantaneous electric power in terms of *abc* variables may be expressed as

$$\begin{aligned} P_e &= \mathbf{v}_{abcs}^{\mathrm{T}}\mathbf{i}_{abcs} \\ &= \left[(\mathbf{K}_s)^{-1}\mathbf{v}_{qd0s}\right]^T(\mathbf{K}_s)^{-1}\mathbf{i}_{qd0s} \\ &= \mathbf{v}_{qd0s}^T\left[(\mathbf{K}_s)^{-1}\right]^T(\mathbf{K}_s)^{-1}\mathbf{i}_{qd0s} \end{aligned} \tag{2.4-25}$$

Carrying out the matrix operations and simplifying

$$P_e = \frac{3}{2}(v_{qs}i_{qs} + v_{ds}i_{ds}) + 3v_{0s}i_{0s} \tag{2.4-26}$$

The preceding equation is valid in any reference frame for steady-state or dynamic operating conditions.

2.5 Transformation Between Reference Frames

In some derivations and analyses, it is convenient to relate variables in one reference frame to variables in another reference frame directly, without involving the

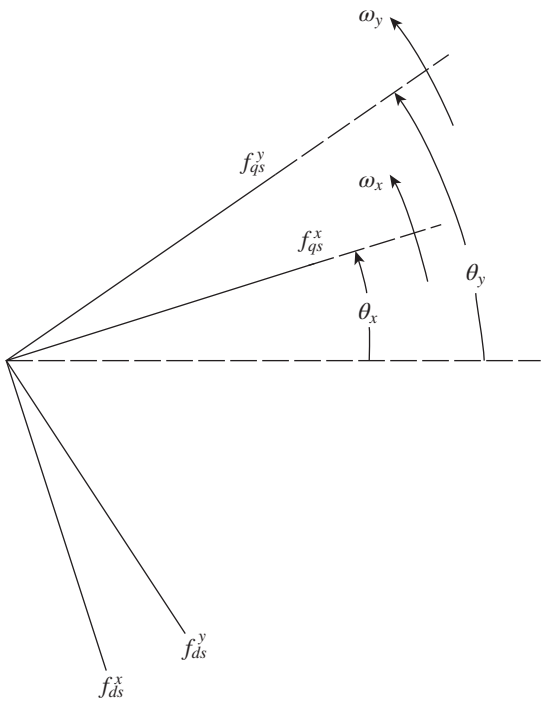

Figure 2.5-1 Transformation between two reference frames portrayed by trigonometric relationships for $\omega \leq \omega_e$.

abc variables in the transformation. To establish this transformation between any two frames of reference, let *x* denotes the reference frame from which the variables are being transformed and *y* denotes the reference frame to which the variables are being transformed. Thus,

$$\mathbf{f}_{qd0s}^{y} = {}^{x}\mathbf{K}^{y}\mathbf{f}_{qd0s}^{x} \tag{2.5-1}$$

From (2.3-6)

$$\mathbf{f}_{qd0s}^{x} = \mathbf{K}_{s}^{x}\mathbf{f}_{abcs} \tag{2.5-2}$$

Substituting (2.5-2) into (2.5-1) yields

$$\mathbf{f}_{qd0s}^{y} = {}^{x}\mathbf{K}^{y}\mathbf{K}_{s}^{x}\mathbf{f}_{abcs} \tag{2.5-3}$$

However, from (2.3-6)

$$\mathbf{f}_{qd0s}^{y} = \mathbf{K}_{s}^{y}\mathbf{f}_{abcs} \tag{2.5-4}$$

Thus

$${}^{x}\mathbf{K}^{y}\mathbf{K}_{s}^{x} = \mathbf{K}_{s}^{y} \tag{2.5-5}$$

from which

$$ {}^{x}\mathbf{K}^{y} = \mathbf{K}_{s}^{y}\left(\mathbf{K}_{s}^{x}\right)^{-1} \tag{2.5-6} $$

The desired transformation is obtained by substituting the appropriate transformations into (2.5-6). Hence

$$ {}^{x}\mathbf{K}^{y} = \begin{bmatrix} \cos(\theta_y - \theta_x) & -\sin(\theta_y - \theta_x) & 0 \\ \sin(\theta_y - \theta_x) & \cos(\theta_y - \theta_x) & 0 \\ 0 & 0 & 1 \end{bmatrix} \tag{2.5-7} $$

Several of the trigonometric identities given in Appendix A are useful in obtaining (2.5–7). This transformation, which is sometimes referred to as a "vector rotator" or simply "rotator," can also be visualized from the trigonometric relationship between two sets of rotating, orthogonal quantities as shown in Fig. 2.5-1. Resolving f_{qs}^{x} and f_{ds}^{x} into f_{qs}^{y} yields the first row of (2.5-7) and resolving f_{qs}^{x} and f_{ds}^{x} into f_{ds}^{y} yields the second row. It is left for the reader to show that

$$ ({}^{x}\mathbf{K}^{y})^{-\mathbf{1}} = ({}^{x}\mathbf{K}^{y})^{\boldsymbol{T}} \tag{2.5-8} $$

2.6 P-Pole Machines

Let us take a minute to see what happens when we have pole pairs larger than two. The magnetic axes of a two-pole and a four-pole three-phase stator are shown in Fig. 2.6-1. The mmf_s may be expressed in the synchronous reference frame for the two-pole device by (2.3-13). The poles are for balanced stator currents with I_{as} positive maximum and I_{bs} and I_{cs} negative at one-half maximum. The mmf_s^e for the four-pole stator may be expressed as

$$ \text{mmf}_s^e = \frac{3}{2}\frac{N_s}{2}\sqrt{2}I_s \cos\left[\theta_{\text{esi}}(0) - \frac{P}{2}\phi_e\right] \tag{2.6-1} $$

Where $P = 4$. Now, the frequency of the stator currents is ω_e; however, the speed of the rotating mmf has been reduced by $\frac{P}{2}$ from the two-pole device.

Although the synchronous speed of the stator variables is ω_e, the synchronous speed of the rotating magnetic field is $\frac{2}{P}\omega_e$. Thus, the electrical angular velocity of the rotating magnetic field is said to be ω_e even though its actual speed is $\frac{2}{P}\omega_e$.

$$ \omega_m = \frac{2}{P}\omega_e \tag{2.6-2} $$

The electrical system is convinced that the rotating magnetic field is traveling at ω_e. This is termed the electrical angular velocity of the magnetic field.

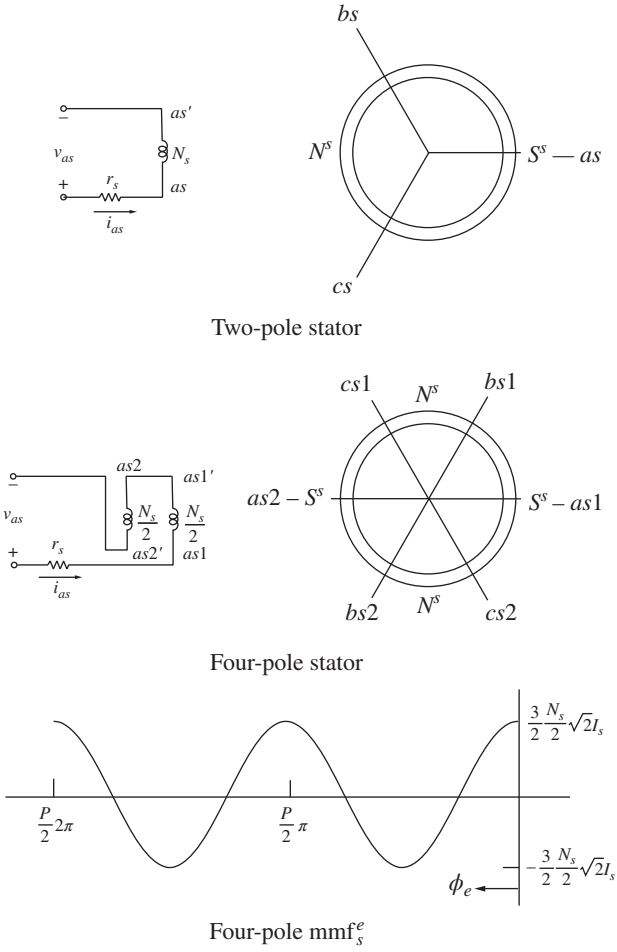

Figure 2.6-1 *P*-pole stator for $\theta_{esi}(0) = 0$.

2.7 Transformation of a Balanced Set

Although the transformation equations are valid regardless of the waveform of the variables, it is instructive to consider the characteristics of the transformation when the three-phase system is symmetrical and the voltages and currents form balanced three-phase sets of ***abc*** sequence as given by (2.7-1)–(2.7-4). A balanced three-phase set is generally defined as a set of equal-amplitude sinusoidal quantities that are displaced by $\frac{2\pi}{3}$. Since the sum of this set is zero, the 0*s* variables are zero.

$$f_{as} = \sqrt{2} f_s \cos \theta_{ef} \tag{2.7-1}$$

$$f_{bs} = \sqrt{2} f_s \cos \left(\theta_{ef} - \frac{2\pi}{3} \right) \tag{2.7-2}$$

$$f_{cs} = \sqrt{2} f_s \cos \left(\theta_{ef} + \frac{2\pi}{3} \right) \tag{2.7-3}$$

where $\boldsymbol{f_s}$ may be a function of time and

$$\frac{d\theta_{ef}}{dt} = \omega_e \tag{2.7-4}$$

Substituting (2.7-1)–(2.7-3) into the transformation to the arbitrary reference frame (2.3-5) yields

$$f_{qs} = \sqrt{2} f_s \cos(\theta_{ef} - \theta) \tag{2.7-5}$$

$$f_{ds} = -\sqrt{2} f_s \sin(\theta_{ef} - \theta) \tag{2.7-6}$$

$$f_{0s} = 0 \tag{2.7-7}$$

With the three-phase variables as given in (2.7-1)–(2.7-3), the *qs* and *ds* variables form a balanced two-phase set in all reference frames except when $\omega = \omega_e$. In this synchronously rotating reference frame, the *qs* and *ds* quantities become

$$f^e_{qs} = \sqrt{2} f_s \cos(\theta_{ef} - \theta_e) \tag{2.7-8}$$

$$f^e_{ds} = -\sqrt{2} f_s \sin(\theta_{ef} - \theta_e) \tag{2.7-9}$$

where θ_e is the angular position of the synchronously rotating reference frame. It is important to note that θ_e and θ_{ef} both have an angular velocity of ω_e. Hence, $\theta_{ef} - \theta_e$ is a constant dependent upon the initial values of the variable being transformed, $\theta_{ef}(0)$, and the initial position of the synchronously rotating reference frame, $\theta_e(0)$. Equations. (2.7-8) and (2.7-9) reveal a property that is noteworthy. Therefore, there is one reference frame where a balanced set will appear as constants if the amplitude f_s is constant. In other words, if a constant-amplitude balanced set appears in any reference frame, then there is another reference frame where this balanced set appears as a set of constants. The converse is also true.

For balanced steady-state conditions, the amplitude and frequency are constants and θ_{ef} becomes $\omega_e t + \theta_{ef}(0)$ whereupon (2.7-1)–(2.7-3) may be expressed as

$$\begin{aligned} F_{as} &= \sqrt{2} F_s \cos \left[\omega_e t + \theta_{ef}(0) \right] \\ &= Re \left[\sqrt{2} F_s e^{j\theta_{ef}(0)} e^{j\omega_e t} \right] \end{aligned} \tag{2.7-10}$$

$$F_{bs} = \sqrt{2}F_s \cos\left[\omega_e t + \theta_{ef}(0) - \frac{2\pi}{3}\right]$$
$$= Re\left[\sqrt{2}F_s e^{j[\theta_{ef}(0)-2\pi/3]} e^{j\omega_e t}\right] \tag{2.7-11}$$

$$F_{cs} = \sqrt{2}F_s \cos\left[\omega_e t + \theta_{ef}(0) + \frac{2\pi}{3}\right]$$
$$= Re\left[\sqrt{2}F_s e^{j[\theta_{ef}(0)+2\pi/3]} e^{j\omega_e t}\right] \tag{2.7-12}$$

where $\theta_{ef}(0)$ corresponds to the time zero value of the three-phase variables. Uppercase notation is used to denote steady-state quantities. If the speed of the arbitrary reference frame is an unspecified constant, then for the balanced steady-state conditions, (2.7-5) and (2.7-6) may be expressed as

$$F_{qs} = \sqrt{2}F_s \cos[(\omega_e - \omega)t + \theta_{ef}(0) - \theta(0)]$$
$$= Re\left[\sqrt{2}F_s e^{j[\theta_{ef}(0)-\theta(0)]} e^{j(\omega_e-\omega)t}\right] \tag{2.7-13}$$

$$F_{ds} = -\sqrt{2}F_s \sin[(\omega_e - \omega)t + \theta_{ef}(0) - \theta(0)]$$
$$= Re\left[j\sqrt{2}F_s e^{j[\theta_{ef}(0)-\theta(0)]} e^{j(\omega_e-\omega)t}\right] \tag{2.7-14}$$

From (2.7-10), the phasor representing the *as* variables is

$$\widetilde{F}_{as} = F_s e^{j\theta_{ef}(0)} \tag{2.7-15}$$

In Section 2.7-3, we denoted the phase angle associated with $I_{as}(t)$ as $\theta_{esi}(0)$ and noted that it is the location of the stator south pole S^s. This implies that we can superimpose S^s at the tip of $\widetilde{I}_{as}$ in a phasor diagram. The north pole N^s is located 180° from S^s.

If $\omega \neq \omega_e$, then F_{qs} and F_{ds} are sinusoidal quantities, and from (2.7-13) and (2.7-14) with $\theta(0) = 0$

$$\widetilde{F}_{qs} = F_s e^{j\theta_{ef}(0)} = \widetilde{F}_{as} \tag{2.7-16}$$

$$\widetilde{F}_{ds} = j\widetilde{F}_{qs} \tag{2.7-17}$$

If we look at (2.7-13) and (2.7-14), we see that when the reference frame speed ω becomes greater then $\omega_e (\omega > \omega_e)$, the frequency of (2.7-13) and (2.7-14) changes sign. This causes mmf_s to rotate cw rather than ccw for $\omega < \omega_e$. In other words, mmf_s always rotates toward ω_e. For $\omega \neq \omega_e$ and $\theta(0) = 0$ (2.7-13) becomes

$$F_{qs} = \text{Re}\{\widetilde{F}_{qs} e^{j(\omega_e-\omega)t}\} \tag{2.7-18}$$

This implies that phasors rotate ccw for $\omega < \omega_e$ and cw for $\omega > \omega_e$. In the synchronously rotating reference frame $\omega = \omega_e$ and $\theta(0) = \theta_e(0)$. If we continue to use uppercase letters to denote the steady-state variables in the synchronously rotating reference frame, then from (2.7-13) and (2.7-14)

$$F_{qs}^{e} = Re\left[\sqrt{2}F_s e^{j[\theta_{ef}(0)-\theta_e(0)]}\right] \tag{2.7-19}$$

$$F_{ds}^{e} = Re\left[j\sqrt{2}F_s e^{j[\theta_{ef}(0)-\theta_e(0)]}\right] \tag{2.7-20}$$

If we let the time-zero position of the reference frame be zero, then $\theta_e(0) = 0$ and

$$F_{qs}^{e} = \sqrt{2}F_s \cos\theta_{ef}(0) \tag{2.7-21}$$

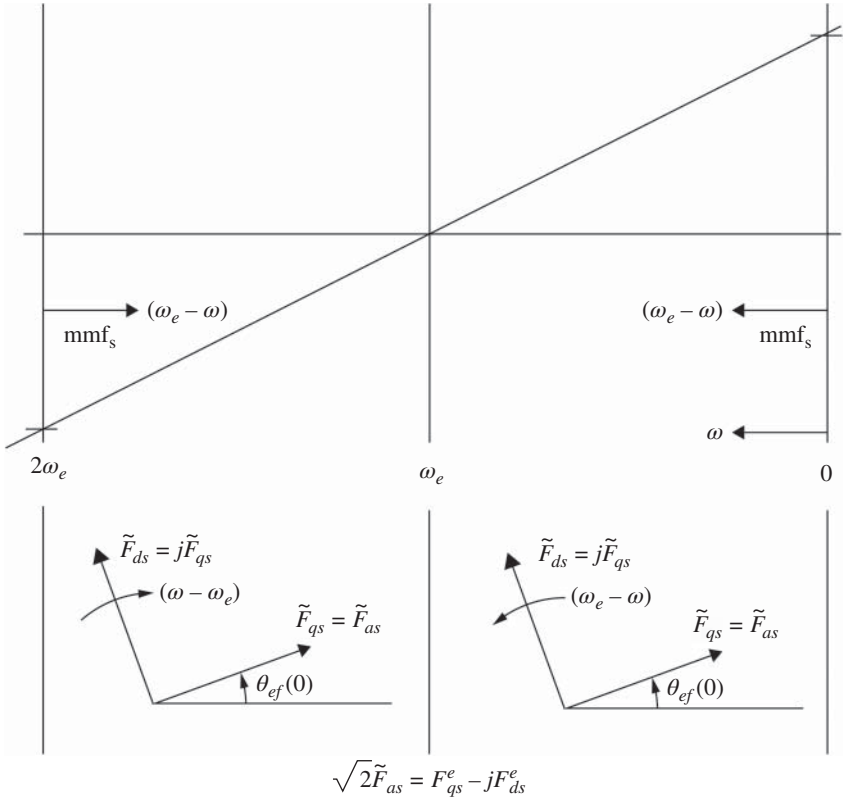

Figure 2.7-1 Direction of rotation of mmf$_s$ and the phase relation between $\tilde{F}_{qs}$ and $\tilde{F}_{ds}$ as viewed from the arbitrary reference frame when $\omega < \omega_e$ and $\omega > \omega_e$ for balanced steady-state conditions.

$$F_{ds}^{e} = -\sqrt{2}F_s \sin\theta_{ef}(0) \tag{2.7-22}$$

Thus, we see from a comparison of (2.7-15) with (2.7-21) and (2.7-22) that

$$\sqrt{2}\widetilde{F}_{as} = F_{qs}^{e} - jF_{ds}^{e} \tag{2.7-23}$$

Since $\widetilde{F}_{as} = \widetilde{F}_{qs}$, (2.7-23) is important in that it relates the synchronously rotating reference-frame variables to a phasor in all other reference frames. $\widetilde{F}_{as}$ is a phasor that represents a sinusoidal quantity; however, F_{qs}^{e} and F_{ds}^{e} are not phasors. They are real quantities representing the constant steady-state variables of the synchronously rotating reference frame. This is all summarized in Fig. 2.7-1. It should be noted that the *ds* variable leads the *qs* variable when $\omega < \omega_e$ and lags it when $\omega > \omega_e$.

2.8 Instantaneous and Steady-State Phasors

The synchronously rotating reference frame can be thought of as a synchronously rotating complex plane as shown in Fig. 2.8-1 whereupon we can think of f_{qs}^{e} and f_{ds}^{e} as $\widetilde{f}_{as}$, an instantaneous phasor of phase *as* variables. This would include the steady-state and transient response for balanced conditions for a three-phase stator. From Fig. 2.8-1, we can write

$$\widetilde{f}_{as}(t) = f_{qs}^{e}(t) - jf_{ds}^{e}(t) \tag{2.8-1}$$

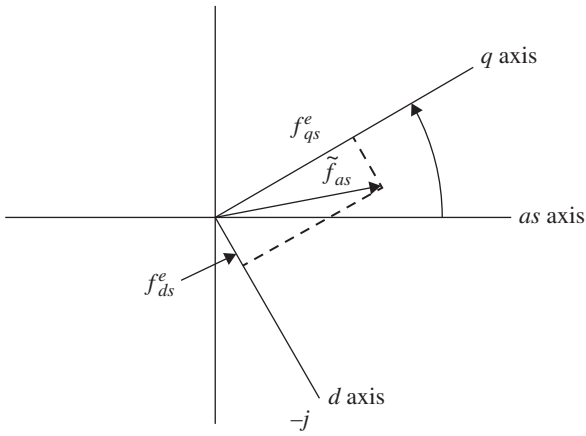

Figure 2.8-1 The q and d complex plane.

Note that in Fig. 2.7-1 we are plotting phases $\widetilde{F}_{qs}$ and $\widetilde{F}_{ds}$ which are equal in magnitude. In Fig. 2.8-1, we are plotting instantaneous values, f^e_{qs} and f^e_{ds}.

Substituting the voltage equations in the synchronously rotating reference frame into (2.8-1) yields, for balanced conditions,

$$v^e_{qs} - jv^e_{ds} = r_s i^e_{qs} + \omega_e \lambda^e_{ds} + p\lambda^e_{qs} - j\left(r_s i^e_{ds} - \omega_e \lambda^e_{qs} + p\lambda^e_{ds}\right) \tag{2.8-2}$$

In terms of instantaneous phasors

$$\widetilde{v}_{as} = r_s \widetilde{i}_{as} + j\omega_e \widetilde{\lambda}_{as} + p\widetilde{\lambda}_{as} \tag{2.8-3}$$

Once the transient subsides, the i^e_{qs} and i^e_{ds} become constant only in the synchronous reference frame and $p\widetilde{\lambda}_{as}$ becomes zero and (2.8-3) becomes

$$\widetilde{v}_{as} = r_s \widetilde{i}_{as} + j\omega_e \widetilde{\lambda}_{as} \tag{2.8-4}$$

Now, (2.8-4) is expressed in instantaneous variables and must be divided by $\sqrt{2}$ to be expressed in terms of steady-state phasors. Also, for a magnetically linear stator and the *rL* circuit being considered

$$\widetilde{\lambda}_{as} = L_{ss}\widetilde{i}_{as} \tag{2.8-5}$$

Thus (2.8-4) becomes

$$\widetilde{V}_{as} = (r + j\omega_e L_{ss})\widetilde{I}_{as} \tag{2.8-6}$$

where

$$L_{ss} = L_{ls} + L_{Ms} \tag{2.8-7}$$

2.9 Variables Observed from Several Frames of Reference

It is instructive to observe the waveform of the variables of the stator shown in Fig. 2.3-1 in commonly used reference frames. For this purpose, we will assume that both $\boldsymbol{r_s}$ and $\boldsymbol{L_{ss}}$ are diagonal matrices each with equal nonzero elements and the applied voltages are of the form

$$v_{as} = \sqrt{2}V_s \cos\omega_e t \tag{2.9-1}$$

$$v_{bs} = \sqrt{2}V_s \cos\left(\omega_e t - \frac{2\pi}{3}\right) \tag{2.9-2}$$

$$v_{cs} = \sqrt{2}V_s \cos\left(\omega_e t + \frac{2\pi}{3}\right) \tag{2.9-3}$$

where ω_e is an unspecified constant. The currents, which are assumed to be zero at $t = 0$, may be expressed as

$$i_{as} = \frac{\sqrt{2}V_s}{|Z_s|}\left[-e^{-t/\tau}\cos\alpha + \cos(\omega_e t - \alpha)\right] \tag{2.9-4}$$

$$i_{bs} = \frac{\sqrt{2}V_s}{|Z_s|}\left[-e^{-t/\tau}\cos\left(\alpha + \frac{2\pi}{3}\right) + \cos\left(\omega_e t - \alpha - \frac{2\pi}{3}\right)\right] \tag{2.9-5}$$

$$i_{cs} = \frac{\sqrt{2}V_s}{|Z_s|}\left[-e^{-t/\tau}\cos\left(\alpha - \frac{2\pi}{3}\right) + \cos\left(\omega_e t - \alpha + \frac{2\pi}{3}\right)\right] \tag{2.9-6}$$

where

$$Z_s = r_s + j\omega_e L_{ss} \tag{2.9-7}$$

$$\tau = \frac{L_{ss}}{r_s} \tag{2.9-8}$$

$$\alpha = \tan^{-1}\frac{\omega_e L_{ss}}{r_s} \tag{2.9-9}$$

It may at first appear necessary to solve the voltage equations in the arbitrary reference frame in order to obtain the expression for the currents in the arbitrary reference frame. This is unnecessary since once the solution is known in one reference frame it is known in all reference frames. In the example at hand, this may be accomplished by transforming (2.9-4)–(2.9-6) to the arbitrary reference frame. If we let ω be an unspecified constant with $\theta(0) = 0$, then $\theta = \omega t$ and in the arbitrary reference frame

$$i_{qs} = \frac{\sqrt{2}V_s}{|Z_s|}\{-e^{-t/\tau}\cos(\omega t - \alpha) + \cos[(\omega_e - \omega)t - \alpha]\} \tag{2.9-10}$$

$$i_{ds} = \frac{\sqrt{2}V_s}{|Z_s|}\{-e^{-t/\tau}\sin(\omega t - \alpha) - \sin[(\omega_e - \omega)t - \alpha]\} \tag{2.9-11}$$

For balanced conditions, the 0*s* variables do not exist. We have taken symmetrical three-phase *rL* circuits each displaced $2\pi/3$ radians and, by the change of variables, converted it to a symmetrical two-phase orthogonal circuit.

Clearly, the state of the electric system is independent of the frame of reference from which it is observed. Although the voltages and currents will appear differently in each reference frame, they will exhibit the same mode of operation (transient or steady state) regardless of the reference frame. In general, (2.9-10) and (2.9-11) contain two balanced sets. One, which represents the electric

transient, decays exponentially at a frequency corresponding to the instantaneous angular velocity of the arbitrary reference frame. In this set, the *qs* variable leads the *ds* variable by $\frac{\pi}{2}$ when $\omega > 0$ and lags by $\frac{\pi}{2}$ when $\omega < 0$. The second balanced set, which represents the steady-state response, has a constant amplitude with a frequency corresponding to the difference in the angular velocity of the voltages applied to the circuits and the angular velocity of the arbitrary reference frame. In this set, the *qs* variable lags the *ds* by $\frac{\pi}{2}$ when $\omega < \omega_e$ and leads by $\frac{\pi}{2}$ when $\omega > \omega_e$.

There are two frames of reference that do not contain both balanced sets. In the stationary reference frame, $\omega = 0$ and $i_{qs}^{s} = i_{as}$. The exponentially decaying balanced set becomes an exponential decay and the constant-amplitude balanced set varies at ω_e. In the synchronously rotating reference frame where $\omega = \omega_e$, the electric transients are represented by an exponentially decaying balanced set varying at $\boldsymbol{\omega_e}$ and the constant amplitude set becomes a set of constants.

The waveforms of the system variables in various reference frames are shown in Figs. 2.9-1–2.9-3. The voltages of the form given by Figs. 2.9-1–2.9-3 are applied to the three-phase circuits with $V_s = \frac{10}{\sqrt{2}}$ V, $r_s = 0.216\,\Omega$, $\omega_e L_{ss} = 1.09\,\Omega$ with $\omega_e = 377$ rad/s. The response, for $t > 0$, of the electric system in the stationary reference frame is shown in Fig. 2.9-1. Since we have selected $\theta(0) = 0, f_{as} = f_{qs}^{s}$ and the plots of v_{qs}^{s} and i_{qs}^{s} are v_{as} and i_{as}, respectively. The variables for the same mode of operation are shown in the synchronously rotating reference frame in Fig. 2.9-2. Note, from Figs. 2.9-1–2.9-3, that we have selected $\theta_{ev}(0) = 0$ and since $\theta(0) = 0$, $v_{qs}^{e} = 10$ V and $v_{ds}^{e} = 0$. In Fig. 2.9-3, with $\theta(0) = 0$, the speed of the reference frame is switched from its original value of -377 rad/s to zero and ramped to 377 rad/s.

There are several features worthy of note. The waveform of the instantaneous electric power is the same in all cases. The electric transient is very evident in the waveforms of the instantaneous electric power and the currents in the synchronously rotating reference frame (Fig. 2.9-2) and since v_{ds}^{e} is zero i_{qs}^{e} is related to the power by a constant $\left(v_{qs}^{e}\right)$. In Fig. 2.9-3, we selected $\theta_{ev}(0) = 0$ and $\theta(0) = 0$. The voltages were applied, and we observed the solution of the differential equations in the reference frame rotating clockwise at ω_e ($\omega = -\omega_e$). The reference frame speed was then stepped from -377 rad/s to zero whereupon the differential equations were solved in the stationary reference frame. However, when switching from one reference frame to another, the variables must be continuous. Therefore, after the switching occurs, the solution continues using the stationary reference frame differential equations with the initial values determined by the instantaneous values of the variables in the previous reference frame ($\boldsymbol{\omega = -\omega_e}$) at the time of switching. It is important to note the change in frequency of the variables as the reference frame speed is ramped from zero to $\boldsymbol{\omega_e}$. Here, the differential equations being

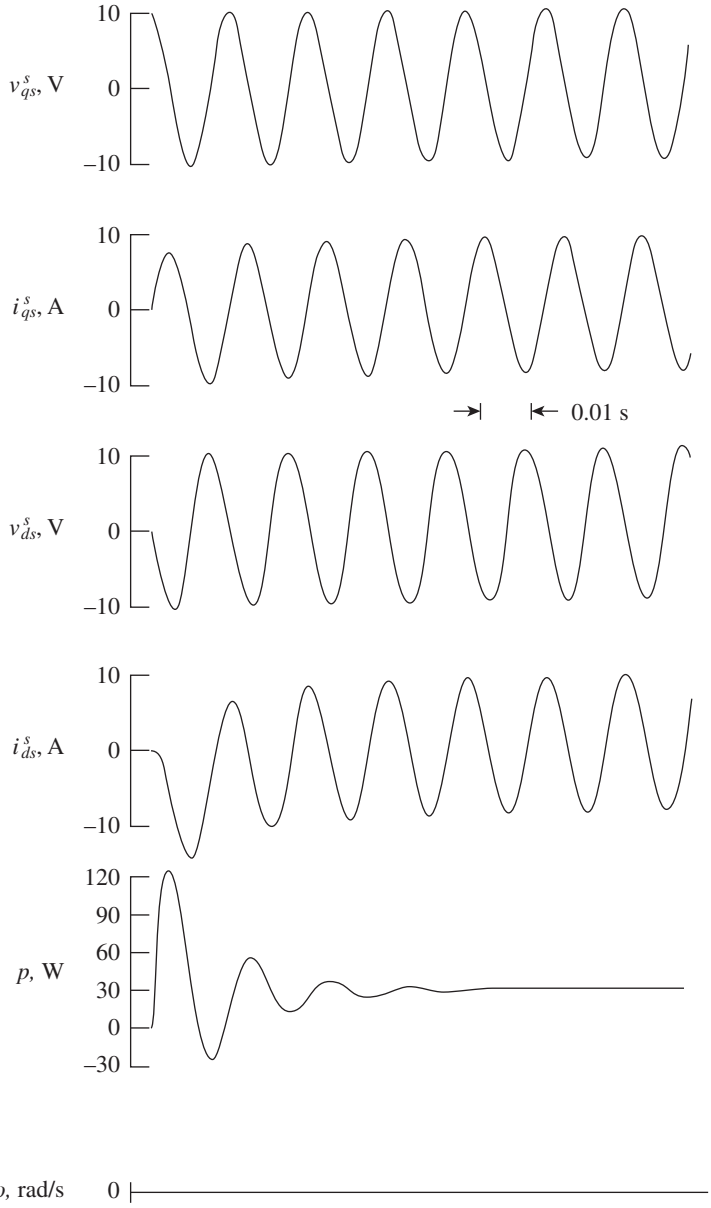

Figure 2.9-1 Variables of three-phase stator circuits in the stationary reference frame.

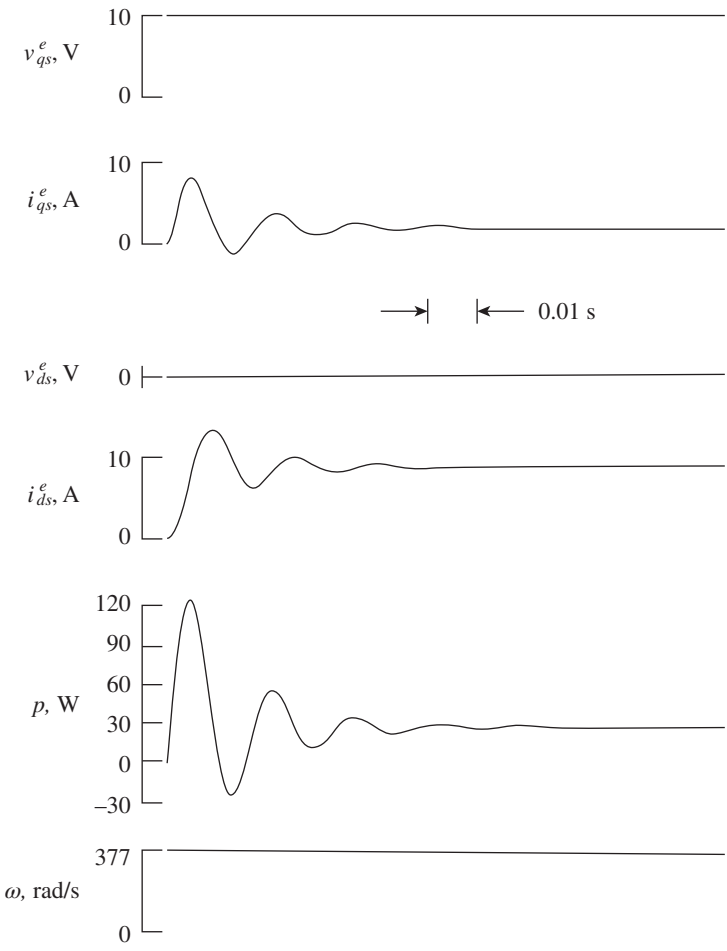

Figure 2.9-2 Variables of three-phase stator circuits in the synchronously rotating frame.

solved are continuously changing while the variables remain continuous. When the reference frame speed reaches synchronous speed, the variables have reached steady state; therefore, they will be constant corresponding to their values when $\boldsymbol{\omega}$ becomes equal to $\boldsymbol{\omega_e}$. In essence, we have applied a balanced three-phase set of voltages to a symmetrical *rL* circuit and in Fig. 2.9-3 we observed the actual variables from various reference frames by first "jumping" and then "running" from one reference frame to another.

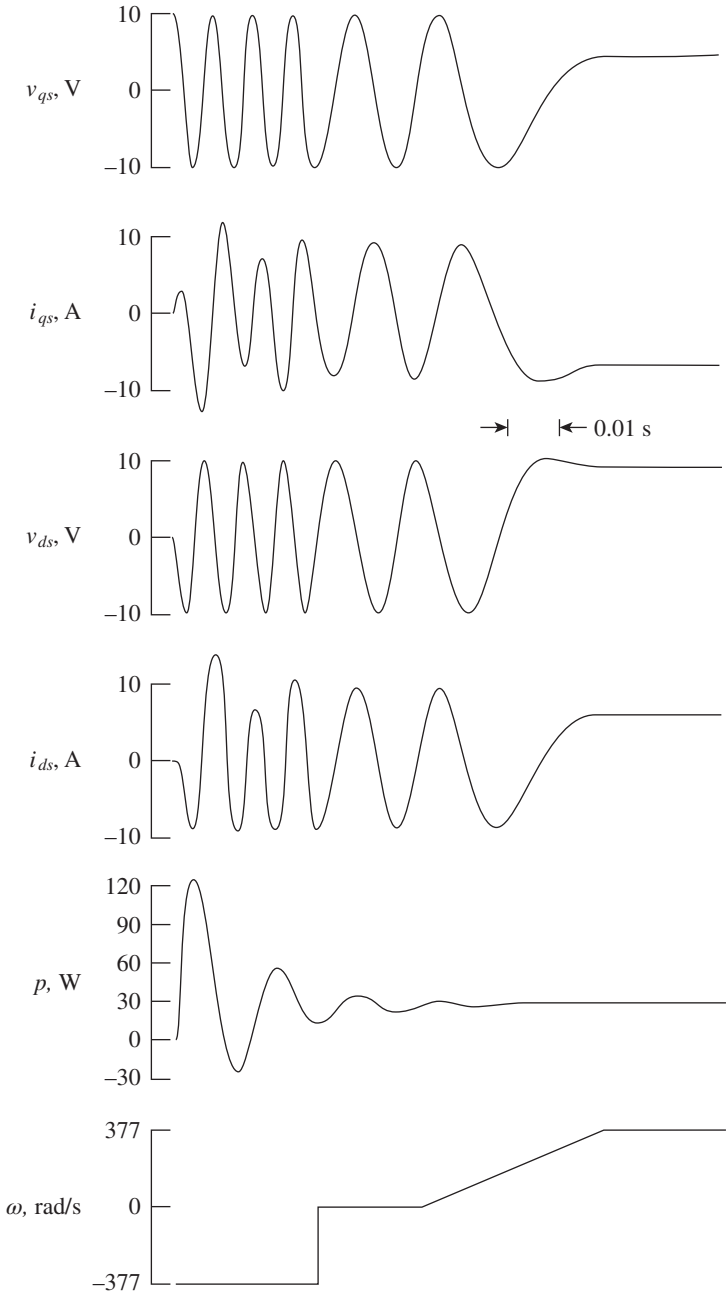

Figure 2.9-3 Variables of three-phase stator circuits. First with $\omega = -\omega$, then $\omega = 0$ followed by a ramp change in reference frame speed to $\omega = \omega_e$.

References

1 R. H. Park, "Two-Reaction Theory of Synchronous Machines – Generalized Method of Analysis –Part 1," *AIEE Trans.* Vol. 48 July 1929, pp. 716–727.
2 P. C. Krause, O. Wasynczuk, T. C. O'Connell, and M. Hasan, "Tesla's Contribution to Electric Machine Analysis," *IEEE PES*, 2018.
3 P. C. Krause, *Reference Frame Theory*, IEEE Press, Wiley, 2020.
4 P. C. Krause, C. H. Thomas, "Simulation of Symmetrical Induction Machinery," *IEEE Trans. Power Apparatus and Systems*, Vol. 84 November 1965, pp. 1038–1053.
5 P. C. Krause, O. Wasynczuk, S. D. Pekarek, and T. C. O'Connell, *Electromechanical Motion Devices*, 3rd Ed. IEEE Press and Wiley, 2020.

Problems

2.1 Plot the mmf for the winding distribution shown in Fig. 2P-1. Let $\theta_{esi}(0) = -20^o$, plot mmf_s^e for a four-pole device.

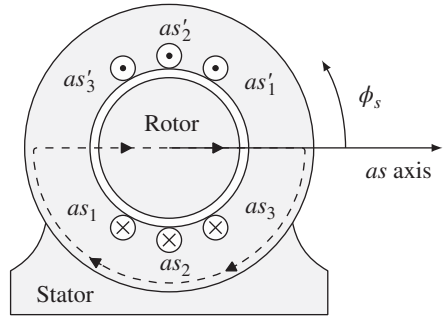

Figure 2P-1 Uniformly distributed winding.

2.2 Justify (2.4–24). What would λ_{qd0s} be for a three-phase load shown in Fig. 2P-2.

2.3 Consider a two-phase stator shown in Fig. 2P-3. Express $\mathbf{K}_s$ and $(\mathbf{K}_s)^{-1}$.

2.4 The two-phase applied stator voltages are

$$v_{as} = V_a \cos \omega_e t$$

$$v_{bs} = V_b \sin \omega_e t$$

where $V_a \neq V_b$. (a) Express v_{qs} and v_{ds} in the arbitrary reference frame. (b) Under what conditions would v_{qs} and v_{ds} be constants?

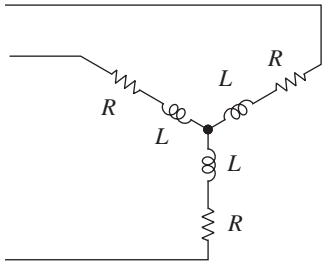

Figure 2P-2 Three-phase RL load.

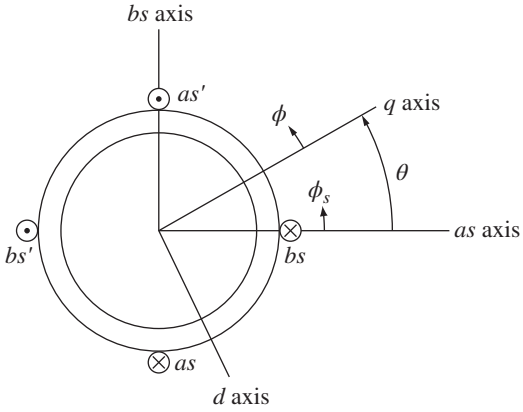

Figure 2P-3 Two-phase stator.

2.5 Equation (2.8-1) is for $\widetilde{f}_{as}$. Express $\widetilde{f}_{bs}$ and $\widetilde{f}_{cs}$.

2.6 Verify (2.5-7).

2.7 Suppose i_{ds} is defined such that (2.3-3) is a positive maximum at $\phi = \frac{\pi}{2}$ instead of $\phi = -\frac{\pi}{2}$ with $i_{qs} = 0$. Express $\mathbf{K}_s$ and $(\mathbf{K}_s)^{-1}$.

2.8 Express $\widetilde{f}_{as}$ for Problem 8.

2.9 Express N_s for Problem 1.

2.10 Consider the two-phase stator of Problem 3. (a) Express v_{qs} and v_{ds} in a form similar to (2.4-12) and (2.4-13). (b) Repeat (a) assuming the *d* axis is located at $\phi = \frac{\pi}{2}$.

2.11 Equation (2.3-5) is for an *abc* sequence. Use this equation for an *acb* sequence and determine v_{qs} and v_{ds} in the arbitrary reference frame.

3

Symmetrical Induction Machine

3.1 Introduction

The induction machine is a major means of converting electric power into mechanical motion. The single-phase induction motor used in household applications and the three-phase induction motor used in large-horsepower applications operate on the same principle. That is, torque is developed by the rotating magnetic field of the stator inducing currents in short-circuit rotor windings. It is the first electric machine that we will consider. We will find that the rotor can be considered a symmetrical system and can be transformed into an arbitrary reference frame. In fact, the symmetrical induction machine has a symmetrical stator and a symmetrical rotor.

3.2 Induction Machine

A cutaway view of a four-pole three-phase 6.5-hp 460 V squirrel-cage induction motor is shown in Fig. 3.2-1. It is a severe-duty motor for use in the chemical, paper, cement, and mining industries. Although it is difficult to discern, the squirrel-cage rotors are made up of laminated punched steel with aluminum bars die casted in the openings of the laminated rotor and the bars terminated at each end of the rotor in an aluminum ring, which is visible in Fig. 3.2-1. The protrusions from the aluminum rings are for cooling purposes. If we remove the steel laminations, the remaining aluminum bars and end rings resemble the rotor (blades) of a "squirrel-cage fan." The question often arises as to how these short-circuited bars produce a rotating magnetic field. Intuitively, the rotor has been considered symmetrical and is shown to be the case in [1].

The two-pole three-phase induction machine shown in Fig. 3.2-2 is the configuration of the machine we will analyze in this chapter. We have already considered the stator in Chapter 2. The rotor is considered to have three-phase sinusoidally

Analysis of Electric Machinery and Drive Systems, Fourth Edition.
Paul C. Krause, Oleg Wasynczuk, Scott D. Sudhoff, and Steven D. Pekarek.

Companion website: www.wiley.com/go/krause_aem4e

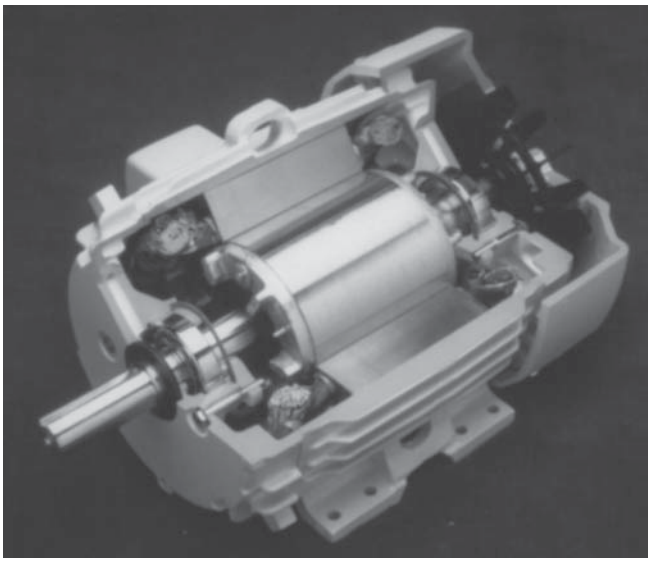

Figure 3.2-1 Four-pole three-phase 6.5-Hp 460 V severe-duty, squirrel-cage induction motor (Courtesy of General Electric).

distributed windings. In most cases, the rotor is a squirrel cage but in a few cases the rotor is wound like the stator and the terminals are available by a slip-ring and brush arrangement. This double-fed induction machine is used in wind energy applications.

Let us talk about the rotor speed of a P-pole machine for just a minute. The rotor must have the same number of poles as the stator. Therefore, the rotor displacement for a P-pole machine is

$$\theta_{rm} = \frac{2}{P}\theta_r \tag{3.2-1}$$

where θ_r is the rotor displacement for a two-pole machine and θ_{rm} is the actual rotor displacement for a P-pole machine. Also,

$$\omega_{rm} = \frac{2}{P}\omega_r \tag{3.2-2}$$

In Chapter 1, we derived force equations for a translatory system given by (1.5-9) and (1.5-12). For a P-pole rotational system, those equations become

$$T_e = -\frac{P}{2}\frac{\partial W_f(\lambda, \theta_r)}{\partial \theta_r} \tag{3.2-3}$$

and

$$T_e = \frac{P}{2}\frac{\partial W_c(i, \theta_r)}{\partial \theta_r} \tag{3.2-4}$$

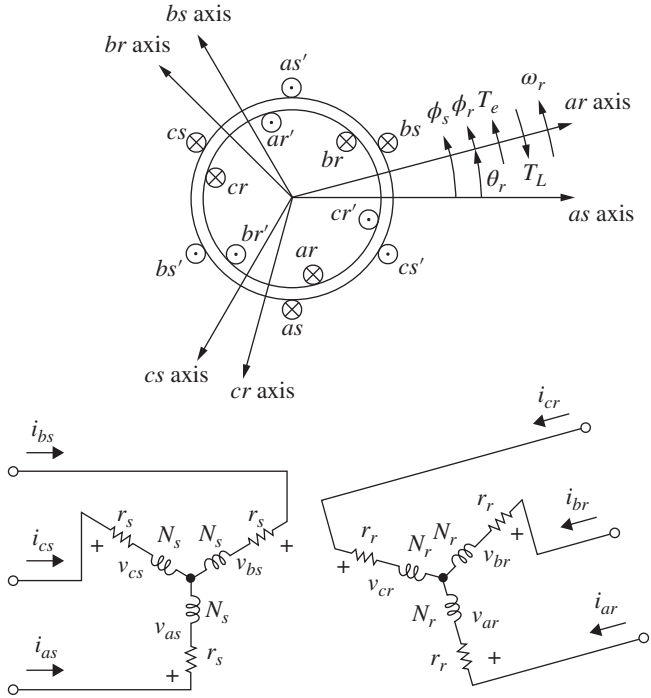

Figure 3.2-2 A two-pole three-phase symmetrical induction machine.

where λ and i are the phase flux linkages and phase currents, respectively. Although (3.2-3) or (3.2-4) can be used to determine the torque, we will establish other means of calculating torque for an electric machine that are more direct.

3.3 Transformation of Rotor Windings to the Arbitrary Reference Frame

In the case of the induction machine, there are two types of rotors, the wound rotor windings and the squirrel-cage rotor. The wound rotor windings are similar to the stator windings with slip rings so that resistors can be inserted during starting of large horsepower machines or to apply a voltage for a double-fed induction machine in wind turbine applications. The squirrel-cage rotor, which is shown in Fig. 3.2-1, is by far the most common.

As we have mentioned, it is difficult to see how the squirrel-cage rotor can be considered for analysis purposes as sinusoidally distributed windings. In order to justify this, we must recall that the stator windings are sinusoidally distributed.

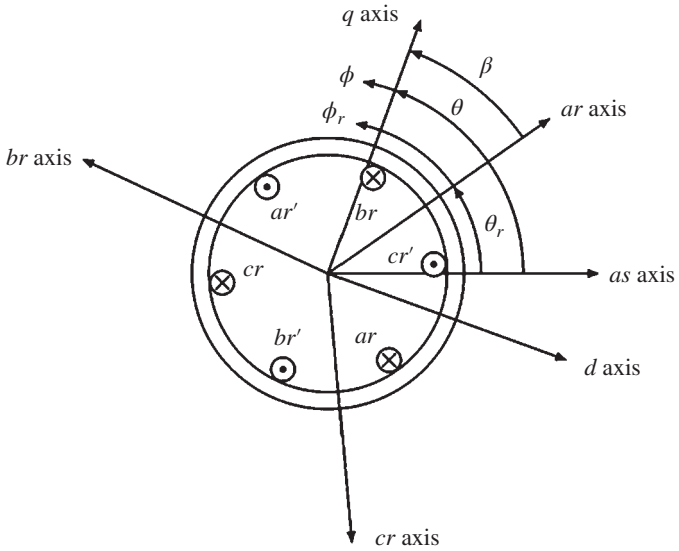

Figure 3.3-1 Elementary two-pole three-phase sinusoidally distributed rotor windings.

With balanced stator currents, we found in Chapter 2 that the rotating magnetic field is a space sinusoid that rotates at ω_e about the air gap. This mmf will induce an mmf in the rotor windings that is similar in form to the stator mmf. Therefore, since the sinusoidally distributed stator windings with balanced stator currents caused the sinusoidal rotating mmfs, it follows that in order to arrive at a sinusoidal rotor mmf, it must have been caused by balanced rotor currents of $\omega_e - \omega_r$ frequency flowing in sinusoidally distributed rotor windings. This has long been the justification for sinusoidal rotor windings. This is shown to be the case in [1]. It is interesting that the rotor can be an empty soda can and it will still rotate. Regardless of the rotor configuration, it can be approximated as two orthogonal sinusoidally distributed rotor (q and d axes) windings. The three-phase rotor circuits are shown in Fig. 3.3-1. We have added the same q and d axes that we used in the analysis of the stator in Chapter 2. We want to develop the transformation between the q and d axes and the *as*, *bs*, and *cs* axes.

In Fig. 3.3-1, θ is the angle between the *as* axis and the q axis and ϕ is the displacement from the q axis so that $\theta + \phi = \theta_r + \phi_r$ where θ_r is the angle between the *as* axis and the *ar* axis, and ϕ_r is the displacement from the *ar* axis. The angle β is the angle between the *ar* axis and the q axis.

The rotor mmf may be expressed from Fig. 3.3-1 as

$$\text{mmf}_r = \frac{N_r}{2}\left[i_{ar}\cos\phi_r + i_{br}\cos\left(\phi_r - \frac{2\pi}{3}\right) + i_{cr}\cos\left(\phi_r + \frac{2\pi}{3}\right)\right] \qquad (3.3\text{-}1)$$

Now,

$$\phi_r = \beta + \phi \tag{3.3-2}$$

where

$$\beta = \theta - \theta_r \tag{3.3-3}$$

Substituting (3.3-2) into (3.3-1) yields

$$\text{mmf}_r = \frac{N_r}{2}\left[i_{ar}\cos(\beta+\phi) + i_{br}\cos\left(\beta+\phi-\frac{2\pi}{3}\right) + i_{cr}\cos\left(\beta+\phi+\frac{2\pi}{3}\right)\right] \tag{3.3-4}$$

After some work, (3.3-4) may be written as

$$\begin{aligned}\text{mmf}_r = {} & \tfrac{N_r}{2}\cos\phi\left[i_{ar}\cos\beta + i_{br}\cos\left(\beta-\tfrac{2\pi}{3}\right) + i_{cr}\cos\left(\beta+\tfrac{2\pi}{3}\right)\right] \\ & -\tfrac{N_r}{2}\sin\phi\left[i_{ar}\sin\beta + i_{br}\sin\left(\beta-\tfrac{2\pi}{3}\right) + i_{cr}\sin\left(\beta+\tfrac{2\pi}{3}\right)\right]\end{aligned} \tag{3.3-5}$$

If we set $\phi = 0$ and define i_{qr} to be the sum of terms within the first [ ], then positive i_{qr} will produce a sinusoidally distributed mmf_r and the corresponding rotor flux that is maximum along the q axis, which is located at $\phi = 0$ [2, 3]. Likewise, if we set $\phi = -\frac{\pi}{2}$ and define i_{dr} to be the sum of terms within the second [ ], then positive i_{dr} will produce a sinusoidally distributed mmf_r and the corresponding rotor flux that is maximum along the d axis, which is located at $\phi = -\frac{\pi}{2}$. The rotor zero current is defined as $i_{0r} = \frac{1}{3}(i_{ar} + i_{br} + i_{cr})$. Although the transformation for rotor currents is motivated by (3.3-5), we will use the same transformation for $f = v$, i, or λ. The transformation for the rotor variables becomes [2, 3]

$$\mathbf{f}_{qd0r} = \mathbf{K}_r\mathbf{f}_{abcr} \tag{3.3-6}$$

where

$$(\mathbf{f}_{qd0r})^T = [f_{qr}\, f_{dr}\, f_{0r}] \tag{3.3-7}$$

$$(\mathbf{f}_{abcr})^T = [f_{ar}\, f_{br}\, f_{cr}] \tag{3.3-8}$$

$$\mathbf{K}_r = \frac{2}{3}\begin{bmatrix}\cos\beta & \cos\left(\beta-\frac{2\pi}{3}\right) & \cos\left(\beta+\frac{2\pi}{3}\right) \\ \sin\beta & \sin\left(\beta-\frac{2\pi}{3}\right) & \sin\left(\beta+\frac{2\pi}{3}\right) \\ \frac{1}{2} & \frac{1}{2} & \frac{1}{2}\end{bmatrix} \tag{3.3-9}$$

$$(\mathbf{K}_r)^{-1} = \begin{bmatrix}\cos\beta & \sin\beta & 1 \\ \cos\left(\beta-\frac{2\pi}{3}\right) & \sin\left(\beta-\frac{2\pi}{3}\right) & 1 \\ \cos\left(\beta+\frac{2\pi}{3}\right) & \sin\left(\beta+\frac{2\pi}{3}\right) & 1\end{bmatrix} \tag{3.3-10}$$

and

$$\frac{d\beta}{dt} = \omega(t) - \omega_r(t) \tag{3.3-11}$$

It is important to note that if we had placed the d axis at $\phi = \frac{\pi}{2}$ and defined i_{dr} to be minus the sum of terms inside the second [ ] in (3.3-5), each of the terms in the second row of $\mathbf{K}_r$ in (3.3-9) and second column of $(\mathbf{K}_r)^{-1}$ in (3.3-10) would include minus signs. In both cases, positive i_{dr} will produce a sinusoidally distributed mmf_r that is maximum along the selected d axis.

Ohm's and Faraday's laws give

$$v_{ar} = r_r i_{ar} + p\lambda_{ar} \tag{3.3-12}$$

$$v_{br} = r_r i_{br} + p\lambda_{br} \tag{3.3-13}$$

$$v_{cr} = r_r i_{cr} + p\lambda_{cr} \tag{3.3-14}$$

If (3.3-12)–(3.3-14) are transformed to the arbitrary reference frame [4], we have

$$v_{qr} = r_r i_{qr} + (\omega - \omega_r)\,\lambda_{dr} + p\lambda_{qr} \tag{3.3-15}$$

$$v_{dr} = r_r i_{dr} - (\omega - \omega_r)\,\lambda_{qr} + p\lambda_{dr} \tag{3.3-16}$$

$$v_{0r} = r_r i_{0r} + p\lambda_{0r} \tag{3.3-17}$$

The rotor has the qr and the dr windings. Now, from (2.3-8) and (3.3-5) and the associated definitions of i_{qs} i_{ds}, i_{qr}, and i_{dr},we can express mmf_s and mmf_r as

$$\text{mmf}_s = \frac{3}{2}\frac{N_s}{2}(i_{qs}\cos\phi_s + i_{ds}\sin\phi_s) \tag{3.3-18}$$

$$\text{mmf}_r = \frac{3}{2}\frac{N_r}{2}(i_{qr}\cos\phi_r + i_{dr}\sin\phi_r) \tag{3.3-19}$$

3.4 Voltage, Flux-Linkage Equations, and Equivalent Circuit

A three-phase symmetrical machine is shown in Fig. 3.2-2. Each stator phase has N_s equivalent turns; each rotor phase has N_r equivalent turns. The flux linkage equations may be written as

$$\begin{bmatrix}\boldsymbol{\lambda}_{abcs}\\ \boldsymbol{\lambda}_{abcr}\end{bmatrix} = \begin{bmatrix}\mathbf{L}_{ss} & \mathbf{L}_{sr}\\ (\mathbf{L}_{sr})^T & \mathbf{L}_{rr}\end{bmatrix}\begin{bmatrix}\mathbf{i}_{abcs}\\ \mathbf{i}_{abcr}\end{bmatrix} \tag{3.4-1}$$

The self-inductances are all constant and can be expressed as (2.2-24) for L_s and similarly for L_r

$$\mathbf{L}_{rr} = \begin{bmatrix} L_{rr} & -\frac{1}{2}L_{mr} & -\frac{1}{2}L_{mr} \\ -\frac{1}{2}L_{mr} & L_{rr} & -\frac{1}{2}L_{mr} \\ -\frac{1}{2}L_{mr} & -\frac{1}{2}L_{mr} & L_{rr} \end{bmatrix} \tag{3.4-2}$$

where $L_{rr} = L_{lr} + L_{mr}$. Also,

$$\mathbf{L}_{sr} = L_{sr} \begin{bmatrix} \cos\theta_r & \cos\left(\theta_r + \frac{2\pi}{3}\right) & \cos\left(\theta_r - \frac{2\pi}{3}\right) \\ \cos\left(\theta_r - \frac{2\pi}{3}\right) & \cos\theta_r & \cos\left(\theta_r + \frac{2\pi}{3}\right) \\ \cos\left(\theta_r + \frac{2\pi}{3}\right) & \cos\left(\theta_r - \frac{2\pi}{3}\right) & \cos\theta_r \end{bmatrix} \tag{3.4-3}$$

where L_{sr} is related to N_s, N_r, and R_m as

$$L_{sr} = \frac{N_s N_r}{R_m} \tag{3.4-4}$$

All rotor variables may be referred to the stator windings by the following turn ratios:

$$\mathbf{i}'_{abcr} = \frac{N_r}{N_s}\mathbf{i}_{abcr} \tag{3.4-5}$$

$$\mathbf{v}'_{abcr} = \frac{N_s}{N_r}\mathbf{v}_{abcr} \tag{3.4-6}$$

$$\boldsymbol{\lambda}'_{abcr} = \frac{N_s}{N_r}\boldsymbol{\lambda}_{abcr} \tag{3.4-7}$$

After substitution into (3.4-1) and some work, the flux linkage equations may be written as

$$\begin{bmatrix} \boldsymbol{\lambda}_{abcs} \\ \boldsymbol{\lambda}'_{abcr} \end{bmatrix} = \begin{bmatrix} \mathbf{L}_{ss} & \mathbf{L}'_{sr} \\ \left(\mathbf{L}'_{sr}\right)^T & \mathbf{L}'_{rr} \end{bmatrix} \begin{bmatrix} \mathbf{i}_{abcs} \\ \mathbf{i}'_{abcr} \end{bmatrix} \tag{3.4-8}$$

where, by definition,

$$\mathbf{L}'_{sr} = \frac{N_s}{N_r}\mathbf{L}_{sr} = \frac{L_{ms}}{L_{sr}}\mathbf{L}_{sr} \tag{3.4-9}$$

and

$$\mathbf{L}'_{rr} = \begin{bmatrix} L'_{lr} + L_{ms} & -\frac{1}{2}L_{ms} & -\frac{1}{2}L_{ms} \\ -\frac{1}{2}L_{ms} & L'_{lr} + L_{ms} & -\frac{1}{2}L_{ms} \\ -\frac{1}{2}L_{ms} & -\frac{1}{2}L_{ms} & L'_{lr} + L_{ms} \end{bmatrix} \tag{3.4-10}$$

In (3.4-10),

$$L'_{lr} = \left(\frac{N_s}{N_r}\right)^2 L_{lr} \tag{3.4-11}$$

A change of variables that formulates a transformation of the three-phase variables of the stationary (stator) circuits to the arbitrary reference frame is given in Chapter 2 and repeated here for convenience.

$$\mathbf{f}_{qd0s} = \mathbf{K}_s \mathbf{f}_{abcs} \tag{3.4-12}$$

where

$$(\mathbf{f}_{qd0s})^T = [f_{qs} \quad f_{ds} \quad f_{0s}] \tag{3.4-13}$$

$$(\mathbf{f}_{abcs})^T = [f_{as} \quad f_{bs} \quad \mathrm{f}_{cs}] \tag{3.4-14}$$

$$\mathbf{K}_s = \frac{2}{3}\begin{bmatrix} \cos\theta & \cos\left(\theta - \frac{2\pi}{3}\right) & \cos\left(\theta + \frac{2\pi}{3}\right) \\ \sin\theta & \sin\left(\theta - \frac{2\pi}{3}\right) & \sin\left(\theta + \frac{2\pi}{3}\right) \\ \frac{1}{2} & \frac{1}{2} & \frac{1}{2} \end{bmatrix} \tag{3.4-15}$$

The time rate-of-change of θ can be expressed as

$$\frac{d\theta(t)}{dt} = \omega(t) \tag{3.4-16}$$

The inverse is

$$(\mathbf{K}_s)^{-1} = \begin{bmatrix} \cos\theta & \sin\theta & 1 \\ \cos\left(\theta - \frac{2\pi}{3}\right) & \sin\left(\theta - \frac{2\pi}{3}\right) & 1 \\ \cos\left(\theta + \frac{2\pi}{3}\right) & \sin\left(\theta + \frac{2\pi}{3}\right) & 1 \end{bmatrix} \tag{3.4-17}$$

The s subscript indicates the variables, parameters, and transformation associated with stationary circuits. Transforming the stator voltage equations yields

$$v_{qs} = r_s i_{qs} + \omega\lambda_{ds} + p\lambda_{qs} \tag{3.4-18}$$

$$v_{ds} = r_s i_{ds} - \omega\lambda_{qs} + p\lambda_{ds} \tag{3.4-19}$$

$$v_{0s} = r_s i_{0s} + p\lambda_{0s} \tag{3.4-20}$$

Applying the transformation of rotor variables given by (3.3-9) to the rotor voltage equations yields

$$v'_{qr} = r'_r i'_{qr} + (\omega - \omega_r)\,\lambda'_{dr} + p\lambda'_{qr} \tag{3.4-21}$$

$$v'_{dr} = r'_r i'_{dr} - (\omega - \omega_r)\,\lambda'_{qr} + p\lambda'_{dr} \tag{3.4-22}$$

$$v'_{0r} = r'_r i'_{0r} + p\lambda'_{0r} \tag{3.4-23}$$

The set of equations is complete once the expressions for the flux linkages are determined. Substituting the equations of transformation into the flux linkage equations expressed in *abc* variables (3.4-8) yields the flux linkage equations for a magnetically linear system [5].

$$\begin{bmatrix} \lambda_{qd0s} \\ \lambda_{qd0r} \end{bmatrix} = \begin{bmatrix} \mathbf{K}_s \mathbf{L}_{ss} (\mathbf{K}_s)^{-1} & \mathbf{K}_s \mathbf{L}'_{sr} (\mathbf{K}_r)^{-1} \\ \mathbf{K}_r \left(\mathbf{L}'_{sr}\right)^T (\mathbf{K}_s)^{-1} & \mathbf{K}_r \mathbf{L}'_{rr} (\mathbf{K}_r)^{-1} \end{bmatrix} \begin{bmatrix} i_{qd0s} \\ i_{qd0r} \end{bmatrix} \tag{3.4-24}$$

We know from Chapter 2 that for L_s of the form given by (2.4-15)

$$\mathbf{K}_s \mathbf{L}_{ss} (\mathbf{K}_s)^{-1} = \begin{bmatrix} L_{ls} + L_{Ms} & 0 & 0 \\ 0 & L_{ls} + L_{Ms} & 0 \\ 0 & 0 & L_{ls} \end{bmatrix} \tag{3.4-25}$$

where

$$L_{Ms} = \frac{3}{2} L_{ms} \tag{3.4-26}$$

Since L'_r is similar in form to L_s, it follows that

$$\mathbf{K}_r \mathbf{L}'_{rr} (\mathbf{K}_r)^{-1} = \begin{bmatrix} L'_{lr} + L_{Ms} & 0 & 0 \\ 0 & L'_{lr} + L_{Ms} & 0 \\ 0 & 0 & L'_{lr} \end{bmatrix} \tag{3.4-27}$$

It can be shown that

$$\mathbf{K}_s \mathbf{L}_{sr} (\mathbf{K}_r)^{-1} = \mathbf{K}_r (\mathbf{L}_{sr})^T (\mathbf{K}_s)^{-1} = \begin{bmatrix} L_{Ms} & 0 & 0 \\ 0 & L_{Ms} & 0 \\ 0 & 0 & 0 \end{bmatrix} \tag{3.4-28}$$

In expanded form, the flux-linkage equations become

$$\lambda_{qs} = L_{ls} i_{qs} + L_{Ms} \left(i_{qs} + i'_{qr}\right) \tag{3.4-29}$$

$$\lambda_{ds} = L_{ls} i_{ds} + L_{Ms} \left(i_{ds} + i'_{dr}\right) \tag{3.4-30}$$

$$\lambda_{0s} = L_{ls} i_{0s} \tag{3.4-31}$$

$$\lambda'_{qr} = L'_{lr} i'_{qr} + L_{Ms} \left(i_{qs} + i'_{qr}\right) \tag{3.4-32}$$

$$\lambda'_{dr} = L'_{lr} i'_{dr} + L_{Ms} \left(i_{ds} + i'_{dr}\right) \tag{3.4-33}$$

$$\lambda'_{0r} = L'_{lr} i'_{0r} \tag{3.4-34}$$

where $L_{Ms} = \frac{3}{2} L_{ms}$ and the *q (d)* fluxes depend on *q (d)* currents.

Equations. (3.4-18)–(3.4-23) and (3.4-29)–(3.4-34) suggest the equivalent circuits shown in Fig. 3.4-1. We can show that other than the voltage equations for the

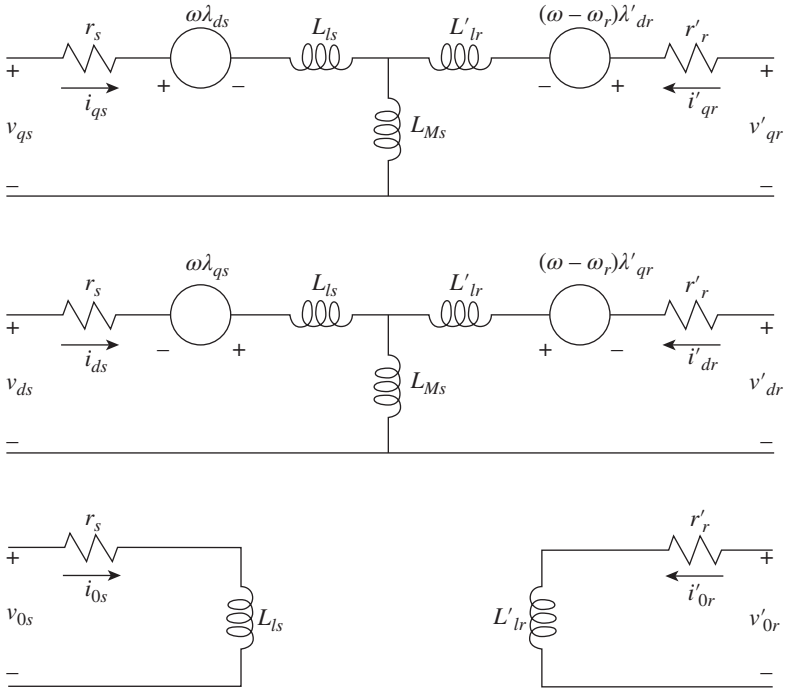

Figure 3.4-1 Arbitrary reference frame equivalent circuits for a three-phase symmetrical machine.

zero-variables and the $\frac{3}{2}$ factor in L_{Ms}, the voltage equations are the same as those for a two-phase machine. Moreover, if the three-phase machine is connected in wye without a neutral connection, as shown in Fig. 3.2-2, the currents i_{0s} and i'_{0r} are identically zero for balanced or unbalanced operation since the sum of the three-phase currents is zero. Therefore, v_{0s} and v'_{0r} are zero since the sum of the three-phase stator and rotor flux linkages will be zero for symmetrical systems. The equivalent circuit is shown in Fig. 3.4-1.

Since machine and power system parameters are nearly always given in ohms, or percent or per unit of a base impedance, it is convenient to express the voltage and flux linkage equations In terms of reactances rather than inductances. Hence, (3.4-18)–(3.4-23) and (3.4-29)–(3.4-34) are often written in terms of X rather than L.

$$v_{qs} = r_s i_{qs} + \frac{\omega}{\omega_b}\psi_{ds} + \frac{p}{\omega_b}\psi_{qs} \tag{3.4-35}$$

$$v_{ds} = r_s i_{ds} - \frac{\omega}{\omega_b}\psi_{qs} + \frac{p}{\omega_b}\psi_{ds} \tag{3.4-36}$$

$$v_{0s} = r_s i_{0s} + \frac{p}{\omega_b}\psi_{0s} \tag{3.4-37}$$

$$v'_{qr} = r'_r i'_{qr} + \left(\frac{\omega - \omega_r}{\omega_b}\right) \psi'_{dr} + \frac{p}{\omega_b}\psi'_{qr} \tag{3.4-38}$$

$$v'_{dr} = r'_r i'_{dr} - \left(\frac{\omega - \omega_r}{\omega_b}\right) \psi'_{qr} + \frac{p}{\omega_b}\psi'_{dr} \tag{3.4-39}$$

$$v'_{0r} = r'_r i'_{0r} + \frac{p}{\omega_b}\psi'_{0r} \tag{3.4-40}$$

where ω_b is the base electrical angular velocity used to calculate the inductive reactances (generally $\omega_b = 2\pi 60$ rad/s in North America or $2\pi 50$ in Europe and Asia). Flux linkages (3.4-29)–(3.4-34) now become flux linkages per second with the units of volts

$$\psi_{qs} = X_{ls} i_{qs} + X_{Ms}\left(i_{qs} + i'_{qr}\right) \tag{3.4-41}$$

$$\psi_{ds} = X_{ls} i_{ds} + X_{Ms}\left(i_{ds} + i'_{dr}\right) \tag{3.4-42}$$

$$\psi_{0s} = X_{ls} i_{0s} \tag{3.4-43}$$

$$\psi'_{qr} = X'_{lr} i'_{qr} + X_{Ms}\left(i_{qs} + i'_{qr}\right) \tag{3.4-44}$$

$$\psi'_{dr} = X'_{lr} i'_{dr} + X_{Ms}\left(i_{ds} + i'_{dr}\right) \tag{3.4-45}$$

$$\psi'_{0r} = X'_{lr} i'_{0r} \tag{3.4-46}$$

In the previous equations, the inductive reactances are obtained by multiplying ω_b times inductance. It is left to the reader to modify the equivalent circuits shown in Fig. 3.4-1 to accommodate the use of reactances rather than inductances in the voltage equations.

3.5 Torque Expressed in Arbitrary Reference Frame Variables

In Chapter 1, we used energy balance to obtain expressions for the electromagnetic torque. We can use those relations to obtain the torque expression for electric machines; however, once a transformation is used, the power balance relations can be used to advantage. In the arbitrary reference frame variables with d axis at $\phi = -\frac{\pi}{2}$, an expression for the stator electric power input can be established by substituting (2.4-12)–(2.4-14) into (2.4-26) and rearranging

$$P_{qd0s} = \frac{3}{2} r_s \left(i_{qs}^2 + i_{ds}^2\right) + \frac{3}{2}(\lambda_{ds} i_{qs} - \lambda_{qs} i_{ds})\omega + \frac{3}{2}(i_{qs} p\lambda_{qs} + i_{ds} p\lambda_{ds}) + 3v_{0s} i_{0s} \tag{3.5-1}$$

Similarly, for the rotor:

$$P_{qd0r} = \frac{3}{2} r'_r \left(i'^2_{qr} + i'^2_{dr}\right) + \frac{3}{2}\left(\lambda'_{dr} i'_{qr} - \lambda'_{qr} i'_{dr}\right)(\omega - \omega_r) + \frac{3}{2}\left(i'_{qr} p\lambda'_{qr} + i'_{dr} p\lambda'_{dr}\right) + 3v'_{0r} i'_{0r} \tag{3.5-2}$$

Now, the power balance equation becomes

$$P_{\text{elec}} = P_{\text{loss}} + \frac{dW_f}{dt} + P_{\text{mech}} \tag{3.5-3}$$

or

$$P_{\text{elec}} - \frac{dW_f}{dt} - P_{\text{loss}} = P_{\text{mech}} \tag{3.5-4}$$

which must hold in any reference frame. The power output positive for motor action is

$$P_{\text{mech}} = T_e \frac{2}{P} \omega_r \tag{3.5-5}$$

Now, the term in P_{qd0s} that is a speed voltage is

$$\frac{3}{2}(\lambda_{ds} i_{qs} - \lambda_{qs} i_{ds})\omega \tag{3.5-6}$$

In P_{qd0r}

$$\frac{3}{2}\left(\lambda'_{dr} i'_{qr} - \lambda'_{qr} i'_{dr}\right)(\omega - \omega_r) \tag{3.5-7}$$

For $\omega \neq \omega_r$, equating coefficients of ω_r we have the torque positive for motor action

$$T_e = \frac{3}{2}\frac{P}{2}\left(\lambda'_{qr} i'_{dr} - \lambda'_{dr} i'_{qr}\right) \tag{3.5-8}$$

For $\omega = \omega_r$, (3.5-7) is zero, and from (3.5-6), we have the T_e positive for motor action

$$T_e = \frac{3}{2}\frac{P}{2}(\lambda_{ds} i_{qs} - \lambda_{qs} i_{ds}) \tag{3.5-9}$$

Both (3.5-8) and (3.5-9) give the T_e positive for motor action as

$$T_e \frac{3}{2}\frac{P}{2} L_{Ms}\left(i'_{dr} i_{qs} - i'_{qr} i_{ds}\right) \tag{3.5-10}$$

There is a problem at the end of this chapter where the d axis is assumed to be located at $\phi = \frac{\pi}{2}$ rather than $\phi = -\frac{\pi}{2}$.

The relation between torque and speed for a two-pole machine is

$$T_e = J\frac{d\omega_r}{dt} + B_m \omega_r + T_L \tag{3.5-11}$$

where J is the inertia of the rotor and lightly connected load. The units are $\text{kg} \cdot \text{m}^2$. The first term on the right-hand side is the inertia torque. The damping coefficient B_m is generally small and often neglected. The units of B_m are $\text{N} \cdot \text{m} \cdot \text{s/rad}$. For a P-pole machine, replace ω_r with $\frac{2}{P}\omega_r$ in (3.5-11).

3.6 Computer Simulation in the Arbitrary Reference Frame

The equations convenient for simulating the symmetrical induction machine in the arbitrary reference frame may be established by first solving the flux linkage equations for currents. This can be accomplished by defining

$$\lambda_{mq} = L_{Ms}\left(i_{qs} + i'_{qr}\right) \tag{3.6-1}$$

$$\lambda_{md} = L_{Ms}\left(i_{ds} + i'_{dr}\right) \tag{3.6-2}$$

From (3.4-29) and (3.6-1), we get

$$i_{qs} = \frac{1}{L_{ls}}(\lambda_{qs} - \lambda_{mq}) \tag{3.6-3}$$

Similarly,

$$i_{ds} = \frac{1}{L_{ls}}(\lambda_{ds} - \lambda_{md}) \tag{3.6-4}$$

$$i'_{qr} = \frac{1}{L'_{lr}}\left(\lambda'_{qr} - \lambda_{mq}\right) \tag{3.6-5}$$

$$i'_{dr} = \frac{1}{L'_{lr}}\left(\lambda'_{dr} - \lambda_{md}\right) \tag{3.6-6}$$

Substituting (3.6-3) and (3.6-5) into (3.6-1) and solving for λ_{mq}

$$\lambda_{mq} = L_a\left(\frac{\lambda_{qs}}{L_{ls}} + \frac{\lambda'_{qr}}{L'_{lr}}\right) \tag{3.6-7}$$

where

$$L_a = \frac{1}{\frac{1}{L_{ls}} + \frac{1}{L'_{lr}} + \frac{1}{L_{Ms}}} \tag{3.6-8}$$

Similarly

$$\lambda_{md} = L_a\left(\frac{\lambda_{ds}}{L_{ls}} + \frac{\lambda'_{dr}}{L'_{lr}}\right) \tag{3.6-9}$$

From (3.4-18)–(3.4-23) may be rewritten as

$$\lambda_{qs} = \int [v_{qs} - \omega\lambda_{ds} - r_s i_{qs}]dt \tag{3.6-10}$$

$$\lambda_{ds} = \int [v_{ds} + \omega\lambda_{qs} - r_s i_{ds}]dt \tag{3.6-11}$$

$$\lambda_{0s} = \int [v_{0s} - r_s i_{0s}]dt \tag{3.6-12}$$

$$\lambda'_{qr} = \int \left[v'_{qr} - (\omega - \omega_r)\lambda'_{dr} - r'_r i'_{qr}\right]dt \tag{3.6-13}$$

$$\lambda'_{dr} = \int \left[v'_{dr} + (\omega - \omega_r)\lambda'_{qr} - r'_r i'_{dr}\right] dt \tag{3.6-14}$$

$$\lambda'_{0r} = \int \left[v'_{0r} - r'_r i'_{dr}\right] dt \tag{3.6-15}$$

Finally, (3.6-3)–(3.6-15) along with the torque equation (3.5-10) can be expressed in the form of a time-domain block diagram as shown in Fig. 3.6-1. The voltages v_{qs}, v_{ds}, and v_{0s} are obtained from v_{as}, v_{bs}, and v_{cs} and (2.3-5). The currents i_{as}, i_{bs}, and i_{cs} are obtained from i_{qs}, i_{ds}, i_{0s} and (2.3-7). The torque and rotor speed is given by (3.5-11).

3.7 Per Unit System

It is convenient, especially in power systems, to express machine parameters and variables as per unit quantities. Base power and base voltage are selected and all parameters and variables are normalized using these base quantities [5]. When the machine is being considered separately, the base power is generally selected as the horsepower rating of the machine in volt-amperes (i.e., horsepower times 746). If, on the other hand, the machine is a part of a power system and if it is desirable to convert the entire system to per unit quantities, then only one power base (VA base) is selected which would most likely be different from the rating of any machine in the system. Here we will consider the machine separately with the rating of the machine taken as base power.

Although we will violate this convention from time to time when dealing with instantaneous quantities, the rms value of the rated phase voltage is generally selected as base voltage for the *abc* variables while the peak value is generally selected as base voltage for the *qd*0 variables. That is, $V_{B(abc)}$ is the rms voltage selected as base voltage for the *abc* variables then $V_{B(qd0)} = \sqrt{2}V_{B(abc)}$. The base power may be expressed as

$$P_B = 3V_{B(abc)}I_{B(abc)} \tag{3.7-1}$$

or

$$P_B = \frac{3}{2}V_{B(qd0)}I_{B(qd0)} \tag{3.7-2}$$

Therefore, since base voltage and base power are selected, base current can be calculated from either (3.7-1) or (3.7-2). It follows that the base impedance may be expressed as

$$Z_B = \frac{V_{B(abc)}}{I_{B(abc)}} = \frac{3V^2_{B(abc)}}{P_B} \tag{3.7-3}$$

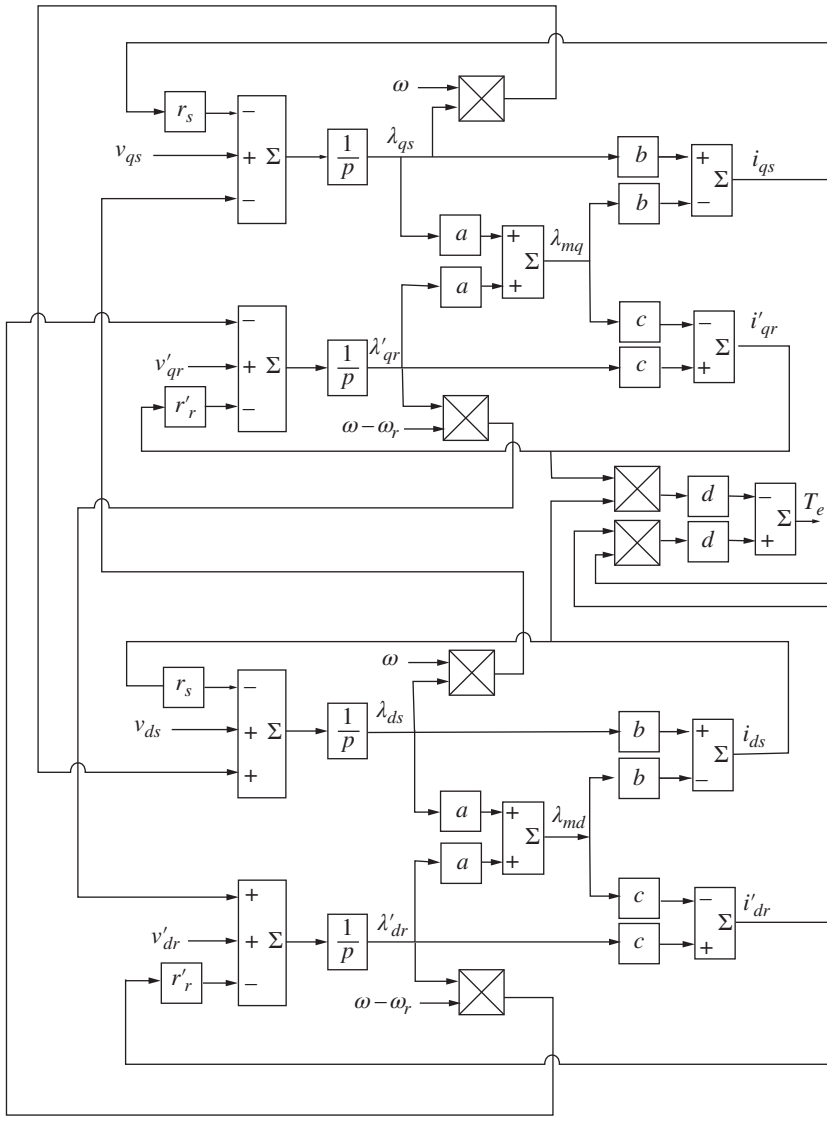

Figure 3.6-1 Time-domain block diagram for induction machine in the arbitrary reference frame. $a = L_a/L_{ls}$, $b = 1/L_{ls}$, $c = 1/L'_{lr}$, $d = \frac{3}{2}\frac{P}{2}L_{Ms}$.

or

$$Z_B = \frac{V_{B(qd0)}}{I_{B(qd0)}} = \left(\frac{3}{2}\right)\frac{V_{B(qd0)}^2}{P_B} \tag{3.7-4}$$

The $qd0$ equations written in terms of reactances, (3.4-41)–(3.4-46), can be readily converted to per unit by dividing the voltages by $V_{B(qd0)}$, the currents by $I_{B(qd0)}$, and the resistances and reactances by Z_B. Note that since a flux linkage per second is a volt, it is per unitized by dividing by base voltage.

Although the voltage and flux linkage per second equations do not change form when per unitized, the torque equation is modified by the per unitizing process. For this purpose, the base torque may be expressed as

$$T_B = \frac{P_B}{(2/P)\omega_b} \tag{3.7-5}$$

where ω_b corresponds to rated or base frequency of the machine (377 rad/s for 60 Hz system). A word of caution is appropriate. If, in (3.7-5), P_B is the rated power output of the machine, then base torque T_B will not be rated torque. We will find that, in the case of an induction machine, rated power output generally occurs at a speed (rated speed) slightly less than synchronous. Hence, T_B will be less than rated torque by the ratio of rated speed to synchronous speed.

If the torque expression given by (3.5-8) is divided by (3.7-5), with (3.7-2) substituted for P_B, the multiplier $\left(\frac{3}{2}\right)(P/2)(1/\omega_b)$ is eliminated and with all quantities expressed in per unit the per unit torque becomes

$$T_e = \psi'_{qr} i'_{dr} - \psi'_{dr} i'_{qr} \tag{3.7-6}$$

If the electrical variables are expressed in volts, amperes, and watts, then the inertia of the rotor is expressed in mks units. If, however, the per unit system is used, the inertia is expressed in seconds. The inertial torque T_{IT} for a P-pole machine may be expressed as

$$T_{IT} = J\left(\frac{2}{P}\right)p\omega_r \tag{3.7-7}$$

where ω_r is the electrical angular velocity of the rotor and J is the inertia of the rotor and connected mechanical load expressed in $\text{kg}\cdot\text{m}^2$. In order to express (3.7-7) in per unit, it is divided by base torque and the rotor speed is normalized to base speed. Thus,

$$T_{IT} = \frac{J(2/P)\omega_b}{T_B} p\frac{\omega_r}{\omega_b} \tag{3.7-8}$$

By definition, the inertia constant expressed in seconds is

$$H = \left(\frac{1}{2}\right)\left(\frac{2}{P}\right)\frac{J\omega_b}{T_B}$$

$$= \left(\frac{1}{2}\right)\left(\frac{2}{P}\right)^2 \frac{J\omega_B^2}{P_B} \tag{3.7-9}$$

Thus, in per unit the torque is related to angular acceleration using

$$T_e = 2Hp\frac{\omega_r}{\omega_b} + T_L \tag{3.7-10}$$

It is important to become familiar with both systems of units and to be able to convert readily from one to the other. We will use both systems interchangeably throughout the text.

3.8 Steady-State Equivalent Circuit and Common Modes of Operation

From (3.4-18), (3.4-19), (3.4-29), and (3.4-30), the voltage equations in the synchronously rotating reference frame for symmetrical machines may be written as

$$v_{qs}^e = r_s i_{qs}^e + \omega_e\left(L_{ss} i_{ds}^e + L_{Ms} i_{dr}'^e\right) + L_{ss} p i_{qs}^e + L_{Ms} p i_{qr}'^e \tag{3.8-1}$$

$$v_{ds}^e = r_s i_{ds}^e - \omega_e\left(L_{ss} i_{qs}^e + L_{Ms} i_{qr}'^e\right) + L_{ss} p i_{ds}^e + L_{Ms} p i_{dr}'^e \tag{3.8-2}$$

$$v_{qr}'^e = r_r' i_{qr}^e + (\omega_e - \omega_r)\left(L_{rr}' i_{dr}'^e + L_{Ms} i_{ds}^e\right) + L_{rr}' p i_{qr}'^e + L_{Ms} p i_{qs}^e \tag{3.8-3}$$

$$v_{dr}'^e = r_r' i_{dr}'^e - (\omega_e - \omega_r)\left(L_{rr}' i_{qr}'^e + L_{Ms} i_{qs}^e\right) + L_{rr}' p i_{dr}'^e + L_{Ms} p i_{ds}^e \tag{3.8-4}$$

Also,

$$\tilde{f}_{as} = f_{qs}^e - j f_{ds}^e \tag{3.8-5}$$

$$\tilde{f}_{ar}' = f'^e_{qr} - j f'^e_{dr} \tag{3.8-6}$$

The instantaneous phasor voltage equations are obtained by substituting (3.8-1)–(3.8-4) into (3.8-5) and (3.8-6), thus

$$\tilde{v}_{as} = r_s \tilde{i}_{as} + j\omega_e L_{ss} \tilde{i}_{as} + j\omega_e L_{Ms} \tilde{i}_{ar}' + pL_{ss} \tilde{i}_{as} + pL_{Ms} \tilde{i}_{ar}' \tag{3.8-7}$$

$$\tilde{v}_{ar}' = r_r' \tilde{i}_{ar}' + j(\omega_e - \omega_r) L_{rr}' \tilde{i}_{ar}' + j(\omega_e - \omega_r) L_{Ms} \tilde{i}_{as} + pL_{rr}' \tilde{i}_{ar}' + pL_{Ms} \tilde{i}_{as} \tag{3.8-8}$$

For steady-state conditions, the last two terms of (3.8-7) and (3.8-8) become zero and we obtain the following steady-state voltage equations.

$$\tilde{V}_{as} = r_s \tilde{I}_{as} + j\omega_e (L_{ls} + L_{Ms}) \tilde{I}_{as} + j\omega_e L_{Ms} \tilde{I}_{ar}' \tag{3.8-9}$$

$$\tilde{V}'_{ar} = r'_r \tilde{I}'_{ar} + j(\omega_e - \omega_r)\left(L'_{lr} + L_{ms}\right)\tilde{I}'_{ar} + j(\omega_e - \omega_r)L_{Ms}\tilde{I}_{as} \tag{3.8-10}$$

The so-called slip is

$$s = \frac{\omega_e - \omega_r}{\omega_e} \tag{3.8-11}$$

We see that slip increases when ω_r decreases, also, if we divide (3.8-10) by the slip, it becomes

$$\frac{\tilde{V}'_{ar}}{s} = \frac{r'_r}{s}\tilde{I}'_{ar} + j\omega_e\left(L'_{lr} + L_{Ms}\right)\tilde{I}'_{ar} + j\omega_e L_{Ms}\tilde{I}_{as} \tag{3.8-12}$$

Equations. (3.8-9) and (3.8-12) suggest the single-phase equivalent T circuit of a three-phase symmetrical machine during steady-state balanced operation shown in Fig. 3.8-1. Note that the inductive reactances are calculated as $X = \omega_e L$. One tends to want to calculate the inductive reactances of the rotor circuit as $X = (\omega_e - \omega_r)L$ and (3.8-10) is of the form we would expect; however, we have divided (3.8-10) by $(\omega_e - \omega_r)$ and multiplied by ω_e to arrive at (3.8-12). With $\tilde{V}'_{ar}$ equal to zero, only $\frac{r'_r}{s}$ changes with rotor speed.

We understand that current is not induced in the rotor windings when $\omega_r = \omega_e$. Since the rotor windings are generally short circuited (v'_{ar} and v'_{br} are zero) and from (3.8-11), the slip is zero and $\frac{r'_r}{s}$ is infinite; hence, the rotor circuit appears to be open circuited thus correctly portraying synchronous speed "operation".

Example 3A The parameters for the equivalent circuit shown in Fig. 3.8-1 may be calculated using electric field theory or determined from tests. The tests generally performed are a dc test, a no-load test, and a blocked-rotor test. The following test data are given for a 5-hp, four-pole, 220 V, three-phase, 60 Hz induction machine where all ac voltages and currents are rms values:

DC test No-load test Blocked-rotor test

$V_{dc} = 13.8$ V $V_{\text{nl}} = 220$ V $V_{\text{br}} = 23.5$ V

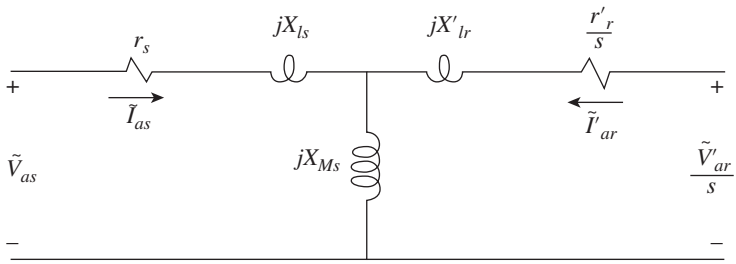

Figure 3.8-1 Equivalent single-phase circuit for a three-phase symmetrical induction machine for balanced steady-state operation.

$I_{dc} = 13.0$ A $I_{\text{nl}} = 3.86$ A $I_{\text{br}} = 12.9$ A
$P_{\text{nl}} = 200$ W $P_{\text{br}} = 469$ W
$f = 60$ Hz $f = 15$ Hz

During the dc test, a dc voltage is applied across two terminals while the machine is at standstill. Thus,

$$r_s = \frac{1}{2}\frac{V_{dc}}{I_{dc}} = \frac{13.8}{2 \times 13} = 0.531\ \Omega \tag{3A-1}$$

The no-load test, which is analogous to the transformer open-circuit test, is performed with balanced three-phase, 60 Hz voltages applied to the stator windings without mechanical load on the machine (no load). The power input during this test is the sum of the stator ohmic losses, the core losses due to hysteresis and eddy current losses, and rotational losses due to friction and windage. The stator ohmic losses are (I_{nl} is a phase current)

$$P_{I^2r_s} = 3I_{\text{nl}}^2 r_s = 3 \times (3.86)^2 \times 0.531 = 23.7\ \text{W} \tag{3A-2}$$

Therefore, the power loss due to friction and windage losses and core losses is

$$P_{f\text{WC}} = P_{\text{nl}} - P_{I^2r_s} = 200 - 23.7 = 176.3\ \text{W} \tag{3A-3}$$

In the equivalent circuit shown in Fig. 3.8-1, this loss is neglected. It is generally small and, in most cases, little error is introduced by neglecting it. It can be taken into account by placing a resistor in parallel with the magnetizing reactance X_{Ms} or by applying a small mechanical load (torque) to the shaft of the machine.

It is noted from the no-load test data that the power factor is very small since the apparent power is (V_{nl} is a line-to-line voltage)

$$|S_{\text{nl}}| = \sqrt{3}V_{\text{nl}}I_{\text{nl}} = \sqrt{3} \times 220 \times 3.86 = 1470.9\ \text{VA} \tag{3A-4}$$

Therefore, the no-load impedance is highly inductive, and its magnitude is assumed to be the sum of the stator leakage reactance and the magnetizing reactance since the rotor speed is essentially synchronous whereupon r_r'/s is much larger than X_{Ms}. Thus

$$X_{ls} + X_{Ms} = \frac{V_{\text{nl}}}{\sqrt{3}I_{\text{nl}}} = \frac{220}{\sqrt{3} \times 3.86} = 32.9 \tag{3A-5}$$

During the blocked-rotor test, which is analogous to the transformer short-circuit test, the rotor is locked by some external means and balanced three-phase stator voltages are applied. The frequency of the applied voltage is often less than rated (15 Hz) in order to obtain a representative value of r_r' since, during normal operation, the frequency of the rotor currents is low and the rotor resistances of some induction machines vary considerably with frequency. During stall, the impedance $r_r' + jX_{lr}'$ is much smaller in magnitude than X_{Ms} whereupon the current flowing in the magnetizing reactance may be neglected. Hence

$$P_{\text{br}} = 3I_{\text{br}}^2 \left(r_s + r_r'\right) \tag{3A-6}$$

From which

$$\begin{aligned} r_r' &= \frac{P_{\text{br}}}{3I_{\text{br}}^2} - r_s \\ &= \frac{469}{3 \times (12.9)^2} - 0.531 = 0.408\ \Omega \end{aligned} \tag{3A-7}$$

The magnitude of the blocked-rotor input impedance is

$$\begin{aligned} |Z_{br}| &= \frac{V_{\text{br}}}{\sqrt{3} I_{\text{br}}} \\ &= \frac{23.5}{\sqrt{3} \times 12.9} = 1.052\ \Omega \end{aligned} \tag{3A-8}$$

Now

$$\left| \left(r_s + r_r'\right) + j\frac{15}{60} \left(X_{ls} + X_{lr}'\right) \right| = 1.052\ \Omega \tag{3A-9}$$

From which

$$\begin{aligned} \left[\frac{15}{16} \left(X_{ls} + X_{lr}'\right)\right]^2 &= (1.052)^2 - \left(r_s + r_r'\right)^2 \\ &= (1.052)^2 - (0.531 + 0.408)^2 \\ &= 0.225\ \Omega \end{aligned} \tag{3A-10}$$

Thus

$$X_{ls} = X_{lr}' = 1.9\ \Omega \tag{3A-11}$$

Generally, X_{ls} and X_{lr}' are assumed equal; however, in some types of induction machines, a different ratio is suggested. We will assume $X_{ls} = X_{lr}'$ whereupon we have determined the machine parameters. In particular, for $\omega_b = 377$ rad/s, the parameters are

$$\begin{aligned} &r_s = 0.531\ \Omega \quad X_{Ms} = 31.95\ \Omega \quad r_r' = 0.408\Omega \\ &X_{ls} = 0.95\ \Omega \qquad\qquad\qquad X_{lr}' = 0.95\ \Omega \end{aligned}$$

An expression for the steady-state electromagnetic torque may be obtained by first writing (3.5-10) in terms of I^e_{qs}, I^e_{ds}, I'^e_{qr}, and I'^e_{dr}, and then express $\tilde{I}_{as}$ and $\tilde{I}'_{ar}$ using

$$\sqrt{2}\tilde{F}_{as} = F^e_{qs} - jF^e_{ds} \tag{3.8-13}$$

$$\sqrt{2}\tilde{F}_{ar} = F^e_{qr} - jF^e_{dr} \tag{3.8-14}$$

The expression may be reduced to

$$T_e = 3\left(\frac{P}{2}\right) L_{Ms} Re\left[j\tilde{I}^*_{as}\tilde{I}'_{ar}\right] \tag{3.8-15}$$

where $\tilde{I}^*_{as}$ is the conjugate of $\tilde{I}_{as}$. The phasor currents may be calculated from the equivalent circuit given in Fig. 3.8-1.

The balanced steady-state torque versus speed or torque versus slip characteristic of a single-fed induction machine warrants discussion. The majority of induction machines in use today are single-fed, wherein electric power is transferred to or from the induction machine through the stator circuits since the rotor windings are short-circuited. Thus

$$\tilde{I}'_{ar} = -\frac{jX_{Ms}}{r'_r/s + j\left(X'_{lr} + X_{Ms}\right)}\tilde{I}_{as} \tag{3.8-16}$$

Substituting (3.8-16) into (3.8-15) yields the following expression for electromagnetic torque of a single-fed three-phase symmetrical induction machine during balanced steady-state operation:

$$T_e = \frac{3(P/2)\left(X^2_{Ms}/\omega_e\right)\left(r'_r/s\right)|\tilde{I}_{as}|^2}{\left(r'_r/s\right)^2 + \left(X'_{lr} + X_{Ms}\right)^2} \tag{3.8-17}$$

It is important to note from (3.8-17) that torque is positive (motor action) when slip is positive which occurs when $\omega_r < \omega_e$ and negative (generator action) when the slip is negative which occurs when the rotor is being driven above synchronous speed, $\omega_r > \omega_e$, and zero when the slip is zero ($\omega_r = \omega_e$).

With the rotor windings short circuited, the input impedance of the equivalent circuit shown in Fig. 3.8-1 is

$$Z = \frac{\left(r_s r'_r/s\right) + \left(X^2_{Ms} - X_{ss}X'_{rr}\right) + j\left[\left(r'_r/s\right)X_{ss} + r_s X'_{rr}\right]}{\left(r'_r/s\right) + jX'_{rr}} \tag{3.8-18}$$

Now $|\tilde{I}_{as}|^2$ is I^2_s and

$$I_s = \frac{|\tilde{V}_{as}|}{|Z|} \tag{3.8-19}$$

Hence, the expression for the steady-state electromagnetic torque for a single-fed three-phase symmetrical induction machine becomes

$$T_e = \frac{3(P/2)\left(X_{Ms}^2/\omega_e\right) r_r' s |\tilde{V}_{as}|^2}{\left[r_s r_r' + s\left(X_{Ms}^2 - X_{ss}X_{rr}'\right)\right]^2 + \left(r_r' X_{ss} + s r_s X_{rr}'\right)^2} \tag{3.8-20}$$

Thus, for a given set of parameters and source frequency ω_e, the steady-state torque varies as the square of the magnitude of the applied voltages.

Figure 3.8-2 shows the steady-state torque speed plot of a typical industrial-type induction motor. Stable operation occurs on the negative slope part of this plot.

In most cases, the load torque is a function of ω_r, say $T_L = K\omega_r^2$, for example. In these cases, the machine can develop sufficient starting torque and, if T_L and T_e match on the negative slope portion, stable operation will occur. If, on the other hand, T_L is constant and greater than T_e at $\omega_r = 0$, we have at least three choices: (1) increase the stator voltage; (2) increase the rotor resistance; or (3) use a different machine. Increasing the rotor resistance to increase the starting torque is something that we have not yet discussed. We will now.

An expression for the slip at maximum torque may be obtained by taking the derivative of (3.8-20) with respect to slip and setting the result equal to zero. In particular,

$$s_m = r_r' G \tag{3.8-21}$$

where s_m is the slip at maximum torque and

$$G = \pm\sqrt{\frac{r_s^2 + X_{ss}^2}{\left(X_{Ms}^2 - X_{ss}X_{rr}'\right)^2 + r_s^2 X_{rr}'^2}} \tag{3.8-22}$$

Two values of slip at maximum torque, s_m, are obtained, one for motor action and one for generator action. It is important to note that G is not a function

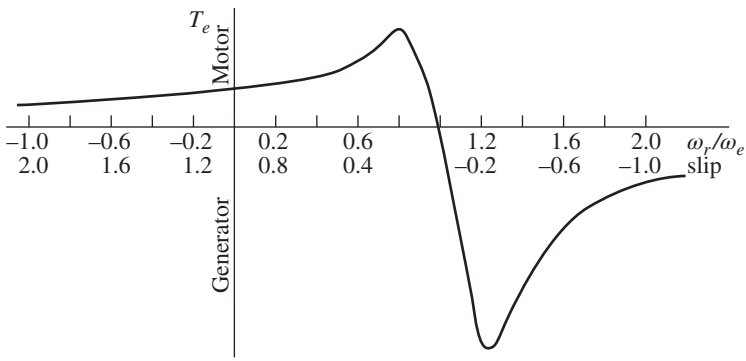

Figure 3.8-2 Steady-state torque versus speed characteristics of a symmetrical induction machine.

of r'_r; thus, the slip at maximum torque, (3.8-21), is directly proportional to r'_r. Consequently, with all other machine parameters constant, the speed at which maximum steady-state torque occurs may be varied by inserting external rotor resistance. This feature is sometimes used when starting large motors that have coil-wound rotor windings with slip rings. In this application, balanced external rotor resistances are placed across the terminals of the rotor windings so that maximum torque occurs near the stall. As the machine speeds up, the external resistors are decreased in value. For unbalanced rotor resistances, see [5]. On the other hand, some induction machines are designed with high resistance rotor windings so that maximum torque is produced at or near stall to provide fast response.

It may at first appear that the magnitude of the maximum torque would be influenced by r'_r. However, if (3.8-21) is substituted into (3.8-20), the maximum torque may be expressed as

$$T_{e,\max} = \frac{3(P/2)\left(X_{Ms}^2/\omega_e\right) G|\tilde{V}_{as}|^2}{\left[r_s + G\left(X_{Ms}^2 - X_{ss}X'_{rr}\right)\right]^2 + \left(X_{ss} + Gr_sX'_{rr}\right)^2} \tag{3.8-23}$$

Equation (3.8-23) is independent of r'_r. Thus, the maximum torque remains constant if only r'_r is varied; however, the slip at which maximum torque is produced varies in accordance with (3.8-21). Figure 3.8-3 illustrates the effect of changing r'_r. Therein, $r'_{r3} > r'_{r2} > r'_{r1}$.

In variable-frequency drive systems, the operating speed of the induction machine is controlled by changing the frequency of the applied voltages by either

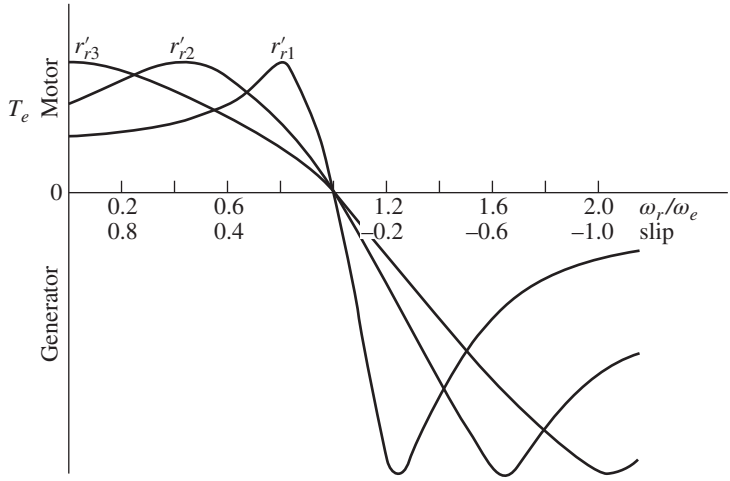

Figure 3.8-3 Steady-state torque versus speed characteristics of a symmetrical induction machine for different values of r'_r.

a converter (solid-state dc-to-ac converter) or a cyc1oconverter (ac frequency changer). The phasor voltage equations are applicable regardless of the frequency of operation. It is only necessary to keep in mind that the reactances given in the steady-state equivalent circuit, Fig. 3.8-1 are defined as the product of ω_e and the inductances. As the frequency is decreased, the time rate-of-change of the steady-state variables is decreased proportionally. Thus, the inductive reactances decrease linearly with frequency. If the amplitude of the applied voltages is maintained at the rated value, the currents will become excessive at the lower frequencies. To prevent these large currents, the magnitude of the stator voltages is decreased as the frequency is decreased. In many applications, the voltage magnitude is reduced linearly with frequency until a low frequency is reached, whereupon the decrease in voltage is programmed in a manner to compensate for the effects of the stator resistance.

The influence of frequency upon the steady-state torque versus speed characteristics is illustrated in Fig. 3.8-4. These characteristics are for a linear relationship between the magnitude of the applied voltages and frequency. This machine is designed to operate at $\omega_e = \omega_b$, where ω_b corresponds to the rated frequency. Rated voltage is applied at rated frequency, that is, when $\omega_e = \omega_b$, $|\widetilde{V}_{as}| = V_B$, where V_B is the base or rated voltage. Since the reactances ($\omega_e L$) decrease with frequency, the voltage is reduced as frequency is reduced to avoid large stator currents. The maximum torque is reduced markedly at $\omega_e/\omega_b = 0.1$. At this frequency, the voltage

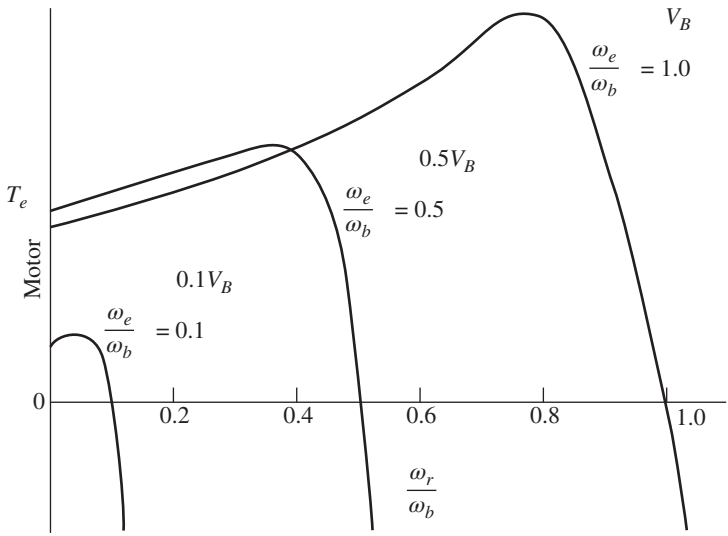

Figure 3.8-4 Steady-state torque versus speed characteristics of a symmetrical induction machine for different operating frequencies.

would probably be increased somewhat so as to obtain a higher torque. Perhaps a voltage of, say, $0.15V_B$ or $0.2V_B$ would be used rather than $0.1V_B$. Saturation of the stator or rotor steel may cause the stator currents to be excessive at this higher voltage. These practical considerations of variable-frequency drives are of major importance but beyond the scope of the present discussion. However, we will encounter variable frequency operation later when we deal with field-oriented control of an induction machine.

3.9 Free-Acceleration Torque Versus Speed Characteristics

It is instructive to observe the performance of several induction machines during free acceleration (no-load) from stall. For this purpose, the nonlinear differential equations that describe the induction machine were simulated on a computer and studies were performed. The parameters of the machines are given in Table 3.9-1. Each machine is a four-pole, 60 Hz, three-phase induction motor. The parameters are expressed in ohms using the 60 Hz value of the reactances. In Table 3.9-1, the voltage is the rated rms line-to-line voltage, the speed is rated speed, and J includes the inertia of the load which is assumed to be equal to the inertia of the rotor. Base torque, as calculated from (3.5-20), and base or rated current (rms) are also given.

The torque versus speed characteristics during free acceleration are shown for each machine in Figs. 3.9-1–3.9-4. In each case, the machine is initially stalled when rated balanced voltages are applied with $v_{as} = \sqrt{2}V_s \cos \omega_e t$. The machine currents along with the electromagnetic torque and speed for the 3- and 2250-hp machines during free acceleration are shown in Figs. 3.9-5 and 3.9-6. Since friction and windage losses are not represented, the machines accelerate at synchronous speed. In all figures, the scales of the currents are given in multiples of rated peak values. The scale of the torque is given in multiples of base torque.

Table 3.9-1 Induction Machine Parameters.

Machine rating			T_B	$I_{B(abc)}$	r_s	X_{ls}	X_{Ms}	X'_{lr}	r'_r	J
hp	volts	rpm	N · m	amps	ohms	ohms	ohms	ohms	ohms	kg · m^2
3	220	1710	11.9	5.8	0.435	0.754	26.13	0.754	0.816	0.089
50	460	1705	198	46.8	0.087	0.302	13.08	0.302	0.228	1.662
500	2300	1773	1.98×10^3	93.6	0.262	1.206	54.02	1.206	0.187	11.06
2250	2300	1786	8.9×10^3	421.2	0.029	0.226	13.04	0.226	0.022	63.87

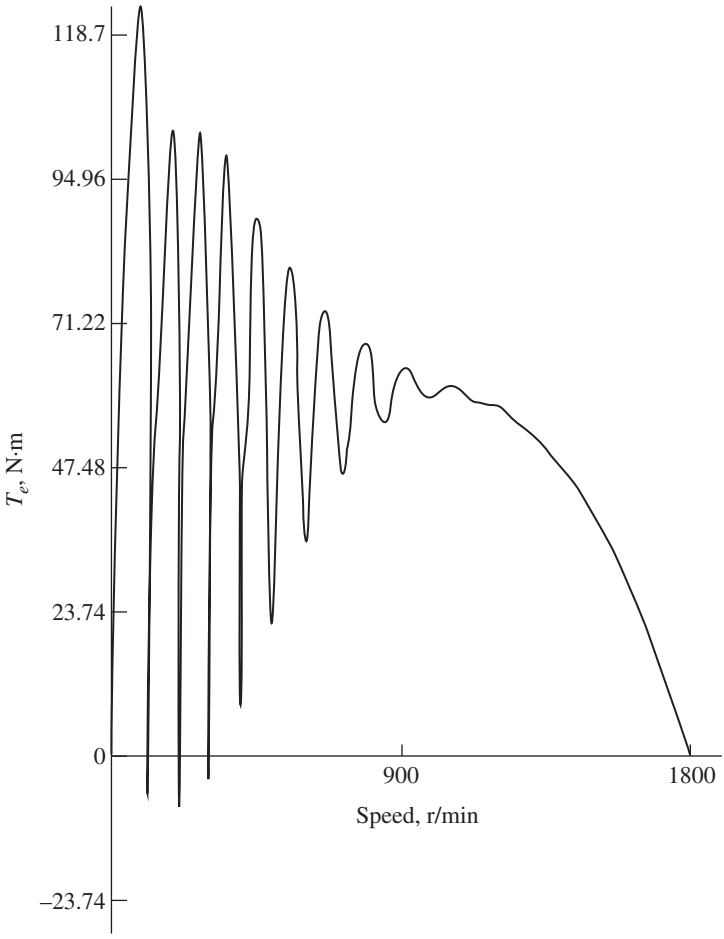

Figure 3.9-1 Torque versus speed characteristics during free acceleration—3-hp induction motor.

At stall, the input impedance of the induction machine is essentially the stator resistance and leakage reactance in series with the rotor resistance and leakage reactance. Consequently, with rated voltage applied the starting current is large, in some cases on the order of 10 times the rated value. Therefore, in practice, a compensator (transformer) is generally used to start large horsepower machines with reduced voltage until the machine has reached 60%–80% of synchronous speed whereupon full voltage is applied.

The 3- and 50-hp machines are relatively high-slip machines, that is, rated torque is developed at a speed considerably less than synchronous speed. On

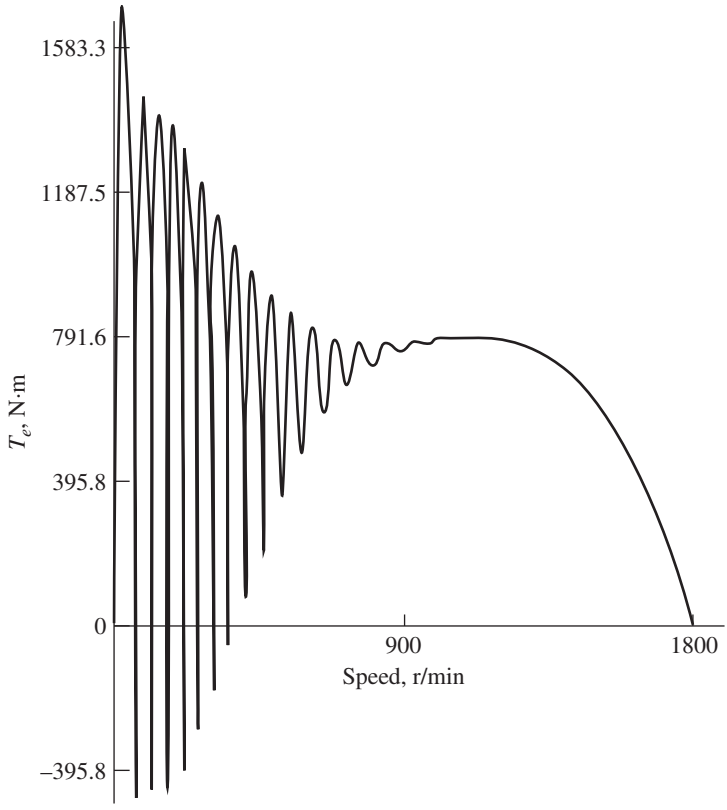

Figure 3.9-2 Torque versus speed characteristics during free acceleration—50-hp induction motor.

the other hand, the 500- and 2250-hp machines are low-slip machines. These characteristics are evident in the torque versus speed characteristics shown in Figs. 3.9-1–3.9-4.

The transient torque versus speed characteristics are different from the steady-state torque versus speed characteristics in several respects. The instantaneous electromagnetic torque, immediately following the application of the stator voltages, varies at 60 Hz about an average positive value. This decaying, 60 Hz variation in the instantaneous torque is due to the transient offset in the stator currents. Although the offset in each of the stator currents depends upon the values of the source voltages at the time of application, the instantaneous torque is independent of the initial values of balanced source voltages since the machine is symmetrical. We also note from the current traces in Figs. 3.9-5 and 3.9-6 that the envelope of the machine currents varies during the transient period. This is due to the interaction of the stator and rotor electric transients [5].

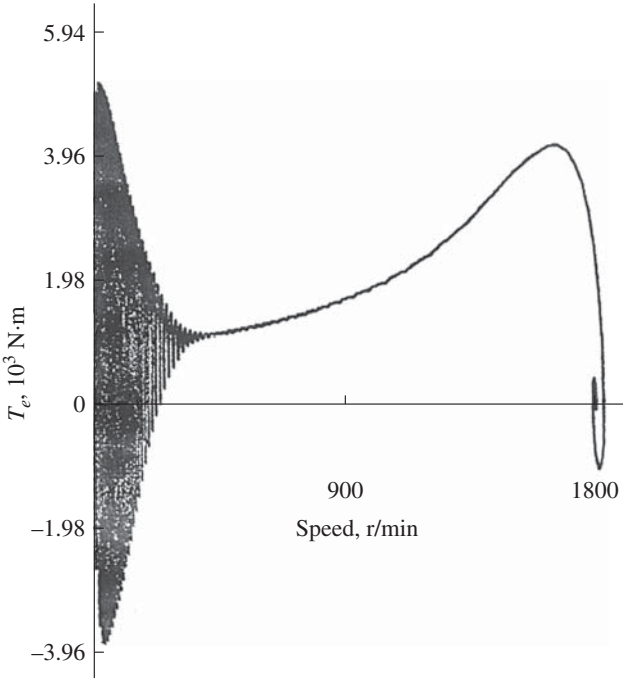

Figure 3.9-3 Torque versus speed characteristics during free acceleration—500-hp induction motor.

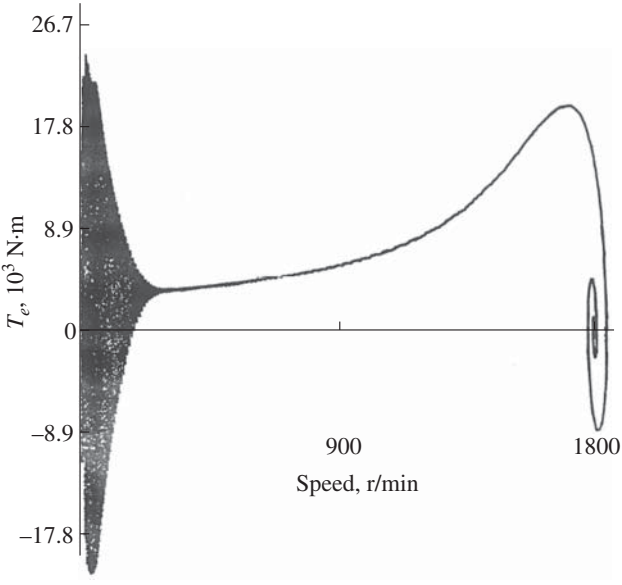

Figure 3.9-4 Torque versus speed characteristics during free acceleration—2250-hp induction motor.

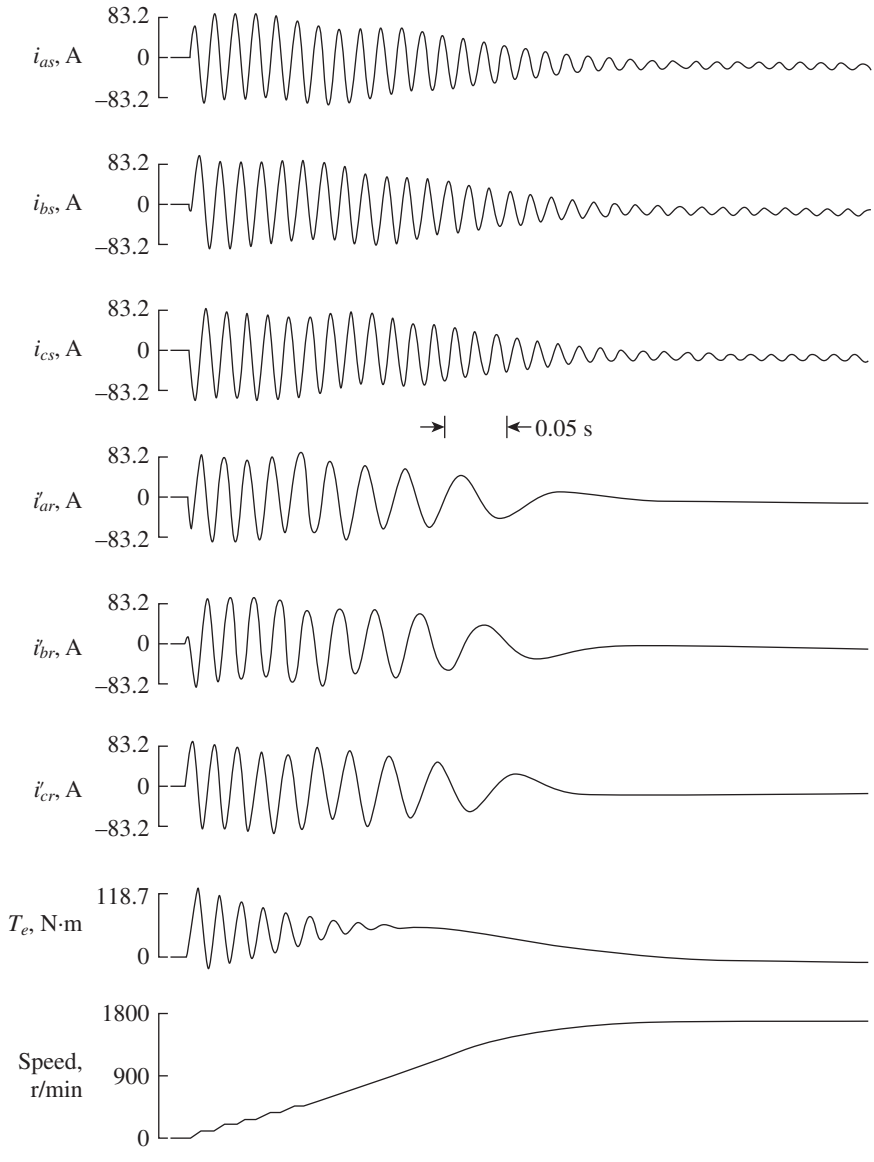

Figure 3.9-5 Machine variables during free acceleration of a 3-hp induction motor.

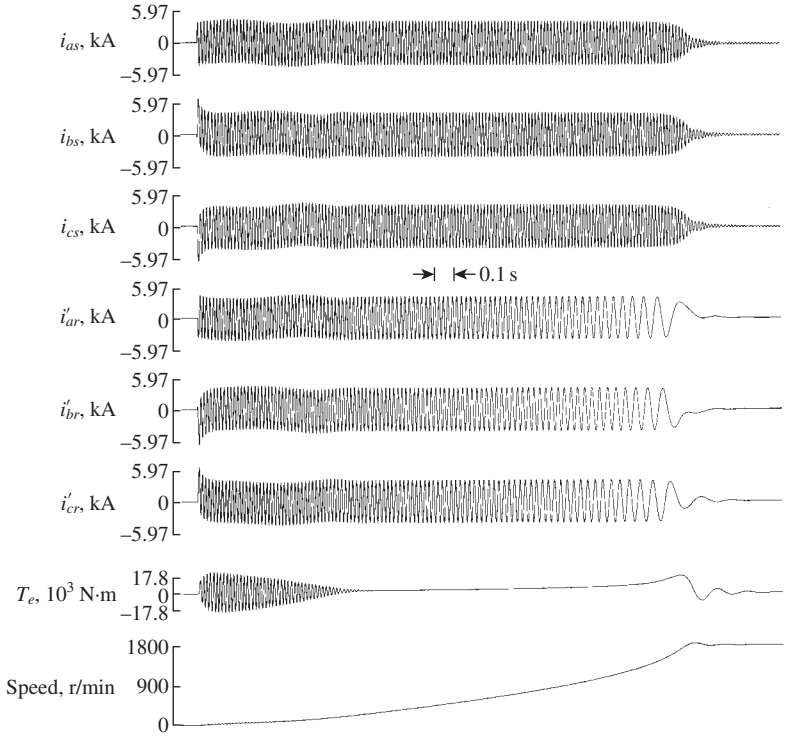

Figure 3.9-6 Machine variables during free acceleration of a 2250-hp induction motor.

Another noticeable difference between the dynamic and steady-state torque versus speed characteristics occurs in the case of the 500- and 2250-hp machines. In particular, the rotor speed overshoots synchronous speed and the instantaneous torque and speed demonstrate decayed oscillations about the final operating point. This characteristic is especially evident in the larger horsepower machines; however, in the case of the 3- and 50-hp machines, the rotor speed is highly damped and the final operating condition is attained without oscillations. It is noted from Table 3.9-1 that the ratio of rotor leakage reactance to rotor resistance is much higher for the larger horsepower machines than for the smaller. The dynamic response associated with the rotor circuits is much less damped in the case of the 500- and 2250-hp machines than in the case of the 3- and 50-hp machines.

If we were to plot the steady-state torque versus speed characteristics of the 3- and 50-hp machines upon the free-acceleration torque versus speed characteristics, we would find that the steady-state torque corresponds very closely to the average of the transient torque. This, however, is not the case for the 500- and 2250-hp machines where the steady-state value of maximum torque

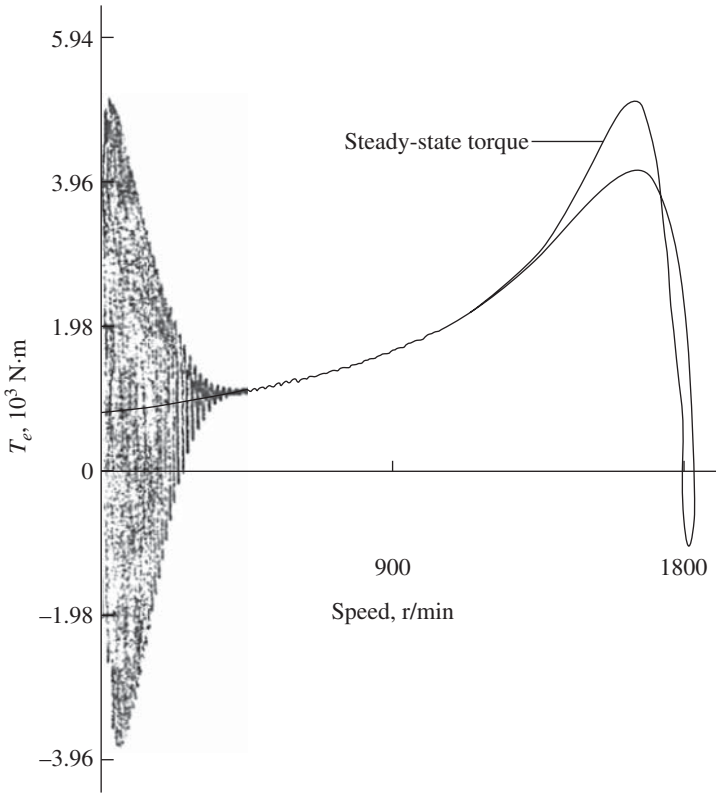

Figure 3.9-7 Comparison of steady-state and free-acceleration torque versus speed characteristics—500-hp induction motor.

is much larger than that observed from the free-acceleration characteristics. This is illustrated in Figs. 3.9-7 and 3.9-8 where the steady-state torque versus speed characteristic is superimposed upon the free-acceleration characteristic for the 500- and 2250-hp machines. This difference is due primarily to the electric transients in the rotor circuits [5].

Example 3B Let us calculate the steady-state torque and current at stall for the 3-hp machine given in Table 3.9-1 and compare these values to those shown in Figs. 3.9-1 and 3.9-5. From (3.8-20) and Table 3.9-1 with $s = 1$

$$T_e = \frac{(3)(4/2)(1)[(26.13)^2/377](0.816)(1)(220/\sqrt{3})^2}{[(0.435)(0.816) + (1)(1)^2(26.13^2 - 26.884 \times 26.884)]^2 + (1)^2(0.816 \times 26.884 + 1 \times 0.435 \times 26.884)^2}$$

$$= 51.9\ \text{N} \cdot \text{m} \qquad \text{(3B-1)}$$

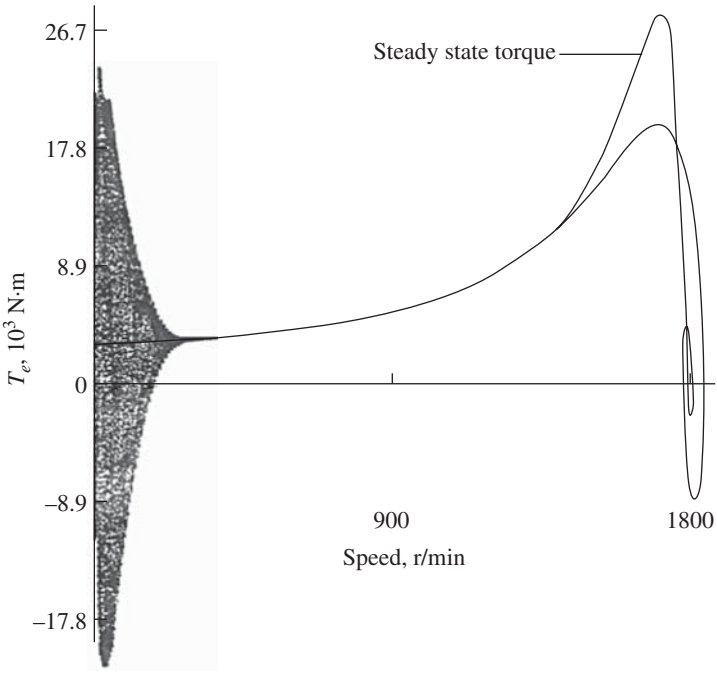

Figure 3.9-8 Comparison of steady-state and free-acceleration torque versus speed characteristics—2250-hp induction motor.

This is approximately the average of the pulsating torque at $\omega_r = 0$ depicted in Figs. 3.9-1 and 3.9-5.

The stall, steady-state current may be calculated from

$$\begin{aligned}\widetilde{I}_{as} &= \frac{\widetilde{V}_{as}}{\left(r_s + r'_r\right) + j\left(X_{ls} + X'_{lr}\right)} \\ &= \frac{(220/\sqrt{3})\underline{/0^{\circ}}}{(0.435 + 0.816) + j(0.754 + 0.754)} \\ &= 64.8\underline{/-50.3^{\circ}} A\end{aligned} \tag{3B-2}$$

This value is the steady-state current that would occur if the rotor is locked and after all electric transients have subsided. It is somewhat difficult to compare this value with that shown in Fig. 3.9-5 since the electric transients cause the currents to be offset in Fig. 3.9-5. However, i_{bs} in Fig. 3.9-5 contains the least offset and it compares quite well. In particular, the rms value of the first cycle of i_{bs} is approximately 69 A, which is in the order of 12 times rated current.

3.10 Free-Acceleration Characteristics Viewed from Various Reference Frames

It is also instructive to observe the variables of an induction machine in various reference frames during free acceleration from stall. The machine simulated on the computer, for this purpose, is a single-excited, six-pole, three-phase, 220 V (line-to-line), 10-hp, 60 Hz induction motor with the following parameters expressed in per unit.

$$r_s = 0.0453 \quad X_{Ms} = 2.042 \quad r'_r = 0.0222$$
$$X_{ls} = 0.0775 \quad X'_{lr} = 0.0322$$

The inertia of the rotor is $H = 0.5$ s.

The machine variables during free acceleration are shown in Fig. 3.10-1. All variables are plotted in per unit with the peak value of the base sinusoidal quantities given as 1.0 pu. If we were to follow the convention set forth in Section 3.7, we would use the rms value as 1.0 pu. However, the selection of peak values as 1.0 pu allows a more direct comparison with the *qd*0*s* variables shown later. Also, base torque rather than rated torque is taken as one per unit torque. At $t = 0$, rated voltage, with v_{as} a cosine, is applied to the machine. As in the studies reported in the previous section, the rotor accelerates from stall with zero load torque and, since friction and windage losses are not taken into account, the machine accelerates to synchronous speed.

The same free-acceleration characteristics are shown in different reference frames in Figs. 3.10-2 through 3.10-4. The stationary reference-frame variables during free acceleration are shown in Fig. 3.10-2. With the reference frame fixed in the stator, the *qs* and *ds* variables are arithmetically related to the *abc* variables. In particular, the zero position of the reference frame is zero; therefore, $f_{as} = f^s_{qs}$. Thus, v^s_{qs} and i^s_{qs} are identical to v_{as} and i_{as} of Fig. 3.10-1. The rotor variables are referred to the stationary reference frame (fictitious circuits) and vary therein at 60 Hz.

The free-acceleration characteristics with the reference frame fixed in the rotor is given in Fig. 3.10-3. Here, the zero position of the rotor and the reference frame are both zero; therefore, $f'_{ar} = f'^{r}_{qr}$. Hence, i'^{r}_{qr} in Fig. 3.10-3 is identical to i'_{ar} of Fig. 3.10-1 and since the stator variables are referred to the fictitious circuit in the rotor and vary at slip frequency. At stall, the rotor reference frame coincides with the stationary reference frame. At synchronous speed, the rotor reference frame becomes the synchronously rotating reference frame. It is important to note that since the machine essentially operates in the steady-state mode upon reaching synchronous speed, the variables become constants corresponding to their instantaneous values at the time the rotor speed becomes equal to synchronous speed.

Free acceleration with the reference frame rotating in synchronism with the electrical angular velocity of the applied voltages is shown in Fig. 3.10-4. Here, the zero position of the reference frame is selected so that v^e_{qs} is the amplitude of the stator applied phase voltages and $v^e_{ds} = 0$.

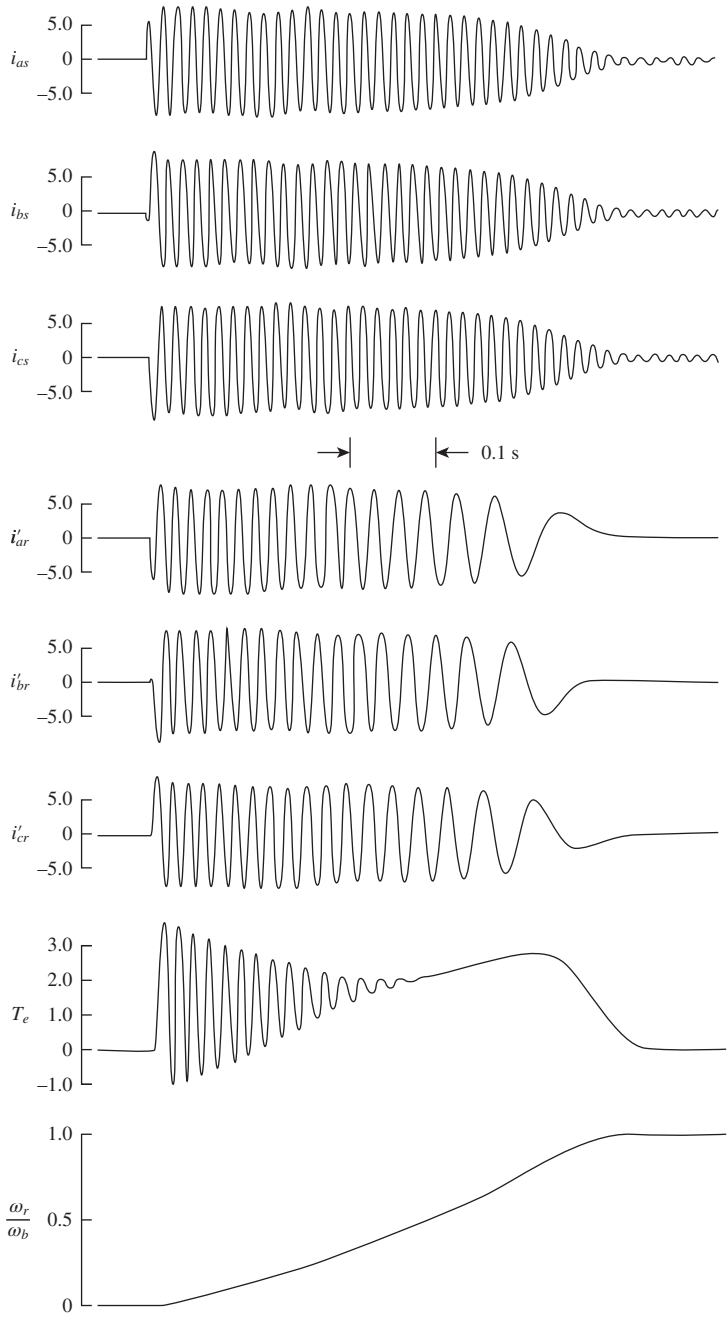

Figure 3.10-1 Free-acceleration characteristics of a 10-hp induction motor in machine variables.

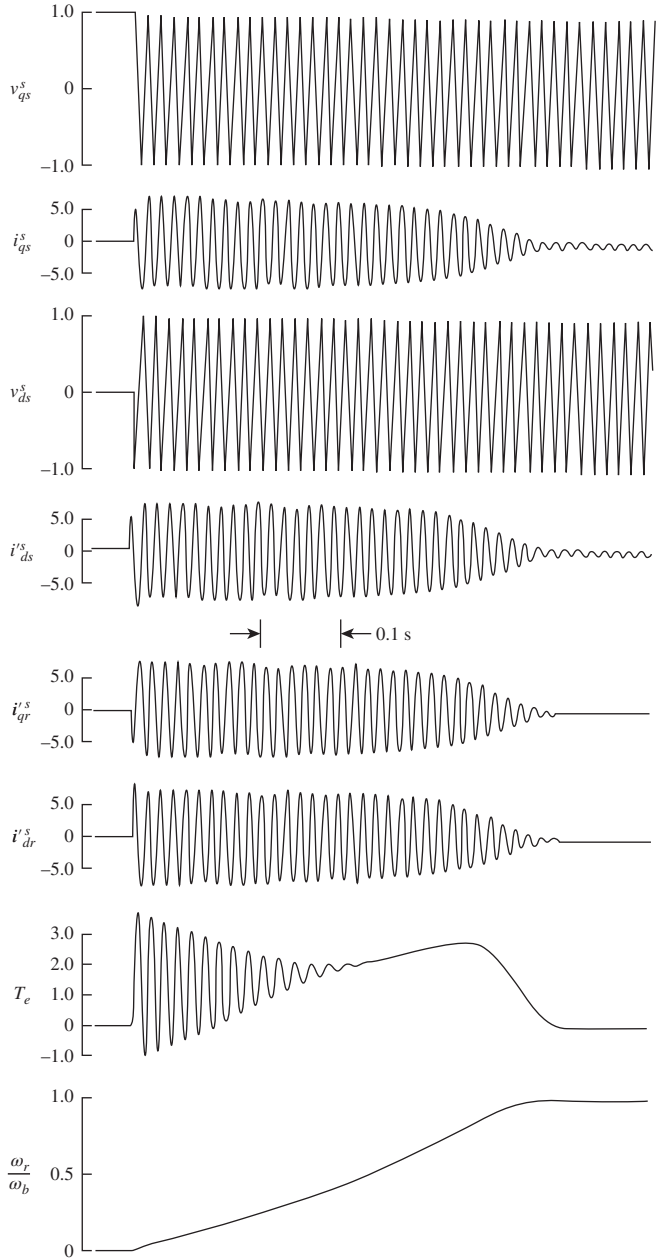

Figure 3.10-2 Free-acceleration characteristics of a 10-hp induction motor in the stationary reference frame.

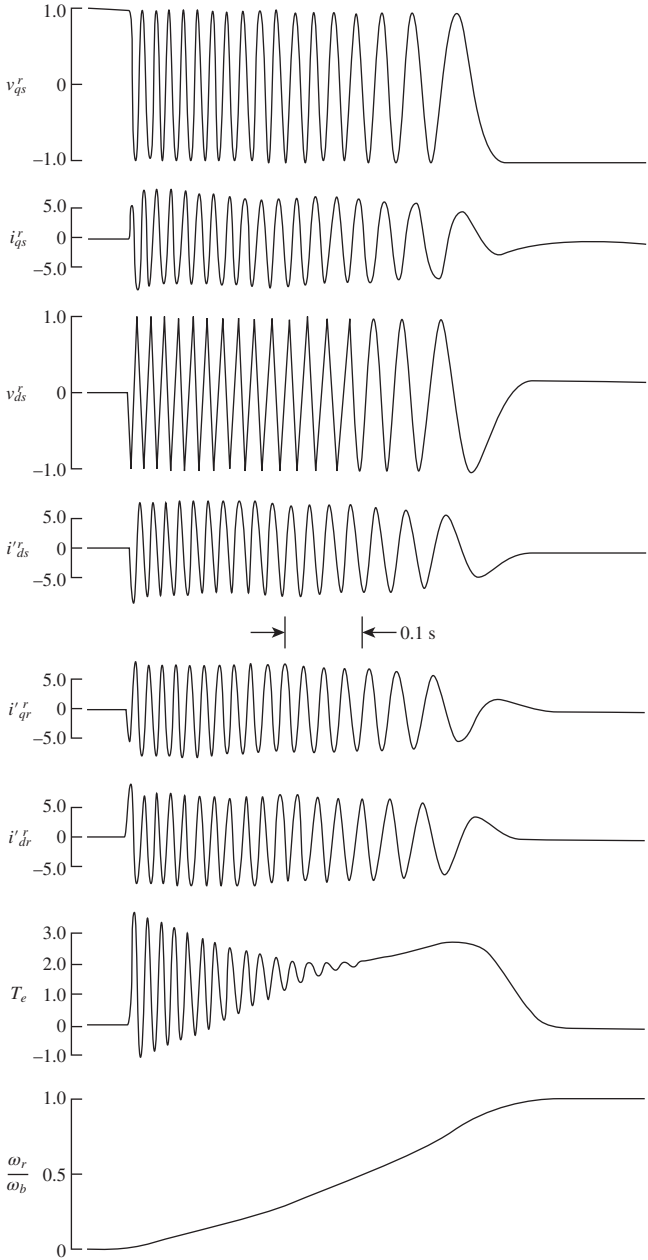

Figure 3.10-3 Free-acceleration characteristics of a 10-hp induction motor in a reference frame fixed in rotor.

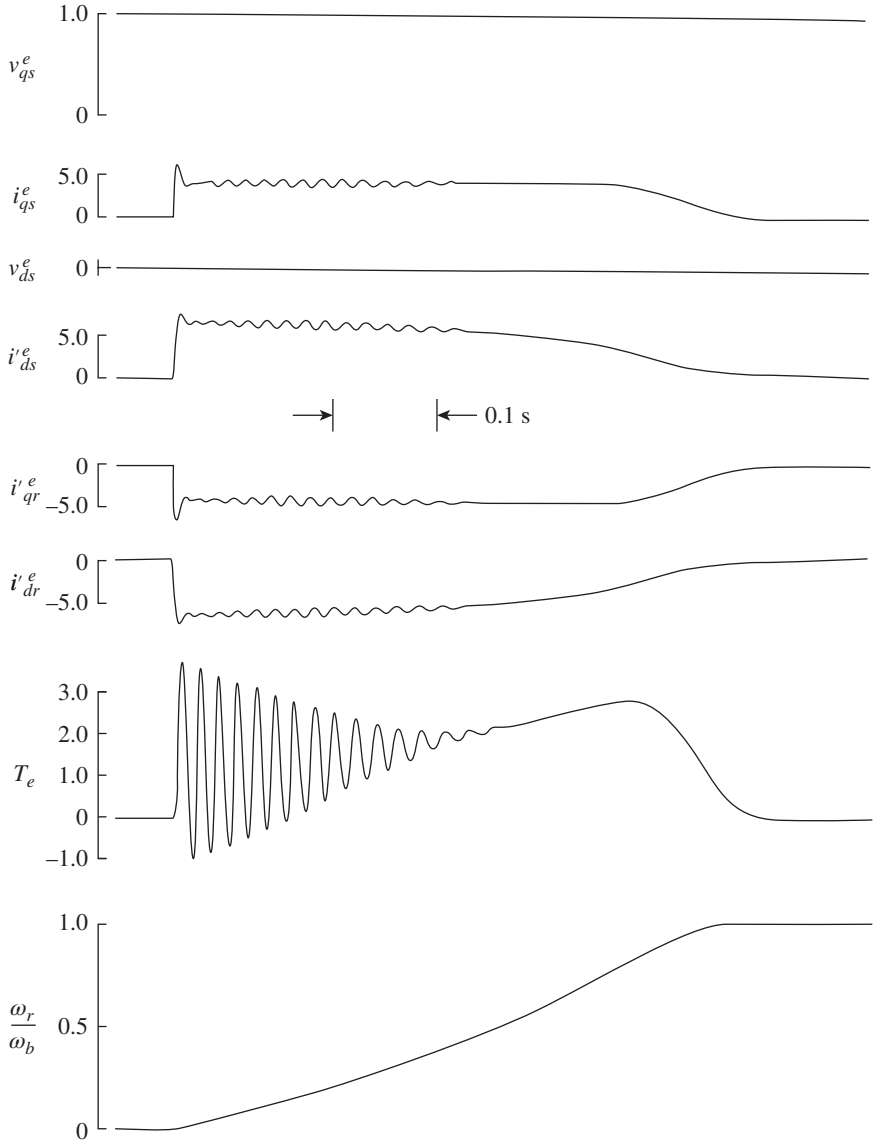

Figure 3.10-4 Free-acceleration characteristics of a 10-hp induction motor in the synchronously rotating reference frame.

3.11 Dynamic Performance During Sudden Changes in Load Torque

The dynamic behavior of the 3- and 2250-hp induction motors during step changes in load torque is shown in Figs. 3.11-1 and 3.11-2, respectively. Initially, each machine is operating at synchronous speed. The load torque is first stepped

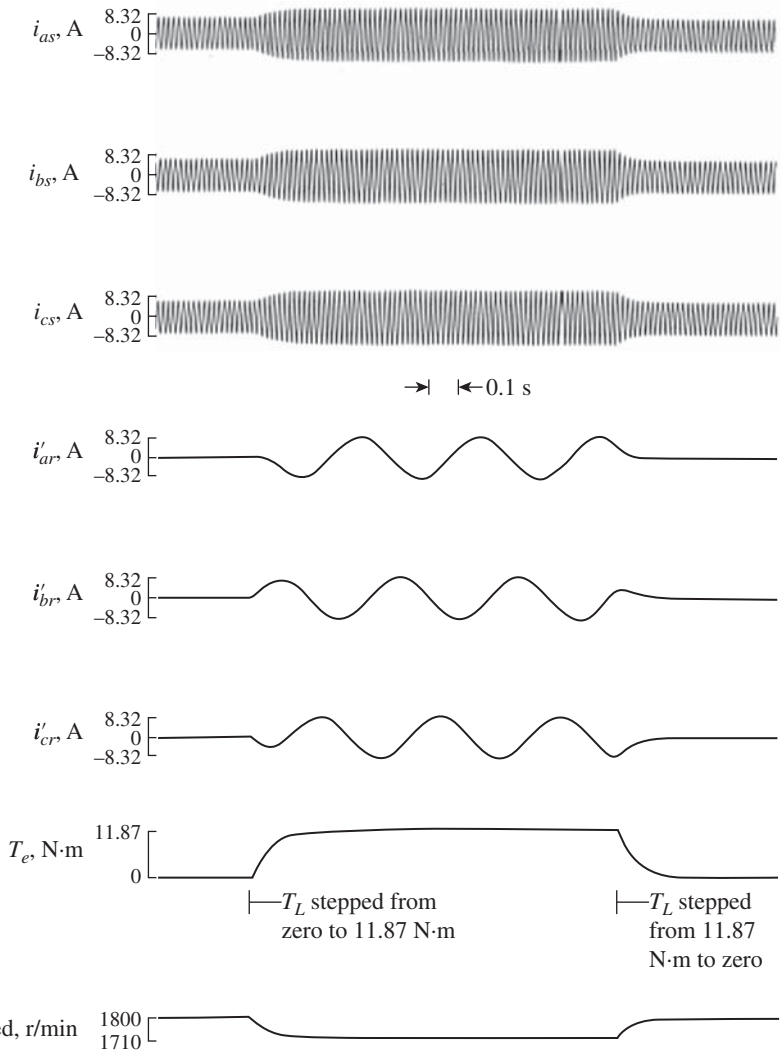

Figure 3.11-1 Dynamic performance of a 3-hp induction motor during step changes in load torque from zero to 11.87 N · m to zero.

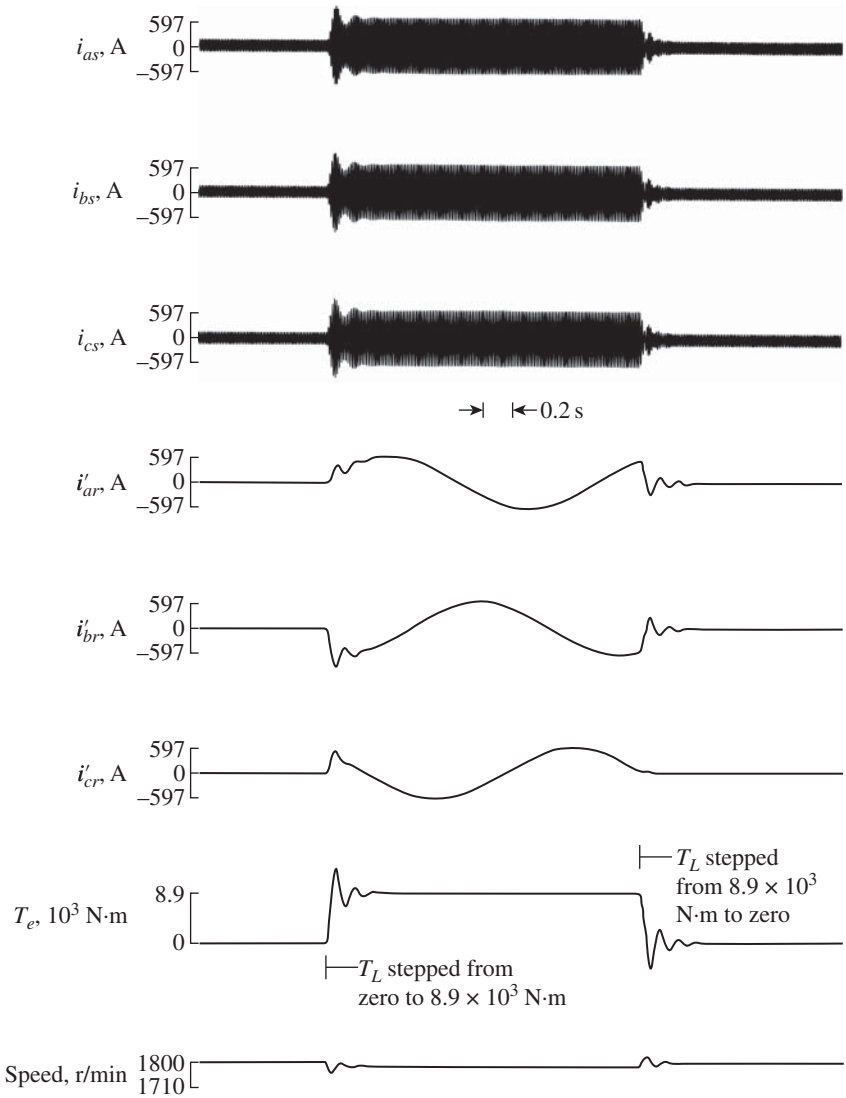

Figure 3.11-2 Dynamic performance of a 2250-hp induction motor during step changes in load torque from zero to 8.9 x 10^3 N · m to zero.

from zero to base torque (slightly less than rated) and the machine is allowed to establish this new operating point. Next, the load torque is stepped from base torque back to zero whereupon the machine reestablishes its original operating condition.

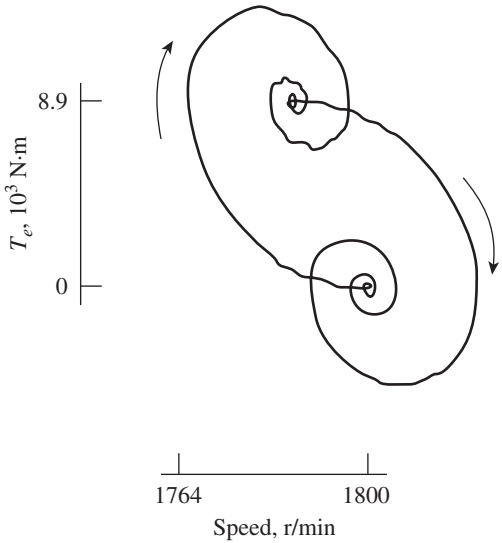

Figure 3.11-3 Torque versus speed for 2250-hp induction motor during load torque changes shown in Fig. 3.11-2.

The variables of the 3-hp machine approach each new operating condition in an overdamped manner. This is characteristic of the 3- and 50-hp machines given in Table 3.9-1. We previously found that for these machines the steady-state torque versus speed characteristic nearly duplicates the free-acceleration characteristic once the electrical transient associated with the stator circuits has subsided; therefore, we are not surprised to find that the dynamics during load torque changes can be predicted adequately by the steady-state torque versus speed characteristics. Indeed, this is the case; the plot of torque versus speed during the load torque changes depicted in Fig. 3.11-1 follows nearly exactly the steady-state torque versus speed curve. Therefore, the dynamic behavior of most smaller induction machines during normal load torque changes can be predicted by using the steady-state voltage and torque equations to calculate the currents and torque.

The dynamic performance of the 2250-hp machine during load torque changes is strongly influenced by the rotor electric transients. The 2250-hp machine exhibits damped oscillations about the new operating point. At best, the steady-state torque versus speed characteristics could approximate the average of this dynamic response; it could not predict the complete dynamics during normal load torque changes for the larger machines. This fact is further emphasized by the plot of torque versus speed for the 2250-hp machine in Fig. 3.11-3. The steady-state torque versus speed characteristic would be nearly a straight line drawn between the two operating points. We, of course, expected this from the previous comparison of the steady-state torque versus speed curve with the free-acceleration characteristics (Fig. 3.9-8).

References

1 A. R. Muñoz and T. A. Lipo, "Complex Vector Model of the Squirrel-Cage, Induction Machine Including Instantaneous Rotor Bar Currents," *IEEE Trans. Ind. App.* Vol. 35, No. 6 Nov. Dec. 1999.

2 P. C. Krause, O. Wasynczuk, T. C. O'Connell, and M. Hasan, "Tesla's Contribution to Electric Machine Analysis," *IEEE PES*, 2018.

3 P. C. Krause, *Reference Frame Theory*, IEEE Press, Wiley, 2020.

4 P. C. Krause, C. H. Thomas, "Simulation of Symmetrical Induction Machinery," *IEEE Trans. PAS*, Vol. 84 Nov. 1965, pp. 1038–1053.

5 Paul Krause, Oleg Wasynczuk, Scott Sudhoff, and Steven Pekarek, *Analysis of Electric Machines and Drive Systems*, 3rd Edition, IEEE Press and Wiley, 2013.

Problems

3.1 Consider the symmetrical two-pole, two-phase symmetrical induction machine shown in Fig. 3P-1. Derive the voltage equations in machine (*ab*) variables.

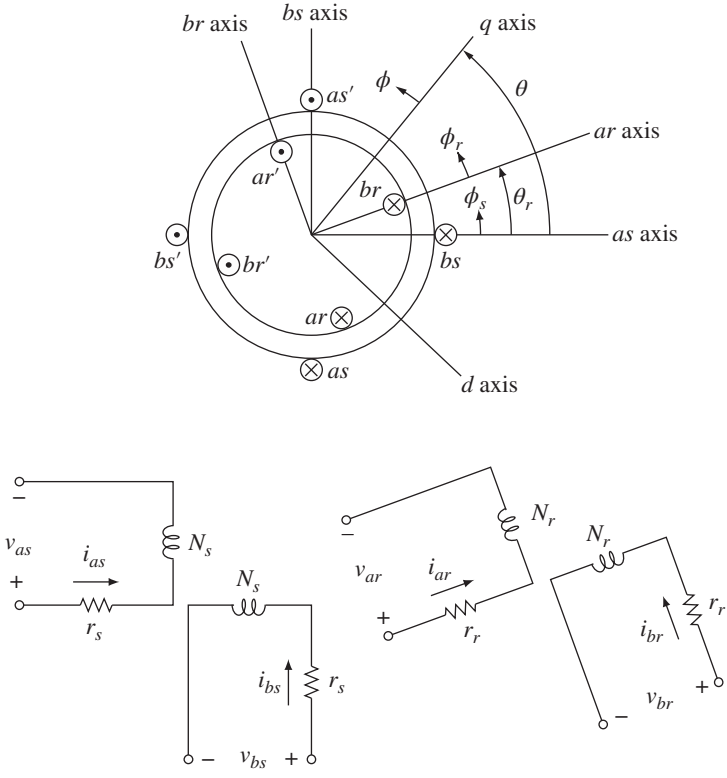

Figure 3P-1 A two-pole two-phase induction machine.

3.2 Prove that for a three-wire wye-connected stator winding $\lambda_{as} + \lambda_{bs} + \lambda_{cs} = 0$. For this to be true, is it necessary for the rotor windings to also be connected in a three-wire wye arrangement?

3.3 Obtain $\mathbf{K}_s$ and $\mathbf{K}_r$ for the two-phase induction motor in Fig. 3P-1 assuming the d axis is located at $\phi = -\frac{\pi}{2}$. Repeat for $\phi = \frac{\pi}{2}$.

3.4 Using the equations of transformation given in Problem 3, derive the voltage equations of a two-phase symmetrical induction machine in the arbitrary reference frame with d axis at $\phi = -\frac{\pi}{2}$.

3.5 An induction machine has a three-phase stator winding as shown in Fig. 3.2-2 and a two-phase rotor winding as shown in Fig. 3P-1. Develop the equivalent circuits for this machine in the arbitrary reference frame.

3.6 Derive an expression for electromagnetic torque in arbitrary reference frame variables for a two-phase machine similar in form to (3.5-10).

3.7 Show that the inertia constant H is equivalent to the stored energy of the rotor at synchronous speed normalized to the base power.

3.8 Devise a relationship that can be used to convert a per unit impedance from one VA base to another.

3.9 Per unitize the machine parameters given in Table 3.9-1.

3.10 Convert the per unit parameters given for the 10-hp machine in Section 3.10 to ohms and henrys and with the inertia in $\text{kg} \cdot \text{m}^2$.

3.11 Derive (3.8-15). What would this expression be in per unit?

3.12 A four-pole, 7.5-hp, three-phase induction motor has the following parameters:

$$r_s = 0.3\,\Omega \quad L_{ms} = 0.035\,\text{H} \quad r'_r = 0.15\,\Omega$$
$$L_{ls} = 0.0015\,\text{H} \qquad\qquad L'_{lr} = 0.0007\,\text{H}$$

The machine is supplied from a 110 V line to neutral 60 Hz source. Calculate the steady-state starting torque and current.

3.13 A four-pole, three-phrase induction machine is operating with $\omega_e = 377$ rad/s, $\omega_r = 350$ rad/s, $\tilde{I}^s_{qr} = 100\underline{/150^o}$, $L_{ls} = L'_{lr} = 1$ mH,

$L_{Ms} = 30$ mH, $r_s = 0.3\ \Omega$, and $r'_r = 0.2\ \Omega$. Assuming mechanical losses are negligible, determine $\tilde{I}_{ar}$, T_L, and I^e_{qs}.

3.14 Calculate the speed at maximum torque (motor action) for the 50-hp machine given in Table 3.9-1 when connected to a source of (a) 120 Hz, (b) 60 Hz, (c) 30 Hz, and (d) 6 Hz.

3.15 The 3-hp induction machine given in Table 3.9-1 is operating at no-load. The sequence of the applied voltages is suddenly changed from *abc* to *acb*. Assume the electrical system establishes steady-state operation before the speed of the rotor has changed appreciably. Calculate the torque.

3.16 Select three identical capacitors so that when they are connected in parallel with the 500-hp induction machine given in Table 3.9-1, the capacitor-induction machine combination operates at a 0.95 lagging power factor at rated power output.

3.17 For the time domain block diagram shown in Fig. 3.6-1, verify λ_{md} and λ_{mq}.

4

Brushless DC Machine

4.1 Introduction

This chapter is devoted to the analysis of a permanent-magnet ac machine supplied from an ideal inverter. This combination is generally referred to as an ideal brushless dc drive. The brushless dc drive is the low- to medium-power drive of choice. The drive is equipped with a means of determining the position of the rotor (permanent magnet) and the inverter is controlled so that the frequency of the applied voltages is equal to the electrical rotor speed. Due to the fast-responding power electronics, the machine essentially operates in synchronism with the applied voltages. Thus, as the mechanical load and speed changes, so does the frequency of the applied voltage. Therefore, it operates as a variable-frequency synchronous machine.

The actual drive is treated in later chapters. Here, we will neglect the harmonics and supply the machine with a three-phase variable (controlled) frequency sinusoidal source. In particular, if we assume that the stator variables (voltages and currents) are sinusoidal and balanced with a frequency equal to the electrical rotor speed, we are able to predict the predominant operating features of all of the modes of operation without becoming involved with the actual switching or control of the inverter. Therefore, in this chapter, we will focus on the performance of the inverter-machine combination assuming that the inverter is designed and controlled appropriately and leave how this is done to a later chapter.

4.2 Voltage Equations in Machine Variables

A four-pole three-phase 28 V $\frac{1}{3}$-hp permanent-magnet ac machine is shown in Fig. 4.2-1. The dissembled motor is shown in Fig. 4.2-1(a). The stator housing is shown in Fig. 4.2-1(b) wherein the stator windings are visible. Housed therein are

Analysis of Electric Machinery and Drive Systems, Fourth Edition.
Paul C. Krause, Oleg Wasynczuk, Scott D. Sudhoff, and Steven D. Pekarek.

Companion website: www.wiley.com/go/krause_aem4e

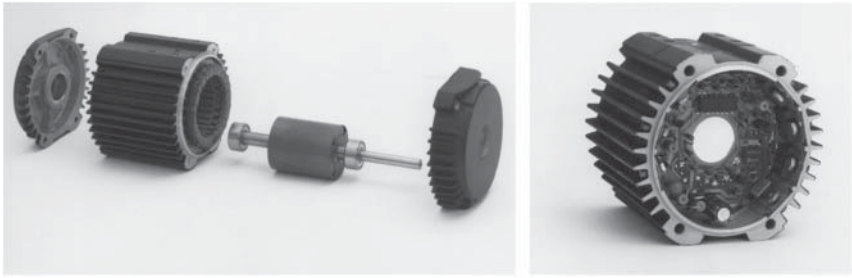

(a) (b)

Figure 4.2-1 (a) Four-pole three-phase 28-V $\frac{1}{3}$-hp permanent-magnet ac machine. (Courtesy EG and G Rotron). (b) Stator housing including electronics.

the Hall-effect sensors, which are used to determine the rotor position, the drive inverter, the filter capacitor, and the logic circuitry.

A two-pole permanent-magnet ac machine is depicted in Fig. 4.2-2. It has three-phase, wye-connected stator windings and a permanent-magnet rotor. The stator windings are identical windings displaced 120°, each with N_s equivalent turns and resistance r_s. For our analysis, we will assume that the stator windings are sinusoidally distributed. The three sensors shown in Fig. 4.2-2 are Hall-effect devices. When the north pole is under a sensor, its output is either zero or nonzero; with a south pole under the sensor, its output is opposite to the north pole. During steady-state operation, the stator windings are supplied from an inverter that is switched at a frequency corresponding to the rotor speed. The states of the three sensors are used to determine the switching logic for the inverter. In the actual machine, the sensors might not be positioned over the rotor as shown in Fig. 4.2-1. Instead, they are placed over a ring that is mounted on the shaft external to the stator windings and magnetized as the rotor. We will return to these sensors and the role they play later.

As shown in Figs. 4.2-1(a) and 4.2-2, the rotor is cylindrical; however, the rotor is unsymmetrical and we must analyze the machine in the rotor reference frame. It is clear that since the rotor is magnetized in one direction, we cannot write transformation equations to a freely rotating q and d axis other than ω_r. In other words, the reference frame must be placed where the asymmetry exists. In this case, the rotor.

Now, although the rotor is cylindrical, the reluctance is not the same along the q and d axes as in the case of the induction machine. In particular, the permanent magnets, which are on the d axis, can have higher reluctance than the iron in the q axis. Therefore, $L_{md} < L_{mq}$. We find in the next chapter that in the case of a synchronous machine (constant frequency) that has a salient-pole rotor with a

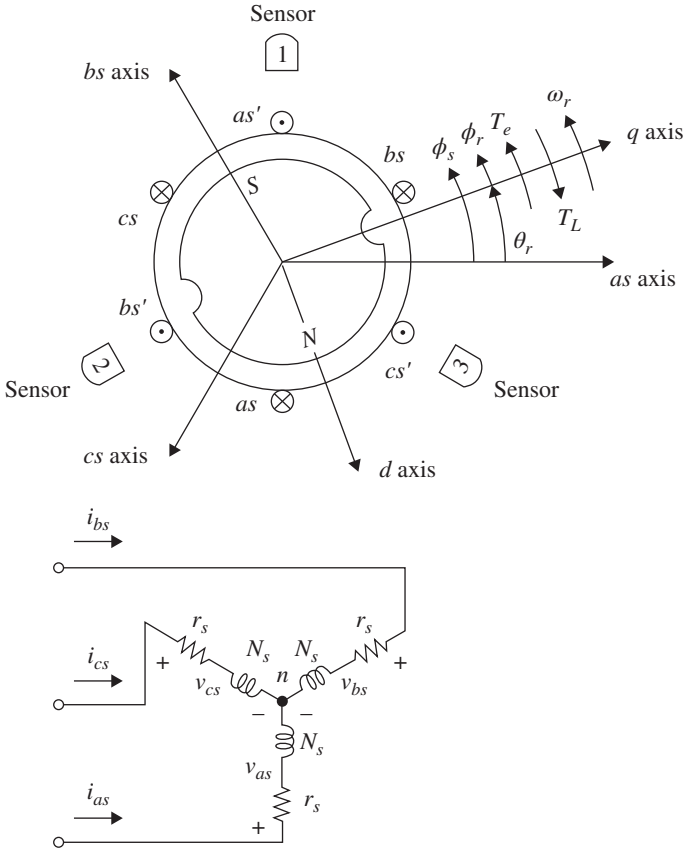

Figure 4.2-2 Two-pole three-phase permanent-magnet ac machine with sensors.

field winding instead of a permanent magnet $L_{mq} < L_{md}$ since the air gap is larger in the q axis. We will see this later.

Now, in the case of the brushless dc machine, the difference in L_{mq} and L_{md} is dependent upon the type of permanent magnets being used. We will write the voltage equations assuming $L_{mq} > L_{md}$.

The voltage equations in machine variables are

$$\mathbf{v}_{abcs} = r_s \mathbf{i}_{abcs} + p\boldsymbol{\lambda}_{abcs} \tag{4.2-1}$$

where

$$(\mathbf{f}_{abcs})^T = [f_{as} \; f_{bs} \; f_{cs}] \tag{4.2-2}$$

The flux linkages may be written as

$$\boldsymbol{\lambda}_{abcs} = \mathbf{L}_s \mathbf{i}_{abcs} + \boldsymbol{\lambda}'_m \tag{4.2-3}$$

where $\mathbf{L}_s$ may be written as

$$\mathbf{L}_s = \begin{bmatrix} L_{ls} + L_A + L_B \cos 2\theta_r & -\frac{1}{2}L_A + L_B \cos 2\left(\theta_r - \frac{\pi}{3}\right) & -\frac{1}{2}L_A + L_B \cos 2\left(\theta_r + \frac{\pi}{3}\right) \\ -\frac{1}{2}L_A + L_B \cos 2\left(\theta_r - \frac{\pi}{3}\right) & L_{ls} + L_A + L_B \cos 2\left(\theta_r - \frac{2\pi}{3}\right) & -\frac{1}{2}L_A + L_B \cos 2(\theta_r - \pi) \\ -\frac{1}{2}L_A + L_B \cos 2\left(\theta_r + \frac{\pi}{3}\right) & -\frac{1}{2}L_A + L_B \cos 2(\theta_r + \pi) & L_{ls} + L_A + L_B \cos 2\left(\theta_r + \frac{2\pi}{3}\right) \end{bmatrix} \tag{4.2-4}$$

where L_A is a positive constant and L_B is the amplitude of variation about L_A and $L_B < L_A$.

The flux linkage $\boldsymbol{\lambda}'_m$ may be expressed as

$$\boldsymbol{\lambda}'_m = \lambda'_m \begin{bmatrix} \sin\theta_r \\ \sin\left(\theta_r - \frac{2\pi}{3}\right) \\ \sin\left(\theta_r + \frac{2\pi}{3}\right) \end{bmatrix} \tag{4.2-5}$$

where λ'_m is the amplitude of the flux linkages established by the permanent magnet as viewed from the stator phase windings. When multiplied by rotor speed it is the back voltage, it does not exist when $\omega_r = 0$. It is the magnetizing flux linkage; it does not include the leakage flux linkages of the permanent magnet of the rotor. That is, $p\boldsymbol{\lambda}'_m$ would be the open-circuit voltage induced in each stator phase winding. We have assumed by (4.2-5) that the voltages induced in the stator windings by the permanent magnet are constant amplitude sinusoidal voltages. For the four-pole machine considered in this chapter, $\lambda_m = 0.0827$ V/rad. This was determined by measuring the voltage across two windings as 60 V at a rotor speed of 1000 r/mm.

The expression for the electromagnetic torque may be written in machine variables as

$$T_e = \left(\frac{P}{2}\right) \frac{\partial W_c(i_{abcs}, \theta_r)}{\partial \theta_r} \tag{4.2-6}$$

However, we will not use this approach to express the torque. Instead, there is a more direct approach once the transformation to the arbitrary reference frame has been made. The torque and speed may be related as

$$T_e = J\left(\frac{2}{P}\right) p\omega_r + B_m \left(\frac{2}{P}\right) \omega_r + T_L \tag{4.2-7}$$

where J is kg·m^2; it is the inertia of the rotor and the connected load. Since we will be concerned primarily with motor action, the torque T_L is positive for a torque load. The constant B_m is a damping coefficient associated with the rotational system of the machine and the mechanical load. It has the units N · m · s per radian of mechanical rotation, and it is generally small and often neglected.

4.3 Voltage and Torque Equations in Rotor Reference Frame Variables

The voltage equations in the rotor reference frame may be written directly from (2.4-10) with $\omega = \omega_r$ [1].

$$\mathbf{v}^r_{qd0s} = \mathbf{r}_s \mathbf{i}^r_{qd0s} + \omega_r \boldsymbol{\lambda}^r_{dqs} + p\boldsymbol{\lambda}^r_{qd0s} \tag{4.3-1}$$

where

$$\left(\boldsymbol{\lambda}^r_{dqs}\right)^T = \begin{bmatrix} \lambda^r_{ds} & -\lambda^r_{qs} & 0 \end{bmatrix} \tag{4.3-2}$$

$$\boldsymbol{\lambda}^r_{qd0s} = \begin{bmatrix} L_{ls} + L_{Mq} & 0 & 0 \\ 0 & L_{ls} + L_{Md} & 0 \\ 0 & 0 & L_{ls} \end{bmatrix} \begin{bmatrix} i^r_{qs} \\ i^r_{ds} \\ i_{0s} \end{bmatrix} + \lambda'^r_m \begin{bmatrix} 0 \\ 1 \\ 0 \end{bmatrix} \tag{4.3-3}$$

where

$$\lambda^r_{qs} = (L_{ls} + L_{Mq}) i^r_{qs} \tag{4.3-4}$$

$$\lambda^r_{ds} = (L_{ls} + L_{Md}) i^r_{ds} + \lambda'^r_m \tag{4.3-5}$$

$$\lambda_{0s} = L_{ls} i_{0s} \tag{4.3-6}$$

The inductance matrix in (4.3-3) can readily be obtained from Fig. 4.2-2, which may be expressed as

$$L_{Mq} = \frac{3}{2}(L_A + L_B) \tag{4.3-7}$$

$$L_{Md} = \frac{3}{2}(L_A - L_B) \tag{4.3-8}$$

where $L_B < L_A$ and L_B is the amplitude of a double angle variation. Also, the first term is from rotor configuration, and the last term of (4.3-3) comes from $\mathbf{K}^r_s \boldsymbol{\lambda}'_m$. The permanent magnet is in the direct axis. To be consistent with our previous notation, we have added the superscript r to λ'_m. Now, λ'^r_m is λ'_m referred to the rotor. They are the same; however, it does not include the leakage flux of the permanent magnet rotor. In expanded form, we have

$$v^r_{qs} = r_s i^r_{qs} + \omega_r \lambda^r_{ds} + p\lambda^r_{qs} \tag{4.3-9}$$

$$v^r_{ds} = r_s i^r_{ds} - \omega_r \lambda^r_{qs} + p\lambda^r_{ds} \tag{4.3-10}$$

$$v_{0s} = r_s i_{0s} + p\lambda_{0s} \tag{4.3-11}$$

where

$$\lambda^r_{qs} = L_q i^r_{qs} \tag{4.3-12}$$

$$\lambda_{ds}^{r} = L_d i_{ds}^{r} + \lambda'^{r}_{m} \tag{4.3-13}$$

$$\lambda_{0s} = L_{ls} i_{0s} \tag{4.3-14}$$

Here, $L_q = L_{ls} + L_{Mq}$ and $L_d = L_{ls} + L_{Md}$.

Substituting (4.3-12)–(4.3-14) into (4.3-9)–(4.3-11), and since $p\lambda'^{r}_{m} = 0$, we can write

$$v_{qs}^{r} = (r_s + pL_q) i_{qs}^{r} + \omega_r L_d i_{ds}^{r} + \omega_r \lambda'^{r}_{m} \tag{4.3-15}$$

$$v_{ds}^{r} = (r_s + pL_d) i_{ds}^{r} - \omega_r L_q i_{qs}^{r} \tag{4.3-16}$$

$$v_{0s} = (r_s + pL_{ls}) i_{0s} \tag{4.3-17}$$

If $L_d = L_q = L_{ss}$, it is useful to define the following time constants:

$$\tau_s = \frac{L_{ss}}{r_s} \tag{4.3-18}$$

$$\tau_v = \frac{\lambda'^{r}_{m}}{\sqrt{2} V_s} \tag{4.3-19}$$

$$\tau_0 = \frac{L_{ls}}{r_s} \tag{4.3-20}$$

Substituting (4.3-18) and (4.3-20) into (4.3-15)–(4.3-17) yields

$$v_{qs}^{r} = r_s (i + \tau_s p) i_{qs}^{r} + r_s \tau_s \omega_r i_{ds}^{r} + \lambda'^{r}_{m} \omega_r \tag{4.3-21}$$

$$v_{ds}^{r} = r_s (i + \tau_s p) i_{ds}^{r} - r_s \tau_s \omega_r i_{qs}^{r} \tag{4.3-22}$$

$$v_{0s} = r_s (i + \tau_0 p) i_{0s} \tag{4.3-23}$$

From Fig. 4.2-2, the sum of phase currents is zero by Kirchoff's current law. This means that the zero current is identically equal to zero making (4.3-17) and (4.3-23) unnecessary.

The expression for electromagnetic torque in terms of substitute variables may be obtained by substituting the expressions for the machine currents in terms of q and d currents into (4.2-10). This procedure is quite labor intensive; however, once we have expressed the voltage equations in terms of reference frame variables, a more direct approach is possible. In particular, the expression for input power is

$$P_{\text{in}} = \frac{3}{2} \left(v_{qs}^{r} i_{qs}^{r} + v_{ds}^{r} i_{ds}^{r} + 2 v_{0s} i_{0s} \right) \tag{4.3-24}$$

Substituting (4.3-9)–(4.3-11) into (4.3-24) gives us

$$P_{\text{in}} = \frac{3}{2} r_s \left(i_{qs}^{r^2} + i_{ds}^{r^2} + 2 i_{0s}^{2} \right) + \frac{3}{2} \left(\lambda_{ds}^{r} i_{qs}^{r} - \lambda_{qs}^{r} i_{ds}^{r} \right) \omega_r + \frac{3}{2} \left(i_{qs}^{r} p \lambda_{qs}^{r} + i_{ds}^{r} p \lambda_{ds}^{r} + 2 i_{0s} p \lambda_{0s} \right) \tag{4.3-25}$$

The first term on the right-hand side of (4.3-25) is the ohmic power loss in the stator windings, the last term is the rate of change of stored magnetic energy. We realize that the coefficient of ω_r is the torque. For a P-pole machine

$$T_e = \left(\frac{3}{2}\right)\left(\frac{P}{2}\right)\left(\lambda^r_{ds} i^r_{qs} - \lambda^r_{qs} i^r_{ds}\right) \tag{4.3-26}$$

Substituting (4.3-12) and (4.3-13) into (4.3-26) yields

$$T_e = \left(\frac{3}{2}\right)\left(\frac{P}{2}\right)\left[\lambda'^r_m i^r_{qs} + (L_d - L_q) i^r_{qs} i^r_{ds}\right] \tag{4.3-27}$$

The electromagnetic torque is positive for motor action.

The relation between torque and speed for a two-pole machine is

$$T_e = J\frac{d\omega_r}{dt} + B_m\omega_r + T_L \tag{4.3-28}$$

where J is the inertia of the rotor and tightly connected load. The units are $\text{kg} \cdot \text{m}^2$. The first term on the right-hand side is the inertia torque. The damping coefficient B_m is generally small and often neglected. The units of B_m are $\text{N} \cdot \text{m} \cdot \text{s/rad}$.

When the machine is supplied with an inverter, it is possible, by controlling the firing of the inverter, to change the values of v^r_{qs} and v^r_{ds}. Mathematically, ω_r is obtained by integrating (4.3-28). In practice, θ_r is determined using Hall effect sensors or a position observer or measured directly using an inline position encoder. For purposes of discussion, let us assume that the applied stator voltages are sinusoidal so that

$$v_{as} = \sqrt{2} v_s \cos\theta_{ev} \tag{4.3-29}$$

$$v_{bs} = \sqrt{2} v_s \cos\left(\theta_{ev} - \frac{2\pi}{3}\right) \tag{4.3-30}$$

$$v_{cs} = \sqrt{2} v_s \cos\left(\theta_{ev} + \frac{2\pi}{3}\right) \tag{4.3-31}$$

When the machine is supplied from an inverter, the stator voltages are controlled such that

$$\theta_{ev} = \theta_r + \phi_v \tag{4.3-32}$$

With power electronics, the voltages will generally have a waveform with switching harmonics included. Nevertheless, as a first approximation, (4.3-29)–(4.3-31) may be considered the fundamental components of these stepped phase voltages.

Transforming (4.3-29)–(4.3-31) to the rotor reference frame yields

$$v^r_{qs} = \sqrt{2} v_s \cos\phi_v \tag{4.3-33}$$

$$v^r_{ds} = -\sqrt{2} v_s \sin\phi_v \tag{4.3-34}$$

where v_s is the rms value.

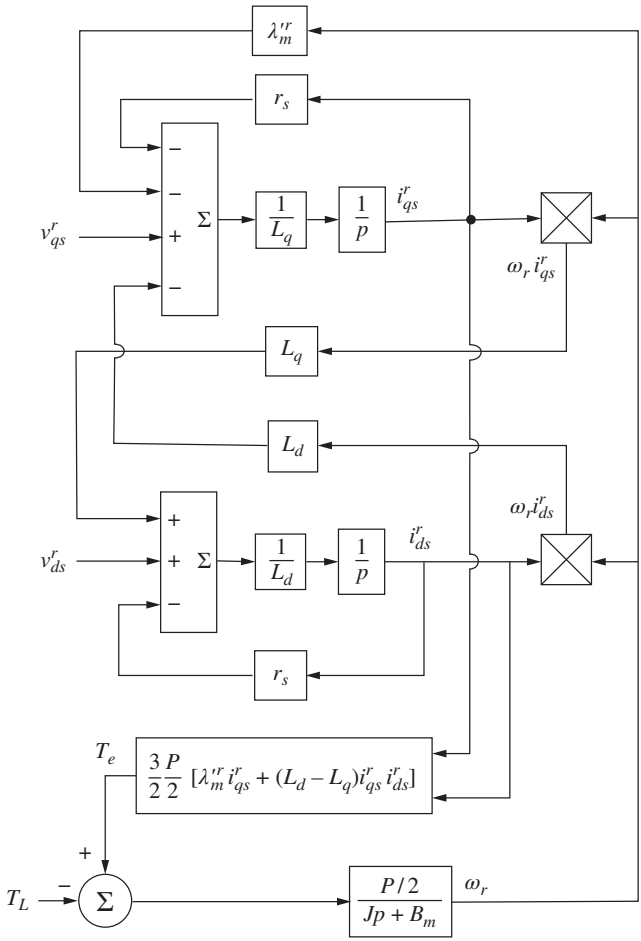

Figure 4.3-1 Time-domain block diagram of brushless dc motor.

The time-domain block diagram is shown in Fig. 4.3-1. It portrays (4.3-15), (4.3-16), and (4.3-27). Eq. (4.3-17) is not portrayed since i_{0s} is zero. The voltages v^r_{qs}, v^r_{ds}, and v_{0s} are obtained from v_{as}, v_{bs}, and v_{cs} by (2.3-5) with $\theta = \theta_r$. The currents i_{as}, i_{bs}, and i_{cs} are obtained from i^r_{qs}, i^r_{ds}, and i_{0s} by (2.3-8) with $\theta = \theta_r$.

4.4 Instantaneous and Steady-State Phasors

We will derive the instantaneous phasor voltage equations by following the work in Chapter 2. From (2.8-1) with $\omega = \omega_r$ and $\omega_r = \omega_e$

$$\tilde{f}_{as} = f^r_{qs} - jf^r_{ds} \tag{4.4-1}$$

Substituting (4.3-15) and (4.3-16) into (4.4-1), for balanced steady-state operation

$$v_{qs}^{r} - jv_{ds}^{r} = r_s i_{qs}^{r} + \omega_r \lambda_{ds}^{r} + p\lambda_{qs}^{r} - j\left(r_s i_{ds}^{r} - \omega_r \lambda_{qs}^{r} + p\lambda_{ds}^{r}\right) \tag{4.4-2}$$

Equation (4.4-2) may be written as

$$\tilde{v}_{as} = r_s \tilde{i}_{as} + \omega_r \left(\lambda_{ds}^{r} + j\lambda_{qs}^{r}\right) - j\omega_r L_q i_{qs}^{r} + p\left(L_q i_{qs} + jL_d i_{ds}^{r}\right) \tag{4.4-3}$$

Now, in the steady state the last term of (4.4-3) is zero and by adding and subtracting $\omega_r L_q i_{ds}^{r}$ to (4.4-3) and dividing by $\sqrt{2}$ to convert to rms, we have

$$\tilde{V}_{as} = (r_s + j\omega_r L_q)\tilde{I}_{as} + \tilde{E}_a \tag{4.4-4}$$

where

$$\tilde{E}_a = \frac{\omega_r}{\sqrt{2}}\left[(L_d - L_q)I_{ds}^{r} + \lambda'^{r}_{m}\right] e^{j0} \tag{4.4-5}$$

Steady-state torque is (4.3-26) with upper case currents.

4.5 Field Orientation of a Brushless DC Drive

In drive applications, the permanent-magnet ac machine is generally supplied from a voltage source inverter that is controlled to synchronize the frequency of the stator applied voltages with the electrical angular velocity of the rotor. In later chapters, we will use an inverter, at this stage we will simulate the inverter with a variable frequency three-phase sinusoidal source. When the torque load on the shaft of the machine is increased, the machine slows and the drive inverter control decreases the frequency of the applied stator voltages, which decreases the inductive reactance's ($\omega_r L$) and $\widetilde{E}_a$. Therefore, the decrease in rotor speed allows the current to increase which, in turn, increases the strength of the stator rotating magnetic field to accommodate the increase in torque load. Although the primary purpose is to control the frequency, the source is also used to orient the rotating magnetic field of the stator relative to the permanent magnet of the rotor. This changes the relative position of the stator poles, which changes the torque characteristics of the machine.

For purposes of establishing the phasor diagram for steady-state operation, $\widetilde{E}_a$ is generally placed at zero degrees and $\widetilde{V}_{as}$, the fundamental component of the *as*-phase voltage, is at the phase angle $\theta_{esv}(0)$. Therefore, in the steady state, $\phi_v = \theta_{esv}(0)$. If, for example, $\phi_v = 0$, then the positive peak value of the fundamental component of v_{as} and the q axis are rotating in unison. That is, $\widetilde{E}_a$ and $\widetilde{V}_{as}$ would be at zero degrees if we stopped rotation of the phasors or observed the phasors each time the q axis is horizontal to the right; i.e., coinciding with the *as* axis or if we are running counterclockwise with the q axis we would always see the peak value of v_{as}. This is the common mode of operation of a brushless dc drive.

In this section, three control strategies are considered with $L_d = L_q = L_{ss}$; $\phi_v = 0$, $\phi_v = \phi_{vMT/V}$, and $\phi_v = \phi_{vMT/A}$. When ϕ_v is controlled at $\phi_{vMT/V}$, the

applied stator voltages are shifted relative to the q axis of the rotor to produce the maximum torque per volt that is possible at the instantaneous speed of the rotor (angular frequency of stator voltages). It is found that $\theta_{vMT/V}$ corresponds to the stator impedance angle which, of course, changes with the frequency of the stator applied voltages (rotor speed). When ϕ_v is controlled at $\phi_{vMT/A}$, the applied stator voltages are shifted in phase relative to the q axis to produce the maximum torque per ampere possible at the instantaneous speed of the rotor. This occurs when $\widetilde{I}_{as}$ is in time phase with the q axis or in other words when $\widetilde{I}_{as}$ is orthogonal to the d axis; thus, the poles of the stator are orthogonal to the permanent magnet.

Before getting further into a discussion of the modes of operation, it is helpful to talk a little more about ϕ_v which is expressed as

$$\phi_v = \theta_{esv} - \theta_r \tag{4.5-1}$$

For steady-state operation, $\theta_{esv} = \omega_e t + \theta_{esv}(0)$, $\theta_r = \omega_r t + \theta_r(0)$ and $\omega_e = \omega_r$. Thus, (4.5-1) becomes

$$\phi_v = \theta_{esv}(0) - \theta_r(0) \tag{4.5-2}$$

Also, for brushless dc machine operation, it is convenient to select $\theta_r(0)$ equal to zero whereupon

$$\phi_v = \theta_{esv}(0) \tag{4.5-3}$$

Therefore, ϕ_v is the phase of $\widetilde{V}_{as}$ and the phase of $\widetilde{E}_a$ is zero degrees since it is controlled to coincide with the q axis.

4.5.1 Brushless dc Motor Operation with $\phi_v = 0$

The parameters of the fractional-horsepower four-pole three-phase permanent-magnet ac machine considered in this section are $r_s = 3.4\ \Omega$, $L_{ls} = 1.1$ mH, $L_{Ms} = 16.5$ mH, $L_{ss} = 17.6$ mH, and $\lambda'_m = 0.0827\ \text{V} \cdot \text{s/rad}$. Here, $L_q = L_d = L_{ss}$ and the reluctance torque is zero. For brushless dc drive operation, ω_e is made equal to ω_r and $\phi_v = 0$ is the common mode of operation, that is, the as-phase voltage phasor is controlled to be "in phase" with the q axis. Thus,

$$V_{as} = \sqrt{2} V_s \cos \omega_r t \tag{4.5-4}$$

with a balanced abc sequence and $V_s = 11.25$ V. With sinusoidal applied voltages and $\phi_v = 0$, the maximum positive value of V_{as} coincides with the q axis and this unison is fixed by controlling the inverter.

The free-acceleration characteristics (starting from stall with $T_L = 0$) of brushless dc drive with $\phi_v = 0$ are shown in Fig 4.5-1. The total inertia J of the rotor and mechanical load is $5 \times 10^{-4}\ \text{kg} \cdot \text{m}^2$, and the damping coefficient B_m is neglected. The torque versus the rotor electrical angular velocity for Fig. 4.5-1 is shown in

Fig. 4.5-2. Here, we see that the steady-state torque resembles that of a dc machine, thus the name brushless dc machine. The steady-state torque is also plotted in Fig. 4.5-2 for comparison purposes. The negative slope of the torque versus speed characteristics ensures stable operation for motor operation. That is, for a given load torque, a slight slowing of the rotor from an operating point will cause T_e to increase, forcing the rotor back to the operating speed where $T_L = T_e$. A small increase in rotor speed causes T_e to decrease whereupon the load torque slows the rotor back to the original operating point, a stable operating condition. Clearly, damper windings are not needed.

The voltage equations for a brushless dc motor during balanced steady-state operation may be obtained by setting V^r_{ds}, the imaginary part of $\widetilde{V}_{as}$, equal to zero. Since $\phi_v = 0$, $V^r_{ds} = 0$ and solving (4.3-16) (with p set to zero for steady state operation) for I^r_{ds} yields

$$I^r_{ds} = \frac{\omega_r L_{ss}}{r_s} \; I^r_{qs} \tag{4.5-5}$$

Substituting (4.5-5) into (4.3-15) with p set to zero gives

$$V^r_{qs} = \frac{r_s^2 + \omega_r^2 L_{ss}^2}{r_s} I^r_{qs} + \omega_r \lambda'^r_m \tag{4.5-6}$$

During steady-state operation, all quantities in (4.5-6) are constants.

There is something that should be mentioned. We have selected the position of the q and d axes that gives the maximum starting torque. Unfortunately, the position of the axes is not known, and the starting torque can be zero. Some means should be implemented to determine the position of the axes. There are various ways to determine this, which is beyond the scope of this text.

If we choose to work with the *abc* variables, the phasor voltage equation is given by

$$\widetilde{V}_{as} = (r_s + j\omega_r L_{ss})\widetilde{I}_{as} + \widetilde{E}_a \tag{4.5-7}$$

where

$$\widetilde{E}_a = \frac{1}{\sqrt{2}} \omega_r \lambda'^r_m \underline{/0^\circ} \tag{4.5-8}$$

With $L_d = L_q$,

$$\begin{aligned} T_e &= \frac{3}{2}\frac{P}{2} \lambda'^r_m i^r_{qs} \\ &= \frac{3}{2}\frac{P}{2} \lambda'^r_m \sqrt{2} I_s [\theta_{esi}(0) - \theta_r(0)] \end{aligned} \tag{4.5-9}$$

where $\theta_r(0) = 0$.

In summary, the brushless dc drive is so named because the torque versus speed characteristics resemble those of a dc motor. Therefore, it seems logical that there is a reference frame where the voltages and currents are dc rather than ac. This is

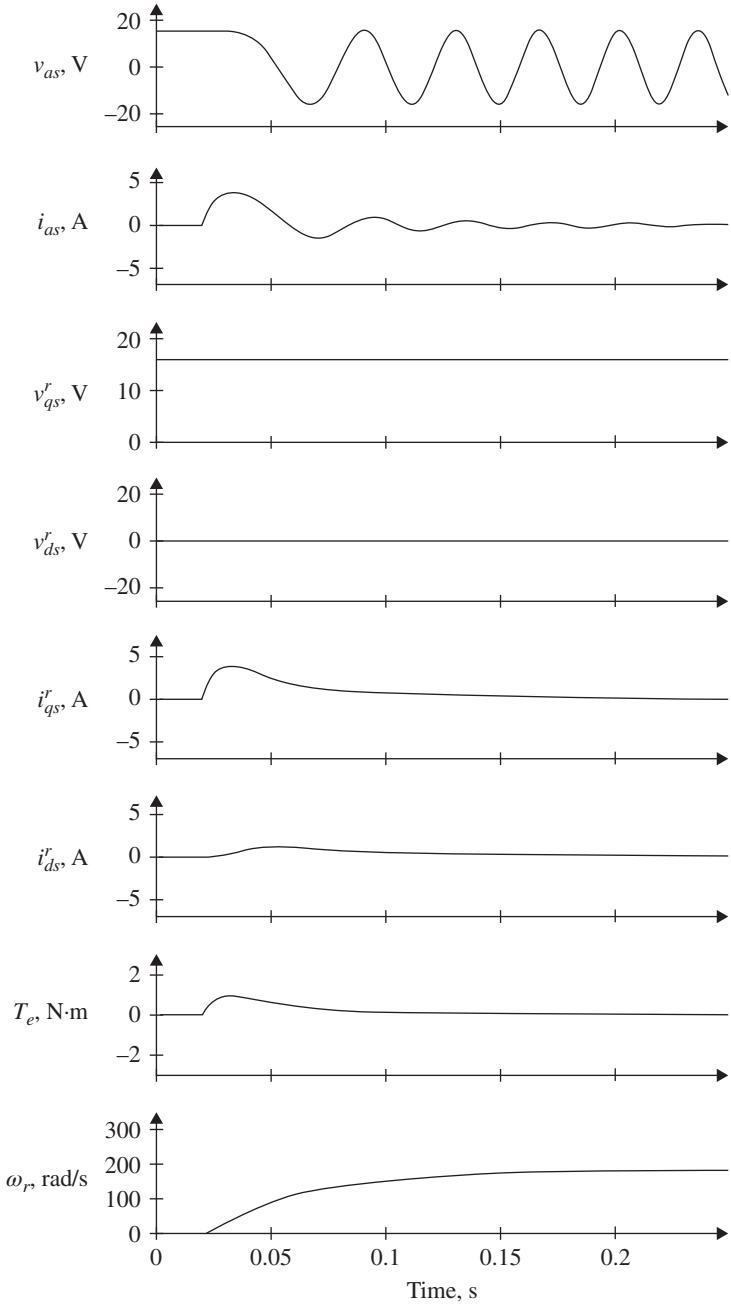

Figure 4.5-1 Free-acceleration characteristics of a brushless dc drive with $\phi_v = 0$ and a total inertia of 5×10^{-4} kg · m^2 ($L_d = L_q$).

very apparent from the traces in Fig. 4.5-1 of v_{qs}^r, i_{qs}^r, i_{ds}^r, and T_e. Since the rotor and synchronous reference frames are the same, these variables are dc in the steady state and the steady-state torque versus speed characteristics (Fig. 4.5-2) resemble those of a dc motor. A phasor diagram for $\omega_r = 50\pi$ rad/s is given in Fig. 4.5-3.

We see from Fig. 4.5-3 that the rotor poles can be considered being "pulled" in the counterclockwise direction by the poles created by the stator currents; motor action.

4.5.2 Maximum-Torque-Per-Volt Operation of a Brushless dc Drive ($\phi_v = \phi_{vMT/V}$)

Although $\phi_v = 0$ is a common mode of operation of the brushless dc drive, researchers in [2, 3] discovered that advancing ϕ_v with respect to the q axis could increase the torque at high rotor speeds. This was shown analytically in [4] and illustrated by simulating the phase shifting (increasing ϕ_v) of the applied voltages to obtain maximum torque per volt ($\phi_v = \phi_{vMT/V}$) at a given speed.

If the applied voltages and thus the stator poles are shifted relative to the magnetic field established by the permanent-magnet rotor, which is fixed in the d axis, the torque versus speed characteristics can be changed over a wide range by shifting ϕ_v from zero to 2π [4]. Here, we will limit our discussion to shifting ϕ_v for the purpose of maximizing torque during motor operation.

Torque is proportional to i_{qs}^r and when ϕ_v is shifted from zero, v_{ds}^r is nonzero as expressed in (4.3-34). For the purpose of deriving an expression for the maximum torque per volt at a given rotor speed ($\phi_{vMT/V}$), we will start with

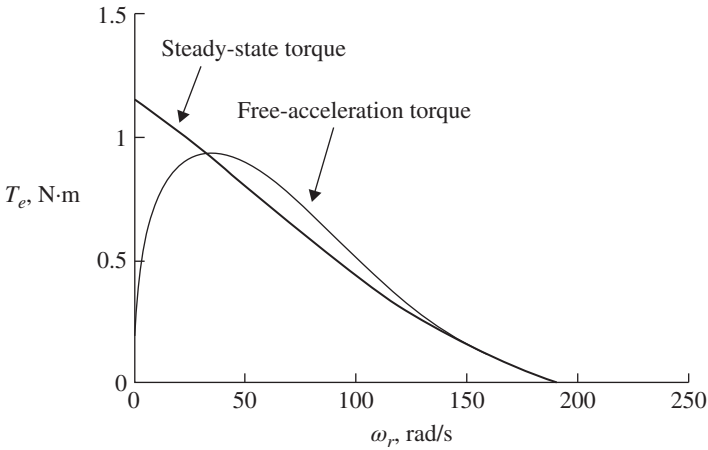

Figure 4.5-2 Torque versus speed characteristics for the free acceleration shown in Fig. 4.5-1 with the steady-state torque shown for comparison purposes.

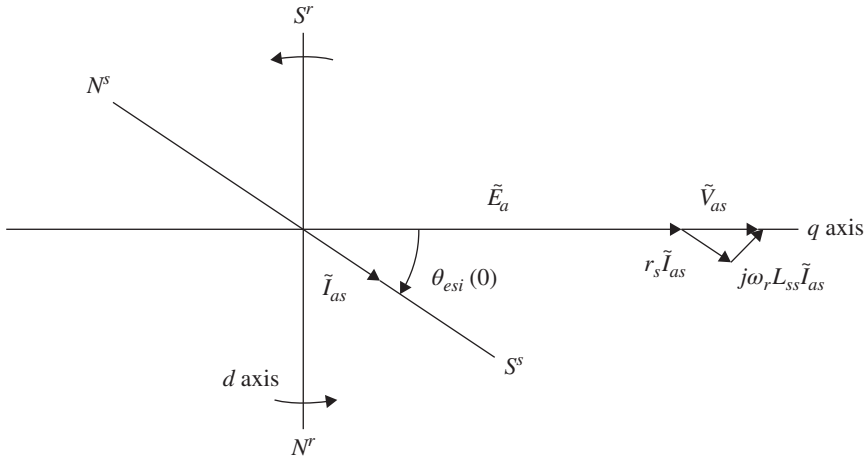

Figure 4.5-3 Phasor diagram for brushless dc drive operation at $\omega_r = 50\pi$ rad/s with $\phi_v = 0$.

(4.5-10) and (4.5-11) for V^r_{qs} and V^r_{ds}, respectively. In particular, for steady-state operation

$$V^r_{qs} = r_s I^r_{qs} + \omega_r L_{ss} I^r_{ds} + \omega_r \lambda'^r_m \tag{4.5-10}$$

$$V^r_{ds} = r_s I^r_{ds} - \omega_r L_{ss} I^r_{qs} \tag{4.5-11}$$

We need the expressions for V^r_{qs} and V^r_{ds} as functions of ϕ_v, which are valid for transient and steady-state operations

$$V^r_{qs} = \sqrt{2} V_s \cos\phi_v \tag{4.5-12}$$

$$V^r_{ds} = -\sqrt{2} V_s \sin\phi_v \tag{4.5-13}$$

Since $\theta_r(0) = 0$, ϕ_v is the angle of $\tilde{V}_{as}$.

Solving (4.5-11) for I^r_{ds} and substituting the result into (4.5-10) yields

$$V^r_{qs} = \frac{r_s^2 + \omega_r^2 L_{ss}^2}{r_s} I^r_{qs} + \frac{\omega_r L_{ss}}{r_s} V^r_{ds} + \omega_r \lambda'^r_m \tag{4.5-14}$$

Now, solving (4.5-14) for I^r_{qs} and substituting (4.5-12) and (4.5-13) for V^r_{qs} and V^r_{ds}, respectively, with $\theta_r(0) = 0$, we have

$$I^r_{qs} = \frac{r_s}{r_s^2 + \omega_r^2 L_{ss}^2} \left(\sqrt{2} V_s \cos\phi_v + \frac{\omega_r L_{ss}}{r_s} \sqrt{2} V_s \sin\phi_v - \omega_r \lambda'^r_m \right) \tag{4.5-15}$$

It is interesting to note from (4.5-14) that negative V_{ds}^{r} aids V_{qs}^{r} to increase $I_{qs}^{r}(T_e)$ for a given rotor speed. Since this results in a negative I_{ds}^{r}, it is often referred to as field weakening even though λ'^{r}_{m} is not decreased in magnitude.

Since T_e is proportional to I_{qs}^{r}, (4.5-9), we can obtain the maximum torque for a given rotor speed by taking the derivative of I_{qs}^{r} with respect to ϕ_v and setting the result equal to zero and then solving for ϕ_v. Thus, from (4.5-15)

$$0 = -\sin\phi_v + \frac{\omega_r L_{ss}}{r_s}\cos\phi_v \tag{4.5-16}$$

whereupon

$$\frac{\sin\phi_v}{\cos\phi_v} = \frac{\omega_r L_{ss}}{r_s} \tag{4.5-17}$$

or

$$\phi_{vMT/V} = \tan^{-1}\frac{\omega_r L_{ss}}{r_s} \tag{4.5-18}$$

Eq. (4.5-18) tells us that for a given positive rotor speed, $\phi_{vMT/V}$ will yield the maximum possible torque per volt at that rotor speed. The free acceleration and steady-state torque versus speed characteristics for maximum-torque-per-volt operation is shown in Fig. 4.5-4. Note the extended speed range with $\phi_{vMT/V}$ (Fig. 4.5-4) compared with $\phi_v = 0$ (Fig. 4.5-2). An increase in torque (I_{qs}^{r}) and speed range occurs due to a decrease in I_{ds}^{r} (a larger negative value). The phasor diagram for $\omega_r = 50$ rad/s is shown in Fig. 4.5-5. From Fig. 4.5-5, we see that the poles created by the stator can be considered "pushing" the rotor poles in the counterclockwise direction.

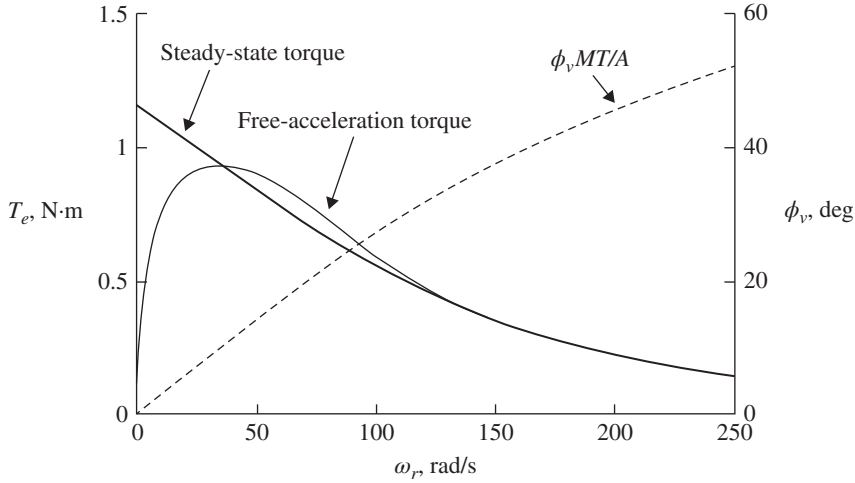

Figure 4.5-4 Torque versus speed characteristics for free acceleration with the steady-state torque versus speed also shown. Compare to Fig. 4.5-2 where $\phi_v = 0$.

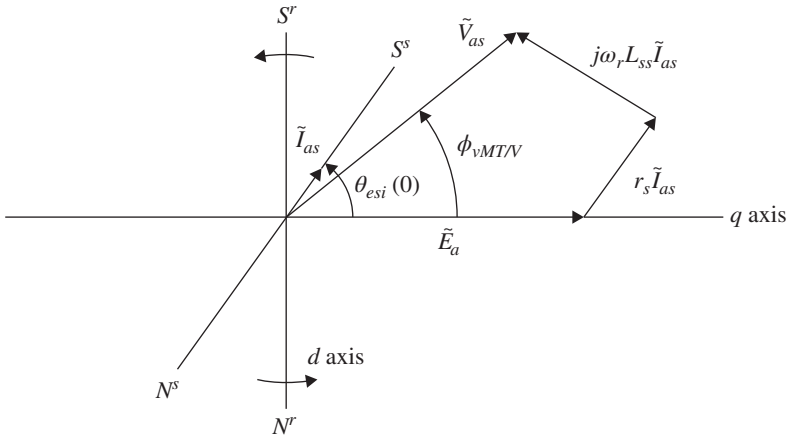

Figure 4.5-5 Phasor diagram for brushless dc drive operation at $\omega_r = 50\pi$ rad/s with $\phi_v = \phi_{vMT/V}$.

4.5.3 Maximum-Torque-Per-Ampere Operation of a Brushless dc Drive ($\phi_v = \phi_{vMT/A}$)

Maximum-torque-per-ampere operation occurs when I^r_{ds} (imaginary part of $\widetilde{I}_{as}$) is made zero by controlling the position of $\widetilde{V}_{as}$ relative to the permanent magnet of the rotor ($\phi_v = \phi_{vMT/A}$). The torque is directly related to the q axis current (real part of $\widetilde{I}_{as}$). The d axis current does contribute to the torque indirectly but decreases the efficiency of the machine as we have seen.

To derive an expression for $\phi_{vMT/A}$ for steady-state operation, we will substitute (4.5-12) and (4.5-13) into (4.5-10) and (4.5-11) for V^r_{qs} and V^r_{ds}, respectively, and solve for $\cos\phi_v$ and $\sin\phi_v$. If $L_d = L_q$ and if we set $I^r_{ds} = 0$ and perform several mathematical manipulations, we can express $\phi_{vMT/A}$, at a given rotor speed, as [5]

$$\phi_{vMT/A} = \tan^{-1}\left[\omega_r\tau_s\left(\frac{-1 \pm \omega_r\tau_v\sqrt{1+\omega_r^2\tau_v^2\left(1-\omega_r^2\tau_v^2\right)}}{\omega_r^4\tau_s^2\tau_v^2 - 1}\right)\right] \tag{4.5-19}$$

where τ_s and τ_v are given by (4.3-18) and (4.3-19).

The free acceleration and steady-state torque versus speed characteristics for maximum-torque-per-ampere operation are shown in Fig. 4.5-6 including a plot of $\phi_{vMT/A}$.

The phasor diagram is shown in Fig 4.5-7. Note that the stator and rotor poles are orthogonal, which yields the maximum torque per ampere for this device at $\omega_r = 50\pi$ rad/s. It is interesting that for this machine, i^r_{ds} is small or zero except for $\phi_{vMT/V}$. Therefore, the reluctance torque is small or zero and the torque calculated using $L_d = L_q$ would be in error for $\phi_{vMT/V}$.

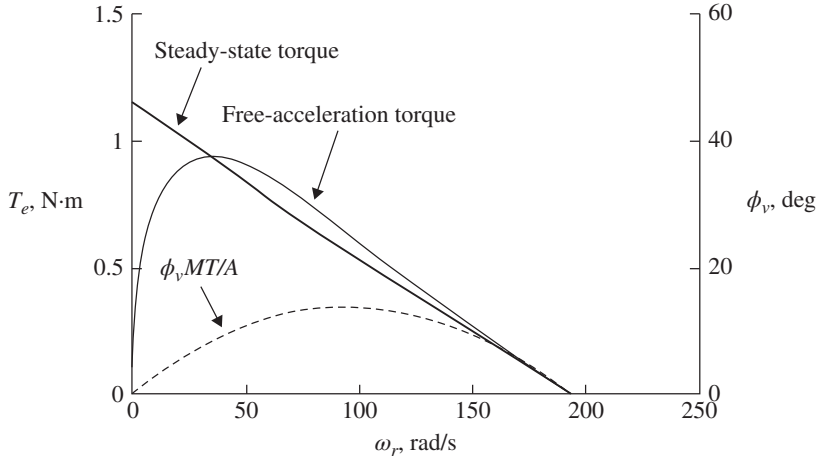

Figure 4.5-6 Torque versus speed characteristics for free acceleration with $\phi_v = \phi_{vMT/A}$.

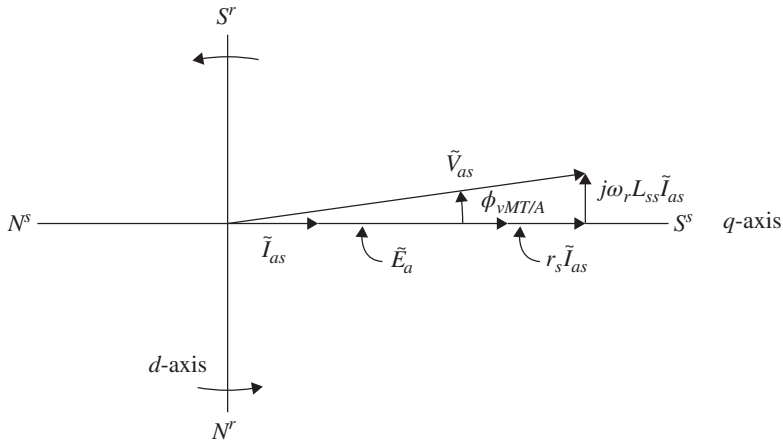

Figure 4.5-7 Phasor diagram for brushless dc drive operation at $\omega_r = 50\pi$ rad/s with $\phi_v = \phi_{vMT/A}$.

References

1 R. H. Park, "Two-Reaction Theory of Synchronous Machines-Generalized Method of Analysis, Part I," *Trans. AIEE*, Vol. 48, July 1929, pp.716–727.

2 T. W. Nehl, F. A. Fouad, and N. A. Demerdash, "Digital Simulation of Power Conditioner– Machine Interaction for Electronically Commutated DC

Permanent Magnet Machines," *IEEE Trans. Magn.,* Vol. 17, November 1981, pp. 3284–3286.

3 T. M. Jahns, "Torque Production in Permanent-Magnet Synchronous Motor Drives with Rectangular Current Excitations," *IAS Conf. Rec.,* Oct. 1983, pp. 476–487.

4 P. C. Krause, *Analysis of Electric Machinery*, McGraw-Hill, 1st Edition, 1986.

5 P. C. Krause, O. Wasynczuk, T. C. O'Connell, and M. Hasan, *Introduction to Power and Drive Systems,* John Wiley and Sons, IEEE Press, New York, 2017.

Problems

4.1 Obtain the last term of (4.3-3).

4.2 Write the voltage equations given by (4.3-15)–(4.3-17) and the torque equation given by (4.3-27) in terms of flux linkages rather than currents.

4.3 Modify Fig. 4.3-1 to account for unbalanced voltages assuming i_{0s} is not restricted to be zero.

4.4 Repeat Problem 3 with v_s, ϕ_v, and T_L as inputs.

4.5 A permanent-magnet *ac* machine has $r_s = 0.1\ \Omega$, $L_q = L_d$, λ'^r_m 0.1 V · s, $P = 4$. A torque of 3 N · m is desired at a speed of $\omega_r = 100$ rad/s. Determine the resulting $\tilde{V}_{as}$.

4.6 The steady-state torque versus speed plots for $\phi_v = 0$ and for $\phi_v = \frac{\pi}{2}$ intersect. Calculate the rotor speed where this intersection occurs.

4.7 A three-phase permanent-magnet ac machine is operating with $I^r_{qs} = 100$ A and $I^r_{ds} = -10$ A. The load is a fan with $T_L = 0.1\omega_r^2$. The parameters of the machine are $P = 4$, $r_s = 0.01\ \Omega$, $L_q = L_d = 1$ mH, $\lambda'^r_m = 0.133$ V · s. Determine V_{as} and the machine efficiency.

5

Synchronous Machines

5.1 Introduction

The electrical and electromechanical behavior of most synchronous machines can be predicted from the equations that describe the three-phase salient-pole synchronous machine. In particular, these equations can be used directly to predict the performance of synchronous motors, hydro-, steam-, or wind-turbine-driven synchronous generators, and, with only slight modifications, reluctance motors.

The rotor of a synchronous machine is equipped with a field winding and one or more damper windings and, in general, each of the rotor windings has different electrical characteristics. Moreover, the rotor of a salient-pole synchronous machine is magnetically unsymmetrical. Due to these rotor asymmetries, a change of variables for the rotor variables offers no advantage. However, a change of variables is beneficial for the stator variables. In most cases, the stator variables are transformed into a reference frame fixed in the rotor (Park's equations) [1]; however, the stator variables may also be expressed in the arbitrary reference frame.

In this chapter, the voltage and electromagnetic torque equations are established from previous work. The equations that describe the steady-state behavior are derived using the procedure established in Chapter 2. The machine equations are arranged in a form convenient for computer simulation. Computer traces are given to illustrate the dynamic behavior of a synchronous machine during motor and generator operation.

Most of the electric power used throughout the world is generated by synchronous generators driven either by hydro, steam, or wind turbines, or by combustion engines. Just as the induction motor is the workhorse when it comes to converting energy from electrical to mechanical, the synchronous machine is the principal means of converting energy from mechanical to electrical. In the power system or electric grid environment, the analysis of the synchronous generator

Analysis of Electric Machinery and Drive Systems, Fourth Edition.
Paul C. Krause, Oleg Wasynczuk, Scott D. Sudhoff, and Steven D. Pekarek.

Companion website: www.wiley.com/go/krause_aem4e

is often carried out assuming positive currents out of the machine. Although this is very convenient for the power systems engineer, it tends to be somewhat confusing for beginning machine analysts and inconvenient for engineers working in the electric drive area. In an effort to make this chapter helpful in both environments, positive stator currents are assumed into the machine as done in the analysis of the induction, brushless dc, permanent-magnet, and synchronous reluctance machines. The assumed positive direction of the stator currents is reversed whereupon high-power synchronous generators that would be used in a power system are considered. The changes in the machine equations necessary to accommodate positive current out of the machine are described. Computer traces are then given to illustrate the dynamic behavior of typical hydro- and steam-turbine-driven generators during sudden changes in input torque and during and following a three-phase fault at the terminals. These dynamic responses are calculated using a detailed set of nonlinear differential equations.

5.2 Windings of a Synchronous Machine

A two-pole, three-phase, wye-connected, salient-pole synchronous machine is shown in Fig. 5.2-1. The stator windings are identical sinusoidally distributed windings, displaced from one another by 120°, each with N_s equivalent turns and resistance r_s. We are familiar with this from Chapter 2. The rotor is equipped with a field winding and three damper windings. The field winding (*fd* winding) has N_{fd} equivalent turns with resistance r_{fd}. One damper winding has the same magnetic axis as the field winding. This winding, the *kd* winding, has N_{kd} equivalent turns with resistance r_{kd}. The magnetic axis of the second and third damper windings, the $kq1$ and $kq2$ windings, is displaced 90° ahead of the magnetic axis of the *fd* and *kd* windings. The $kq1$ and $kq2$ windings have N_{kq1} and N_{kq2} equivalent turns, respectively, with resistances r_{kq1} and r_{kq2}.

We see from Fig. 5.2-1 that for analysis purposes the stator is the same as in the induction and permanent-magnet synchronous machines. The rotor has different single-phase windings. Thus, the rotor is unsymmetrical, and we cannot transfer these windings to another reference frame. We must use the rotor reference frame as we did in the case of the permanent-magnet machine.

Now, the rotor shown in Fig. 5.2-1 is referred to as a salient-pole rotor, which is common for high-power machines with a large number of poles. Lower power machines may have cylindrical rotors with damper windings similar to the induction machine with only two damper windings. Although the damper windings are shown with provisions to apply a voltage, they are, in fact, short-circuited windings that represent paths for induced rotor currents. Currents may flow either in cage-type windings similar to the squirrel-cage windings or in the actual

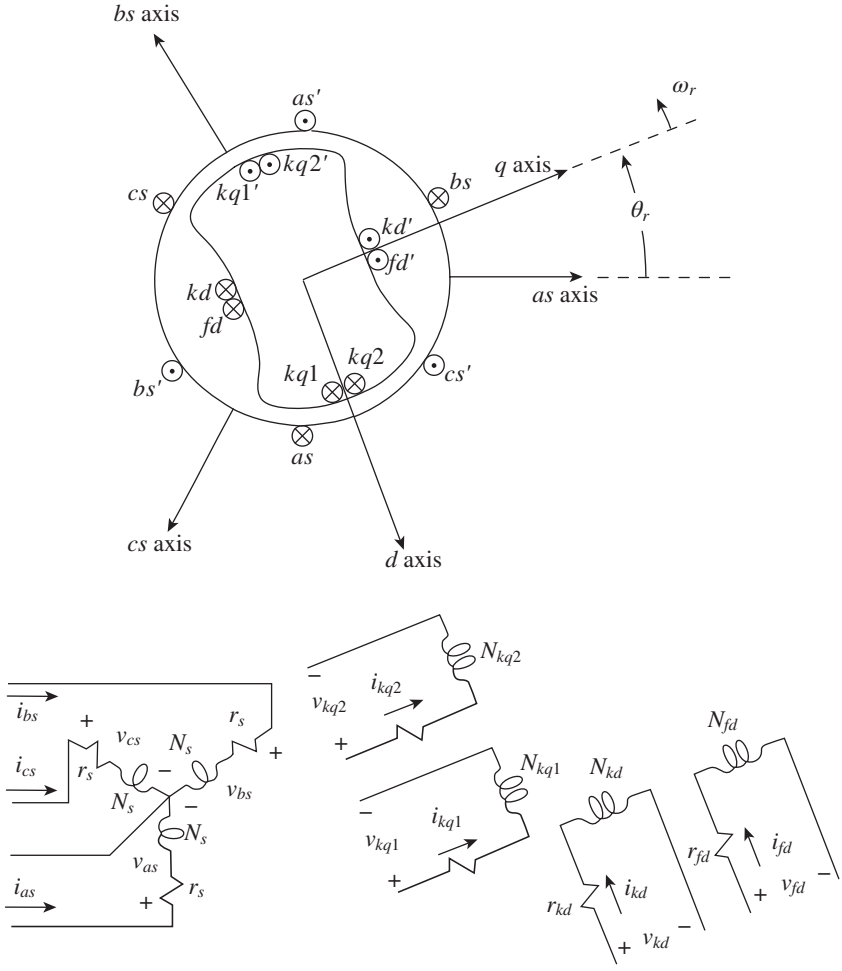

Figure 5.2-1 Two-pole, three-phase, wye-connected salient-pole synchronous machine.

iron of the rotor. In salient-pole machines, the rotor is composed of laminations that are electrically insulated from one another and the damper winding currents are confined, for the most part, to the cage windings embedded in the rotor. In high-speed two- or four-pole machines, the rotor is cylindrical, made of solid iron with a field winding. Some may have cage-type winding embedded in rotor slots, which produces a magnetic field oriented along the q axes. Here, currents can flow either in the cage winding or in the solid iron. The field winding current exists to create a magnetic field; the damper winding and induced rotor iron currents exist only when $\omega_r \neq \omega_e$.

The performance of nearly all types of synchronous machines may be adequately described by straightforward modifications of the equations describing the performance of the machine shown in Fig. 5.2-1. For example, the behavior of low-speed hydro-turbine generators, which are always salient-pole machines, is generally predicted sufficiently by one equivalent damper winding in the q axis. Hence, the performance of this type of machine may be described from the equations derived for the machine shown in Fig. 5.2-1 by eliminating all terms involving one of the kq windings. The reluctance machine, which has no field winding and generally only one damper winding in the q axis, may be described by eliminating the terms involving the fd winding and one of the kq windings. Also, it is necessary, in most cases, to include all three damper windings in order to portray adequately the transient characteristics of the stator variables and the electromagnetic torque of solid iron rotor machines [2].

5.3 Voltage Equations in Rotor Reference Frame Variables

R.H. Park was the first to incorporate a change of variables in the analysis of synchronous machines [1]. He transformed the stator variables to the rotor reference frame, which eliminates the position-varying inductances in the voltage equations. Park assumed a positive stator current out of the machine, which was convenient for generator action. Thus far, we have assumed a positive stator current into the machine since we have been dealing with motor action. Let us continue with motor action. The equivalent circuits for positive stator currents into the machine are shown in Fig. 5.3-1.

From Chapter 2, for the wye-connected stator circuits:

$$L_q = L_{ls} + \frac{3}{2}(L_A - L_B) = L_{ls} + L_{Mq} \tag{5.3-1}$$

$$L_d = L_{ls} + \frac{3}{2}(L_A + L_B) = L_{ls} + L_{Md} \tag{5.3-2}$$

Here, $L_q < L_d$ which is opposite from what we had in Chapter 4 for the permanent-magnet machine. Also,

$$i'_j = \frac{2}{3}\frac{N_j}{N_s} i_j \tag{5.3-3}$$

$$v'_j = \frac{N_s}{N_j} v_j \tag{5.3-4}$$

$$\lambda'_j = \frac{N_s}{N_j} \lambda_j \tag{5.3-5}$$

$$r'_j = \left(\frac{3}{2}\frac{N_s}{N_j}\right)^2 r_j \tag{5.3-6}$$

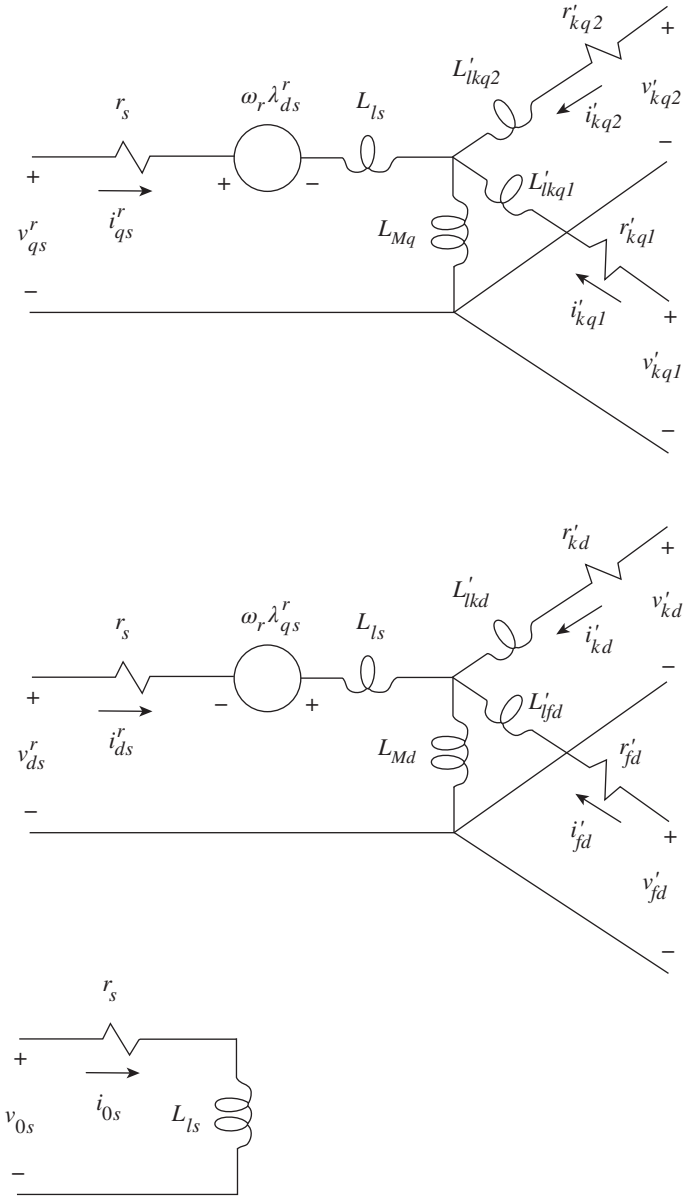

Figure 5.3-1 Equivalent circuits of a three-phase synchronous machine with the reference frame fixed in rotor.

$$L'_{lj} = \left(\frac{3}{2}\frac{N_s}{N_j}\right)^2 L_{lj} \tag{5.3-7}$$

where j may be *kq*1, *kq*2, *fd*, or *kd*. We can write the voltage and flux linkage equations as

$$v^r_{qs} = r_s i^r_{qs} + \omega_r \lambda^r_{ds} + p\lambda^r_{qs} \tag{5.3-8}$$

$$v^r_{ds} = r_s i^r_{ds} - \omega_r \lambda^r_{qs} + p\lambda^r_{ds} \tag{5.3-9}$$

$$v_{0s} = r_s i_{0s} + p\lambda_{0s} \tag{5.3-10}$$

$$v'^r_{kq1} = r'^r_{kq1} i'^r_{kq1} + p\lambda'^r_{kq1} \tag{5.3-11}$$

$$v'^r_{kq2} = r'^r_{kq2} i'^r_{kq2} + p\lambda'^r_{kq2} \tag{5.3-12}$$

$$v'^r_{fd} = r'^r_{fd} i'^r_{fd} + p\lambda'^r_{fd} \tag{5.3-13}$$

$$v'^r_{kd} = r'^r_{kd} i'^r_{kd} + p\lambda'^r_{kd} \tag{5.3-14}$$

where

$$\lambda^r_{qs} = L_{ls} i^r_{qs} + L_{Mq}\left(i^r_{qs} + i'^r_{kq1} + i'^r_{kq2}\right) \tag{5.3-15}$$

$$\lambda^r_{ds} = L_{ls} i^r_{ds} + L_{Md}\left(i^r_{ds} + i'^r_{fd} + i'^r_{kd}\right) \tag{5.3-16}$$

$$\lambda_{0s} = L_{ls} i_{0s} \tag{5.3-17}$$

$$\lambda'^r_{kq1} = L'_{lkq1} i'^r_{kq1} + L_{Mq}\left(i^r_{qs} + i'^r_{kq1} + i'^r_{kq2}\right) \tag{5.3-18}$$

$$\lambda'^r_{kq2} = L'_{lkq2} i'^r_{kq2} + L_{Mq}\left(i^r_{qs} + i'^r_{kq1} + i'^r_{kq2}\right) \tag{5.3-19}$$

$$\lambda'^r_{fd} = L'_{lfd} i'^r_{fd} + L_{Md}\left(i^r_{ds} + i'^r_{fd} + i'^r_{kd}\right) \tag{5.3-20}$$

$$\lambda'^r_{kd} = L'_{lkd} i'^r_{kd} + L_{Md}\left(i^r_{ds} + i'^r_{fd} + i'^r_{kd}\right) \tag{5.3-21}$$

Also, $L_{Mq} = \frac{3}{2}(L_A - L_B)$ and $L_{Md} = \frac{3}{2}(L_A + L_B)$ where L_A is greater than L_B. For cylindrical rotors, $L_B = 0$. Only the stator variables are expressed in the rotor reference frame. Rotor voltages, currents, and fluxes are not transformed.

As in the case of the induction machine, it is often convenient to express the voltage and flux linkage equations in terms of reactances rather than inductances. This can be done by following a similar procedure given in Section 3.1.

5.4 Torque Expressions Positive for Motor Action

Now, we see from the voltage equations (5.3-8)–(5.3-14) that the only terms containing ω_r are from (5.3-8) and (5.3-9). Therefore, we can write

$$\frac{2}{3}\frac{2}{P}T_e\omega_r = \left(\lambda^r_{ds}i^r_{qs} - \lambda^r_{qs}i^r_{ds}\right)\omega_r \tag{5.4-1}$$

Thus, the torque positive for motor action is

$$T_e = \left(\frac{3}{2}\right)\left(\frac{P}{2}\right)\left(\lambda^r_{ds}i^r_{qs} - \lambda^r_{qs}i^r_{ds}\right) \tag{5.4-2}$$

where the $\left(\frac{3}{2}\right)$ factor is due to the $\left(\frac{2}{3}\right)$ factor in $\mathbf{K}^r_s$ (2.3-6). The $\left(\frac{P}{2}\right)$ factor is the number of pole pairs. We can also express the torque from (5.4-2) as

$$T_e = \left(\frac{3}{2}\right)\left(\frac{P}{2}\right)\left[L_{Md}\left(i^r_{ds} + i'^r_{fd} + i'^r_{kd}\right)i^r_{qs} + L_{Mq}\left(i^r_{qs} + i'^r_{kq1} + i'^r_{kq2}\right)i^r_{ds}\right] \tag{5.4-3}$$

The torque and rotor speed are related by

$$T_e = J\frac{2}{P}p\omega_r + B_m\frac{2}{P}\omega_r + T_L \tag{5.4-4}$$

5.5 Time-Domain Block Diagram

The equations convenient for simulating the synchronous machine in the rotor reference frame may be established by first solving the flux linkage equations for currents. This can be accomplished by defining

$$\lambda^r_{mq} = L_{Mq}\left(i^r_{qs} + i'^r_{kq1} + i'^r_{kq2}\right) \tag{5.5-1}$$

$$\lambda^r_{md} = L_{Md}\left(i^r_{ds} + i'^r_{kd} + i'^r_{fd}\right) \tag{5.5-2}$$

From (5.3-15), we get

$$i^r_{qs} = \frac{1}{L_{ls}}\left(\lambda^r_{qs} - \lambda^r_{mq}\right) \tag{5.5-3}$$

Similarly,

$$i^r_{ds} = \frac{1}{L_{ls}}\left(\lambda^r_{ds} - \lambda^r_{md}\right) \tag{5.5-4}$$

$$i'_{kq1} = \frac{1}{L'_{lkq1}}\left(\lambda'_{kq1} - \lambda^r_{mq}\right) \tag{5.5-5}$$

$$i'_{kq2} = \frac{1}{L'_{lkq2}}\left(\lambda'_{kq2} - \lambda^r_{mq}\right) \tag{5.5-6}$$

$$i'_{fd} = \frac{1}{L'_{lfd}}\left(\lambda'_{fd} - \lambda^r_{md}\right) \tag{5.5-7}$$

$$i'_{kd} = \frac{1}{L'_{lkd}}\left(\lambda'_{kd} - \lambda^r_{md}\right) \tag{5.5-8}$$

Substituting (5.5-3), (5.5-5), and (5.5-6) into (5.5-1) and solving for λ^r_{mq}

$$\lambda^r_{mq} = L_{aq}\left(\frac{\lambda^r_{qs}}{L_{ls}} + \frac{\lambda'^r_{kq1}}{L'_{lkq1}} + \frac{\lambda'^r_{kq2}}{L'_{lkq2}}\right) \tag{5.5-9}$$

where

$$L_{aq} = \frac{1}{\frac{1}{L_{ls}} + \frac{1}{L'_{lkq1}} + \frac{1}{L'_{lkq2}} + \frac{1}{L_{Mq}}} \tag{5.5-10}$$

Similarly

$$\lambda^r_{md} = L_{ad}\left(\frac{\lambda^r_{ds}}{L_{ls}} + \frac{\lambda'^r_{kd}}{L'_{lkd}} + \frac{\lambda'^r_{fd}}{L'_{lfd}}\right) \tag{5.5-11}$$

where

$$L_{ad} = \frac{1}{\frac{1}{L_{ls}} + \frac{1}{L'_{lkd}} + \frac{1}{L'_{lfd}} + \frac{1}{L_{Md}}} \tag{5.5-12}$$

Now (5.3-8) and (5.3-9) may be rewritten as

$$\lambda^r_{qs} = \int \left[v^r_{qs} - \omega_r\lambda^r_{ds} - r_s i^r_{qs}\right] dt \tag{5.5-13}$$

$$\lambda^r_{ds} = \int \left[v^r_{ds} + \omega_r\lambda^r_{qs} - r_s i^r_{ds}\right] dt \tag{5.5-14}$$

Setting $v'^r_{kd} = v'^r_{kq1} = v'^r_{kq2} = 0$ in (5.3-11)–(5.3-14), and substituting (5.5-5)–(5.5-8) for the currents yields

$$\lambda'^r_{kq1} = \int \frac{r'_{kq1}}{L'_{lkq1}}\left(\lambda^r_{mq} - \lambda'^r_{kq1}\right) dt \tag{5.5-15}$$

$$\lambda'^r_{kq2} = \int \frac{r'_{kq2}}{L'_{lkq2}}\left(\lambda^r_{mq} - \lambda'^r_{kq2}\right) dt \tag{5.5-16}$$

$$\lambda'^r_{fd} = \int v'^r_{fd} + \frac{r'_{fd}}{L'_{lfd}}\left(\lambda^r_{md} - \lambda'^r_{fd}\right) dt \tag{5.5-17}$$

$$\lambda'^r_{kd} = \int \frac{r'_{kd}}{L'_{lkd}}\left(\lambda^r_{md} - \lambda'^r_{kd}\right) dt \tag{5.5-18}$$

Finally, (5.5-13)–(5.5-18) along with the torque equation (5.4-2) can be expressed in the form of a time-domain block diagram as shown in Fig. 5.5-1. The torque and rotor speed is given by (5.4-4). The voltages v^r_{qs} and v^r_{ds} are obtained from v_{as}, v_{bs}, and v_{cs} using (2.3-5). The currents i_{as}, i_{bs}, and i_{cs} are obtained from

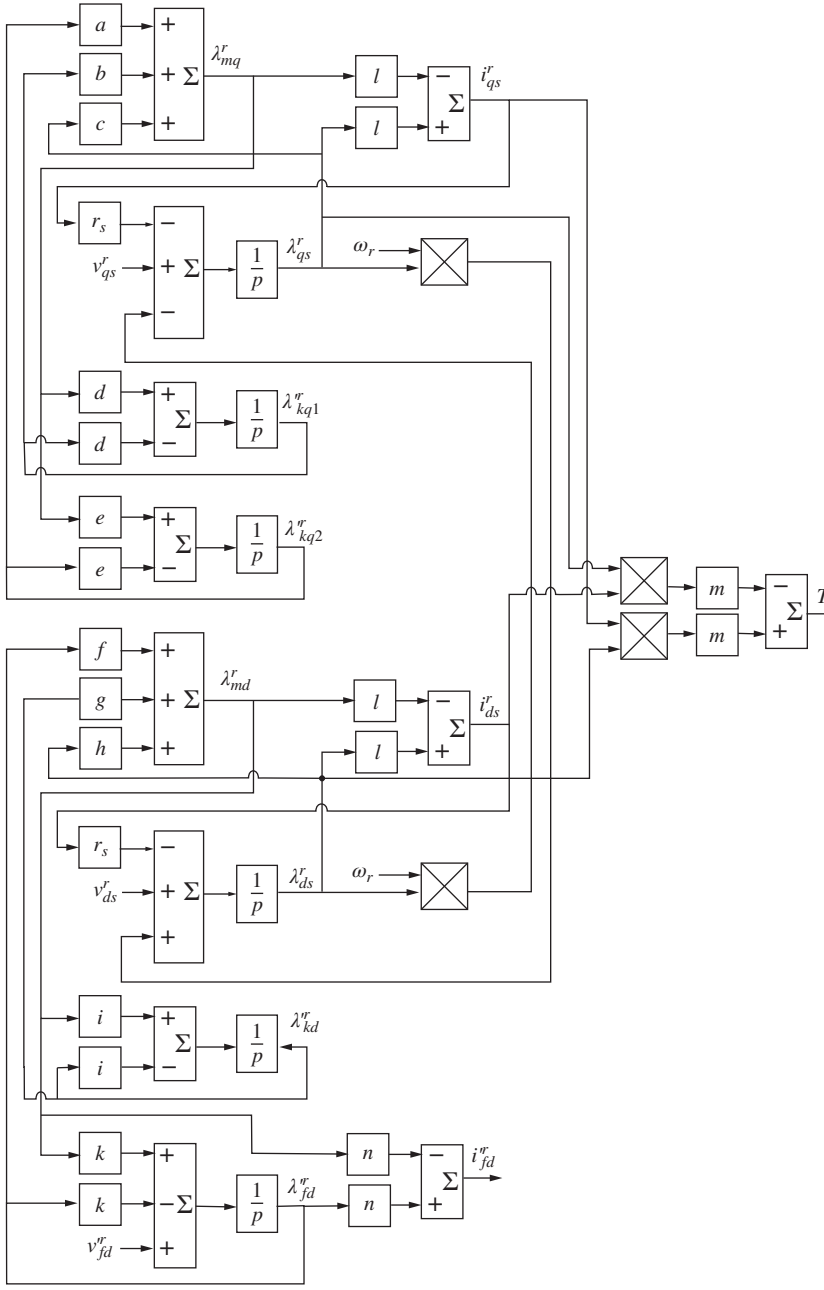

Figure 5.5-1 Time-domain block diagram for synchronous machines in the rotor reference frame. $a = \frac{L_{aq}}{L'_{lkq2}}$, $b = \frac{L_{aq}}{L'_{lkq1}}$, $c = \frac{L_{aq}}{L_{ls}}$, $d = \frac{r'_{kq1}}{L'_{lkq1}}$, $e = \frac{r'_{kq2}}{L'_{lkq2}}$, $f = \frac{L_{ad}}{L'_{lfd}}$, $g = \frac{L_{ad}}{L'_{lkd}}$, $h = \frac{L_{ad}}{L_{ls}}$, $i = \frac{r'_{kd}}{L'_{lkd}}$, $k = \frac{r'_{fd}}{L'_{lfd}}$, $l = \frac{1}{L_{ls}}$, $m = \left(\frac{3}{2}\right)\left(\frac{P}{2}\right)$, $n = \frac{1}{L'_{lfd}}$.

i^r_{qs} and i^r_{ds} using (2.3-7). If the stator windings are connected in delta or wye with ungrounded neutral, the 0s voltages, currents, and flux linkages are all identically equal to zero. It is left as an exercise for the reader to update the time-domain block diagram to include the 0s variables if the neutral is grounded and unbalanced operation is to be studied.

5.6 Rotor Angle and Angle Between Rotors

Except for isolated operations, it is convenient for analysis and interpretation purposes to relate the position of the rotor of a synchronous machine to a system voltage. If the machine is in a system environment, the electrical angular displacement of the rotor relative to its terminal (system) voltage is defined as the rotor angle. In particular, the rotor angle is the displacement of the rotor generally referenced to the maximum positive value of the fundamental component of the terminal (system) voltage of phase a. Therefore, the electrical angle of the rotor expressed in radians is

$$\delta = \theta_r - \theta_{ev} \tag{5.6-1}$$

The electrical angular speed of the rotor is ω_r; ω_e is the electrical frequency of the terminal voltages.

Let us take a minute to talk about an equation from Chapter 4, which dealt with variable-speed (and frequency) operation of permanent-magnet ac machines. From (4.3-32), we have $\phi_v = \theta_{ev} - \theta_r$ where ϕ_v is the controlled position of the terminal voltage $\widetilde{V}_{as}$, which is constant in the steady state. For analysis purposes, $\theta_r(0)$ (hence the time-zero position of the q axis) was assumed to be zero. Now, (5.6-1) is the rotor angle relative to the terminal voltages, which is the negative of ϕ_v. In Chapter 4, we caused an angle to occur between $\widetilde{V}_{as}$ and the q axis in the phasor diagram by moving $\widetilde{V}_{as}$ and holding the q axis at zero. In this chapter, the frequency of the terminal voltages is assumed fixed, and for analysis purposes, we will assume $\theta_{ev}(0) = 0$. Thus, from (5.6-1), the time-zero position of θ_r is δ, which like ϕ_v is constant in the steady state. With this assumption, $\widetilde{V}_{as}$ is at zero degrees in the phasor diagram and the q axis is at δ. However, it is important to note that, unlike ϕ_v in Chapter 4, δ is not directly controlled. Its value will be shown in Section 5.8 as a function of the load or prime mover torque.

The rotor angle δ is often used as the argument in the transformation between the rotor and synchronously rotating reference frames since ω_e is the speed of the synchronously rotating reference frame and is also the rate-of-change of θ_{ev}. From (2.5-1)

$$\mathbf{f}^r_{qd0s} = {}^e\mathbf{K}^r\,\mathbf{f}^e_{qd0s} \tag{5.6-2}$$

where

$$ {}^{e}\mathbf{K}^{r} = \begin{bmatrix} \cos\delta & -\sin\delta & 0 \\ \sin\delta & \cos\delta & 0 \\ 0 & 0 & 1 \end{bmatrix} \tag{5.6-3} $$

The rotor angle is often used in relating torque and rotor speed. In particular, if ω_e is constant, then (5.4-4) may be written as

$$ T_e = J\left(\frac{2}{P}\right)p^2\delta + B_m p\delta + T_L \tag{5.6-4} $$

where δ is expressed in radians.

5.7 Per Unit System

The equations for a synchronous machine may be written in per unit by following the same procedure as in the case of the induction machine. Base voltage is generally selected as the rms value of the rated phase voltage for the *abc* variables and the peak value for the *qd*0 variables. However, we will often use the same base value when comparing *abc* and *qd*0 variables. When considering the machine separately, the power base is selected as its volt-ampere rating. When considering power systems, a system power base (system base) is selected that is generally different from the power base of the machine (machine base).

Once the base quantities are established, the corresponding base current and base impedance may be calculated. Park's equations written in terms of flux-linkages-per-second and reactances are readily per unitized by dividing each term by the peak of the base voltage (or the peak value of the base current times base impedance). The form of these equations remains unchanged as a result of per unitizing.

Base torque is the base power divided by the synchronous speed of the rotor. Thus,

$$ \begin{aligned} T_B &= \frac{P_B}{(2/P)\omega_B} \\ &= \frac{\left(\frac{3}{2}\right)V_{B(qd0)}I_{B(qd0)}}{(2/P)\omega_B} \end{aligned} \tag{5.7-1} $$

where ω_B corresponds to rated or base frequency, P_B is the base power, $V_{B(qd0)}$ is the peak value of the base phase voltage, and $I_{B(qd0)}$ is the peak value of the base phase current. In this text, we will use ω_e and ω_B which are the same, i.e., 377 rad/s for a 60 Hz system. Dividing the torque equations by (5.7-1) yields the torque expressed in per unit. For example, (5.4-2) with all quantities expressed in per unit becomes

$$ T_e = \psi_{ds}^{r} i_{qs}^{r} - \psi_{qs}^{r} i_{ds}^{r} \tag{5.7-2} $$

where $\Psi = \omega_B \lambda$.

Eq. (5.4-4), which relates torque and speed, is expressed in per unit with B_m neglected as

$$T_e = 2Hp\frac{\omega_r}{\omega_B} + T_L \tag{5.7-3}$$

If ω_e is constant, then this relationship becomes

$$T_e = \frac{2H}{\omega_B}p^2\delta + T_L \tag{5.7-4}$$

where δ is the electrical rotor angle in radians. The inertia constant H is in seconds. It is defined as

$$\begin{aligned} H &= \left(\frac{1}{2}\right)\left(\frac{2}{P}\right)\frac{J\omega_B}{T_B} \\ &= \left(\frac{1}{2}\right)\left(\frac{2}{P}\right)^2\frac{J\omega_B^2}{P_B} \end{aligned} \tag{5.7-5}$$

where J is often the combined inertia of the rotor and prime mover expressed in $\text{kg}\cdot\text{m}^2$ or given as the quantity WR^2 in $\text{lb}\cdot\text{ft}^2$.

5.8 Analysis of Steady-State Operation

For balanced conditions, the 0s quantities are zero and the electrical angular velocity of the rotor is constant and equal to ω_e. Therefore, the electrical angular velocity of the rotor reference frame becomes the electrical angular velocity of the synchronously rotating reference frame. In this mode of operation, the rotor windings do not experience a change of flux linkages, hence current is not flowing in the short-circuited damper windings and λ_{qs}^r and λ_{ds}^r are constant.

For balanced operation, the stator variables may be expressed as

$$f_{as} = \sqrt{2}f_s\cos\,\theta_{ef} \tag{5.8-1}$$

$$f_{bs} = \sqrt{2}f_s\cos\left(\theta_{ef} - \frac{2\pi}{3}\right) \tag{5.8-2}$$

$$f_{cs} = \sqrt{2}f_s\cos\left(\theta_{ef} + \frac{2\pi}{3}\right) \tag{5.8-3}$$

These variables may be expressed in the rotor reference frame as

$$f_{qs}^r = \sqrt{2}f_s\cos(\theta_{ef} - \theta_r) \tag{5.8-4}$$

$$f_{ds}^r = -\sqrt{2}f_s\sin(\theta_{ef} - \theta_r) \tag{5.8-5}$$

If the rotor angle from (5.6-1) is substituted into (5.8-4) and (5.8-5), we obtain

$$f_{qs}^r = \sqrt{2}f_s\cos(\theta_{ef} - \theta_{ev} - \delta) \tag{5.8-6}$$

$$f_{ds}^{r} = -\sqrt{2} f_s \sin(\theta_{ef} - \theta_{ev} - \delta) \tag{5.8-7}$$

The only restriction on (5.8-6) and (5.8-7) is that the stator variables form a balanced set. These equations are valid for transient and steady-state operation, that is, f_s and δ may both be functions of time. For balanced steady-state conditions, (5.8-6) and (5.8-7) are constants since f_s and the argument to the trigonometric functions are generally both constants. From (5.8-6) and (5.8-7),

$$\begin{aligned} f_{qs}^{r} - jf_{ds}^{r} &= \sqrt{2} f_s [\cos(\theta_{ef} - \theta_{ev} - \delta) + j \sin(\theta_{ef} - \theta_{ev} - \delta)] \\ &= \sqrt{2} f_s e^{j(\theta_{ef} - \theta_{ev} - \delta)} \end{aligned} \tag{5.8-8}$$

The position of $\tilde{V}_{as}$, i.e., $\theta_{ev}(0)$, is selected to be zero; this is generally determined by the power system to which it is connected. Thus, in the steady state $\theta_{ef} - \theta_{ev} = \theta_{ef}(0)$ and

$$\begin{aligned} F_{qs}^{r} - jF_{ds}^{r} &= \sqrt{2} F_s e^{j(\theta_{ef}(0) - \delta)} \\ &= \sqrt{2} \tilde{F}_{as} e^{-j\delta} \end{aligned} \tag{5.8-9}$$

From (5.3-8) and (5.3-9) and since in the steady state $\omega_r = \omega_e$, we can write

$$v_{qs}^{r} = r_s i_{qs}^{r} + \omega_e \lambda_{ds}^{r} \tag{5.8-10}$$

$$v_{ds}^{r} = r_s i_{ds}^{r} - \omega_e \lambda_{qs}^{r} \tag{5.8-11}$$

where

$$\begin{aligned} \lambda_{qs}^{r} &= L_{ls} i_{qs}^{r} + L_{Mq} i_{qs}^{r} \\ &= L_q i_{qs}^{r} \end{aligned} \tag{5.8-12}$$

$$\begin{aligned} \lambda_{ds}^{r} &= L_{ls} i_{ds}^{r} + L_{Md} \left(i_{ds}^{r} + i_{fd}^{\prime r} \right) \\ &= L_d i_{ds}^{r} + L_{Md} i_{fd}^{\prime r} \end{aligned} \tag{5.8-13}$$

Substituting (5.8-12) and (5.8-13) into (5.8-10) and (5.8-11) and using (5.8-9), we have

$$\sqrt{2} \tilde{V}_{as} e^{-j\delta} = r_s \sqrt{2} \tilde{I}_{as} e^{-j\delta} + \omega_e L_d I_{ds}^{r} + \omega_e L_{Md} I_{fd}^{\prime r} - j\omega_e L_q i_{qs}^{r} \tag{5.8-14}$$

Now from (5.8-9)

$$j\sqrt{2} \tilde{I}_{as} e^{-j\delta} = I_{ds}^{r} + jI_{qs}^{r} \tag{5.8-15}$$

If we now add and subtract $\omega_e L_q I_{ds}^{r}$ to the right-hand side of (5.8-14) and divide each side by $\sqrt{2} e^{-j\delta}$

$$\tilde{V}_{as} = (r_s + j\omega_e L_q) \tilde{I}_{as} + \frac{1}{\sqrt{2}} \left[\omega_e (L_d - L_q) I_{ds}^{r} + \omega_e L_{Md} I_{fd}^{\prime r} \right] e^{j\delta} \tag{5.8-16}$$

Now, in terms of X rather than $\omega_e L$, we have

$$\tilde{V}_{as} = (r_s + jX_q)\tilde{I}_{as} + \frac{1}{\sqrt{2}}\left[(X_d - X_q)I^r_{ds} + X_{Md}I'^r_{fd}\right]e^{j\delta} \tag{5.8-17}$$

We can write (5.8-17) as

$$\tilde{V}_{as} = (r_s + jX_q)\tilde{I}_{as} + \tilde{E}_a \tag{5.8-18}$$

where $\tilde{E}_a$ is

$$\tilde{E}_a = \frac{1}{\sqrt{2}}\left[(X_d - X_q)I^r_{ds} + X_{Md}I'^r_{fd}\right]e^{j\delta} \tag{5.8-19}$$

Now, $\tilde{E}_a$ is oriented along the q axis, but where is the q axis? Well, we can make use of the rotor angle given by (5.6-1). So (5.6-1) may be written with $\theta_{ev}(0) = 0$ as

$$\delta = \theta_r(0) \tag{5.8-20}$$

We see from Fig. 5.2-1 that θ_r is the displacement angle of the q axis. Thus, the last term of (5.8-18) is at δ or $\theta_r(0)$.

Before proceeding, it is noted that for balanced steady-state operation, we can write the excitation voltage as

$$E'^r_{xfd} = X_{Md}I'^r_{fd} \tag{5.8-21}$$

Although the excitation voltage is sometimes substituted into the above steady-state voltage equations, it is most often used in the expression for torque. In particular, if (5.8-19) and the steady-state versions of (5.8-17) and (5.8-18) are used and if r_s is neglected the torque may be expressed as

$$T_e = -\left(\frac{3}{2}\right)\left(\frac{P}{2}\right)\left(\frac{1}{\omega_e}\right)\left[\frac{E'^r_{xfd}\sqrt{2}V_s}{X_d}\sin\delta + \left(\frac{1}{2}\right)\left(\frac{1}{X_q} - \frac{1}{X_d}\right)(\sqrt{2}V_s)^2\sin 2\delta\right] \tag{5.8-22}$$

In per unit, (5.8-22) becomes

$$T_e = -\frac{E'^r_{xfd}V_s}{X_d}\sin\delta - \left(\frac{1}{2}\right)\left(\frac{1}{X_q} - \frac{1}{X_d}\right)V_s^2\sin 2\delta \tag{5.8-23}$$

In (5.8-22) and (5.8-23), the rotor angle appears since $\tilde{V}_{as}$ is fixed and the rotor (q and d axes) moves relative to the applied voltages. In the case of the permanent-magnet ac machine (Chapter 4), the applied voltages move with the rotor. Neglecting r_s is justified if r_s is small relative to the reactances of the machine. In variable-frequency drive systems, this may not be the case at low frequencies. With the stator resistance neglected, steady-state power and torque are related by rotor speed, and if torque and power are expressed in per unit, they are equal during steady-state operation.

Although (5.8-22) is valid only for balanced steady-state operation and if the stator resistance is small relative to the magnetizing reactances (X_{Mq} and X_{Md}) of the machine, it permits a quantitative description of the nature of the steady-state electromagnetic torque of a synchronous machine. The first term on the right-hand side of (5.8-22) is due to the interaction of the magnetic system produced by the currents flowing in the stator windings and the magnetic system produced by the current flowing in the field winding. The second term is due to the saliency of the rotor. This component is commonly referred to as the reluctance torque. The predominant torque is the torque due to the interaction of the stator and rotor magnetic fields. The amplitude of this component is proportional to the magnitudes of the stator voltage V_s, and the voltage applied to the field. In power systems, it is desirable to maintain the stator voltage near rated. This is achieved by automatically adjusting the voltage applied to the field winding. Hence, the amplitude of this torque component varies as E'^r_{xfd} is varied to maintain the terminal voltage at or near rated and/or to control reactive power flow. The reluctance torque component is generally a relatively small part of the total torque. In power systems where the terminal voltage is maintained nearly constant, the amplitude of the reluctance torque would also be nearly constant, a function only of the parameters of the machine and rotor angle. A steady-state reluctance torque does not exist in round or cylindrical rotor synchronous machines since $X_q = X_d$. On the other hand, a reluctance machine is a device that is not equipped with a field winding; hence, the only torque produced is reluctance torque.

Let us return for a moment to the steady-state voltage equation given by (5.8-17). With $\theta_{ev}(0) = 0$, $\tilde{V}_{as}$ lies along the positive real axis of a phasor diagram. Since δ is the angle associated with $\tilde{E}_a$ (5.8-19), its position relative to $\tilde{V}_{as}$ is also the position of the q axis of the machine relative to $\tilde{V}_{as}$ if $\theta_r(0) = 0$. Therefore, we can superimpose the q and d axes of the synchronous machine upon the phasor diagram.

If T_L is assumed zero and if we neglect friction and windage losses along with the stator resistance, then T_e and δ are also zero and the machine will theoretically run at synchronous speed without absorbing energy from either the electrical or mechanical system. Although this mode of operation is not feasible in practice since the machine will actually absorb some small amount of energy to satisfy the ohmic, friction, and windage losses, it is convenient for purposes of explanation. With the machine "floating on the line," the field voltage can be adjusted to establish the desired terminal conditions. Three situations may exist: (1) $|\tilde{E}_a| = |\tilde{V}_{as}|$, whereupon $\tilde{I}_{as} = 0$; (2) $|\tilde{E}_a| > |\tilde{V}_{as}|$, whereupon $\tilde{I}_{as}$ leads $\tilde{V}_{as}$; the synchronous machine appears as a capacitor supplying reactive power to the system; or (3) $|\tilde{E}_a| < |\tilde{V}_{as}|$ with $\tilde{I}_{as}$ lagging $\tilde{V}_{as}$, whereupon the machine is absorbing reactive power appearing as an inductor to the system. If you plot the amplitude

of stator current versus field winding current, you will get the well-known V curve.

To maintain the voltage in a power system at rated value, the synchronous generators are normally operated in the overexcited mode with $|\tilde{E}_a| > |\tilde{V}_{as}|$ since they are the main source of reactive power for the inductive loads throughout the system. In the past, some synchronous machines were often placed in the power system for the sole purpose of supplying reactive power without any provision to provide real power. During peak load conditions when the system voltage is depressed, these so-called synchronous condensers were brought online and the field voltage was adjusted to help increase the system voltage. In this mode of operation, the synchronous machine behaves like an adjustable capacitor. Although the synchronous condenser is not used as widely as in the past, it is an instructive example. On the other hand, it may be necessary for a generator to absorb reactive power in order to regulate voltage in a high-voltage transmission system during light load conditions. This mode of operation is, however, not desirable and should be avoided since machine oscillations become less damped as the reactive power required is decreased. This is shown in [3].

Example 5A A four-pole, three-phase, salient-pole synchronous machine is supplied from a 440 V (rms) line-to-line, 60 Hz source. The machine is operated as a motor with a total input power of 4 kW at the terminals. The parameters are

$$r_s = 0.3\,\Omega \; L_{Md} = 0.015\text{ H}$$

$$L_{ls} = 0.001\text{ H} \; L_{Mq} = 0.008\text{ H}$$

Assume the positive direction of current is into the stator terminals.

(a) The excitation is adjusted so that $\tilde{I}_{as}$ lags $\tilde{V}_{as}$ by 30°. Calculate $\tilde{E}_a$ and the reactive power Q.
(b) Repeat (a) with the excitation adjusted so that $\tilde{I}_{as}$ is in phase with $\tilde{V}_{as}$.
(c) Repeat (a) with the excitation adjusted so that $\tilde{I}_{as}$ leads $\tilde{V}_{as}$ by 30°.

(a) $P = 3|\tilde{V}_{as}||\tilde{I}_{as}|\cos\phi$, $|\tilde{I}_{as}| = 90.61$ A, where ϕ is the angle between $\tilde{V}_{as}$ and $\tilde{I}_{as}$.

$$\tilde{E}_a = \tilde{V}_{as} - (r_s + jX_q)\tilde{I}_{as} = 216.59 \underline{/ -51.28^\circ}\text{ A} \tag{5A-1}$$

$$Q = 3|V_a||I_a|\sin\phi = 23.096\text{ kVAR} \tag{5A-2}$$

(b) $\phi = 0$, $Q = 0$

$$|\tilde{I}_{as}| = 52.49\text{ A} \tag{5A-3}$$

$$\tilde{E}_a = 297.50 \underline{/ -36.77^\circ} \tag{5A-4}$$

(c) $|\tilde{I}_{as}| = 60.61$ A

$$\tilde{E}_a = 389.10 \angle -28.75\text{V} \tag{5A-5}$$

$$Q = -23.096 \text{ kVAR} \tag{5A-6}$$

5.9 Stator Currents Positive out of Machine—Synchronous Generator Operation

The early power system engineers and analysts chose to assume positive stator currents out of the synchronous machine perhaps because the main application was generator action. This notation is still used predominately in power system analysis and therefore warrants consideration. The synchronous machine is shown in Fig. 5.9-1 and the equivalent circuits shown in Fig. 5.9-2 depict positive stator currents out of the machine. It is important to note that the field and damper winding currents are positive into the machine. It may at first appear that it would be a huge task to modify the analysis used thus far in this chapter to accommodate this change in the assumed direction of positive current. We would hope not to be forced to repeat the entire derivation. Fortunately, we will not have to do this. First, let us consider the changes necessary in order to make the steady-state equations compatible with assumed positive stator currents out of the machine.

The steady-state voltage and torque equations for positive stator currents out of the machine are obtained by simply changing the sign of stator current, $\tilde{I}_{as}$, or the substitute variables, I^r_{qs} and I^r_{ds}. From Section 5.8,

$$\tilde{V}_{as} = -(r_s + jX_q)\tilde{I}_{as} + \tilde{E}_a \tag{5.9-1}$$

$$\tilde{E}_a = \frac{1}{\sqrt{2}}\left[-(X_d - X_q)I^r_{ds} + X_{md}I'^{\text{r}}_{fd}\right]e^{j\delta} \tag{5.9-2}$$

The steady-state torque, positive for generator action, is the negative of (5.8-22) or (5.8-23).

We realize that this changes the sense of the torque versus angle plot from a negative sign to a positive sign. Along with this change is the change in the concept of stable operation. In particular, when we assumed positive currents into the machine, stable operation occurred on the negative slope part of the torque versus angle plot; now stable operation is on the positive slope portion.

For generator action, the torque and rotor speed relationship is generally written as

$$T_e = -J\left(\frac{2}{P}\right)p\omega_r + B_m\left(\frac{2}{P}\right)\omega_r + T_I \tag{5.9-3}$$

where T_e is positive for generator action and T_I is the input torque, which is positive for a torque input to the shaft of the synchronous generator. Torque

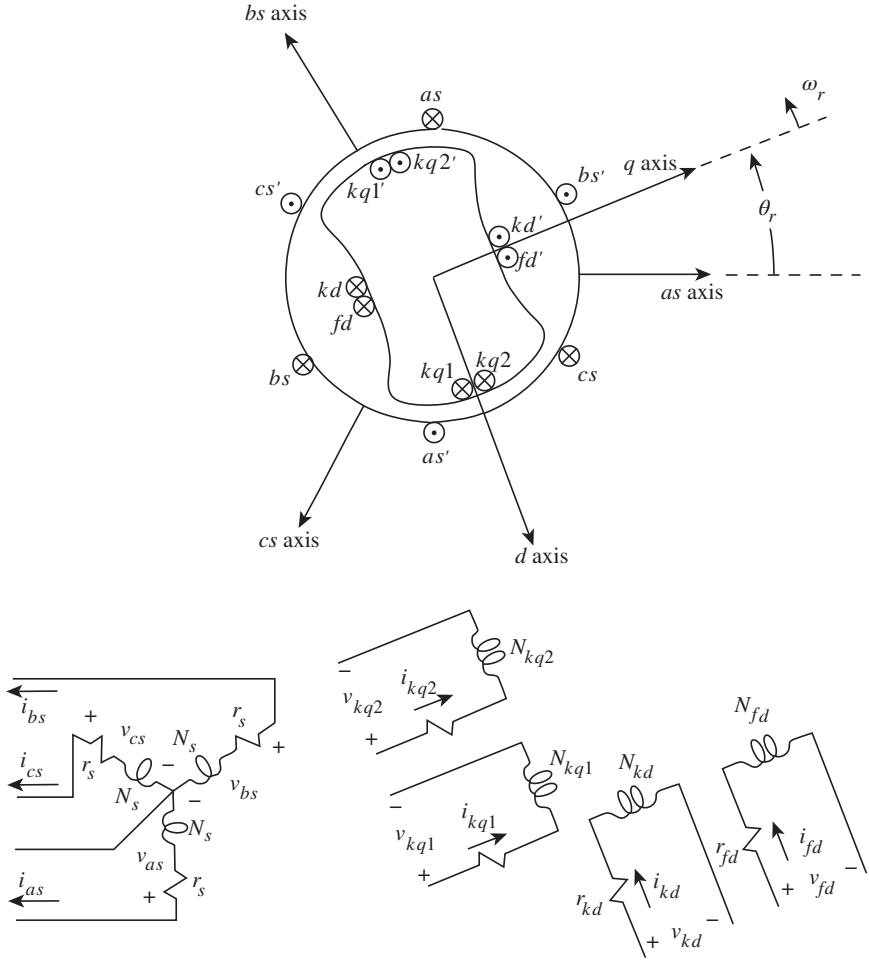

Figure 5.9-1 Two-pole three-phase wye-connected salient-pole synchronous machine with currents defined positive out of the phase windings.

versus speed relationships expressed in per unit are, neglecting B_m,

$$T_e = -2Hp\frac{\omega_r}{\omega_B} + T_I \tag{5.9-4}$$

If ω_e (ω_B) is constant, then (5.9-4) may be written as

$$T_e = -\frac{2H}{\omega_B}p^2\delta + T_I \tag{5.9-5}$$

where H is in seconds and δ is in electrical radians. A typical phasor diagram for generator action with positive stator currents out of the machine is shown in

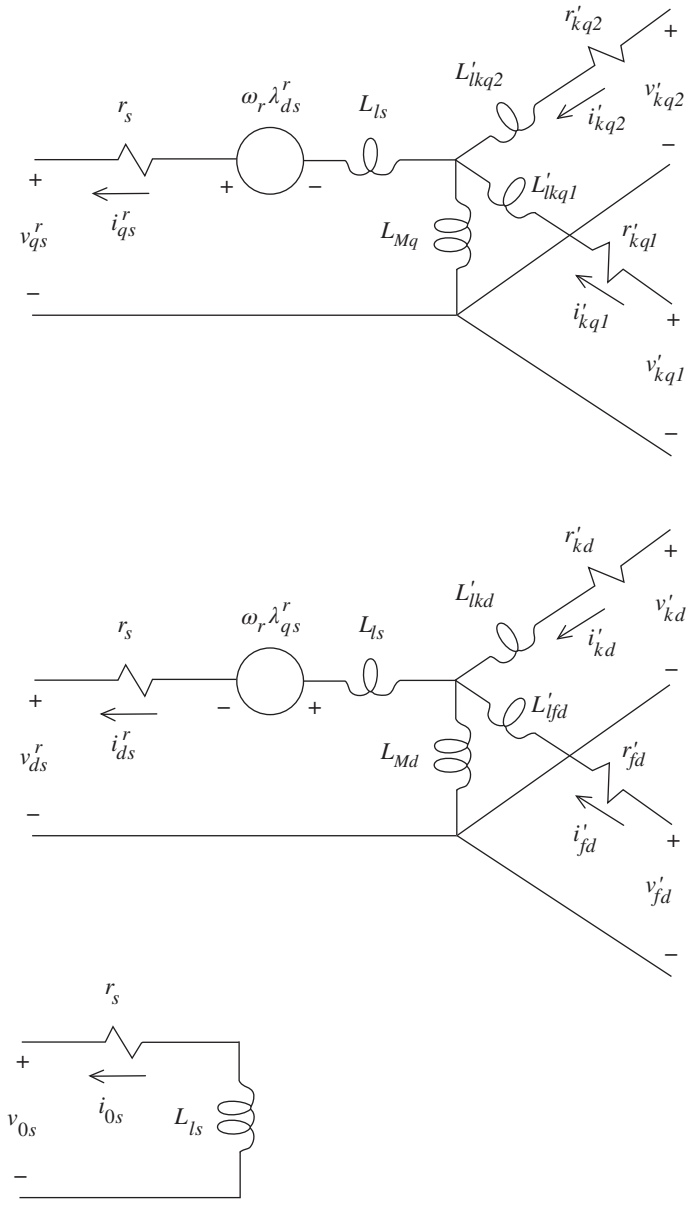

Figure 5.9-2 Equivalent circuits of a three-phase synchronous machine with the reference frame fixed in rotor—Park's equations with currents defined positive out of the phase windings.

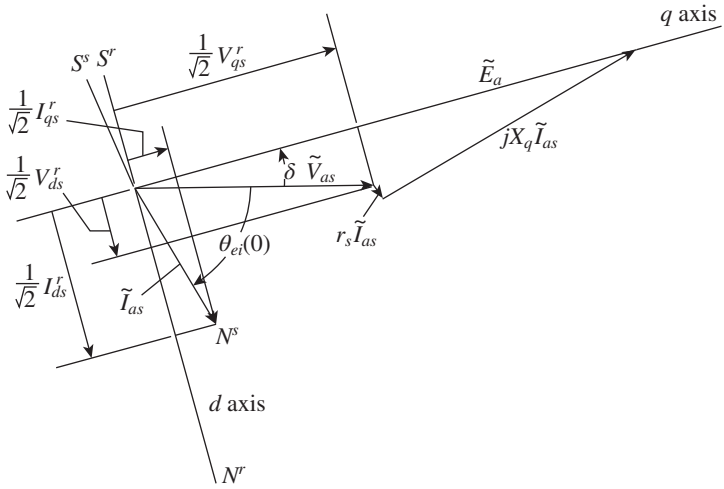

Figure 5.9-3 Phasor diagram for generator operation with currents defined positive out of the phase windings.

Fig. 5.9-3. Note that the stator poles change from motor action. It appears that we are now prepared to consider generator operation compatible with the convention used in power system analysis.

Example 5B A three-phase, 64-pole, hydro-turbine generator is rated at 325 MVA, with 20 kV line-to-line voltage and a power factor of 0.85 lagging. The machine parameters in ohms at 60 Hz are $r_s = 0.00234\ \Omega$, $X_q = 0.5911\ \Omega$, and $X_d = 1.0467\ \Omega$. For balanced, steady-state rated conditions, calculate (*a*) $\tilde{E}_a$, (*b*) E'^r_{xfd}, and (*c*) T_e.

The apparent power $|S|$ is

$$|S| = 3|\tilde{V}_{as}|\,|\tilde{I}_{as}| \tag{5B-1}$$

Thus,

$$\begin{aligned} |\tilde{I}_{as}| &= \frac{|\mathrm{S}|}{3|\tilde{V}_{as}|} \\ &= \frac{325 \times 10^6}{(3 \times 20 \times 10^3)/\sqrt{3}} \\ &= 9.37\ \mathrm{kA} \end{aligned} \tag{5B-2}$$

The power factor angle is $\cos^{-1}0.85 = 31.\ 8°$. Since current is positive out of the terminals of the generator, reactive power is delivered by the generator when the current is lagging the terminal voltage. Thus, $\tilde{I}_{as} = 9.37\underline{/-31.8°}$ kA. Therefore,

from (5.9-1), we can obtain the answer to part (*a*).

$$\begin{aligned}\tilde{E}_a &= \tilde{V}_{as} + (r_s + jX_q)\tilde{I}_{as} \\ &= \frac{20\times10^3}{\sqrt{3}}\underline{/0^\circ} + (0.00234 + j0.591)\,9.37\times10^3\underline{/-31.8^\circ} \\ &= 15.2\underline{/18^\circ}\ \text{kV}\end{aligned} \tag{5B-3}$$

Hence, $\delta = 18^\circ$.

We can solve for E''^r_{xfd} by first substituting (5.8-21) into (5.9-2); however, I^r_{ds} is required before E''^r_{xfd} can be evaluated. Thus,

$$\begin{aligned}I^r_{ds} &= -\sqrt{2}I_s \sin[\theta_{ei}(0) - \theta_{ev}(0) - \delta] \\ &= -\sqrt{2}|\tilde{I}_{as}|\sin[-31.8^\circ - 0 - 18^\circ] \\ &= -\sqrt{2}(9.37\times10^3)\sin[-49.8^\circ] \\ &= 10.12\ \text{kA}\end{aligned} \tag{5B-4}$$

From (5.9-2) and (5.8-21)

$$\begin{aligned}E''^r_{xfd} &= \sqrt{2}\tilde{E}_a + (X_d - X_q)I^r_{ds} \\ &= \sqrt{2}(15.2\times10^3) + (1.0467 - 0.591)10.12\times10^3 \\ &= 26.1\ \text{kV}\end{aligned} \tag{5B-5}$$

Since r_s is small, T_e may be calculated by substitution into the negative of (5.7-23)

$$\begin{aligned}T_e &= \left(\frac{3}{2}\right)\left(\frac{P}{2}\right)\left(\frac{1}{\omega_e}\right)\left[\frac{E''^r_{xfd}\sqrt{2}|\tilde{V}_{as}|}{X_d}\sin\delta\right] + \left(\frac{1}{2}\right)\left(\frac{1}{X_q} - \frac{1}{X_d}\right)\left(\sqrt{2}|\tilde{V}_{as}|\right)^2\sin 2\delta \\ &= \left(\frac{3}{2}\right)\left(\frac{64}{2}\right)\left(\frac{1}{377}\right)\left[\frac{(26.1\times10^3)\sqrt{2}(20\times10^3)/\sqrt{3}}{1.0467}\sin 18^\circ\right] \\ &\quad + \left(\frac{1}{2}\right)\left(\frac{1}{0.5911} - \frac{1}{1.0467}\right)\left(\sqrt{2}\frac{20\times10^3}{\sqrt{3}}\right)^2\sin 36^\circ \\ &= 23.4\times10^6\ \text{N}\cdot\text{m}\end{aligned} \tag{5B-6}$$

5.9.1 Dynamic Performance during a Sudden Change in Input Torque

It is instructive to observe the dynamic performance of a synchronous machine during a step change in input torque. For this purpose, the differential equations that describe the synchronous machine were programmed on a computer and a study was performed [3]. Two large machines are considered: a low-speed hydro-turbine generator and a high-speed steam-turbine generator. Information regarding each machine is given in Tables 5.9-1 and 5.9-2. In the case of the

Table 5.9-1 Hydro Turbine Generator.

Rating: 325 MVA
Line-to-line voltage: 20 kV
Power factor: 0.85
Poles: 64
Speed: 112.5 rev/min
Combined inertia of generator and turbine:
$J = 35.1 \times 10^6$ J · s^2, or $WR^2 = 833.1 \times 10^6$lbm · ft^2 $\quad H = 7.5$ s
Parameters in ohms and per unit:
$r_s = 0.00234\ \Omega$, 0.0019 pu
$X_{ls} = 0.1478\ \Omega$, 0.120 pu
$X_q = 0.5911\ \Omega$, 0.480 pu $\quad X_d = 1.0467\ \Omega$, 0.850 pu
$r'_{fd} = 0.00050\ \Omega$, 0.00041 pu
$X'_{lfd} = 0.2523\ \Omega$, 0.2049 pu
$r'_{kq1} = 0.01675\ \Omega$, 0.0136 pu $\quad r'_{kd} = 0.01736\ \Omega$, 0.0141 pu
$X'_{lkq1} = 0.1267\ \Omega$, 0.1029 pu $\quad X'_{lkd} = 0.1970\ \Omega$, 0.160 pu

hydro-turbine generator, parameters are given for only one damper winding in the q axis.

The computer traces shown in Figs. 5.9-4 and 5.9-5 illustrate the dynamic behavior of the hydro-turbine generator following a step change in input torque from zero to 27.6×10^6 N · m (rated torque for unity power factor). The dynamic behavior of the steam-turbine generator is depicted in Figs. 5.9-6 and 5.9-7. In this case, the step change in input torque is from zero to 1.11×10^6 N · m (50% rated). In Figs. 5.9-4 and 5.9-5, the following variables are plotted: i_{as}, v^r_{qs}, i^r_{qs}, v^r_{ds}, i^r_{ds}, i'^r_{fd}, T_e, ω_r, and δ, where ω_r is expressed in radians per second and δ in degrees. Figures 5.9-5 and 5.9-7 illustrate the dynamic torque versus rotor-angle characteristics. In all figures, the scales of the voltages and currents are given in multiples of peak rated values and $\omega_b = 377$ rad/s.

In each study, it is assumed that the machine is connected to a bus whose voltage and frequency remain constant, at their rated values, regardless of the stator current. This is commonly referred to as an infinite bus, since its characteristics do not change regardless of the power supplied or consumed by any device connected to it. Although an infinite bus cannot be realized in practice, its characteristics are approached if the power delivery capability of the system, at the point where the machine is connected, is much larger than the rating of the machine.

Table 5.9-2 Steam Turbine Generator.

Rating: 835 MVA
Line-to-line voltage: 26 kV
Power factor: 0.85
Poles: 64
Speed: 112.5 r/min
Combined inertia of generator and turbine:
$J = 0.0658$ x 10^6 J · s^2, or $WR^2 = 1.56$ x 10^6 lbm · ft^2 $H = 5.6$ s
Parameters in ohms and per unit:
$r_s = 0.00243\ \Omega$, 0.003 pu
$X_{ls} = 0.1538\ \Omega$, 0.19 pu
$X_q = 1.457\ \Omega$, 1.8 pu $\quad X_d = 1.457\ \Omega$, 1.8 pu
$r'_{kq1} = 0.00144\ \Omega, 0.00178$ pu $\quad r'_{fd} = 0.00075\ \Omega, 0.000929$ pu
$X'_{lkq1} = 0.6578\ \Omega, 0.8125$ pu $\quad X'_{lfd} = 0.1145\ \Omega, 0.1414$ pu
$r'_{kq2} = 0.00681\ \Omega, 0.00841$ pu $\quad r'_{kd} = 0.01080\ \Omega, 0.01334$ pu
$X'_{lkq2} = 0.07602\ \Omega, 0.0939$ pu $\quad X'_{lkd} = 0.06577\ \Omega, 0.08125$ pu

Initially, each machine is operating with zero input torque with the excitation held fixed at the value that gives rated open-circuit terminal voltage at synchronous speed. It is instructive to observe the plots of T_e, ω_r, and δ following the step change input torque. In particular, consider the response of the hydro-turbine generator (Fig. 5.9-4) where the machine is subjected to a step increase in input torque from zero to 27.6×10^6 N · m. The rotor speed begins to increase immediately following the step increase in input torque as predicted by (5.9-5) whereupon the rotor angle increases in accordance with (5.6-1). The rotor speeds up until the accelerating torque on the rotor is zero. As noted in Fig. 5.9-4, the electrical speed increases to approximately 380 radians per second at which time T_e is equal to T_I since the change of ω_r is zero and hence the inertial torque (T_{IT}) is zero. Even though the accelerating torque is zero at this time, the rotor is running above synchronous speed, hence δ, and thus T_e, will continue to increase. The increase in T_e, which corresponds to an increase in the power output of the machine, causes the rotor to decelerate toward synchronous speed. However, when synchronous speed is reached, the magnitude of δ has become larger than necessary to satisfy the input torque. Note that at the first synchronous speed crossing of ω_r after the change in input torque, δ is approximately 42 electrical degrees and T_e approximately 47×10^6 N · m. Hence, the rotor continues to decelerate below synchronous speed and consequently δ begins to decrease which

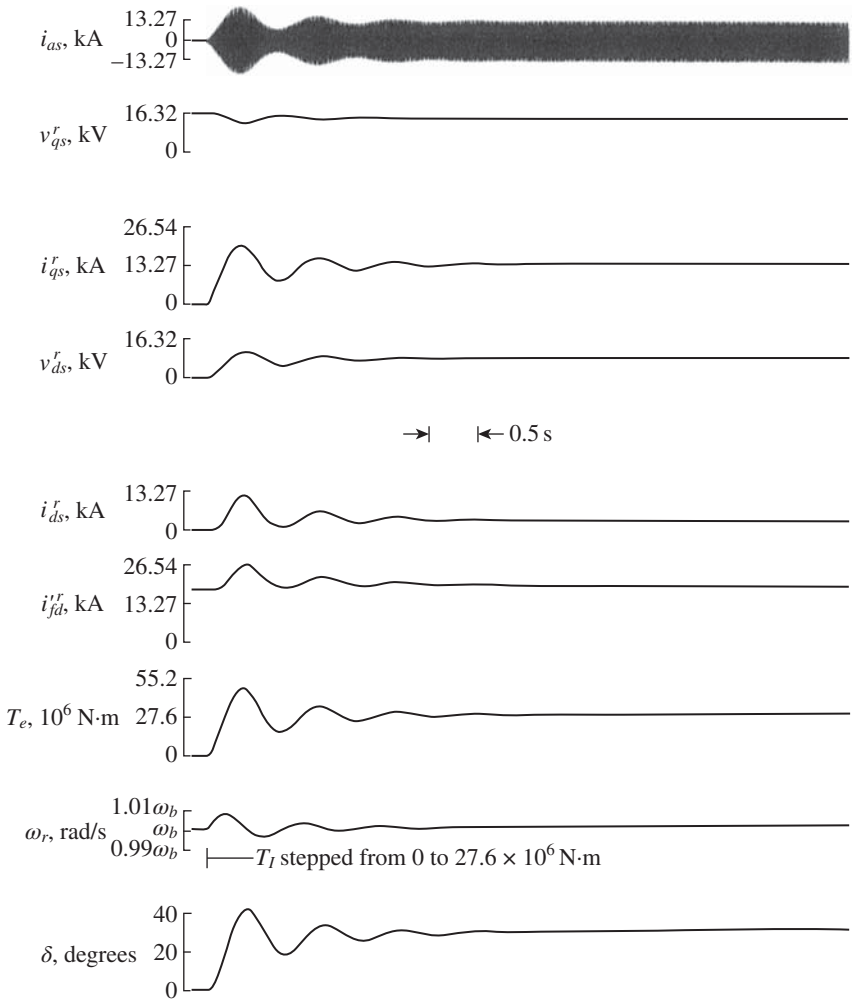

Figure 5.9-4 Dynamic performance of a hydro-turbine generator following a step increase in input torque from zero to rated.

in turn decreases T_e. Damped oscillations of the machine variables continue until a new steady-state operating point is finally attained.

In the case of the hydro-turbine generator (Fig. 5.9-4), the oscillations in machine variables subside in a matter of two or three seconds and the machine establishes the new steady-state operating point within eight to ten seconds. In the case of the steam-turbine generator (Fig. 5.9-5), the oscillations subside rapidly but the new steady-state operating point is slowly approached. The damping is,

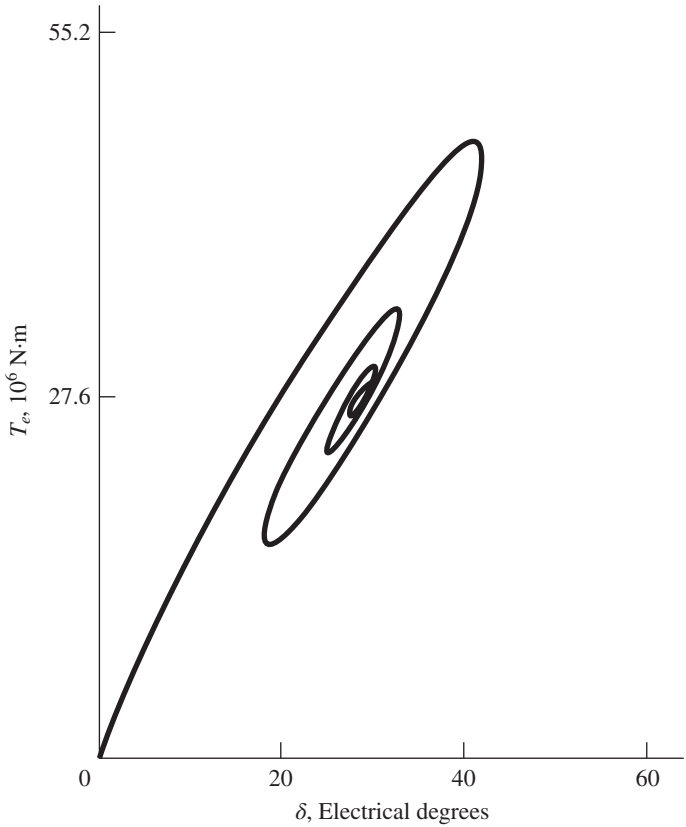

Figure 5.9-5 Torque versus rotor-angle characteristics for the study shown in Fig, 5.9–4.

of course, a function of the damper windings and can be determined from an eigenvalue analysis. The point of interest here is the time required for the machine variables to reestablish steady-state operation after the torque disturbance. This rather slow approach to the new steady-state operating point in the case of the steam-turbine generator is also apparent from the plot of T_e versus δ (Fig. 5.9-7).

Let us consider, for a moment, the expression for steady-state torque, (5.8-22) (remember to change the sign). For the hydro-turbine generator with $E'^{r}_{xfd} = \sqrt{\frac{2}{3}}\,20\,\text{kV}$

$$T_e = (32.5 \sin\delta + 12.5 \sin 2\delta) \times 10^6\ \text{N} \cdot \text{m} \tag{5.9-6}$$

and for the steam-turbine generator with $E'^{r}_{xfd} = \sqrt{\frac{2}{3}}\,26\,\text{kV}$

$$T_e = 1.23 \times 10^6\ \sin\ \delta\ \text{N} \cdot \text{m} \tag{5.9-7}$$

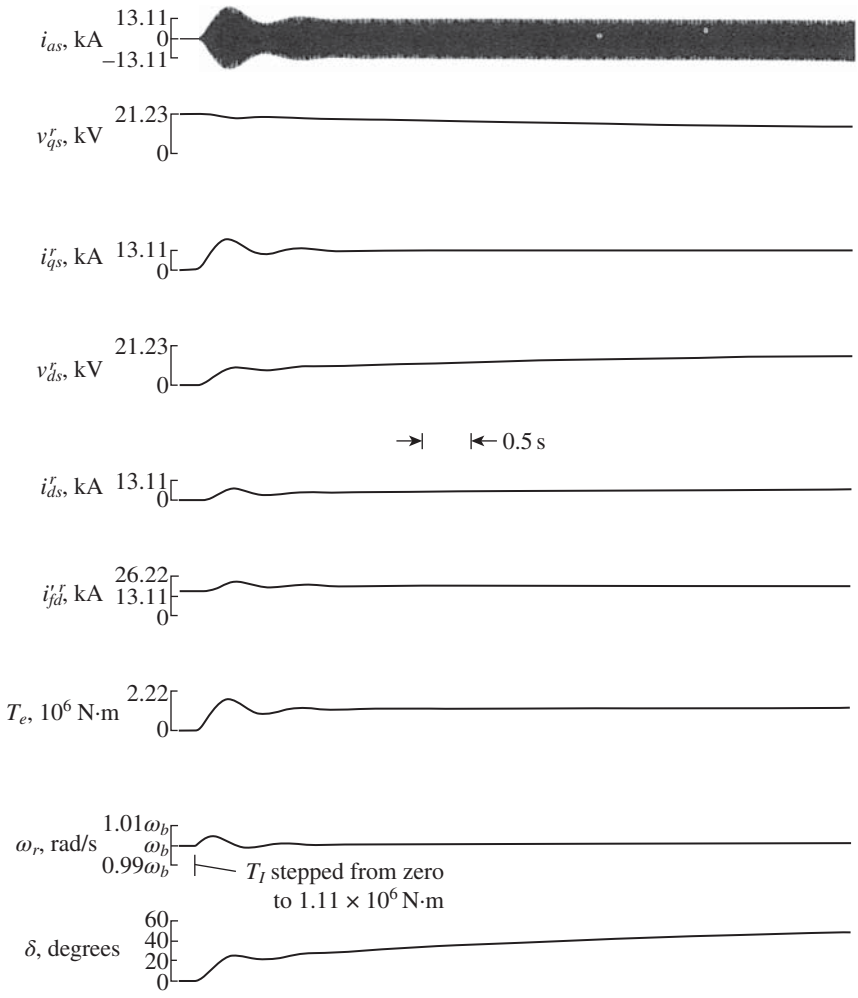

Figure 5.9-6 Dynamic performance of a steam-turbine generator following a step increase in input torque.

The steady-state T_e versus δ curves will pass through the final value of the dynamic T_e versus δ plots of Figs. 5.9-5 and 5.9-7. However, the dynamic torque versus angle characteristics immediately following the input torque disturbance yields a much larger T_e for a given value of δ than does the steady-state characteristic. In other words, the dynamic or transient torque versus angle characteristic, which can only be established by solving nonlinear differential equations, is

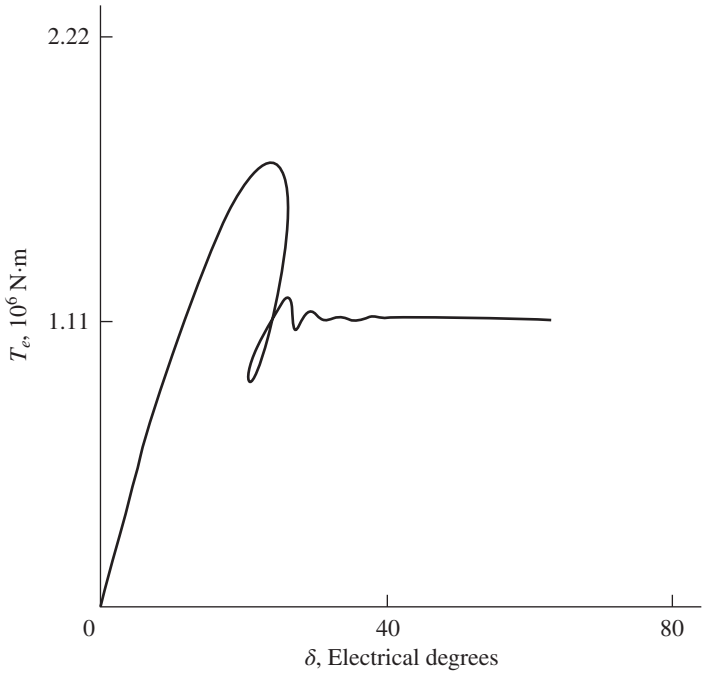

Figure 5.9-7 Torque versus rotor-angle characteristics for the study shown in Fig. 5.9-6.

considerably different from the steady-state characteristic and the steady-state T_e versus δ curve applies only after all transients have subsided [4].

5.9.2 Dynamic Performance during a Three-Phase Fault at the Machine Terminals

The stability of synchronous machines throughout the power system following a fault is of major concern. A three-phase fault or short-circuit rarely occurs and a three-phase fault at the machine terminals is even more uncommon; nevertheless, it is instructive to observe the dynamic performance of a synchronous machine during this type of fault.

The computer traces shown in Figs. 5.9-8 and 5.9-9 illustrate the dynamic behavior of the hydro-turbine generator during and following a three-phase fault at the terminals. The dynamic behavior of the steam-turbine generator as a result of a three-phase terminal fault is shown in Figs. 5.9-10 and 5.9-11. In Figs. 5.9-8 and 5.9-10, the following variables are plotted: i_{as}, v^r_{qs}, i^r_{qs}, v^r_{ds}, i^r_{ds}, i'^r_{fd}, T_e, ω_r, and δ. Figures 5.9-9 and 5.9-11 illustrate the dynamic torque versus angle characteristics during and following the three-phase fault. In each case, the machine is initially

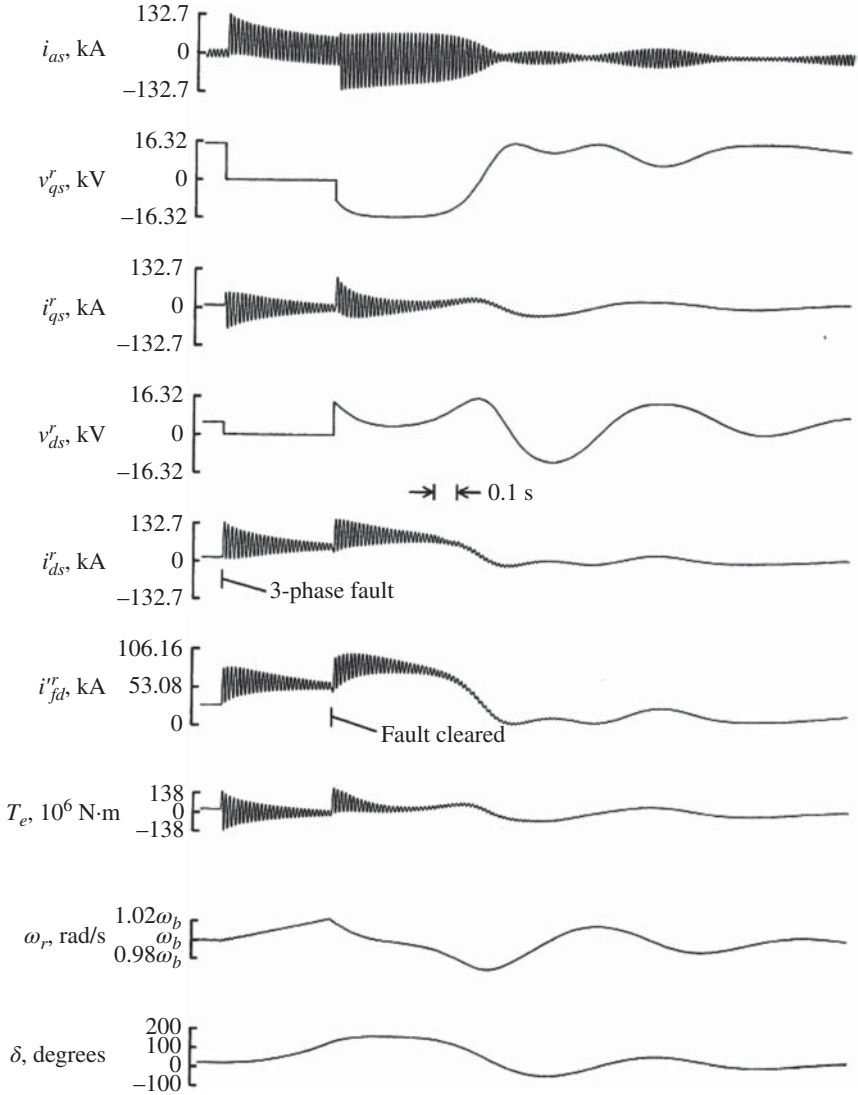

Figure 5.9-8 Dynamic performance of a hydro-turbine generator during and following a three-phase fault at the terminals.

connected to an infinite bus delivering rated MVA at rated power factor. In the case of the hydro-turbine generator, the input torque is held constant at (0.85) 27.6×10^6 N·m with E'^r_{xfd} fixed at (1.6)$\sqrt{\frac{2}{3}}$ 20 kV; for the steam-turbine generator

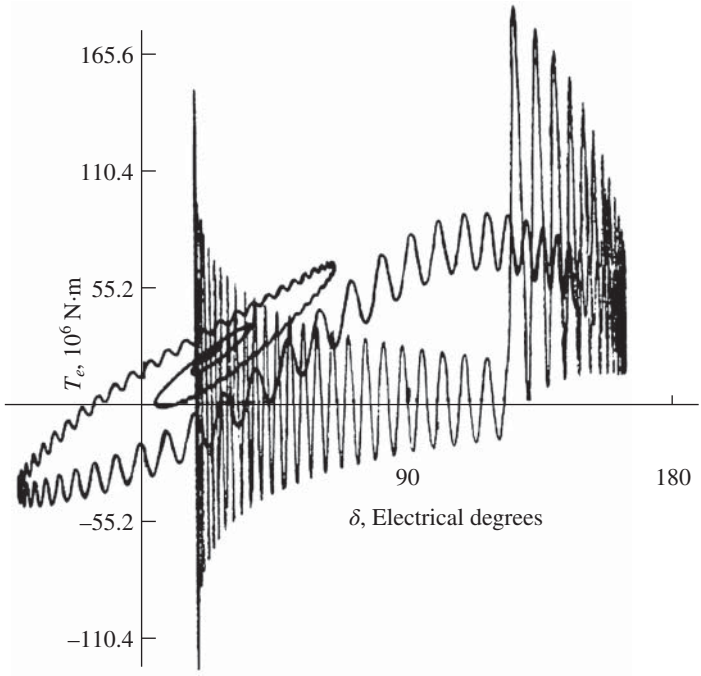

Figure 5.9-9 Torque versus rotor-angle characteristics for the study shown in Fig. 5.9-8.

$T_I = (0.85)2.22 \times 10^6$ N·m and $E''^r_{xfd} = (2.48)\sqrt{\frac{2}{3}}$ 26 kV. (Rated operating conditions for the hydro-turbine generator are calculated in Example 5B.) With the machines operating in this steady-state condition, a three-phase terminal fault is simulated by setting v_{as}, v_{bs}, and v_{cs} to zero at the instant v_{as} passes through zero going positive. The transient offset in the phase currents is reflected into the rotor reference frame variables and the instantaneous torque as a decaying 60 Hz pulsation. Since the terminal voltage is zero during the three-phase fault, the machine is unable to transmit power to the system. Hence, all of the input torque, with the exception of the ohmic losses, accelerates the rotor.

In the case of the hydro-turbine generator, the fault is removed in 0.466 seconds, 0.362 seconds in the case of the steam-turbine generator. If the fault had been allowed to remain on the system slightly longer, the machines would have become unstable, that is, they would either not have returned to synchronous speed after removal of the fault or slipped poles before returning to synchronous speed.

When the fault is cleared, the system voltages are reapplied to the machine; offsets again occur in the phase currents giving rise to the decaying 60 Hz oscillations in the rotor reference frame variables and the instantaneous torque. The dynamic

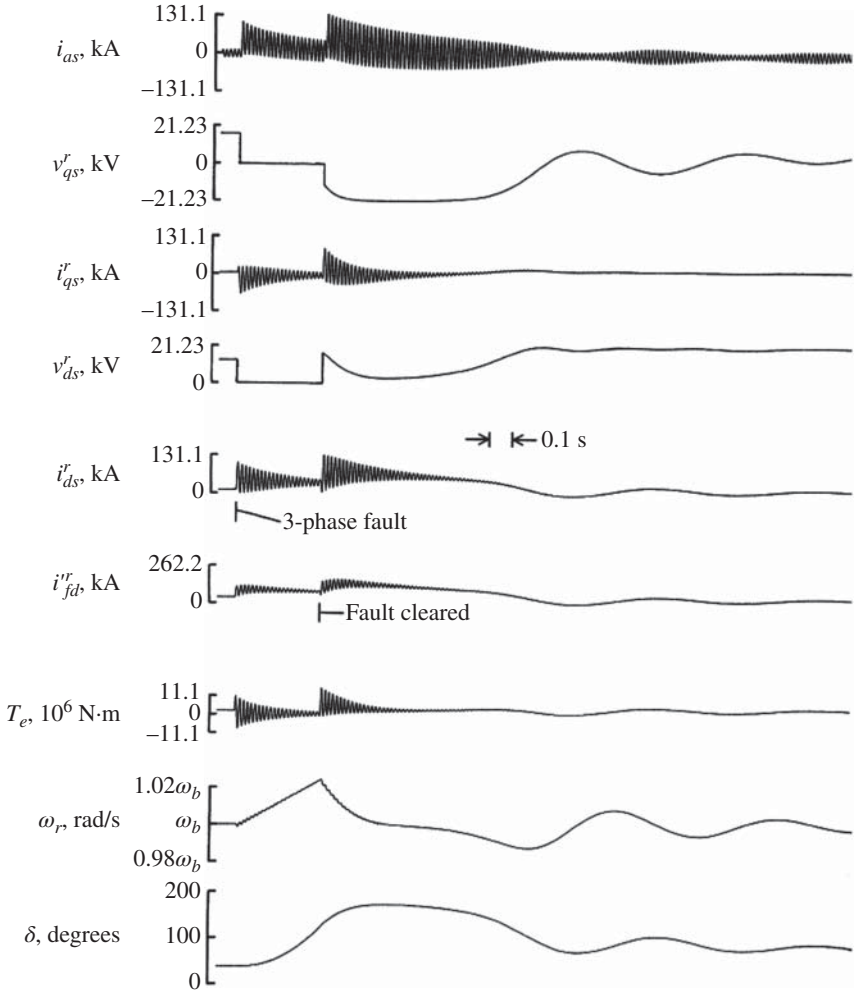

Figure 5.9-10 Dynamic performance of a steam-turbine generator during and following a three-phase fault at the terminals.

torque versus angle characteristics shown in Figs. 5.9-9 and 5.9-11 yield a very lucid illustration of the fault and switching sequence and the return of the machine to its original operating condition after the fault is cleared. The torque versus angle plots of the steam-turbine generator are shown later with the stator electric transients neglected, which eliminates the 60 Hz pulsating electromagnetic torque and permits the average torque to be more clearly depicted.

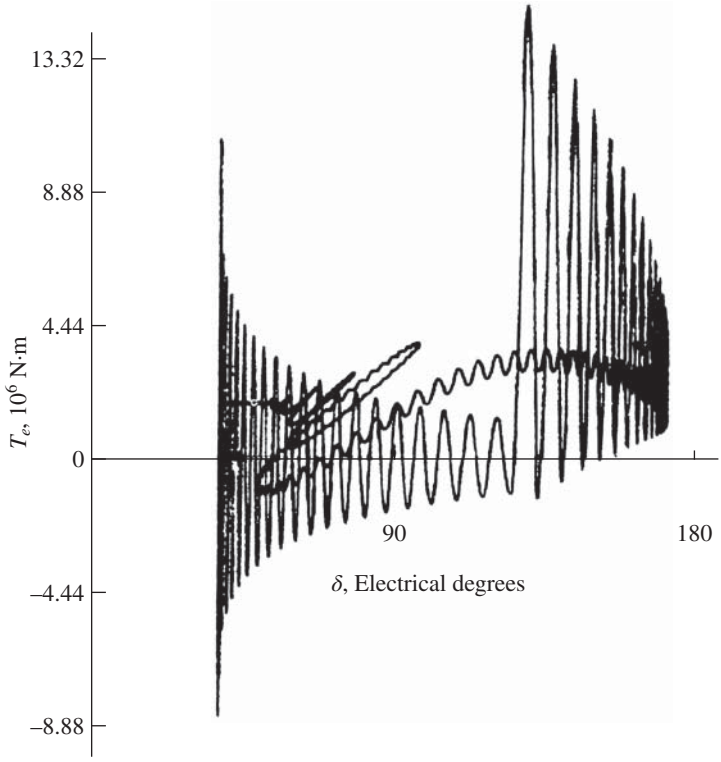

Figure 5.9-11 Torque versus rotor-angle characteristics for the study shown in Fig. 5.9-10.

It is perhaps appropriate to mention that this example is somewhat impractical. In the case of a three-phase fault close to a fully loaded machine, the circuit breakers would likely remove the machine from the system and reclosing would be prohibited since the machine would accelerate beyond speed limits before it would be physically possible to reclose the circuit breakers. A practical situation that is approximated by the example might be a three-phase fault on a large transmission line close to the machine terminals. Clearing or "switching out" of this line would then remove the fault from the system. However, the generator remains connected to the system through other unfaulted transmission lines.

The expression for the steady-state torque versus angle characteristic for the hydro-turbine generator is

$$T_e = (52.1 \sin \delta + 12.5 \sin 2\delta) \times 10^6 \text{ N} \cdot \text{m} \tag{5.9-8}$$

For the steam-turbine generator

$$T_e = 3.05 \times 10^6 \sin \delta \, \text{N} \cdot \text{m} \tag{5.9-9}$$

If these steady-state torque versus angle characteristics are plotted in Figs. 5.9-9 and 5.9-11, respectively, they would pass through only the initial or final steady-state operating point. As in the case of a sudden change in input torque, the instantaneous and/or average value of the dynamic or transient torque versus angle characteristics differ markedly from the steady-state torque versus angle characteristics.

The approximate torque versus angle characteristics were used to study transient stability of power systems before the advent of the computer. This method along with Equal-Area Criterion is covered in [3, 4]. We will not cover these methods that have long since been replaced by the computer.

References

1 R. H. Park, "Two-Reaction Theory of Synchronous Machines – Generalized Method of Analysis – Part I," *AIEE Trans.*, Vol. 48, July 1929, pp. 716–727.

2 D. R. Brown and P. C. Krause, "Modeling of Transient Electrical Torques in Solid Iron Rotor Turbogenerators," *IEEE Trans. Power Apparatus Systems*, Vol. 98, September/October 1979, pp. 1502–1508.

3 P. C. Krause, O. Wasynczuk, and S. D. Sudhoff, *Analysis of Electric Machinery*, IEEE Press, Piscataway, NJ, 1995.

4 R. E. Doherty and C. A. Nickle, "Synchronous Machines – III, Torque-Angle Characteristics Under Transient Conditions," *AIEE Trans.*, Vol. 46, January 1927, pp. 1–8.

Problems

5.1 A two-pole two-phase, salient-pole synchronous machine is shown in Fig. 5P-1. In case of a two-phase machine, the magnetizing inductances are defined as

$$L_{mq} = L_A - L_B$$

$$L_{md} = L_A + L_B$$

Write the voltage and flux linkage equations in the rotor reference frame.

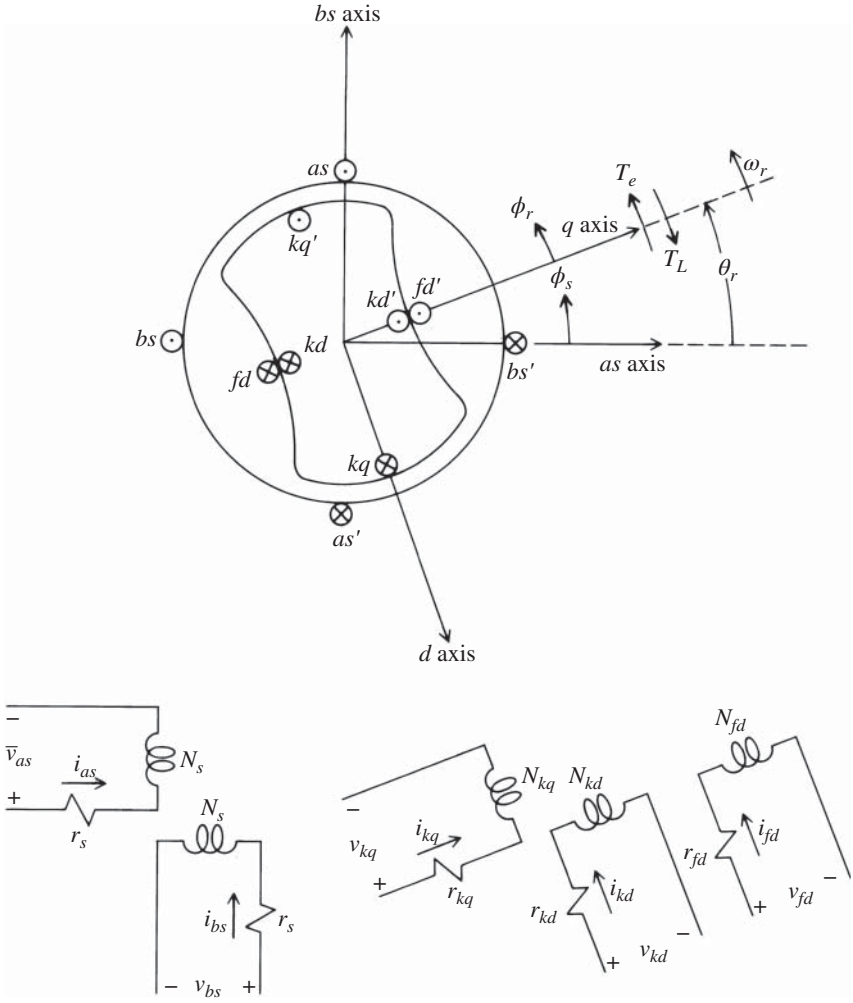

Figure 5P-1 Two-pole, two-phase synchronous machine.

5.2 In the case of a three-phase synchronous machine, L_{Mq} and L_{Md} are defined with a 3/2 factor. This factor is unity in the case of the two-phase machine. Why?

5.3 Modify the voltage equations in Problem 1 to describe a two-phase reluctance machine with damper windings.

5.4 Derive the expression for electromagnetic torque in machine variables for the two-phase synchronous machine shown in Fig. 5P-1.

5.5 Determine $\mathbf{K}_s\mathbf{L}_{ss}(\mathbf{K}_s)^{-1}$ for the machine shown in Fig. 5P-1. Show that θ must equal θ_r for the result to be a constant matrix.

5.6 Repeat Problem 5 for $\left(\mathbf{L}'_{sr}\right)^T\left(\mathbf{K}_s^r\right)^{-1}$.

5.7 Express the transformation of stator variables from the arbitrary reference frame into the rotor reference frame in terms of θ and θ_r.

5.8 What are the differences between Park's stator voltage equations and (5.3-8)–(5.3-10).

5.9 Consider the hydro-turbine generator given in Section 5.9. Select the rated MVA as the base power. Determine the base voltage, base current, and base impedance. Check the parameters given in per unit.

5.10 Repeat Problem 9 for the steam turbine generator given in Section 5.9.

5.11 Modify the steady-state voltage and torque equations for the synchronous machine given in Section 5.8 for the machine shown in Fig. 5P-1.

5.12 A four-pole three-phase salient-pole synchronous machine is supplied from a 440 V (rms) line-to-line, 60 Hz source. The machine is operated as a motor with a total input power of 40 kW at the terminals. The parameters are

$$r_s = 0.3\,\Omega \qquad L_{Md} = 0.015\,\text{H}$$
$$L_{ls} = 0.001\,\text{H} \qquad L_{Mq} = 0.008\,\text{H}$$

Assume the positive direction of current is into the stator terminals.

(a) The excitation is adjusted so that $\tilde{I}_{as}$ lags $\tilde{V}_{as}$ by 30°. Calculate $\tilde{E}_a$ and the reactive power Q. Draw the phasor diagram.
(b) Repeat a with the excitation adjusted so that $\tilde{I}_{as}$ is in phase with $\tilde{V}_{as}$.
(c) Repeat a with the excitation adjusted so that $\tilde{I}_{as}$ leads $\tilde{V}_{as}$ by 30°.

5.13 A two-pole, 220 V (rms, line-to-line), 5 hp., three-phase reluctance motor has the following parameters:

$$r_s = 1\,\Omega \qquad L_{Md} = 0.10\,\text{H}$$
$$L_{ls} = 0.005\,\text{H} \qquad L_{Mq} = 0.02\,\text{H}$$

(a) The machine is supplied from 60 Hz, 220 V source with zero load torque. Calculate δ and $\tilde{I}_{as}$.
(b) Repeat *a* with the machine connected to a 6 Hz, 22 V source.

5.14 The line-to-neutral voltage of phase *a* at one end of a three-phase transmission line is $\tilde{V}_{a1} = V_1\underline{/\theta_1}$. At the other end, $\tilde{V}_{a2} = V_2\underline{/\theta_2}$. The per phase impedance of the transmission line is X_l. Derive an expression for the steady-state power flowing over the transmission line in terms of V_1, V_2, θ_1, θ_2, and X_l.

5.15 The stator terminals of two synchronous machines are connected in a phase-to-phase arrangement. Let $\tilde{E}_{a1} = E_{a1}\underline{/\delta_1}$ and $\tilde{E}_{a2} = E_{a2}\underline{/\delta_2}$. Derive an expression for the steady-state power flowing between the two machines in terms of E_{a1}, E_{a2}, δ_1, δ_2, and the appropriate reactances of each machine. Neglect the stator resistance of both machines.

5.16 Calculate the steady-state $\tilde{I}_{as}$ and δ for the hydro-turbine generator for the final operating condition depicted in Figs. 5.9-4 and 5.9-5.

5.17 Repeat Problem 16 for the final operating conditions for the steam-turbine generator depicted in Figs. 5.9-6 and 5.9-7.

5.18 Calculate the initial, prefault values of all variables of the steam-turbine generator for the condition shown in Fig. 5.9-10.

6

Neglecting Electric Transients

6.1 Introduction

In transient stability studies, the stator and network electric transients are generally neglected. The network is generally simulated in the synchronous reference frame with the $p\lambda$ terms neglected. This eliminates the need to integrate for each inductance in the network. Since the synchronous machine must be simulated in the rotor reference frame, there was a question as to what terms should be neglected in these equations in order to neglect the electric transients in the stator when $\omega_r \neq \omega_e$. This chapter is devoted to this subject starting with neglecting stator transients in the arbitrary reference frame. This is the last chapter that we will deal with power system concerns.

Now in order to do this, we must disregard the rotor circuits since in the case of the synchronous machine, the rotor circuits are not transformed to any reference frame other than the rotor. This of course is not the case with an induction machine where both the stator and rotor circuits may be transformed to the arbitrary reference frame. Therefore, neglecting stator transients in the stator of a synchronous machine allows us to neglect the transients associated with the stator but not the transients associated with the rotor circuit variables.

6.2 Neglecting Stator Electric Transients

The theory of neglecting electric transients is set forth in [1]. To establish this theory, let us return for a moment to the work in Section 2.4 where the variables associated with the stator resistance and inductance elements were transformed to the arbitrary reference frame. It is obvious that the instantaneous voltage equations for the three-phase resistance are in the same form for either transient or steady-state conditions. However, it is not obvious that the equations describing the behavior of a three-phase inductance with the electric transients neglected

Analysis of Electric Machinery and Drive Systems, Fourth Edition.
Paul C. Krause, Oleg Wasynczuk, Scott D. Sudhoff, and Steven D. Pekarek.

Companion website: www.wiley.com/go/krause_aem4e

(steady-state behavior) may be arranged so that the instantaneous voltages and currents are related algebraically without the operator d/dt.

First, let us express the voltage equations of a symmetrical stator, which includes the synchronous and induction machines, in the synchronously rotating reference frame. From (2.4-12) and (2.4-13) with $\omega = \omega_e$.

$$v_{qs}^e = r_s i_{qs}^e + \omega_e \lambda_{ds}^e + p\lambda_{qs}^e \tag{6.2-1}$$

$$v_{ds}^e = r_s i_{ds}^e - \omega_e \lambda_{qs}^e + p\lambda_{ds}^e \tag{6.2-2}$$

We are not including the unsymmetrical rotor circuits. For balanced steady-state conditions, the variables in the synchronously rotating reference frame are constants. Hence, we can neglect the electric transients by neglecting the last terms of (6.2-1) and (6.2-2) that is $p\lambda_{qs}^e$ and $p\lambda_{ds}^e$. Our purpose is to obtain algebraically related instantaneous voltage equations in the arbitrary reference frame that may be used to portray the behavior with the stator electric transients neglected (steady-state behavior). To this end, it is helpful to determine the arbitrary reference frame equivalent of neglecting $p\lambda_{qs}^e$ and $p\lambda_{ds}^e$. This may be accomplished by noting from (2.5-1) that the synchronous rotating and arbitrary reference frame variables are related by

$$\mathbf{f}_{qd0s} = {}^e\mathbf{K}_s \, \mathbf{f}_{qd0s}^e \tag{6.2-3}$$

Now from (2.5-7) and since this is valid only for balanced conditions the f_{0s} does not exist.

$${}^e\mathbf{K} = \begin{bmatrix} \cos\alpha & -\sin\alpha \\ \sin\alpha & \cos\alpha \end{bmatrix} \tag{6.2-4}$$

and

$${}^e\mathbf{K}^{-1} = \begin{bmatrix} \cos\alpha & \sin\alpha \\ -\sin\alpha & \cos\alpha \end{bmatrix} \tag{6.2-5}$$

where α is $(\theta - \theta_e)$. It is recalled that the arbitrary reference frame variables do not carry a raised index. We understand that the stator is a symmetrical system that can be expressed in an arbitrary reference frame.

The voltage equations in the arbitrary reference frame may be expressed from (6.2-3) as

$$\mathbf{v}_{qd0s} = {}^e\mathbf{K} \, \mathbf{v}_{qd0s}^e \tag{6.2-6}$$

Since there is no v_{0s}, we have

$$\begin{aligned} \mathbf{v}_{qds} = {} & {}^e\mathbf{K} r_s \, ({}^e\mathbf{K})^{-1} \mathbf{i}_{qds} + {}^e\mathbf{K} \, ({}^e\mathbf{K})^{-1} \omega_e \begin{bmatrix} \lambda_{ds} \\ -\lambda_{qs} \end{bmatrix} \\ & + {}^e\mathbf{K} p \, ({}^e\mathbf{K})^{-1} \boldsymbol{\lambda}_{qds} + {}^e\mathbf{K} \, ({}^e\mathbf{K})^{-1} p\boldsymbol{\lambda}_{qds} \end{aligned} \tag{6.2-7}$$

Now the third and fourth terms on the right-hand side are due to neglecting $p\lambda^e_{qds}$ of the stator that must be set to zero. Thus,

$$v_{qs} = r_s i_{qs} + \omega_e \lambda_{ds} \tag{6.2-8}$$

$$v_{ds} = r_s i_{ds} - \omega_e \lambda_{qs} \tag{6.2-9}$$

What have we done? Well, since the stator is assumed to be a symmetrical system, the voltage equations in the arbitrary reference frame are

$$v_{qs} = r_s i_{qs} + \omega \lambda_{ds} + p\lambda_{qs} \tag{6.2-10}$$

$$v_{ds} = r_s i_{ds} - \omega \lambda_{qs} + p\lambda_{ds} \tag{6.2-11}$$

Now with $p\lambda^e_{qd0s}$ of the stator neglected, the voltage equations in the arbitrary reference frame are (6.2-8) and (6.2-9). We have replaced the last two terms of (6.2-10) with $\omega_e \lambda_{ds}$ and the last two terms of (6.2-11) with $-\omega_e \lambda_{qs}$.

For a three-phase coupled circuit with no rotor windings in the arbitrary reference frame

$$\lambda_{qs} = L_{Ms} i_{qs} \tag{6.2-12}$$

$$\lambda_{ds} = L_{Ms} i_{ds} \tag{6.2-13}$$

In summary, the arbitrary reference frame voltage equations have been established for inductive circuits with the electric transients neglected, by neglecting the change of flux linkages in the synchronously rotating reference frame. However, during unbalanced conditions, such as unbalanced voltages applied to the symmetrical circuits, the voltages in the synchronously rotating reference frame will vary with time. For example, 60 Hz unbalanced stator voltages give rise to a constant and a double-frequency voltage in the synchronously rotating reference frame. Therefore, the flux linkages in the synchronously rotating reference frame will also contain a double-frequency component. It follows that, during unbalanced conditions, neglecting the change in the synchronously rotating reference frame flux linkages results in neglecting something more than just the electric transients. Therefore, the voltage equations that have been derived by neglecting the change in the flux linkages in the synchronously rotating reference frame apply for balanced or symmetrical conditions such as simultaneous application of balanced voltages, a change in either load or input torque, and a three-phase fault. Consequently, the zero quantities are not involved in the machine equations given in this chapter.

It is interesting that if we neglect $p\lambda^e_{qs}$ and $p\lambda^e_{ds}$ in (6.2-1) and (6.2-2) and if we remove the raised "e" on the rest of the terms of (6.2-1) and (6.2-2), we have (6.2-8) and (6.2-9).

6.3 Induction Machine with Stator Transients Neglected

The voltage equations written in the arbitrary reference frame for an induction machine with the electric transients of the stator voltage equations neglected may be written from (3.4-18) through (3.4-34) with the zero quantities eliminated and (6.2-8) and (6.2-9) appropriately taken into account [2].

$$v_{qs} = r_s i_{qs} + \omega_e \lambda_{ds} \tag{6.3-1}$$

$$v_{ds} = r_s i_{ds} - \omega_e \lambda_{qs} \tag{6.3-2}$$

$$v'_{qr} = r'_r i'_{qr} + (\omega - \omega_r)\, \lambda'_{dr} + p\lambda'_{qr} \tag{6.3-3}$$

$$v'_{dr} = r'_r i'_{dr} - (\omega - \omega_r)\, \lambda'_{qr} + p\lambda'_{dr} \tag{6.3-4}$$

where

$$\lambda_{qs} = L_{ls} i_{qs} + L_{Ms} \left(i_{qs} + i'_{qr}\right) \tag{6.3-5}$$

$$\lambda_{ds} = L_{ls} i_{ds} + L_{Ms} \left(i_{ds} + i'_{dr}\right) \tag{6.3-6}$$

$$\lambda'_{qr} = L'_{lr} i'_{qr} + L_{Ms} \left(i_{qs} + i'_{qr}\right) \tag{6.3-7}$$

$$\lambda'_{dr} = L'_{lr} i'_{dr} + L_{Ms} \left(i_{ds} + i'_{dr}\right) \tag{6.3-8}$$

Although the reference frame speed appears in the speed voltages in the rotor voltage equations, it does not appear in the stator voltage equations.

6.3.1 Free-Acceleration Characteristics

The free-acceleration characteristics predicted for the 3- and 2250-hp induction motors with the electric transients neglected in the stator voltage equations are given in Figs. 6.3-1–6.3-4. The parameters and operating conditions are identical to those used in Chapter 3. A comparison of the torque versus speed characteristics shown in Figs. 6.3-1 and 6.3-2 with those shown in Figs. 3.9-1 and 3.9-4 reveals that the only significant difference is in the initial starting transient. Although a transient occurs in the instantaneous starting torque, it is much less pronounced when the stator electric transients are neglected. Our first reaction is to assume that the transient that remains is due to the rotor circuits. Although this is essentially the case, we must be careful with such an interpretation since we are imposing a condition upon the voltage equations that is difficult to be realized in practice. We are aware that the stator electric transient gives rise to a 60 Hz pulsating torque. Since

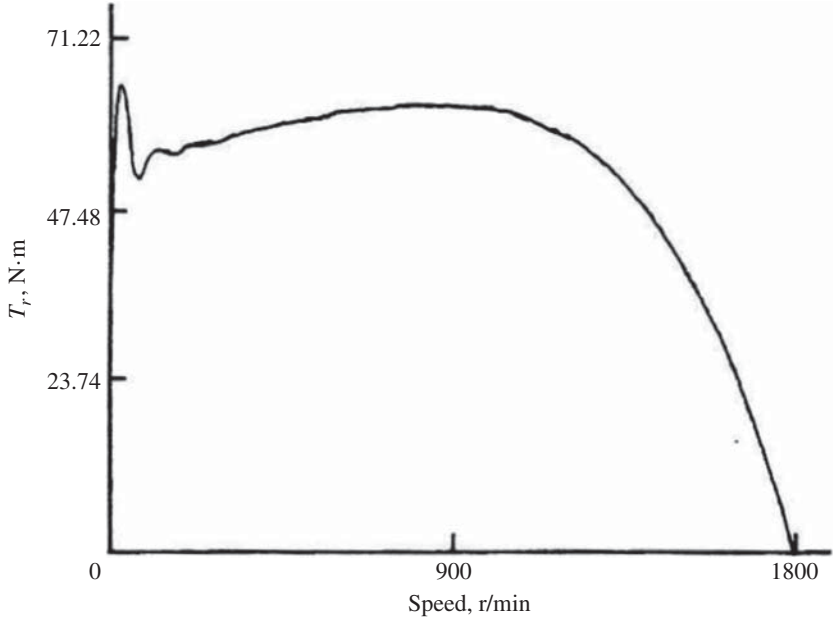

Figure 6.3-1 Torque versus speed characteristics during free acceleration predicted with stator electric transients neglected—3-hp induction motor.

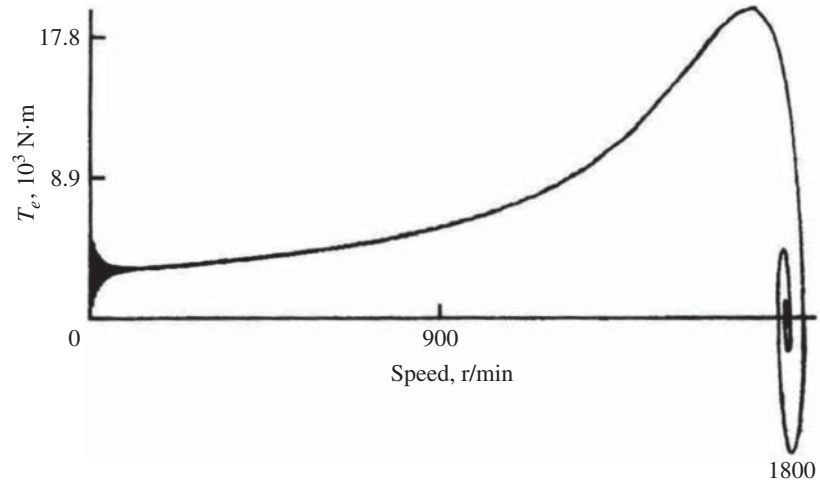

Figure 6.3-2 Torque versus speed characteristics during free acceleration predicted with stator electric transients neglected—2200-hp induction motor.

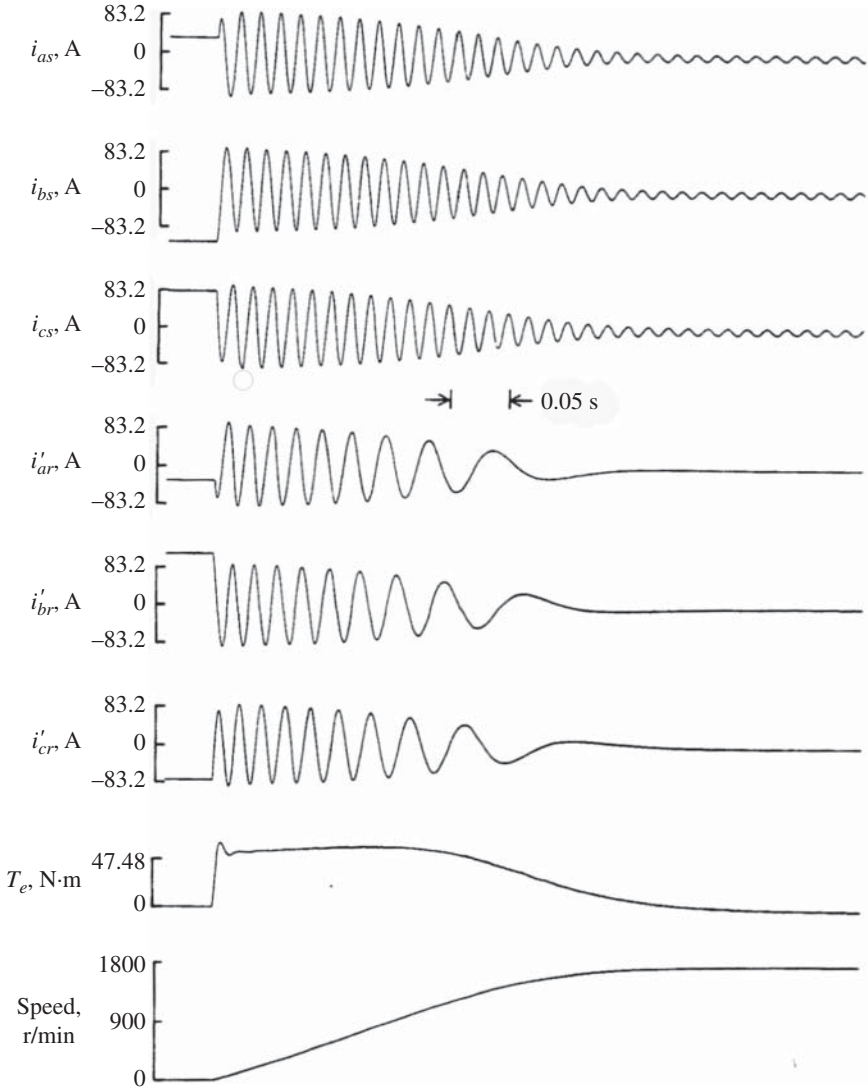

Figure 6.3-3 Machine variables during free acceleration of a 3-hp induction machine predicted with stator electric transients neglected.

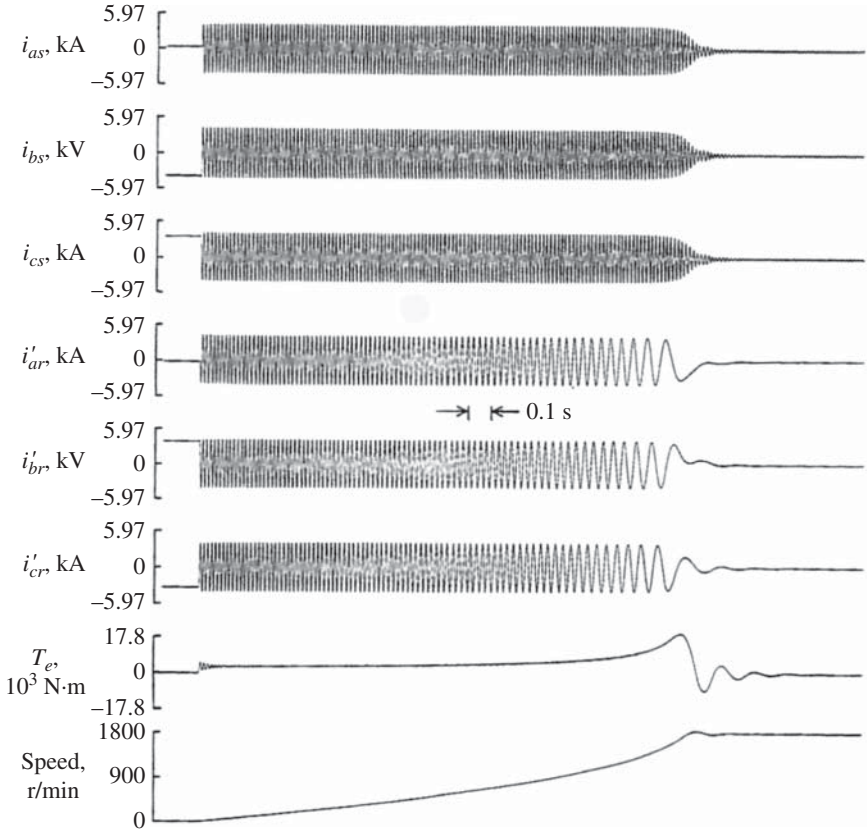

Figure 6.3-4 Machine variables during free acceleration of a 2250-hp induction machine predicted with stator electric transients neglected.

we are neglecting the electric transients in the stator voltage equations, we would expect discrepancies to occur whenever this transient is excited and whenever it influences the behavior of the machine. In effect, this is what we observe when comparing Figs. 6.3-1 and 6.3-4 with Figs. 3.9-1 and 3.9-4. Once the stator electric transient subsides, the torque versus speed characteristics are identical for all practical purposes. For the machine studied, the speed is not significantly influenced by the 60 Hz transient torque during free acceleration. If the inertia was relatively small or if the frequency of the stator voltages was considerably less than rated, as may occur in variable-speed drive systems, the pulsating electromagnetic torque could have a significant influence on the behavior of the machine.

The oscillation about synchronous speed, which is determined primarily by the rotor circuits, is still present as is clearly illustrated in the case of the 2250-hp

machine (Fig. 6.3-2). This oscillation does not occur when the electric transients of the rotor circuits are neglected.

Another interesting feature regarding the transient characteristics of the induction machine is apparent in Figs. 6.3-3 and 6.3-4. The varying envelope of the machine currents during free acceleration does not occur when the stator electric transients are neglected. Therefore, we must conclude that the varying current envelope depicted in Figs. 3.7-5 and 3.7-6 occurs due to the interaction of stator and rotor electric transients.

A word of explanation regarding Figs. 6.3-3 and 6.3-4 is necessary. Although this has no influence upon the solution that follows, we can see the ambiguity that occurs when imposing impossible restrictions upon the behavior of electric circuits. Here, we see that the stator voltages are algebraically related to all machine currents since the stator and rotor currents change instantaneously when the stator voltages are applied in the initial condition mode. It is interesting that this situation, which is impossible practically, does not give rise to an initial torque.

6.4 The Synchronous Machine with Stator Transients Neglected

The stator voltage equations of the synchronous machine written in the arbitrary reference frame are given by (6.2-1) and (6.2-2). As illustrated by (6.2-8) and (6.2-9), the electric transients are neglected in the stator voltage equations by neglecting the derivative of flux linkages in the arbitrary reference frame and setting $\omega = \omega_e$. Thus, with the electric transients neglected, the stator voltage equations of the synchronous machine with positive current assumed out of the terminals of the synchronous machine are of the same form as (6.3-1) and (6.3-2). It follows that the voltage equations for the synchronous machine in the rotor reference frame with the stator electric transients neglected are obtained by neglecting the derivative of the flux linkages in Park's equations and setting $\omega_r = \omega_e$. Thus, with the 0s quantities omitted

$$v_{qs}^{r} = -r_s i_{qs}^{r} + \omega_e \lambda'_{ds} \tag{6.4-1}$$

$$v_{ds}^{r} = -r_s i_{ds}^{r} - \omega_e \lambda_{qs}^{r} \tag{6.4-2}$$

$$v'^{r}_{kq1} = r'^{r}_{kq1} i'^{r}_{kq1} + p\lambda'^{r}_{kq1} \tag{6.4-3}$$

$$v'^{r}_{kq2} = r'^{r}_{kq2} i'^{r}_{kq2} + p\lambda'^{r}_{kq2} \tag{6.4-4}$$

$$v'^{r}_{fd} = r'^{r}_{fd} i'^{r}_{fd} + p\lambda'^{r}_{fd} \tag{6.4-5}$$

$$v'^{r}_{kd} = r'^{r}_{kd} i'^{r}_{kd} + p\lambda'^{r}_{kd} \tag{6.4-6}$$

where

$$\lambda^{r}_{qs} = L_{ls} i^{r}_{qs} + L_{Mq}\left(-i^{r}_{qs} + i'^{r}_{kq1} + i'^{r}_{kq2}\right) \tag{6.4-7}$$

$$\lambda'^{r}_{kq1} = L'_{lkq1} i'^{r}_{kq1} + L_{Mq}\left(-i^{r}_{qs} + i'^{r}_{kq1} + i'^{r}_{kq2}\right) \tag{6.4-8}$$

$$\lambda'^{r}_{kq2} = L'_{lkq2} i'^{r}_{kq2} + L_{Mq}\left(-i^{r}_{qs} + i'^{r}_{kq1} + i'^{r}_{kq2}\right) \tag{6.4-9}$$

$$\lambda'^{r}_{fd} = L'_{lfd} i'^{r}_{fd} + L_{Md}\left(-i^{r}_{ds} + i'^{r}_{fd} + i'^{r}_{kd}\right) \tag{6.4-10}$$

$$\lambda'^{r}_{kd} = L'_{lkd} i'^{r}_{kd} + L_{Md}\left(-i^{r}_{ds} + i'^{r}_{fd} + i'^{r}_{kd}\right) \tag{6.4-11}$$

Also, $L_{Mq} = \frac{3}{2}(L_A - L_B)$ and $L_{Md} = \frac{3}{2}(L_A + L_B)$.

The reduced-order model of the synchronous machine obtained by neglecting the stator electric transients is used widely in the power industry as an analysis tool. Therefore, it is important to compare the performance of the synchronous machine predicted by the reduced-order equations with that predicted by the detailed model (Chapter 5), especially for disturbances common in transient stability studies.

6.4.1 Three-Phase Fault at Machine Terminals

The dynamic behavior of the hydro-turbine generator during and following a three-phase fault at the terminals, predicted with the electric transients neglected in the stator voltage equations, is shown in Figs. 6.4-1 and 6.4-2. The behavior predicted for the steam-turbine generator is shown in Figs. 6.4-3 and 6.4-4. An indication of the accuracy of this reduced-order model can be obtained by comparing the behavior depicted in these figures to that shown in Figs. 5.9-8–5.9-11. The machines and operating conditions are identical in both cases. Initially, each machine is connected to an infinite bus delivering rated MVA at rated power factor. (Machine data are given in Section 5.9.) In the case of the hydro-turbine generator, the input torque is held constant at (0.85) 27.6×10^6 N·m with E'_{xfd} fixed at (1.6)$\sqrt{\frac{2}{3}}$20 kV; for the steam-turbine generator, $T_I = (0.85)\ 2.22 \times 10^6$ N·m and $E'_{xfd} = (2.48)\sqrt{\frac{2}{3}}26$ kV. With the machines operating in this steady-state condition, a three-phase fault at the terminals is simulated by setting v_{as}, v_{bs}, and v_{cs} to zero at the instant v_{as} passes through zero going positive. The instantaneous changes in the machine currents and torque at the initiation and removal

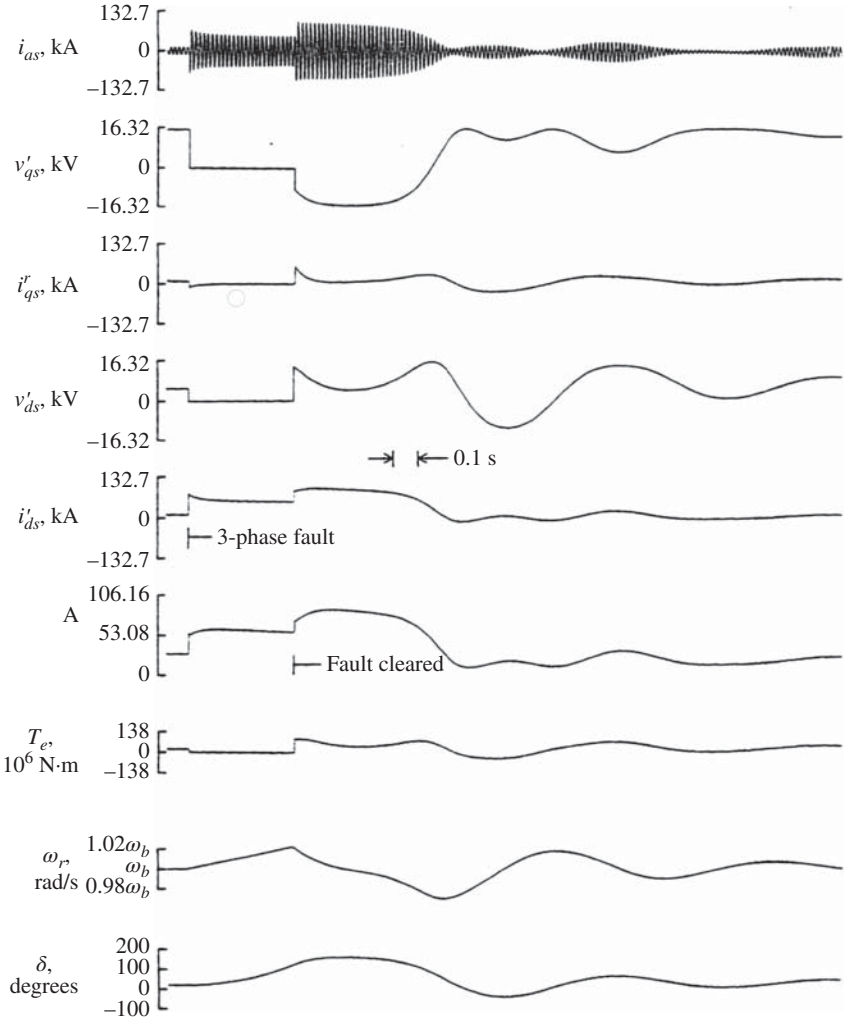

Figure 6.4-1 Dynamic performance of a hydro-turbine generator during a three-phase fault at the terminals predicted with stator transients neglected.

of the fault demonstrate the algebraic relationship between stator voltages and machine currents.

With the stator electric transients neglected, the offset transients do not appear and consequently the 60 Hz pulsating electromagnetic torque is not present during and following the three-phase fault. The absence of the 60 Hz transient torque is especially apparent in the torque versus rotor-angle characteristics given in Figs. 6.4-2 and 6.4-4. These should be compared to Figs. 5.9-9 and 5.9-11.

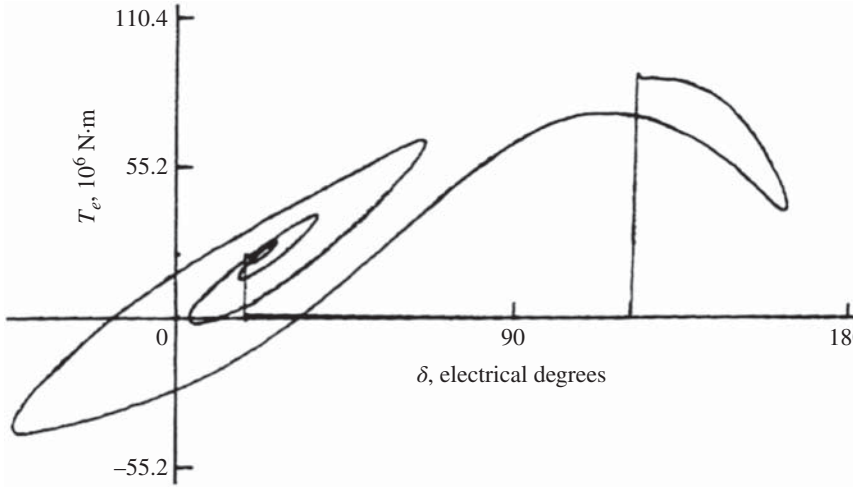

Figure 6.4-2 Torque versus rotor-angle characteristics for the study shown in Fig. 6.4-1.

From all outward appearances, it would seem that other than the pulsating electromagnetic torque there is little difference between the behavior predicted neglecting stator transients or detailed models. Therefore, one would expect the model to be sufficiently accurate in predicting this performance during and following a three-phase fault. There is, however, a difference that occurs when determining the critical clearing time. The situation portrayed in Figs. 5.9-8–5.9-11 and likewise in Figs. 6.4-1–6.4-4 is one where only a slight increase in the fault time would cause the machines to become unstable. That is, if the three-phase fault were allowed to persist slightly longer, the rotor speed would not return to synchronous after the fault is cleared. Using the detailed model in Chapter 5, this critical clearing time was determined to be 0.466 s for the hydro unit and 0.362 s for the steam unit. For the reduced model, the critical clearing time for the hydro unit is 0.424 s and 0.334 s for the steam unit. The longer critical clearing times predicted by the detailed models are due primarily to the pulsating 60 Hz torque that occurs immediately following the occurrence of the fault. The initial torque pulsation causes the rotor to slow down very slightly, which has the effect of delaying the increase in the "average" rotor speed. This effect can be observed in Figs. 5.9-8 and 5.9-10 where the rotor speed remains at ω_e longer than in Figs. 6.4-1 and 6.4-3. With the stator electric transients neglected, the 60 Hz pulsating torque is absent and hence the initial "backswing" does not occur [3]. There are two points that warrant mentioning in defense of this apparent inaccuracy of the reduced-order model. First, it will typically yield conservative results. Second, a three-phase fault seldom if ever occurs instantaneously. That

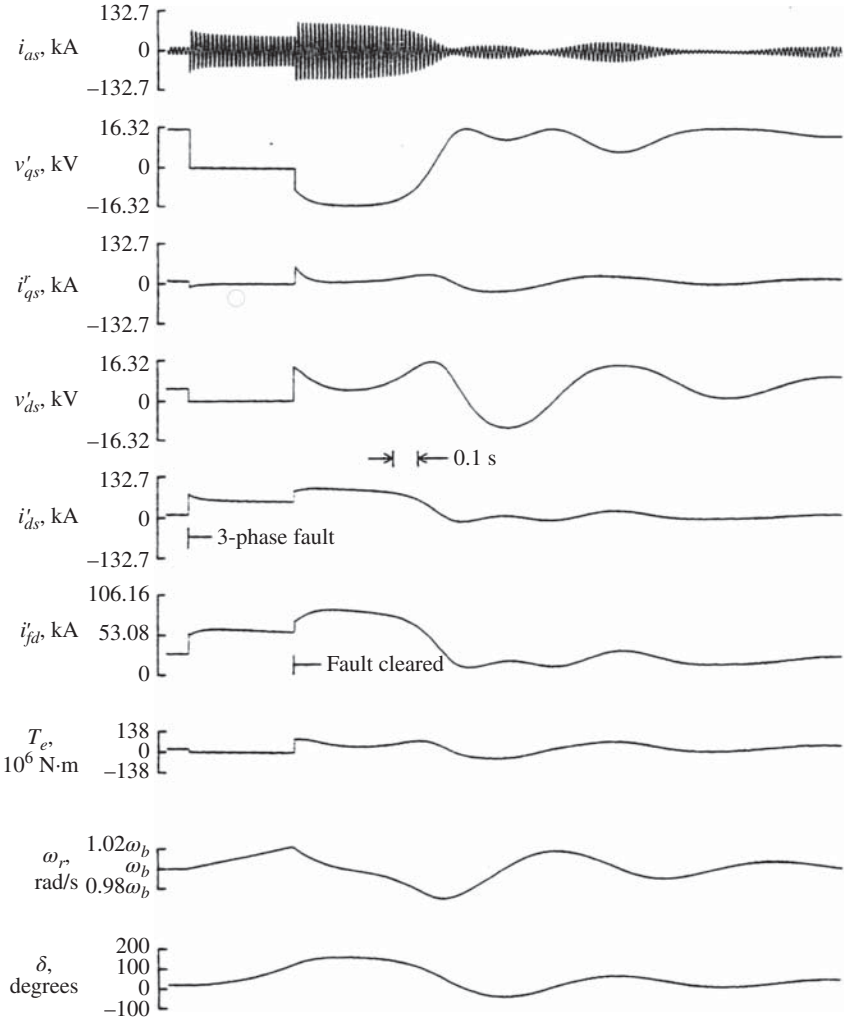

Figure 6.4-3 Dynamic performance of a steam-turbine generator during a three-phase fault at the terminals predicted with stator transients neglected.

is, a fault generally starts as a single line-to-ground or as a phase-to-phase fault, and then it may progress rapidly to a three-phase fault. Hence, the instantaneous pulsation in electromagnetic torque is generally not sufficient in the practical case to cause the slowing down of the rotor as depicted in Figs. 5.9-8 and 5.9-10. In this regard, the effect of the 60 Hz pulsating torque resulting from an instantaneous three-phase fault is perhaps more of academic than of practical interest.

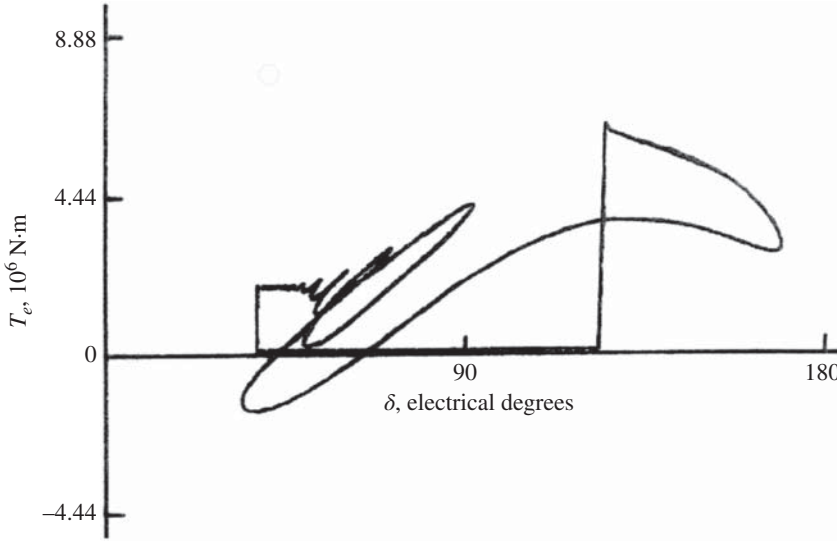

Figure 6.4-4 Torque versus rotor-angle characteristics for the study shown in Fig. 6.4-3.

References

1 P. C. Krause, F. Nozari, T. L. Skvarenina, and D. W. Olive, "The Theory of Neglecting Stator Transients," *IEEE Trans. Power Apparatus and Systems*, Vol. 98, January/February 1979, pp. 141–148.

2 T. L. Skvarenina and P. C. Krause, "Accuracy of a Reduced Order Model of Induction Machines in Dynamic Stability Studies," *IEEE Trans. Power Apparatus and Systems*, Vol. 98, July/August 1979, pp. 1192–1197.

3 R. G. Harley and B. Adkins, "Calculations of the Angular Back Swing Following a Short-Circuit of a Loaded Alternator," *Proc. IEE*, Vol. 117, No. 2, February 1970, pp. 377–386.

Problems

6.1 Express the rotor voltage equations of an induction machine in the arbitrary reference frame with the stator and rotor electric transients neglected.

6.2 Neglect the electric transients in the stator and rotor of a synchronous machine. From these voltage equations, derive the familiar steady-state voltage equation given by (5.8-17).

6.3 In the chapter, we have considered only three-phase machines. Explain the changes that must be made so that this material will apply to *(a)* two-phase induction machines and *(b)* two-phase synchronous machines.

6.4 Is it appropriate to neglect stator transients when analyzing an induction machine with unbalanced stator applied voltages? Why?

7

Machine Equations in Operational Impedances and Time Constants

7.1 Introduction

In Chapter 5, we assumed that the electrical characteristics of the rotor of a synchronous machine could be portrayed by two windings in each axis. This type of a representation is sufficient for most applications; however, there are instances where a more refined model may be necessary. For example, when representing solid iron rotor machines, it may be necessary to use three or more rotor windings in each axis so that transient dynamics are accurately represented. This may also be required to accurately capture switching dynamics when modeling machine/rectifier systems.

R. H. Park [1], in his original paper, did not specify the number of rotor circuits. Instead, he expressed the stator flux linkages in terms of operational impedances and a transfer function relating stator flux linkages to field voltage. In other words, Park recognized that, in general, the rotor of a synchronous machine appears as a distributed parameter system when viewed from the stator. The fact that an accurate, equivalent lumped parameter circuit representation of the rotor of a synchronous machine might require two, three, or four damper windings was more or less of academic interest until digital computers became available. Prior to the 1970s, the damper windings were seldom considered in stability studies; however, as the capability of computers increased, it became desirable to represent the machine in more detail.

The standard short-circuit test, which involves monitoring the stator short-circuit currents, provides information from which the parameters of the field winding and one damper winding in the d-axis can be determined. The parameters for the q-axis damper winding are calculated from design data. Due to the need for more accurate parameters, frequency–response data are now being used as means of measuring the operational impedances from which the parameters can be obtained for any number of rotor windings in both axes.

Analysis of Electric Machinery and Drive Systems, Fourth Edition.
Paul C. Krause, Oleg Wasynczuk, Scott D. Sudhoff, and Steven D. Pekarek.

Companion website: www.wiley.com/go/krause_aem4e

In this chapter, the operational impedances as set forth by Park [1] are described. The standard and derived synchronous machine time constants are defined and their relationship to the operational impedances established. Finally, a method of approximating the measured operational impedances by lumped parameter rotor circuits is presented. It is important to note that, for notational convenience, the magnetizing reactances will be denoted in this chapter as X_{mq} and X_{md} for both two- and three-phase synchronous machines.

7.2 Park's Equations in Operational form

R.H. Park [1] published the original $qd0$-voltage equations in the form

$$v_{qs}^{r} = -r_s i_{qs}^{r} + \frac{\omega_r}{\omega_b}\psi_{ds}^{r} + \frac{p}{\omega_b}\psi_{qs}^{r} \tag{7.2-1}$$

$$v_{ds}^{r} = -r_s i_{ds}^{r} - \frac{\omega_r}{\omega_b}\psi_{qs}^{r} + \frac{p}{\omega_b}\psi_{ds}^{r} \tag{7.2-2}$$

$$v_{0s} = -r_s i_{0s} + \frac{p}{\omega_b}\psi_{0s} \tag{7.2-3}$$

where

$$\psi_{qs}^{r} = -X_q(p) i_{qs}^{r} \tag{7.2-4}$$

$$\psi_{ds}^{r} = -X_d(p) i_{ds}^{r} + G(p) v'^{r}_{fd} \tag{7.2-5}$$

$$\psi_{0s} = -X_{ls} i_{0s} \tag{7.2-6}$$

In these equations, positive stator current is assumed out of the machine, the operator $X_q(p)$ is referred to as the q-axis operational impedance, $X_d(p)$ is the d-axis operational impedance, and $G(p)$ is a dimensionless transfer function relating stator flux linkages per second to field voltage.

With the equations written in this form, the rotor of a synchronous machine can be considered as either a distributed or lumped parameter system. Over the years, the electrical characteristics of the rotor have often been approximated by three lumped parameter circuits, one field winding and two damper windings, one in each axis. Although this type of representation is generally adequate for salient-pole machines, it does not suffice for a solid iron rotor machine. It now appears that for dynamic and transient stability considerations, at least two and perhaps three damper windings should be used in the q-axis for solid rotor machines with a field and two damper windings in the d-axis [2].

7.3 Operational Impedances and $G(P)$ for a Synchronous Machine with Four Rotor Windings

In Chapter 5, the synchronous machine was represented with a field winding and one damper winding in the d-axis and with two damper windings in

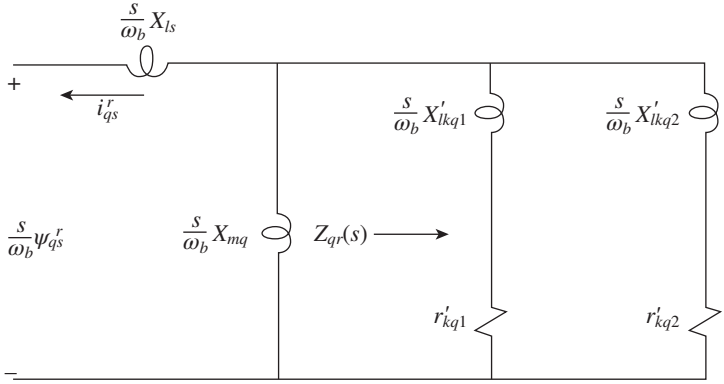

Figure 7.3-1 Equivalent circuit with two damper windings in the quadrature axis.

the q-axis. It is helpful to determine $X_q(p)$, $X_d(p)$, and $G(p)$ for this type of rotor representation before deriving the lumped parameter approximations from measured frequency-response data. For this purpose, it is convenient to consider the network shown in Figure 7.3-1. It is helpful in this and in the following derivations to express the input impedance of the rotor circuits in the form

$$Z_{qr}(s) = R_{eq}\frac{(1+\tau_{qa}s)(1+\tau_{qb}s)}{(1+\tau_{Qa}s)} \tag{7.3-1}$$

Since it is customary to use the Laplace operator s rather than the operator p, Laplace notation will be employed hereafter. In (7.3-1)

$$R_{eq} = \frac{r'_{kq1}r'_{kq2}}{r'_{kq1}+r'_{kq2}} \tag{7.3-2}$$

$$\tau_{qa} = \frac{X'_{lkq1}}{\omega_b r'_{kq1}} \tag{7.3-3}$$

$$\tau_{qb} = \frac{X'_{lkq2}}{\omega_b r'_{kq2}} \tag{7.3-4}$$

$$\begin{aligned}\tau_{Qa} &= \frac{X'_{lkq1}+X'_{lkq2}}{\omega_b\left(r'_{kq1}+r'_{kq2}\right)} \\ &= R_{eq}\left(\frac{\tau_{qa}}{r'_{kq2}}+\frac{\tau_{qb}}{r'_{kq1}}\right)\end{aligned} \tag{7.3-5}$$

From Figure 7.3-1

$$\frac{sX_q(s)}{\omega_b} = \frac{sX_{ls}}{\omega_b} + \frac{(sX_{mq}/\omega_b)Z_{qr}(s)}{Z_{qr}(s) + (sX_{mq}/\omega_b)} \tag{7.3-6}$$

Solving the above equation for $X_q(s)$ yields the operational impedance for two damper windings in the q-axis, which can be expressed

$$X_q(s) = X_q \frac{1 + (\tau_{q4} + \tau_{q5})s + \tau_{q4}\tau_{q6}s^2}{1 + (\tau_{q1} + \tau_{q2})s + \tau_{q1}\tau_{q3}s^2} \tag{7.3-7}$$

where

$$\tau_{q1} = \frac{1}{\omega_b r'_{kq1}} \left(X'_{lkq1} + X_{mq} \right) \tag{7.3-8}$$

$$\tau_{q2} = \frac{1}{\omega_b r'_{kq2}} \left(X'_{lkq2} + X_{mq} \right) \tag{7.3-9}$$

$$\tau_{q3} = \frac{1}{\omega_b r'_{kq2}} \left(X'_{lkq2} + \frac{X_{mq}X'_{lkq1}}{X'_{lkq1} + X_{mq}} \right) \tag{7.3-10}$$

$$\tau_{q4} = \frac{1}{\omega_b r'_{kq1}} \left(X'_{lkq1} + \frac{X_{mq}X_{ls}}{X_{ls} + X_{mq}} \right) \tag{7.3-11}$$

$$\tau_{q5} = \frac{1}{\omega_b r'_{kq2}} \left(X'_{lkq2} + \frac{X_{mq}X_{ls}}{X_{ls} + X_{mq}} \right) \tag{7.3-12}$$

$$\tau_{q6} = \frac{1}{\omega_b r'_{kq2}} \left(X'_{lkq2} + \frac{X_{mq}X_{ls}X'_{lkq1}}{X_{mq}X_{ls} + X_{mq}X'_{lkq1} + X_{ls}X'_{lkq1}} \right) \tag{7.3-13}$$

The d-axis operational impedance $X_d(s)$ may be calculated for the machine with a field and a damper winding by the same procedure. In particular, from Figure 7.3-2a

$$Z_{dr}(s) = R_{ed} \frac{(1 + \tau_{da}s)(1 + \tau_{db}s)}{(1 + \tau_{Da}s)} \tag{7.3-14}$$

where

$$R_{ed} = \frac{r'_{fd}r'_{kd}}{r'_{fd} + r'_{kd}} \tag{7.3-15}$$

$$\tau_{da} = \frac{X'_{lfd}}{\omega_b r'_{fd}} \tag{7.3-16}$$

$$\tau_{db} = \frac{X'_{lkd}}{\omega_b r'_{kd}} \tag{7.3-17}$$

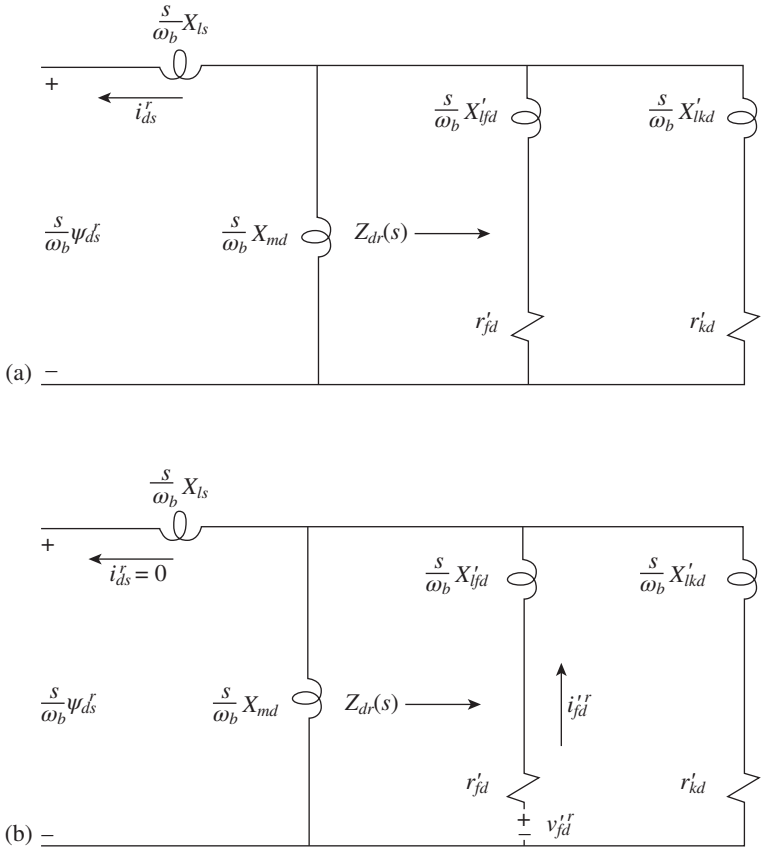

Figure 7.3-2 Calculation of $X_d(s)$ and $G(s)$ for two rotor windings in direct axis. (a) Calculation of $X_d(s)$; $v'^r_{fd} = 0$; (b) calculation of $G(s)$; $i^r_{ds} = 0$.

$$\tau_{Da} = \frac{X'_{lfd} + X'_{lkd}}{\omega_b \left(r'_{fd} + r'_{kd} \right)}$$
$$= R_{ed} \left(\frac{\tau_{da}}{r'_{kd}} + \frac{\tau_{db}}{r'_{fd}} \right) \tag{7.3-18}$$

The operational impedance for a field and damper winding in the d-axis can be obtained by setting v'^r_{fd} to zero and following the same procedure, as in the case of the q-axis. The final expression is

$$X_d(s) = X_d \frac{1 + (\tau_{d4} + \tau_{d5})s + \tau_{d4}\tau_{d6}s^2}{1 + (\tau_{d1} + \tau_{d2})s + \tau_{d1}\tau_{d3}s^2} \tag{7.3-19}$$

where

$$\tau_{d1} = \frac{1}{\omega_b r'_{fd}} \left(X'_{lfd} + X_{md} \right) \tag{7.3-20}$$

$$\tau_{d2} = \frac{1}{\omega_b r'_{kd}} \left(X'_{lkd} + X_{md} \right) \tag{7.3-21}$$

$$\tau_{d3} = \frac{1}{\omega_b r'_{kd}} \left(X'_{lkd} + \frac{X_{md} X'_{lfd}}{X'_{lfd} + X_{md}} \right) \tag{7.3-22}$$

$$\tau_{d4} = \frac{1}{\omega_b r'_{fd}} \left(X'_{lfd} + \frac{X_{md} X_{ls}}{X_{ls} + X_{md}} \right) \tag{7.3-23}$$

$$\tau_{d5} = \frac{1}{\omega_b r'_{kd}} \left(X'_{lkd} + \frac{X_{md} X_{ls}}{X_{ls} + X_{md}} \right) \tag{7.3-24}$$

$$\tau_{d6} = \frac{1}{\omega_b r'_{kd}} \left(X'_{lkd} + \frac{X_{md} X_{ls} X'_{lfd}}{X_{md} X_{ls} + X_{md} X'_{lfd} + X_{ls} X'_{lfd}} \right) \tag{7.3-25}$$

The transfer function $G(s)$ may be evaluated by expressing the relationship between stator flux linkages per second to field voltage, v'^r_{fd}, with i^r_{ds} equal to zero. Hence, from (7.2-25)

$$G(s) = \left. \frac{\psi^r_{ds}}{v'^r_{fd}} \right|_{i^r_{ds}=0} \tag{7.3-26}$$

From Figure 7.3-2b, this yields

$$G(s) = \frac{X_{md}}{r'_{fd}} \frac{1 + \tau_{db} s}{1 + (\tau_{d1} + \tau_{d2}) s + \tau_{d1} \tau_{d3} s^2} \tag{7.3-27}$$

where τ_{db} is defined by (7.3-17).

7.4 Standard Synchronous Machine Reactances

It is instructive to set forth the commonly used reactances for the four-winding rotor synchronous machine and to relate these reactances to the operational impedances whenever appropriate. The q- and d-axis reactances are

$$X_q = X_{ls} + X_{mq} \tag{7.4-1}$$

$$X_d = X_{ls} + X_{md} \tag{7.4-2}$$

These reactances were defined in Section 5.3. They characterize the machine during balanced steady-state operation whereupon variables in the rotor reference frame are constants. The zero frequency value of $X_q(s)$ or $X_d(s)$ is found by

replacing the operator s with zero. Hence, the operational impedances for balanced steady-state operation are

$$X_q(0) = X_q \tag{7.4-3}$$

$$X_d(0) = X_d \tag{7.4-4}$$

Similarly, the steady-state value of the transfer function is

$$G(0) = \frac{X_{md}}{r'_{fd}} \tag{7.4-5}$$

The q- and d-axis transient reactances are defined as

$$X'_q = X_{ls} + \frac{X_{mq}X'_{lkq1}}{X'_{lkq1} + X_{mq}} \tag{7.4-6}$$

$$X'_d = X_{ls} + \frac{X_{md}X'_{lfd}}{X'_{lfd} + X_{md}} \tag{7.4-7}$$

Although X'_q has not been defined previously, we did encounter the d-axis transient reactance in the derivation of the approximate transient torque-angle characteristic in Chapter 5.

The q- and d-axis subtransient reactances are defined as

$$X''_q = X_{ls} + \frac{X_{mq}X'_{lkq1}X'_{lkq2}}{X_{mq}X'_{lkq1} + X_{mq}X'_{lkq2} + X'_{lkq1}X'_{lkq2}} \tag{7.4-8}$$

$$X''_d = X_{ls} + \frac{X_{md}X'_{lfd}X'_{lkd}}{X_{md}X'_{lfd} + X_{md}X'_{lkd} + X'_{lfd}X'_{lkd}} \tag{7.4-9}$$

These reactances are the high-frequency asymptotes of the operational impedances. That is

$$X_q(\infty) = X''_q \tag{7.4-10}$$

$$X_d(\infty) = X''_d \tag{7.4-11}$$

The high-frequency response of the machine is characterized by these reactances. It is interesting that $G(\infty)$ is zero, which indicates that the stator flux linkages are essentially insensitive to high frequency changes in field voltage. Primes are used to denote transient and subtransient quantities, which can be confused with rotor quantities referred to the stator windings by a turns ratio. Hopefully, this confusion is minimized by the fact that X'_d and X'_q are the only single-primed parameters that are not referred impedances.

Although the steady-state and subtransient reactances can be related to the operational impedances, this is not the case with the transient reactances.

It appears that the *d*-axis transient reactance evolved from Doherty and Nickle's [3] development of an approximate transient torque-angle characteristic where the effects of *d*-axis damper windings are neglected. The *q*-axis transient reactance has come into use when it became desirable to portray more accurately the dynamic characteristics of the solid iron rotor machine in transient stability studies. In many of the early studies, only one damper winding was used to describe the electrical characteristics of the *q*-axis, which is generally adequate in the case of salient-pole machines. In our earlier development, we implied a notational correspondence between the *kq*1 and the *fd* windings and between the *kq*2 and the *kd* windings. In this chapter, we have associated the *kq*1 winding with the transient reactance (7.4-6), and the *kq*2 winding with the subtransient reactance (7.4-8). Therefore, it seems logical to use only the *kq*2 winding when one damper winding is deemed adequate to portray the electrical characteristics of the *q* axis. It is recalled that in Chapter 5, we chose to use the *kq*2 winding rather than the *kq*1 winding in the case of the salient-pole hydro turbine generator.

It is perhaps apparent that the subtransient reactances characterize the equivalent reactances of the machine during a very short period of time following an electrical disturbance. After a period, of perhaps a few milliseconds, the machine equivalent reactances approach the values of the transient reactances, and even though they are not directly related to $X_q(s)$ and $X_d(s)$, their values lie between the subtransient and steady-state values. As more time elapses after a disturbance, the transient reactances give way to the steady-state reactances. In Chapter 5, we observed the impedance of the machine "changing" from transient to steady state following a system disturbance. Clearly, the use of the transient and subtransient quantities to portray the behavior of the machine over specific time intervals was a direct result of the need to simplify the machine equations so that precomputer computational techniques could be used.

7.5 Standard Synchronous Machine Time Constants

The standard time constants associated with a four-rotor winding synchronous machine are given in Table 7.5-1. These time constants are defined as

τ'_{qo} and τ'_{do} are the *q*- and *d*-axis transient open-circuit time constants.
τ''_{qo} and τ''_{do} are the *q*- and *d*-axis subtransient open-circuit time constants.
τ'_{q} and τ'_{d} are the *q*- and *d*-axis transient short-circuit time constants.
τ''_{q} and τ''_{d} are the *q*- and *d*-axis subtransient short-circuit time constants.

In the above definitions, open and short circuit refers to the conditions of the stator circuits. All of these time constants are approximations of the actual time

Table 7.5-1 Standard Synchronous Machine Time Constants.

Open-Circuit Time Constants
$\tau'_{qo} = \frac{1}{\omega_b r'_{kq1}} \left(X'_{lkq1} + X_{mq} \right)$
$\tau'_{do} = \frac{1}{\omega_b r'_{fd}} \left(X'_{lfd} + X_{md} \right)$
$\tau''_{qo} = \frac{1}{\omega_b r'_{kq2}} \left(X'_{lkq2} + \frac{X_{mq} X'_{lkq1}}{X_{mq} + X'_{lkq1}} \right)$
$\tau''_{do} = \frac{1}{\omega_b r'_{kd}} \left(X'_{lkd} + \frac{X_{md} X'_{lfd}}{X_{md} + X'_{lfd}} \right)$
Short-Circuit Time Constants
$\tau'_{q} = \frac{1}{\omega_b r'_{kq1}} \left(X'_{lkq1} + \frac{X_{mq} X_{ls}}{X_{mq} + X_{ls}} \right)$
$\tau'_{d} = \frac{1}{\omega_b r'_{fd}} \left(X'_{lfd} + \frac{X_{md} X_{ls}}{X_{md} + X_{ls}} \right)$
$\tau''_{q} = \frac{1}{\omega_b r'_{kq2}} \left(X'_{lkq2} + \frac{X_{mq} X_{ls} X'_{lkq1}}{X_{mq} X_{ls} + X_{mq} X'_{lkq1} + X_{ls} X'_{lkq1}} \right)$
$\tau''_{d} = \frac{1}{\omega_b r'_{kd}} \left(X'_{lkd} + \frac{X_{md} X_{ls} X'_{lfd}}{X_{md} X_{ls} + X_{md} X'_{lfd} + X_{ls} X'_{lfd}} \right)$

constants, and when used to determine the machine parameters, they can lead to substantial errors in predicting the dynamic behavior of a synchronous machine. More accurate expressions for the time constants are derived in the following section.

7.6 Derived Synchronous Machine Time Constants

The open-circuit time constants, which characterize the duration of transient changes of machine variables during open-circuit conditions, are the reciprocals of the roots of the characteristic equation associated with the operational impedances, which, of course, are the poles of the operational impedances. The roots of the denominators of $X_q(s)$ and $X_d(s)$ can be found by setting these second-order polynomials equal to zero. From $X_q(s)$, (7.3-7)

$$s^2 + \frac{\tau_{q1} + \tau_{q2}}{\tau_{q1}\tau_{q3}} s + \frac{1}{\tau_{q1}\tau_{q3}} = 0 \tag{7.6-1}$$

From $X_d(s)$, (7.3-19)

$$s^2 + \frac{\tau_{d1} + \tau_{d2}}{\tau_{d1}\tau_{d3}} s + \frac{1}{\tau_{d1}\tau_{d3}} = 0 \tag{7.6-2}$$

The roots are of the form

$$s = -\frac{b}{2} \pm \frac{b}{2}\sqrt{1 - \frac{4c}{b^2}} \tag{7.6-3}$$

The exact solution of (7.6-3) is quite involved. It can be simplified, however, if the quantity $4c/b^2$ is much less than unity [4]. In the case of the q-axis

$$\frac{4c}{b^2} = \frac{4\tau_{q1}\tau_{q3}}{(\tau_{q1} + \tau_{q2})^2} \tag{7.6-4}$$

It can be shown that

$$\frac{4\tau_{q1}\tau_{q3}}{(\tau_{q1} + \tau_{q2})^2} \approx \frac{4r'_{kq1}r'_{kq2}\left(X'_{lkq1} + X'_{lkq2}\right)}{X_{mq}\left(r'_{kq1} + r'_{kq2}\right)^2} \tag{7.6-5}$$

In the case of the d-axis

$$\frac{4\tau_{d1}\tau_{d3}}{(\tau_{d1} + \tau_{d2})^2} \approx \frac{4r'_{fd}r'_{kd}\left(X'_{lfd} + X'_{lkd}\right)}{X_{md}\left(r'_{fd} + r'_{kd}\right)^2} \tag{7.6-6}$$

In most cases, the right-hand side of (7.6-5) and (7.6-6) is much less than unity. Hence, the solution of (7.6-3) with $4c/b^2 \ll 1$ and $c/b \ll b$ is obtained by employing the binomial expansion, from which

$$s_1 = -\frac{c}{b} \tag{7.6-7}$$

$$s_2 = -b \tag{7.6-8}$$

Now, the reciprocals of the roots are the time constants, and if we define the transient open-circuit time constant as the largest time constant and the subtransient open-circuit time constant as the smallest, then

$$\tau'_{qo} = \frac{b}{c}$$
$$= \tau_{q1} + \tau_{q2} \tag{7.6-9}$$

and

$$\tau''_{qo} = \frac{1}{b}$$
$$= \frac{\tau_{q3}}{1 + \tau_{q2}/\tau_{q1}} \tag{7.6-10}$$

Similarly, the d-axis open-circuit time constants are

$$\tau'_{do} = \tau_{d1} + \tau_{d2} \tag{7.6-11}$$

$$\tau''_{do} = \frac{\tau_{d3}}{1 + \tau_{d2}/\tau_{d1}} \tag{7.6-12}$$

Table 7.6-1 Derived Synchronous Machine Time Constants.

Open-Circuit Time Constants

$$\tau'_{qo} = \frac{1}{\omega_b r'_{kq1}}\left(X'_{lkq1} + X_{mq}\right) + \frac{1}{\omega_b r'_{kq2}}\left(X'_{lkq2} + X_{mq}\right)$$

$$\tau'_{do} = \frac{1}{\omega_b r'_{fd}}\left(X'_{lfd} + X_{md}\right) + \frac{1}{\omega_b r'_{kd}}\left(X'_{lkd} + X_{md}\right)$$

$$\tau''_{qo} = \frac{\frac{1}{\omega_b r'_{kq2}}\left(X'_{lkq2} + \frac{X_{mq}X'_{lkq1}}{X'_{lkq1}+X_{mq}}\right)}{1+\frac{\frac{1}{\omega_b r'_{kq2}}\left(X'_{lkq2}+X_{mq}\right)}{\frac{1}{\omega_b r'_{kq1}}\left(X'_{lkq1}+X_{mq}\right)}}$$

$$\tau''_{do} = \frac{\frac{1}{\omega_b r'_{kd}}\left(X'_{lkd} + \frac{X_{md}X'_{lfd}}{X'_{lfd}+X_{md}}\right)}{1+\frac{\frac{1}{\omega_b r'_{kd}}\left(X'_{lkd}+X_{md}\right)}{\frac{1}{\omega_b r'_{fd}}\left(X'_{lfd}+X_{md}\right)}}$$

Short-Circuit Time Constants

$$\tau'_{q} = \frac{1}{\omega_b r'_{kq1}}\left(X'_{lkq1} + \frac{X_{mq}X_{ls}}{X_{ls}+X_{mq}}\right) + \frac{1}{\omega_b r'_{kq2}}\left(X'_{lkq2} + \frac{X_{mq}X_{ls}}{X_{ls}+X_{mq}}\right)$$

$$\tau'_{d} = \frac{1}{\omega_b r'_{fd}}\left(X'_{lfd} + \frac{X_{md}X_{ls}}{X_{ls}+X_{md}}\right) + \frac{1}{\omega_b r'_{kd}}\left(X'_{lkd} + \frac{X_{md}X_{ls}}{X_{ls}+X_{md}}\right)$$

$$\tau''_{q} = \frac{\frac{1}{\omega_b r'_{kq2}}\left(X'_{lkq2} + \frac{X_{mq}X_{ls}X'_{lkq1}}{X_{mq}X_{ls}+X_{mq}X'_{lkq1}+X_{ls}X'_{lkq1}}\right)}{1+\frac{\frac{1}{\omega_b r'_{kq2}}\left(X'_{lkq2}+\frac{X_{mq}X_{ls}}{X_{ls}+X_{mq}}\right)}{\frac{1}{\omega_b r'_{kq1}}\left(X'_{lkq1}+\frac{X_{mq}X_{ls}}{X_{ls}+X_{mq}}\right)}}$$

$$\tau''_{d} = \frac{\frac{1}{\omega_b r'_{kd}}\left(X'_{lkd} + \frac{X_{md}X_{ls}X'_{lfd}}{X_{md}X_{ls}+X_{md}X'_{lfd}+X_{ls}X'_{lfd}}\right)}{1+\frac{\frac{1}{\omega_b r'_{kd}}\left(X'_{lkd}+\frac{X_{md}X_{ls}}{X_{ls}+X_{md}}\right)}{\frac{1}{\omega_b r'_{fd}}\left(X'_{lfd}+\frac{X_{md}X_{ls}}{X_{ls}+X_{md}}\right)}}$$

The above derived open-circuit time constants are expressed in terms of machine parameters in Table 7.6-1.

The short-circuit time constants are defined as the reciprocals of the roots of the numerator of the operational impedances. Although the stator resistance should be included in the calculation of the short-circuit time constants; its influence is generally small. From $X_q(s)$, (7.3-7)

$$s^2 + \frac{\tau_{q4} + \tau_{q5}}{\tau_{q4}\tau_{q6}}s + \frac{1}{\tau_{q4}\tau_{q6}} = 0 \tag{7.6-13}$$

From $X_d(s)$, given by (7.3-19)

$$s^2 + \frac{\tau_{d4} + \tau_{d5}}{\tau_{d4}\tau_{d6}}s + \frac{1}{\tau_{d4}\tau_{d6}} = 0 \tag{7.6-14}$$

The roots are of the form given by (7.6-3) and, as in the case of the open-circuit time constants, $4c/b^2 \ll 1$ and $c/b \ll b$. Hence

$$\tau'_q = \tau_{q4} + \tau_{q5} \tag{7.6-15}$$

$$\tau''_q = \frac{\tau_{q6}}{1 + \tau_{q5}/\tau_{q4}} \tag{7.6-16}$$

$$\tau'_d = \tau_{d4} + \tau_{d5} \tag{7.6-17}$$

$$\tau''_d = \frac{\tau_{d6}}{1 + \tau_{d5}/\tau_{d4}} \tag{7.6-18}$$

The above derived synchronous machine time constants are given in Table 7.6-1 in terms of machine parameters. It is important to note that the standard machine time constants given in Table 7.5-1 are considerably different from the more accurate derived time constants. The standard time constants are acceptable approximations of the derived time constants if

$$r'_{kq2} >> r'_{kq1} \tag{7.6-19}$$

and

$$r'_{kd} >> r'_{fd} \tag{7.6-20}$$

In the lumped parameter approximation of the rotor circuits, r'_{kd} is generally much larger than r'_{fd}, and therefore the standard d-axis time constants are often good approximations of the derived time constants. This is not the case for the q-axis lumped parameter approximation of the rotor circuits. That is, r'_{kq2} is seldom if ever larger than r'_{kq1}, hence the standard q-axis time constants are generally poor approximations of the derived time constants.

7.7 Parameters from Short-Circuit Characteristics

For much of the twentieth century, results from a short-circuit test performed on an unloaded synchronous machine were used to establish the d-axis parameters [5]. Alternative techniques have for the most part replaced short-circuit characterization. Despite being replaced, many of the terms, such as the short-circuit time-constants, have roots in the analytical derivation of the short circuit response of a machine. Thus, it is useful to briefly describe the test herein.

If the speed of the machine is constant, then (7.2-1)–(7.2–6) form a set of linear differential equations that can be solved using linear system theory. Prior to the short circuit of the stator terminals, the machine variables are in the steady state and the stator terminals are open-circuited. If the field voltage is held fixed at its prefault value, then the Laplace transform of the change in v'^r_{fd} is zero. Hence, if the terms involving r_s^2 are neglected, the Laplace transform of the fault currents

(defined positive out of the machine), for the constant speed operation ($\omega_r = \omega_b$), may be expressed

$$i^r_{qs}(s) = -\frac{1/X_q(s)}{s^2 + 2\alpha s + \omega_b^2}\left[\frac{\omega_b^2 r_s v^r_{qs}(s)}{X_d(s)} + \omega_b s v^r_{qs}(s) - \omega_b^2 v^r_{ds}(s)\right] \tag{7.7-1}$$

$$i^r_{ds}(s) = -\frac{1/X_d(s)}{s^2 + 2\alpha s + \omega_b^2}\left[\frac{\omega_b^2 r_s v^r_{ds}(s)}{X_q(s)} + \omega_b s v^r_{ds}(s) + \omega_b^2 v^r_{qs}(s)\right] \tag{7.7-2}$$

where

$$\alpha = \frac{\omega_b r_s}{2}\left(\frac{1}{X_q(s)} + \frac{1}{X_d(s)}\right) \tag{7.7-3}$$

It is clear that the 0 quantities are zero for a three-phase fault at the stator terminals. It is also clear that ω_r, ω_b, and ω_e are all equal in this example.

Initially, the machine is operating open-circuited, hence

$$v^r_{qs} = \sqrt{2}V_s \tag{7.7-4}$$

$$v^r_{ds} = 0 \tag{7.7-5}$$

The three-phase fault appears as a step decrease in v^r_{qs} to zero. Therefore, the Laplace transform of the change in the voltages from the prefault to fault values are

$$v^r_{qs}(s) = -\frac{\sqrt{2}V_s}{s} \tag{7.7-6}$$

$$v^r_{ds}(s) = 0 \tag{7.7-7}$$

If (7.7-6) and (7.7-7) are substituted into (7.7-1) and (7.7-2), and if the terms involving r_s are neglected except for α, wherein the operational impedances are replaced by their high-frequency asymptotes, the Laplace transform of the short-circuit currents becomes

$$i^r_{qs}(s) = \frac{1/X_q(s)}{s^2 + 2\alpha s + \omega_b^2}(\omega_b\sqrt{2}V_s) \tag{7.7-8}$$

$$i^r_{ds}(s) = \frac{1/X_d(s)}{s^2 + 2\alpha s + \omega_b^2}\left(\frac{\omega_b^2\sqrt{2}V_s}{s}\right) \tag{7.7-9}$$

where

$$\alpha = \frac{\omega_b r_s}{2}\left(\frac{1}{X_q(\infty)} + \frac{1}{X_d(\infty)}\right) \tag{7.7-10}$$

Replacing the operational impedances with their high frequency asymptotes in α is equivalent to neglecting the effects of the rotor resistances in α.

If we now assume that the electrical characteristics of the synchronous machine can be portrayed by two rotor windings in each axis, then we can express the operational impedances in terms of time constants. It is recalled that the open- and short-circuit time constants are respectively the reciprocals of the roots of the denominator and numerator of the operational impedances. Therefore, the reciprocals of the operational impedances may be expressed

$$\frac{1}{X_q(s)} = \frac{1}{X_q} \frac{\left(1+\tau'_{qo}s\right)\left(1+\tau''_{qo}s\right)}{\left(1+\tau'_{q}s\right)\left(1+\tau''_{q}s\right)} \tag{7.7-11}$$

$$\frac{1}{X_d(s)} = \frac{1}{X_d} \frac{\left(1+\tau'_{do}s\right)\left(1+\tau''_{do}s\right)}{\left(1+\tau'_{d}s\right)\left(1+\tau''_{d}s\right)} \tag{7.7-12}$$

These expressions may be written as [6]

$$\frac{1}{X_q(s)} = \frac{1}{X_q}\left(1 + \frac{As}{1+\tau'_q s} + \frac{Bs}{1+\tau''_q s}\right) \tag{7.7-13}$$

$$\frac{1}{X_d(s)} = \frac{1}{X_d}\left(1 + \frac{Cs}{1+\tau'_d s} + \frac{Ds}{1+\tau''_d s}\right) \tag{7.7-14}$$

where

$$A = -\frac{\tau'_q\left(1-\tau'_{qo}/\tau'_q\right)\left(1-\tau''_{qo}/\tau'_q\right)}{1-\tau''_q/\tau'_q} \tag{7.7-15}$$

$$B = -\frac{\tau''_q\left(1-\tau'_{qo}/\tau''_q\right)\left(1-\tau''_{qo}/\tau''_q\right)}{1-\tau'_q/\tau''_q} \tag{7.7-16}$$

The constants C and D are identical to A and B, respectively, with the q subscript replaced by d in all time constants.

Since the subtransient time constants are considerably smaller than the transient time constants, (7.7-13) and (7.7-14) may be approximated by

$$\frac{1}{X_q(s)} = \frac{1}{X_q} + \left(\frac{\tau'_{qo}}{\tau'_q}\frac{1}{X_q} - \frac{1}{X_q}\right)\frac{\tau'_q s}{1+\tau'_q s} + \left(\frac{1}{X''_q} - \frac{\tau'_{qo}}{\tau'_q}\frac{1}{X_q}\right)\frac{\tau''_q s}{1+\tau''_q s} \tag{7.7-17}$$

$$\frac{1}{X_d(s)} = \frac{1}{X_d} + \left(\frac{\tau'_{do}}{\tau'_d}\frac{1}{X_d} - \frac{1}{X_d}\right)\frac{\tau'_d s}{1+\tau'_d s} + \left(\frac{1}{X''_d} - \frac{\tau'_{do}}{\tau'_d}\frac{1}{X_d}\right)\frac{\tau''_d s}{1+\tau''_d s} \tag{7.7-18}$$

Although the assumption that the subtransient time constants are much smaller than the transient time constants is appropriate in the case of the d-axis time constants, the difference is not as large in the case of the q-axis time constants.

Hence, (7.7-17) is a less acceptable approximation than is (7.7-18). This inaccuracy will not influence our work in this section, however. Also, since we have not restricted the derivation as far as time constants are concerned, either the standard or derived time constants can be used in the equations given in this section. However, if the approximate standard time constants are used, $\left(\tau'_{qo}/\tau'_q\right)(1/X_q)$ and $\left(\tau'_{do}/\tau'_d\right)(1/X_d)$ can be replaced by $1/X'_q$ and $1/X'_d$, respectively.

If (7.7-17) and (7.7-18) are appropriately substituted into (7.7-8) and (7.7-9), the fault currents in terms of the Laplace operator become

$$i^r_{qs}(s) = \left(\frac{\sqrt{2}V_s}{s}\right)\left(\frac{\omega_b s}{s^2+2\alpha s+\omega_b^2}\right)\left[\frac{1}{X_q}+\left(\frac{\tau'_{qo}}{\tau'_q}\frac{1}{X_q}-\frac{1}{X_q}\right)\frac{\tau'_q s}{1+\tau'_q s}\right.$$
$$\left.+\left(\frac{1}{X''_q}-\frac{\tau'_{qo}}{\tau'_q}\frac{1}{X_q}\right)\frac{\tau''_q s}{1+\tau''_q s}\right] \tag{7.7-19}$$

$$i^r_{ds}(s) = \left(\frac{\sqrt{2}V_s}{s}\right)\left(\frac{\omega_b^2}{s^2+2\alpha s+\omega_b^2}\right)\left[\frac{1}{X_d}+\left(\frac{\tau'_{do}}{\tau'_d}\frac{1}{X_d}-\frac{1}{X_d}\right)\frac{\tau'_d s}{1+\tau'_d s}\right.$$
$$\left.+\left(\frac{1}{X''_d}-\frac{\tau'_{do}}{\tau'_d}\frac{1}{X_d}\right)\frac{\tau''_d s}{1+\tau''_d s}\right] \tag{7.7-20}$$

Equations (7.7-19) and (7.7-20) may be transformed to the time domain by the following inverse Laplace transforms. If a and α are much less than ω_b, then

$$L^{-1}\left[\frac{\omega_b s}{(s+a)\left(s^2+2\alpha s+\omega_b^2\right)}\right] = e^{-\alpha t}\sin\omega_b t \tag{7.7-21}$$

$$L^{-1}\left[\frac{\omega_b^2}{(s+a)\left(s^2+2\alpha s+\omega_b^2\right)}\right] = e^{-at}-e^{-\alpha t}\cos\omega_b t \tag{7.7-22}$$

If (7.7-21) is applied term by term to (7.7-19) with a set equal to zero for the term $1/X_q$ and then $1/\tau'_q$ and $1/\tau''_q$ for successive terms, and if (7.7-22) is applied in a similar manner to (7.7-20), we obtain [6]

$$i^r_{qs} = \frac{\sqrt{2}V_s}{X''_q}e^{-\alpha t}\sin\omega_b t \tag{7.7-23}$$

$$i^r_{ds} = \sqrt{2}V_s\left[\frac{1}{X_d}+\left(\frac{\tau'_{do}}{\tau'_d}\frac{1}{X_d}-\frac{1}{X_d}\right)e^{-t/\tau'_d}+\left(\frac{1}{X''_d}-\frac{\tau'_{do}}{\tau'_d}\frac{1}{X_d}\right)e^{-t/\tau''_d}\right]$$
$$-\frac{\sqrt{2}V_s}{X''_d}e^{-\alpha t}\cos\omega_b t \tag{7.7-24}$$

It is clear that ω_b may be replaced by ω_e in the above equations.

Initially, the machine is operating open-circuited with the time zero position of the q- and d-axis selected so that the a-phase voltage is maximum at the time

the q-axis coincides with the axis of the a phase. If we now select time zero at the instant of the short-circuit, and if the speed of the rotor is held fixed at synchronous speed then

$$\theta_r = \omega_b t + \theta_r(0) \tag{7.7-25}$$

where $\theta_r(0)$ is the position of the rotor relative to the magnetic axis of the as winding at the time of the fault. In other words, the point on the a-phase sinusoidal voltage relative to its maximum value. Substituting (7.7-25) into the transformation given by (2.3-7) yields the a-phase short-circuit current

$$\begin{aligned} i_{as} = \sqrt{2}V_s \left[\frac{1}{X_d} + \left(\frac{\tau'_{do}}{\tau'_d} \frac{1}{X_d} - \frac{1}{X_d} \right) e^{-t/\tau'_d} + \left(\frac{1}{X''_d} - \frac{\tau'_{do}}{\tau'_d} \frac{1}{X_d} \right) e^{-t/\tau''_d} \right] \\ \times \sin[\omega_b t + \theta_r(0)] \\ - \frac{\sqrt{2}V_s}{2} \left(\frac{1}{X''_d} + \frac{1}{X''_q} \right) e^{-\alpha t} \sin\theta_r(0) - \frac{\sqrt{2}V_s}{2} \left(\frac{1}{X''_d} + \frac{1}{X''_q} \right) e^{-\alpha t} \\ \times \sin[2\omega_b t + \theta_r(0)] \end{aligned} \tag{7.7-26}$$

The short-circuit currents in phases b and c may be expressed by displacing each term of (7.7-26) by $-2\pi/3$ and $2\pi/3$ electrical degrees, respectively.

Let us take a moment to discuss the terms of (7.7-26) and their relationship to the terms of (7.7-23) and (7.7-24). Since the rotor speed is held fixed at synchronous, the rotor reference frame is the synchronously rotating reference frame. In Section 2.7, we showed that a balanced three-phase set appears in the synchronously rotating reference frame as variables proportional to the amplitude of the three-phase balanced set, (2.7-5) and (2.7-6) which may be time varying. Therefore, we would expect that all terms on the right-hand side of (7.7-24), except the cosine term, would be the amplitude of the fundamental frequency-balanced three-phase set. We see from (7.7-26) that this is indeed the case. The amplitude of the balanced three-phase set contains the information necessary to determine the d-axis parameters. Later, we will return to describe the technique of extracting this information.

From the material presented in Section 2.9, we would expect the exponentially decaying offset occurring in the abc variables to appear as an exponentially decaying balanced two-phase set in the synchronously rotating reference frame as illustrated by (2.9-10) and (2.9-11). In particular, if we consider only the exponentially decaying term of the abc variables, then

$$i^*_{as} = -\frac{\sqrt{2}V_s}{2} \left(\frac{1}{X''_d} + \frac{1}{X''_q} \right) e^{-\alpha t} \sin\theta_r(0) \tag{7.7-27}$$

$$i_{bs}^{*} = -\frac{\sqrt{2}V_s}{2}\left(\frac{1}{X_d''} + \frac{1}{X_q''}\right)e^{-\alpha t}\sin\left[\theta_r(0) - \frac{2\pi}{3}\right] \tag{7.7-28}$$

$$i_{cs}^{*} = -\frac{\sqrt{2}V_s}{2}\left(\frac{1}{X_d''} + \frac{1}{X_q''}\right)e^{-\alpha t}\sin\left[\theta_r(0) + \frac{2\pi}{3}\right] \tag{7.7-29}$$

where the asterisk is used to denote the exponentially decaying component of the short-circuit stator currents. If these currents are transformed to the rotor (synchronous) reference frame by (2.3-5), the following q- and d-axis currents are obtained:

$$i_{qs}^{r*} = \frac{\sqrt{2}V_s}{2}\left(\frac{1}{X_d''} + \frac{1}{X_q''}\right)e^{-\alpha t}\sin\omega_b t \tag{7.7-30}$$

$$i_{ds}^{r*} = -\frac{\sqrt{2}V_s}{2}\left(\frac{1}{X_d''} + \frac{1}{X_q''}\right)e^{-\alpha t}\cos\omega_b t \tag{7.7-31}$$

These expressions do not appear in this form in (7.7-23) and (7.7-24); however, before becoming too alarmed, let us consider the double-frequency term occurring in the short-circuit stator currents. In particular, from (7.7-26)

$$i_{as}^{**} = -\frac{\sqrt{2}V_s}{2}\left(\frac{1}{X_d''} - \frac{1}{X_q''}\right)e^{-\alpha t}\sin[2\omega_b t + \theta_r(0)] \tag{7.7-32}$$

Therefore

$$i_{bs}^{**} = -\frac{\sqrt{2}V_s}{2}\left(\frac{1}{X_d''} - \frac{1}{X_q''}\right)e^{-\alpha t}\sin\left[2\omega_b t + \theta_r(0) - \frac{2\pi}{3}\right] \tag{7.7-33}$$

$$i_{cs}^{**} = -\frac{\sqrt{2}V_s}{2}\left(\frac{1}{X_d''} - \frac{1}{X_q''}\right)e^{-\alpha t}\sin\left[2\omega_b t + \theta_r(0) + \frac{2\pi}{3}\right] \tag{7.7-34}$$

where the superscript ** denotes the double-frequency components of the short-circuit stator currents. These terms form a double-frequency, balanced three-phase set in the *abc* variables. We would expect this set to appear as a balanced two-phase set of fundamental frequency in the synchronously rotating reference frame ($\omega = \omega_b$ or ω_e) and as decaying exponentials in a reference frame rotating at $2\omega_b$. Thus

$$i_{qs}^{r**} = -\frac{\sqrt{2}V_s}{2}\left(\frac{1}{X_d''} - \frac{1}{X_q''}\right)e^{-\alpha t}\sin\omega_b t \tag{7.7-35}$$

$$i_{ds}^{r**} = -\frac{\sqrt{2}V_s}{2}\left(\frac{1}{X_d''} - \frac{1}{X_q''}\right)e^{-\alpha t}\cos\omega_b t \tag{7.7-36}$$

We now see that if we add i_{qs}^{r*}, (7.7-30), and i_{qs}^{r**}, (7.7-35), we obtain (7.7-23). Similarly, if we add i_{ds}^{r*}, (7.7-31), and i_{ds}^{r**}, (7.7-36), we obtain the last term of (7.7-24). In other words, (7.7-23) and (7.7-24) can be written as

$$i_{qs}^{r} = \frac{\sqrt{2}V_s}{2}\left(\frac{1}{X_d''} + \frac{1}{X_q''}\right)e^{-\alpha t}\sin\omega_b t - \frac{\sqrt{2}V_s}{2}\left(\frac{1}{X_d''} - \frac{1}{X_q''}\right)e^{-\alpha t}\sin\omega_b t \tag{7.7-37}$$

$$i_{ds}^{r} = \sqrt{2}V_s\left[\frac{1}{X_d} + \left(\frac{\tau_{do}'}{\tau_d'}\frac{1}{X_d} - \frac{1}{X_d}\right)e^{-t/\tau_d'} + \left(\frac{1}{X_d''} - \frac{\tau_{do}'}{\tau_d'}\frac{1}{X_d}\right)e^{-t/\tau_d''}\right]$$
$$-\frac{\sqrt{2}V_s}{2}\left(\frac{1}{X_d''} + \frac{1}{X_q''}\right)e^{-\alpha t}\cos\omega_b t - \frac{\sqrt{2}V_s}{2}\left(\frac{1}{X_d''} - \frac{1}{X_q''}\right)e^{-\alpha t}\cos\omega_b t \tag{7.7-38}$$

If (7.7-23) and (7.7-24) had originally been written in this form, perhaps we could have written i_{as} by inspection or at least accepted the resulting form of i_{as} without questioning the theory that we had established in Chapter 2.

Let us now return to the expression for the short-circuit current i_{as} given by (7.7-26). In most machines, X_d'' and X_q'' are comparable in magnitude, hence the double-frequency component of the short-circuit stator currents is small. Consequently, the short-circuit current is predominately the combination of a decaying fundamental frequency component and a decaying offset. We first observed the waveform of the short-circuit current in Figure 5.9-8 and Figure 5.9-10. Although the initial conditions were different in that the machine was loaded and the speed of the machine increased slightly during the three-phase fault, the two predominate components of (7.7-26) are evident in these traces.

As mentioned previously, the amplitude or the envelope of the fundamental frequency component of each phase current contains the information necessary to determine the *d*-axis parameters. For purposes of explanation, let

$$i_{sc} = \sqrt{2}V_s\left[\frac{1}{X_d} + \left(\frac{\tau_{do}'}{\tau_d'}\frac{1}{X_d} - \frac{1}{X_d}\right)e^{-t/\tau_d'} + \left(\frac{1}{X_d''} - \frac{\tau_{do}'}{\tau_d'}\frac{1}{X_d}\right)e^{-t/\tau_d''}\right] \tag{7.7-39}$$

where i_{sc} is the envelope of the fundamental component of the short-circuit stator currents. This can be readily determined from a plot of any one of the instantaneous phase currents.

Now, at the instant of the fault

$$i_{sc}(t = 0^+) = \frac{\sqrt{2}V_s}{X_d''} \tag{7.7-40}$$

At the final or steady state value

$$i_{sc}(t \to \infty) = \frac{\sqrt{2}V_s}{X_d} \tag{7.7-41}$$

Hence, if we know the prefault voltage and if we can determine the initial and final values of the current envelope, X_d'' and X_d can be calculated.

It is helpful to break up i_{sc} into three components

$$i_{sc} = i_{ss} + i_t + i_{st} \tag{7.7-42}$$

where i_{ss} is the steady-state component, i_t is the transient component that decays according to τ_d', and i_{st} is the subtransient component with the time constant τ_d''. It is customary to subtract the steady-state component i_{ss} from the envelope and plot $(i_t + i_{st})$ on semilog paper as illustrated in Figure 7.7-1. Since $\tau_d' > \tau_d''$, the plot of $(i_t + i_{st})$ is determined by i_t as time increases, and since the plot is on the semi-log paper, this decay is a straight line. If the transient component is extended to the y-axis as shown by the dashed line in Figure 7.7-1, the initial value of the transient component is obtained

$$i_t(t = 0^+) = \sqrt{2}V_s \left(\frac{\tau_{do}'}{\tau_d'} \frac{1}{X_d} - \frac{1}{X_d} \right) \tag{7.7-43}$$

Since X_d is determined from (7.7-41), we can now determine $\left(\tau_{do}'/\tau_d'\right)(1/X_d)$, or if we choose to use the standard time constants, $\left(\tau_{do}'/\tau_d'\right)(1/X_d)$ is replaced by $1/X_d'$.

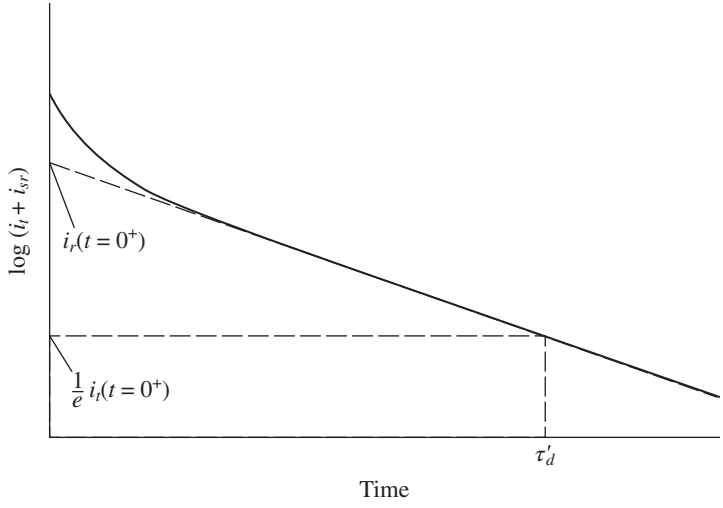

Figure 7.7-1 Plot of transient and subtransient components of the envelope of the short-circuit stator current.

The time constant τ'_d can also be determined from the plot shown in Figure 3. In particular, τ'_d is the time it takes for i_t to decrease to $1/e$ (0.368) of its original value. Thus, we now know X''_d, X_d, and τ'_d. Also, X'_d is known if we wish to use the standard, approximate time constants for τ'_{do} if we wish to use the derived time constants to calculate the d-axis parameters.

We can now extract the subtransient component from Figure 7.7-1 by subtracting the dashed-line extension of the straight-line portion, which is i_t, from the plot of $(i_t + i_{st})$. This difference will also yield a straight line when plotted on semilog paper from which the initial value of the subtransient component, $i_{st}(t = 0^+)$, and the time constant τ''_d can be determined.

Thus we have determined X'_d, X_d, τ'_d, τ''_d, and τ'_{do}.The stator leakage reactance X_{ls} can be calculated from the winding arrangement or from tests, or a reasonable value can be assumed. Hence, with a value of X_{ls}, we can determine the d-axis parameters. If $r'_{fd} << r'_{kd}$, it is generally sufficient to use X'_d and the standard time constants which, of course, markedly reduces the calculations involved.

7.8 Parameters from Frequency-Response Characteristics

Toward the end of the twentieth century, a transition was made to determine the machine parameters for dynamic and transient stability studies from measured frequency-response data rather than short-circuit tests [7–10]. These tests are generally performed by applying a low voltage across two terminals of the stator windings, with the rotor at standstill and either the q- or d-axis aligned with the resultant magnetic axis established by the two stator windings. The frequency of the applied voltage is varied from a very low value of the order of 10^{-3} Hz up to approximately 100 Hz. From these data $X_q(s)$, $X_d(s)$, and $G(s)$ are determined. An advantage of this method is that one can gain information regarding both the q- and d-axes, unlike the short-circuit test, which provides information on the parameters of only the d-axis. Moreover, the frequency-response test provides data from which the rotor can be represented by as many rotor windings in each axis as is required to obtain an acceptable match of the measured operational impedances and $G(s)$. Although popular, it has been shown that a number of issues can hinder the frequency response testing [11–13]. These include that minor hysteresis loops are traversed in the machine core under the small signal injection. As a result, the measured magnetizing inductances correspond to incremental permeability values, which lead to lower inductance than that predicted by the slope of an anhysteretic magnetizing curve. In addition, the low-level currents do not provide typical rotor heating or magnetic biasing, so that respective damper winding resistance and leakage inductances do not correspond

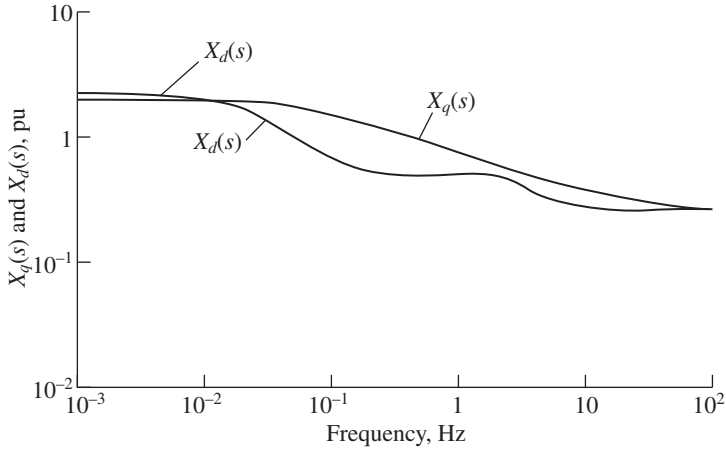

Figure 7.8-1 Plot of $X_q(s)$ and $X_d(s)$ versus frequency for a solid iron synchronous machine.

to what would be experienced under load. These issues, along with techniques to characterize models that include saturation and an arbitrary rotor network representation using a combination of magnetization and frequency response testing, are described in Reference 14. Existing industry standards, which rely heavily on frequency response testing, are detailed in Reference 15.

To gain understanding of frequency response methods, plots of measured $X_q(s)$ and $X_d(s)$ versus frequency similar to those given in Reference 10 are shown in Figure 7.8-1 for a solid iron rotor machine. Figure 7.8-2 and Figure 7.8-3 show,

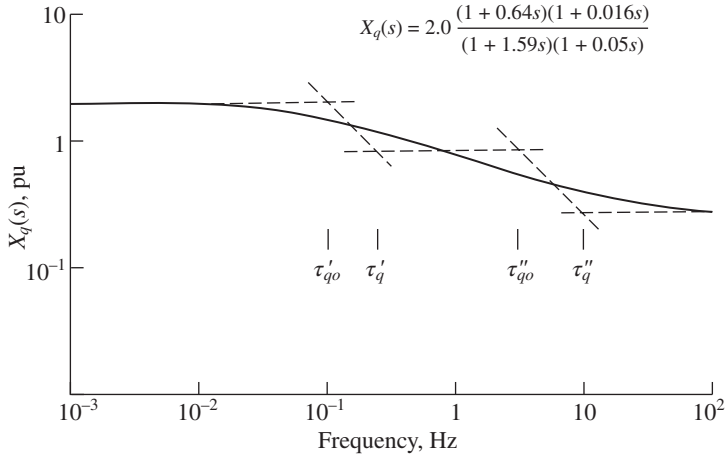

Figure 7.8-2 Two-rotor winding approximation of $X_q(s)$.

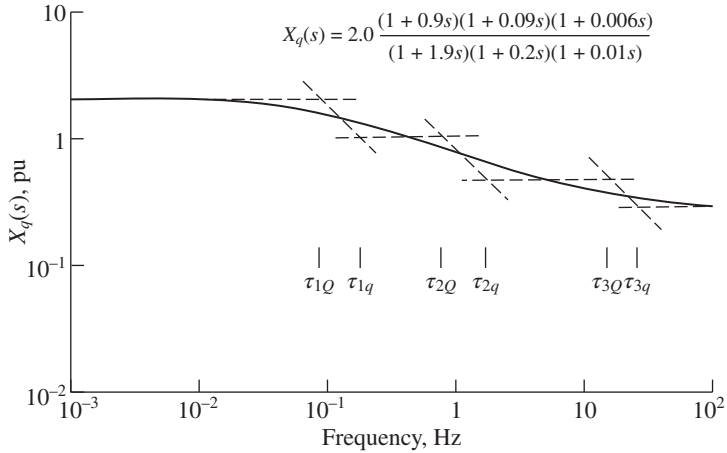

Figure 7.8-3 Three-rotor winding approximation of $X_q(s)$.

respectively, a two-rotor winding and a three-rotor winding approximation of $X_q(s)$. It is recalled from (7.7-11) that for two rotor windings

$$X_q(s) = X_q \frac{\left(1+\tau'_q s\right)\left(1+\tau''_q s\right)}{\left(1+\tau'_{qo} s\right)\left(1+\tau''_{qo} s\right)} \tag{7.8-1}$$

As illustrated in Figure 7.8-2 and Figure 7.8-3, the asymptotic approximation of $(1+\tau s)$ is used to match the plot of the magnitude of $X_q(s)$ versus frequency. Although a computer program could be used to perform curve fitting, the asymptotic approximation is sufficient for our purposes. It is important, however, that regardless of the matching procedure employed, care must be taken to match the operational impedances as closely as possible over the frequency range from 0.05 to 5 Hz, since it has been determined that matching over this range is critical in achieving accuracy in dynamic and transient stability studies [10].

The asymptotic approximation of $(1+j\omega\tau)$, where s has been replaced by $j\omega$, is that for $\omega\tau < 1$, $(1+j\omega\tau)$ is approximated by 1, and for $\omega\tau > 1$, $(1+j\omega\tau)$ is approximated by $j\omega\tau$. The corner frequency or "breakpoint" is at $\omega\tau = 1$, from which the time constant may be determined. At the corner frequency, the slope of the asymptotic approximation of $(1+j\omega\tau)$ changes from zero to a positive value increasing by one decade in amplitude (a gain of 20 dB) for every decade increase in frequency. It follows that the asymptotic approximation of $(1+j\omega\tau)^{-1}$ is a zero slope line to the corner frequency whereupon the slope becomes negative, decreasing in amplitude by one decade for every decade increase in frequency.

To obtain a lumped parameter approximation of $X_q(s)$ by using this procedure, we start at the low-frequency asymptote, extending this zero slope line to a point

where it appears that a breakpoint and thus a negative slope should occur in order to follow the measured value of $X_q(s)$. Since it is necessary that a negative slope occur after the breakpoint, a $(1 + \tau s)$ factor must be present in the denominator. Hence, this corner frequency determines the largest time constant in the denominator, which is τ'_{qo} in the case of the two-rotor winding approximation. We now continue on the negative slope asymptote until it is deemed necessary to again resume a zero slope asymptote in order to match the $X_q(s)$ plot. This swing back to a zero slope line gives rise to a $(1 + \tau s)$ factor in the numerator. This corner frequency determines the largest time constant in the numerator, τ'_q in the case of the two-rotor winding approximation. It follows that τ''_{qo} and τ''_q are determined by the same procedure.

The phase angle of $X_q(s)$ can also be measured at the same time that the magnitude of $X_q(s)$ is measured. However, the phase angle was not made use of in the curve-fitting process. Although the measured phase angle does provide a check on the asymptotic approximation of $X_q(s)$, it is not necessary in this "minimum phase" system, where the magnitude of $X_q(s)$ as a function of frequency is sufficient to determine the phase $X_q(s)$ [9]. Hence, the asymptotic approximation provides an approximation of the magnitude and phase of $X_q(s)$.

The stator leakage reactance, X_{ls}, can be determined by tests or taken as the value recommended by the manufacturer that is generally calculated or approximated from design data. The value of X_{ls} should not be larger than the subtransient reactances since this choice could result in negative rotor leakage reactances that are not commonly used. For the machine under consideration, X_{ls} of 0.15 per unit is used. Once a value of X_{ls} is selected, the parameters may be determined from the information gained from the frequency-response tests. In particular, from Figure 7.8-2

$$\begin{aligned} X_q &= 2 \text{ pu} & X''_q &= 0.25 \text{ pu} \\ \tau'_{qo} &= 1.59 \text{ second} & \tau''_{qo} &= 0.05 \text{ second} \\ \tau'_q &= 0.64 \text{ second} & \tau''_q &= 0.016 \text{ second} \end{aligned}$$

with X_{ls} selected as 0.15 pu, X_{mq} becomes 1.85 pu. Four parameters remain to be determined r'_{kq1}, X'_{lkq1}, r'_{kq2}, and X'_{lkq2}. These may be determined from the expressions of the derived q-axis time constants given in Table 7.6-1.

There is another approach by which the parameters of the lumped-circuit approximation of $X_q(s)$ may be determined that is especially useful when it is necessary to represent the rotor with more than two windings in an axis. By a curve-fitting procedure, such as illustrated in Figure 7.8-2 and Figure 7.8-3, it is possible to approximate $X_q(s)$ by

$$X_q(s) = X_q \frac{N_x(s)}{D_x(s)} \tag{7.8-2}$$

where in general

$$N_x(s) = (1 + \tau_{1q}s)(1 + \tau_{2q}s)\cdots \tag{7.8-3}$$

$$D_x(s) = (1 + \tau_{1Q}s)(1 + \tau_{2Q}s)\cdots \tag{7.8-4}$$

The input impedance for a two-rotor winding circuit is expressed by (7.3-1). For any number of rotor circuits

$$Z_{qr}(s) = R_{eq}\frac{N_z(s)}{D_z(s)} \tag{7.8-5}$$

where

$$\frac{1}{R_{eq}} = \frac{1}{R_{qa}} + \frac{1}{R_{qb}} + \cdots \tag{7.8-6}$$

$$N_z(s) = (1 + \tau_{qa}s)(1 + \tau_{qb}s)\cdots \tag{7.8-7}$$

$$D_z(s) = (1 + \tau_{Qa}s)\cdots \tag{7.8-8}$$

It is clear that (7.3-6) is valid regardless of the number of rotor windings. Thus, if we substitute (7.8-2) into (7.3-6) and solve for $Z_{qr}(s)$, we obtain [7]

$$Z_{qr}(s) = \frac{sX_{mq}/\omega_b[N_x(s) - (X_{ls}/X_q)D_x(s)]}{D_x(s) - N_x(s)} \tag{7.8-9}$$

Since the time constants of (7.8-3) and (7.8-4) can be obtained by a curve-fitting procedure, and since X_q is readily obtained from $X_q(s)$, all elements of (7.8-9) are known once X_{ls} is selected. Hence, values can be substituted into (7.8-9), and after some algebraic manipulation, it is possible to put (7.8-9) in the form of (7.8-5), whereupon R_{eq} and the time constants of (7.8-7) and (7.8-8) are known. The parameters of the lumped circuit approximation can then be determined. For example, in the case of the two-winding approximation

$$\begin{bmatrix} 1 & 1 \\ \tau_{qb} & \tau_{qa} \end{bmatrix} \begin{bmatrix} \frac{1}{r'_{kq1}} \\ \frac{1}{r'_{kq2}} \end{bmatrix} = \frac{1}{R_{eq}} \begin{bmatrix} 1 \\ \tau_{Qa} \end{bmatrix} \tag{7.8-10}$$

where the second row of (7.8-10) is (7.3-5). Thus, r'_{kq1} and r'_{kq2} can be evaluated from (7.8-10), and then X'_{lkq1} and X'_{lkq2} from (7.3-3), and (7.3-4), respectively.

In the case of the three-rotor winding approximation in the q-axis [7], (7.8-10) becomes

$$\begin{bmatrix} 1 & 1 & 1 \\ \tau_{qb} + \tau_{qc} & \tau_{qa} + \tau_{qc} & \tau_{qa} + \tau_{qb} \\ \tau_{qb}\tau_{qc} & \tau_{qa}\tau_{qc} & \tau_{qa}\tau_{qb} \end{bmatrix} \begin{bmatrix} \frac{1}{r'_{kq1}} \\ \frac{1}{r'_{kq2}} \\ \frac{1}{r'_{kq3}} \end{bmatrix} = \frac{1}{R_{eq}} \begin{bmatrix} 1 \\ \tau_{Qa} + \tau_{Qb} \\ \tau_{Qa}\tau_{Qb} \end{bmatrix} \tag{7.8-11}$$

It is left to the reader to express $Z_{qr}(s)$ for three-rotor windings.

In the development of the lumped parameter circuit approximation, there is generally no need to preserve the identity of a winding that might physically exist in the q-axis of the rotor, since the interest is to portray the electrical characteristics of this axis as viewed from the stator. However, in the d-axis, we view the characteristics of the rotor from the stator by the operation impedance $X_d(s)$ and the transfer function $G(s)$. If a lumped parameter circuit approximation is developed from only $X_d(s)$, the stator electrical characteristics may be accurately portrayed; however, the field-induced voltage during a disturbance could be quite different from that which occurs in the actual machine, especially if the measured $G(s)$, and the $G(s)$ which results when using only $X_d(s)$, do not correspond. A representation of this type, wherein only $X_d(s)$ is used to determine the lumped parameter approximation of the d-axis and the winding with the largest time constant is designated as the field winding, is quite adequate when the electrical characteristics of the field have only secondary influence upon the study being performed. Most dynamic and transient stability studies fall into this category. It has been shown that if the electrical characteristics of the stator are accurately portrayed, then the electromagnetic torque is also accurately portrayed even though the simulated field variables may be markedly different from those which actually occur [16]. In Reference 16, it is shown that this correspondence still holds even when a high initial response excitation system is used.

When the induced field voltage is of interest, as in the rating and control of solid-state switching devices that might be used in fast response excitation systems, it may be necessary to represent more accurately the electrical characteristics of the field circuit. Several researchers have considered this problem [9, 17, 18]. I.M. Canay [17] suggested the use of an additional rotor leakage inductance whereupon the d-axis circuit for a two-rotor winding approximation would appear as shown in Figure 7.8-4. The additional rotor leakage reactance or the "cross-mutual" reactance provides a means to account for the fact that the mutual inductance between the rotor and the stator windings is not necessarily the same as that between the rotor field winding and equivalent damper windings [10]. I.M. Canay [17] showed that with additional rotor leakage reactance, both the stator and the field electrical variables could be accurately portrayed. However, in order to determine the parameters for this type of d-axis lumped parameter approximation, both $X_d(s)$ and $G(s)$ must be used [6, 9].

There are several reasons for not considering the issue of the additional rotor leakage reactance further at this time. Instead, we will determine the lumped parameter circuit approximation for the d-axis from only $X_d(s)$ using the same techniques as in the case of $X_q(s)$ and designate the rotor winding with the largest time constant as the field winding. There are many cases where the measured $X_d(s)$ yields a winding arrangement that results in a $G(s)$ essentially

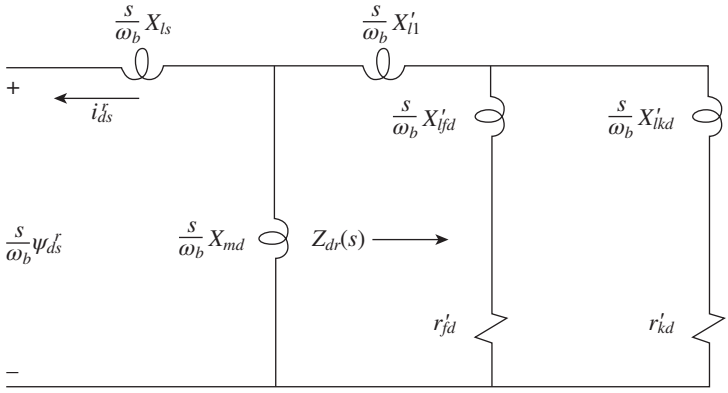

Figure 7.8-4 Two-rotor winding direct-axis circuit with unequal coupling.

the same as the measured $G(s)$, hence the additional rotor leakage reactance is small. Also, most studies do not require this degree of refinement in the machine representation, that is, the accuracy of the simulated field variables is of secondary or minor importance to the system performance of interest. In cases in which this refinement is necessary, an attractive approach is to forego the use of lumped parameters and use the arbitrary rotor network representation proposed in Reference 19. For those who have a need to develop a model of a power system without having access to machine parameter values, Kimbark [20] provides a typical range of per-unit values of synchronous machine parameters and time constants that can be a helpful place to start an analysis.

References

1 R. H. Park, "Two-Reaction Theory of Synchronous Machines—Generalized Method of Analysis—Part I," *AIEE Trans.*, Vol. 48, July 1929, pp. 716–727.

2 R. P. Schulz, W. D. Jones, and D. W. Ewart, "Dynamic Models of Turbine Generators Derived from Solid Rotor Equivalent Circuits," *IEEE Trans. Power App. Syst.*, Vol. 92, May/June 1973, pp. 926–933.

3 R. E. Doherty and C. A. Nickle, "Synchronous Machines—III, Torque-Angle Characteristics under Transient Conditions," *AIEE Trans.*, Vol. 46, January 1927, pp. 1–8.

4 G. Shackshaft, "New Approach to the Determination of Synchronous Machine Parameters from Tests," *Proc. IEE*, Vol. 121, November 1974, pp. 1385–1392.

5 *IEEE Standard Dictionary of Electrical and Electronic Terms*, 2nd ed., John Wiley and Sons, New York, 1978.

6 B. Adkins and R. G. Harley, *The General Theory of Alternating Current Machines*, Chapman and Hall, London, 1975.

7 W. Watson and G. Manchur, "Synchronous Machine Operational Impedance from Low Voltage Measurements at the Stator Terminals," *IEEE Trans. Power App. Syst.*, Vol. 93, May/June 1974, pp. 777–784.

8 P. L. Dandeno and P. Kundur, "Stability Performance of 555 MVA Turboalternators—Digital Comparisons with System Operating Tests," *IEEE Trans. Power App. Syst.*, Vol. 93, May/June 1974, pp. 767–776.

9 S. D. Umans, J. A. Malleck, and G. L. Wilson, "Modeling of Solid Rotor Turbogenerators—Parts I and II," *IEEE Trans. Power App. Syst.*, Vol. 97, January/February 1978, pp. 269–296.

10 IEEE Committee Report, "Supplementary Definitions and Associated Test Methods for Obtaining Parameters for Synchronous Machine Stability and Study Simulations," *IEEE Trans. Power App. Syst.*, Vol. 99, July/August 1980, pp. 1625–1633.

11 F. P. de Mello and L. N. Hannett, "Determination of Synchronous Machine Electrical Characteristics by Test," *IEEE Trans. Power App. Syst.*, Vol. 102, December 1983, pp. 1625–1633.

12 S. H. Minnich, "Small Signals, Large Signals, and Saturation in Generator Modeling," *IEEE Trans. Energy Convers.*, Vol. 1, March 1986, pp. 94–102.

13 A. G. Jack and T. J. Bedford, "A Study of the Frequency Response of Turbogenerators with Special Reference to Nanticoke G. S.," *IEEE Trans. Energy Convers.*, Vol. EC-2, September 1987, pp. 496–505.

14 D. C. Aliprantis, S. D. Sudhoff, and B. T. Kuhn, "Experimental Characterization Procedure for a Synchronous Machine Model with Saturation and Arbitrary Rotor Network Representation," *IEEE Trans. Energy Convers.*, Vol. 20, September 2005, pp. 595–603.

15 IEEE Standard115, Test Procedure for Synchronous Machines Part 2: Test Procedures and Parameter Determination for Dynamic Analysis, 2009.

16 D. R. Brown and P. C. Krause, "Modeling of Transient Electrical Torques in Solid Iron Rotor Turbogenerators," *IEEE Trans. Power App. Syst.*, Vol. 98, September/October 1979, pp. 1502–1508.

17 I. M. Canay, "Causes of Discrepancies on Calculation of Rotor Quantities and Exact Equivalent Diagrams of the Synchronous Machine," *IEEE Trans. Power App. Syst.*, Vol. 88, July 1969, pp. 1114–1120.

18 Y. Tabeda and B. Adkins, "Determination of Synchronous Machine Parameters Allowing for Unequal Mutual Inductances," *Proc. IEE*, Vol. 121, December 1974, pp. 1501–1504.

19 D.C. Aliprantis, S.D. Sudhoff, and B.T. Kuhn, "A Synchronous Machine Model with Saturation and Arbitrary Rotor Network Representation," *IEEE Trans. Energy Convers.*, Vol. 20, September 2005, pp. 584–594.

20 E. W. Kimbark, *Power System Stability: Synchronous Machines*, Vol. 3, Dover Publications, New York, 1968.

Problems

7.1 Derive expressions for the short-circuit time constants with the stator resistance included.

7.2 Calculate and compare the standard and derived time constants for the hydro turbine generator given in Chapter 5.

7.3 Repeat Problem 7.2 for the steam turbine generator given in Chapter 5.

7.4 Derive an expression for the instantaneous electromagnetic torque during a three-phase short circuit at the terminals. Assume the stator terminals of the machine are initially open-circuited and the speed does not change during the fault.

7.5 Derive an expression for the instantaneous field current for a three-phase short circuit at the terminals. As in Problem 7.4, assume that the machine is initially operating with the stator open-circuited and that the speed remains constant during the fault.

7.6 Consider the short-circuit stator currents shown in Figure 7P-1. The machine is originally operating open-circuited at rated voltage. The speed is fixed during the fault. Assume $r_s = 0.0037$ pu, $X_d = 1.7$ pu, and $X_{ls} = 0.19$ pu. Determine the remaining d-axis circuit parameters using (a) the derived time constants and (b) the standard time constants.

7.7 For two-rotor windings in the d-axis, show that $i'^r_{fd} = pG(p)i^r_{ds}$ for $v'^r_{fd} = 0$.

7.8 Determine r'_{kq1}, X'_{lkq1}, r'_{kq2}, and X'_{lkq2} for the two-rotor winding approximation of $X_q(s)$ given in Figure 7.8-2 by using (a) the derived time constants and (b)(7.8-10), (7.3-3), and (7.3-4).

7.9 Determine the parameters of a two-rotor winding approximation of $X_d(s)$ given in Figure 7.8-1.

7.10 Express $Z_{qr}(s)$ for a three-rotor winding approximation. Compare the terms in the denominator to the last two rows of (7.8-11).

7.11 Determine the time constants of $X_d(s)$ given in Figure 7.8-1 for a three-rotor winding approximation.

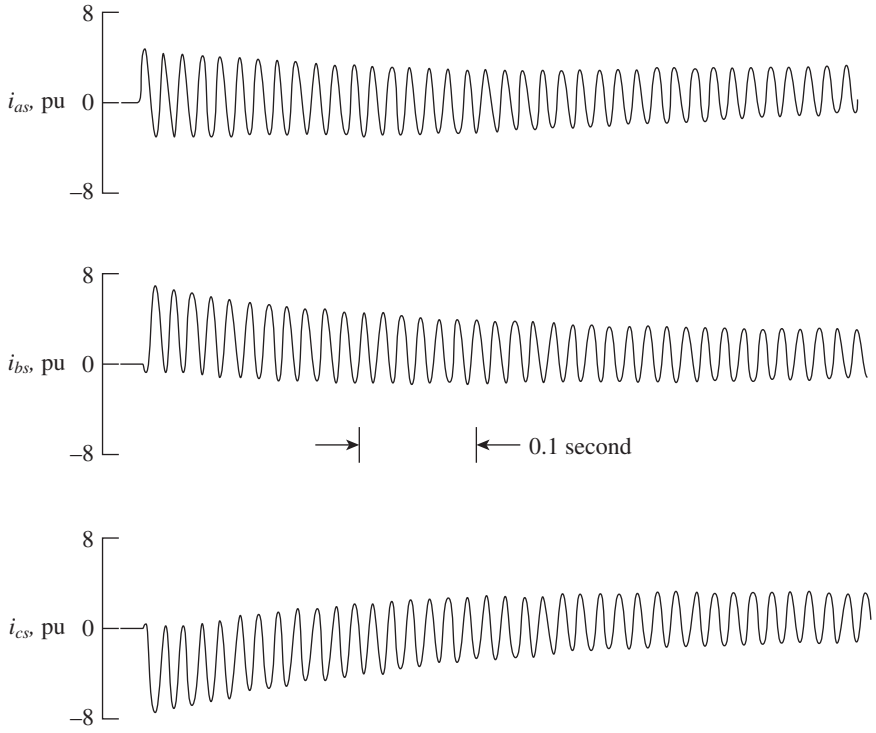

Figure 7P-1 Short-circuit stator currents.

7.12 Determine the parameters of a three-rotor winding approximation of $X_q(s)$ shown in Figure 7.8-2.

7.13 Repeat Problem 7.12 for $X_d(s)$ in Figure 7.8-1.

7.14 Write Park's equations for a synchronous machine represented by three damper windings in the q-axis and two damper windings and a field winding in the d-axis.

7.15 Derive $X_d(s)$ and $G(s)$ for the d-axis circuit with the additional rotor leakage reactance shown in Figure 7.8-4. Show that both have the same denominator.

7.16 Write the voltage equations in the rotor reference frame for the d-axis circuit with the additional rotor leakage reactance shown in Figure 7.8-4.

7.17 Plot the $X_d(s)$ and $X_q(s)$ for the steam and hydroturbine generators whose parameters are given in Chapter 5.

8

Eigenvalues and Voltage-Behind-Reactance Machine Equations

8.1 Introduction

There are alternative formulations of induction and synchronous machine equations that warrant consideration since each has a specific useful purpose. In particular, (1) linearized or small-displacement formulation for operating point stability issues; (2) neglecting stator electric transients for large-excursion transient stability studies, which was considered in Chapter 6; and (3) voltage-behind-reactance (VBR) formulation convenient for machine-converter analysis and simulation. The first and third formulations are considered in this chapter.

Although standard computer algorithms may be used to automatically linearize machine equations, it is important to be aware of the steps necessary to perform linearization. This procedure is set forth by applying Taylor expansion about an operating point. The resulting set of linear differential equations describes the dynamic behavior during small displacements or small excursions about an operating point, whereupon the basic linear system theory can be used to calculate eigenvalues. In the first sections of this chapter, the nonlinear equations of induction and synchronous machines are linearized, and the eigenvalues are calculated. Although these equations are valid for operation with stator voltages of any frequency, only rated frequency operation is considered in detail.

Over the years, there has been considerable attention given to the development of simplified models primarily for the purpose of predicting the dynamic behavior of electric machines during large excursions in some or all of the machine variables. Before the 1960s, the dynamic behavior of induction machines was generally predicted using the steady-state voltage equations and the dynamic relationship between rotor speed and torque. Similarly, the large-excursion behavior of synchronous machines was predicted using a set of steady-state voltage equations with modifications to account for transient conditions, as presented in

Analysis of Electric Machinery and Drive Systems, Fourth Edition.
Paul C. Krause, Oleg Wasynczuk, Scott D. Sudhoff, and Steven D. Pekarek.

Companion website: www.wiley.com/go/krause_aem4e

Chapter 5, along with the dynamic relationship between rotor angle and torque. With the advent of the computer, these models have given way to more accurate representations. In some cases, the machine equations are programmed in detail; however, in the vast majority of cases, a reduced-order model is used in computer simulations of power systems.

In an increasing number of applications, electric machines are coupled to power electronic circuits. In Chapters 4–6, a great deal of the focus was placed upon utilizing reference-frame theory to eliminate rotor-dependent inductances (or flux linkage in the case of the permanent-magnet machine). Although reference-frame theory enables analytical evaluation of steady-state performance and provides the basis for most modern electric drive controls, it can be difficult to apply a transformation to some power system components, particularly power electronic converters. In such cases, one is forced to establish a coupling between a machine modeled in a reference frame and a power converter modeled in terms of physical variables. As an alternative, it can be convenient to represent a machine in terms of physical variables using a VBR model. In this chapter, the derivation of a physical-variable voltage-behind-reactance (PVVBR) model of the synchronous machine is provided, along with the explanation of its potential application and advantages over alternative model structures. In addition, approximate forms of the VBR model are described in which rotor-position-dependent inductances are eliminated, which greatly simplifies the modeling of machines in physical variables.

8.2 Machine Equations to be Linearized

The linearized machine equations are conveniently derived from voltage equations expressed in terms of constant parameters with constant driving forces, independent of time. During steady-state balanced conditions, these requirements are satisfied, in the case of the induction machine, by the voltage equations expressed in the synchronously rotating reference frame and by the voltage equations in the rotor reference frame in the case of the synchronous machine. Since the currents and flux linkages are not independent variables, the machine equations can be written using either currents or flux linkages, or flux linkages per second, as state variables. The choice is generally determined by the application. Currents are selected here. Formulating the small-displacement equations in terms of flux linkages per second is left as an exercise for the reader.

8.2.1 Induction Machine

The voltage equations for the induction machine with currents as state variables may be written in the synchronously rotating reference frame by setting $\omega = \omega_e$ [1]

$$\begin{bmatrix} v_{qs}^{e} \\ v_{ds}^{e} \\ v_{qr}^{\prime e} \\ v_{dr}^{\prime e} \end{bmatrix} = \begin{bmatrix} r_s + \frac{p}{\omega_b}X_{ss} & \frac{\omega_e}{\omega_b}X_{ss} & \frac{p}{\omega_b}X_{Ms} & \frac{\omega_e}{\omega_b}X_{Ms} \\ -\frac{\omega_e}{\omega_b}X_{ss} & r_s + \frac{p}{\omega_b}X_{ss} & -\frac{\omega_e}{\omega_b}X_{Ms} & \frac{p}{\omega_b}X_{Ms} \\ \frac{p}{\omega_b}X_{Ms} & s\frac{\omega_e}{\omega_b}X_{Ms} & r_r^{\prime} + \frac{p}{\omega_b}X_{rr}^{\prime} & s\frac{\omega_e}{\omega_b}X_{rr}^{\prime} \\ -s\frac{\omega_e}{\omega_b}X_{Ms} & \frac{p}{\omega_b}X_{Ms} & -s\frac{\omega_e}{\omega_b}X_{rr}^{\prime} & r_r^{\prime} + \frac{p}{\omega_b}X_{rr}^{\prime} \end{bmatrix} \begin{bmatrix} i_{qs}^{e} \\ i_{ds}^{e} \\ i_{qr}^{\prime e} \\ i_{dr}^{\prime e} \end{bmatrix} \tag{8.2-1}$$

where s is the slip defined by (3.8-11) and the zero quantities have been omitted since only balanced conditions are considered. The reactances X_{ss} and $X_{rr}^{\prime}$ are established by multiplying the diagonal entries in (3.4-25) and (3.4-27) by ω_b.

Since we have selected currents as state variables, the electromagnetic torque is most conveniently expressed as

$$T_e = X_{Ms}\left(i_{qs}^{e} i_{dr}^{\prime e} - i_{ds}^{e} i_{qr}^{\prime e}\right) \tag{8.2-2}$$

Here, the per unit version of (3.5-10) is selected for compactness. The per unit relationship between torque and speed is (3.7-10), which is written here for convenience [1]

$$T_e = 2Hp\frac{\omega_r}{\omega_b} + T_L \tag{8.2-3}$$

8.2.2 Synchronous Machine

The voltage equations for the synchronous machine in the rotor reference frame may be written from Section 5.3

$$\begin{bmatrix} v_{qs}^{r} \\ v_{ds}^{r} \\ v_{kq1}^{\prime r} \\ v_{kq2}^{\prime r} \\ e_{xfd}^{\prime r} \\ v_{kd}^{\prime r} \end{bmatrix} = \begin{bmatrix} r_s + \frac{p}{\omega_b}X_q & \frac{\omega_r}{\omega_b}X_d & \frac{p}{\omega_b}X_{Mq} & \frac{p}{\omega_b}X_{Mq} & \frac{\omega_r}{\omega_b}X_{Md} & \frac{\omega_r}{\omega_b}X_{Md} \\ -\frac{\omega_r}{\omega_b}X_q & r_s + \frac{p}{\omega_b}X_d & -\frac{\omega_r}{\omega_b}X_{Mq} & -\frac{\omega_r}{\omega_b}X_{Mq} & \frac{p}{\omega_b}X_{Md} & \frac{p}{\omega_b}X_{Md} \\ \frac{p}{\omega_b}X_{Mq} & 0 & r_{kq1}^{\prime} + \frac{p}{\omega_b}X_{kq1}^{\prime} & \frac{p}{\omega_b}X_{mq} & 0 & 0 \\ \frac{p}{\omega_b}X_{Mq} & 0 & \frac{p}{\omega_b}X_{Mq} & r_{kq2}^{\prime} + \frac{p}{\omega_b}X_{kq2}^{\prime} & 0 & 0 \\ 0 & \frac{X_{Md}}{r_{fd}^{\prime}}\left(\frac{p}{\omega_b}X_{Md}\right) & 0 & 0 & \frac{X_{Md}}{r_{fd}^{\prime}}\left(r_{fd}^{\prime} + \frac{p}{\omega_b}X_{fd}^{\prime}\right) & \frac{X_{Md}}{r_{fd}^{\prime}}\left(\frac{p}{\omega_b}X_{Md}\right) \\ 0 & \frac{p}{\omega_b}X_{Md} & 0 & 0 & \frac{p}{\omega_b}X_{Md} & r_{kd}^{\prime} + \frac{p}{\omega_b}X_{kd}^{\prime} \end{bmatrix} \begin{bmatrix} i_{qs}^{r} \\ i_{ds}^{r} \\ i_{kq1}^{\prime r} \\ i_{kq2}^{\prime r} \\ i_{fd}^{\prime r} \\ i_{kd}^{\prime r} \end{bmatrix} \tag{8.2-4}$$

where positive currents are assumed into the machine and the reactances are defined by multiplying the inductances in (5.3-1) and (5.3-2) by ω_b.

With the currents as state variables, the per unit electromagnetic torque positive for motor action is expressed from (5.7-2) as

$$T_e = X_{Md}\left(i^r_{ds} + i'^r_{fd} + i'_{kd}\right) i^r_{qs} - X_{Mq}\left(i^r_{qs} + i'^r_{kq1} + i'^r_{kq2}\right) i^r_{ds} \tag{8.2-5}$$

The per unit relationship between torque and rotor speed is given by (5.7-3), which is

$$T_e = 2Hp\frac{\omega_r}{\omega_b} + T_L \tag{8.2-6}$$

The rotor angle is expressed from (5.6-1) as

$$\delta = \frac{\omega_b}{p}\left(\frac{\omega_r - \omega_e}{\omega_b}\right) \tag{8.2-7}$$

It is necessary, in the following analysis, to relate variables in the synchronously rotating reference frame to variables in the rotor reference frame. This is accomplished by using (5.6-3) with the zero quantities omitted. Thus,

$$\begin{bmatrix} f^r_{qs} \\ f^r_{ds} \end{bmatrix} = \begin{bmatrix} \cos\delta & -\sin\delta \\ \sin\delta & \cos\delta \end{bmatrix} \begin{bmatrix} f^e_{qs} \\ f^e_{ds} \end{bmatrix} \tag{8.2-8}$$

8.3 Linearization of Machine Equations

There are two procedures that can be followed to obtain the linearized machine equations. One is to employ Taylor's expansion about a fixed value or operating point. That is, any machine variable f_i can be written in terms of a Taylor expansion about its fixed value, f_{io}, as [1]

$$g(f_i) = g(f_{io}) + g'(f_{io})\Delta f_i + \frac{g''(f_{io})}{2!}\Delta f_i^2 + \cdots \tag{8.3-1}$$

where

$$f_i = f_{io} + \Delta f_i \tag{8.3-2}$$

If only a small excursion from the fixed point is experienced, all terms higher than the first order may be neglected and $g(f_i)$ may be approximated by

$$g(f_i) \approx g(f_{io}) + g'(f_{io})\,\Delta f_i \tag{8.3-3}$$

Hence, the small-displacement characteristics of the system are given by the first-order terms of Taylor's series,

$$\Delta g(f_i) = g'(f_{io})\,\Delta f_i \tag{8.3-4}$$

For functions of two variables, the same argument applies

$$g(f_1,f_2) \approx g(f_{1o},f_{2o}) + \frac{\partial}{\partial f_1} g(f_{1o},f_{2o})\,\Delta f_1 + \frac{\partial}{\partial f_2} g(f_{1o},f_{2o})\,\Delta f_2 \tag{8.3-5}$$

where $\Delta g(f_1, f_2)$ is the last two terms of (8.3-5).

If, for example, we apply this method to the expression for induction machine torque, (8.2-2), then

$$\begin{aligned} T_e\left(i^e_{qs}, i^e_{ds}, i'^e_{qr}, i'^e_{dr}\right) \approx\ & T_e\left(i^e_{qso}, i^e_{dso}, i'^e_{qro}, i'^e_{dro}\right) \\ & + \frac{\partial T_e\left(i^e_{qso}, i^e_{dso}, i'^e_{qro}, i'^e_{dro}\right)}{\partial i^e_{qs}}\,\Delta i^e_{qs} \\ & + \text{etc.} \end{aligned} \tag{8.3-6}$$

whereupon the small-displacement expression for torque becomes

$$\Delta T_e = X_M\left(i^e_{qso}\Delta i'^e_{dr} + i'^e_{dro}\Delta i^e_{qs} - i^e_{dso}\Delta i'^e_{qr} - i'^e_{qro}\Delta i^e_{ds}\right) \tag{8.3-7}$$

where the added subscript *o* denotes steady-state quantities.

An equivalent method of linearizing nonlinear equations is to write all variables in the form given by (8.3-2). If all multiplications are then performed and the steady-state expressions canceled from both sides of the equations and if all products of small-displacement terms ($\Delta f_1 \Delta f_2$, for example) are neglected, the small-displacement equations are obtained. It is left to the reader to obtain (8.3-7) by this technique.

8.3.1 Induction Machine

If either of the above-described methods of linearization is employed to (8.2-1)–(8.2-3), the linear differential equations of an induction machine become

$$\begin{bmatrix} \Delta v^e_{qs} \\ \Delta v^e_{ds} \\ \Delta v'^e_{qr} \\ \Delta v'^e_{dr} \\ \Delta T_L \end{bmatrix} = \begin{bmatrix} r_s + \frac{p}{\omega_b}X_{ss} & \frac{\omega_e}{\omega_b}X_{ss} & \frac{p}{\omega_b}X_{Ms} & \frac{\omega_e}{\omega_b}X_{Ms} & 0 \\ -\frac{\omega_e}{\omega_b}X_{ss} & r_s + \frac{p}{\omega_b}X_{ss} & -\frac{\omega_e}{\omega_b}X_{Ms} & \frac{p}{\omega_b}X_{Ms} & 0 \\ \frac{p}{\omega_b}X_{Ms} & s_o\frac{\omega_e}{\omega_b}X_{Ms} & r'_r + \frac{p}{\omega_b}X'_{rr} & s_o\frac{\omega_e}{\omega_b}X'_{rr} & -X_{Ms}i^e_{dso} - X'_{rr}i'^e_{dro} \\ -s_o\frac{\omega_e}{\omega_b}X_{Ms} & \frac{p}{\omega_b}X_{Ms} & -s_o\frac{\omega_e}{\omega_b}X'_{rr} & r'_r + \frac{p}{\omega_b}X'_{rr} & X_{Ms}i^e_{qso} + X'_{rr}i'^e_{qro} \\ X_{Ms}i'^e_{dro} & -X_{Ms}i'^e_{qro} & -X_{Ms}i^e_{dso} & X_{Ms}i^e_{qso} & -2Hp \end{bmatrix} \begin{bmatrix} \Delta i^e_{qs} \\ \Delta i^e_{ds} \\ \Delta i'^e_{qr} \\ \Delta i'^e_{dr} \\ \frac{\Delta\omega_r}{\omega_b} \end{bmatrix} \tag{8.3-8}$$

where

$$s_o = \frac{\omega_e - \omega_{ro}}{\omega_e} \tag{8.3-9}$$

It is clear that with applied voltages of rated frequency the ratio of ω_e to ω_b is unity. However, (8.3-8) and (8.3-9) are written with ω_e included explicitly so as to accommodate applied voltages of a constant frequency other than rated as would occur in variable-speed drive systems. The frequency of the applied stator voltages in variable-speed drive systems is varied by controlling the firing of the source converter. Therefore, in some applications, the frequency of the stator voltages may be a controlled variable. It is recalled from Chapter 3 that variable-frequency operation may be investigated in the synchronously rotating reference frame by simply changing the speed of the reference frame corresponding to the change in frequency. Therefore, if frequency is a system input variable, then a small displacement in frequency may be taken into account by allowing the reference-frame speed to change by replacing ω_e with $\omega_{eo} + \Delta\omega_e$.

It is convenient to separate out the derivative terms and write (8.3-8) in the form

$$\mathbf{E}p\mathbf{x} = \mathbf{F}\mathbf{x} + \mathbf{u} \tag{8.3-10}$$

where

$$(\mathbf{x})^T = \begin{bmatrix} \Delta i^e_{qs} & \Delta i^e_{ds} & \Delta i'^e_{qr} & \Delta i'^e_{dr} & \dfrac{\Delta\omega_r}{\omega_b} \end{bmatrix} \tag{8.3-11}$$

$$(\mathbf{u})^T = \begin{bmatrix} \Delta v^e_{qs} & \Delta v^e_{ds} & \Delta v'^e_{qr} & \Delta v'^e_{dr} & \Delta T_L \end{bmatrix} \tag{8.3-12}$$

$$\mathbf{E} = \frac{1}{\omega_b} \begin{bmatrix} X_{ss} & 0 & X_M & 0 & 0 \\ 0 & X_{ss} & 0 & X_M & 0 \\ X_M & 0 & X'_{rr} & 0 & 0 \\ 0 & X_M & 0 & X'_{rr} & 0 \\ 0 & 0 & 0 & 0 & -2H\omega_b \end{bmatrix} \tag{8.3-13}$$

$$\mathbf{F} = -\begin{bmatrix} r_s & \frac{\omega_e}{\omega_b}X_{ss} & 0 & \frac{\omega_e}{\omega_b}X_{Ms} & 0 \\ -\frac{\omega_e}{\omega_b}X_{ss} & r_s & -\frac{\omega_e}{\omega_b}X_{Ms} & 0 & 0 \\ 0 & s_o\frac{\omega_e}{\omega_b}X_{Ms} & r'_r & s_o\frac{\omega_e}{\omega_b}X'_{rr} & -X_{Ms}i^e_{dso} - X'_{rr}i'^e_{dro} \\ -s_o\frac{\omega_e}{\omega_b}X_{Ms} & 0 & -s_o\frac{\omega_e}{\omega_b}X'_{rr} & r'_r & X_{Ms}i^e_{qso} + X'_{rr}i'^e_{qro} \\ X_{Ms}i'^e_{dro} & -X_{Ms}i'^e_{qro} & -X_M i^e_{dso} & X_{Ms}i^e_{qso} & 0 \end{bmatrix} \tag{8.3-14}$$

In the analysis of linear systems, it is convenient to express the linear differential equations in the form

$$p\mathbf{x} = \mathbf{A}\mathbf{x} + \mathbf{B}\mathbf{u} \tag{8.3-15}$$

Equation (8.3-15) is the fundamental form of the linear differential equations. It is commonly referred to as the state equation.

Equation (8.3-10) may be written as

$$p\mathbf{x} = (\mathbf{E})^{-1}\mathbf{F}\mathbf{x} + (\mathbf{E})^{-1}\mathbf{u} \tag{8.3-16}$$

which is in the form of (8.3-15) with

$$\mathbf{A} = (\mathbf{E})^{-1}\mathbf{F} \tag{8.3-17}$$

$$\mathbf{B} = (\mathbf{E})^{-1} \tag{8.3-18}$$

8.3.2 Synchronous Machines

Linearizing (8.2-4)–(8.2-8) yields (8.3-19). Since the steady-state damper winding currents (i'^{r}_{kdo}, i'^{r}_{kq1o} and i'^{r}_{kq2o}) are zero, they are not included in (8.3-19). Since the synchronous machine is generally connected to an electric system such as a power system and since it is advantageous to linearize the system voltage equations in the synchronously rotating reference frame, it is convenient to include the relationship between $\Delta\omega_r$ and $\Delta\delta$ in (8.3-19). As in the case of linearized equations for the induction machine, ω_e is included explicitly in (8.3-19) so that the equations are in a form convenient for voltages of any constant frequency. Small, controlled changes in the frequency of the applied stator voltages, as is possible in variable-speed drive systems, may be taken into account analytically by replacing ω_e with $\omega_{eo} + \Delta\omega_e$ in the expression for δ given by (8.2-7).

$$\begin{bmatrix} \Delta v^r_{qs} \\ \Delta v^r_{ds} \\ \Delta v'^r_{kq1} \\ \Delta v'^r_{kq2} \\ \Delta e'^r_{xfd} \\ \Delta v'^r_{kd} \\ \Delta T_L \\ 0 \end{bmatrix} = \begin{bmatrix} r_s + \frac{p}{\omega_b}X_q & \frac{\omega_e}{\omega_b}X_d & \frac{p}{\omega_b}X_{Mq} & \frac{p}{\omega_b}X_{Mq} \\ -\frac{\omega_e}{\omega_b}X_q & r_s + \frac{p}{\omega_b}X_d & -\frac{\omega_e}{\omega_b}X_{Mq} & -\frac{\omega_e}{\omega_b}X_{Mq} \\ \frac{p}{\omega_b}X_{Mq} & 0 & r'_{kq1} + \frac{p}{\omega_b}X'_{kq1} & \frac{p}{\omega_b}X_q \\ \frac{p}{\omega_b}X_{Mq} & 0 & \frac{p}{\omega_b}X_{Mq} & r'_{kq2} + \frac{p}{\omega_b}X'_{kq2} \\ 0 & \frac{X_{Md}}{r'_{fd}}\left(\frac{p}{\omega_b}X_{Md}\right) & 0 & 0 \\ 0 & \frac{p}{\omega_b}X_{Md} & 0 & 0 \\ -X_{Mq}i^r_{dso} + X_{Md}\left(i^r_{dso} - i'^r_{fdo}\right) & X_{Md}i^r_{qso} - X_{Mq}i^r_{qso} & -X_{Mq}i^r_{dso} & -X_{Mq}i^r_{dso} \\ 0 & 0 & 0 & 0 \end{bmatrix}$$

$$\begin{bmatrix} \frac{\omega_e}{\omega_b}X_{Md} & \frac{\omega_e}{\omega_b}X_{Md} & -X_d i^r_{dso} + X_{Md}i'^r_{fdo} & 0 \\ \frac{p}{\omega_b}X_{Md} & \frac{p}{\omega_b}X_{Md} & X_q i^r_{qso} & 0 \\ 0 & 0 & 0 & 0 \\ 0 & 0 & 0 & 0 \\ \frac{X_{Md}}{r'_{fd}}\left(r'_{fd} + \frac{p}{\omega_b}X'_{fd}\right) & \frac{X_{Md}}{r'_{fd}}\left(\frac{p}{\omega_b}X_{Md}\right) & 0 & 0 \\ \frac{p}{\omega_b}X_{Md} & r'_{kd} + \frac{p}{\omega_b}X'_{kd} & 0 & 0 \\ X_{Md}i^r_{qso} & X_{Md}i^r_{qso} & -2Hp & 0 \\ 0 & 0 & -\omega_b & p \end{bmatrix} \begin{bmatrix} \Delta i^r_{qs} \\ \Delta i^r_{ds} \\ \Delta i'^r_{kq1} \\ \Delta i'^r_{kq2} \\ \Delta i'^r_{fd} \\ \Delta i'^r_{kd} \\ \frac{\Delta\omega_r}{\omega_b} \\ \Delta\delta \end{bmatrix} \tag{8.3-19}$$

In most cases, the synchronous machine is connected to a power system whereupon the voltages v_{qs}^r and v_{ds}^r, which are functions of the state variable δ, will vary as the rotor angle varies during a disturbance. It is of course necessary to account for the dependence of the driving forces on the state variables before expressing the linear differential equations in fundamental form. In power system analysis, it is often assumed that at some place in the system there is a balanced source that can be considered a constant amplitude, constant frequency, and zero impedance source (infinite bus). This would be a balanced independent driving force, which would be represented as constant voltages in the synchronously rotating reference frame. Hence, it is necessary to relate the synchronously rotating reference-frame variables, where the independent driving force exists, to the variables in the rotor reference frame. The transformation given by (8.2-8) is nonlinear. To incorporate it into a linear set of differential equations, it must be linearized. By employing the approximations that $\cos \Delta\delta = 1$ and $\sin \Delta\delta = \Delta\delta$, the linearized version of (8.2-8) is

$$\begin{bmatrix} \Delta f_{qs}^r \\ \Delta f_{ds}^r \end{bmatrix} = \begin{bmatrix} \cos \delta_o & -\sin \delta_o \\ \sin \delta_o & \cos \delta_o \end{bmatrix} \begin{bmatrix} \Delta f_{qs}^e \\ \Delta f_{ds}^e \end{bmatrix} + \begin{bmatrix} -f_{dso}^r \\ f_{qso}^r \end{bmatrix} \Delta\delta \tag{8.3-20}$$

Linearizing the inverse transformation yields

$$\begin{bmatrix} \Delta f_{qs}^e \\ \Delta f_{ds}^e \end{bmatrix} = \begin{bmatrix} \cos \delta_o & \sin \delta_o \\ -\sin \delta_o & \cos \delta_o \end{bmatrix} \begin{bmatrix} \Delta f_{qs}^r \\ \Delta f_{ds}^r \end{bmatrix} + \begin{bmatrix} f_{dso}^e \\ -f_{qso}^e \end{bmatrix} \Delta\delta \tag{8.3-21}$$

It is convenient to write the above equations in the form

$$\Delta \mathbf{f}_{qds}^r = \mathbf{T}\, \Delta \mathbf{f}_{qds}^e + \mathbf{F}^r\, \Delta\delta \tag{8.3-22}$$

$$\Delta \mathbf{f}_{qds}^e = (\mathbf{T})^{-1}\, \Delta \mathbf{f}_{qds}^r + \mathbf{F}\, \Delta\delta \tag{8.3-23}$$

It is instructive to view the interconnections of the above relationships as shown in Fig. 8.3-1. With the equations as shown in Fig. 8.3-1, a change in $\Delta \mathbf{v}_{qds}^e$ is reflected through the transformation to the voltage equations in the rotor reference frame and finally back to the synchronously rotating reference-frame currents $\Delta \mathbf{i}_{qds}^e$. The detail shown in Fig. 8.3-1 is more than is generally necessary. If, for example, the objective is to study the small-displacement dynamics of a synchronous machine with its terminals connected to an infinite bus, then $\Delta \mathbf{v}_{qds}^e$ is zero and $\Delta \mathbf{v}_{qds}^r$ changes due only to $\Delta\delta$. Also, in this case, it is unnecessary to transform the rotor reference-frame currents to the synchronously rotating reference frame since the source (infinite bus) has zero impedance.

If the machine is connected through a transmission line to a large system (infinite bus), the small-displacement dynamics of the transmission system must be taken into account. If only the machine is connected to the transmission line and if it is not equipped with a voltage regulator, then it is convenient to transform the equations of the transmission line to the rotor reference frame. In such a case,

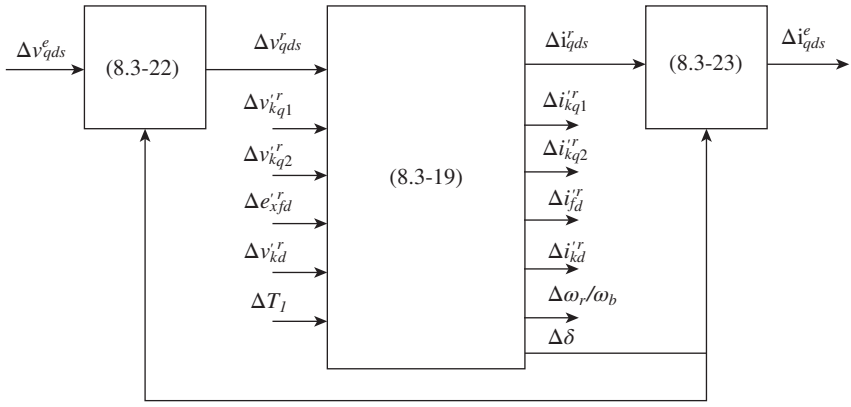

Figure 8.3-1 Interconnection of small-displacement equations of a synchronous machine: Park's equations.

the machine and transmission line can be considered in much the same way as a machine connected to an infinite bus. If, however, the machine is equipped with a voltage regulator or more than one machine is connected to the same transmission line, it is generally preferable to express the dynamics of the transmission system in the synchronously rotating reference frame and transform to and from the rotor reference frame of each machine as depicted in Fig 8.3-1.

If the machine is equipped with a voltage regulator, the dynamic behavior of the regulator will affect the dynamic characteristics of the machine. Therefore, the small-displacement dynamics of the regulator must be taken into account. When regulators are employed, the change in field voltage $\Delta e'^r_{xfd}$ is dynamically related to the change in terminal voltage, which is a function of $\Delta \mathbf{v}^e_{qds}$ (or $\Delta \mathbf{v}^r_{qds}$), the change in field current Δi^r_{fd}, and perhaps the change in rotor speed $\Delta\omega_r/\omega_b$ if the excitation system is equipped with a control to help damp rotor oscillations by means of field voltage control. This type of damping control is referred to as a power system stabilizer (PSS).

In some investigations, it is necessary to incorporate the small-displacement dynamics of the prime mover system. The change of input torque (negative load torque) is a function of the change in rotor speed $\Delta\omega_r/\omega_b$, which in turn is a function of the dynamics of the masses, shafts, and damping associated with the mechanical system and, if long-term transients are of interest, the steam or hydro dynamics and associated controls.

Although a more detailed discussion of the dynamics of the excitation and prime mover systems would be helpful, it is clear, from the above discussion, that the equations which describe the operation and control of a synchronous machine equipped with a voltage regulator and a prime mover system are very

involved. This becomes readily apparent when it is necessary to arrange the small-displacement equations of the complete system into the fundamental form. Rather than performing this task by hand, it is preferable to take advantage of analytical techniques that involve formulating the equations of each component (machine, excitation system, prime mover system, etc.) in fundamental form. A computer routine can be used to arrange the small-displacement equations along with the interconnecting transformations of the complete system into the fundamental form.

8.4 Small-Displacement Stability—Eigenvalues

With the linear differential equations written in state variable form, the **u** vector represents the forcing functions. If **u** is set equal to zero, the general solution of the homogeneous or force-free linear differential equations becomes [1]

$$\mathbf{x} = e^{\mathbf{A}t}\mathbf{K} \tag{8.4-1}$$

where **K** is a vector formed by an arbitrary set of initial conditions. The exponential $e^{\mathbf{A}t}$ represents the unforced response of the system. It is called the state transition matrix. Small-displacement stability is assured if all elements of the transition matrix approach zero asymptotically as time approaches infinity. Asymptotic behavior of all elements of the matrix occurs whenever all of the roots of the characteristic equation of **A** have negative real parts where the characteristic equation of **A** is defined

$$\det(\mathbf{A} - \lambda\,\mathbf{I}) = 0 \tag{8.4-2}$$

In (8.4-2), **I** is the identity matrix and λ are the roots of the characteristic equation of **A** referred to as characteristic roots, latent roots, or eigenvalues. Herein, we will use the latter designation. One should not confuse the λ used here to denote eigenvalues with the same notation used to denote flux linkages.

The eigenvalues provide a simple means of predicting the behavior of an induction or synchronous machine at any balanced operating condition. Eigenvalues may be either real or complex and when complex they occur as conjugate pairs signifying a mode of oscillation of the state variables. Negative real parts correspond to state variables or oscillations of state variables, which decrease exponentially with time. Positive real parts indicate an exponential increase with time, an unstable condition.

8.5 Eigenvalues of Typical Induction Machines

The eigenvalues of an induction machine can be obtained by using a standard eigenvalue computer routine to calculate the roots of **A** given by (8.3-17).

Table 8.5-1 Induction Machine Eigenvalues.

Rating, hp	Stall	Rated speed	No load
3	$-4.57 \pm j377$	$-85.6 \pm j313$	$-89.2 \pm j316$
	$-313 \pm j\ 377$	$-223 \pm j83.9$	$-218 \pm j60.3$
	1.46	−16.8	−19.5
50	$-2.02 \pm j\ 377$	$-49.4 \pm j356$	$-50.1 \pm j357$
	$-198 \pm j377$	$-142 \pm j42.5$	$-140 \pm j18.2$
	1.18	−14.4	−17.0
500	$-0.872 \pm j377$	$-41.8 \pm j374$	$-41.8 \pm j374$
	$-70.3 \pm j377$	$-15.4 \pm j41.5$	$-14.3 \pm j42.8$
	0.397	−27.5	−29.6
2250	$-0.428 \pm j377$	$-24.5 \pm j376$	$-24.6 \pm j376$
	$-42.6 \pm j377$	$-9.36 \pm j41.7$	$-9.05 \pm j42.5$
	0.241	−17.9	−18.5

The eigenvalues given in Table 8.5-1 are for the machines listed in Table 3.9-1. The induction machine, as we have perceived it, is described by five state variables and hence five eigenvalues. Sets of eigenvalues for each machine at stall, rated, and no-load speeds are given in Table 8.5-1 for rated frequency operation. Plots of the eigenvalues (real part and only the positive imaginary part) for rotor speeds from stall to synchronous are given in Figs. 8.5-1 and 8.5-2 for the 3- and 2250-hp induction motors, respectively.

At stall, the two complex conjugate pairs of eigenvalues have a frequency (imaginary part) corresponding to ω_b. The frequency of one complex conjugate pair decreases as the speed increases from stall while the frequency of the other complex conjugate pair remains at approximately ω_b, in fact, nearly equal to ω_b for the larger horsepower machines. The eigenvalues are dependent on the parameters of the machine, and it is difficult to relate analytically a change in an eigenvalue with a change in a specific machine parameter. It is possible, however, to identify an association between eigenvalues and the machine variables. For example, the complex conjugate pair that remains at a frequency close to ω_b is primarily associated with the transient offset currents in the stator windings, which reflects into the synchronously rotating reference as a decaying 60 Hz variation. This complex conjugate pair, which is denoted as the "stator" eigenvalues in Figs. 8.5-1 and 8.5-2, is not present when the electric transients are neglected in the stator voltage equations. It follows that the transient response of the machine is influenced by this complex conjugate eigenvalue pair whenever a disturbance

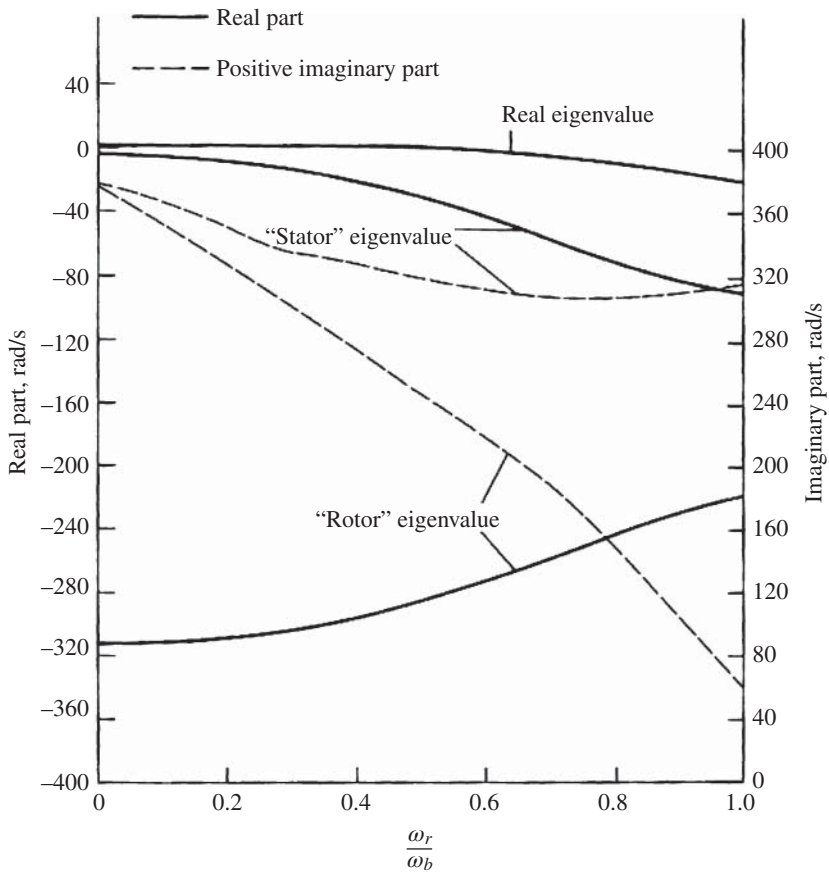

Figure 8.5-1 Plot of eigenvalues for a 3-hp induction motor.

causes a transient offset in the stator currents. It is recalled that, in Chapter 3, we noted a transient pulsation in the instantaneous torque of 60 Hz during free acceleration and following a three-phase fault at the terminals with the machine initially operating at near-rated conditions. We also noted that the pulsations were more damped in the case of the smaller horsepower machines than for the larger horsepower machines. It is noted in Table 8.5-1 that the magnitudes of the real part of the complex eigenvalues with a frequency corresponding to ω_b are larger, signifying more damping, for the smaller horsepower machine than for the larger machines.

The complex conjugate pair that changes in frequency as the rotor speed varies is associated primarily with the electric transients in the rotor circuits and is denoted in Figs. 8.5-1 and 8.5-2 as the "rotor" eigenvalue. This complex

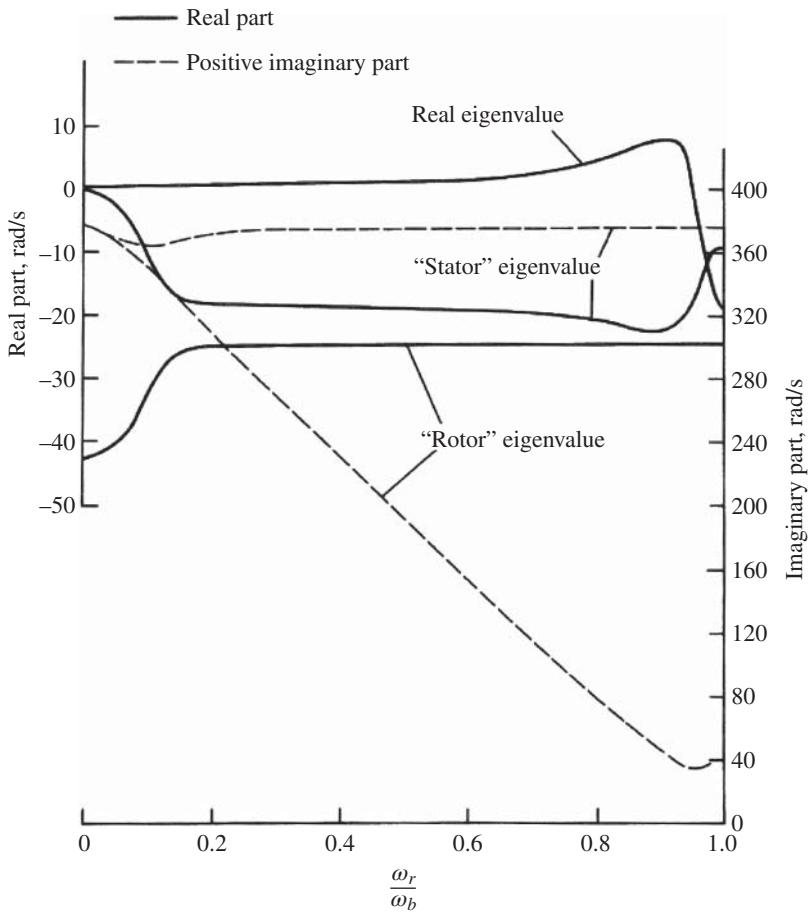

Figure 8.5-2 Plot of eigenvalues for a 2250-hp induction motor.

conjugate pair is not present when the rotor electric transients are neglected. The damping associated with this complex conjugate pair is less for the larger horsepower machines than for the smaller machines. It is recalled that, during free acceleration, the 3- and 50-hp machines approached synchronous speed in a well-damped manner while the 500- and 2250-hp machines demonstrated damped oscillations about synchronous speed. Similar behavior was noted as the machines approached their final operating point following a load torque change or a three-phase terminal fault. This behavior corresponds to that predicted by this eigenvalue. It is interesting to note that this eigenvalue is reflected noticeably in the rotor speed, whereas the higher-frequency "stator" eigenvalue is not.

This, of course, is due to the fact that for a given inertia and torque amplitude, a low-frequency torque component will cause a larger amplitude variation in rotor speed than a high-frequency component.

The real eigenvalue signifies an exponential response. It would characterize the behavior of the induction machine equations if all electric transients are mathematically neglected or if, in the actual machine, the electric transients are highly damped as in the case of the smaller horsepower machines. Perhaps, the most interesting feature of this eigenvalue, which is denoted as the real eigenvalue in Figs. 8.5-1 and 8.5-2, is that it can be related to the steady-state torque-speed curve. If we think for a moment about the torque–speed characteristics, we realize that an induction machine can operate stably only in the negative-slope portion of the torque–speed curve. If we were to assume an operating point on the positive-slope portion of the torque–speed curve, we would find that a small disturbance would cause the machine to move away from this operating point, either accelerating to the negative-slope region or decelerating to stall and perhaps reversing the direction of rotation depending on the nature of the load torque. A positive eigenvalue signifies a system that would move away from an assumed operating point. Note that this eigenvalue is positive over the positive-slope region of the torque–speed curve, becoming negative after maximum steady-state torque.

8.6 Eigenvalues of Typical Synchronous Machines

The linearized transformations, (8.3-22) and (8.3-23), and the machine equations (8.3-19) may each be considered components as shown in Fig. 8.3-1. The eigenvalues of the two synchronous machines, each connected to an infinite bus, studied in Section 5.9 are given in Table 8.6-1 for rated operation.

The complex conjugate pair with the frequency (imaginary part) approximately equal to ω_b is associated with the transient offset currents in the stator

Table 8.6-1 Synchronous Machine Eigenvalues for Rated Conditions.

Hydro-turbine generator	Steam-turbine generator
$-3.58 \pm j377$	$-4.45 \pm j377$
$-133 \pm j8.68$	$-1.70 \pm j10.5$
−24.4	−32.2
−22.9	−11.1
−0.453	−0.349
	−0.855

windings which cause the 60 Hz pulsation in electromagnetic torque. This pulsation in torque is evident in the computer traces of a three-phase fault at the machine terminals shown in Figs. 5.9-8 and 5.9-10. Although operation therein is initially at rated conditions, the three-phase fault and subsequent switching cause the operating condition to change significantly from rated conditions. Nevertheless, we note that the 60 Hz pulsation is damped slightly more in the case of the steam-turbine generators than in the case of the hydro-turbine generator. Correspondingly, the relative values of the real parts of the "stator" eigenvalues given in Table 8.6-1 indicate that the stator electric transients of the steam unit are damped more than the stator transients of the hydro unit.

The remaining complex conjugate pair is similar to the "rotor" eigenvalue in the case of the induction machine. However, in the case of the synchronous machine, this mode of oscillation is commonly referred to as the hunting or swing mode, which is the principal mode of oscillation of the rotor of the machine relative to the electrical angular velocity of the electrical system (the infinite bus in the case of studies made in Chapter 5). This mode of oscillation is apparent in the machine variables, especially the rotor speed, in Figs. 5.9-8 and 5.9-10 during the "settling out" period following reclosing. As indicated by this complex conjugate eigenvalue, the "settling out" rotor oscillation of the steam unit (Fig. 5.9-10) is more damped and of higher frequency than the corresponding rotor oscillation of the hydro unit.

The real eigenvalues are associated with the decay of the offset currents in the rotor circuits and therefore associated with the inverse of the effective time constant of these circuits. It follows that since the field winding has the largest time constant it gives rise to the smallest of the real eigenvalues. In [1], it is shown that the "stator" eigenvalue and the real eigenvalues do not change significantly in value as the real and reactive power loading conditions change.

8.7 Detailed Voltage-Behind-Reactance Model

Many software packages exist to simulate the performance of electric machines within power systems. Examples of state-variable-based solvers include ACSL [2], Easy5 [3], Eurostag [4], and MATLAB/Simulink [5]. Specialized packages such as SimPowerSystems [6], RT-Lab [7], PLECS [8], and ASMG [9] come with circuit interfaces that enable relatively straightforward assembly of system models using canonical branch circuits, such as the one shown in Fig. 8.10-1 [9].

The creation of such tools has enabled the simulation of complicated systems; however, their optimal use requires some thought as to model structure and implementation. In Chapters 3, 5, and 6, a great deal of the focus is to

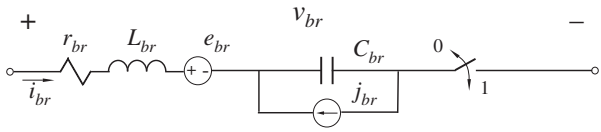

Figure 8.7-1 Example canonical branch circuit element.

apply reference-frame theory to simplify the models of electric machinery by eliminating rotor-position-dependent inductances. A key result of applying the respective transformations are the *q*- and *d*-circuit representations of wound rotor synchronous and induction machines shown in Figs. 5.3-1 and 3.4-1. Both have constant inductances and are readily implemented within circuit simulators using the branch element form of Fig. 8.7-1. However, when simulating systems in which electric machines are coupled to power electronic circuits, a challenge arises. Specifically, it is difficult to apply the reference-frame transformation to the models of most power electronic circuits. As a result, coupling the *q*- and *d*-model of a machine to a power electronic circuit represented in terms of physical variables requires one to create a *q*- and *d*- to *abc* circuit interface. A similar challenge is encountered in power system models in which a transmission line/network is represented in terms of phase quantities, as is common, for example, in electromagnetic transient program EMTP-type solvers. In general, the interface that is utilized is software dependent. For example, in PSCAD/EMTDC, the machine model is coupled to the network model using a Norton current source/impedance [10].

An alternative is to model a respective machine using a physical-variable coupled-circuit (PVCC) form, i.e., machine variables. The PVCC model of the induction machine is provided in (2.4-4) and (3.4-1). The PVCC model of the synchronous machine is given by (2.4-4), (5.3-11)–(5.3-14), and (5.3-18)–(5.3-21). An example of the use of the PVCC of the synchronous machine is shown in Fig. 8.7-2, wherein a machine is coupled to a diode rectifier using the branch elements of Fig. 8.7-1. Both the stator and rotor circuits are represented using inductive branches. The stator branches are directly connected to those of the diode circuit. The field winding branch is connected to a voltage source. The damper windings are short circuited. The θ_r in Fig. 8.7-2 is used to denote that the coupling between windings is rotor-position-dependent. In the case of a salient-pole synchronous machine, the stator inductances are also rotor-position-dependent. Although the application of the PVCC model eliminates the need to establish a *q*- and *d*- to *abc* coupling, the position-dependent inductances and the additional branches/elements of the PVCC model add computational cost.

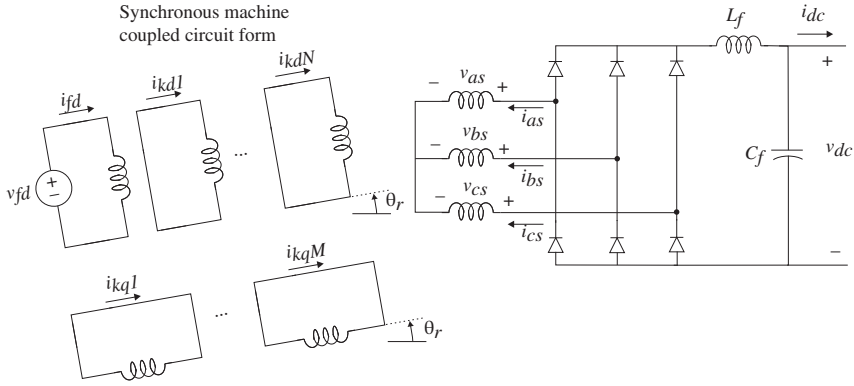

Figure 8.7-2 Machine/rectifier model using PVCC form.

An alternative to the PVCC is a PVVBR formulation that was initially shown to provide advantages in modeling synchronous machines in state-model-based solvers in [11]. The PVVBR model was subsequently shown to have advantages in EMTP-type solvers in [12]. In this section, the PVVBR model is derived. A similar derivation is readily applied to the model of the induction machine and has been documented in [13] and [14].

Prior to deriving the PVVBR model, a few details of notation are necessary. A prime notation ($'$) is used to denote a rotor variable that had been referred to the stator through an appropriate turns ratio. However, it is common in analyzing synchronous machines, that a primed quantity is used to denote a time constant, or inductance associated with the "transient" interval. This is used, for example, in Chapters 5 and 7. Along the same line, a double prime ($''$) is often used to denote a "subtransient" inductance or time constant. Subtransient inductances and time constants are typically expressed assuming there are two damper windings in the q axis and a single damper winding in the d axis. During the "subtransient" interval, all damper windings are active. In this section, all rotor variables are indeed referred to the stator quantities through the turn ratios defined in Chapter 5. However, since here we have introduced additional primed variables, the turn ratio prime is dropped to avoid confusion and the double prime $''$ is applied to denote a dynamic inductance for a machine with arbitrary damper windings in each axis. In the case in which a machine is modeled using a single damper in the d axis and two in the q axis, the dynamic inductances are the traditional subtransient inductances. Finally, since this model is often applied in drive system applications, we take positive stator currents into the machine.

Interestingly, the derivation of the PVVBR for the synchronous machine begins in the rotor frame of reference. Specifically, the q- and d-axis magnetizing flux

linkages

$$\lambda_{mq} = L_{Mq}\left(i^r_{qs} + \sum_{j=1}^{M} i_{kqj}\right) \tag{8.7-1}$$

$$\lambda_{md} = L_{Md}\left(i^r_{ds} + i_{fd} + \sum_{j=1}^{N} i_{kdj}\right) \tag{8.7-2}$$

for a machine with M damper windings in the q-axis and N damper windings in the d-axis are first expressed in terms of rotor flux linkages using the relationship that

$$i_{kqj} = (\lambda_{kqj} - \lambda_{mq})/L_{lkqj} \qquad j = kq1, \ldots, kqM \tag{8.7-3}$$

$$i_{kdj} = (\lambda_{kdj} - \lambda_{md})/L_{lkdj} \qquad j = kd1, \ldots, kdN \tag{8.7-4}$$

$$i_{fd} = (\lambda_{fd} - \lambda_{md})/L_{lfd} \tag{8.7-5}$$

Substituting (8.7-3)–(8.7-5) into (8.7-1) and (8.7-2) with some rearrangement results in

$$\lambda_{mq} = L''_{mq} i^r_{qs} + \lambda''_q \tag{8.7-6}$$

$$\lambda_{md} = L''_{md} i^r_{ds} + \lambda''_d \tag{8.7-7}$$

where

$$L''_{mq} = \frac{1}{L_{Mq}} + \sum_{j=1}^{M} \frac{1}{L_{lkqj}} \tag{8.7-8}$$

$$L''_{md} = \frac{1}{L_{Md}} + \frac{1}{L_{lfd}} + \sum_{j=1}^{N} \frac{1}{L_{lkdj}} \tag{8.7-9}$$

Using (8.7-6) and (8.7-7), the stator flux linkages are then expressed as

$$\lambda^r_{qs} = L''_q i^r_{qs} + \lambda''_q \tag{8.7-10}$$

$$\lambda^r_{ds} = L''_d i^r_{ds} + \lambda''_d \tag{8.7-11}$$

where $L''_q = L_{ls} + L''_{mq}$ and $L''_d = L_{ls} + L''_{md}$ are the dynamic inductances. The dynamic flux linkages are given by

$$\lambda''_q = L''_{mq}\left(\sum_{j=1}^{M} \frac{\lambda_{kqj}}{L_{lkqj}}\right) \tag{8.7-12}$$

$$\lambda''_d = L''_{md}\left(\frac{\lambda_{fd}}{L_{lfd}} + \sum_{j=1}^{N} \frac{\lambda_{kdj}}{L_{lkdj}}\right) \tag{8.7-13}$$

Using (8.7-10) and (8.7-11), the q- and d-axis stator voltage equations of (5.3-8) and (5.3-9) can be written as

$$v_{qs}^r = r_s i_{qs}^r + \omega_r \left(L_d'' i_{ds}^r + \lambda_d''\right) + p\left(L_q'' i_{qs}^r + \lambda_q''\right) \tag{8.7-14}$$

$$v_{ds}^r = r_s i_{ds}^r - \omega_r \left(L_q'' i_{qs}^r + \lambda_q''\right) + p\left(L_d'' i_{ds}^r + \lambda_d''\right) \tag{8.7-15}$$

The terms

$$p\lambda_q'' = -L_{mq}'' \sum_{j=1}^{M} \frac{r_{kqj} i_{kqj}}{L_{lkqj}} \tag{8.7-16}$$

$$p\lambda_d'' = L_{md}'' \left(\frac{v_{fd} - r_{fd} i_{fd}}{L_{lfd}} - \sum_{j=1}^{N} \frac{r_{kdj} i_{kdj}}{L_{lkdj}} \right) \tag{8.7-17}$$

are then expressed in terms of stator current and rotor flux linkages by substituting (8.7-3)–(8.7-5) into (8.7-16) and (8.7-17) and applying the relation (8.7-6) and (8.7-7) to the result. The stator voltage equations are then expressed in a form

$$v_{qs}^r = r_q'' i_{qs}^r + \omega_r L_d'' i_{ds}^r + p L_d'' i_{qs}^r + e_q'' \tag{8.7-18}$$

$$v_{ds}^r = r_d'' i_{ds}^r - \omega_r L_d'' i_{qs}^r + p L_d'' i_{ds}^r + e_d'' \tag{8.7-19}$$

where

$$r_q'' = r_s + L''^2_{mq} \left(\sum_{j=1}^{M} \frac{r_{kqj}}{L_{lkqj}^2} \right) \tag{8.7-20}$$

$$r_d'' = r_s + L''^2_{md} \frac{r_{fd}}{L_{lfd}^2} + L''^2_{md} \left(\sum_{j=1}^{N} \frac{r_{kdj}}{L_{lkdj}^2} \right) \tag{8.7-21}$$

and

$$e_q'' = \omega_r \lambda_d'' + \sum_{j=1}^{M} \left(\frac{L_{mq}'' r_{kqj}}{L_{lkqj}^2} \left(\lambda_q'' - \lambda_{kqj}\right) \right) \tag{8.7-22}$$

$$e_d'' = -\omega_r \lambda_q'' + \sum_{j=1}^{N} \left(\frac{L_{md}'' r_{kdj}}{L_{lkdj}^2} \left(\lambda_d'' - \lambda_{kdj}\right) \right) + \frac{L_{md}''}{L_{lfd}} v_{fd} + \frac{L_{md}'' r_{fd}}{L_{lfd}^2} \left(\lambda_d'' - \lambda_{fd}\right) \tag{8.7-23}$$

Applying the inverse Park's transformation to (8.7-18), (8.7-19), and the zero-sequence voltage equation of (5.3-10) yields

$$\boldsymbol{v}_{abcs} = \boldsymbol{r}_{abcs}''(\theta_r)\boldsymbol{i}_{abcs} + p\left[\boldsymbol{L}_{abcs}''(\theta_r)\boldsymbol{i}_{abcs}\right] + \boldsymbol{e}_{abcs}'' \tag{8.7-24}$$

where $\boldsymbol{L}''_{abcs}$ is an inductance matrix containing dynamic inductances defined as

$$\boldsymbol{L}''_{abcs}(\theta_r) = \begin{bmatrix} L''_S(2\theta_r) & L''_M\left(2\theta_r - \frac{2\pi}{3}\right) & L''_M\left(2\theta_r + \frac{2\pi}{3}\right) \\ L''_M\left(2\theta_r - \frac{2\pi}{3}\right) & L''_S\left(2\theta_r - \frac{4\pi}{3}\right) & L''_M(2\theta_r) \\ L''_M\left(2\theta_r + \frac{2\pi}{3}\right) & L''_M(2\theta_r) & L''_S\left(2\theta_r + \frac{4\pi}{3}\right) \end{bmatrix} \tag{8.7-25}$$

The entries are expressed using $\cdot$ to denote $2\theta_r$, $2\theta_r - \frac{2\pi}{3}$, $2\theta_r + \frac{2\pi}{3}$, respectively, as

$$L''_S(\cdot) = L_{ls} + L''_a - L''_b \cos(\cdot) \tag{8.7-26}$$

$$L''_M(\cdot) = -\frac{L''_a}{2} - L''_b \cos(\cdot) \tag{8.7-27}$$

$$L''_a = \frac{\left(L''_{md} + L''_{mq}\right)}{3} \tag{8.7-28}$$

$$L''_b = \frac{\left(L''_{md} - L''_{mq}\right)}{3} \tag{8.7-29}$$

The resistance matrix is

$$\boldsymbol{r}''_{abcs}(\theta_r) = \begin{bmatrix} r''_S(2\theta_r) & r''_M\left(2\theta_r - \frac{2\pi}{3}\right) & r''_M\left(2\theta_r + \frac{2\pi}{3}\right) \\ r''_M\left(2\theta_r - \frac{2\pi}{3}\right) & r''_S\left(2\theta_r - \frac{4\pi}{3}\right) & r''_M(2\theta_r) \\ r''_M\left(2\theta_r + \frac{2\pi}{3}\right) & r''_M(2\theta_r) & r''_S\left(2\theta_r + \frac{4\pi}{3}\right) \end{bmatrix} \tag{8.7-30}$$

where the entries are defined as follows:

$$r''_S(\cdot) = r_s + r''_a - r''_b \cos(\cdot) \tag{8.7-31}$$

$$r''_M(\cdot) = \frac{-r''_a}{2} - r''_b \cos(\cdot) \tag{8.7-32}$$

$$r''_a = \frac{r''_d + r''_q}{3} - \frac{2}{3} r_s \tag{8.7-33}$$

$$r''_b = \frac{r''_d - r''_q}{3} \tag{8.7-34}$$

The stator voltage equations given in (8.7-24), along with the rotor state equations

$$p\lambda_{kqj} = -\frac{r_{kqj}}{L_{lkqj}}(\lambda_{kqj} - \lambda_{mq}); \;\; j = 1, \cdots M \tag{8.7-35}$$

$$p\lambda_{kdj} = -\frac{r_{kdj}}{L_{lkdj}}(\lambda_{kdj} - \lambda_{md}) \; ; \; j = 1, \cdots N \tag{8.7-36}$$

$$p\lambda_{fd} = -\frac{r_{fd}}{L_{lfd}}(\lambda_{fd} - \lambda_{md}) + v_{fd} \tag{8.7-37}$$

where λ_{mq} and λ_{md} are given by (8.7-6) and (8.7-7), define a detailed PVVBR model of the synchronous machine. When implementing the PVVBR model, the stator windings are included in defining the circuit topology using the canonical branch circuit elements of Fig. 8.7-1. The rotor voltage equations are expressed explicitly in state model form with flux linkages as state variables. The subtransient voltages e''_q and e''_d represent outputs of the rotor model and are incorporated into the stator circuit as dependent sources. The stator branch currents are transformed to the rotor reference frame and represent inputs to the rotor state model. This is shown pictorially in Fig. 8.7-3.

A few comments are in order regarding the PVVBR model. First, the assumptions upon which the model is based are identical to those of the traditional q- and d-model and the PVCC model. Thus, neglecting numerical error, the responses predicted using all three models should be the same. In addition, no assumptions have been made in regard to winding configuration. The windings may be connected in wye, delta, or the individual windings may be supplied by isolated converter circuits. Among the advantages, the PVVBR form has over a PVCC form is the reduced computation burden, due to a reduction in the number of nodes/branches required to characterize the stator windings. In addition, the eigenstructure of the PVVBR yields improved numerical accuracy, which is highlighted in [11] and explained in further detail in [12]. Of course, each application and computer language presents its own challenges, and thus the choice of the model structure, state variables, and reference frame often requires experience and engineering judgment.

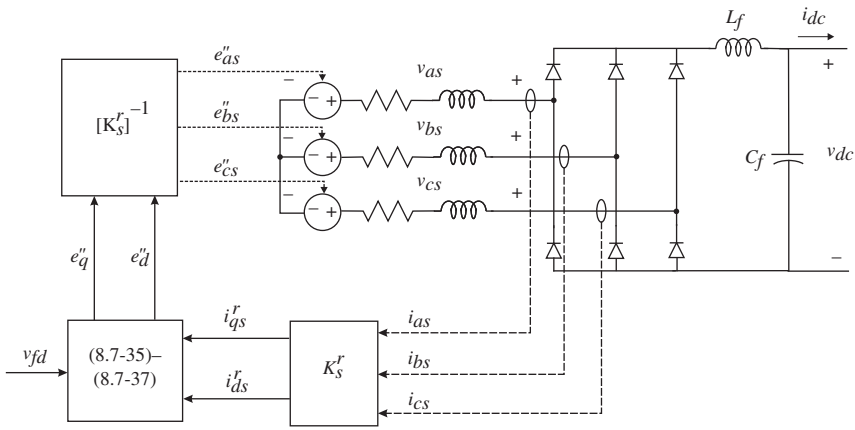

Figure 8.7-3 Machine/rectifier model using the PVVBR model.

Among the challenges that can be faced when implementing the PVVBR model are the rotor-dependent resistances and inductances. The rotor-dependent resistances can be eliminated by restructuring the model slightly. Specifically, the terms $\left(\sum_{j=1}^{M} \frac{r_{kqj}}{L_{lkqj}^2}\right) L_{mq}''^2 i_{qs}^r$ and $\left(\frac{r_{fd}}{L_{lfd}^2} + \sum_{j=1}^{N} \frac{r_{kdj}}{L_{lkdj}^2}\right) L_{md}''^2 i_{ds}^r$ that are represented using resistances in (8.7-18) and (8.7-19) can be incorporated into the back-emf expressions in any simulation packages that allow current-based voltage sources in series with inductive branches. Doing so also eliminates resistive coupling between windings. An alternative, that has been applied in the derivation of average-value models of machine-rectifier systems [15], is to neglect the $p\lambda_q''$ and $p\lambda_d''$ in (8.7-14) and (8.7-15). The justification is that the rotor flux linkages are relatively constant over a switching interval. Particular care must be applied in making such an approximation in that it has been shown in [16] that the resulting model can be unstable.

Eliminating the rotor-dependent inductances represents a more unique challenge and is related to the neglect of dynamic saliency in transient stability formulations. In the PVVBR model, the rotor-position-dependent inductances are eliminated if the assumption

$$L_b'' = \frac{\left(L_{md}'' - L_{mq}''\right)}{3} \cong 0 \tag{8.7-38}$$

is made. Determining mathematical bounds for the error resulting from such an approximation is a tedious, if not intractable, task. In [17], the effect of applying the approximation of (8.7-38) was considered in the frequency domain by comparing the q- and d-axis operational impedance of the PVVBR models with/without the approximation. Example results are shown in Fig. 8.7-4. Comparing the impedances of the PVVBR and approximate PVVBR models shows the frequency-domain errors associated with making the approximation of (8.7-38). In particular, the curves are both shifted by $\left|X_d'' - X_q''\right|/2$ over the entire frequency range. An alternative to the approximation of (8.7-38) was proposed in [17]. Therein, an additional damper winding is placed along the q axis. The additional damper winding is used to fit machine parameters to approximate impedance curves that have equal dynamic reactances but match the original operational impedances for frequencies less than a user-specified fit frequency, f_r. The impact of doing so is shown in the frequency domain in Fig. 8.7-5. In applying such an approximation, the user must balance between error and numerical stiffness. Specifically, as f_r is increased, the error between the salient and nonsalient versions of the PVVBR model reduces. However, the time constant associated with the additional damper winding increases. In [17], it is shown that a reasonable balance between error and stiffness can be made and that the resulting model yields much less error in the time-domain responses compared to a model in which (8.7-38) is applied.

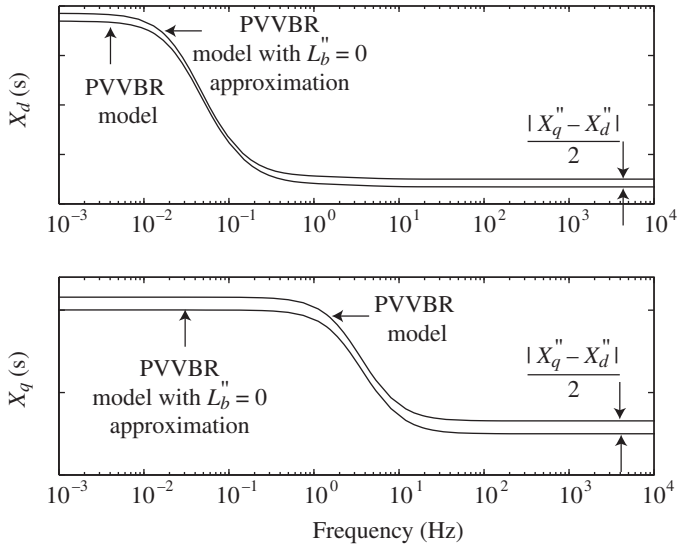

Figure 8.7-4 Operational impedance of PVVBR model and PVVBR model with approximation of $L_b'' \cong 0$.

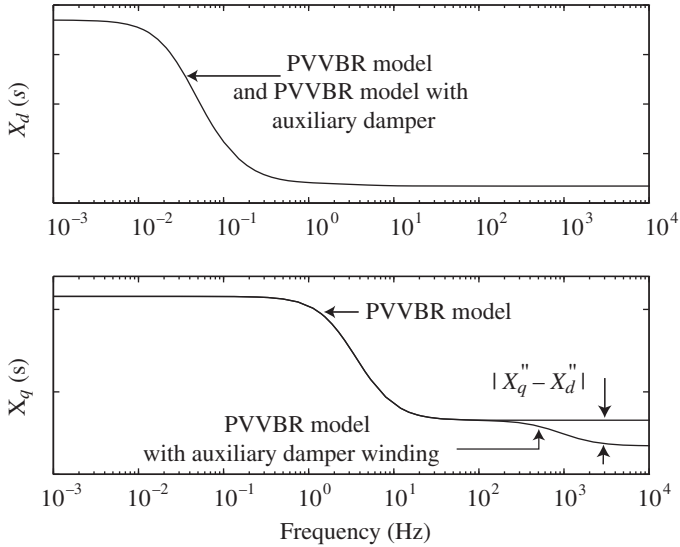

Figure 8.7-5 Operational impedance of PVVBR model and PVVBR model with auxiliary damper winding to force $L_b'' = 0$.

A question that often arises is how to model saturation in the physical variable models. Specifically, at first glance, it appears to be a challenge, since all stator self and mutual inductances are impacted. A relatively straightforward method of incorporating *d*-axis saturation within the PVVBR model has been shown in [18]. A more general approach in which saturation is modeled in both axis and transfer functions to represent rotor dynamics is presented in [19].

8.8 Reduced-Order Voltage-Behind-Reactance Model

As indicated in Section 6.4, a common practice in modeling power systems is to neglect electric transients of the stator voltage equations. The resulting reduced-order model can be represented in a VBR model form. Specifically, by expressing (6.4-1) and (6.4-2) in terms of dynamic inductances and flux linkages, the reduced-order stator voltage equations can be written as

$$v_{qs}^r = -r_s i_{qs}^r - \omega_e L_d'' i_{ds}^r + e_q'' \tag{8.8-1}$$

$$v_{ds}^r = -r_s i_{ds}^r + \omega_e L_q'' i_{qs}^r + e_d'' \tag{8.8-2}$$

where

$$e_q'' = \omega_e \lambda_d'' \tag{8.8-3}$$

$$e_d'' = -\omega_e \lambda_q'' \tag{8.8-4}$$

Equations (8.8-1) and (8.8-2), together with the state equations of the rotor flux linkages of (8.7-35)–(8.7-37) form a reduced-order VBR model. If the stator voltages are expressed as

$$v_{qs}^r = \sqrt{2} v_s \cos\delta \tag{8.8-5}$$

$$v_{ds}^r = \sqrt{2} v_s \sin\delta \tag{8.8-6}$$

and the stator resistance neglected, an approximate expression for electromagnetic torque commonly used in transient stability analysis can be derived using (8.8-1) and (8.8-2) to express stator current in terms of stator voltage and using the result in the expression for torque (5.8-22). The approximate torque is expressed as

$$T_e = \frac{3}{4}\frac{P}{\omega_e^2}\left(-\frac{\sqrt{2} v_s e_d''}{L_q''}\cos\delta + \frac{\sqrt{2} v_s e_q''}{L_d''}\sin\delta + \left(\frac{1}{L_q''} - \frac{1}{L_d''}\right) v_s^2 \sin 2\delta\right) \tag{8.8-7}$$

References

1 P. C. Krause, *Analysis of Electric Machinery*, McGraw-Hill, 1st Ed., 1986.

2 *ACSLX, Advanced Continuous Simulation Language, User's Guide*, Version 2.4, The AEgis Technologies Group, Inc., March 2008. Available: http://www.acslsim.com.

3 *EASY5 Engineering Software for the Design, Analysis and Simulation*, MSC SimEnterprise, Inc. Available: http://www.mscsoftware.com

4 *EUROSTAG: Software for Simulation of Large Electric Power Systems*, Tractebel Energy Engineering. Available: http://www.eurostag.be and www.tractebel-engineering.com.

5 *Simulink Dynamic System Simulation Software – Users Manual*, MathWorks, Inc., Natick, Massachusetts, 2009. Available: http://www.mathworks.com.

6 Simulink Dynamic System Simulation Software–SymPowerSystems Manual, The MathWorks, Inc., Natick, Massachusetts, 2009.

7 *RT-Lab User's Manual*, Opal-RT Technologies, Montréal, Québec, Canada, Available: http://www.opal-rt.com.

8 *Piecewise Linear Electrical Circuit Simulation (PLECS) User Manual, Version*. 1.5, Plexim GmbH, 2006. Available: www.plexim.com.

9 *Automated State Model Generator (ASMG), Reference Manual*, Version 2, PC Krause and Associates Inc. www.pcka.com, 2002.

10 *EMTDC User's Guide*. Winnipeg, MB, Canada: Manitoba HVDC Research Center Inc., 2004.

11 S. D. Pekarek, O. Wasynczuk, H. J. Hegner, "An Efficient and Accurate Model for the Simulation and Analysis of Synchronous Machine/Converter Systems," *IEEE PES*, Vol. 13, No. 1, pp. 42–48, March 1998.

12 L. Wang and J. Jatskevich, "A Voltage-Behind-Reactance Synchronous Machine Model for the EMTP-type Solution," *IEEE Trans. Power Systems*, Vol. 21, No. 4, pp. 1539–1549, November 2006.

13 L. Wang, J. Jatskevich, S. D. Pekarek, "Modeling of Induction Machines Using a Voltage-Behind-Reactance Formulation," *IEEE PES*, Vol. 23, No. 2, pp. 382–392, June 2008.

14 L. Wang, J. Jatskevich, C. Wang, and P. Li, "A Voltage-Behind-Reactance Induction Machine Model for the EMTP-type Solution," *IEEE Trans. Power Systems*, Vol. 23, No. 3, pp. 1226–1238, August 2008.

15 S. D. Sudhoff, O. Wasynczuk, "Analysis and Average-Value Modeling of Line-Commutated Converter Synchronous Machine Systems," *IEEE PES*, Vol. 8, No. 1, pp. 92–99, March 1993.

16 S. D. Pekarek, A Partitioned State Model of Synchronous Machines for Simulation/Analysis of Power/Drive Systems, Ph.D. Thesis, Purdue University, 1996.

17 S. D. Pekarek, E. A. Walters, "An Accurate Method of Neglecting Dynamic Saliency of Synchronous Machines in Power Electronic Based Systems," *IEEE PES*, Vol. 14, No. 4, pp. 1177–1183, December 1999.

18 S. D. Pekarek, E. A. Walters, B. T. Kuhn, "An Efficient and Accurate Method of Representing Saturation in Physical-Variable Models of Synchronous Machines," *IEEE PES*, Vol. 14, No. 1, pp. 72–29, March 1999.

19 D. C. Aliprantis, O. Wasynczuk, C. D. Rodriguez Valdez, "A Voltage-Behind-Reactance Synchronous Machine Model With Saturation and Arbitrary Rotor Network Representation," *IEEE PES*, Vol. 23, No. 2, pp. 499–508, June 2008.

Problems

8.1 Derive the small-displacement equations of an induction machine with flux linkages per second as state variables. Express the equations in fundamental form.

8.2 Repeat Problem 1 for a synchronous machine.

8.3 Write the small-displacement equations for an induction machine with currents as state variables and with a small displacement in ω_e where $\Delta\omega_e$ is an input variable. It is clear that the resulting equations are valid for small changes in the frequency of the applied stator voltages.

8.4 Repeat Problem 3 for a synchronous machine.

8.5 Derive the PVVBR model of the three-phase induction machine.

8.6 Assume the stator windings of an induction machine are connected in wye. Simplify the PVVBR model derived in Problem 5, using the fact that $i_{0s} = 0$.

8.7 In the case of a three-phase synchronous machine, L_{Mq} and L_{Md} are defined with a 3/2 factor. This factor is unity in the case of the two-phase machine. Why?

9

Semi-Controlled Bridge Converters

9.1 Introduction

A brief analysis of single- and three-phase semi-controlled bridge converters is presented in this chapter. This type of converter is also commonly referred to as a line-commutated converter. The objective is to provide a basic background in converter operation without becoming overly involved. For this reason, only the constant-current operation is considered. A more detailed analysis of these and other converters can be found in References 1–4. Finally, to set the stage for the analysis of dc and ac drive systems in later chapters, an average-value model of the three-phase semi-controlled bridge converter is derived. This model can be used to predict the average-value performance during steady-state and transient operating conditions.

9.2 Single-Phase Load Commutated Converter

A single-phase line-commutated full-bridge converter is shown in Figure 9.2-1. The ac source voltage and current are denoted e_{ga} and i_{ga}, respectively. The series inductance (commutating inductance) is denoted l_c. The thyristors are numbered $T1$ through $T4$, and the associated gating or firing signals are denoted e_{f1} through e_{f4}. The converter output voltage and current are v_d and i_d. The following simplifying assumptions are made in this analysis: (1) the ac source contains only one frequency, (2) the output current i_d is constant, (3) the thyristor is an infinite impedance device when in the reverse bias mode (cathode positive) or when the gating signal to allow current flow has not occurred, and (4) when conducting, the voltage drop across the thyristor is negligibly small.

Analysis of Electric Machinery and Drive Systems, Fourth Edition.
Paul C. Krause, Oleg Wasynczuk, Scott D. Sudhoff, and Steven D. Pekarek.

Companion website: www.wiley.com/go/krause_aem4e

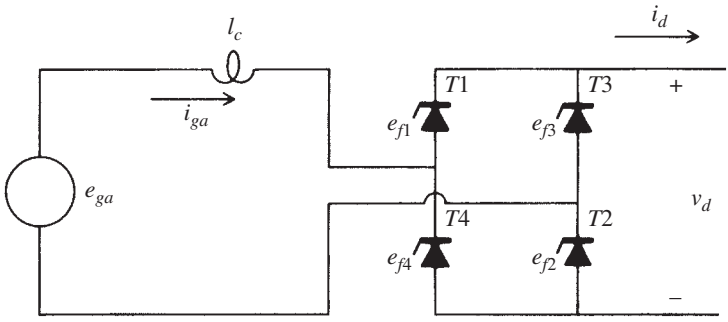

Figure 9.2-1 Single-phase full-bridge converter.

Operation without Commutating Inductance or Firing Delay

It is convenient to analyze converter operation in steps starting with the simplest case where the commutating inductance is not present and there is no firing delay. In this case, it can be assumed that the gating signals are always present, whereupon the thyristors will conduct whenever they become forward biased (anode positive) just as if they were diodes. Converter operation for constant i_d with $l_c = 0$ and without firing delay is depicted in Figure 9.2-2. The thyristor in the upper part of the converter (*T1* or *T3*) that conducts is the one with the greatest anode voltage. Similarly, the thyristor that conducts in the lower part of the converter ($T2$ or $T4$) is the one whose cathode voltage is the most negative. In this case, the converter operates as a full-wave rectifier.

Let us begin our analysis assuming that the source voltage may be described by

$$e_{ga} = \sqrt{2}E\cos\theta_g \tag{9.2-1}$$

where

$$\theta_g = \omega_g t + \phi_g \tag{9.2-2}$$

In (9.2-2), ω_g and ϕ_g are the radian frequency and phase of the source, respectively. We wish to compute the steady-state average-value of v_d, which is defined as

$$\overline{V}_d = \frac{1}{2\pi}\int_{-\pi}^{\pi} v_d d\theta_g \tag{9.2-3}$$

It is noted that the output voltage is made up of two identical π intervals per cycle of the source voltage. For the interval $-\pi/2 \le \theta_g \le \pi/2$

$$v_d = e_{ga} \tag{9.2-4}$$

Using symmetry and (9.2-1)–(9.2-4), the average output voltage may be determined by finding the average of (9.2-3) over the interval $-\pi/2 \le \theta_g \le \pi/2$. Thus,

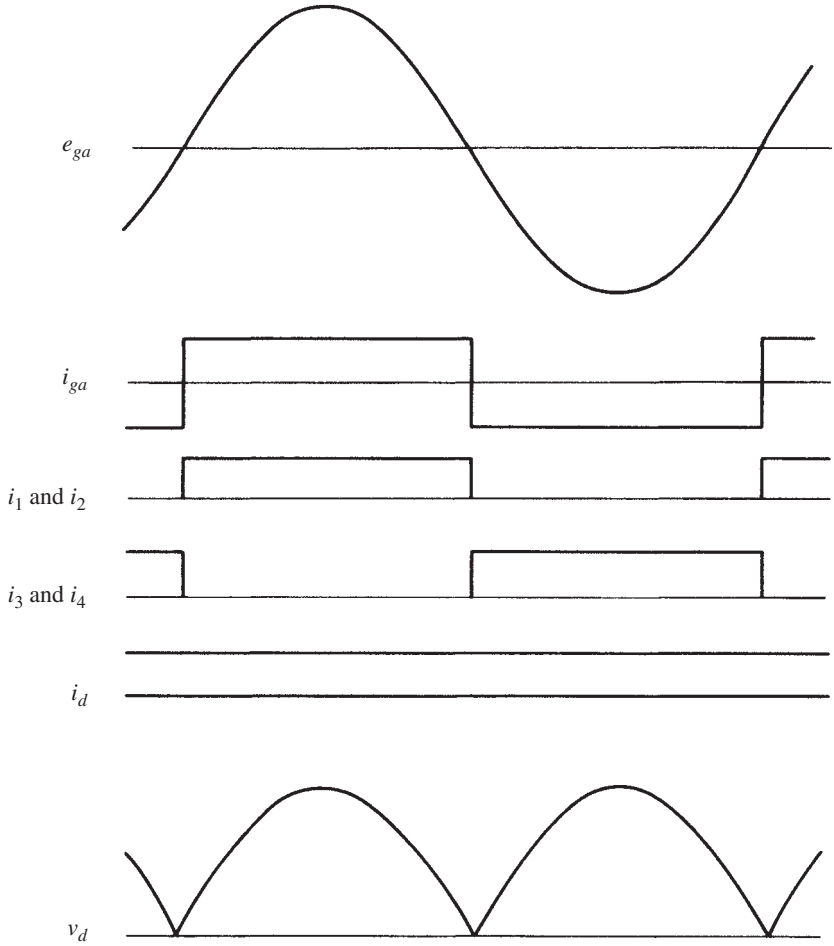

Figure 9.2-2 Single-phase, full-bridge converter operation for constant output current without l_c and firing delay.

the average-value of v_d may be expressed

$$\overline{V}_d = V_{d0} = \frac{1}{\pi}\int_{-\pi/2}^{\pi/2} \sqrt{2}E\cos\theta_g d\theta_g$$
$$= \frac{2\sqrt{2}}{\pi}E \tag{9.2-5}$$

where E is the rms value of the source voltage. We will use V_{d0} to denote the average output voltage without commutation inductance and without firing delay.

Operation with Commutating Inductance and without Firing Delay

When l_c is zero, the process of "current switching" from one thyristor to the other in either the upper or lower part of the converter ($T1$ to $T3$ to $T1$ to . . . , etc., and $T2$ to $T4$ to $T2$ to . . . , etc.) takes place instantaneously. Instantaneous commutation cannot occur in practice since there is always some inductance between the source and the converter. The operation of the converter with commutating inductance and without firing delay is shown in Figure 9.2-3. During commutation, the source is short-circuited simultaneously through $T1$ and $T3$ and through $T2$ and $T4$. Hence, if we consider the commutation from $T1$ to $T3$

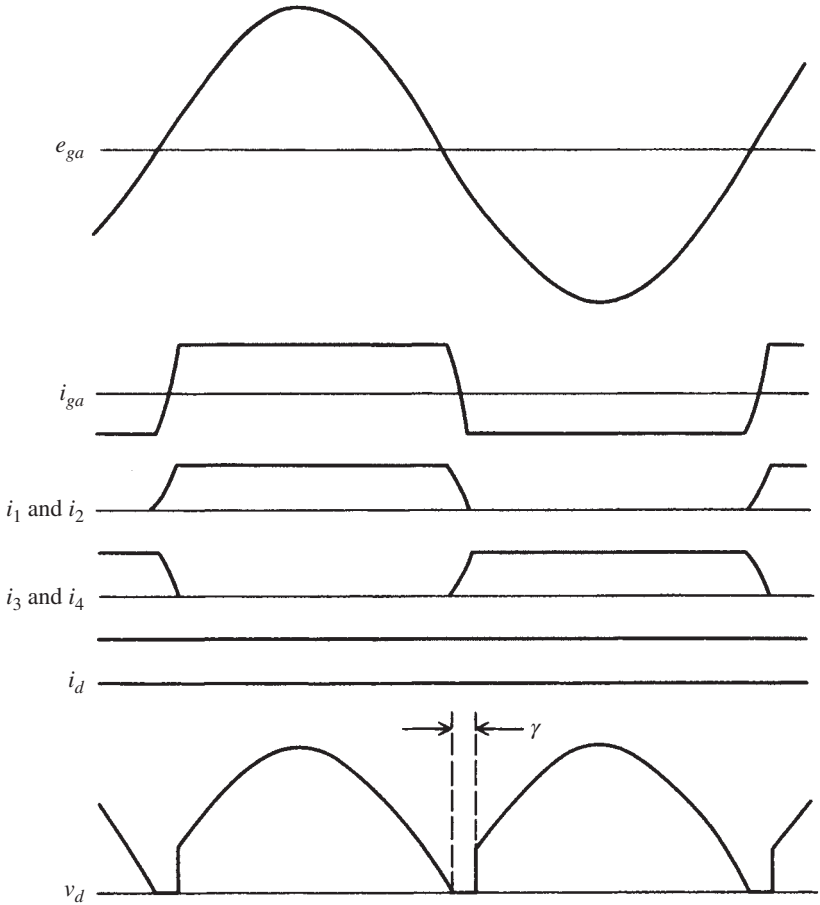

Figure 9.2-3 Single-phase, full-bridge converter operation for constant output current with l_c and without firing delay.

and $T2$ to $T4$ and if we assume that the short-circuit current during commutation is positive through $T3$, then

$$e_{ga} = -l_c \frac{di_3}{dt} \tag{9.2-6}$$

where i_3 is the current in thyristor T3. Substituting (9.2-1) into (9.2-6) and solving for i_3 yields

$$\begin{aligned} i_3 &= -\frac{1}{l_c} \int \sqrt{2}E \cos\theta_g dt \\ &= -\frac{\sqrt{2}E}{\omega_g l_c} \sin\theta_g + C \end{aligned} \tag{9.2-7}$$

At $\theta_g = \pi/2$, $i_3 = 0$, therefore

$$C = \frac{\sqrt{2}E}{\omega_g l_c} \tag{9.2-8}$$

whereupon

$$i_3 = \frac{\sqrt{2}E}{\omega_g l_c}(1 - \sin\theta_g) \tag{9.2-9}$$

At the end of commutation $\theta_g = \pi/2 + \gamma$ and $i_3 = I_d$, therefore

$$I_d = \frac{\sqrt{2}E}{\omega_g l_c}(1 - \cos\gamma) \tag{9.2-10}$$

where γ is the commutation angle (Fig. 9.2-3). The uppercase (I_d) is used to denote constant or steady-state quantities. During commutation, the converter output voltage v_d is zero. Once commutation is completed, the short-circuit paths are broken, and the output voltage jumps to the value of the source voltage since i_d, and hence i_{ga}, are assumed constant after commutation. Since i_{ga} is constant, zero voltage is dropped across the inductance l_c. It is recalled that V_{d0} given by (9.2-5) is the average converter output voltage when l_c is zero. When l_c is considered, the output voltage is zero during commutation. Hence, the average output voltage decreases due to commutation. The average converter output voltage may be determined by

$$\begin{aligned} \overline{V}_d &= \frac{1}{\pi} \int_{-\pi/2+\gamma}^{\pi/2} \sqrt{2}E \cos\theta_g d\theta_g \\ &= \frac{V_{d0}}{2}(1 + \cos\gamma) \end{aligned} \tag{9.2-11}$$

If (9.2-10) is solved for $\cos\gamma$ and the result substituted into (9.2-11), the average converter output voltage with commutating inductance but without firing delay becomes

$$\overline{V}_d = V_{d0} - \frac{\omega_g l_c}{\pi} I_d \tag{9.2-12}$$

It is interesting to note that commutation appears as a voltage drop as if the converter had an internal resistance of $\omega_g l_c/\pi$. However, this is not a resistance in the sense that it does not dissipate energy.

Operation without Commutating Inductance and with Firing Delay

Thus far, we have considered the thyristor as a diode and hence have only considered rectifier operation of the converter. However, the thyristor will conduct only if the anode voltage is positive and it has received a gating signal. Hence, the conduction of a thyristor may be delayed after the anode has become positive by delaying the gating signal (firing signal). Converter operation with firing delay but without commutating inductance is shown in Figure 9.2-4.

We can determine the average output by

$$\begin{aligned}\overline{V}_d &= \frac{1}{\pi}\int_{-\pi/2+\alpha}^{\pi/2+\alpha} \sqrt{2}E\cos\theta_g d\theta_g \\ &= \frac{2\sqrt{2}}{\pi}E\cos\alpha \\ &= V_{d0}\cos\alpha\end{aligned} \tag{9.2-13}$$

where α is the firing delay angle (Fig. 9.2-4). If the current is maintained constant, the average output voltage will become negative for α greater than $\pi/2$. This is referred to as inverter operation, wherein average power is being transferred from the dc part of the circuit to the ac part of the circuit.

Operation with Commutating Inductance and Firing Delay

Converter operation with both commutating inductance and firing delay is shown in Figure 9.2-5. The calculation of i_3 and $\overline{V}_d$ are identical to that given by (9.2-6)–(9.2-12), except that the intervals of evaluation are different. In particular, (9.2-7) applies, but it is at $\theta_g = \pi/2 + \alpha$, where $i_3 = 0$, thus

$$C = \frac{\sqrt{2}E}{\omega_g l_c}\cos\alpha \tag{9.2-14}$$

Commutation ends at $\theta_g = \pi/2 + \alpha + \gamma$, whereupon $i_3 = I_d$, thus

$$I_d = \frac{\sqrt{2}E}{\omega_g l_c}[\cos\alpha - \cos(\alpha+\gamma)] \tag{9.2-15}$$

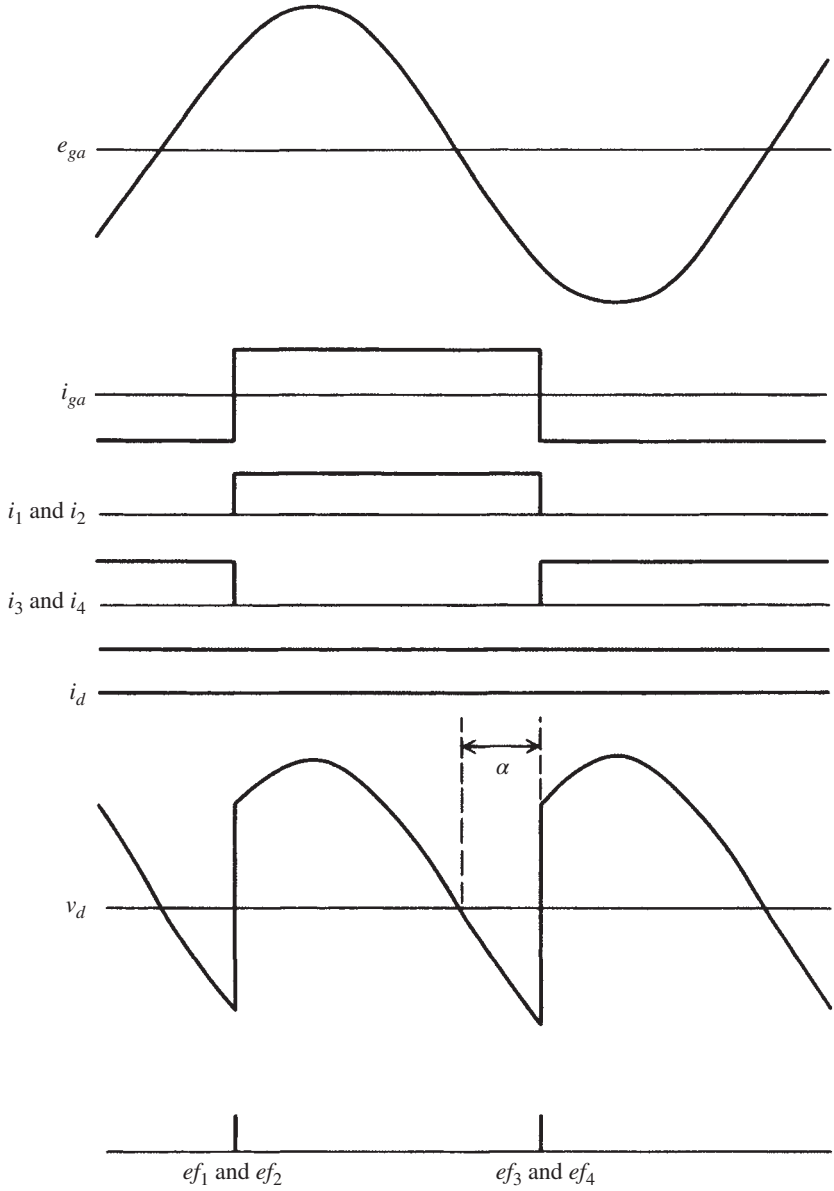

Figure 9.2-4 Single-phase, full-bridge converter operation for constant output current with l_c and firing delay.

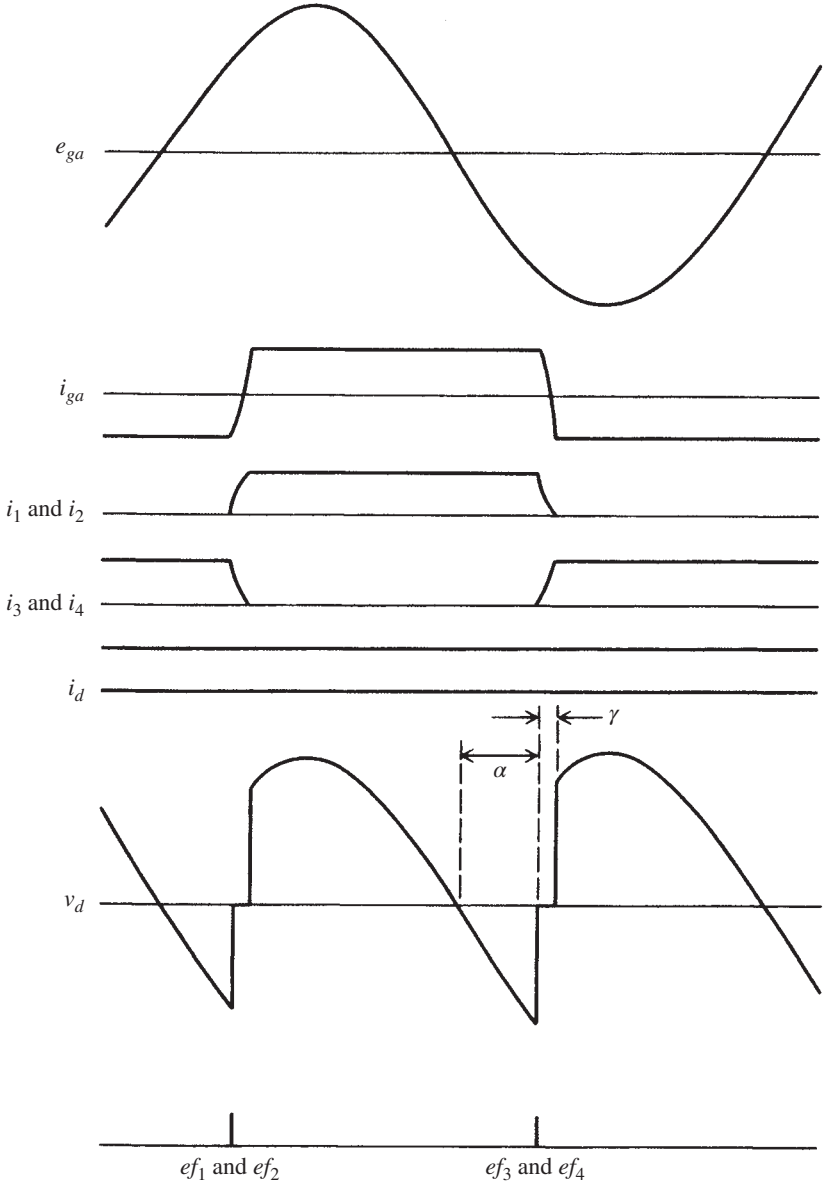

Figure 9.2-5 Single-phase, full-bridge converter operation for constant output current with l_c and firing delay.

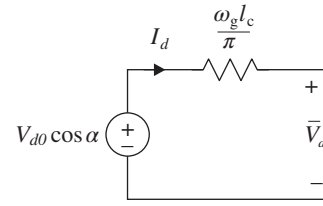

Figure 9.2-6 Average-value equivalent circuit for a single-phase full-bridge converter.

From (9.2-13)

$$V_d = \frac{1}{\pi}\int_{-\pi/2+\alpha+\gamma}^{\pi/2+\alpha} \sqrt{2}E\cos\theta_g d\theta_g$$
$$= \frac{V_{d0}}{2}[\cos\alpha + \cos(\alpha+\gamma)] \tag{9.2-16}$$

Solving (9.2-15) for $\cos(\alpha+\gamma)$ and substituting the results into (9.2-16) yields the following expression for the average output voltage with commutating inductance and firing delay.

$$\overline{V}_d = V_{d0}\cos\alpha - \frac{\omega_g l_c}{\pi} I_d \tag{9.2-17}$$

The equivalent circuit suggested by (9.2-17) is shown in Figure 9.2-6.

The average-value relations and corresponding equivalent circuit depicted in Figure 9.2-6 were developed based upon the assumptions that (1) the rms amplitude of the ac source voltage, E, is constant, and (2) the dc load current i_d is constant and hence denoted I_d. This equivalent circuit provides a reasonable approximation of the average dc voltage even if E and i_d vary with respect to time provided that the variations from one conduction interval to the next are small.

Modes of Operation

Various modes of operation of a single-phase, full-bridge converter are illustrated by simulation results in Figure 9.2-7, Figure 9.2-8, and Figure 9.2-9. The source voltage is 280 V (rms) and the commutating inductance in 1.4 mH. In each case, e_{ga}, i_{ga}, i_1, i_3, v_d, and i_d are plotted, where i_1 and i_3 are the currents through thyristors $T1$ and $T3$, respectively. In Figure 9.2-7a, the converter is operating with a series RL load connected across the output terminals, where $R = 3\,\Omega$ and $L = 40$ mH. In Figure 9.2-7a, the converter is operating without firing delay. In Figure 9.2-7b, the firing delay angle is 45°. In Figure 9.2-7c, the firing delay is slightly less than 90°; the current i_d is discontinuous. The output current is nearly constant when the converter is operating without firing delay due to the large-load inductance.

In the case shown in Figure 9.2-8, the combination of a series RL ($R = 3\,\Omega$, $L = 40$ mH) connected in series with a constant 200-V source is connected across

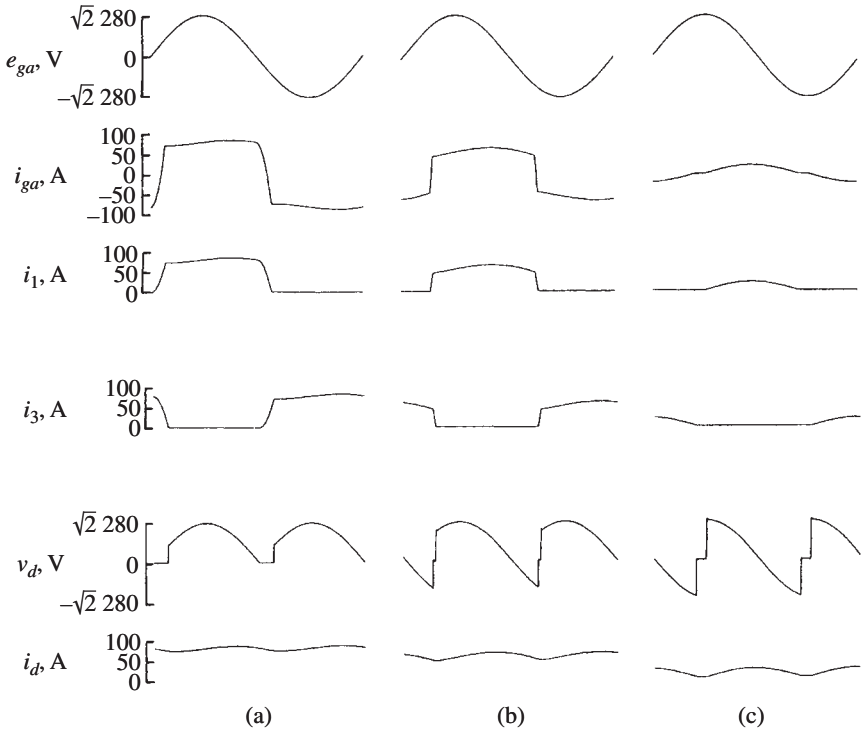

Figure 9.2-7 Single-phase, full-bridge converter operation with RL load. (a) $\alpha = 0°$; (b) $\alpha = 45°$; (c) $\alpha \approx 90°$, discontinuous operation.

the output terminals of the converter. The dc source is connected so that it opposes a positive v_d. In Figure 9.2-8a, the converter is operating without firing delay, while in Figure 9.2-8b, the firing delay angle is 60°. During the zero-current portion of operation, v_d is equal to 200 V, the magnitude of the series-connected dc source.

Inverter operation is depicted in Figure 9.2-9. In this case, the combination of the RL load and dc source is still connected across the output terminals of the converter, but the polarity of the dc source is reversed. In Figure 9.2-9a, the firing delay angle is 108°. In Figure 9b, the firing delay angle is 126°.

Although (9.2-17) was derived for a constant output current, it is quite accurate for determining the average values of converter voltage and current, especially if the current is not discontinuous. The reader should take the time to compare the calculated converter output voltage and current using (9.2-17) with the average-values shown in Figure 9.2-7, Figure 9.2-8, and Figure 9.2-9, and to qualitatively justify any differences that may occur.

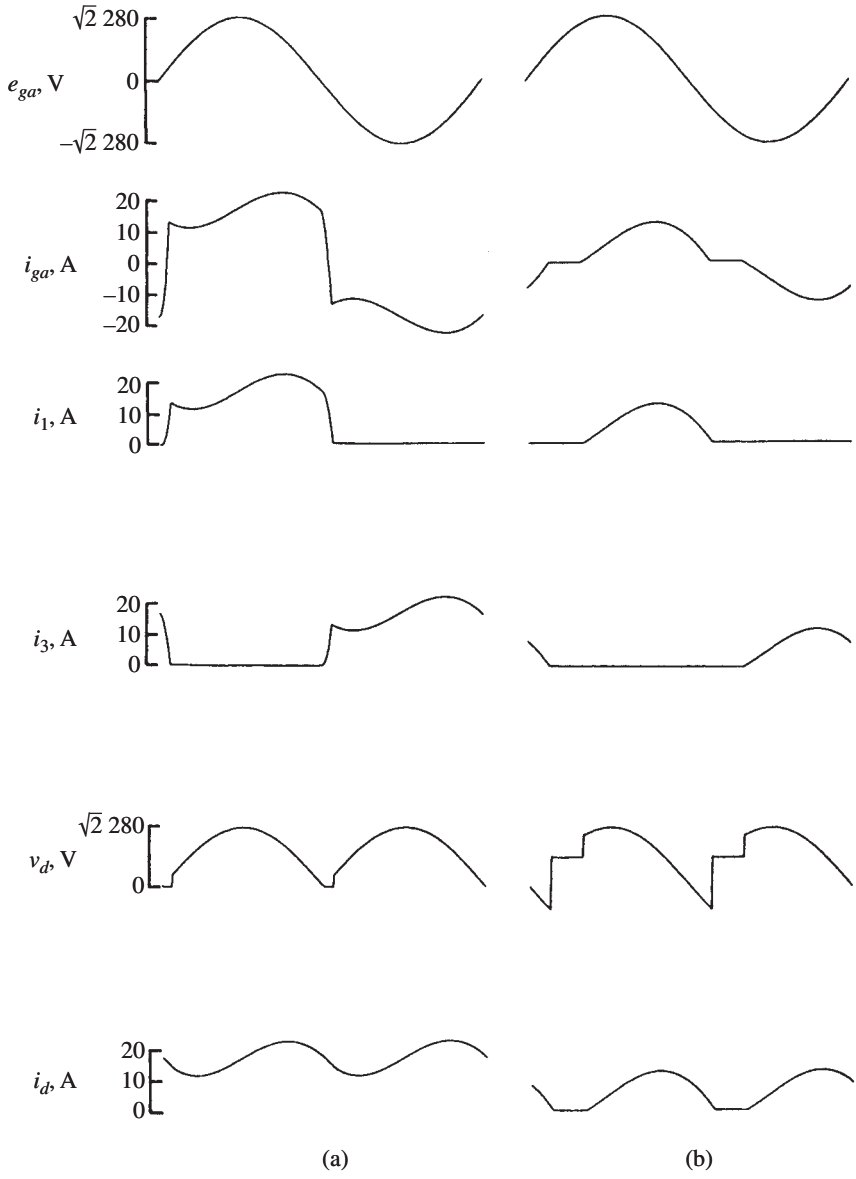

Figure 9.2-8 Single-phase, full-bridge converter operation with RL and an opposing dc source connected in series across the converter terminals. (a) $\alpha = 0°$; (b) $\alpha = 60°$.

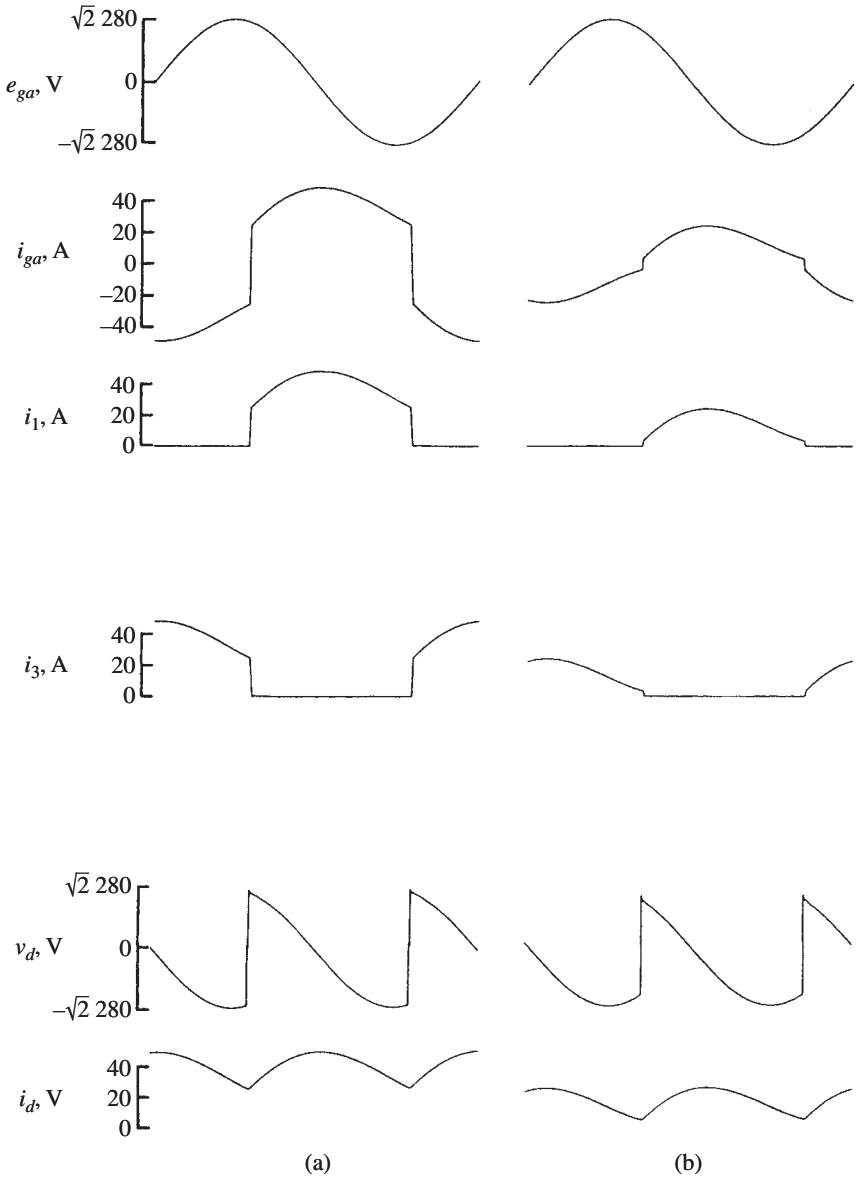

Figure 9.2-9 Single-phase, full-bridge converter operation with RL and an aiding dc source connected in series across the converter terminals. (a) $\alpha = 108°$; (b) $\alpha = 126°$.

9.3 Three-Phase Load Commutated Converter

A three-phase, line-commutated, full-bridge converter is shown in Figure 9.3-1. The voltages of the three-phase, ac source are denoted e_{ga}, e_{gb}, and e_{gc}, and the phase currents i_{ag}, i_{bg}, and i_{cg}. The ac source voltages may be expressed as

$$e_{ga} = \sqrt{2}E\cos\theta_g \tag{9.3-1}$$

$$e_{bg} = \sqrt{2}E\cos\left(\theta_g - \frac{2\pi}{3}\right) \tag{9.3-2}$$

$$e_{cg} = \sqrt{2}E\cos\left(\theta_g + \frac{2\pi}{3}\right) \tag{9.3-3}$$

where E is the rms magnitude of the source voltage, θ_g is given by (9.2-2) and is the angular position of the source voltages, and the source frequency is $\omega_g = p\theta_g$. The ac side inductance (commutating inductance) is denoted as l_c. The thyristors are numbered $T1$ through $T6$ in the order in which they are turned on and the gating or firing signals for the thyristors are e_{f1} through e_{f6}. The converter output voltage and current are denoted v_d and i_d, respectively. This circuit also includes a dc inductor and resistor, L_{dc} and r_{dc}, that may represent the armature inductance and resistance of a dc machine or the inductance and resistance of a filtering circuit. Likewise, the voltage e_d may represent the back emf of a dc machine or the capacitor voltage in a dc filter.

Modes of Operation

Before analyzing the converter, it is instructive to consider several modes of operation of a three-phase, full-bridge converter illustrated in Figure 9.3-2, Figure 9.3-3, and Figure 9.3-4 by simulation results. The line-to-line ac source voltage is 208 V (rms) and the commutating inductance is 45 μH. In each case, e_{ga}, $i_{ga} = -i_{ag}$, i_1, i_3, v_d, and i_d are plotted where the currents i_1 and i_3 are the currents through thyristors $T1$ and $T3$, respectively.

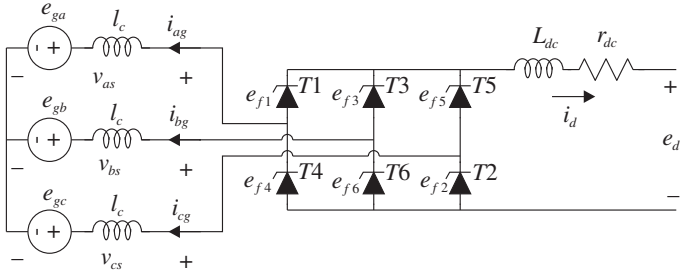

Figure 9.3-1 Three-phase full-bridge converter.

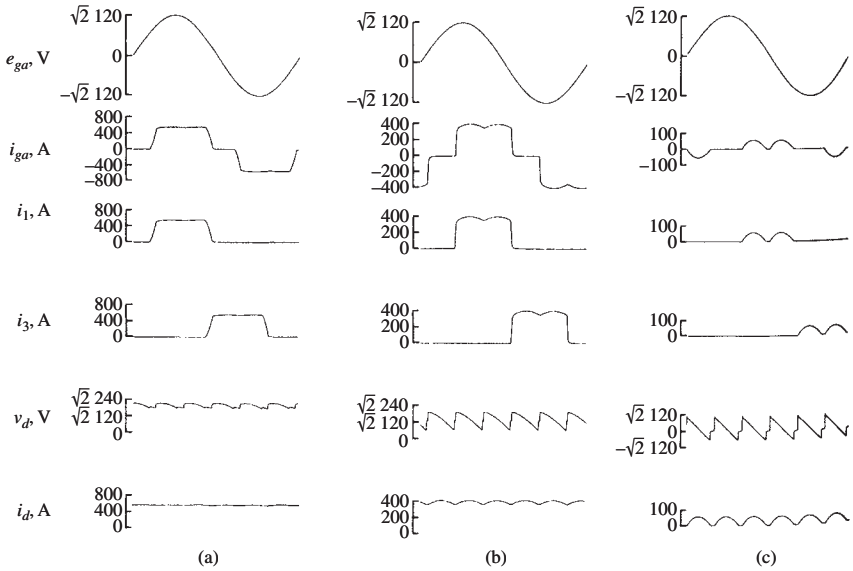

Figure 9.3-2 Three-phase, full-bridge converter operation with RL load. (a) $\alpha = 0°$; (b) $\alpha = 45°$; (c) $\alpha = 90°$.

In Figure 9.3-2, the converter is operating with $r_{dc} = 0.5\,\Omega$, $L_{dc} = 1.33$ mH, and $e_d = 0$. In Figure 9.3-2a, the converter is operating without firing delay. It is interesting to note that the output current is nearly constant. In this study, there are alternately two or three thyristors conducting; hence, this will be referred to as 2-3 mode, which is the normal mode of operation. The firing delay angle is 45° in Figure 9.3-1b (again 2-3 mode) and 90° in Figure 9.3-1c where the output current i_d is discontinuous. Note, when i_d is zero, v_d is also zero. In this case, there are alternately 2 and 0 thyristors conducting; hence, this will be referred to as 2-0 mode.

In the case depicted in Figure 9.3-3, the combination of a $r_{dc} = 50$ mΩ and $L_{dc} = 133$ μH is connected in series with a $e_d = 260$ V dc source is connected across the output terminals of the converter. In Figure 9.3-2a (2-3 mode), the converter is operating without firing delay. In Figure 9.3-2b, the firing delay angle is 35°, and the output current is discontinuous (2-0 Mode). Note that when i_d is zero, v_d is 260 V.

Inverter operation is illustrated in Figure 9.3-4. In this case, $r_{dc} = 50$ mΩ, $L_{dc} = 133$ μH, and $e_d = -260$ V. In Figure 9.3-4a, the firing delay angle is 140° (2-3 mode). The firing delay angle in Figure 9.3-4b is 160° where discontinuous output current occurs (2-0 mode). Clearly, when i_d is zero, v_d is −260 V.

Note that while these studies depict 2-3 and 2-0 modes, other modes exist. In 3-3 mode, which we will consider later, there are always three thyristors conducting.

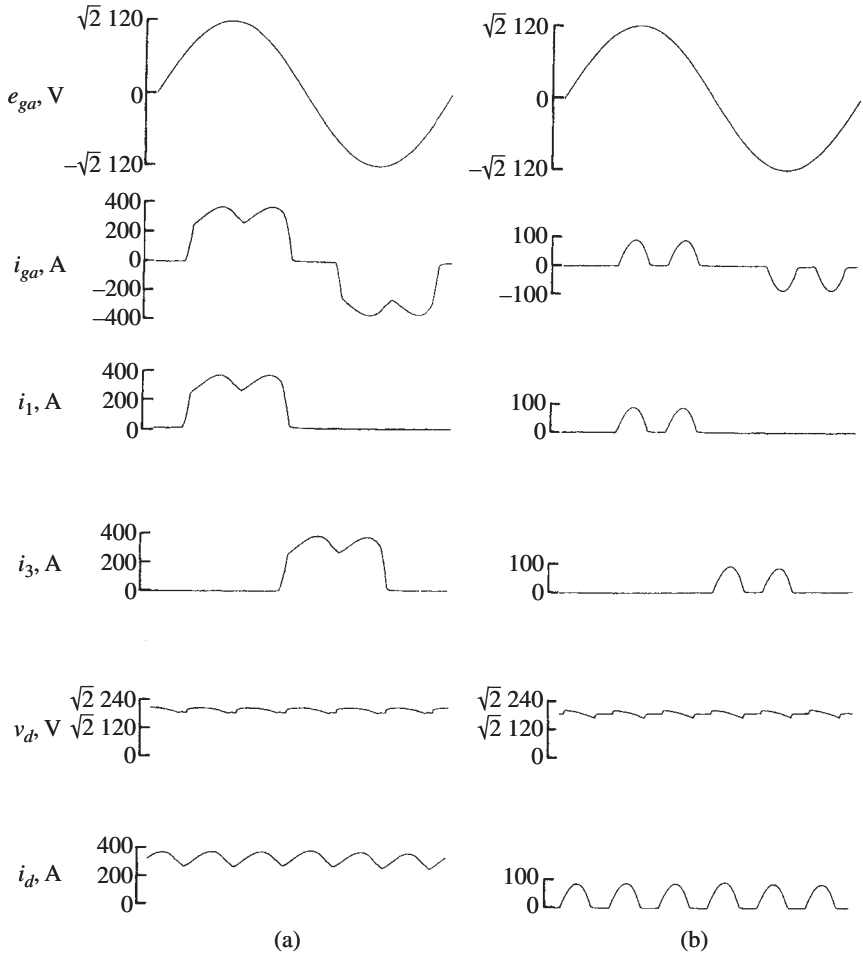

Figure 9.3-3 Three-phase, full-bridge converter operation with RL and an opposing dc source connected in series across the converter terminals. (a) $\alpha = 0°$; (b) $\alpha = 35°$.

In 3-4 mode, which occurs under heavy rectifier loads, there are alternately three and four thyristors conducting. In this case, the dc link becomes periodically shorted as in the single-phase case.

Analysis and Average-Value Model

Unlike our work in Section 9.2, herein we use a *qd* framework for our analysis, and include the derivation for the ac currents (represented in terms of *qd* variables). The explicit consideration of a slowly varying i_d will yield a dynamic

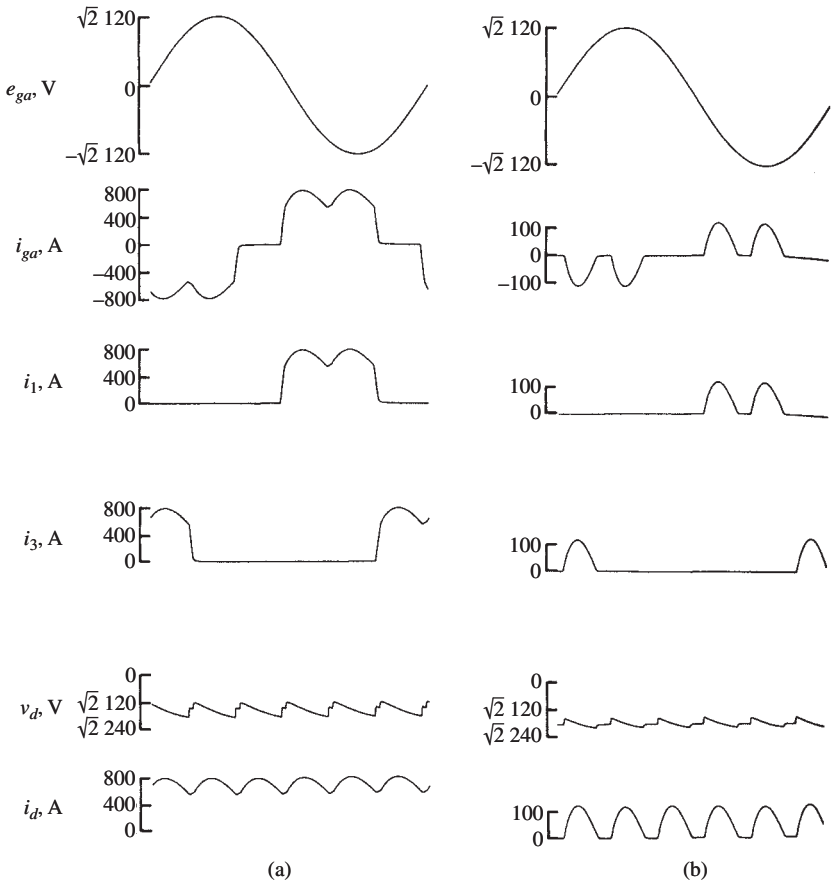

Figure 9.3-4 Three-phase, full-bridge converter operation with RL and an aiding dc source connected in series across the converter terminals. (a) $\alpha = 140°$; (b) $\alpha = 160°$.

average-value model of the load-commutated inverter that more accurately predicts the average dc voltage during transients. The consideration of the average *q*- and *d*-axis components of the ac source currents allows the model to be used in a system context and to calculate the real, apparent, and/or reactive power supplied by the ac source using expressions developed in Chapter 2. The use of *qd* variables is desirable because by suitable choice of reference frame, the *qd* state variables will be constant in the steady-state, which facilitates a variety of analyses. The following simplifying assumptions are made herein: (1) the three-phase source is balanced, (2) the current i_d is varying slowly relative to the converter switching frequency, (3) the thyristor is an infinite impedance device when reverse biased or when the gating signal to allow current flow has not

occurred, (4) when conducting the voltage drop across the thyristor is negligibly small and (5) operation is in the 2-3 or 3-3 modes.

In order to put our work into a *qd* framework, let us transform the source voltages (9.3-1)–(9.3-3) to *qd* variables using the reference-frame transformation. In particular,

$$\mathbf{v}_{qd}^{g} = \begin{bmatrix} v_{qg}^{g} \\ v_{dg}^{g} \end{bmatrix} = \mathbf{K}_{s}^{g}\Big|_{utr} \begin{bmatrix} e_{ag} \\ e_{bg} \\ e_{cg} \end{bmatrix} \tag{9.3-4}$$

where the "g" superscript denotes a reference frame wherein $\theta = \theta_g$ and "utr" denotes upper two rows. This yields

$$v_{qg}^{g} = \sqrt{2}E \tag{9.3-5}$$

$$v_{dg}^{g} = 0 \tag{9.3-6}$$

A goal of the model herein will be to accept *q*- and *d*-voltages in an arbitrary reference frame and then to find the currents in that same reference frame. For *q*- and *d*-voltages in an arbitrary reference frame (emphasized with a superscript "a" herein), in which (9.3-5) and (9.3-6) do not hold, we can utilize a frame-to-frame transformation. In particular, if the *q*- and *d*-axis components of the source voltages are given in the arbitrary reference frame, the transformation into the reference frame wherein (9.3-6) and 23 hold may be deduced from the frame-to-frame transformation

$$\mathbf{f}_{qd}^{g} = {}^{a}\mathbf{K}^{g}\mathbf{f}_{qd}^{a} \tag{9.3-7}$$

where, from Chapter 3,

$${}^{a}\mathbf{K}^{g} = \begin{bmatrix} \cos\theta_{ga} & -\sin\theta_{ga} \\ \sin\theta_{ga} & \cos\theta_{ga} \end{bmatrix} \tag{9.3-8}$$

and where $\mathbf{f} = [f_q f_d]^T$ can be a voltage *v* or current *i*, and $\theta_{ga} = \theta_g - \theta_a$, where θ_a is the position of the arbitrary reference frame. Manipulating (9.3-5) through (9.3-8),

$$\theta_{ga} = -\text{angle}\left(v_{qg}^{a} - jv_{dg}^{a}\right) \tag{9.3-9}$$

$$E = \frac{1}{\sqrt{2}}\sqrt{\left(v_{qg}^{a}\right)^2 + \left(v_{dg}^{a}\right)^2} \tag{9.3-10}$$

where v_{qg}^{a} and v_{dg}^{a} are the *q*- and *d*-axis voltages to the left of the ac side inductor l_c in Figure 9.3-1.

The next step is to derive an expression for the average dc voltage. All dc side and *qd* variables are periodic in $\pi/3$ of θ_g. Thus, the average-values may be established for any $\pi/3$ interval of θ_g. It is convenient to consider the $\pi/3$ interval that begins

when $T3$ begins to conduct and ends when $T4$ begins to conduct. The average dc voltage over this interval may be expressed

$$\hat{v}_d = \frac{3}{\pi}\int_{\frac{\pi}{3}+\alpha}^{\frac{2\pi}{3}+\alpha} (v_{bs} - v_{cs})d\theta_g \tag{9.3-11}$$

In (9.3-11), the "∧" is used to denote the average-value during dynamical conditions wherein the dc current i_d and/or the amplitude of the ac voltages E are allowed to vary, provided that the variation from one switching interval to the next is relatively small. In other words, the averaging interval in (9.3-11) is assumed to be small relative to the longer-term dynamics associated with the variations in E and/or i_d. Thus, (9.3-11) may be interpreted as the short-term average of v_d. Likewise, the short-term average of i_d (average of i_d over a $\pi/3$ interval) will be denoted as $\hat{i}_d$. The firing delay angle α in (9.3-11) is defined such that $T3$ fires when

$$\theta_g = \frac{\pi}{3} + \alpha \tag{9.3-12}$$

The average dc voltage indicated in (9.3-11) may be evaluated by noting from Figure 9.3-1 that

$$v_{as} = e_{ga} + l_c\frac{di_{ag}}{dt} \tag{9.3-13}$$

$$v_{bs} = e_{gb} + l_c\frac{di_{bg}}{dt} \tag{9.3-14}$$

$$v_{cs} = e_{gc} + l_c\frac{di_{cg}}{dt} \tag{9.3-15}$$

Substituting (9.3-13)–(9.3-15) into (9.3-11) yields

$$\hat{v}_d = \frac{3}{\pi}\int_{\frac{\pi}{3}+\alpha}^{\frac{2\pi}{3}+\alpha} (e_{gb} - e_{gc})d\theta_g + \frac{3}{\pi}l_c\omega_g(i_{bg} - i_{cg})\Big|_{\frac{\pi}{3}+\alpha}^{\frac{2\pi}{3}+\alpha} \tag{9.3-16}$$

Substituting (9.3-2) and (9.3-3) into (9.3-16) and simplifying yields

$$\hat{v}_d = \frac{3\sqrt{6}}{\pi}E\cos\alpha + \frac{3}{\pi}l_c\omega_g(i_{bg} - i_{cg})\Big|_{\frac{\pi}{3}+\alpha}^{\frac{2\pi}{3}+\alpha} \tag{9.3-17}$$

Further simplification can be obtained by observing that prior to the instant when $T3$ begins to conduct, only $T1$ and $T2$ are conducting. Therefore,

$$\mathbf{i}_{abcg}\Big|_{\theta_g=\frac{\pi}{3}+\alpha} = [-\hat{i}_d \;\; 0 \;\; \hat{i}_d]^T \tag{9.3-18}$$

Similarly, immediately prior to the instant when $T4$ begins to conduct, only $T2$ and $T3$ are on, therefore

$$\mathbf{i}_{abcg}\Big|_{\theta_g=\frac{2\pi}{3}+\alpha} = \left[\begin{array}{ccc} 0 & -\hat{i}_d - \Delta\hat{i}_d & \hat{i}_d + \Delta\hat{i}_d \end{array}\right]^T \tag{9.3-19}$$

In 9.3-19, $\Delta\hat{i}_d$ represents the change in average dc current over the given conduction interval due to long-term dynamics. It follows from this definition that the derivative of the dynamic-average rectifier current may be approximated as

$$\frac{d\hat{i}_d}{dt} = \frac{\Delta\hat{i}_d}{\pi/3}\omega_g \tag{9.3-20}$$

Substituting (9.3-18)–(9.3-20) into (9.3-17) and simplifying yields

$$\hat{v}_d = \frac{3\sqrt{6}}{\pi}E\cos\alpha - \frac{3}{\pi}l_c\omega_g\hat{i}_d - 2l_c\frac{d\hat{i}_d}{dt} \tag{9.3-21}$$

From Figure 9.3-1, $\hat{v}_d$ can be related to $\hat{i}_d$ and e_d using

$$\hat{v}_d = r_{dc}\hat{i}_d + L_{dc}\frac{d\hat{i}_d}{dt} + e_d \tag{9.3-22}$$

Combining (9.3-21) and (9.3-22) yields

$$\frac{d\hat{i}_d}{dt} = \frac{\frac{3\sqrt{6}}{\pi}E\cos\alpha - \left(r_{dc} + \frac{3}{\pi}l_c\omega_g\right)\hat{i}_d - e_d}{L_{dc} + 2l_c} \tag{9.3-23}$$

To establish the average q- and d-axis components of the ac currents, it is assumed that the rectifier current is constant throughout the interval and equal to $\hat{i}_d$. It is convenient to divide the interval into two subintervals; the commutation interval during which the current is transferred from $T1$ to $T3$, and the conduction interval during which only $T2$ and $T3$ are conducting. During the commutation interval, $T1$, $T2$, and $T3$ are conducting. Therefore, the current into the ac source must be of the form

$$\mathbf{i}_{abcg} = \begin{bmatrix} i_{ag} & -\hat{i}_d - i_{ag} & \hat{i}_d \end{bmatrix}^T \tag{9.3-24}$$

and

$$v_{as} = v_{bs} = 0 \tag{9.3-25}$$

Algebraically manipulating (9.2-2), (9.3-1), (9.3-2), (9.3-13), (9.3-14), (9.3-24), and (9.3-25), it is possible to show that

$$\frac{di_{ag}}{dt} = \frac{\sqrt{6}E}{2l_c\omega_g}\cos\left(\theta_g - \frac{5\pi}{6}\right) \tag{9.3-26}$$

From (9.3-26) and noting that at $\theta_g = \alpha + \pi/3$, we have that $i_{ag} = -\hat{i}_d$, we conclude that

$$i_{ag}(\theta_g) = -\hat{i}_d + \frac{\sqrt{6}}{2l_c\omega_g}E\left[\cos\alpha - \cos\left(\theta_g - \frac{\pi}{3}\right)\right] \tag{9.3-27}$$

The commutation subinterval ends when the current in $T1$, which is the a-phase current, becomes zero. The angle from the time $T3$ is turned on and $T1$ is turned

off is known as the commutation angle γ. It can be found by setting (9.3-27) equal to zero. In particular,

$$\gamma = -\alpha + \arccos\left(\cos\alpha - \frac{2l_c\omega_g\hat{i}_d}{\sqrt{6}E}\right) \tag{9.3-28}$$

For (9.3-27) to be applicable, several conditions need to be met. First, for (9.3-28) to be defined

$$\left|\cos\alpha - \frac{2l_c\omega_g\hat{i}_d}{\sqrt{6}E}\right| \leq 1 \tag{9.3-29}$$

However, this is not the only condition which must be met. Note that $T3$ turns on at

$$\theta_g = \frac{\pi}{3} + \alpha \tag{9.3-30}$$

For $T3$ to turn on, the time derivative of i_{ag} must be positive, so that the current in $T3$ will increase. Substitution of (9.3-30) into (9.3-26), we conclude

$$\alpha \geq 0 \tag{9.3-31}$$

Similarly, the end of commutation occurs at

$$\theta_g = \frac{\pi}{3} + \alpha + \gamma \tag{9.3-32}$$

For commutation to complete, the time derivative of i_{ag} must be positive at the end of commutation as well. Substitution of (9.3-32) into (9.3-26) and requiring the time derivative to be positive,

$$\alpha + \gamma \leq \pi \tag{9.3-33}$$

This requirement is particularly relevant to inverter operation in which α is large. Finally, for 2-3 mode, we must have

$$\gamma \leq \frac{\pi}{3} \tag{9.3-34}$$

Because of these restrictions, it is useful to differentiate between the actual firing delay α and the intended (or commanded) firing delay angle α^*. Suppose we take $\alpha = \alpha^*$ in our analysis (9.3-28)–(9.3-34). If all constraints are met, then this is indeed the case. If the constraints are not met, then the converter is either in another mode or is not operating properly (and is, e.g., experiencing commutation failures). While our approach is not valid for these other modes, we can extend it to 3-3 mode. In this mode, the commutation angle is exactly $\pi/3$, and the firing delay is increased from the intended value to the value that corresponds to the

aforementioned commutation angle. Setting $\gamma = \pi/3$ in (9.3-28) and solving for the firing angle

$$\alpha = \frac{\pi}{3} - \arccos\left(\frac{2l_c\omega_g\hat{i}_d}{\sqrt{6}E}\right) \tag{9.3-35}$$

Note that mathematically, there is another solution with a change of sign on the arccos() term; however, this alternate solution does not make sense physically since such a solution would yield a firing delay that decreases with increasing $\hat{i}_d$. Note that for (9.3-35) to be valid,

$$\frac{1}{2} \le \frac{2l_c\omega_g\hat{i}_d}{\sqrt{6}E} \le 1 \tag{9.3-36}$$

or α will be negative or the argument to the arccos() function will be out of range.

Summarizing, these results, we have

$$\alpha = \begin{cases} \alpha^* & \text{valid} \quad 2\text{-}3 \quad \text{mode} \\ \frac{\pi}{3} - \arccos\left(\frac{2l_c\omega_g\hat{i}_d}{\sqrt{6}E}\right) & \text{valid} \quad 3\text{-}3 \quad \text{mode} \end{cases} \tag{9.3-37}$$

In other words, if we assume $\alpha = \alpha^*$ and it yields valid 2-3 mode of operation, then indeed $\alpha = \alpha^*$. If this does not yield valid operation, then we can find α from (9.3-35). If this yields valid 3-3 mode, then this is the firing delay. If neither assumption yields a valid result, the operation is in another mode (e.g., 3-4 mode, wherein the converter operates between three and four thyristors on) or the converter is not operating in a periodic fashion.

The next step in our analysis is to determine an expression for the ac side currents. The average q- and d-axis components can be established using

$$\hat{i}^g_{qg} = \frac{3}{\pi}\int_{\frac{\pi}{3}+\alpha}^{\frac{2\pi}{3}+\alpha} i^g_{qg}(\theta_g)d\theta_g \tag{9.3-38}$$

$$\hat{i}^g_{dg} = \frac{3}{\pi}\int_{\frac{\pi}{3}+\alpha}^{\frac{2\pi}{3}+\alpha} i^g_{dg}(\theta_g)d\theta_g \tag{9.3-39}$$

Since the expressions for the ac currents are different during the conduction interval than in the commutation interval, it is convenient to break up (9.3-38) and (9.3-39) into components corresponding to these two intervals. In particular,

$$\hat{i}^g_{qg} = \hat{i}^g_{qg,com} + \hat{i}^g_{qg,cond} \tag{9.3-40}$$

$$\hat{i}^g_{dg} = \hat{i}^g_{dg,com} + \hat{i}^g_{dg,cond} \tag{9.3-41}$$

where

$$\hat{i}^g_{qg,\text{com}} = \frac{3}{\pi}\int_{\frac{\pi}{3}+\alpha}^{\frac{\pi}{3}+\alpha+\gamma} i^g_{qg}(\theta_g)d\theta_g \tag{9.3-42}$$

$$\hat{i}^g_{qg,\text{cond}} = \frac{3}{\pi}\int_{\frac{\pi}{3}+\alpha+\gamma}^{\frac{2\pi}{3}+\alpha} i^g_{qg}(\theta_g)d\theta_g \tag{9.3-43}$$

$$\hat{i}^g_{dg,\text{com}} = \frac{3}{\pi}\int_{\frac{\pi}{3}+\alpha}^{\frac{\pi}{3}+\alpha+\gamma} i^g_{dg}(\theta_g)d\theta_g \tag{9.3-44}$$

$$\hat{i}^g_{dg,\text{cond}} = \frac{3}{\pi}\int_{\frac{\pi}{3}+\alpha+\gamma}^{\frac{2\pi}{3}+\alpha} i^g_{dg}(\theta_g)d\theta_g \tag{9.3-45}$$

The commutation component of the current may be found by substituting (9.3-27) into (9.3-24), applying the reference-frame transformation (3.3-1) with $\theta = \theta_g$, and integrating in accordance with (9.3-42) and (9.3-44). After considerable manipulation,

$$\begin{aligned}\hat{i}^g_{qg,com} = {} & \frac{2\sqrt{3}}{\pi}\hat{i}_d\left[\sin\left(\gamma+\alpha-\frac{5\pi}{6}\right)-\sin\left(\alpha-\frac{5\pi}{6}\right)\right] \\ & + \frac{3}{\pi}\frac{\sqrt{2E}}{l_c\omega_g}\cos\alpha[\cos(\gamma+\alpha)-\cos(\alpha)] \\ & + \frac{1}{4}\frac{3}{\pi}\frac{\sqrt{2E}}{l_c\omega_g}[\cos 2\alpha-\cos(2\alpha+2\gamma)]\end{aligned} \tag{9.3-46}$$

$$\begin{aligned}\hat{i}^g_{dg,com} = {} & \frac{2\sqrt{3}}{\pi}\hat{i}_d\left[-\cos\left(\gamma+\alpha-\frac{5\pi}{6}\right)+\cos\left(\alpha-\frac{5\pi}{6}\right)\right] \\ & + \frac{3}{\pi}\frac{\sqrt{2E}}{l_c\omega_g}\cos\alpha[\sin(\gamma+\alpha)-\sin(\alpha)] \\ & + \frac{1}{4}\frac{3}{\pi}\frac{\sqrt{2E}}{l_c\omega_g}[\sin 2\alpha-\sin(2\alpha+2\gamma)] - \frac{3}{\pi}\frac{\sqrt{2E}}{l_c\omega_g}\frac{1}{2}\gamma\end{aligned} \tag{9.3-47}$$

To compute the conduction component of the average currents, note that after commutation, the a-phase current remains at zero; therefore

$$\mathbf{i}_{abcg} = \begin{bmatrix}0 & -\hat{i}_d & \hat{i}_d\end{bmatrix}^T \tag{9.3-48}$$

Transforming (9.3-48) to the $\theta = \theta_g$ reference frame and utilizing (9.3-43) and (9.3-45),

$$\hat{i}^g_{qg,cond} = \frac{2\sqrt{3}}{\pi}\hat{i}_d\left[\sin\left(\alpha+\frac{7\pi}{6}\right)-\sin\left(\alpha+\gamma+\frac{5\pi}{6}\right)\right] \tag{9.3-49}$$

$$\hat{i}^g_{dg,cond} = \frac{2\sqrt{3}}{\pi}\hat{i}_d\left[-\cos\left(\alpha+\frac{7\pi}{6}\right)+\cos\left(\alpha+\gamma+\frac{5\pi}{6}\right)\right] \tag{9.3-50}$$

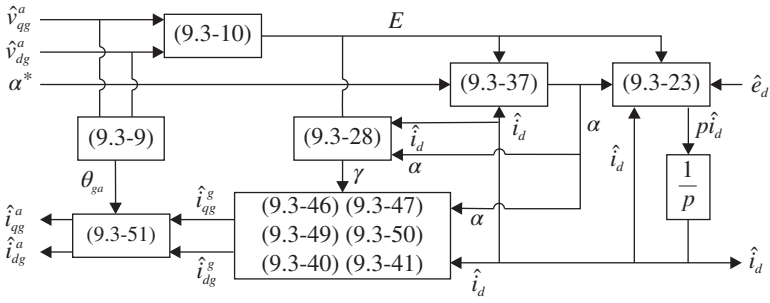

Figure 9.3-5 Average-value model of three-phase full-bridge converter.

At this point, the total q- and d-axis current may be found using (9.3-40) and (9.3-41). The resulting currents can then be transformed back to the desired reference frame using

$$\hat{\mathbf{i}}^a_{qd} = {}^g\mathbf{K}^a\,\hat{\mathbf{i}}^g_{qd} = [{}^g\mathbf{K}^a]^{-1}\hat{\mathbf{i}}^g_{qd} \tag{9.3-51}$$

The relationships between the previous equations are conveniently summarized in the block diagram illustrated in Figure 9.3-5, which represents an average-value model of the load commutated converter. The inputs to this model include the commanded firing delay α^*, the q- and d-axis components of the source voltage in the arbitrary reference frame, and the dc source voltage e_d. The outputs of the model include the dynamic-average of the rectifier current $\hat{i}_d$ and the dynamic-average of the q- and d-axis components of the ac currents in the arbitrary reference frame.

To illustrate the dynamic response that is established using the average-value model, it is assumed that the rated line-to-line source voltage is 208 V (rms). The commutating inductance l_c is 45 μH. Also, $r_{dc} = 0.5\,\Omega$, $L_{dc} = 1.33$ mH, and $e_d = 0$. In the following study, the dc and ac currents are initially zero, and rated voltages are suddenly applied at $t = 0$ with the firing delay angle α set to zero. The dynamic response is shown in Figure 9.3-6, wherein the following variables are plotted: i_d—the dc current, i^g_{qg}—the q-axis component of the ac current, and i^g_{dg}—the d-axis component of the ac current. The ac currents are expressed in the reference frame wherein $v^g_{dg} = 0$. The variables indicated with an "$\wedge$" correspond to the average-value model in Figure 9.3-5, while those that do not include the "$\wedge$" correspond to the actual response. At the instant of time indicated in Figure 9.3-6, the firing delay angle is stepped to 45°. As shown, the average-value model accurately portrays the dynamic-average dynamic response for the given study. The steady-state waveforms for $\alpha = 0$ and $\alpha = 45°$ are shown in Figure 9.3-2a,b, respectively.

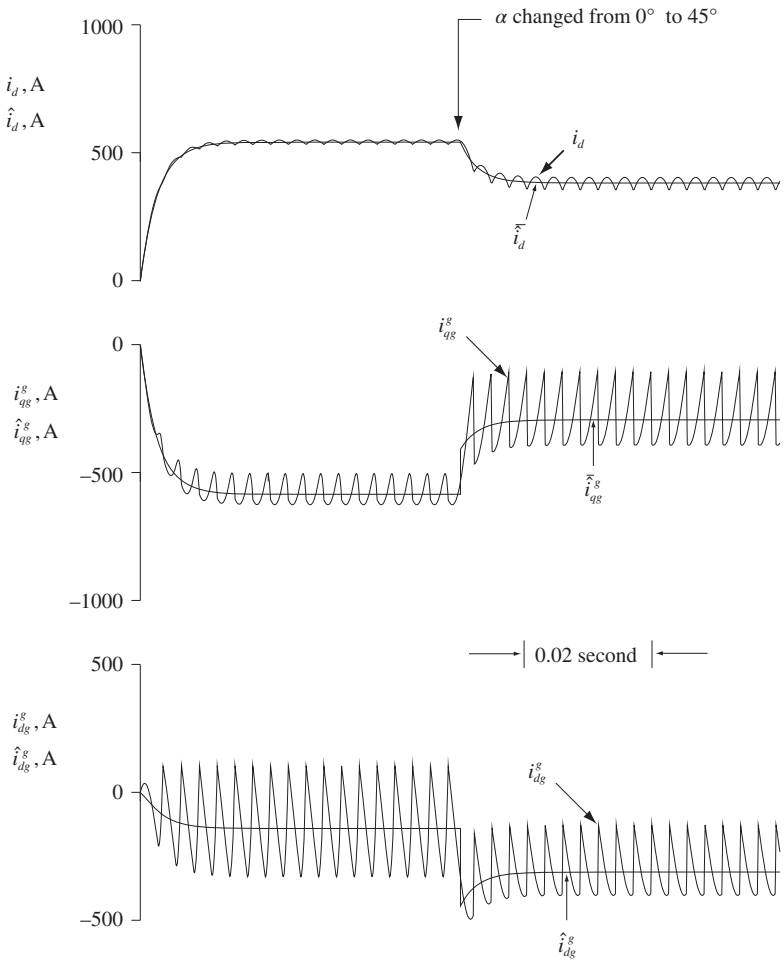

Figure 9.3-6 Comparison of average-value dynamic response with actual response.

9.4 Conclusions and Extensions

The focus of this chapter has been the development of average-value and dynamic average-value models of line-commutated converters connected to an ideal source. A natural extension of this work is the consideration of the connection of line-commutated converters to synchronous machines. One approach to doing this is set forth in References 5 and 6. An extension of the methodology to a six-phase rectifier connected to a sic-phase machine is set forth in Reference 7. In Reference 8, a method of determining instantaneous waveforms from an

average-value model is considered using a procedure referred to as waveform reconstruction. Throughout this work, it was assumed that enough dc link inductance was included so that the dc current could be considered constant. An analysis of line-commutated converter systems in which no dc-link is present is set forth in Reference 9. Finally, it is appropriate to consider methods for the detailed simulation of line-commutated inverters. While the literature is rich in this subject, a particularly computationally efficient methodology is set forth in Reference 10.

References

1 C. Adamson and N. G. Hingarani, *High Voltage Direct Current Power Transmission*, Garroway Limited, London, 1960.

2 E. W. Kimbark, *Direct Current Transmission—Vol. 1*, John Wiley and Sons, New York, 1971.

3 S. B. Dewan and A. Straughen, *Power Semiconductor Circuits*, John Wiley and Sons, New York, 1975.

4 P. Wood, *Switching Power Converters*, Van Nostrand Reinhold Co., New York, 1981.

5 S. D. Sudhoff and O. Wasynczuk, "Analysis and Average-Value Modeling of Line-Commutated Converter—Synchronous Machine Systems," *IEEE Trans. Energy Conversion*, Vol. 8, No. 1, March 1993, pp. 92–99.

6 S. D. Sudhoff, K. A. Corzine, H. J. Hegner, and D. E. Delisle, "Transient and Dynamic Average-Value Modeling of Synchronous Machine Fed Load-Commutated Converters," *IEEE Trans. Energy Conversion*, Vol. 11, No. 3, September 1996, pp. 508–514.

7 S. D. Sudhoff, "Analysis and Average-Value Modeling of Dual Line-Commutated Converter—6-Phase Synchronous Machine Systems," *IEEE Trans. Energy Conversion*, Vol. 8, No. 3, September 1993, pp. 411–417.

8 S. D. Sudhoff, "Waveform Reconstruction in the Average-Value Modeling of Line-Commutated Converter—Synchronous Machine Systems," *IEEE Trans. Energy Conversion*, Vol. 8, No. 3, September 1993, pp. 404–410.

9 J. T. Alt, S. D. Sudhoff, and B. E. Ladd, "Analysis and Average-Value Modeling of an Inductorless Synchronous Machine Load Commutated Converter System," *IEEE Trans. Energy Conversion*, Vol. 14, No. 1, March 1999, pp. 37–43.

10 O. Wasynczuk and S. D. Sudhoff, "Automated State Model Generation Algorithm for Power Circuits and Systems," *IEEE Trans. Power Systems*, Vol. 11, No. 4, November 1996, pp. 1951–1956.

Problems

9.1 Using the average-value equations derived in Section 9.2, calculate the average dc voltage and current for each of the conditions in Figure 9.2-7. Compare with the average-values plotted in Figure 9.2-7.

9.2 Using the average-value equations derived in Section 9.3, calculate the average dc voltage and current for each of the conditions in Figure 9.3-2. Compare with the average-values plotted in Figure 9.3-2.

9.3 Assume that the ac source voltage applied to the three-phase load commutated converter have an *acb* phase sequence. Indicate the sequence in which the thyristors should be fired.

9.4 Derive (9.3-9) and (9.3-10).

9.5 Starting with (9.3-26) obtain (9.3-27).

9.6 Using (9.3-26) and (9.3-32), infer (9.3-33).

9.7 Perform the detailed mathematical manipulation needed to obtain (9.3-46).

9.8 Perform the detailed mathematical manipulation needed to obtain (9.3-47).

9.9 Perform the detailed mathematical manipulation needed to obtain (9.3-49).

9.10 Perform the detailed mathematical manipulation needed to obtain (9.3-50).

10

Fully Controlled Three-Phase Bridge Converters

10.1 Introduction

In our study of induction, synchronous, and permanent-magnet ac machines, we set forth control strategies that assumed the machine was driven by a three-phase, variable-frequency voltage or current source without mention of how such a source is actually obtained, or what its characteristics might be. In this chapter, the operation of a three-phase fully controlled bridge converter is set forth. It is shown that by suitable control, this device can be used to achieve either a three-phase controllable voltage source or a three-phase controllable current source, as was assumed to exist in previous chapters.

10.2 The Three-Phase Bridge Converter

The converter topology that serves as the basis for many three-phase variable speed drive systems is shown in Figure 10.2-1. This type of converter is comprised of six controllable switches labeled T1–T6. Physically, bipolar junction transistors (BJTs), metal–oxide–semiconductor field-effect transistors (MOSFETs), insulated-gate bipolar junction transistors (IGBTs), and MOS controlled thyristors (MCTs) are just a few of the devices that can be used as switches. Across each switch is an antiparallel diode used to ensure that there is a path for inductive current in the event that a switch which would normally conduct current of that polarity is turned off. This type of converter is often referred to as an inverter when power flow is from the dc system to the ac system. If power flow is from the ac system to the dc system, which is also possible, the converter is often referred to as an active rectifier.

In Figure 10.2-1, v_{dc} denotes the dc voltage applied to the converter bridge, and i_{dc} designates the dc current flowing into the bridge. The bridge is divided

Analysis of Electric Machinery and Drive Systems, Fourth Edition.
Paul C. Krause, Oleg Wasynczuk, Scott D. Sudhoff, and Steven D. Pekarek.

Companion website: www.wiley.com/go/krause_aem4e

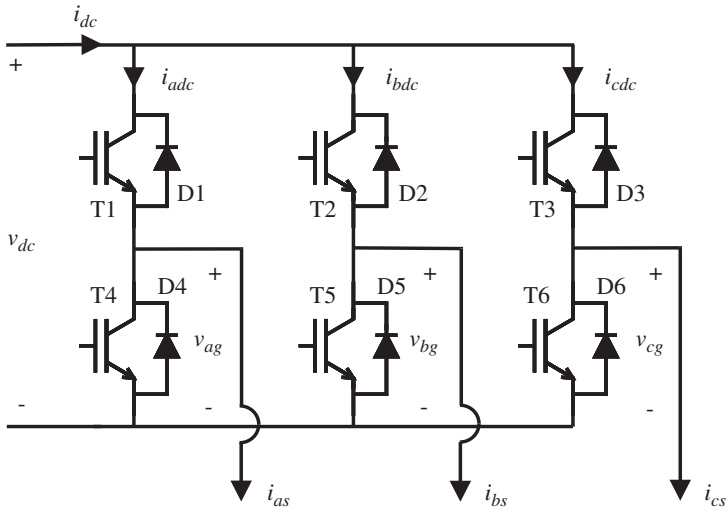

Figure 10.2-1 The three-phase bridge converter topology.

into three legs, one for each phase of the load. The line-to-ground voltage of the *a*-, *b*-, and *c*-phase legs of the converter are denoted v_{ag}, v_{bg}, and v_{cg} respectively. In this text, the load current will generally be the stator current into a synchronous, induction, or permanent-magnet ac machine; therefore, i_{as}, i_{bs}, and i_{cs} are used to represent the current into each phase of the load. Finally, the dc currents from the upper rail into the top of each phase leg are designated i_{adc}, i_{bdc}, and i_{cdc}.

To understand the operation of this basic topology, it must first be understood that none of the semiconductor devices shown are ever intentionally operated in the active region of their *i*–*v* characteristics. Their operating point is either in the saturated region (on) or in the cutoff region (off). If the devices were operated in their active region, then by applying a suitable gate voltage to each device, the line-to-ground voltage of each leg could be continuously varied from 0 to v_{dc}. At first, such control appears advantageous, since each leg of the converter could be used as a controllable voltage source. The disadvantage of this strategy is that, if the switching devices are allowed to operate in their active region, there will be both a voltage across and current through each semiconductor device, resulting in power loss. On the other hand, if each semiconductor is either on or off, then either there is a current through the device but no voltage, or a voltage across the device but no current. Neither case results in power loss. Of course, in a real device, there will be some power losses due to the small voltage drop that occurs even when the device is in saturation (on), and due to losses that are associated with turning the switching devices on or off (switching losses); nevertheless, inverter efficiencies greater than 95% are readily obtained.

In this study of the operation of the converter bridge, it will be assumed that either the upper switch or lower switch of each leg is gated on, except during switching transients (the result of turning one switch on while turning another off). Ideally, the leg-to-ground voltage of a given phase will be v_{dc} if the upper switch is on and the lower switch is turned off, or 0 if the lower switch is turned on and the upper switch is off. This assumption is often useful for analysis purposes, as well as for time–domain simulation of systems, in which the dc supply voltage is much greater than the semiconductor voltage drops. If a more detailed analysis or simulation is desired (and hence the voltage drops across the semiconductors are not neglected), then the line-to-ground voltage is determined both by the switching devices turned on and the phase current.

To illustrate this, consider the diagram of one leg of the bridge as is shown in Figure 10.2-2. Therein, x can be a, b, or c, to represent the a-, b-, or c-phase, respectively. Figure 10.2-3a illustrates the effective equivalent circuit shown in Figure 10.2-2 if the upper transistor is on and the current i_{xs} is positive. For this condition, it can be seen that the line-to-ground voltage v_{xg} will be equal to the dc supply voltage v_{dc} less the voltage drop across the switch v_{sw}. The voltage drop across the switch is generally in the range of 0.7–3.0 V. Although the voltage drop is actually a function of the switch current, it can often be represented as a constant. From Figure 10.2-3a, the dc current into the bridge, i_{xdc}, is equal to the phase current i_{xs}.

If the upper transistor is on and the phase current is negative, then the equivalent circuit is as shown in Figure 10.2-3b. In this case, the dc current into the leg i_{xdc} is again equal to the phase current i_{xs}. However, since the current is now flowing through the diode, the line-to-ground voltage v_{xg} is equal to the dc supply voltage v_{dc} plus the diode forward voltage drop v_d. If the upper switch is on and the phase current is zero, it seems reasonable to assume that the line-to-ground voltage is equal to the supply voltage as indicated in Figure 10.2-3c. Although other

Figure 10.2-2 One phase leg.

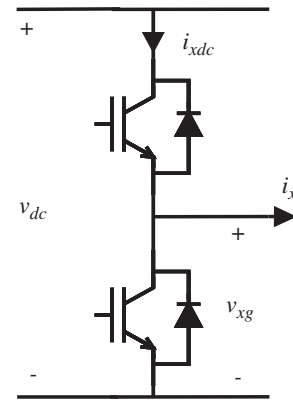

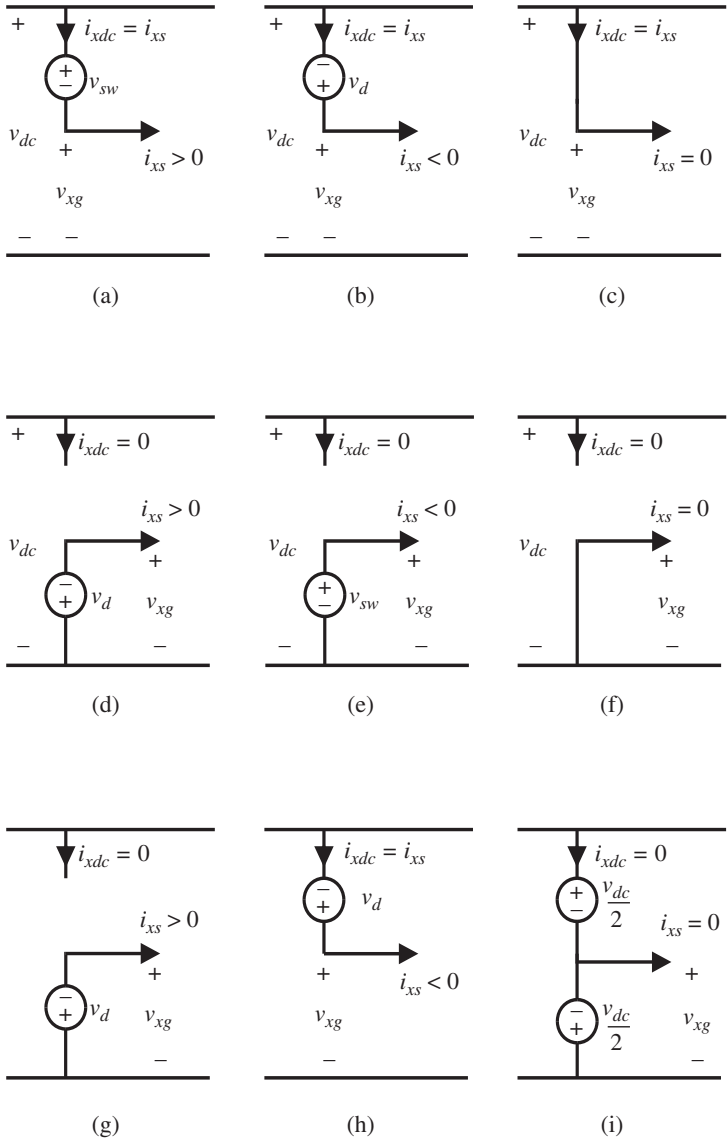

Figure 10.2-3 Phase leg equivalent circuits. (a) Upper switch on; $i_{xs} > 0$. (b) Upper switch on; $i_{xs} < 0$. (c) Upper switch on; $i_{xs} = 0$. (d) Lower switch on; $i_{xs} > 0$. (e) Lower switch on; $i_{xs} < 0$. (f) Lower switch on; $i_{xs} = 0$. (g) Neither switch on; $i_{xs} > 0$. (h) Neither switch on; $i_{xs} < 0$. (i) Neither switch on; $i_{xs} = 0$.

estimates could be argued (such as averaging the voltage from the positive and negative current conditions), it must be remembered that this is a rare condition, so a small inaccuracy will not have a perceptible effect on the results.

The positive, negative, and zero current equivalent circuits, which represent the phase leg when the lower switching device is on and the upper switching device is off, are illustrated in Figure 10.2-3d,e,f, respectively. The situation is entirely analogous to the case in which the upper switch is on.

One final possibility is the case in which neither transistor is turned on. As stated previously, it is assumed that in the drives considered herein, either the upper or lower transistor is turned on. However, there is a delay between the time a switch is commanded to turn off and the time it actually turns off, as well as a delay between the time a switch is commanded to turn on and the time it actually turns on. Sophisticated semiconductor device models are required to predict the exact voltage and current waveforms associated with the turn-on and turn-off transients of the switching devices [1–5]. However, as an approximate representation, it can be assumed that a device turns on with a delay T_{on} after the control logic commands it to turn on, and turns off after a delay T_{off} after the control logic commands it to turn off. The turn-off time is generally longer than the turn-on time. Unless the turn-on time and turn-off time are identical, there will be an interval in which either no device in a leg is turned on or both devices in a leg are turned on. The latter possibility is known as "shoot-through" and is extremely undesirable; therefore, an extra delay is incorporated into the control logic such that the device being turned off will do so before the complementary device is turned on (see Problem 10). Therefore, it may be necessary to represent the condition in which neither device of a leg is turned on.

If neither device of a phase leg is turned on and the current is positive, then the situation is as in Figure 10.2-3g. Since neither switching device is conducting, the current must flow through the lower diode. Thus, the line-to-ground voltage v_{xg} is equal to $-v_d$ and the dc current into the leg i_{xdc} is zero. Conversely, if the phase current is negative, then the upper diode must conduct as is indicated in Figure 10.2-3h. In this case, the line-to-ground voltage is $v_{dc} + v_d$ and the dc current into the leg i_{xdc} is equal to phase current into the load i_{xs}. In the event that neither transistor is on, and that the phase current into the load is zero, it is difficult to identify what the line-to-ground voltage will be since it will become a function of the back emf of the machine to which the converter is connected. If, however, it is assumed that the period during which neither switching device is gated on is brief (on the order of a microsecond), then assuming that the line-to-ground voltage is $v_{dc}/2$ is an acceptable approximation. Note that this approximation cannot be used if the period during which neither switching device is gated on is extended. An example of the type of analysis that must be conducted if both the upper and lower switching devices are off for an extended period appears in References [6–8].

Table 10.2-1 Converter Voltages and Currents.

Switch On	Current Polarity	v_{xg}	i_{xdc}
Upper	Positive	$v_{dc} - v_{sw}$	i_{xs}
	Negative	$v_{dc} + v_d$	i_{xs}
	Zero	v_{dc}	i_{xs}
Lower	Positive	$-v_d$	0
	Negative	v_{sw}	0
	Zero	0	0
Neither	Positive	$-v_d$	0
	Negative	$v_{dc} + v_d$	i_{xs}
	Zero	$v_{dc}/2$	0

Table 10.2-1 summarizes the calculation of line-to-ground voltage and dc current into each leg of the bridge for each possible condition. Once each of the line-to-ground voltages are found, the line-to-line voltages may be calculated. In particular,

$$v_{abs} = v_{ag} - v_{bg} \tag{10.2-1}$$

$$v_{bcs} = v_{bg} - v_{cg} \tag{10.2-2}$$

$$v_{cas} = v_{cg} - v_{ag} \tag{10.2-3}$$

and from Figure 10.2-1, the total dc current into the bridge is given by

$$i_{dc} = i_{adc} + i_{bdc} + i_{cdc} \tag{10.2-4}$$

Since machines are often wye-connected, it is useful to derive equations for the line-to-neutral voltages produced by the three-phase bridge. If the converter of Figure 10.2-1 is connected to a wye-connected load, then the line-to-ground voltages are related to the line-to-neutral voltages and the neutral-to-ground voltage by

$$v_{ag} = v_{as} + v_{ng} \tag{10.2-5}$$

$$v_{bg} = v_{bs} + v_{ng} \tag{10.2-6}$$

$$v_{cg} = v_{cs} + v_{ng} \tag{10.2-7}$$

Summing (10.2-5)–(10.2-7) and rearranging yields

$$v_{ng} = \frac{1}{3}(v_{ag} + v_{bg} + v_{cg}) - \frac{1}{3}(v_{as} + v_{bs} + v_{cs}) \tag{10.2-8}$$

The final term in (10.2-8) is recognized as the zero-sequence voltage of the machine, thus

$$v_{ng} = \frac{1}{3}(v_{ag} + v_{bg} + v_{cg}) - v_{0s} \tag{10.2-9}$$

For a balanced, wye-connected machine, such as a synchronous machine, induction machine, or permanent-magnet ac machine, summing the line-to-neutral voltage equations indicates that the zero-sequence voltage is zero. However, if the machine is unbalanced, this would not be the case. Another practical example of a case in which the zero-sequence voltage is not identically equal to zero is a permanent-magnet ac machine with a square-wave or trapezoidal back emf, in which case the sum of the three-phase back emfs is not zero. However, for the machines considered in this text in which the zero-sequence voltage must be zero, (10.2-9) reduces to

$$v_{ng} = \frac{1}{3}(v_{ag} + v_{bg} + v_{cg}) \tag{10.2-10}$$

Substitution of (10.2-10) into (10.2-5)–(10.2-7) and solving for the line-to-neutral voltages yields

$$v_{as} = \frac{2}{3}v_{ag} - \frac{1}{3}v_{bg} - \frac{1}{3}v_{cg} \tag{10.2-11}$$

$$v_{bs} = \frac{2}{3}v_{bg} - \frac{1}{3}v_{ag} - \frac{1}{3}v_{cg} \tag{10.2-12}$$

$$v_{cs} = \frac{2}{3}v_{cg} - \frac{1}{3}v_{ag} - \frac{1}{3}v_{bg} \tag{10.2-13}$$

10.3 Six-Step Operation

In the previous section, the basic voltage and current relationships needed to analyze the three-phase bridge were set forth with no discussion as to how the bridge would enable operation of a three-phase ac machine from a dc supply. In this section, a basic method of accomplishing the dc to ac power conversion is set forth. This method will be referred to as six-step operation, and is also commonly referred to as 180° voltage-source operation. In this mode of operation, the converter appears as a three-phase voltage source to the ac system, and so six-step operation is classified as a voltage-source control scheme.

The operation of a six-stepped three-phase bridge is shown in Figure 10.3-1. Therein, the first three traces illustrate switching signals applied to the power electronic devices, which are a function of θ_c, the converter angle. The definition of the converter angle is dependent upon the type of machine the given converter is driving. For the present, the converter angle can be taken to be $\omega_c t$, where t is time and ω_c is the radian frequency of the three-phase output. In subsequent

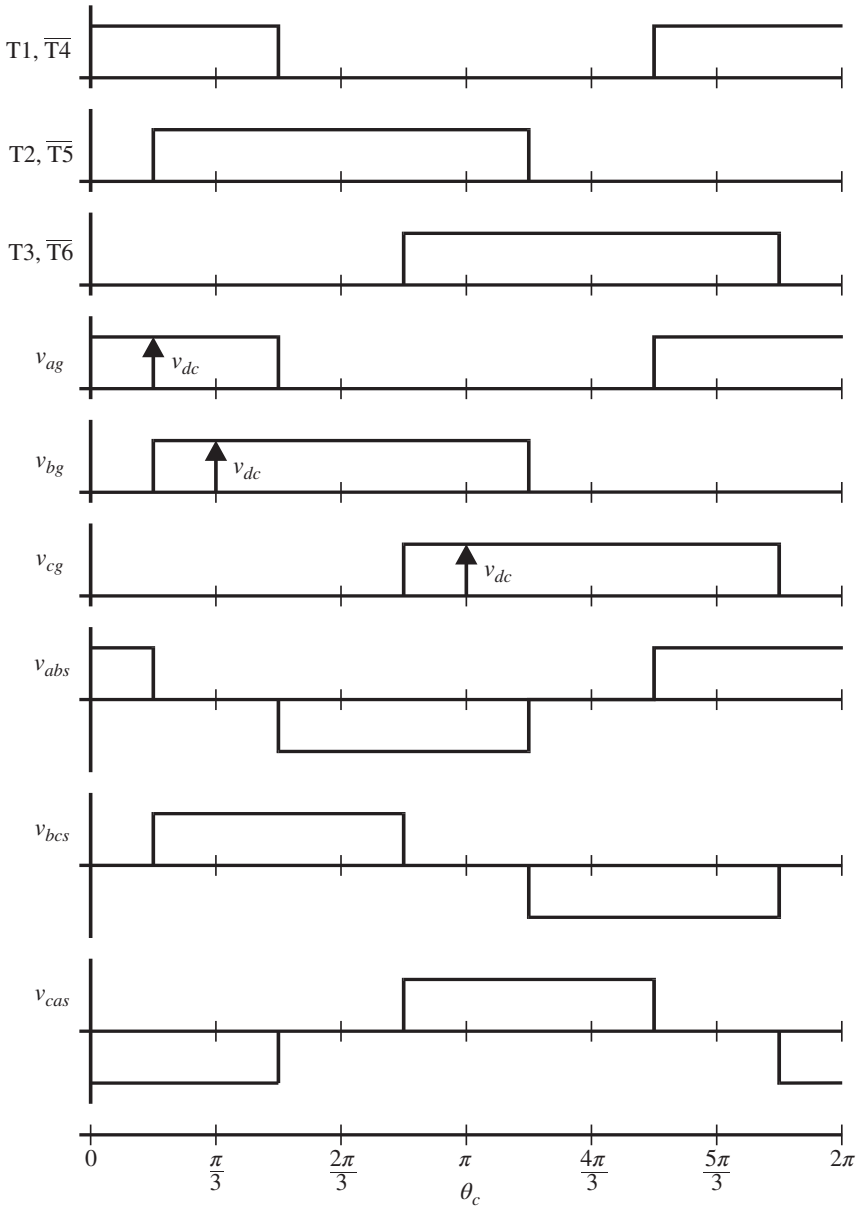

Figure 10.3-1 Line-to-line voltages for six-step operation.

chapters, the converter angle will be related to the electrical rotor position or the position of the synchronous reference frame depending upon the type of machine. Referring to Figure 10.3-1, the logical complement of the switching command to the lower device of each leg is shown for convenience, since this signal is equal to the switch command of the upper device if switching times are neglected. For purposes of explanation, it is further assumed that the diode and switching devices are ideal—that is, that they are perfect conductors when turned on or perfect insulators when turned off. With these assumptions, the line-to-ground voltages are as shown in the central three traces of Figure 10.3-1. From the line-to-ground voltages, the line-to-line voltages may be calculated from (10.2-1)–(10.2-3), which are illustrated in the final three traces. Since the waveforms are square waves rather than sine waves, the three-phase bridge produces considerable harmonic content in the ac output when operated in this fashion. In particular, using Fourier series techniques, the a- to b-phase line-to-line voltage may be expressed as

$$v_{abs} = \frac{2\sqrt{3}}{\pi} v_{dc} \cos\left(\theta_c + \frac{\pi}{6}\right) + \frac{2\sqrt{3}}{\pi} v_{dc} \left(\sum_{j=1}^{\infty} \left(-\frac{1}{6j-1} \cos\left((6j-1)\left(\theta_c + \frac{\pi}{6}\right)\right) + \frac{1}{6j+1} \cos\left((6j+1)\left(\theta_c + \frac{\pi}{6}\right)\right)\right)\right) \tag{10.3-1}$$

From (10.3-1), it can be seen that the line-to-line voltage contains a fundamental component, as well as the 5th, 7th, 9th, 11th, 13th, 17th, 19th … harmonic components. There are no even harmonics or odd harmonics that are a multiple of three. The effect of harmonics depends on the machine. In the case of a permanent-magnet ac machine with a sinusoidal back emf, the harmonics will result in torque harmonics but will not have any effect on the average torque. In the case of the induction motor, torque harmonics will again result; however, in this case the average torque will be affected. In particular, it can be shown that the $6j-1$ harmonics form an *acb* sequence that will reduce the average torque, while the $6j+1$ harmonics form an *abc* sequence that increases the average torque. The net result is usually a small decrease in average torque. In all cases, harmonics will result in increased machine losses.

Figure 10.3-2 again illustrates six-stepped operation, except that the formulation of the line-to-neutral voltages is considered. From the line-to-ground voltage, the neutral-to-ground voltage v_{ng} is calculated using (10.2-10). The line-to-neutral voltages are calculated using the line-to-ground voltages and line-to-neutral voltage from (10.2-5)–(10.2-7). From Figure 10.3-2, the a-phase line-to-neutral voltage

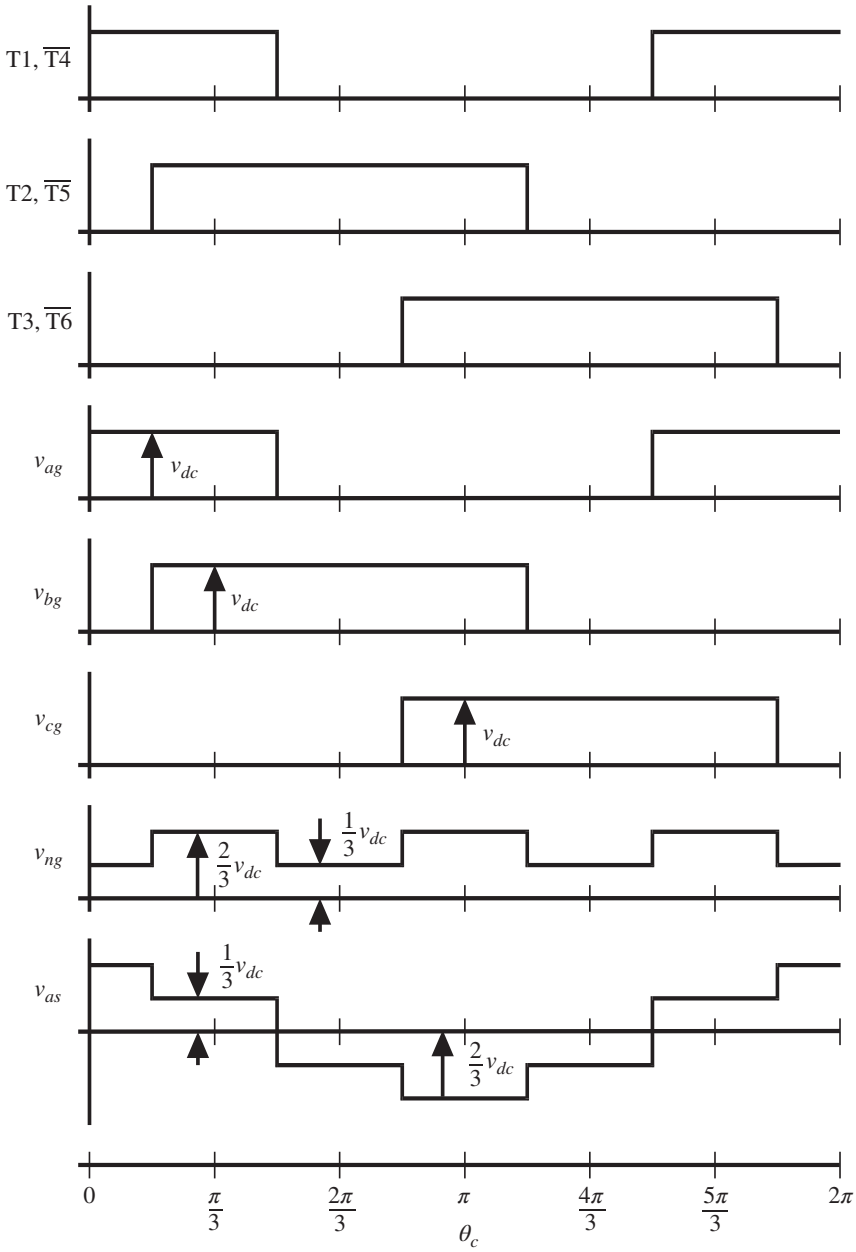

Figure 10.3-2 Line-to-neutral voltage for six-step operation.

may be expressed as a Fourier series of the form

$$v_{as} = \frac{2}{\pi} v_{dc} \cos\theta_c + \frac{2}{\pi} v_{dc} \sum_{j=1}^{\infty} \left(\frac{(-1)^{j+1}}{6j-1} \cos((6j-1)\theta_c) + \frac{(-1)^j}{6j+1} \cos((6j+1)\theta_c) \right) \tag{10.3-2}$$

Relative to the fundamental component, each harmonic component of the line-to-neutral voltage waveform has the same amplitude as in the line-to-line voltage. The frequency spectrum of both the line-to-line and line-to-neutral voltages is illustrated in Figure 10.3-3.

The effect of these harmonics on the current waveforms is illustrated in Figure 10.3-4. In this study, a three-phase bridge supplies a wye-connected load consisting of a 2-Ω resistor in series with a 1-mH inductor in each phase. The dc voltage is 100 V and the frequency is 100 Hz. The *a*-phase voltage has the waveshape depicted in Figure 10.3-2, and the impact of the *a*-phase voltage harmonics on the *a*-phase current is clearly evident. Because of the harmonic content of the waveforms, the power going into the three-phase load is not constant, which implies that the power into the converter, and hence the dc current into the converter, is not constant. As can be seen, the dc current waveform repeats every 60 electrical degrees; this same pattern will also be shown to be evident in *q*- and *d*-axis variables.

Since the analysis of electric machinery is based on reference-frame theory, it is convenient to determine *q*- and *d*-axis voltages produced by the converter. To do this, we will define the converter reference frame to be a reference frame in which

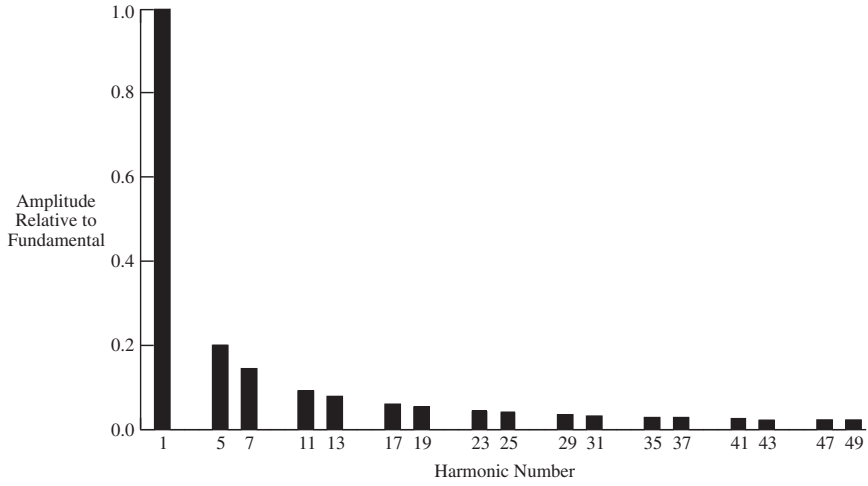

Figure 10.3-3 Frequency spectrum of six-step operation.

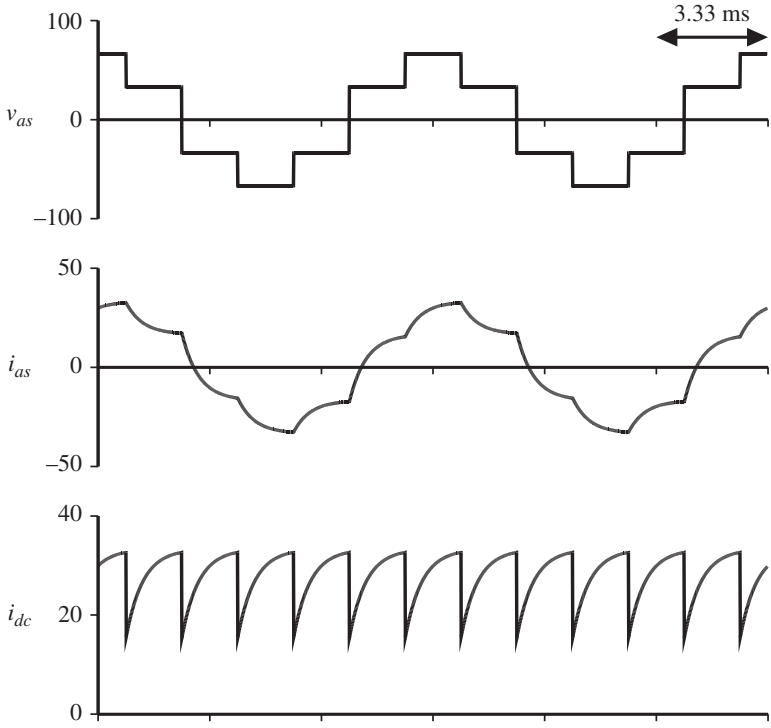

Figure 10.3-4 Voltage and current waveforms for a six-stepped converter feeding an RL load.

θ of (3.3-4) is equal to θ_c. In this reference frame, the average q-axis voltage is equal to the peak value of the fundamental component of the applied line-to-neutral voltage and the average d-axis voltage is zero. This transformation will be designated $\mathbf{K}_s^c$. Usually, the converter reference frame will be the rotor reference frame in the case of a permanent magnet ac machine or the synchronously rotating reference frame in the case of an induction motor. Deriving expressions analogous to (10.3-2) for the b- and c-phase line-to-neutral voltages and transforming these voltages to the converter reference frame yields

$$v_{qs}^c = \frac{2}{\pi} v_{dc} - \frac{2}{\pi} v_{dc} \sum_{j=1}^{\infty} \frac{2(-1)^j}{36j^2 - 1} \cos(6j\theta_c) \tag{10.3-3}$$

$$v_{ds}^c = \frac{2}{\pi} v_{dc} \sum_{j=1}^{\infty} \frac{12j}{36j^2 - 1} \sin(6j\theta_c) \tag{10.3-4}$$

From (10.3-3) and (10.3-4), it can be seen that the q- and d-axis variables will contain a dc component in addition to multiples of the sixth harmonic. In addition

to being evident in *qd* variables, the 6th harmonic is also apparent in the torque waveforms of machines connected to six-stepped converters.

For the purposes of machine analysis, it is often convenient to derive an average-value model of the machine in which harmonics are neglected. From (10.3-3) and (10.3-4), the average *q*- and *d*-axis voltage may be expressed

$$\overline{v}_{qs}^{c} = \frac{2}{\pi} v_{dc} \tag{10.3-5}$$

$$\overline{v}_{qs}^{c} = 0 \tag{10.3-6}$$

where the line above the variables denotes average value.

It is interesting to compare the line-to-neutral voltage to the *q*- and *d*-axis voltage. Such a comparison appears in Figure 10.3-5. As can be seen, the *q*- and *d*-axis voltages repeat every 60 electrical degrees, which is consistent with the fact that these waveforms only contain a dc component and harmonics that are a multiple of six. The *qd* currents, *qd* flux linkages, and electromagnetic torque also possess the property of repeating every 60 electrical degrees.

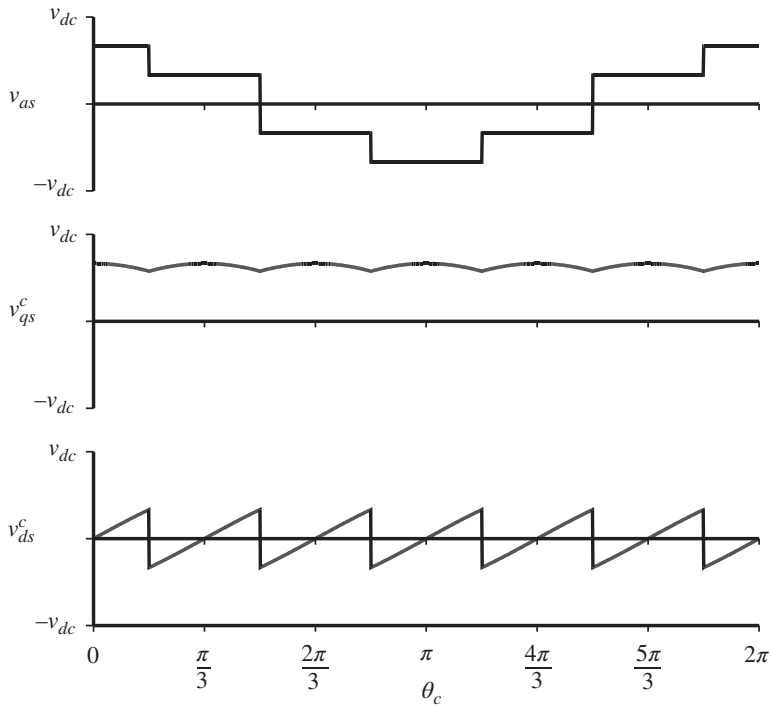

Figure 10.3-5 Comparison of *a*-phase voltage to *q*- and *d*-axis voltage.

In order to calculate the average dc current into the inverter, note that the instantaneous power into the inverter is given by

$$P_{\text{in}} = i_{dc} v_{dc} \tag{10.3-7}$$

The power out of the inverter is given by

$$P_{\text{out}} = \frac{3}{2}(v_{qs} i_{qs} + v_{ds} i_{ds}) \tag{10.3-8}$$

Neglecting inverter losses, the input power must equal the output power, therefore

$$i_{dc} = \frac{3(v_{qs} i_{qs} + v_{ds} i_{ds})}{2 v_{dc}} \tag{10.3-9}$$

Equation (10.3-9) is true on an instantaneous basis in any reference frame. Therefore, it is also true on average, thus

$$\bar{i}_{dc} = \frac{3}{2}\left(\frac{\overline{v_{qs} i_{qs} + v_{ds} i_{ds}}}{v_{dc}}\right) \tag{10.3-10}$$

In a reference frame in which the fundamental components of the applied voltages are constant and if the power transmitted through the bridge via the harmonics of the voltage and current waveforms is neglected, (10.3-10) may be approximated as

$$\bar{i}_{dc} = \frac{3}{2}\frac{\bar{v}_{ds}\bar{i}_{qs} + \bar{v}_{ds}\bar{i}_{qs}}{\bar{v}_{dc}} \tag{10.3-11}$$

It should be emphasized that (10.3-11) is only valid in a reference frame in which the variables are constant in the steady state (the converter reference frame, rotor reference frame of a synchronous or permanent magnet ac machine, or the synchronous reference frame) and when the harmonic power can be neglected.

Example 10A Suppose a six-step bridge converter drives a three-phase RL load. The system parameters are as follows: $v_{dc} = 100$ V, $r = 1.0\ \Omega$, $l = 1.0$ mH, and $\omega_c = 2\pi 100$ rad/s. Estimate the average dc current into the inverter. From (10.3-5) and (10.3-6), we have that $\bar{v}^c_{qs} = 63.7$ V and $\bar{v}^c_{qs} = 0$ V. From the steady-state equations representing the RL circuit in the converter reference frame,

$$\begin{bmatrix} \bar{i}^c_{qs} \\ \bar{i}^c_{ds} \end{bmatrix} = \begin{bmatrix} r & \omega_c l \\ -\omega_c l & r \end{bmatrix}^{-1} \begin{bmatrix} \bar{v}^c_{qs} \\ \bar{v}^c_{ds} \end{bmatrix} \tag{10A-1}$$

from which we obtain $\bar{i}_{qc} = 45.6$ A and $\bar{i}^c_{ds} = 28.7$ A. From (10.3-11), we have that $\bar{i}_{dc} = 43.6$ A. It is instructive to do this calculation somewhat more accurately by

including the harmonic power. In particular, from (10.3-2), the harmonic content of the voltage waveform can be calculated, which can then be used to find the total power being supplied by the load as

$$p_{\text{out}} = \frac{3}{2} r \left(\left| \frac{\frac{2}{\pi} v_{dc}}{r + j\omega_c l} \right|^2 + \sum_{i=1}^{\infty} \left(\left| \frac{\frac{2}{\pi(6k-1)} v_{dc}}{r + j(6k-1)\omega_c l} \right|^2 + \left| \frac{\frac{2}{\pi(6k+1)} v_{dc}}{r + j(6k+1)\omega_c l} \right|^2 \right) \right) \tag{10A-2}$$

This yields $P_{\text{out}} = 4389$ W, which requires an average dc current of 43.9 A. Thus, at least for this load, the approximations made in deriving (10.3-11) are valid.

Six-step operation is the simplest strategy for controlling the three-phase bridge topology so as to synthesize a three-phase ac voltage source from a single-phase dc voltage source. By varying ω_c, variable frequency operation is readily achieved. Nevertheless, there are two distinct disadvantages of this type of operation. First, the only way that the amplitude of the fundamental component can be achieved is by varying v_{dc}. Although this is certainly possible by using a controllable dc source, appropriate control of the power electronic switches can also be used, which allows the use of a less expensive uncontrolled dc supply. Such a method is considered in the following section. Second, the harmonic content inevitably lowers the machine efficiency. An appropriate switching strategy can substantially alleviate this problem. Thus, although the control strategy just considered is simple, more sophisticated methods of control are generally preferred. The one advantage of the method besides its simplicity is that the amplitude of the fundamental component of the voltage is the largest possible with the topology considered. For this reason, many other control strategies effectively approach six-step operation as the desired output voltage increases.

10.4 Six-Step Modulation

In this section, a refinement of six-step operation is presented. In particular, one of several pulse-width modulation (PWM) control strategies that allows the amplitude of the fundamental component of the voltage to be readily controlled is set forth in this section. As in the case of six-step operation, the converter will appear as a voltage-source to the system, and so six-step modulation is also described as a voltage-source modulation scheme.

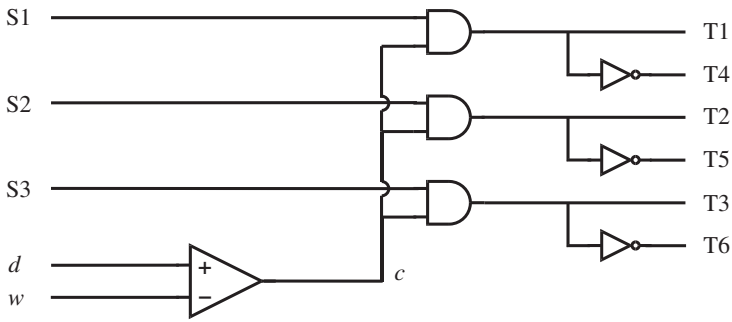

Figure 10.4-1 Six-step modulation control schematic (deadtime logic not shown).

Figure 10.4-1 illustrates the logic control strategy for six-step modulation. Therein, the logic signals S1–S3 are the same as the switching signals T1–T3 for six-step operation. The control input to the converter is the duty cycle d, which may be varied from 0 to 1. The signal w is a triangle waveform that also varies between 0 and 1. The duty cycle d and triangle wave w are inputs of a comparator, the output of which will be denoted c. The comparator output is logically added with S1–S3 to yield the control signals for the semiconductor devices.

The operation of this control circuit is illustrated in Figure 10.4-2. As alluded to previously, the signals S1–S3 are identical to T1–T3 in six-step operation. The duty cycle d is assumed to be constant or to vary slowly relative to the triangle wave. The frequency of the triangle wave is the switching frequency f_{sw} (the number of times each switching device is turned on per second), which should be much greater than the frequency of the fundamental component of the output. The output of the comparator c is a square wave whose average value is d. When c is high, the switching signals to the transistors T1–T3, and hence the voltages, are all identical to those of six-step operation. When c is low, all the voltages are zero.

In order to analyze six-step modulation, it is convenient to make use of the fact that the voltages produced by this control strategy are equal to voltages applied in the six-step operation multiplied by the output of the comparator. Using Fourier series techniques, the comparator output may be expressed as

$$c = d + 2d\sum_{k=1}^{\infty}\text{sinc}(kd)\cos(k\theta_{sw}) \tag{10.4-1}$$

where θ_{sw} is the switching angle defined by

$$p\theta_{sw} = \omega_{sw} \tag{10.4-2}$$

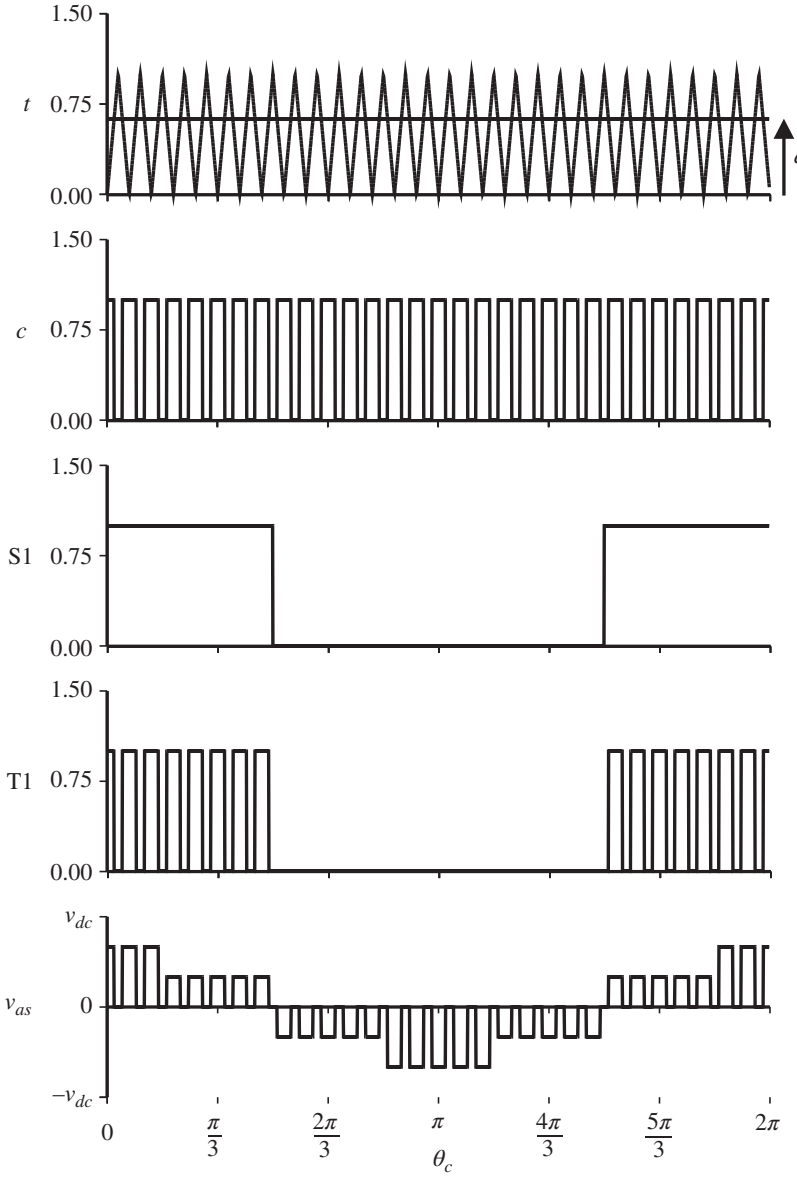

Figure 10.4-2 Six-step modulation control signals.

where $\omega_{sw} = 2\pi f_{sw}$. Multiplying (10.4-1) by (10.3-2) yields a Fourier series expression for the a-phase line-to-neutral voltage:

$$
\begin{aligned}
v_{as} = \&\frac{2dv_{dc}}{\pi}\left(\cos\theta_c + \sum_{j=1}^{\infty}\left(\frac{(-1)^{j+1}}{6j-1}\cos((6j-1)\theta_c) + \frac{(-1)^j}{6j+1}\cos((6j+\mathbf{1})\theta_c)\right)\right) \\
&+ \frac{2dv_{dc}}{\pi}\sum_{k=1}^{\infty}\text{sinc}(kd)\cos(k\theta_{sw} - \theta_c) \\
&+ \frac{2dv_{dc}}{\pi}\sum_{k=1}^{\infty}\text{sinc}(kd)\sum_{j=1}^{\infty} \\
&\left(\frac{(-1)^{j+1}}{6j-1}\cos(k\theta_{sw} - (6j-1)\theta_c) + \frac{(-1)^j}{6j+1}\cos(k\theta_{sw} - (6j+1)\theta_c)\right) \\
&+ \frac{2dv_{dc}}{\pi}\sum_{k=1}^{\infty}\text{sinc}(kd)\cos(k\theta_{sw} + \theta_c) \\
&+ \frac{2dv_{dc}}{\pi}\sum_{k=1}^{\infty}\text{sinc}(kd)\sum_{j=1}^{\infty} \\
&\left(\frac{(-1)^{j+1}}{6j-1}\cos(k\theta_{sw} + (6j-1)\theta_c) + \frac{(-1)^j}{6j+1}\cos(k\theta_{sw} + (6j+1)\theta_c)\right) \qquad (10.4\text{-}3)
\end{aligned}
$$

As can be seen, (10.4-3) is quite involved. The first line indicates that the PWM drive will produce all the harmonics produced by six-step operation, except that all components, including the fundamental, will be scaled by the duty cycle. The next two lines represent the spectrum produced by six-step operation as projected onto the lower side band of the fundamental and harmonics of the switching frequency. The final two lines represent the spectrum produced by six-step operation as projected onto the upper side band of the fundamental and harmonics of the switching frequency. Although the high-frequency harmonic components are not of direct interest for machine analysis, the location of these harmonics is important in the identification of acoustic and electromagnetic noise.

From (10.4-3), it is apparent that the fundamental component of the applied voltage is given by

$$|v_{as}|_{\text{fund}} = d\frac{2}{\pi}v_{dc}\cos\theta_c \qquad (10.4\text{-}4)$$

From (10.4-4), it follows that the average q- and d-axis voltage are given by

$$\bar{v}_{qs}^{c} = \frac{2}{\pi}dv_{dc} \qquad (10.4\text{-}5)$$

$$\bar{v}_{ds}^{c} = 0 \qquad (10.4\text{-}6)$$

Thus, by varying the duty-cycle, the amplitude of the fundamental component of the inverter voltage is readily achieved with a fixed dc supply voltage.

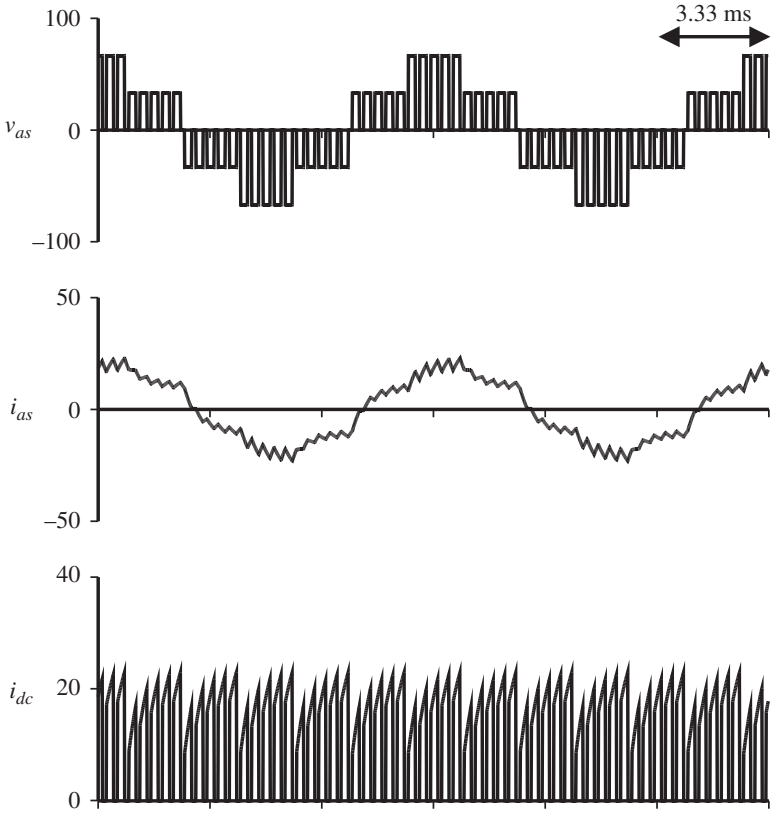

Figure 10.4-3 Voltage and current waveforms for six-step modulated converter feeding an RL load.

Figure 10-4.3 illustrates the voltage and current waveforms obtained using six-step modulation. The system parameters are the same as for Figure 10.3-4, except that the duty cycle is 0.628 and the switching frequency is 3000 Hz. As can be seen, the a-phase current waveform is approximately 0.628 times the current waveform in Figure 10.3-4 if the higher-frequency components of the a-phase current are neglected.

Although this control strategy allows the fundamental component of the applied voltage to be readily controlled, the disadvantage of this method is that the low-frequency harmonic content adversely affects the performance of the drive. The next modulation scheme considered, sine-triangle modulation, also allows for the control of the applied voltage. However, in this case, there is relatively little low-frequency harmonic content, resulting in nearly ideal machine performance.

10.5 Sine-Triangle Modulation

In the previous section, a method to control the amplitude of the applied voltages was set forth. Although straightforward, considerable low-frequency harmonics were generated. The sine-triangle modulation strategy illustrated in Figure 10.5-1 does not share this drawback. Like six-step and six-step modulated operation, this control strategy again makes the converter appear as a voltage-source to the ac system, and so it is again classified as a voltage-source modulation strategy.

In Figure 10.5-1, the signals d_a, d_b, and d_c represent duty cycles that vary in a sinusoidal fashion and w is a triangle wave that varies between -1 and 1 with a period T_{sw}. In practice, each of these variables is typically scaled such that the actual voltage levels make the best use of the hardware on which they are implemented.

Figure 10.5-2 illustrates the triangle wave w, a-phase duty cycle, and resulting a-phase line-to-ground voltage. Therein, the a-phase duty cycle is shown as being constant even though it is sinusoidal. This is because the triangle wave is assumed to be of a much higher switching frequency than the duty cycle signals, so that on the time scale shown, the a-phase duty cycle appears to be constant. For the purposes of analysis, it is convenient to define the "dynamic average" of a variable—that is, the average value over a period of time T_{sw}—as

$$\hat{x}(t) = \frac{1}{T_{sw}} \int_{t-T_{sw}}^{t} x(t)dt \tag{10.5-1}$$

From Figure 10.5-1 and (10.5-1), it can be shown that

$$\hat{v}_{ag} = \frac{1}{2}(1 + d_a)v_{dc} \tag{10.5-2}$$

Similarly,

$$\hat{v}_{bg} = \frac{1}{2}(1 + d_b)v_{dc} \tag{10.5-3}$$

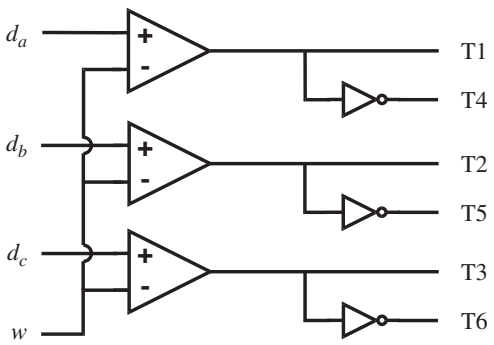

Figure 10.5-1 Sine-triangle modulation control schematic (deadtime logic not shown).

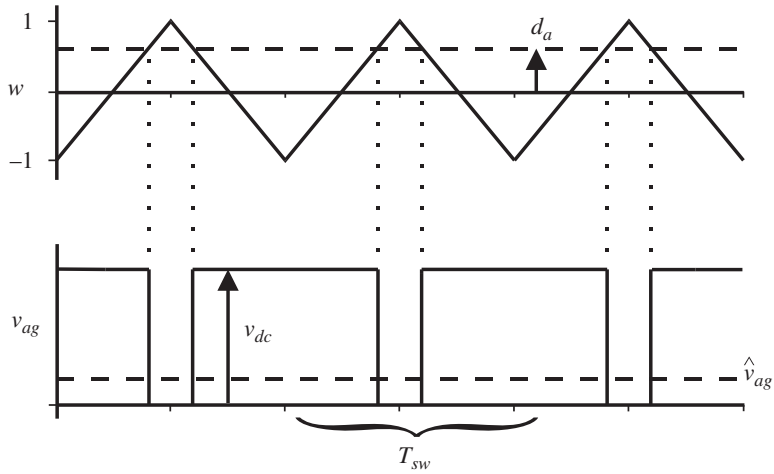

Figure 10.5-2 Operation of a sine-triangle modulator.

$$\hat{v}_{cg} = \frac{1}{2}(1 + d_c)v_{dc} \tag{10.5-4}$$

If d_a, d_b, and d_c form a balanced three-phase set, then these three signals must sum to zero. Making use of this fact, substitution of (10.5-2)–(10.5-4) into (10.2-11)–(10.2-13) yields

$$\hat{v}_{as} = \frac{1}{2}d_a v_{dc} \tag{10.5-5}$$

$$\hat{v}_{bs} = \frac{1}{2}d_b v_{dc} \tag{10.5-6}$$

$$\hat{v}_{cs} = \frac{1}{2}d_c v_{dc} \tag{10.5-7}$$

Although it has been assumed that the duty cycles are sinusoidal, (10.5-5)–(10.5-7) hold whenever the sum of the duty cycles is zero. If the duty cycles are specified as

$$d_a = d\cos\theta_c \tag{10.5-8}$$

$$d_b = d\cos\left(\theta_c - \frac{2\pi}{3}\right) \tag{10.5-9}$$

$$d_c = d\cos\left(\theta_c + \frac{2\pi}{3}\right) \tag{10.5-10}$$

It follows from (10.5-5)–(10.5-7) that

$$\hat{v}_{as} = \frac{1}{2}dv_{dc}\cos\theta_c \tag{10.5-11}$$

$$\hat{v}_{bs} = \frac{1}{2}dv_{dc}\cos\left(\theta_c - \frac{2\pi}{3}\right) \tag{10.5-12}$$

$$\hat{v}_{cs} = \frac{1}{2} d v_{dc} \cos\left(\theta_c + \frac{2\pi}{3}\right) \tag{10.5-13}$$

Recall that the "∧" denotes the dynamic-average value. Thus, assuming that the frequency of the triangle wave is much higher than the frequency of the desired waveform, the sine-triangle modulation strategy does not produce any low-frequency harmonics. Transforming (10.5-11)–(10.5-13) to the converter reference frame yields

$$\hat{v}_{qs}^{c} = \frac{1}{2} d v_{dc} \tag{10.5-14}$$

$$\hat{v}_{ds}^{c} = 0 \tag{10.5-15}$$

Equation (10.5-14) and Equation (10.5-15) serve as both steady-state average-value, and, since there are no low-frequency harmonics, dynamic-average-value expressions.

Figure 10.5-3 illustrates the performance of a sine-triangle modulated converter feeding an RL load. The system parameters are identical to the study in

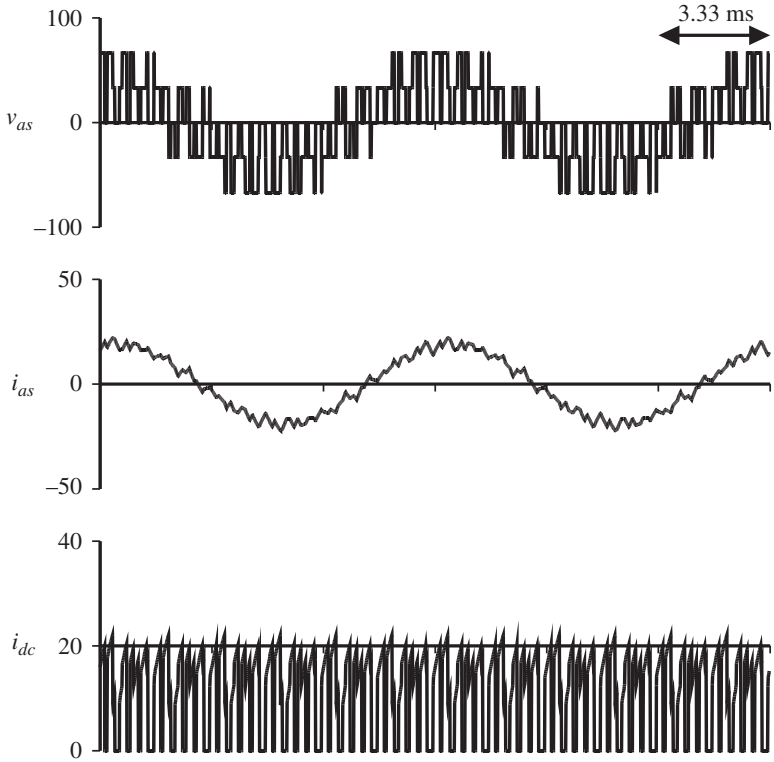

Figure 10.5-3 Voltage and current waveforms using sine-triangle modulation.

Figure 10.4-3, except that $d = 0.4$, which results in the voltage waveform with the same fundamental component as in Figure 10.4-3. Comparing Figure 10.5-3 with Figure 10.4-3, it is evident that the sine-triangle modulation strategy results in greatly reduced low-frequency current harmonics. This is even more evident as the switching frequency is increased.

From (10.5-11)–(10.5-13) or (10.5-14) and (10.5-15), it can be seen that if d is limited to values between 0 and 1, then the amplitude of the applied voltage varies from 0 to $v_{dc}/2$, whereas in the case of pulse width modulation, the amplitude varies between 0 and $2v_{dc}/\pi$. The maximum amplitude produced by the sine-triangle modulation scheme can be increased to the same value as for six-step modulation by increasing d to a value greater than 1, a mode of operation known as overmodulation.

Figure 10.5-4 illustrates overmodulated operation. In the upper trace, the two lines indicate the envelope of the triangle wave. The action of the comparators, given the value of the duty cycle relative the envelope of the triangle wave in the upper trace of Figure 10.5-4, results in the following description of the dynamic-average of the a-phase line-to-ground voltage

$$\hat{v}_{ag} = \begin{cases} v_{dc} & d_a > 1 \\ \dfrac{1}{2}(1 + d_a)v_{dc} & -1 \le d_a \le 1 \\ 0 & d_a < 1 \end{cases} \tag{10.5-16}$$

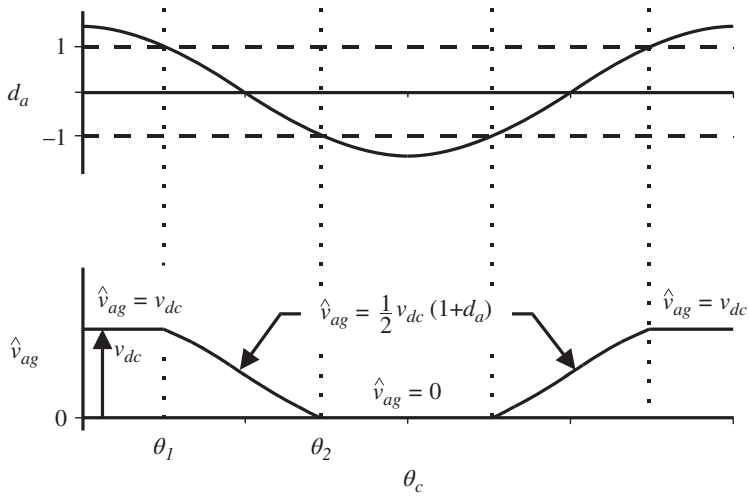

Figure 10.5-4 Overmodulation.

This is illustrated in the second trace of Figure 10.5-4, wherein the angles θ_1 and θ_2 mark the points at which the a-phase duty cycle is equal to 1 and -1, respectively. Using Fourier analysis, v_{ag} may be expressed in terms of its average-value and fundamental component as

$$|v_{ag}|_{\text{avg+fund}} = \frac{v_{dc}}{2} + \frac{2v_{dc}}{\pi} f(d) \cos\theta_c \tag{10.5-17}$$

where

$$f(d) = \frac{1}{2}\sqrt{1 - \left(\frac{1}{d}\right)^2} + \frac{1}{4} d \left(\pi - 2\arccos\left(\frac{1}{d}\right)\right) \tag{10.5-18}$$

and d must be greater than unity (overmodulated). The b- and c-phase voltages may be similarly expressed by subtracting and adding 120° from θ_c in (10.5-17), respectively, whereupon (10.2-11)–(10.2-13) may be used to express the line-to-neutral voltages. This yields that

$$|v_{as}|_{\text{fund}} = \frac{2v_{dc}}{\pi} f(d) \cos(\theta_c) \tag{10.5-19}$$

As d varies from one to infinity, $f(d)$ varies from $\pi/4$ to 1. Thus, the amplitude of the fundamental component increases as the duty cycle becomes greater than 1. However, this increase is at a cost; low-frequency harmonics will be present and will increase with duty cycle. In particular, at a duty cycle of 1, no low-frequency harmonics will be present, but at $d = \infty$, the harmonics are equal to those produced by six-step operation.

Expressing the b- and c-phase voltages analogously to (10.5-19) and transforming to the converter reference frame yields

$$\overline{v}_{qs}^{c} = \frac{2v_{dc}}{\pi} f(d) \quad d \geq 1 \tag{10.5-20}$$

$$\overline{v}_{ds}^{c} = 0 \quad d \geq 0 \tag{10.5-21}$$

It is interesting to observe the performance of the overmodulated sine-triangle modulated bridge. Figure 10.5-5 illustrates system performance for the same conditions as illustrated in Figure 10.5-3, except that d has been increased to 2. As can be seen, the fundamental component of the voltage and current waveforms has increased; however, this is at the expense of a slight increase in the low-frequency harmonics. As the duty cycle is further increased, the voltage and current waveforms will approach those shown in Figure 10.3-4.

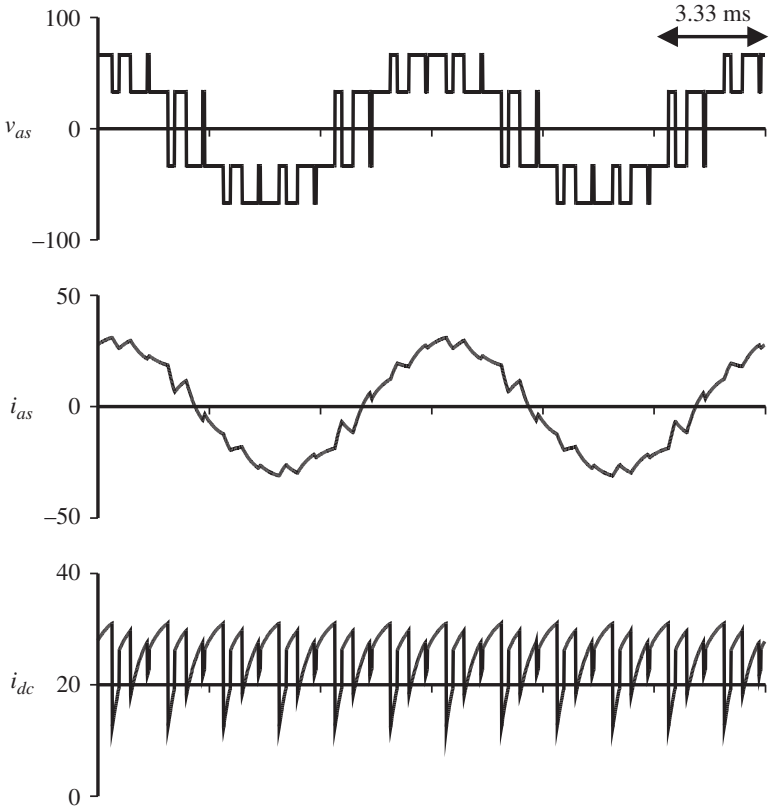

Figure 10.5-5 Voltage and current waveforms during overmodulated operation.

10.6 Extended Sine-Triangle Modulation

One of the chief limitations of sine-triangle modulation is that the peak value of the fundamental component of the line-to-neutral voltage is limited to $v_{dc}/2$. As it turns out, this limit can be increased by changing the duty cycle waveforms from the expression given by (10.5-8)–(10.5-10) to the following:

$$d_a = d\cos\theta_c - d_3\cos(3\theta_c) \tag{10.6-1}$$

$$d_b = d\cos\left(\theta_c - \frac{2\pi}{3}\right) - d_3\cos(3\theta_c) \tag{10.6-2}$$

$$d_c = d\cos\left(\theta_c + \frac{2\pi}{3}\right) - d_3\cos(3\theta_c) \tag{10.6-3}$$

Doing this will allow us to use values of d greater than 1. This scheme will be referred to as extended sine-triangle modulation, which is also classified as a voltage-source modulation scheme.

In order to understand why (10.6-1)–(10.6-3) can be used to increase the maximum fundamental component of the line-to-neutral voltage, note that applying the dynamic-average definition to (10.2-10) yields

$$\hat{v}_{ng} = \frac{1}{3}(\hat{v}_{ag} + \hat{v}_{bg} + \hat{v}_{cg}) \tag{10.6-4}$$

Applying the same dynamic-average definition to (10.2-5)–(10.2-7) and solving for the line-to-neutral voltage yields

$$\hat{v}_{as} = \hat{v}_{ag} - \hat{v}_{ng} \tag{10.6-5}$$

$$\hat{v}_{bs} = \hat{v}_{bg} - \hat{v}_{ng} \tag{10.6-6}$$

$$\hat{v}_{cs} = \hat{v}_{cg} - \hat{v}_{ng} \tag{10.6-7}$$

Substitution of (10.6-1)–(10.6-3) into (10.5-2)–(10.5-4), and then substituting the resulting expressions for $\hat{v}_{ag}$, $\hat{v}_{bg}$, and $\hat{v}_{cg}$ into (10.6-4) and then (10.6-5)–(10.6-7) yields

$$\hat{v}_{as} = \frac{1}{2}d\hat{v}_{dc}\cos\theta_c \tag{10.6-8}$$

$$\hat{v}_{bs} = \frac{1}{2}d\hat{v}_{dc}\cos\left(\theta_c - \frac{2\pi}{3}\right) \tag{10.6-9}$$

$$\hat{v}_{cs} = \frac{1}{2}d\hat{v}_{dc}\cos\left(\theta_c + \frac{2\pi}{3}\right) \tag{10.6-10}$$

This is the same result as was obtained for sine-triangle modulation in the previous section, (10.5-11), (10.5-12), and (10.5-13), and like the previous result is valid provided $|d_a|$, $|d_b|$, and $|d_c|$ are less than unity for all θ_c. The difference is that this requirement on $|d_a|$, $|d_b|$, and $|d_c|$ is met. In particular, in the case of sine-triangle modulation, ensuring that $|d_a|$, $|d_b|$, and $|d_c|$ are all less than unity is met by requiring $|d| < 1$, which forces the fundamental component of the line-to-neutral voltage to be limited to $v_{dc}/2$. In the case of extended sine-triangle modulation, the requirement that $|d_a|$, $|d_b|$, and $|d_c|$ are all less than unity can be met with $d > 1$, because the third-harmonic term can be used to reduce the peak value of the phase duty cycle waveforms.

It remains to establish the maximum value of d and the value that should be used for d_3. Because of symmetry, these quantities can be determined by considering just the a-phase over the range $0 \le \theta_c \le \pi/6$. Note that over this range, the effect of the third-harmonic term is to reduce the magnitude of d_a (provided that d is positive). However, at $\theta_c = \pi/6$, $\cos 3\theta_c$ is zero and so the amount of the reduction is zero. Evaluating (10.6-1) at $\theta_c = \pi/6$ leads to the requirement that

$$d\cos(\pi/6) \le 1 \tag{10.6-11}$$

which means that

$$d \leq \frac{2}{\sqrt{3}} \tag{10.6-12}$$

for the strategy to work correctly. The next step is to establish the value of d_3. To derive this value, requiring that (10.6-1) has a peak value less than unity for all θ_c when d is its maximum value of $2/\sqrt{3}$ yields $d_3 = 1/(3\sqrt{3})$. For this reason, it is common to select $d_3 = d/6$. This answer is unique; any other value will result in overmodulation when $d = 2/\sqrt{3}$.

The primary advantage of this strategy is the increase in available voltage, which can be obtained. In particular, substituting $d = 2/\sqrt{3}$ into (10.6-8), the fundamental component of the line-to-neutral voltage is increased to $v_{dc}/\sqrt{3}$, a 15% increase in amplitude over sine-triangle modulation. In regard to the average value modeling of this strategy, (10.5-14) and (10.5-15) are valid provided that $d \leq 2/\sqrt{3}$.

10.7 Space-Vector Modulation

Another voltage-source PWM strategy for achieving three-phase voltage waveforms that are devoid of low-frequency harmonic content is space-vector modulation [9]. This modulation strategy is designed to work with voltage commands expressed in terms of *qd* variables. In particular, in this strategy, voltage commands expressed in a stationary reference frame (v_{qs}^{s*} and v_{ds}^{s*}) are sampled at the beginning of each switching cycle, and then the inverter semiconductors are switched in such a way that the dynamic average of the actual q- and d-axis voltages in the stationary reference frame ($\widehat{v}_{qs}^{s}$ and $\widehat{v}_{ds}^{s}$) are obtained over the ensuing switching period.

When describing the space-vector modulator algorithm, it is convenient to define the q- and d-axis modulation indexes as the q- and d-axis voltages in the stationary reference frame normalized to the dc voltage

$$m_q^s = \widehat{v}_q^s / v_{dc} \tag{10.7-1}$$

$$m_d^s = \widehat{v}_d^s / v_{dc} \tag{10.7-2}$$

It is likewise convenient to define the commanded modulation indexes as

$$m_q^{s*} = v_q^{s*} / v_{dc} \tag{10.7-3}$$

$$m_d^{s*} = v_d^{s*} / v_{dc} \tag{10.7-4}$$

Assuming that the dc voltage is constant, or at least slowly varying compared with the switching frequency, it is apparent that the dynamic-average of the q- and d-axis voltage will be equal to the commanded voltages if the dynamic average of the q- and d-axis modulation index is equal to the commanded modulation index.

The space-vector modulation strategy can now be explained in terms of the space-vector diagram illustrated in Figure 10.7-1. Therein, the q- and d-axis modulation index vector corresponding to each of the eight possible switching states of the converter is shown. The numerical values of the q- and d-axis modulation index corresponding to the i'th state, $m_{q,x}$ and $m_{d,x}$, respectively, along with the on/off status of the inverter transistors corresponding to that state, are listed in Table 10.7-1.

In order to determine the sequence of states required to achieve the desired modulation index for a switching cycle, the following steps are performed. First, given the q- and d-axis voltage command in the stationary reference frame, the q- and d-axis modulation index command is calculated using (10.7-3) and (10.7-4). The next step is to limit the magnitude of the modulation index command to reflect the voltage limitation applied to the converter. The magnitude of the modulation

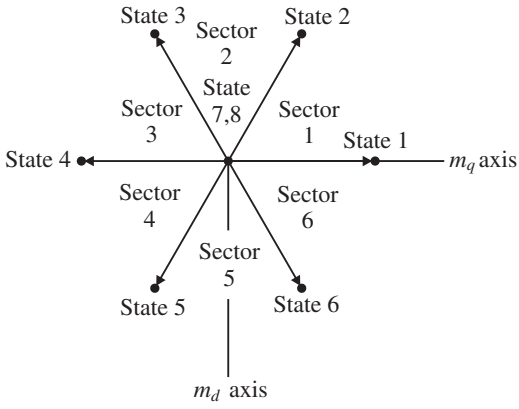

Figure 10.7-1 Space-vector diagram.

Table 10.7-1 Modulation Indices versus State.

State	$T1/\overline{T4}$	$T2/\overline{T5}$	$T3/\overline{T6}$	$m_{q,x}$	$m_{d,x}$
1	1	0	0	$2/3\cos(0°)$	$-2/3\sin(0°)$
2	1	1	0	$2/3\cos(60°)$	$-2/3\sin(60°)$
3	0	1	0	$2/3\cos(120°)$	$-2/3\sin(120°)$
4	0	1	1	$2/3\cos(180°)$	$-2/3\sin(180°)$
5	0	0	1	$2/3\cos(240°)$	$-2/3\sin(240°)$
6	1	0	1	$2/3\cos(300°)$	$-2/3\sin(300°)$
7	1	1	1	0	0
8	0	0	0	0	0

index command is defined as

$$m^* = \sqrt{\left(m_q^{s*}\right)^2 + \left(m_d^{s*}\right)^2} \tag{10.7-5}$$

In the stationary reference frame, the modulation index command vector has a magnitude of $m^*$and rotates in the qd plane at the desired electrical frequency. The largest magnitude that can be achieved without introducing low-frequency harmonics corresponds to the radius of the largest circle that can be circumscribed within the boundaries of the hexagon connecting the switching state vectors in Figure 10.7-1. This radius is given by

$$m_{max} = \frac{1}{\sqrt{3}} \tag{10.7-6}$$

The limited modulation index command is next found as follows. First, the magnitude of the raw command is computed using (10.7-5). Then the conditioned modulation index commands are calculated as follows:

$$m_q^{**} = \begin{cases} m_q^* & m^* \le m_{\max} \\ m_{max}\dfrac{m_q^*}{|m^*|} & m^* > m_{\max} \end{cases} \tag{10.7-7}$$

$$m_d^{**} = \begin{cases} m_d^* & m^* \le m_{\max} \\ m_{\max}\dfrac{m_d^*}{|m^*|} & m^* > m_{\max} \end{cases} \tag{10.7-8}$$

The next step is to compute the sector of the conditioned modulation command. This is readily calculated from

$$\text{Sector} = \text{ceil}\left(\frac{\text{angle}\left(m_q^{**} - jm_d^{**}\right)3}{\pi}\right) \tag{10.7-9}$$

where angle() returns the angle of its complex argument and has a range of 0–2π and ceil() returns the next greatest integer.

Once the sector has been determined, the sequence of states used in the ensuing switching cycle are as set forth in Table 10.7-2. This sequence consists of four states: the initial state denoted α, the second state denoted β, the third state denoted γ, and the final state denoted δ. The initial state is always 7 or 8, and the final state will be 8 if the initial state is 7 and will be 7 if the initial state is 8. Therefore, the switching state always begins and ends in a state in which the instantaneous modulation indexes are zero. Another property of the listed state sequence is that only the three states (with states 7 and 8 counted as a single state since they produce identical voltages) with modulation indexes spatially closest to the desired modulation index are used. It is also interesting to observe that with the state sequence listed, the transition between each state

Table 10.7-2 State Sequence.

Sector	Initial State (α)	2nd State (β)	3rd State (γ)	Final State (δ)
1	7	2	1	8
2	7	2	3	8
3	7	4	3	8
4	7	4	5	8
5	7	6	5	8
6	7	6	1	8
1	8	1	2	7
2	8	3	2	7
3	8	3	4	7
4	8	5	4	7
5	8	5	6	7
6	8	1	6	7

and the following state is always achieved by switching the semiconductors in a single converter leg. This is an important feature because it minimizes switching frequency.

After the state sequence has been determined, the time to be spent in each state has to be determined. It can be shown that the dynamic average of the modulation index is given by

$$\hat{m}_q = \frac{t_\beta}{T_{sw}} m_{q,\beta} + \frac{t_\gamma}{T_{sw}} m_{q,\gamma} \tag{10.7-10}$$

$$\hat{m}_d = \frac{t_\beta}{T_{sw}} m_{d,\beta} + \frac{t_\gamma}{T_{sw}} m_{d,\gamma} \tag{10.7-11}$$

where t_β and t_γ denote the amount of time spent in the second and third states of the sequence, β and γ denote index (1–6, see Table 10.7-1) of the second and third states of the sequence as determined from Table 10.7-2, and T_{sw} denotes the switching period. Setting the dynamic-average modulation indexes equal to the limited modulation index commands and solving (10.7-10) and (10.7-11) for the switching times yields

$$t_\beta = T_{sw} \left(m_{d,\gamma} m_q^{**} - m_{q,\gamma} m_d^{**} \right) / D \tag{10.7-12}$$

$$t_\gamma = T_{sw} \left(-m_{d,\beta} m_q^{**} + m_{q,\beta} m_d^{**} \right) / D \tag{10.7-13}$$

where

$$D = m_{q,\beta} m_{d,\gamma} - m_{q,\gamma} m_{d,\beta} \tag{10.7-14}$$

Once t_β and t_γ have been found, the last step is to determine the instants at which the state transitions will occur. To this end, it is convenient to define $t = 0$ as the beginning of the switching cycle and to define t_A, t_B, and t_C as the times at which the transition from state α to β, β to γ, and γ to δ, respectively, are made. These times are determined in accordance with

$$t_A = (T_{sw} - t_\beta - t_\gamma)/2 \tag{10.7-15}$$

$$t_B = t_A + t_\beta \tag{10.7-16}$$

$$t_C = t_B + t_\gamma \tag{10.7-17}$$

In summary, the space-vector modulator operates as follows. At the beginning of a switching cycle, the commanded modulation indexes are calculated using (10.7-3) and (10.7-4). Next, the conditioned modulation index commands are limited using (10.7-5)–(10.7-8) in order to reflect the voltage limitations of the converter. Next, the sector of the modulation command is determined using (10.7-9) from which the state sequence is established using Table 10.7-2. At this point, (10.7-12)–(10.7-14) are used to determine the amount of time spent in each state, and then (10.7-15)–(10.7-17) are used to calculate the actual transition times.

The modeling of this switching algorithm is quite straightforward. In particular, neglecting deadtime and voltage drops, it may be assumed that the output voltage in the stationary reference frame may be expressed as

$$\hat{v}_{qs}^{s} = m_q^{**} v_{dc} \tag{10.7-18}$$

$$\hat{v}_{ds}^{s} = m_d^{**} v_{dc} \tag{10.7-19}$$

It is interesting to note that because of the limitation on the magnitude of the modulation index (10.7-6), the limit on the peak value of the fundamental component of the line-to-neutral voltage that can be produced is $v_{dc}/\sqrt{3}$, which is identical to that of extended sine-triangle modulation.

10.8 Hysteresis Modulation

Thus far, all the bridge control strategies considered have resulted in a three-phase voltage source. Thus, those strategies may all be described as voltage-source. However, it is also possible for the bridge to be controlled so as to appear to be, at some level, and for some conditions, as a current source. Hysteresis modulation is one of these current-source control schemes. In particular, let i_{as}^*, i_{bs}^*, and i_{cs}^* denote the desired machine or load currents. In order that the actual a-phase current be maintained within a certain tolerance of the desired a-phase currents, the control strategy depicted in Figure 10.8-1, known as a hysteresis modulator, is used. As can be seen, if the a-phase current becomes greater than the reference current plus the

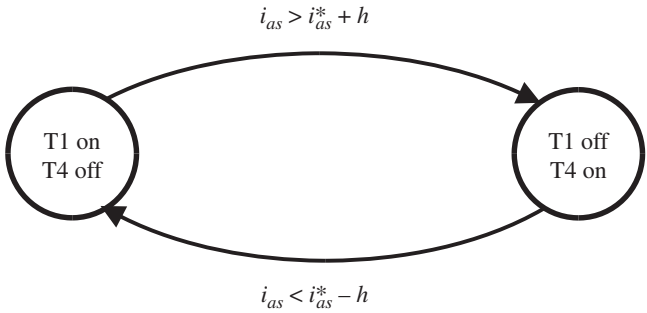

Figure 10.8-1 State transition diagram.

hysteresis level h, the lower transistor of the a-phase leg is turned on, which tends to reduce the current. If the a-phase current becomes less than the reference current minus the hysteresis level h, the upper transistor is turned on, which tends to increase the a-phase current. The b- and c-phases are likewise controlled. The net effect is that the a-phase current is within the hysteresis level of the desired current, as is illustrated in Figure 10.8-2. As can be seen, the a-phase current tends to wander back and forth between the two error bands. However, the a-phase current has inflections even when the current is not against one of the error bands; these are due to the switching in the other phase legs.

The performance of the hysteresis modulator is illustrated in Figure 10.8-3 for the same conditions illustrated in Figure 10.4-3 and Figure 10.5-3. In this case, the commanded a-phase current is

$$i_{as}^* = 19.1\cos(\theta_c - 17.4°)$$

and the b- and c-phase reference currents lag the a-phase reference currents by 120° and 240°, respectively. This current command is the fundamental component of the current obtained in Figure 10.4-3 and Figure 10.5-3. The hysteresis level is set at 2 A. As can be seen, as in the case of the sine-triangle modulated converter, relatively little low-frequency harmonic content is generated.

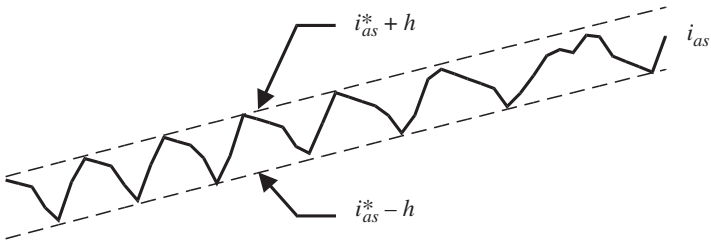

Figure 10.8-2 Allowable current band.

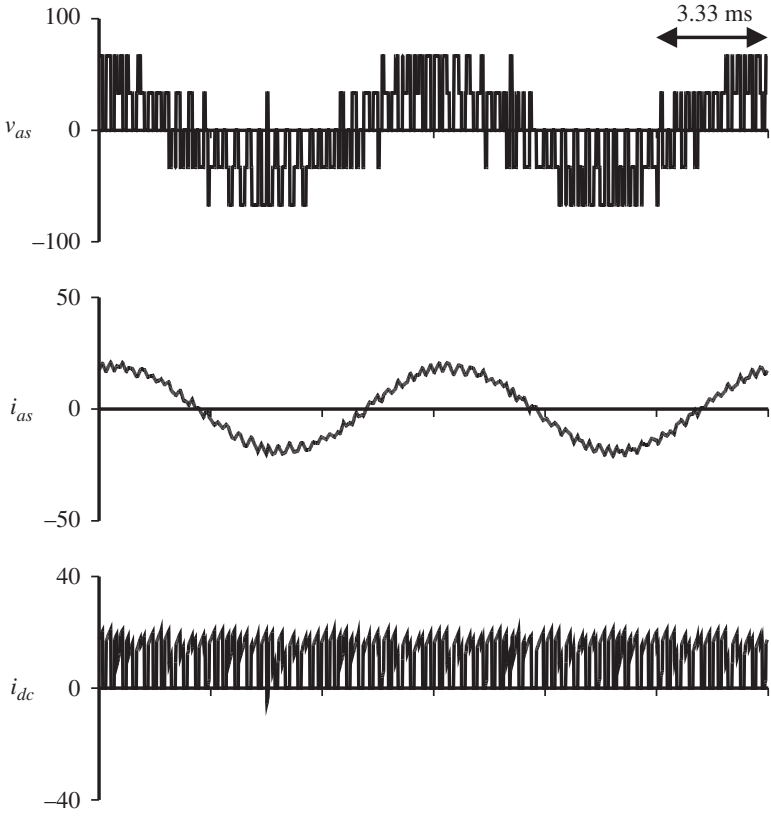

Figure 10.8-3 Voltage and current waveforms using a hysteresis modulator.

Although the concept of having a controllable current source is attractive in that it allows us to ignore the stator dynamics, there are several limitations of hysteresis modulation. First, there is a limit on the range of currents that can actually be commanded. In particular, assume that for a given current command, the peak line-to-neutral terminal voltage is v_{pk}. Since the peak line-to-neutral voltage the bridge can supply is $2v_{dc}/3$, it is apparent that v_{pk} must be less than $2v_{dc}/3$ if the commanded current is to be obtained. There is another constraint, which is that the peak line-to-line voltage $\sqrt{3}v_{pk}$ must be less than the peak line-to-line voltage the converter can achieve, which is equal to v_{dc}. This requirement is more restrictive and defines the steady-state range over which we can expect the currents to be tracked. In particular,

$$v_{pk} < \frac{v_{dc}}{\sqrt{3}} \tag{10.8-1}$$

Note that the maximum voltage achieved using hysteresis modulation is greater than that which is achieved using sine-triangle modulation, but equal to that of extended sine-triangle or space-vector modulation.

In addition to the steady-state limitation on whether the commanded currents will be tracked, there is also a dynamic limitation. In particular, since the stator currents of a machine are algebraically related to the state variables, they cannot be changed instantaneously. Therefore, current tracking will be lost during any step change in commanded currents. When the current command is being changed in a continuous fashion, then current tracking will be maintained provided the peak line-to-neutral voltage necessary to achieve the commanded currents does not exceed (10.8-1).

One disadvantage of the hysteresis-controlled modulation scheme is that the switching frequency cannot be directly controlled. Indirectly, it can be controlled by setting h to an appropriate level—making h smaller increases the switching frequency and making h larger decreases the switching frequency; however, once h is set, the switching frequency will vary depending on the machine parameters and the operating point. For this reason, current-regulated operation is sometimes synthesized by using suitable control of a voltage-regulated modulation scheme with current feedback.

In regard to average-value modeling, the most straightforward approach is to assume that the actual currents are equal to the commanded currents. Since this involves neglecting the dynamics associated with the load, such an approach constitutes a reduced-order model. When taking this approach, a check should be conducted to make sure that sufficient voltage is available to actually achieve the current command because such a modeling approach is not valid if sufficient voltage is not present. In the event that a more sophisticated model is required, the reader is referred to References 10 and 11, which describe how to include dynamics of hysteresis modulation and how to model the effects of loss of current tracking due to insufficient inverter voltage, respectively.

10.9 Delta Modulation

Delta modulation is another current-source modulation strategy. This strategy has an advantage over hysteresis modulation in that a maximum switching frequency is set. The disadvantage is that there is no guarantee on how closely the actual current will track the commanded current.

In this strategy, the current error of each phase is calculated in accordance with

$$e_{xs} = i^*_{xs} - i_{xs} \tag{10.9-1}$$

Every T_{sw} seconds (the switching period), the current error is sampled. If the current error is positive, the upper switch is turned on; if it is negative, the lower switch is turned on. Clearly, as the switching period is decreased, the actual current will track the desired current more and more closely. It should be observed that since the sign of the error does not necessarily change from one sampling to the next, the phase leg involved will not necessarily switch at every sampling. In addition, since a semiconductor must be turned off before being turned back on, the switching frequency is less than $1/(2T_{sw})$.

There are two variations of this strategy. In the first, the three phase legs are sampled and switched simultaneously. In the second, the switching between phases is staggered. The second method is preferred because it provides slightly higher bandwidth and is more robust with respect to electromagnetic compatibility concerns since the switching in one phase will not interfere with the switching in another. This robustness, coupled with its extreme simplicity in regard to hardware implementation, make this strategy very attractive.

As in the case of hysteresis modulation, there are limitations on how well and under what conditions a current waveform can be achieved. The limitations arising from available voltage are precisely the same as for hysteresis modulation, and so no further discussion will be given in this regard. However, in the case of delta modulation, there is an additional limitation in that there is no guarantee on how closely the waveform will track the reference. This must be addressed through careful selection of the switching frequency. Trading off waveform quality versus the switching frequency, while keeping in mind that the actual switching frequency will be lower than the set switching frequency, is a trade-off best made through the use of a waveform-level simulation of the converter machine system.

10.10 Open-Loop Voltage and Current Regulation

In the previous sections, a variety of modulation strategies were set forth that achieve voltages or currents of a certain magnitude and frequency. For each of these, a method to predict the dynamic average of the q- and d-axis voltages or currents in the converter reference frame was set forth. In this section, we examine the inverse problem—that of obtaining the appropriate duty cycle(s) and the converter reference-frame position in order to achieve a desired dynamic-average synchronous reference frame q- and d-axis voltage or current.

Six-step modulation, extended sine-triangle modulation, and space-vector modulation are all voltage-source modulation schemes. In our development, we will use these schemes to develop an open-loop voltage-regulated converter. Hysteresis modulation and delta modulation are both current source-based schemes.

These will be used as the basis of developing an open-loop current-regulated converter.

The first modulation strategy considered in this chapter that was capable of achieving a q- and d-axis voltage command was six-step modulation. In order to see how the variables associated with this modulation strategy are related to a voltage command, observe that with $v_{0s} = 0$, we have

$$\begin{bmatrix} v_{qs}^{e} \\ v_{ds}^{e} \end{bmatrix} = \begin{bmatrix} \cos\theta_{ce} & \sin\theta_{ce} \\ -\sin\theta_{ce} & \cos\theta_{ce} \end{bmatrix} \begin{bmatrix} v_{qs}^{c} \\ v_{ds}^{c} \end{bmatrix} \tag{10.10-1}$$

where θ_{ce} is angular displacement of the synchronous reference frame from the converter reference frame, that is,

$$\theta_{ce} = \theta_{c} - \theta_{e} \tag{10.10-2}$$

Replacing v_{qs}^{e} with the commanded value v_{qs}^{e*}, v_{ds}^{e} with the commanded value v_{ds}^{e*}, and v_{qs}^{c} and v_{ds}^{c} with the average values expressions given by (10.4-5) and (10.4-6) in (10.10-1) yields

$$\begin{bmatrix} v_{qs}^{e*} \\ v_{ds}^{e*} \end{bmatrix} = \begin{bmatrix} \cos\theta_{ce} & \sin\theta_{ce} \\ -\sin\theta_{ce} & \cos\theta_{ce} \end{bmatrix} \begin{bmatrix} \frac{2}{\pi} d v_{dc} \\ 0 \end{bmatrix} \tag{10.10-3}$$

From (10.10-3), we obtain

$$d = \frac{\pi}{2 v_{dc}} \sqrt{\left(v_{qs}^{e*}\right)^2 + \left(v_{ds}^{e*}\right)^2} \tag{10.10-4}$$

$$\theta_{ce} = \text{angle}\left(v_{qs}^{e*} - j v_{ds}^{e*}\right) \tag{10.10-5}$$

Together, (10.10-4) and (10.10-5) suggest the control strategy illustrated in Figure 10.10-1. Therein the inputs are the q- and d-axis voltage commands in the synchronous reference frame v_{qs}^{e*} and v_{ds}^{e*}, the dc input voltage to the inverter v_{dc}, and the position of the synchronous reference frame θ_e. The outputs are the duty

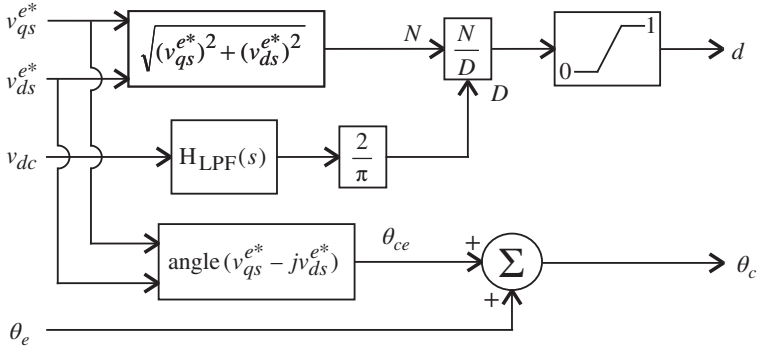

Figure 10.10-1 Voltage regulation using a six-step modulator.

cycle d, and the position of the converter reference frame θ_c, as required by the switch level control defined by Figure 10.4-1 (in which S1, S2, and S3 are defined in the same way as T1, T2, and T3 in Fig. 10.3-1). As can be seen in Figure 10.10-1, the duty cycle is essentially calculated in accordance with (10.10-4) with the exception that the dc voltage is filtered through a transfer function $H_{LPF}(s)$ to eliminate noise and for the purposes of stability. In addition, a limit is placed on the duty cycle d. The position of the converter reference frame is established by simply adding θ_{ce} as set forth in (10.10-5) to the position of the synchronous reference frame θ_e.

The next modulation strategy considered was sine-triangle modulation. However, sine-triangle modulation is rarely used in its pure form; it is normally utilized in conjunction with the extended sine-triangle modulation since this yields the potential for a greater ac voltage for a given dc voltage than sine-triangle modulation. The development of a strategy to generate the duty cycle and the position of the converter reference frame from the q- and d-axis voltage command is nearly identical to the case for six-step modulation except that (10.5-14) and (10.5-15) replace (10.4-5) and (10.4-6) in the development, which results in a change in the gain following the low-pass filter output from $2/\pi$ to $1/2$, the change of the limit on the duty cycle from 1 to $2/\sqrt{3}$, and the introduction of the duty cycle d_3. These modifications are reflected in Figure 10.10-2. Using the output of this block, the gating of the transistors is readily determined as explained in Section 10.5 and Section 10.6.

In the case of space-vector modulation, the situation is more straightforward since this switching algorithm is based on a q- and d-axis voltage command, albeit in the stationary reference frame. In this case, the q- and d-axis voltage in the stationary reference frame is calculated from the q- and d-axis command in the stationary reference frame using the frame-to-frame transformation; in particular,

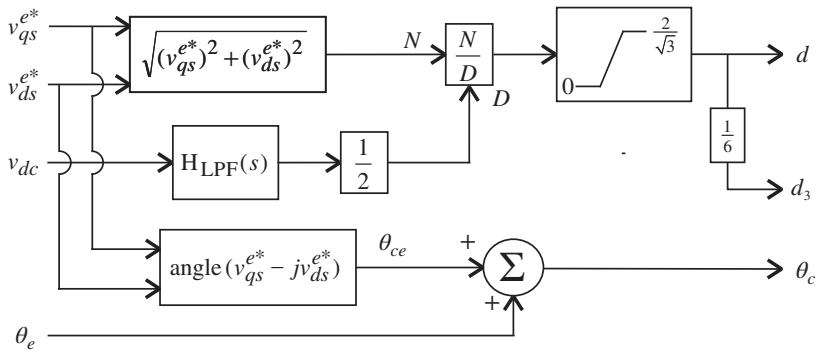

Figure 10.10-2 Voltage regulation using an extended sine-triangle modulator.

this yields,

$$v_{qs}^{s*} = v_{qs}^{e*}\cos\theta_e + v_{ds}^{e*}\sin\theta_e \tag{10.10-6}$$

$$v_{ds}^{s*} = -v_{qs}^{e*}\sin\theta_e + v_{ds}^{e*}\cos\theta_e \tag{10.10-7}$$

Let us now consider the problem of obtaining an open-loop current-regulated converter using one of the current source-based modulation schemes. Both hysteresis and delta modulation are based on an *abc* variable current command, which is readily computed in terms of a *q*- and *d*-axis current command in the synchronous reference, and the position of the synchronous reference frame, θ_e, using the inverse transformation. In particular, this yields

$$i_{abcs}^{*} = \mathbf{K}_s^{e^{-1}} i_{qd0s}^{e*} \tag{10.10-8}$$

10.11 Closed-Loop Voltage and Current Regulation

In the previous section, several strategies for obtaining *q*- and *d*-axis voltage and current commands were discussed. However, each of these methods was open-loop. In the case of the voltage control strategies, errors will arise because of logic propagation delays, switching deadtime, and the voltage drop across the semiconductors. In the case of current control, even if the inverter is operated in an ideal sense, there will still be a deviation between the actual and commanded current that will have the net effect that the average *q*- and *d*-axis current obtained will not be equal to the commanded values.

In this section, closed-loop methods of regulating *q*- and *d*-axis voltages and currents are set forth. These methods stem from the synchronous regulator concept set forth in Reference 10. This concept is based on the observation that integral feedback loop is most effective if implemented in the synchronous reference frame. Because of the integral feedback, there will be no error for dc terms provided the inverter can produce the required voltage. In other words, the average value of the voltages or currents (as expressed in the synchronous reference frame) will be exactly achieved. Since the average value in the synchronous reference frame corresponds to the fundamental component in *abc* variables, it can be seen that integral feedback loop implemented in a synchronous reference frame will ensure that the desired fundamental component of the applied voltages or currents is precisely achieved.

Figure 10.11-1 illustrates a method whereby integral feedback can be used to form a closed-loop voltage-regulated converter using a voltage-source modulator or a closed-loop current-regulated converter using a current-source modulator. Therein, f can denote either voltage v or current i. The superscript ** designates

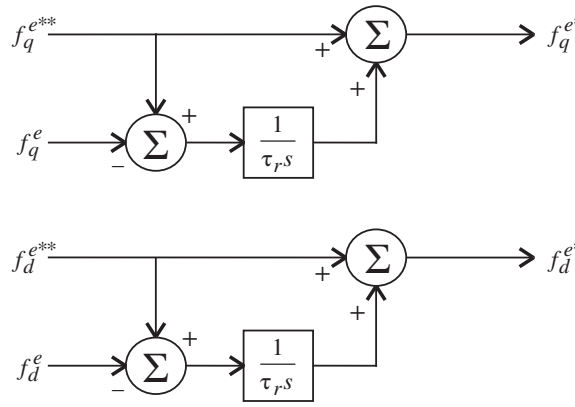

Figure 10.11-1
Synchronous regulator.

a physically desired value, whereas the superscript * designates the inverter command (which will be used in accordance with one of the modulation strategies described in Section 10.10). Note that the strategy is dependent upon the measured value of voltage or current in the synchronous reference frame, f_q^e and f_d^e. These variables are obtained by measuring the *abc* voltages or currents and transforming them to the synchronous reference frame.

For the purposes of analysis, it is sufficient to consider the q-axis loop (as the d-axis will yield identical results), whereupon it is convenient to assume that q-axis quantity f_q^e will be equal to the q-axis inverter command f_q^{e*} plus an error term; in particular,

$$f_q^e = f_q^{e*} + f_{q,\text{err}}^e \tag{10.11-1}$$

Incorporating (10.11-1) into Figure 10.11-1, it is straightforward to show that the transfer function between the q-axis quantity f_q^e, the command f_q^{e**}, and the error $f_{q,err}^e$ is given by

$$f_q^e = f_q^{e**} + \frac{\tau_r s}{\tau_r s + 1} f_{q,\text{err}}^e \tag{10.11-2}$$

From (10.11-2), it is readily seen that in the steady state, the average value of the q-axis quantity f_q^e will be equal to the q-axis command f_q^{e**}. It is also possible to see that from the perspective of (10.11-2), it is desirable to make time constant τ_r as small as possible since this decreases the frequency range and extent to which $f_{q,err}^e$ can corrupt f_q^e.

However, there is a constraint on how small τ_r can be made. In particular, again using (10.11-1) in conjunction with Figure 10.11-1, it can be shown that

$$f_q^{e*} = f_q^{e**} + \frac{1}{\tau_r s + 1} f_{q,\text{err}}^e \tag{10.11-3}$$

As this point, it is important to keep in mind that f_{qs}^{e*} should be relatively free from harmonic content or otherwise distortions in the switching pattern will result. Since $f_{q,\text{err}}^{e}$ contains considerable high-frequency switching components, τ_r must be large enough so that significant switching harmonics are not present in f_q^{e*}.

The selection of τ_r is a function of the modulation strategy. For example, if this strategy is used for current regulation using a current-source modulator, then selecting

$$\tau_r \approx \frac{5}{2\pi f_{sw,\text{est}}} \tag{10.11-4}$$

where $f_{sw,\text{est}}$ is the estimated switching frequency (which can be determined through a waveform-level simulation), should normally produce adequate attenuation of the switching ripple in the inverter command.

However, if the scheme is being used for voltage-regulation in conjunction with a extended sine-triangle or space-vector voltage-source modulator, then there will be considerable voltage error ripple, whereupon selecting

$$\tau_r \approx \frac{20}{2\pi f_{sw}} \tag{10.11-5}$$

where f_{sw} is the switching frequency is more appropriate. Finally, for six-step modulation, the presence of low-frequency harmonics necessitates an even larger time constant, perhaps on the order of

$$\tau_r \approx \frac{20}{2\pi 6 f_{\min}} \tag{10.11-6}$$

where $f_{\min}$ denotes the minimum frequency of the fundamental component of the applied waveform that will be used (this can require a very long time constant and implies poor transient performance).

The regulator shown in Figure 10.11-1 is designed as a trimming loop wherein a voltage-source modulation strategy (i.e., six-step, sine-triangle, extended sine-triangle, or space-vector modulators) is used to create a voltage-source converter, or in which a current-based modulation strategy (hysteresis or delta modulators) is used in a current-regulated inverter. However, it is sometimes the case that a voltage-based modulation strategy will be used to regulate current. The advantage of this approach to obtaining a current command is that it allows a fixed switching frequency modulation strategy to be used.

One approach to achieving a voltage-source-modulator-based current regulator is depicted in Figure 10.11-2. Inputs to this control are the q- and d-axis current commands i_{qs}^{e*} and i_{ds}^{e*}, the measured q- and d-axis currents i_{qs}^{e} and i_{ds}^{e} (obtained by measuring the *abc* currents and transforming to the synchronous reference frame), and finally the speed of the synchronous reference frame ω_e. The outputs of the control are the q- and d-axis voltage commands in a synchronous reference frame

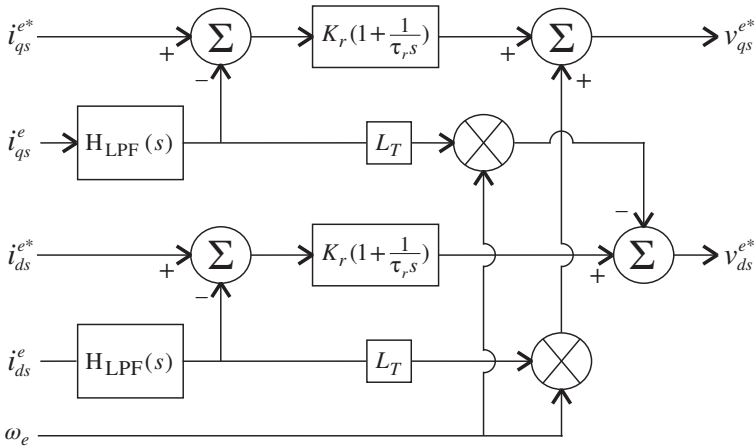

Figure 10.11-2 Voltage-source modulator based current regulator.

v_{qs}^{e*} and v_{ds}^{e*}, which are achieved using one of the open-loop control strategies discussed in Section 10.10. Parameters associated with this strategy are the regulator gain K_r, time constant τ_r, and a Thevenin equivalent inductance of the load L_T. The low-pass filter $H_{LPF}(s)$ is designed to have unity gain at dc with a cut-off frequency somewhat below the switching frequency.

In order to gain insight into the operation of this control loop, let us assume that the actual q- and d-axis voltages v_{qs}^{e} and v_{ds}^{e} are equal to their commanded values v_{qs}^{e*} and v_{ds}^{e*}, that the low pass filter has dynamics that are appreciably faster than those of this regulator so that they may be ignored for the purpose of designing this control loop, and that on the time scale that this control loop operates (which is much faster than the typical fundamental component of the waveforms in *abc* variables but slower than the switching frequency), the load on the inverter may be approximated as

$$v_{qs}^{e} = \omega_e L_T i_{ds}^{e} + L_T p i_{qs}^{e} + e_{qT} \tag{10.11-7}$$

$$v_{ds}^{e} = -\omega_e L_T i_{qs}^{e} + L_T p i_{ds}^{e} + e_{dT} \tag{10.11-8}$$

where e_{qT} and e_{dT} are slowly varying quantities. In essence, this is the model of a voltage-behind-inductance load. Many machines, including permanent-magnet ac machines (see Problem 19) and induction machines (see Problem 20), can have their stator equation approximated by this form for fast transients. Incorporating these assumptions into Figure 10.11-2 yields

$$i_{qs}^{e} = \frac{K_r(\tau_r s + 1) i_{qs}^{e*} + \tau_r s e_{qT}^{e}}{L_T \tau_r \left(s^2 + \frac{K_r}{L_T} s + \frac{K_v}{L_T \tau_v} \right)} \tag{10.11-9}$$

A similar result can be derived for the d-axis. Inspection of (10.11-9) reveals that there will be no steady-state error and that there is no interaction between the q- and d-axis. This interaction was eliminated by the L_T term in the control. Of course, if this term is not used, or if the value used is not equal to the Thevenin equivalent inductance, then interaction between the q- and d-axis will exist and can be quite pronounced.

The gain K_r and time constant τ_r may be readily chosen using pole-placement techniques. In particular, if it is desired that the pole locations be at $s = -s_1$ and $s = -s_2$, wherein s_1 and s_2 are chosen to be as fast as possible, subject to the constraint that the two poles will be considerably slower than the low pass filter and the switching frequency, then the gain and time constant may be readily expressed as

$$K_r = L_T(s_1 + s_2) \tag{10.11-10}$$

$$\tau_r = \frac{1}{s_1} + \frac{1}{s_2} \tag{10.11-11}$$

In utilizing (10.11-10) and (10.11-11), one choice is to make the system critically damped and chose

$$s_1 = s_2 \approx \frac{\pi f_{sw}}{5} \tag{10.11-12}$$

where f_{sw} is the switching frequency. A numerical example in applying this design procedure to the design of the current control loops of a large induction motor drive is set forth in Reference 13, and the application of the same general technique to an ac power supply is set forth in Reference 14; this latter reference includes an excellent discussion of the decoupling mechanism.

Any of the techniques used in this section will guarantee that provided enough dc voltage is present, the desired fundamental component of the applied voltage or current will be exactly obtained. Of course, low levels of low frequency harmonics (including negative sequence terms, fifth and seventh harmonics, etc.) and high frequency switching harmonics will still be present. A method of eliminating low-frequency harmonics is set forth in References 15 and 16.

References

1 J. G. Kassakian, M. F. Schlecht, and G. C. Verghese, *Principals of Power Electronics*, Addison-Wesley, Reading, MA, 1991.

2 N. Mohan, T. M. Undeland, and W. P. Robbins, *Power Electronics*, 2nd ed., John Wiley & Sons/IEEE Press, New York, 1995.

3 M. H. Rashid, *Power Electronics*, 2nd ed., Prentice-Hall, Englewood Cliffs, NJ, 1993.

4 R. S. Ramshaw, *Power Electronics Semiconductor Switches*, 2nd ed., Chapman & Hall, London, 1993.

5 J. T. Tichenor, S. D. Sudhoff, and J. L. Drewniak, "Behavioral IGBT Modeling for Prediction of High Frequency Effects in Motor Drives," Proceedings of the 1997 Naval Symposium on Electric Machines, July 28–31, 1997, Newport, RI, pp. 69–75.

6 R. R. Nucera, S. D. Sudhoff, and P. C. Krause, "Computation of Steady-State Performance of an Electronically Commutated Motor," *IEEE Trans. Industry Applications*, Vol. 25, November/December 1989, pp. 1110–1117.

7 S. D. Sudhoff and P. C. Krause, "Average-Value Model of the Brushless DC 120° Inverter System," *IEEE Trans. Energy Conversion*, Vol. 5, September 1990, pp. 553–557.

8 S. D. Sudhoff and P. C. Krause, "Operating Modes of the Brushless DC Motor with a 120° Inverter," *IEEE Trans. Energy Conversion*, Vol. 5, September 1990, pp. 558–564.

9 H. W. Van Der Broek, H. Ch. Skudelny, and G. Stanke, "Analysis and Realization of a Pulse Width Modulator Based on Voltage Space Vectors," *IEEE Trans. Industry Applications*, Vol. 24, No. 1, January/February 1988, pp. 142–150.

10 S. F. Glover, S. D. Sudhoff, H. J. Hegner, and H. N. Robey, Jr., "Average Value Modeling of a Hysteresis Controlled DC/DC Converter for Use in Electrochemical System Studies," Proceedings of the 1997 Naval Symposium on Electric Machines, July 28–31, 1997, Newport, RI, pp. 77–84.

11 K. A. Corzine, S. D. Sudhoff, and H. J. Hegner, "Analysis of a Current-Regulated Brushless DC Drive," *IEEE Trans. Energy Conversion*, Vol. 10, No. 3, September 1995, pp. 438–445.

12 T. M. Rowan and R. J. Kerkman, "A New Synchronous Current Regulator and an Analysis of Current-Regulated Inverters," *IEEE Trans. Industry Applications*, Vol. IA-22, No. 4, 1986, pp. 678–690.

13 S. D. Sudhoff, J. T. Alt, H. J. Hegner, and H. N. Robey, Jr., "Control of a 15-Phase Induction Motor Drive System," Proceedings of the 1997 National Symposium on Electric Machines, July 28–31, 1997, Newport, RI, pp. 103–110.

14 O. Wasynczuk, S. D. Sudhoff, T. D. Tran, D. H. Clayton, and H. J. Hegner, "A Voltage Control Strategy for Current-Regulated PWM Inverters," *IEEE Trans. Power Electronics*, Vol. 11, No. 1, January 1996, pp. 7–15.

15 P. L. Chapman and S. D. Sudhoff, "A Multiple Reference Frame Synchronous Estimator/Regulator," *IEEE Trans. Energy Conversion*, Vol. 15, No. 2, June 2000, pp. 197–202.

16 P. L. Chapman and S. D. Sudhoff, "Optimal Control of Permanent-Magnet AC Drives with a Novel Multiple Reference Frame Synchronous Estimator/Regulator," Proceedings of the 34th Industry Applications Society Annual Meeting, 1999.

Problems

10.1 Show that v_{0s} is zero for a balanced three-phase induction motor.

10.2 Show that v_{0s} is zero for a balanced three-phase synchronous machine.

10.3 Show that v_{0s} is zero for a balanced three-phase permanent magnet ac machine with a sinusoidal back emf.

10.4 Figure 10P-1 illustrates the a-phase line-to-ground voltage of a three-phase bridge converter. Determine the diode and transistor forward voltage drops.

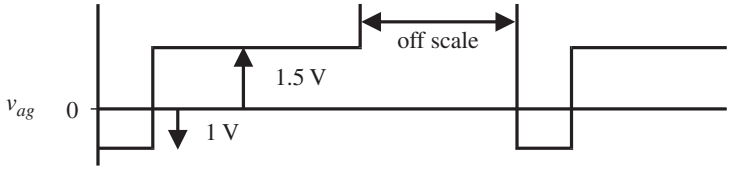

Figure 10P-1 The a-phase line-to-ground voltage of a three-phase bridge converter.

10.5 From Figure 10.3-1, derive (10.3-1).

10.6 From (10.3-1), deduce analogous expressions for v_{bcs} and v_{cas}.

10.7 From Figure 10.3-2, derive (10.3-2).

10.8 From (10.3-2), deduce analogous expressions for v_{bs} and v_{cs}.

10.9 Consider a three-phase bridge supplying a wye-connected load in which the a-phase, b-phase, and c-phase resistances are 2, 4, and 4 Ω, respectively. Given that the dc supply voltage is 100 V and the control strategy is six-step operation, sketch the a-phase line-to-neutral voltage waveform.

10.10 Figure 10P-2 illustrates a circuit that can be used to avoid shoot-through. If 5 V logic is used, the gate threshold turn-on voltage is 3.4 V, and the resistor is 1 kΩ, compute the capacitance necessary to assure that gate turn-off will occur 1.5 μs before the second transistor of the pair is gated on.

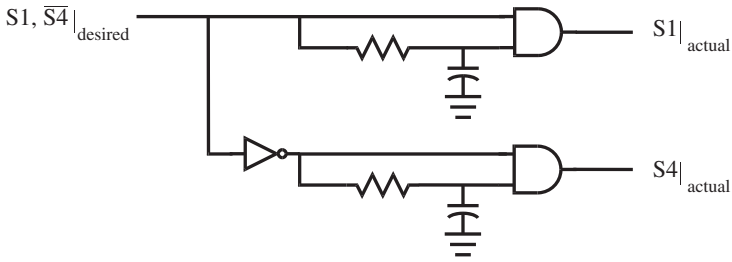

Figure 10P-2 Circuit than can be used to avoid shoot-through.

10.11 Consider the 3-hp induction motor whose parameters are listed in Table 6.10-1. Plot the torque-speed and dc current-speed curves if it is being fed from a three-phase bridge in six-step operation, assuming that the dc voltage is 560 V and the frequency is 120 Hz. Neglect harmonics.

10.12 Consider the system discussed in Problem 11. Compute the effect of the fifth and seventh harmonics on the average torque if the machine is operating at a slip of 0.025 relative to the fundamental component of the applied voltages.

10.13 A six-step modulated drive with a dc voltage of 600 V and a duty cycle of 0.75 is used to drive a permanent-magnet ac machine. At a certain operating speed, the fundamental component of the stator frequency is 300 Hz. If the switching frequency is 10 kHz, compute the amplitude of the strongest two harmonics in the region of 50 kHz.

10.14 A permanent magnet ac machine is to be operated from the six-step modulated three-phase bridge. The dc voltage is 100 V, and the desired q- and d-axis voltages are $v_{qs}^r = 50$ V and $v_{ds}^r = 10$ V. Specify the duty-cycle d and the relationship between θ_c and θ_r such that these voltages are obtained.

10.15 Derive (10.5-17) and (10.5-18) from Figure 10.5-4.

10.16 Consider the 3-hp induction motor in Table 3.9-1. The machine is being fed from a sine-triangle modulated three-phase bridge with $v_{dc} = 280$ V. If the machine is being operated at a speed of 1710 rpm and the frequency of the fundamental component of the applied voltages is 60 Hz, plot the torque versus duty cycle as the duty-cycle d is varied from 0 to 5.

10.17 A three-phase four-pole permanent magnet ac machine has the parameters $r_s = 2.99\ \Omega$, $L_{ss} = 11.35$ mH, and $\lambda'_m = 0.156\ \text{V} \cdot \text{s/rad}$ is operated from a current-source modulated inverter with $v_{dc} = 140$ V. If it is being operated at 2670 rpm, plot the locus of points in the q-axis current command versus d-axis current command plane that describes the limits of the region over which the current command can be expected to be obtained.

10.18 Rederive (10.11-9)–(10.11-11) if a resistive term is included in the load model (10.11-7) and (10.11-8).

10.19 Ignoring stator resistance, and taking the synchronous reference frame to be the rotor reference frame, express L_T, e_{qT}, and e_{dT} in terms of electrical rotor speed for a surface mounted (nonsalient) permanent magnet ac machine.

10.20 Ignoring stator resistance, and assuming that the rotor flux linkages in the synchronous reference frame are constants, express L_T, e_{qT}, and e_{dT} for an induction machine in terms of the q- and d-axis rotor flux linkages and the electrical rotor speed. As an aside, because the rotor winding are shorted, their time derivative tends to be small, which leads to this approximation—it is akin to putting the model in subtransient form in the case of synchronous machines.

11

Direct-Current Machine and Drive

11.1 Introduction

The direct-current (dc) machine is not as widely used today as it once was. The dc generator has been replaced by power electronics, which convert alternating current into direct current with provisions to control the magnitude of the dc voltage. In drive applications, the dc motor is being replaced by the voltage-controlled permanent-magnet ac machine (brushless dc drive) and/or the field-orientated induction motor. Although the analysis of a dc machine does not require a change of variables, it is still desirable to devote some time to the dc machine and dc drive since it is sometimes used as a low-power drive motor. There is another and perhaps more important reason to consider the dc machine. Although maintenance issues hamper the use of dc machines, this device is the only electric machine that is designed with the stator and rotor mmf's orthogonal to one another, which inherently produces maximum torque per ampere. With the advent of power electronics, there has become a huge effort to control the permanent-magnet ac and induction machines so as to emulate the characteristics of the dc motor. In this chapter, we will treat the dc machines sufficiently to introduce the reader to the operating principles of dc machines with a focus on the shunt-connected and permanent-magnet dc machine and drive, thus setting the stage for a comparison of the operating characteristics with the voltage-controlled brushless dc drive and the field-oriented induction motor drive.

A disassembled two-pole 0.1-hp 6 V 12,000 r/min permanent-magnet dc motor is shown in Fig. 11.1-1. The magnets, which replace the stator field winding, are samarium cobalt and the device is used to drive hand-held battery-operated surgical instruments.

Analysis of Electric Machinery and Drive Systems, Fourth Edition.
Paul C. Krause, Oleg Wasynczuk, Scott D. Sudhoff, and Steven D. Pekarek.

Companion website: www.wiley.com/go/krause_aem4e

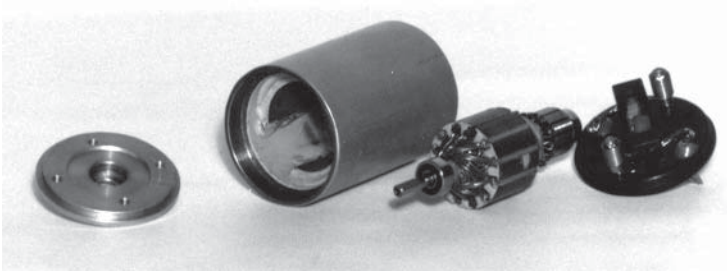

Figure 11.1-1 Two-pole 0.1-hp 8 V 12,000 r/min permanent-magnet dc motor (Courtesy Vick ElectroMech.)

11.2 Commutation

An elementary dc machine is shown in cross section in Figs. 11.2-1 and 11.2-2. The field winding is carrying a direct current i_f into the paper at f_1 and out at f_1' and then in at f_2 and out at f_2'. A voltage v_f is applied across f_1 and f_2'. With positive i_f, the field winding creates a mmf that is stationary and positive in the f axis.

The armature or rotor consists of two parallel windings: the a winding and the A winding. Each winding has four coils with each coil connected to two segments of the commutator. The commutator is fixed to the rotor and makes contact with carbon brushes. As the rotor rotates, the commutator segments slide against the brushes. This action connects the rotating circuits (a and A windings) to stationary terminals denoted as v_a, which are connected to a dc source or to a load if the device is operating as a generator. Note that in Fig. 11.2-1 the dc i_a is flowing into the top brush, which is straddling two of the eight segments of the commutator. Each segment is insulated from the others. The top brush is short-circuiting the A_4 coil; the bottom brush is short-circuiting the a_4 coil. In Fig. 11.2-2, the brushes are not commutating any windings. Sinusoidal voltages are induced in each of the coils due to the constant field current or permanent magnet producing a stationary mmf_s and the windings rotating in this constant mmf_s. Due to the action of the commutator, the mmf_r (a axis) of the rotor is also essentially stationary and orthogonal to the field mmf_s (f axis).

The full-wave rectified voltages in Figs. 11.2-1 and 11.2-2 are the open-circuit voltages of one parallel path between brushes. This is referred to as the back voltage or back emf. This induced voltage exists only when the rotor is turning. Many of the comments made in Chapter 4 can be made here regarding the back voltage. In Figs. 11.2-1 and 11.2-2, the parallel windings of each consist of four coils and produce an mmf that is orthogonal to the mmf produced by the stator winding, the f winding.

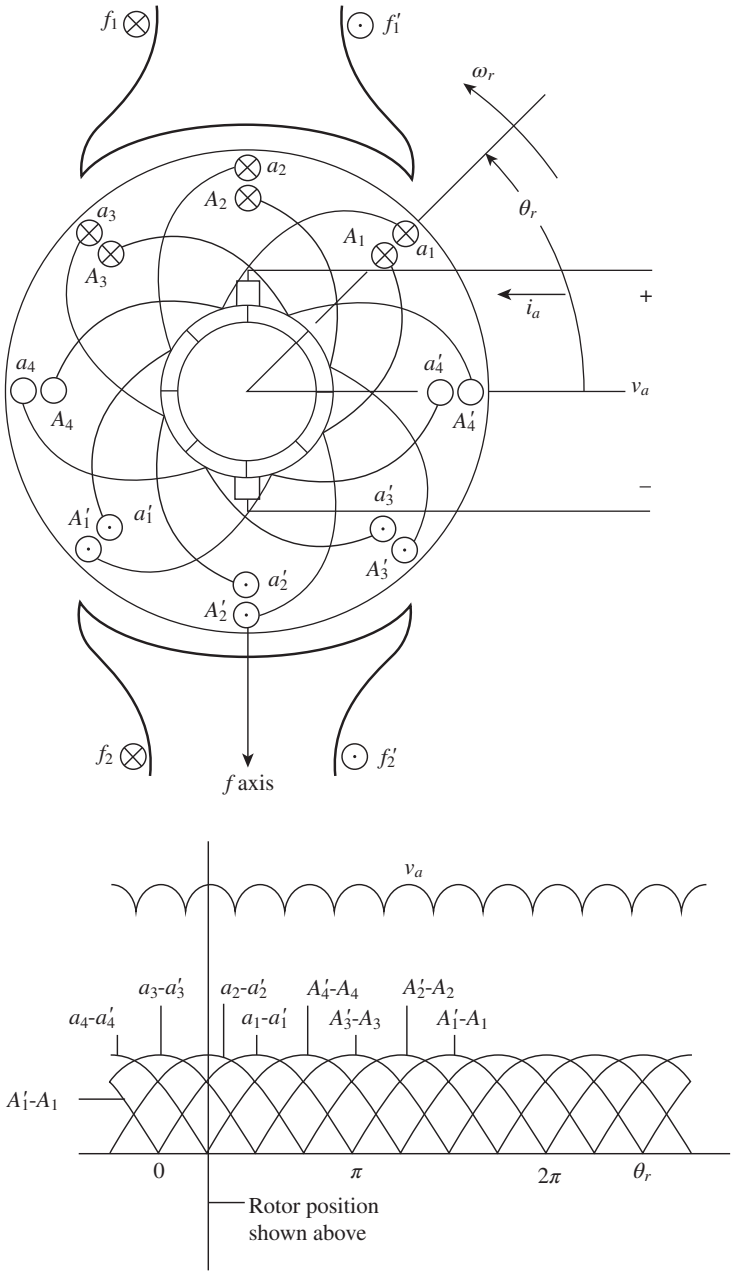

Figure 11.2-1 A dc machine with parallel armature windings.

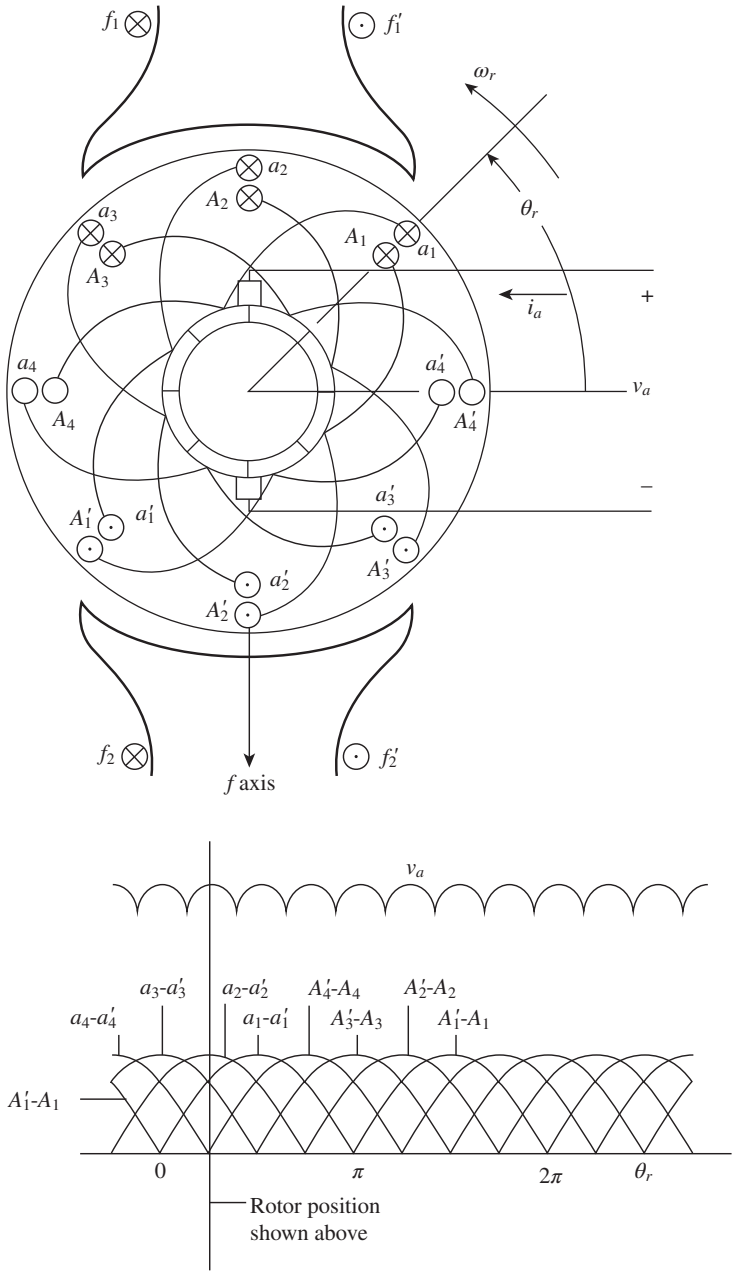

Figure 11.2-2 Same as Fig. 11.2-1 with rotor advanced approximately 22.5° counterclockwise.

It is important to understand that the commutator and brush combination is to change the direction of current flow in the rotor windings so that positive current into the machine flows into the paper over the top part of the rotor and out over the bottom part for motor action. The current is reversed for generator action.

11.3 Voltage and Torque Equations

It is advantageous to first consider the dc machine with a field and armature winding before turning to the permanent-magnet device exclusively. Although rigorous derivation of the voltage and torque equations is possible, it is rather lengthy, and little is gained since these relationships may be deduced. The armature coils revolve in a stationary magnetic field established by a current flowing in the field winding. We have established that a voltage is induced in these coils by virtue of this rotation. However, the action of the commutator causes the armature coils to appear as a stationary winding with its magnetic axis orthogonal to the magnetic axis of the field winding. In other words, the stator and rotor mmf's are orthogonal. Therefore, voltages are not induced in one winding due to the time rate-of-change of the current flowing in the other (transformer action). Mindful of these conditions, we can write the field and armature voltage equations in matrix form as

$$\begin{bmatrix} v_f \\ v_a \end{bmatrix} = \begin{bmatrix} r_f + pL_{FF} & 0 \\ \omega_r L_{AF} & r_a + pL_{AA} \end{bmatrix} \begin{bmatrix} i_f \\ i_a \end{bmatrix} \tag{11.3-1}$$

where L_{FF} and L_{AA} are the self-inductances of the field and armature windings, respectively, and p is the short-hand notation for the operator d/dt. The rotor speed is denoted as ω_r, and L_{AF} is the mutual inductance between the field and the rotating armature coils that is readily determined from the open-circuited voltage. The above equation suggests the equivalent circuit shown in Fig. 11.3-1. The voltage induced in the armature circuit, $\omega_r L_{AF} i_f$, is commonly referred to as the counter or back voltage. It also represents the open-circuit armature voltage from which

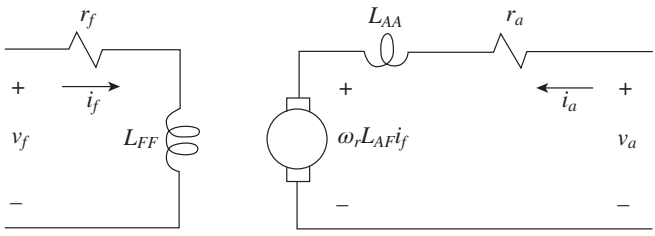

Figure 11.3-1 Equivalent circuit of a dc machine.

L_{AF} can be readily determined. The equivalent circuit shown in Fig. 11.3-1 is for a separately excited machine where v_f is from a separate dc source. When the field and armature are connected to the same dc source, $v_f = v_a$, it is a shunt machine.

A substitute variable that is often used is

$$k_v = L_{AF} i_f \tag{11.3-2}$$

We will find that this substitute variable is particularly convenient and frequently used. Even though a permanent-magnet dc machine has no field circuit, the constant field flux produced by the permanent magnet is analogous to a dc machine with a constant k_v.

An expression for torque can be established by noting that the electric power supplied to the armature can be expressed as $v_a i_a$. The voltage dropped across the armature resistance in Fig. 11.3-1 is $r_a i_a$, which when multiplied by i_a is the armature resistive power loss. The voltage $\omega_r L_{AF} i_f$ in Fig. 11.3-1, when multiplied by i_a, represents the power supplied to the mechanical system, which can also be expressed as $T_e \omega_r$. Equating these two expressions

$$T_e \omega_r = \omega_r L_{AF} i_f i_a \tag{11.3-3}$$

Dividing both sides by ω_r,

$$T_e = L_{AF} i_f i_a \tag{11.3-4}$$

The torque and rotor speed are related by

$$T_e = J \frac{d\omega_r}{dt} + B_m \omega_r + T_L \tag{11.3-5}$$

where J is the inertia of the rotor and rigidly connected mechanical load. The units of the inertia are $\text{kg} \cdot \text{m}^2$ or $\text{N} \cdot \text{m} \cdot \text{s}^2$. A positive electromagnetic torque T_e acts to turn the rotor in the direction of increasing θ_r. The load torque T_L is positive for a torque, on the shaft of the rotor, that opposes the positive electromagnetic torque T_e. The constant B_m is a damping coefficient associated with the mechanical rotational system of the machine. It has the units of $\text{N} \cdot \text{m} \cdot \text{s}$ /rad, and it is generally small and often neglected.

Although we will focus on the permanent-magnet dc motor, it is worthwhile to take a moment to mention that we have established the basis for several types of dc machines. In particular, the machine shown in Fig. 11.3-1 is a separately excited dc machine. If we connect the field winding in parallel with the armature winding, it becomes a shunt-connected dc machine. If the field winding is connected in series with the armature winding, it is a series-connected dc machine. If two windings are used, one in parallel with and another in series with the armature, it is referred to as a compound-connected dc machine. Clearly, this is an overly simplistic description, and the reader is referred to [1] for a more detailed consideration of these machine types.

Before proceeding, it is appropriate to briefly mention generator action even though the dc generator has been replaced by the ac-to-dc converter. We see from Fig. 11.3-1 that if $\omega_r L_{AF} i_f$ is greater than v_a, i_a is reversed and we have generator action. In this case, T_L is negative since the dc machine is being driven and T_e, (11.3-4), is also negative. In (11.3-5), $\frac{d\omega_r}{dt}$ is zero in the steady state and B_m is typically small.

11.4 Permanent-Magnet dc Machine

In the case of the permanent-magnet dc machine, $L_{AF} I_f$ is replaced with k_v whereupon the steady-state armature voltage equation becomes

$$V_a = r_a I_a + k_v \omega_r \tag{11.4-1}$$

If (11.4-1) is solved for I_a and submitted into (11.3-4) with $L_{AF} I_f$ replaced by k_v, the steady-state torque may be expressed as

$$\begin{aligned} T_e &= k_v I_a \\ &= \frac{k_v V_a - k_v^2 \omega_r}{r_a} \end{aligned} \tag{11.4-2}$$

The steady-state torque versus speed characteristic is shown in Fig. 11.4-1.

It is apparent from Fig. 11.4-1 that the stall ($\omega_r = 0$) torque could be made larger for a given armature voltage by reducing r_a. Although the machine may be designed with a smaller armature resistance, there is a problem since, at stall, the steady-state armature current is limited by the armature resistance, hence, for a constant V_a, reducing r_a will result in a larger I_a at stall which can cause damage to the armature winding, commutator, and/or brushes. On the other hand, increasing the starting torque by reducing r_a causes the torque versus speed characteristics to have a steeper slope that results in a smaller change in speed for a given change in load torque during normal (near-rated) operation. If, however,

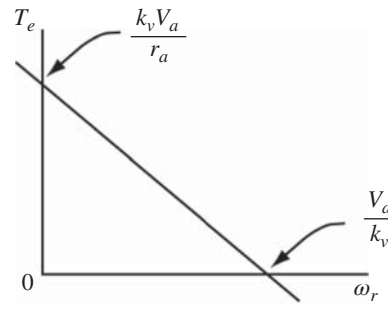

Figure 11.4-1 Steady-state torque versus speed characteristic of a permanent-magnet dc machine.

the armature voltage is reduced during the starting period to protect the brushes, the desirable characteristic of a small speed change for load torque variations during normal operation could be achieved. In fact, controlled regulation of the armature voltage is generally employed for large horsepower machines by using a converter; however, low-power permanent-magnet dc machines are often supplied from a battery and, therefore, a large armature resistance is necessary in order to prevent any damage during the early part of the stating period. Fortunately, a small speed variation during load torque changes is not required in many applications of the permanent-magnet dc machine; therefore, steep torque versus speed characteristics are not necessary.

Example 11A ***Calculating machine parameters.***
A permanent-magnet dc motor is rated at 8 V with the following parameters: $r_a = 7\ \Omega$, $L_{AA} = 120$ mH, $k_T = 2$ oz · in/A, and $J = 150\ \mu$ oz · in · s^2. (a) Determine the stall torque and the no-load speed. (b) A torque load of 0.5 oz · in is applied, determine the steady-state ω_r. (c) Determine the efficiency at this load.

First, let us convert k_T and J to units that we have been using. In this regard, we will convert the inertia to kg · m^2, which is the same as N · m · s^2. To do this, we must convert ounces to Newtons and inches to meters. Thus,

$$J = \frac{150 \times 10^{-6}}{(3.6)(39.37)} = 1.06 \times 10^{-6}\ \text{kg} \cdot \text{m}^2 \tag{11A-1}$$

We have not seen k_T before. It is the torque constant and, if expressed in the appropriate units, it is numerically equal to k_v. When k_v is used in the expression for $T_e (T_e = k_v i_a)$, it is often referred to as the *torque constant* and denoted k_T. When used in the voltage equation, it is typically denoted k_v. Now, we must convert oz · in to N · m, whereupon k_T equals our k_v; hence,

$$k_v = \frac{2}{(3.6)(39.37)} = 1.41 \times 10^{-2}\ \text{N} \cdot \text{m/A} = 1.41 \times 10^{-2}\ \text{V} \cdot \text{s/rad} \tag{11A-2}$$

(a) The stall torque is

$$T_e = \frac{k_v V_a}{r_a} = \frac{(1.41 \times 10^{-2})(6)}{7} = 1.21 \times 10^{-2}\ \text{N} \cdot \text{m} \tag{11A-3}$$

The no-load speed is

$$\omega_r = \frac{V_a}{k_v} = \frac{6}{1.41 \times 10^{-2}} = 425.5\ \text{rad/s} \tag{11A-4}$$

(b)

$$T_L = \frac{0.5}{(3.6)(39.37)} = 3.5 \times 10^{-3}\ \text{N} \cdot \text{m} \tag{11A-5}$$

From (11.4-1) with $T_e = T_L$

$$\omega_r = \frac{V_a}{k_v} - \frac{T_L r_a}{k_v^2} = \frac{6}{1.41 \times 10^{-2}} - \frac{(3.5 \times 10^{-3})(7)}{(1.41 \times 10^{-2})^2}$$

$$= 425.5 - 123.2 = 302.3 \text{ rad/s} \tag{11A-6}$$

(c)

$$T_e = k_v I_a$$

$$3.5 \times 10^{-3} = (1.41 \times 10^{-2}) I_a$$

$$I_a = \frac{3.5 \times 10^{-3}}{1.41 \times 10^{-2}} = 0.248 \text{ A} \tag{11A-7}$$

$$P_{\text{loss}} = r_a I_a^2 = (7)(0.248)^2 = 0.431 \text{ W} \tag{11A-8}$$

$$P_{\text{in}} = V_a I_a = (6)(0.248) = 1.488 \text{ W} \tag{11A-9}$$

$$P_{\text{out}} = P_{\text{in}} - P_{\text{loss}} = 1.488 - 0.431 = 1.057 \text{ W} \tag{11A-10}$$

$$\text{Eff.} = \frac{P_{\text{out}}}{P_{\text{in}}} \times 100 = \frac{1.058}{1.488} \times 100 = 71\% \tag{11A-11}$$

Note that

$$P_{\text{out}} = T_e \omega_r = 3.5 \times 10^{-3} \times 302.3 = 1.058 \text{ W} \tag{11A-12}$$

which is essentially equal to (7A-10).

11.5 dc Drive

Since the dc machine plays a role in some drive applications, a brief look at a voltage controlled drive is appropriate. Our focus will be on the permanent-magnet dc machine supplied from a two-quadrant dc-to-dc converter. Dynamic and steady-state performances are illustrated. Since the dc-to-dc converters used in dc drive systems are often called choppers, we will use dc-to-dc converter and chopper interchangeably. In this section, we will analyze the operation and establish the average-value model for a two-quadrant chopper drive.

A two-quadrant dc converter is depicted in Fig. 11.5-1. The switches $S1$ and $S2$ are transistors. They are assumed to be ideal; that is, if $S1$ or $S2$ is closed, current is allowed to flow in the direction of the arrow; current is not permitted to flow opposite to the arrow. If $S1$ or $S2$ is open, current is not allowed to flow in either direction regardless of the voltage across the switch. If $S1$ or $S2$ is closed and the

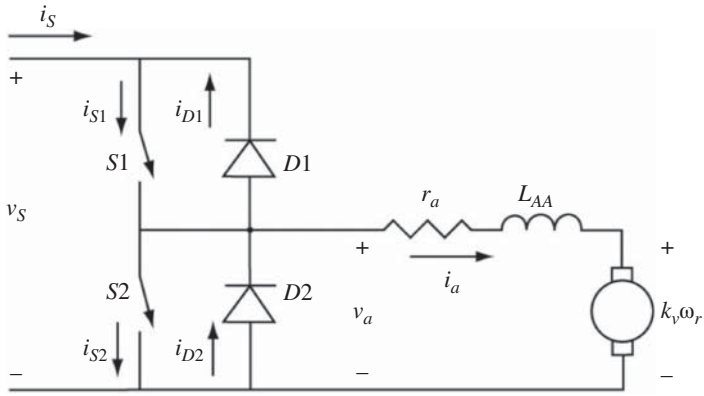

Figure 11.5-1 Two-quadrant chopper drive.

current is positive, the voltage drop across the switch is assumed to be zero. Similarly, the diodes $D1$ and $D2$ are ideal. Therefore, if the diode current i_{D1} or i_{D2} is greater than zero, the voltage across the diode is zero. The diode current can never be less than zero.

Waveforms of the converter variables during steady-state operation are shown in Fig. 11.5-2. Therein, the switching period T is made large relative to the armature time constant $\tau_a = L_{AA}/r_a$ for the purpose of depicting the transient of the armature current. Normally, the switching period is much smaller than the armature time constant and the switching segments of i_a are essentially sawtooth in shape. This is portrayed later in this section. With a two-quadrant chopper, the armature voltage cannot be negative ($v_a \geq 0$); however, the armature current can be positive or negative. That is, I_1 and I_2 (Fig. 11.5-2) can both be positive, or I_1 can be negative and I_2 positive, or I_1 and I_2 can both be negative. In Fig. 11.5-2, I_1 is negative with I_2 positive and the average value of i_a is positive. The mode of operation depicted is motor action if ω_r is positive (ccw).

During interval *A*, $S1$ is closed and $S2$ is open and, at the start of interval *A*, $i_a = I_1$, which is negative. Since $S2$ is open, a negative i_a (I_1) can only flow through $D1$. It is important to note that $-i_{D1}$ and $-i_{S2}$ are plotted in Fig. 11.5-2 to allow ready comparison with the waveform of i_a, since they are opposite to positive i_a. Let us go back to the start of interval *A*. How did i_a become negative? Well, during the interval *B* in the preceding period, $S2$ was closed with $S1$ open. With $S2$ closed, the armature terminals are in effect short-circuited and the counter emf has driven i_a negative. Therefore, when $S1$ is closed and $S2$ is opened at the start of interval *A*, the source voltage has to contend with this negative I_1. We see from Fig. 11.5-2 that the average value of i_a is slightly positive; therefore, v_S is larger than

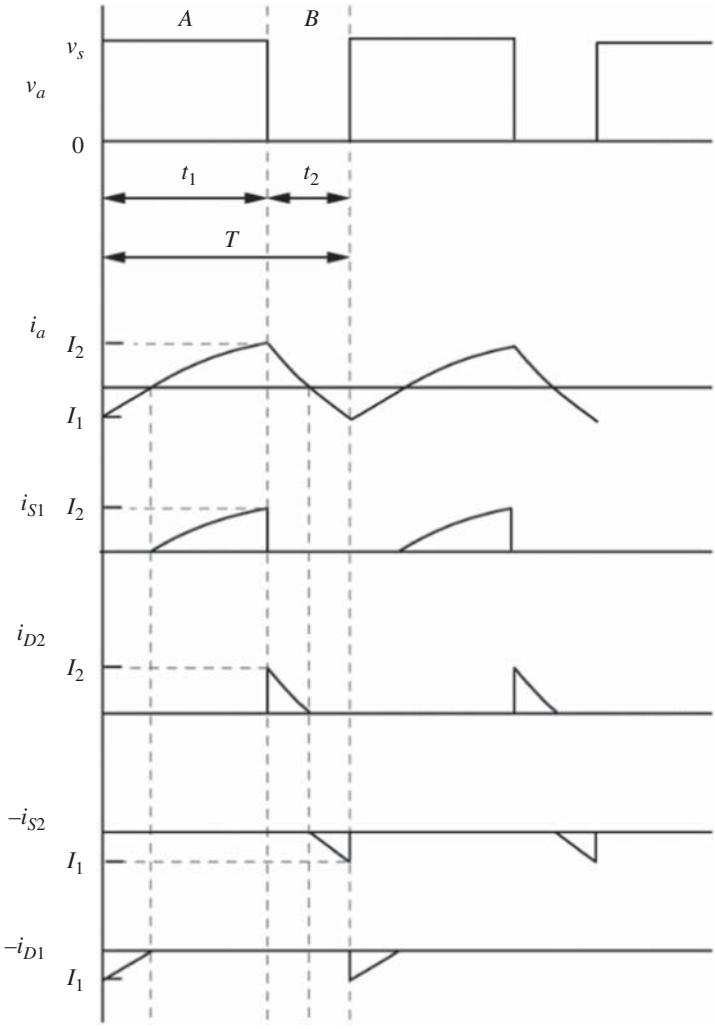

Figure 11.5-2 Steady-state operation of a two-quadrant dc converter drive.

the counter emf and at the start of interval A when v_S is applied to the machine the armature current begins to increase toward zero from the negative value of I_1. Once i_a reaches zero, the diode D_1 blocks the current flow. That is, i_{D1} cannot become negative (cannot conduct positive i_a); however, $S1$ has been closed since the start of interval A and since i_{S1} can only be positive, $S1$ is ready to carry the positive i_a. The armature current, which is now i_{S1}, continues to increase until the end of interval A (I_2).

At the beginning of interval *B, S*1 is opened and *S*2 is closed; however, *S*2 cannot conduct a positive armature current. Therefore, the positive current (I_2) is diverted to diode *D*2, which is short-circuiting the armature terminals. Now, the counter emf has the positive current (I_2) with which to contend. It is clear that if the armature terminals were permanently short-circuited, the counter emf would drive i_a negative. At the start of interval *B*, the counter emf begins to do just that; however, when i_a becomes zero, diode *D*2 blocks i_{D2} and the negative armature current is picked up by *S*2, which has been closed since the beginning of interval *B,* waiting to be called upon to conduct a negative armature current. This continues until the end of interval *B*, whereupon we are back to where we started.

It is apparent that if the mode of operation is such that I_1 and I_2 are both positive, then the machine is acting as a motor with a substantial load torque if ω_r is positive (ccw). In this mode, either *S*1 or *D*2 will carry current during a switching period *T*. If both I_1 and I_2 are negative, the machine is operating as a generator, delivering power to the source if ω_r is driven ccw. In this case, either *S*2 or *D*1 will carry current during a switching period.

11.5.1 Average-Value Time-Domain Block Diagram

The average-value time-domain block diagram for the two-quadrant chopper drive system is shown in Fig. 11.5-3. From Fig. 11.5-2, the average armature voltage may be determined as

$$\bar{v}_a = \frac{1}{T}\left[\int_0^{t_1} v_S\, d\xi + \int_{t_1}^{T} 0\, d\xi\right] \tag{11.5-1}$$

Since $t_1 = kT$, where k is referred to as the duty cycle, the average armature voltage becomes

$$\bar{v}_a = kv_S \tag{11.5-2}$$

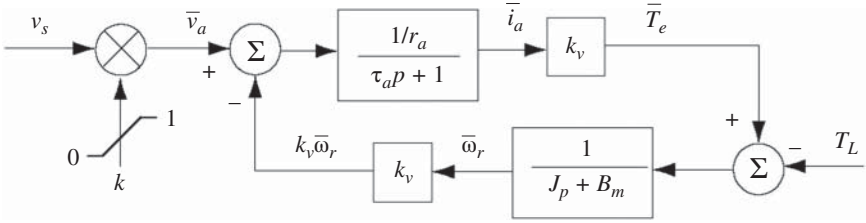

Figure 11.5-3 Average-value model of two-quadrant dc converter drive.

In Fig. 11.5-3, the bars over the variables denote average values.

The starting characteristics of a permanent-magnet dc machine with a two-quadrant chopper drive are depicted in Fig. 11.5-4. The machine parameters are $r_a = 7\ \Omega$, $L_{AA} = 120$ mH, $k_v = 1.41 \times 10^{-2}$ V · s/rad, and $J = 1.06 \times 10^{-6}$ kg · m^2; rated voltage is 6 V. Here, the switching frequency f_s is set to 200 Hz and the source voltage to 10 V. Typically, the switching frequency is much higher, generally greater than 20 kHz. The frequency was selected to illustrate the dynamics introduced by the converter. Even at this low switching frequency, the switching period T is much less than the armature time constant τ_a. Thus, the armature current essentially consists of piecewise linear segments about an average response. In Fig. 11.5-4, the duty cycle is stepped from 0 to 0.6, corresponding to a step increase in average applied voltage from 0 to 6 V. The start-up response established using the average-value model is superimposed for purposes of comparison. As shown, the only salient difference between the two responses is the "sawtooth" behavior of the armature current due to converter switching. The difference in rotor speeds is indistinguishable.

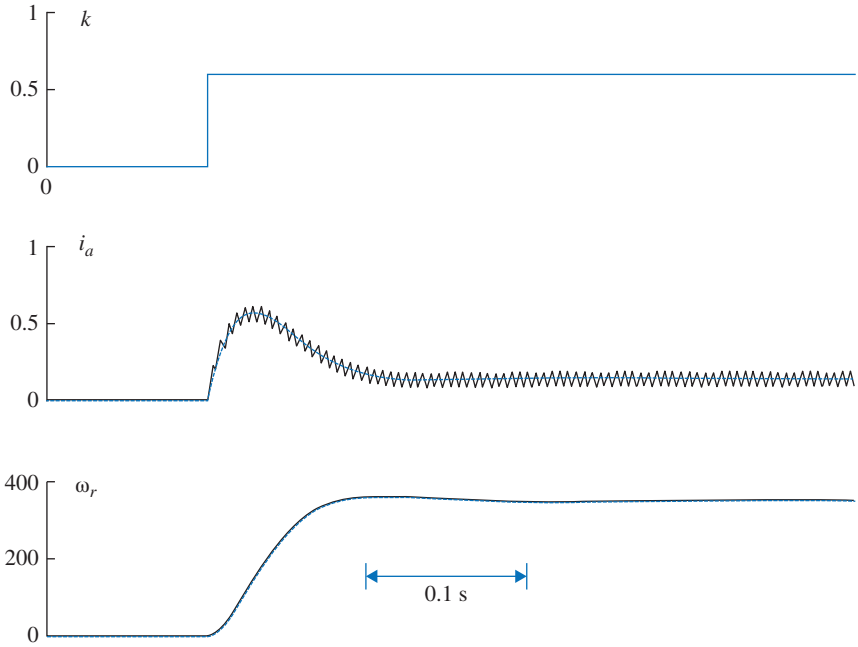

Figure 11.5-4 Starting characteristics of a permanent-magnet dc machine with a two-quadrant dc/dc converter drive.

11.5.2 Torque Control

The parameters of a permanent-magnet dc machine are $V_a = 6$ V (rated), $r_a = 7\ \Omega$, $k_v = 1.41 \times 10^{-2}$ V·s/rad, $L_{AA} = 120$ mH, $J = 1.06$ kg·m^2, and $B_m = 6.04 \times 10^{-6}$ N·m·s. We are to limit the commanded torque T_e^* to 0.423×10^{-2} N·m or $I_a^* = 0.3$ A where the asterisk denotes commanded values. The control is shown symbolically in Fig. 11.5-5.

Since the current is controlled, the electric dynamics are neglected; therefore, only the mechanical dynamics are considered. The equations involved in Fig. 11.5-5 are

$$V_a = r_a I_a^* + \omega_r k_v \tag{11.5-3}$$

$$T_e^* = J\frac{d\omega_r}{dt} + B_m\omega_r + T_L \tag{11.5-4}$$

where $T_e^* = k_v I_a^* = 0.423 \times 10^{-2}$ N·m. The load line is

$$T_L = K\omega_r^2 \tag{11.5-5}$$

where

$$K = 5.529 \times 10^{-8}\ \text{N} \cdot \text{m} \cdot \text{s}^2 \tag{11.5-6}$$

This intersects rated-V_a current versus speed plot at Operating Point 1 where $\omega_r = 276.6$ rad/s, as shown in Fig. 11.5-6.

The dc machine is operating at Point 1. The commanded torque is suddenly switched to $\frac{1}{2}$ the original value which intersects the limiting torque $\left(I_a^*\right)$ at Operating Point 2 where $\omega_r = 195.6$ rad/s. The electromechanical dynamics are

$$T_e^* = J\frac{d\omega_r}{dt} + B_m\omega_r + T_L \tag{11.5-7}$$

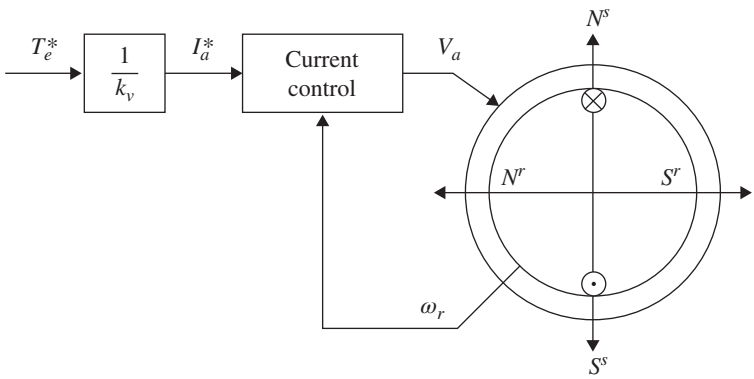

Figure 11.5-5 Torque control.

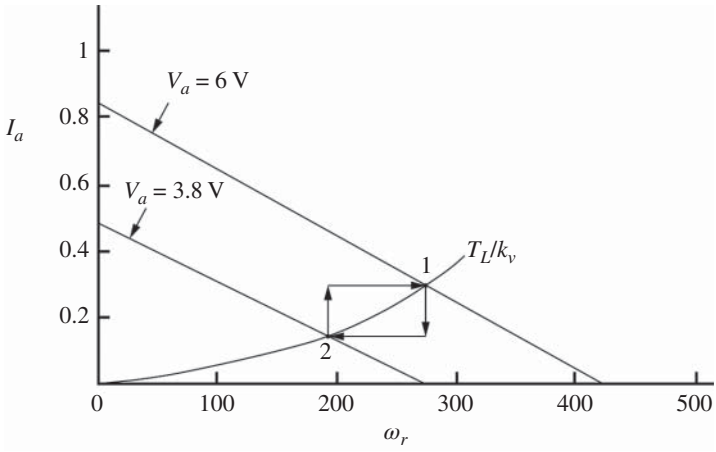

Figure 11.5-6 Armature current versus speed trajectory during T_e^* switching.

Assuming the torque control is functioning perfectly, the rotor slows and the steady state is reached at Operating Point 2. The voltage at Operating Point 2 is

$$\begin{aligned} V_a &= \mathrm{r}_a I_a^* + k_v \omega_r \\ &= (7)(0.15) + (1.41 \times 10^{-2})(195.6) \\ &= 1.05 + 2.76 = 3.8\ \mathrm{V} \end{aligned} \tag{11.5-8}$$

The commanded torque T_e^* is then returned to the original value. The rotor speeds up and reaches the steady state at Operating Point 1. The trajectory from Operating Point 1 to Operating Point 2 and then back to 1 is shown in Fig. 11.5-6.

Reference

1 P. C. Krause, *Analysis of Electric Machinery*, New York, McGraw-Hill Book Company, 1986.

Problems

11.1 A permanent-magnet dc motor has the following parameters: $r_a = 8\ \Omega$ and $k_v = 0.01\ \mathrm{V \cdot s/rad}$. The shaft load torque is approximated as $T_L = K\omega_r$, where $K = 5 \times 10^{-6}\ \mathrm{N \cdot m \cdot s}$. The applied voltage is 8 V and $B_m = 0$. Calculate the steady-state rotor speed ω_r in rad/s.

11.2 A permanent-magnet dc motor is driven by a mechanical source at 3820 rev/min. The measured open-circuit armature voltage is 7 V. The mechanical source is disconnected, and a 12 V electric source is connected to the armature. With zero-load torque, $I_a = 0.1$ A and $\omega_r = 650$ rad/s. Calculate k_v, B_m, and r_a.

11.3 The parameters of a permanent-magnet dc machine are $r_a = 6\ \Omega$ and $k_v = 2 \times 10^{-2}$ V · s/rad. V_a can be varied from zero to 10 V. The device is to be operated in the constant-torque mode with $T_e = 4 \times 10^{-3}$ N · m. (a) Determine V_a for $\omega_r = 0$. (b) Determine the maximum ω_r range of the constant-torque mode of operation (maximum ω_r with $T_e = 4 \times 10^{-3}$ N · m and $V_a = 10$ V).

11.4 Sketch Fig. 11.5-2 for generator action; i.e., i_{S1} and i_{D2} equal to zero.

12

Torque Control of Permanent-Magnet and Synchronous Reluctance Machines

12.1 Introduction

In an electric vehicle, the accelerating force is proportional to the electromagnetic torque of the propulsion motor(s). The angle of the accelerator pedal determines the desired accelerating or tractive force, which, in turn, determines the desired electromagnetic torque of the motor. This chapter describes an approach to torque control of permanent-magnet and reluctance machines, which are used in many automotive applications. The control is power electronic based, which controls the amplitude and frequency of the applied stator voltages and currents. This is accomplished very fast compared to the mechanical dynamics of the vehicle. Hence, it is reasonable to neglect the electrical dynamics associated with the motor and associated power electronic controls. That is, even though the motor speed and/or torque vary with respect to time, the steady-state equations of the motor may be used to predict the mechanical dynamics of the vehicle (e.g., its acceleration/deceleration).

In Chapter 4, we considered the brushless dc machine with L_q and L_d being equal. However, in the permanent-magnet motors commonly used in electric vehicles, these inductances are considerably different, which gives rise to a reluctance torque that can be significant. The device no longer operates as a brushless dc machine; however, many of the equations given in Chapter 4 apply equally well to this device.

In a reluctance machine, we no longer have a permanent magnet $\left(\lambda_m'^r = 0\right)$; we have only reluctance torque. In this case, the device becomes a synchronous reluctance machine, which is also treated in this chapter.

Analysis of Electric Machinery and Drive Systems, Fourth Edition.
Paul C. Krause, Oleg Wasynczuk, Scott D. Sudhoff, and Steven D. Pekarek.

Companion website: www.wiley.com/go/krause_aem4e

12.2 Torque Control of a Permanent-Magnet AC Machine

In earlier introductory texts [1, 2], we considered torque control of a small permanent-magnet machine with $L_q = L_d$. Therein, it was assumed that the current control was very fast. Thus, the stator currents settled to their steady-state values a few milliseconds after a step change in torque command. This, along with the assumption that $L_q = L_d$, made it easy to establish the response of the drive.

In this section, we will consider a much larger machine similar to that used in an automotive electric drive [3]. It is an interior permanent-magnet (IPM) machine with the following parameters: $P = 8$, $\sqrt{2}\, I_{s,\,\max} = 222$ A, $\sqrt{2}\, V_{s,\,\max} = 230.9$ V, $\lambda'_m = 0.2\,\text{V}\cdot\text{s}$, $r_s = 0.09\ \Omega$, $L_d = 2$ mH, and $L_q = 3.3$ mH. A cross-sectional view of a two-pole IPM machine is shown in Fig. 12.2-1. Note that $L_q > L_d$ since the magnets are embedded in the direct axis of the rotor (there is less magnetic steel along the direct axis), whereas in [1, 2], arc-shaped magnets were mounted on the surface of the rotor and $L_d \approx L_q$. The equations of the eight-pole machine considered herein are the same as for the two-pole machine in Fig. 12.2-1 with the usual substitutions $\theta_r = \frac{P}{2}\theta_{rm}$ and $\omega_r = \frac{P}{2}\omega_{rm}$.

From (4.3-27), the steady-state torque can be expressed in terms of the q- and d-axis components of the stator current as

$$T_e = \left(\frac{3}{2}\right)\left(\frac{P}{2}\right)\left[\lambda'^r_m I^r_{qs} + (L_d - L_q) I^r_{qs} I^r_{ds}\right] \tag{12.2-1}$$

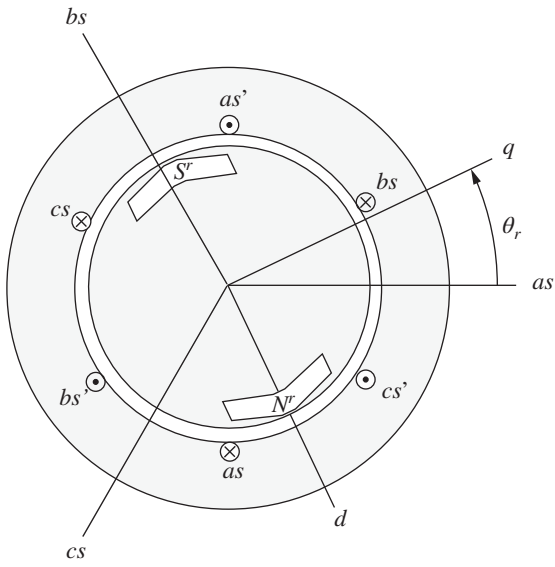

Figure 12.2-1 Two-pole interior permanent-magnet ac machine.

Although this expression is valid for dynamic as well as steady-state operating conditions, we will initially consider steady-state operation. The peak value of the stator currents is typically constrained to be less than the maximum value. Mathematically,

$$\sqrt{2}I_s = \sqrt{\left(I_{qs}^r\right)^2 + \left(I_{ds}^r\right)^2} \leq \sqrt{2}I_{s,\max} \tag{12.2-2}$$

There is an infinite number of values for I_{qs}^r and I_{ds}^r that give the same value of T_e as shown in Fig. 12.2-2. Therein, the dashed circles represent constant-I_s contours. Operating conditions A, B, and C are the optimal I_{qs}^r and I_{ds}^r for T_e values of 100, 200, and 400 N · m, respectively. These optimal operating points occur when a constant-T_e contour is tangent to a constant-I_s contour. The plots in Fig. 12.2-2 are independent of rotor speed and positive and negative torque form a mirror image. The plots shown in Fig. 12.2-3 are the optimal currents versus torque for $I_s \leq I_{s,\max}$. Therein, it is assumed that (12.2.2) is the only constraint present. If there is an additional voltage constraint, it may not be possible to achieve the currents needed to produce the desired torque at high rotational speeds. For example, if we assume $\omega_r = 2000$ rad/s and it is desirable to have 400 N · m of torque, it would

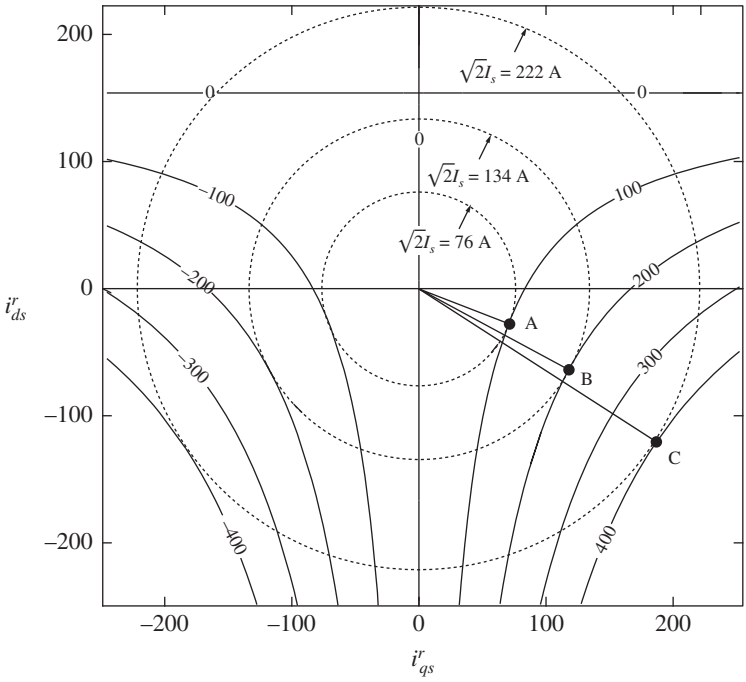

Figure 12.2-2 Contour plot for various values of torque, T_e. Points A, B, and C give optimal currents for T_e = 100, 200, and 400 N · m.

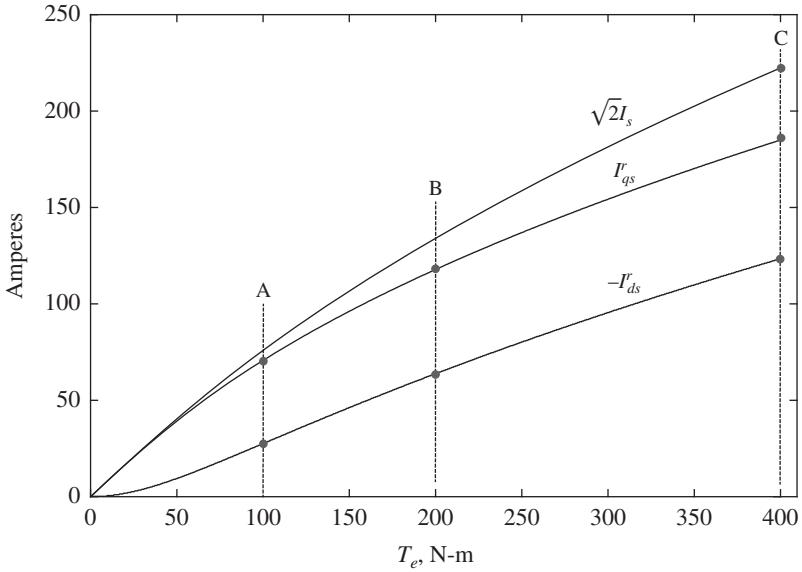

Figure 12.2-3 Optimal currents versus torque for $I_s \leq I_{s,\max}$ assuming there is no constraint on voltage.

require more than 1000 V of V^r_{ds} in order to obtain the desired current shown in Fig. 12.2-3. Clearly, this is far above the maximum peak voltage of 230.9 V.

12.2.1 Maximum Steady-State Torque Versus Speed

In addition to the current constraint given by (12.2-2), the peak ac voltage is also constrained to be less than a maximum value. Mathematically,

$$\sqrt{2}V_s = \sqrt{\left(V^r_{qs}\right)^2 + \left(V^r_{ds}\right)^2} \leq \sqrt{2}V_{s,\max} \tag{12.2-3}$$

where

$$V^r_{qs} = r_s I^r_{qs} + \omega_r L_d I^r_{ds} + \omega_r \lambda'^r_m \tag{12.2-4}$$

$$V^r_{ds} = r_s I^r_{ds} - \omega_r L_q I^r_{qs} \tag{12.2-5}$$

Equations (12.2-2) and (12.2-3) represent inequality constraints, whereas (12.2-4) and (12.2-5) are called equality constraints. Of practical importance is the maximum and minimum torque that can be developed by the machine with all constraints satisfied. Since (12.2-4) and (12.2-5) involve rotor speed, the maximum and minimum torque will be functions of speed. Equation (12.2-1) is called an objective function (function to be maximized or minimized) while (12.2-2)–(12.2-5) are constraint equations. Finding the maximum or

minimum torque with all constraints satisfied is difficult to accomplish analytically; however, there are several programs such as MATLAB [4] and Python [5], for example, that can be used to do this numerically and quickly. A systematic step-by-step procedure for calculating maximum and minimum torque as a function of speed is shown below.

1) For $0 \le \omega_r \le \omega_{r,\,\max}$
2) Using MATLAB's `fmincon` function, find I^r_{qs} and I^r_{ds} that **maximizes** $T_e = \left(\frac{3}{2}\right)\left(\frac{P}{2}\right)\left[\lambda'^r_m I^r_{qs} + (L_d - L_q) I^r_{qs} I^r_{ds}\right]$ while satisfying all constraints
3) Calculate corresponding $T_{e,\,\max}(\omega_r)$, V^r_{qs}, and V^r_{ds}. Resulting $T_{e,\,\max}(\omega_r)$ is plotted in Fig 12.2-4. The corresponding I^r_{qs} and I^r_{ds} are plotted in Fig. 12.2-5, and the corresponding V^r_{qs}, and V^r_{ds} are plotted in Fig. 12.2-6.
4) Using MATLAB's `fmincon` function, find I^r_{qs} and I^r_{ds} that **minimizes** $T_e = \left(\frac{3}{2}\right)\left(\frac{P}{2}\right)\left[\lambda'^r_m I^r_{qs} + (L_d - L_q) I^r_{qs} I^r_{ds}\right]$ while satisfying all constraints
5) Calculate corresponding $T_{e,\,\min}(\omega_r)$ (plotted in Fig 12.2-4).

The maximum and minimum torque are plotted as a function of electrical rotor speed in Fig. 12.2-4 for speeds up to $\omega_r = 2000$ rad/s. As shown, the largest positive and negative torque that can be developed occurs when the electrical rotor speed is less than 360.7 rad/s, where only the 222 A stator current limit comes into play. In this range, $T_{e,\,\min}(\omega_r)$ is the mirror image of $T_{e,\,\max}(\omega_r)$. Also, it is readily verified that the reluctance component of torque is 44% of the total torque.

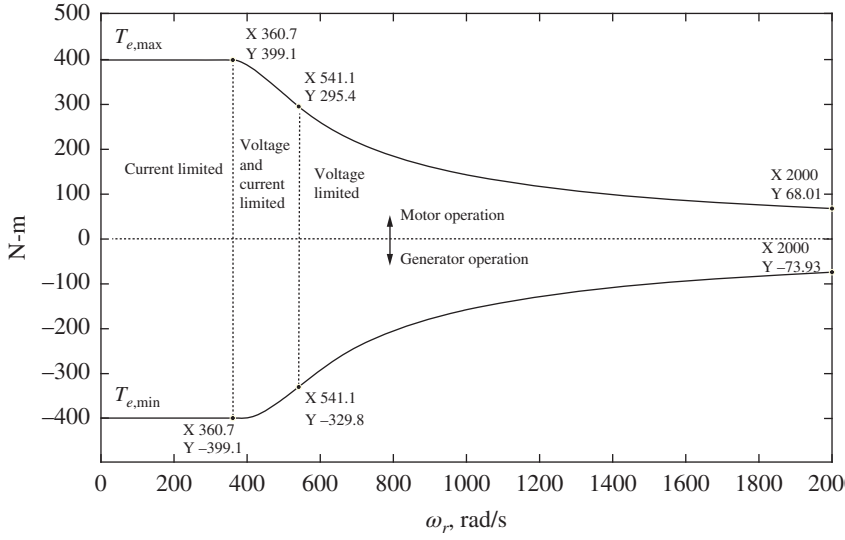

Figure 12.2-4 Maximum and minimum torque as a function of electrical rotor speed.

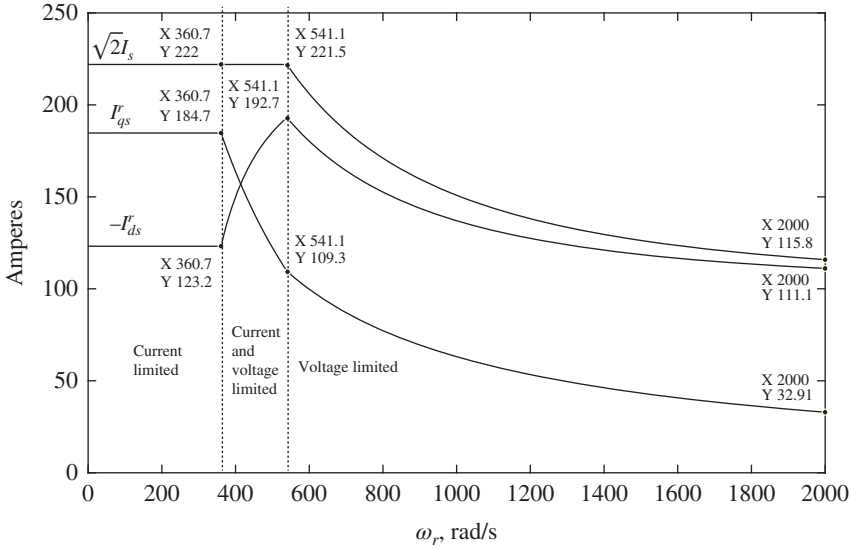

Figure 12.2-5 Stator currents for maximum torque.

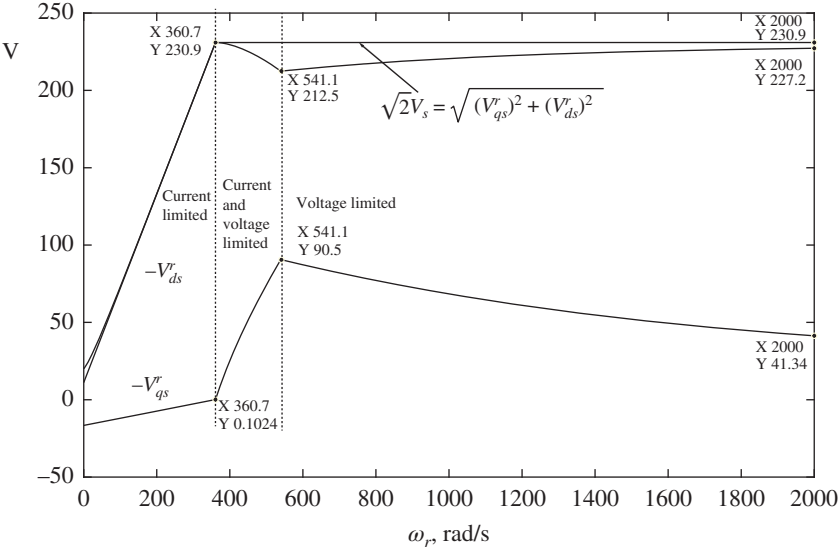

Figure 12.2-6 Stator voltages for maximum torque.

As shown in Fig. 12.2-6, as the rotor speed increases, the voltages needed to produce the required currents increase in magnitude. At an electrical rotor speed of 360.7 rad/s, the stator voltage limit of 230.9 V is reached. For rotor speeds between 360.7 and 541.1 rad/s, the motor operates at the maximum current and voltage as shown in Figs 12.2-5 and 12.2-6, respectively. That is, $V_s = V_{s,\max}$ and $I_s = I_{s,\max}$. Although I_s is constant in this interval, the magnitude of I_{qs}^r decreases and I_{ds}^r increases with the corresponding torque decreasing as ω_r increases. Similarly, V_s is constant; however, V_{qs}^r and V_{ds}^r both change as a function of speed. As shown in Fig. 12.2-4, the absolute magnitudes of the maximum and minimum torque differ slightly when the voltage limit is involved due to the resistive drop in voltage. At the end of the region (ω_r = 541.1 rad/s), the reluctance torque is 55.6% of the total maximum torque.

For rotor speeds greater than 541.1 rad/s, the motor continues to operate at its voltage limit $V_s = V_{s,\max}$; however, the current is now less than the maximum, $I_s < I_{s,\max}$ as shown in Fig. 12.2-5. Although a larger current could produce a larger torque, the voltage constraint limits the peak current I_s to a value less than rated. At the end of the region, the reluctance torque makes up 41.8% of the total torque.

The maximum mechanical power (product of maximum torque and **mechanical** speed) and efficiency (mechanical power out divided by electric power in) are shown in Figs. 12.2-7 and 12.2-8, respectively, for motor action. The power increases linearly for rotor speeds up to 360.7 rad/s. Maximum power is

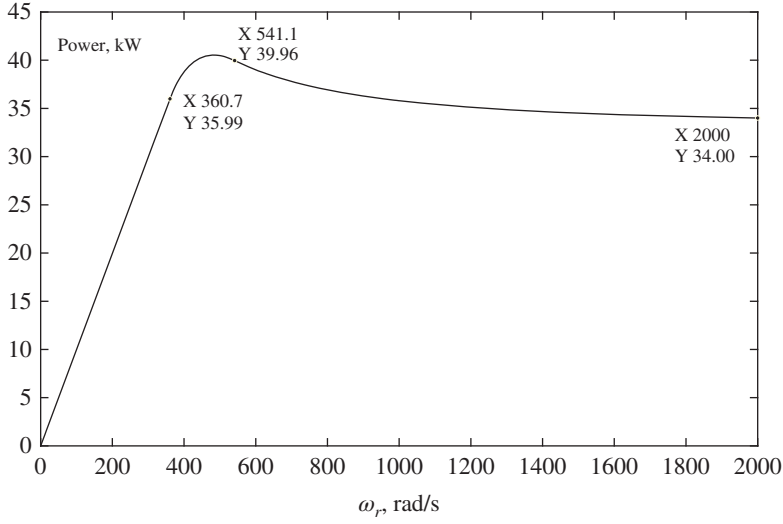

Figure 12.2-7 Maximum mechanical power versus rotor speed.

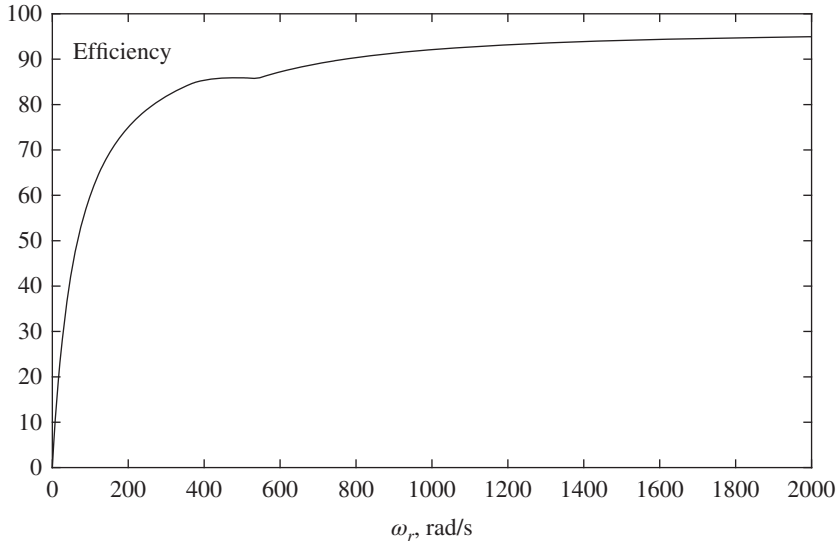

Figure 12.2-8 Efficiency for maximum T_e.

approximately 40 kW, which occurs at a rotor speed of approximately 450 rad/s. For larger speeds, maximum power falls off slightly approaching 34 kW at an electrical rotor speed of 2000 rad/s. Maximum efficiency of 95% is achieved at 2000 rad/s. It is important to note that only the stator resistive losses have been considered here. Core losses (hysteresis and eddy current) in both the stator and rotor will also exist in practice lowering the efficiency somewhat. A more detailed analysis of losses and efficiency for an IPM motor used in hybrid vehicles is provided in [8].

Before considering the phasor diagrams, let us step back and talk about the notation being used. Due to the power electronics control, the change in frequency of applied voltages is nearly instantaneous; however, the change in rotor speed is much slower. Therefore, the electrical variables of the machine are essentially always in synchronism with the applied voltages. That is, $\omega_e = \omega_r$, where ω_r is the electrical angular velocity of the rotor. Perhaps we should use an "e" superscript instead of "r" on the electrical variables; however, we will continue with "r" and realize that $\omega_r = \omega_e$.

Now, the phasor diagrams are shown in Fig. 12.2-9 for $\omega_r = 0$, 360.7, 541.1, and 2000 rad/s. The phasors are determined using

$$\sqrt{2}\tilde{F}_{as} = F^r_{qs} - jF^r_{ds} \tag{12.2-6}$$

where F is either V or I. In each case, we see motor action. That is, the torque acts in the counterclockwise direction (direction of rotation).

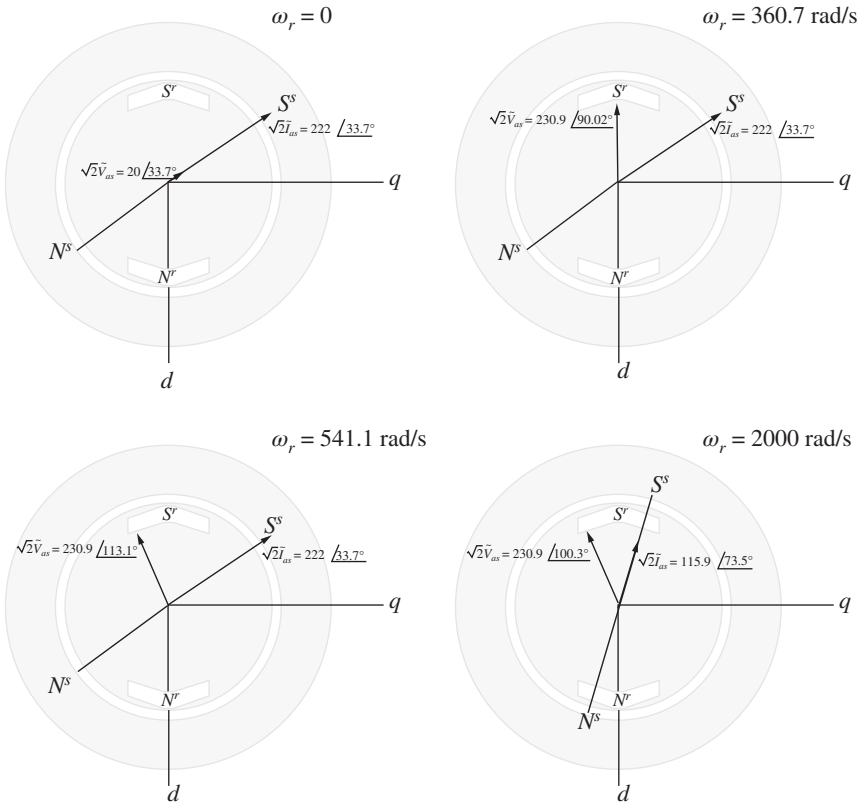

Figure 12.2-9 Phasor diagrams at maximum torque for $\omega_r = 0$, 360.7, 541.1, and 2000 rad/s.

It is important to note that $T_{e,\max}(\omega_r)$ and $T_{e,\min}(\omega_r)$ are, respectively, the maximum and minimum torque that can be developed at a given rotor speed. Typically, the desired or commanded torque, denoted T_e^*, is somewhere in between these limits. In this case, it is desired to select I_{qs}^r and I_{ds}^r that **minimizes**

$$\sqrt{2}I_s = \sqrt{\left(I_{qs}^r\right)^2 + \left(I_{ds}^r\right)^2} \tag{12.2-7}$$

while satisfying the following constraints

$$T_e^* = \left(\frac{3}{2}\right)\left(\frac{P}{2}\right)\left[\lambda'^r_m I_{qs}^r + (L_d - L_q) I_{qs}^r I_{ds}^r\right] \tag{12.2-8}$$

$$\sqrt{\left(V_{qs}^r\right)^2 + \left(V_{ds}^r\right)^2} \le \sqrt{2}V_{s,\max} \tag{12.2-9}$$

where V_{qs}^r and V_{qs}^r are given by (12.2-4) and (12.2-5). Note that (12.2-2) is no longer a constraint. Instead, (12.2-7) becomes the new objective function (to be

minimized). Equations (12.2-8) and (12.2-9) along with (12.2-4) and (12.2-5) form the new set of constraint equations. Optimal I_{qs}^{r} and I_{ds}^{r} will be functions of both T_e^* and ω_r since both variables appear in the constraint equations. A procedure for calculating optimal I_{qs}^{r} and I_{ds}^{r} is shown below.

1 For $0 \le \omega_r \le \omega_{r,\max}$
2 For $T_{e,\min}(\omega_r = 0) \le T_e^* \le T_{e,\max}(\omega_r = 0)$
3 If $T_e^* \ge T_{e,\max}(\omega_r)$ (desired T_e^* cannot be achieved at given ω_r)
4 Set $I_{qs}^{r*}(\omega_r, T_e^*) = I_{qs}^{r}$ calculated previously (set to a value that maximizes T_e)
5 Set $I_{ds}^{r*}(\omega_r, T_e^*) = I_{ds}^{r}$ calculated previously (set to a value that maximizes T_e)
6 If $T_e^* \le T_{e,\min}(\omega_r)$ (desired T_e^* cannot be achieved at given ω_r)
7 Set $I_{qs}^{r*}(\omega_r, T_e^*) = I_{qs}^{r}$ calculated previously (set to a value that minimizes T_e)
8 Set $I_{ds}^{r*}(\omega_r, T_e^*) = I_{ds}^{r}$ calculated previously (set to a value that minimizes T_e)
9 If $T_{e,\min}(\omega_r) \le T_e^* \le T_{e,\max}(\omega_r)$
10 Using MATLAB's `fmincon` function, find I_{qs}^{r} and I_{ds}^{r} that minimizes $\sqrt{(I_{qs}^{r})^2 + (I_{ds}^{r})^2}$ with a set of new constraints satisfied
11 Set $I_{qs}^{r*}(\omega_r, T_e^*) = I_{qs}^{r}$.
12 Set $I_{\mathrm{ds}}^{r*}(\omega_r, T_e^*) = I_{\mathrm{ds}}^{r}$

The resulting optimal I_{qs}^{r*} and I_{ds}^{r*} are plotted as a function of desired torque T_e^* and electrical rotor speed ω_r in Figs. 12.2-10 and 12.2-11, respectively.

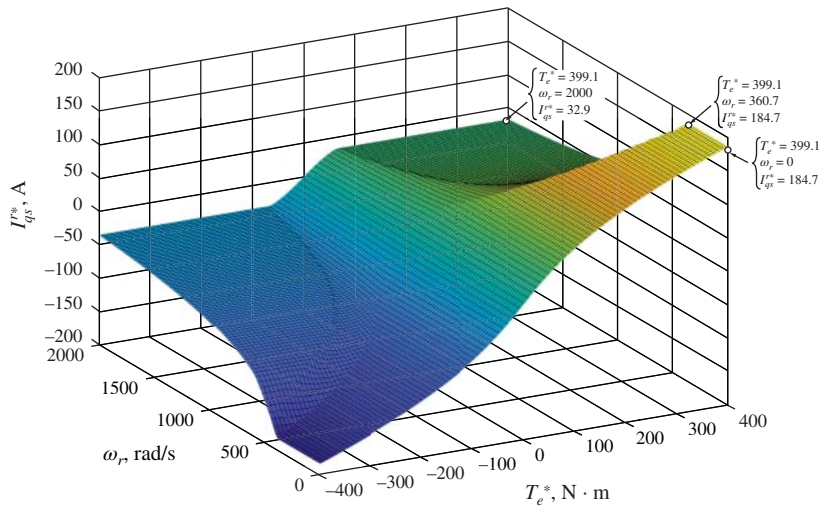

Figure 12.2-10 Plot of $I_{qs}^{r*}(\omega_r, T_e^*)$.

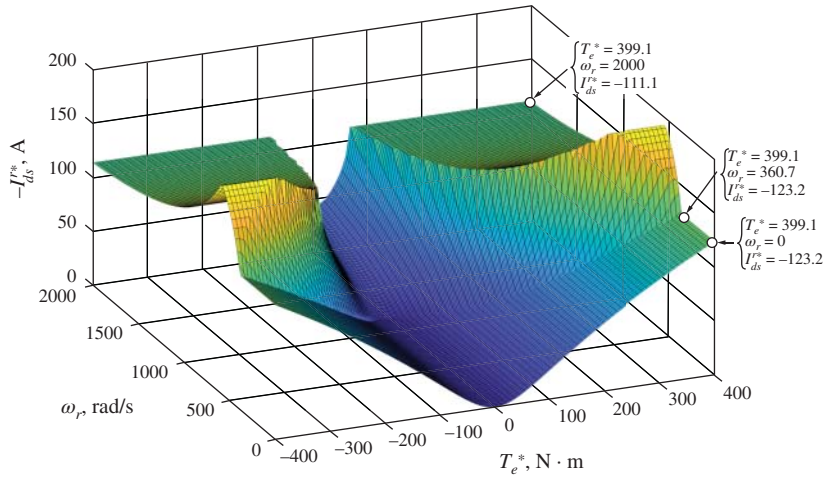

Figure 12.2-11 Plot of $-I_{ds}^{r*}(\omega_r, T_e^*)$.

The numerical data used to generate these figures can be implemented as two-dimensional look-up tables in a torque control system as described in the next section. As shown in Figs. 12.2-10 and 12.2-11, for rotor speeds less than 360.7 rad/s, I_{qs}^{r*} and I_{ds}^{r*} are independent of speed and depend only on T_e^*, consistent with Fig. 12.2-3. However, when the rotor speed becomes larger than 360.7 rad/s, the voltage constraint comes into play, whereupon I_{qs}^{r*} and I_{ds}^{r*} become functions of both T_e^* and ω_r.

12.3 Simulation of a Permanent-Magnet AC Machine with Torque Control

We are now able to establish a reduced-order model of a permanent-magnet ac machine with torque control. It is assumed that the inverter operates very fast, nearly instantaneously, to establish v_{qs}^r and v_{ds}^r. In fact, we are going to assume that v_{qs}^r and v_{ds}^r are equal to their desired or commanded values v_{qs}^{r*} and v_{ds}^{r*} that are established by a current controller. Lower-case variables are used here since we are no longer restricting operation to steady-state operation at constant speed and torque.

A block diagram of the drive system is shown in Fig. 12.3-1. As shown, the system includes a permanent-magnet ac machine, an inverter and modulator, a current controller, and a table lookup block that establishes the desired (commanded) i_{qs}^{r*} and i_{ds}^{r*}. The commanded currents are supplied to a current control

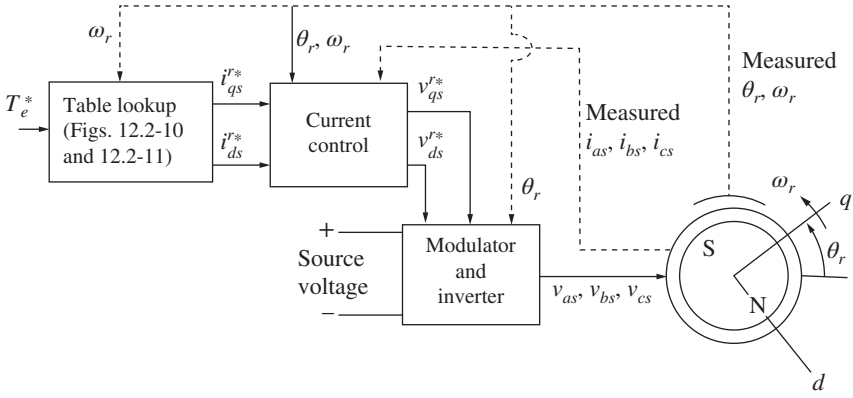

Figure 12.3-1 Block diagram of torque-controlled drive system.

block that determines the commanded v_{qs}^{r*} and v_{ds}^{r*}, which are supplied to the modulator and inverter. Detailed descriptions of the inverter and modulator are provided in Chapter 10. As noted previously, we are going to assume that v_{qs}^{r} and v_{ds}^{r} are equal to their commanded values v_{qs}^{r*} and v_{ds}^{r*}, which will later be shown to be a very reasonable assumption.

The current controller is detailed in Fig. 12.3-2. The outputs of the current control are v_{qs}^{r*} and v_{ds}^{r*}, which are supplied to the modulator and inverter. The

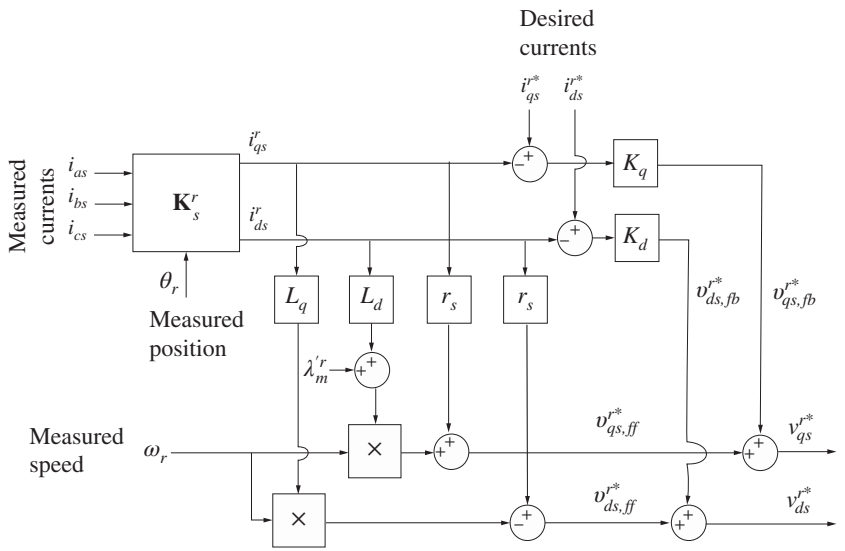

Figure 12.3-2 Current control.

commanded voltages of each have two components: a feedforward component and a feedback component. The feedforward components are

$$v_{qs,ff}^{r*} = r_s i_{qs}^r + \omega_r \left(\lambda'_m + L_d i_{ds}^r\right) \tag{12.3-1}$$

$$v_{ds,ff}^{r*} = r_s i_{ds}^r - \omega_r L_q i_{qs}^r \tag{12.3-2}$$

which represent the resistive and speed-voltage terms of the stator voltage equations. The feedback components are

$$v_{qs,fb}^{r*} = K_q \left(i_{qs}^{r*} - i_{qs}^r\right) \tag{12.3-3}$$

$$v_{ds,fb}^{r*} = K_d \left(i_{ds}^{r*} - i_{ds}^r\right) \tag{12.3-4}$$

Under the assumption that v_{qs}^r and v_{ds}^r are equal to v_{qs}^{r*} and v_{ds}^{r*}, it can readily be shown (left as a homework exercise) that the dynamic relationships between actual and commanded currents can be expressed as

$$K_q i_{qs}^{r*} = L_q p i_{qs}^r + K_q i_{qs}^r \tag{12.3-5}$$

$$K_d i_{ds}^{r*} = L_d p i_{ds}^r + K_d i_{ds}^r \tag{12.3-6}$$

which represent first-order differential equations with time constants of L_q/K_q and L_d/K_d. In the steady state, $I_{qs}^r = I_{qs}^{r*}$ and $I_{ds}^r = I_{ds}^{r*}$. A small time constant is needed to yield a fast response. However, the time constant should be at least an order of magnitude larger than the switching period of the inverter (50 μs for an inverter with a switching frequency of 20 kHz). In the following studies, the values of K_q and K_d were selected to yield a time constant of 2 ms, which is much larger than the switching period but is still negligible when compared to typical mechanical time constants, thus justifying the use of the steady-state equations for the electric machine and associated torque control in a reduced-order simulation of the overall drive system.

12.3.1 Electrical Dynamics

The dynamic equations of a permanent-magnet ac machine were described in Chapter 4. The equations can be manipulated and expressed in the form of a time-domain block diagram as shown in Fig. 12.3-3. The inputs are v_{qs}^r, v_{ds}^r, and ω_r. The outputs are i_{qs}^r, i_{ds}^r, and T_e.

12.3.2 Mechanical Dynamics

In a terrestrial vehicle (electric or otherwise), the opposing (load) forces are typically characterized as rolling resistance (due to tire deflection), grade (gravitational forces when going up or down hill), and aerodynamic drag, which is related to

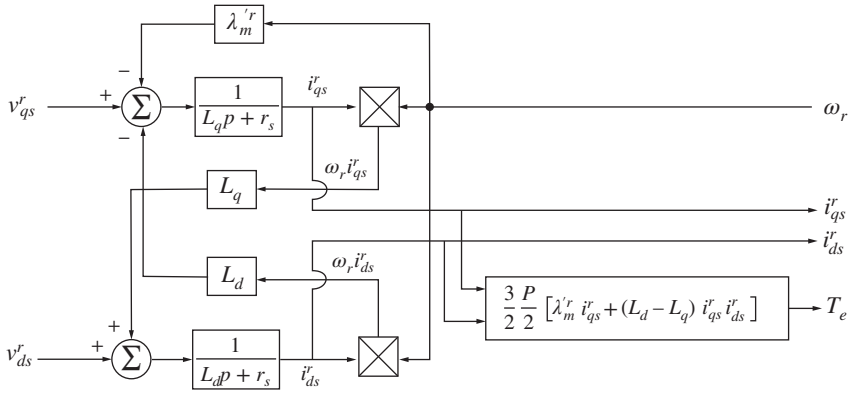

Figure 12.3-3 Time-domain block diagram of permanent-magnet ac machine with salient rotor.

vehicle speed and is affected by head or tail winds. The motor load torque is proportional to the net load force with the proportionality constant being related to tire radius and gear ratios associated with the drive train. The motor load torque is often expressed in the form

$$T_L = K_1 + K_2\omega_r + K_3\omega_r^2 \tag{12.3-7}$$

where K_1 is related to rolling resistance and grade forces, K_2 to friction, and K_3 to aerodynamic drag, which is a nonlinear function of vehicle and/or wind speed. The values of K_1 through K_3 depend on the vehicle as well as the terrain and one may become as detailed as necessary. Although the values of K_1 through K_3 depend on the situation being simulated, we selected $K_1 = 6.57\ \text{N}\cdot\text{m}$, $K_2 = 0.0193\ \text{N}\cdot\text{m}\cdot\text{s}$, and $K_3 = 9.37\times10^{-6}\ \text{N}\cdot\text{m}\cdot\text{s}^2$ corresponding to a flat (zero grade), smooth terrain with no head or tail wind.

Under the assumption that the drive train is rigid (mechanical compliance in shafts or gears neglected), the electromagnetic and load torques are related by

$$T_e = J_m p\omega_r + T_L \tag{12.3-8}$$

where J_m is the sum of the rotational inertia of the motor and the vehicle mass reflected into an equivalent rotational inertia as viewed by the motor. The value of J_m assumed in subsequent studies is $8.16\ \text{kg}\cdot\text{m}^2$.

12.3.3 System-Level Simulation Block Diagram

A system-level simulation block diagram that includes the mechanical, electrical, and control system dynamics is depicted in Fig. 12.3-4. This diagram is in a form that can be readily implemented in Simulink.

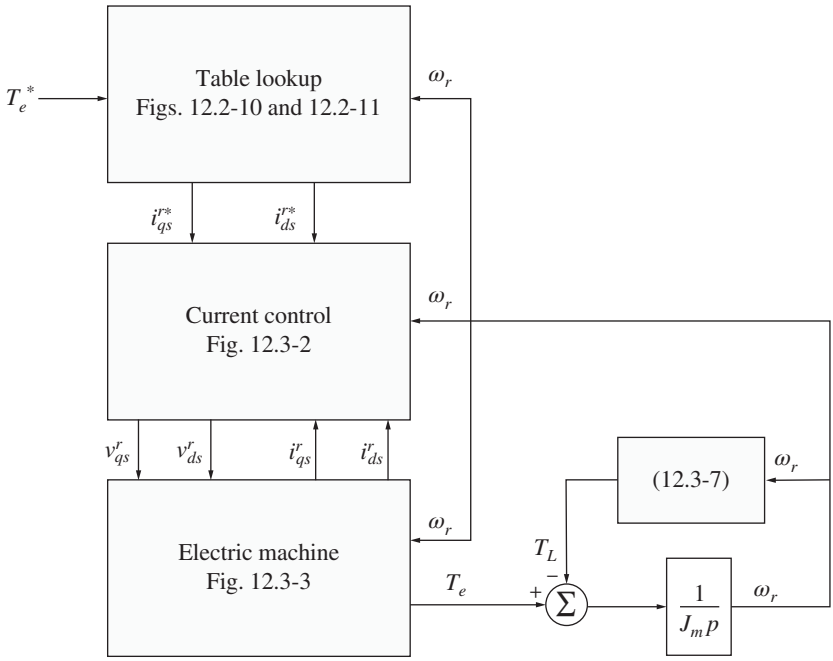

Figure 12.3-4 System-level simulation block diagram.

12.3.4 System Studies

In the following study, it is assumed that the vehicle is initially at rest ($\omega_r = 0$) and $T_e^* = 6.57\ \text{N} \cdot \text{m}$. Then, at $t = 2$ s, the torque command is switched to $400\ \text{N} \cdot \text{m}$, which is slightly larger than maximum torque, causing the motor and vehicle to accelerate as rapidly as possible. At $t = 10\ s$, the torque command is switched to $-400\ \text{N} \cdot \text{m}$, causing the vehicle to decelerate as rapidly as possible. This represents a regenerative-braking event where the kinetic energy of the vehicle and motor is converted back to electrical energy used to recharge the battery. Figs. 12.3-5, 12.3-6, and 12.3-7 show the resulting response.

Initially, the load and commanded torque are both $6.57\ \text{N} \cdot \text{m}$. At $t = 2$ s (point A in Fig. 12.3-5), the torque command T_e^* is switched to $400\ \text{N} \cdot \text{m}$. In approximately 10 ms thereafter, the actual torque T_e settles to a value very close to maximum ($399.1\ \text{N} \cdot \text{m}$), which is point B. At $t = 10$ s (point C), the torque command is switched to $-400\ \text{N} \cdot \text{m}$. In approximately 10 ms thereafter, the actual torque settles to a value close to its minimum (negative maximum) at the given rotor speed (point D). When the speed decelerates to zero speed at 16.151 s, the commanded torque is switched back to $6.57\ \text{N} \cdot \text{m}$.

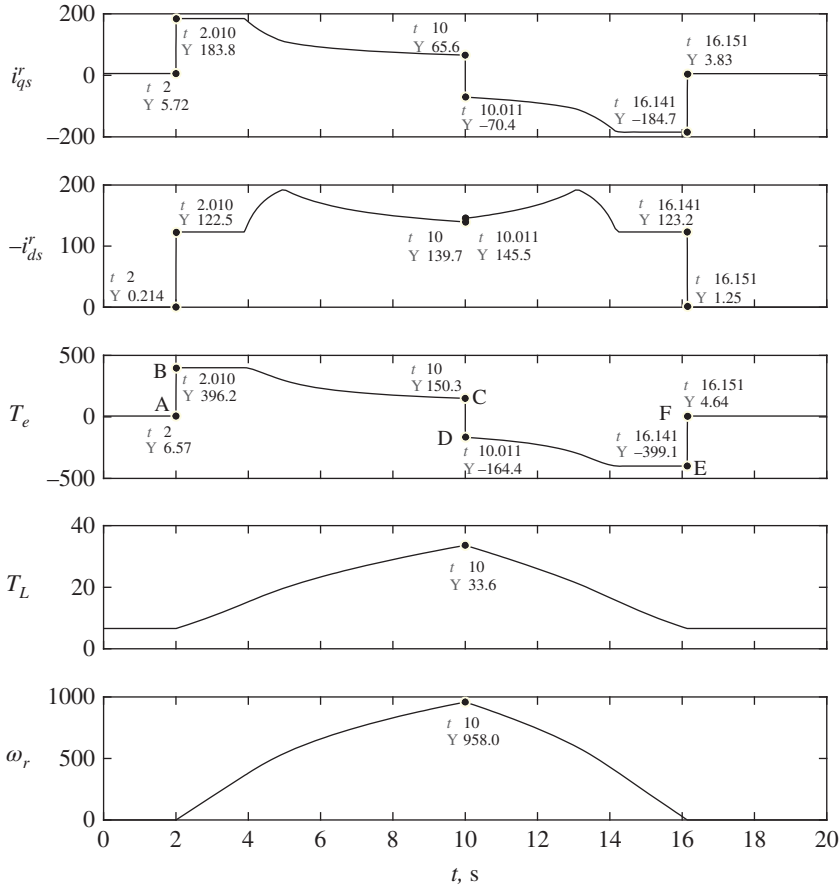

Figure 12.3-5 Torque command stepped from 6.57 to 400 N · m at $t = 2$ *s*, then to −400 at $t = 10$ *s*.

The transient response near 2 and 10 s is expanded in Fig. 12.3-6. Therein, it is seen that the electrical and control transients subside in approximately 10 ms. During these transients, the rotor speed and load torque do not change very significantly. However, the electromagnetic torque changes very rapidly achieving its new quasi-steady-state value approximately 10 ms following the step change in commanded torque. This strongly suggests that the electrical transient may be neglected when predicting the longer-term mechanical response.

The electromagnetic and load torque are plotted as a function of rotor speed in Fig. 12.3-7 (torque versus speed trajectory). Therein, the electrical and control transients from A to B and from C to D are not observable. It appears the change in electromagnetic torque is instantaneous.

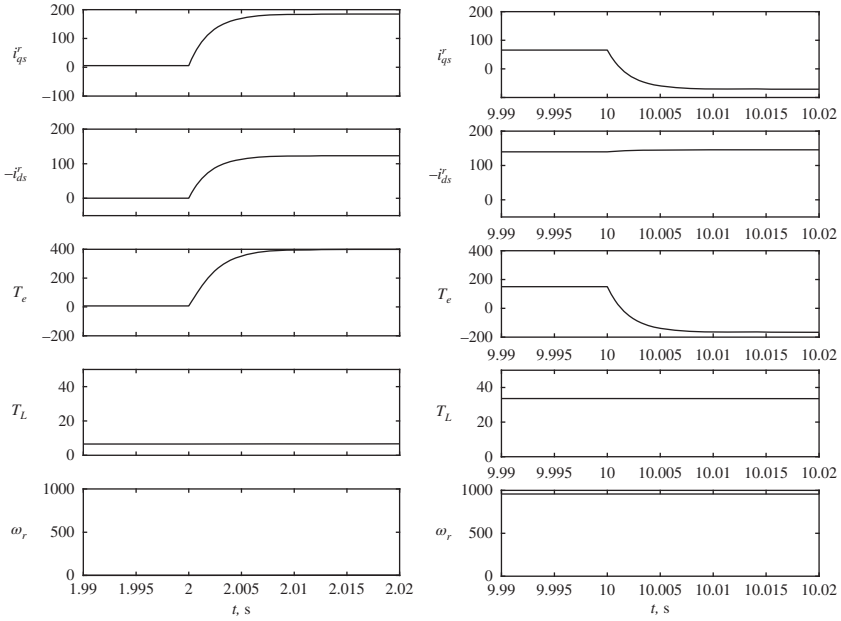

Figure 12.3-6 Expanded view near 2 and 10 s. Electrical and control transients subside in approximately 10 ms.

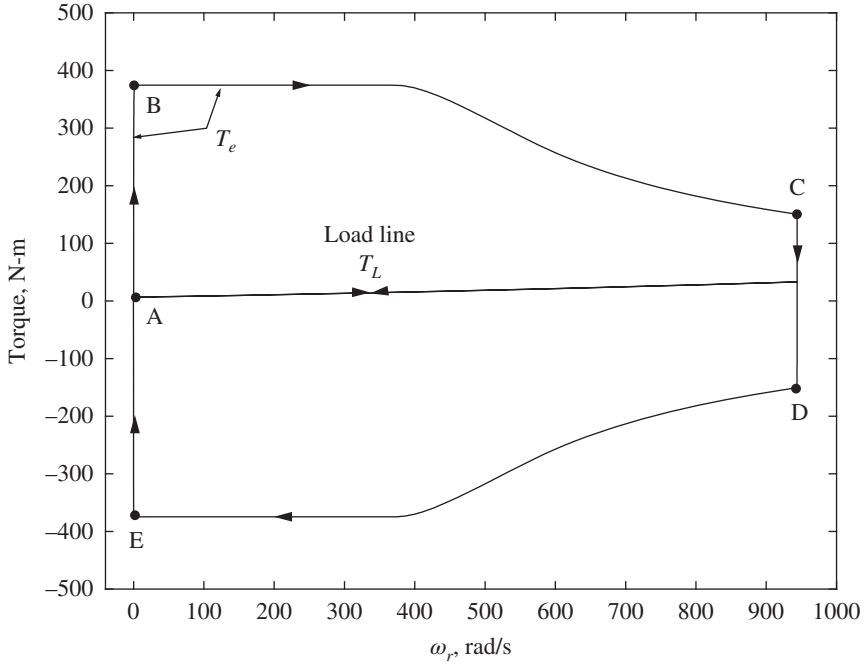

Figure 12.3-7 Torque versus speed trajectories for step changes in torque command.

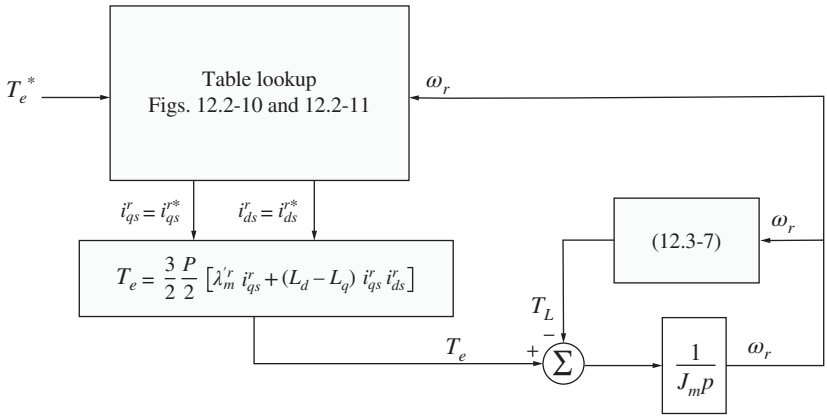

Figure 12.3-8 Reduced-order simulation block diagram.

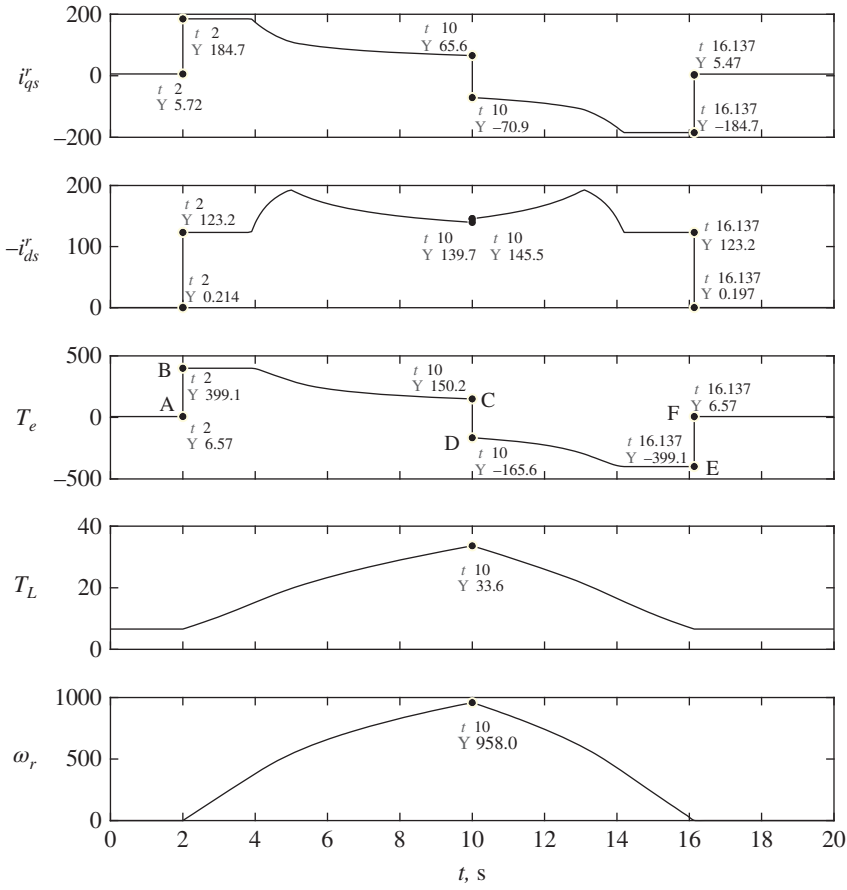

Figure 12.3-9 Same as Fig. 12.3-5 with the electric machine and control transients neglected.

12.3.5 Reduced-Order Simulation

In the previous simulation, the motor's electrical and current control system transients were included. However, the electrical transients are very short-lived, suggesting that they can be neglected. A reduced-order simulation block diagram with electrical and control transients neglected is shown in Fig. 12.3-8.

The previous study was repeated, and the resulting response is shown in Fig. 12.3-9. Clearly, Figs. 12.3-5 and 12.3-9 appear identical with relatively small differences in the numerical values of the variables at the indicated instants of time.

12.4 Torque Control of a Synchronous Reluctance Machine

There is another machine that is a sister to the permanent-magnet ac machine and warrants some consideration. If we let $\lambda'_m = 0$, the permanent-magnet ac machine becomes a synchronous reluctance machine [6, 7]. In such a machine, the rotor is constructed so that the amount of magnetic steel along the q and d axes differ as much as possible, while maintaining structural integrity. This results in a large difference between the values of L_d and L_q. In the literature, L_d/L_q ratios between 5 and 9 have been reported [6]. In the following studies, L_d is set to 3.3 mH, which is equal to the value of L_q in the permanent-magnet machine considered in the previous sections, and $L_q = \frac{3.3}{5} = 0.66$ mH. All other parameters are assumed to be the same: $P = 8$, $\sqrt{2}\, I_{s,\max} = 222$ A, $\sqrt{2}\, V_{s,\max} = 230.9$ V, and $r_s = 0.09\ \Omega$. These parameters would be representative of a machine with the same stator as the permanent-magnet machine considered previously, with the permanent magnet in the rotor removed and additional magnetic steel cut out of the rotor to increase the reluctance and decrease the inductance along the d axis. Finally, the d and q subscripts are assumed to be interchanged in this section to make $L_d > L_q$. The last step is arbitrary and not necessary; however, in legacy motors and generators with salient rotors, L_d is typically larger than L_q.

In a synchronous reluctance machine, the torque equation becomes

$$T_e = \left(\frac{3}{2}\right)\left(\frac{P}{2}\right)(L_d - L_q)\, I^r_{qs} I^r_{ds} \tag{12.4-1}$$

There is an infinite number of values for I^r_{qs} and I^r_{ds} that give the same value of T_e as shown in Fig. 12.4-1 for T_e values of 100, 200, 300, and 400 N · m. The plots in Fig. 12.4-1 are independent of rotor speed and positive and negative torque form a mirror image. In the reluctance machine, the shape of a constant-T_e contour is a hyperbola.

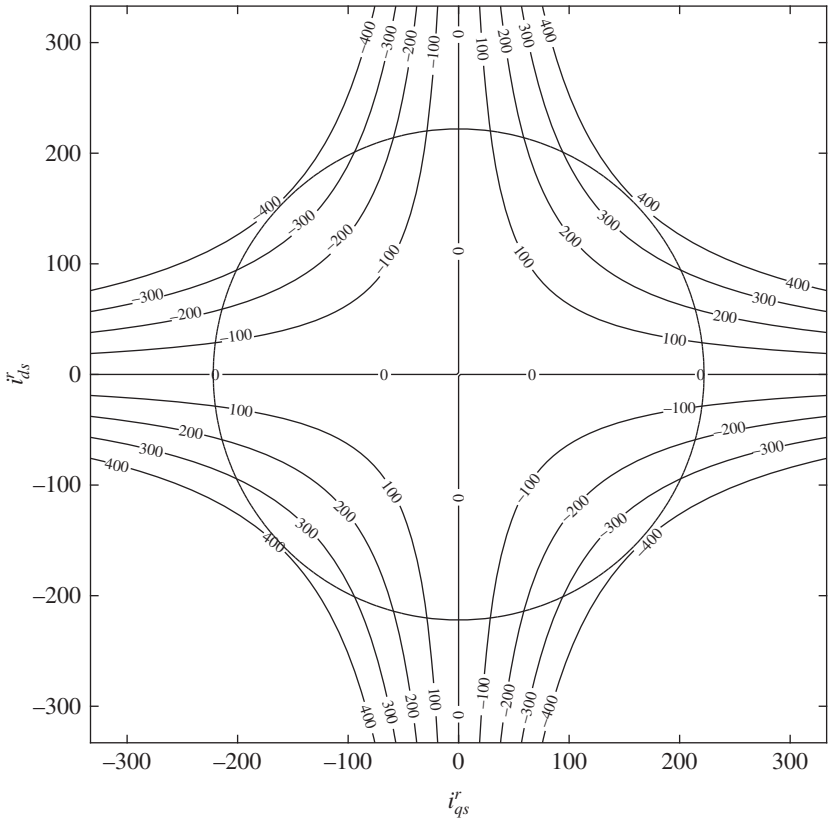

Figure 12.4-1 Contour plots for various values of torque, T_e.

It is readily shown analytically that for a given value of T_e, I^r_{qs} should be set equal to I^r_{ds} in order to minimize $I_s = \sqrt{\left(I^r_{qs}\right)^2 + \left(I^r_{ds}\right)^2}$ (left as a homework exercise for the reader). The optimal currents are plotted in Fig. 12.4-2 as a function of torque, assuming there is no voltage constraint that would limit the currents.

When a voltage constraint is involved, however, the situation is analytically more complicated and a numerical procedure to establish the maximum and minimum torque and the optimal currents is warranted. Fortunately, the procedure previously used to establish these for a permanent-magnet machine may also be used for the reluctance machine with only minor modifications. The current and voltage limits given by (12.2-2) and (12.2-3) are the same for the synchronous reluctance machine. However, the steady-state voltage (constraint) equations are now

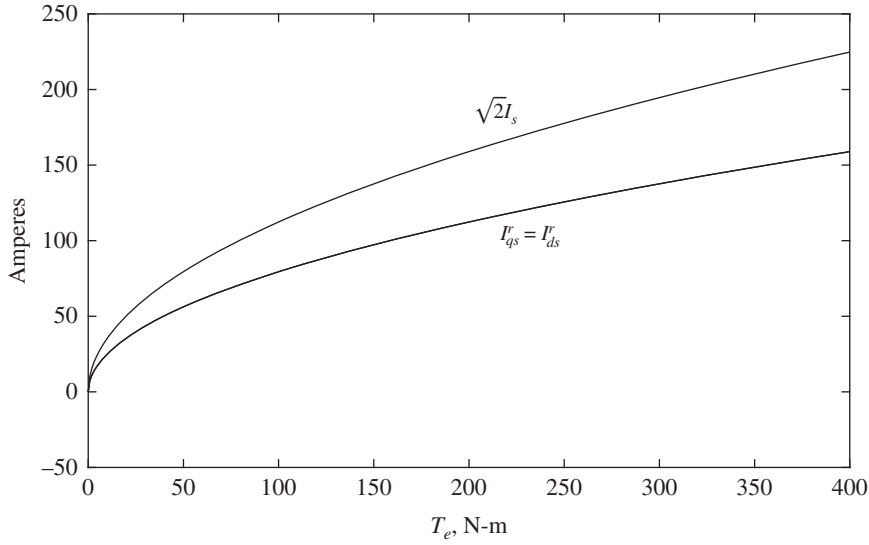

Figure 12.4-2 Optimal currents versus torque without voltage constraint.

$$V^r_{qs} = r_s I^r_{qs} + \omega_r L_d I^r_{ds} \tag{12.4-2}$$

$$V^r_{ds} = r_s I^r_{ds} - \omega_r L_q I^r_{qs} \tag{12.4-3}$$

which is the same as in the permanent-magnet machine less the $\omega_r \lambda_m$ term. Repeating the procedure used for the permanent-magnet machine, the maximum and minimum torque are plotted as a function of electrical rotor speed in Fig. 12.4-3, which can be compared to Fig. 12.2-4. The currents and voltages needed to produce maximum torque are shown in Figs. 12.4-4 and 12.4-5, respectively.

The maximum mechanical power and the efficiency at maximum power are plotted as a function of electrical rotor speed in Figs. 12.4-6 and 12.4-7, respectively. These can be compared with Figs. 12.2-7 and 12.2-8 for the permanent-magnet machine. The general shape of the maximum torque and maximum power versus speed plots is very similar; only the numerical values differ. Interestingly, maximum torque is comparable, and the maximum power is somewhat larger in the synchronous reluctance machine than in the permanent-magnet machine with the same voltage and current constraints. However, the maximum power decreases more rapidly as the rotor speed increases with a value of 22.9 kW at 2000 rad/s. The maximum efficiency is also somewhat lower.

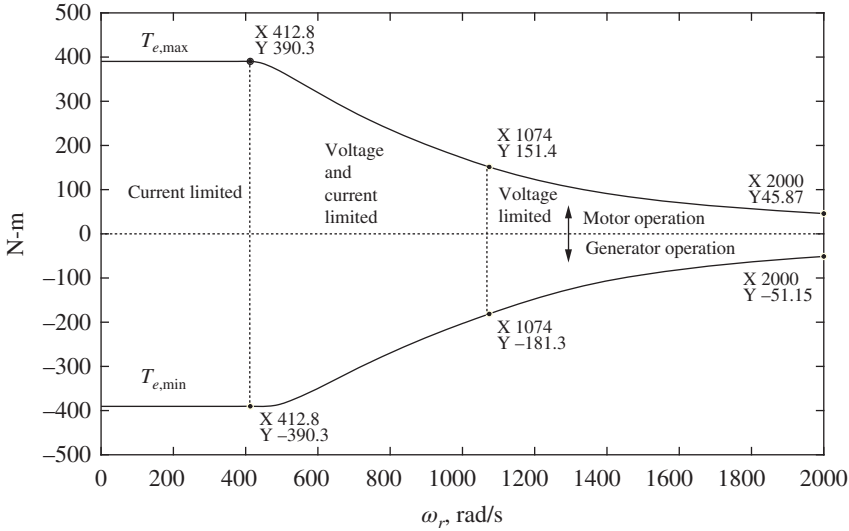

Figure 12.4-3 Maximum and minimum torque as a function of electrical rotor speed.

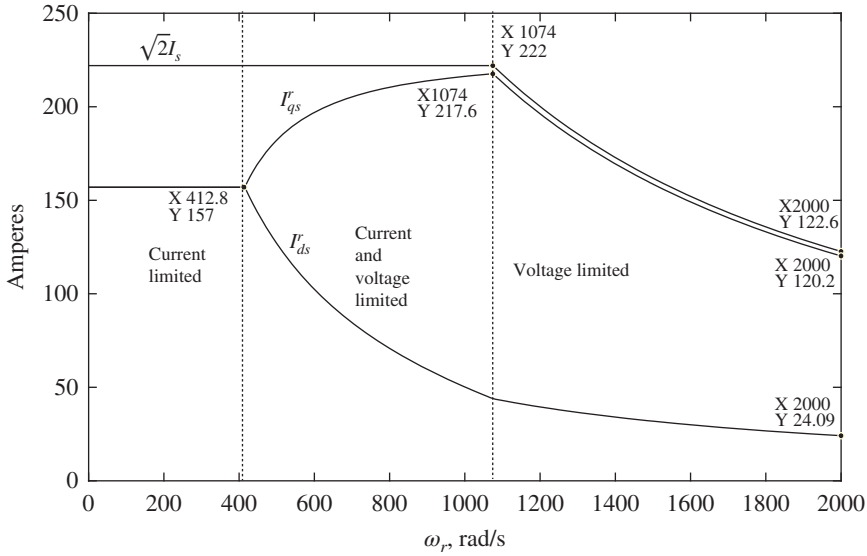

Figure 12.4-4 Optimum stator currents versus speed for maximum torque.

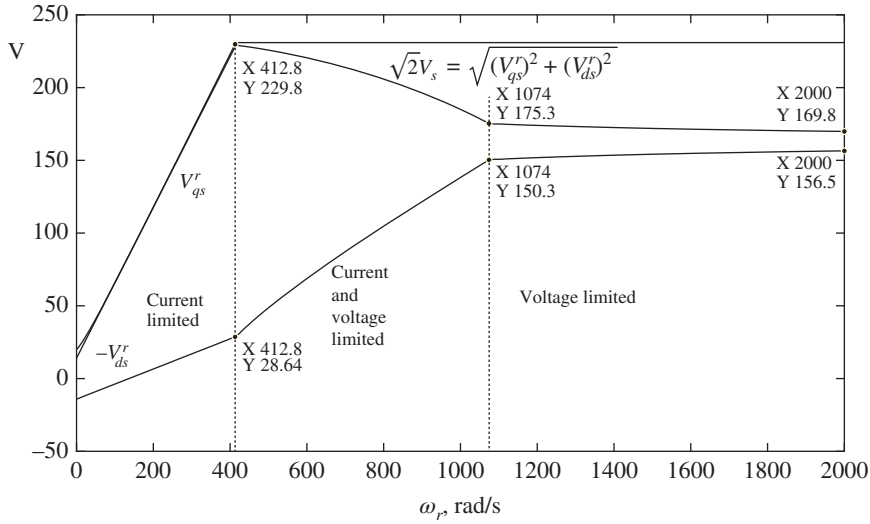

Figure 12.4-5 Voltages needed for maximum torque.

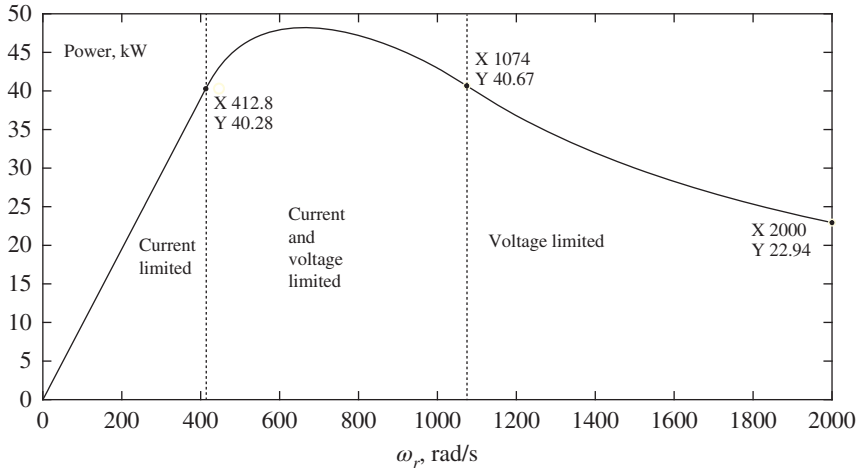

Figure 12.4-6 Maximum mechanical power versus rotor speed.

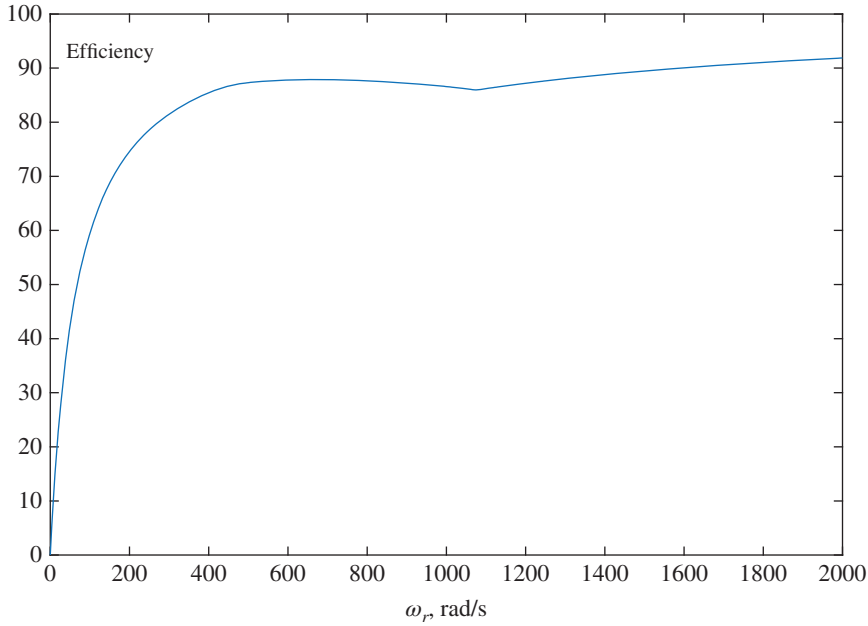

Figure 12.4-7 Efficiency for maximum T_e.

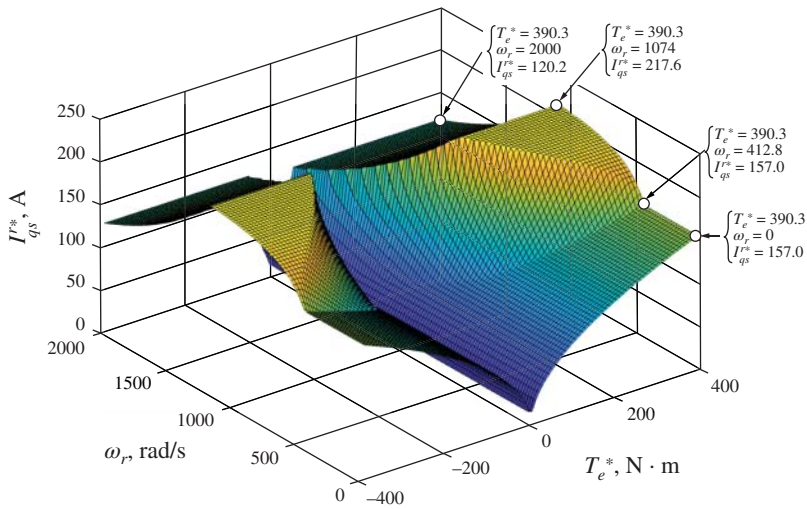

Figure 12.4-8 Plot of $I_{qs}^{r*}\left(\omega_r, T_e^*\right)$.

In the preceding figures, it is assumed that the motor is operating at maximum or minimum torque. Typically, however, the desired torque will lie somewhere between these values. To minimize stator winding losses, it is desired to select I_{qs}^{r*} and I_{ds}^{r*} that produces the desired torque T_e^* with minimum peak stator current. As in the permanent-magnet machine, I_{qs}^{r*} and I_{ds}^{r*} will, in general, be functions of both T_e^* and ω_r for the same reasons. Moreover, the same procedure used to generate $I_{qs}^{r*}\left(T_e^*, \omega_r\right)$ and $I_{ds}^{r*}\left(T_e^*, \omega_r\right)$ for the permanent-magnet machine can be used for the synchronous reluctance machine. The results are shown in Figs. 12.4-8 and 12.4-9. Interestingly, the general shapes of the optimal $I_{qs}^{r*}\left(T_e^*, \omega_r\right)$ and $I_{ds}^{r*}\left(T_e^*, \omega_r\right)$ plots for the reluctance machine are, respectively, similar to $I_{ds}^{r*}\left(T_e^*, \omega_r\right)$ and $I_{qs}^{r*}\left(T_e^*, \omega_r\right)$ for the permanent-magnet machine. The reader is reminded that the q and d subscripts were interchanged by choice earlier in this section. The data used to generate Figs. 12.4-8 and 12.4-9 can be stored in lookup tables as part of a torque control system.

The method of torque control described for the permanent-magnet machine can also be used for the synchronous reluctance machine. Figures 12.3-1–12.3-4 and 12.3-8 may be applied to the synchronous reluctance machine simply by setting $\lambda_m'^r$ to zero in Figs. 12.3-2 and 12.3-3 and updating the lookup tables in Figs. 12.3-1, 12.3-4, and 12.3-8 to correspond to the data plotted in Figs. 12.4-8 and 12.4-9. These modifications are so minor that these figures will not be repeated here.

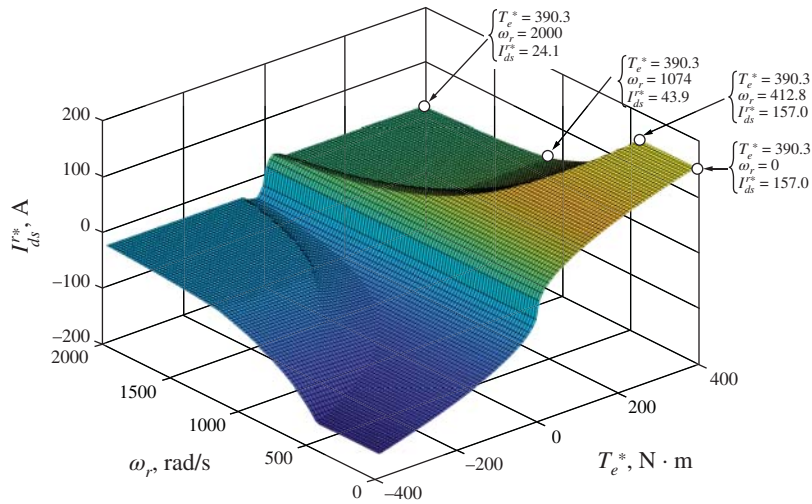

Figure 12.4-9 Plot of $I_{ds}^{r*}\left(\omega_r, T_e^*\right)$.

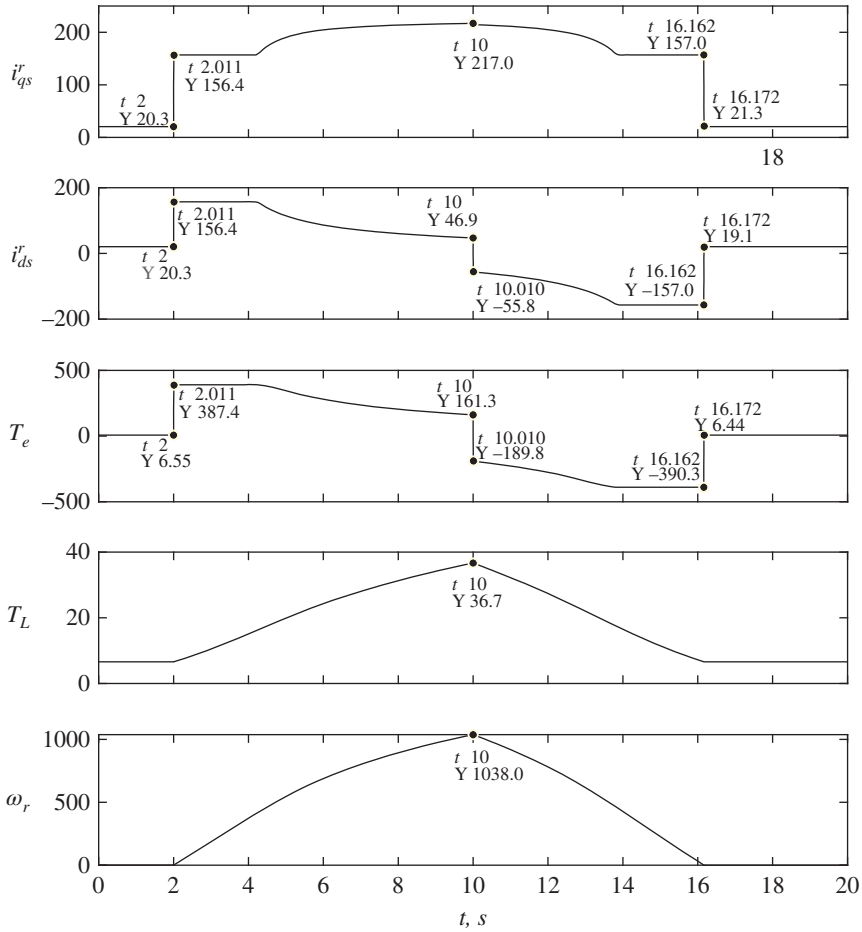

Figure 12.4-10 Torque command stepped from 6.57 to 400 N · m at $t = 2$ s, then to −400 at $t = 10$ s.

The simulation studies portrayed in Figs. 12.3-5 and 12.3-8 were repeated for the synchronous reluctance machine. The results are shown in Figs. 12.4-10 (full-order model) and 12.4-11 (reduced-order model with electric and control transients neglected). The responses are very similar in appearance to those shown in Figs. 12.3-5 and 12.3-9; only the numerical values are different. As in the permanent-magnet machine, the electric machine and control transients are short-lived and do not significantly affect the longer-term mechanical response.

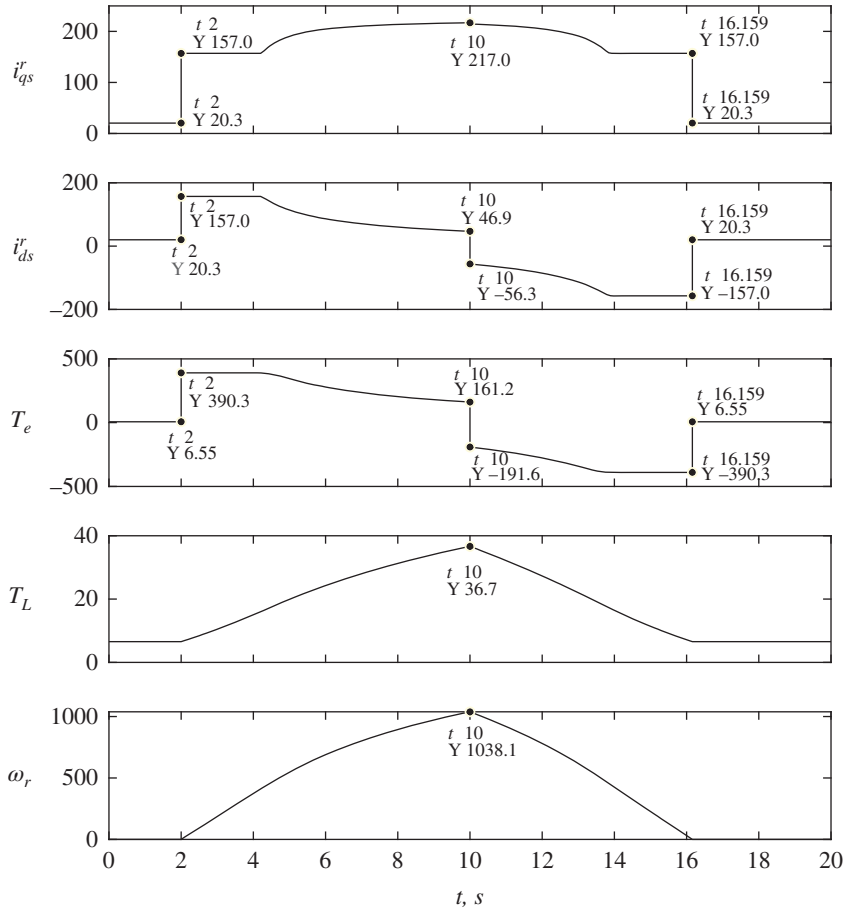

Figure 12.4-11 Same as Fig. 12.4-10 with the electric machine and control transients neglected.

References

1 P. Krause, O. Wasynczuk, S. Pekarek, T. O'Connell, *Electromechanical Motion Devices*, IEEE Press and John Wiley, 2022.

2 P. Krause, T. Krause, *Introduction to Modern Analysis of Electric Machines and Devices*, IEEE Press and John Wiley, 2023.

3 J. H. Hsu, C. W. Ayers, C. L. Coomer, R. H. Wiles, S. L. Campbell, K. T. Lowe, R. T. Michelhaugh. Report on Toyota/Prius Motor Torque Capability,

Torque-Property, No-load Back EMF and Mechanical Losses. United States Department of Energy, 2004.
4 https://www.mathworks.com/help/optim/ug/fmincon.html
5 https://docs.scipy.org/doc/scipy/reference/generated/scipy.optimize.minimize.html
6 E. S. Calvo and D. Potoradi. "Synchronous Reluctance Motors With and Without Permanent Magnets for High Performance Low Cost Electrical Drives." In 2015 5th International Electric Drives Production Conference (EDPC), pp. 1–7. IEEE, 2015.
7 N. Bianchi, S. Bolognani, E. Carraro, M. Castiello, and E. Fornasiero. "Electric Vehicle Traction Based on Synchronous Reluctance Motors." *IEEE Trans. Ind. Appl.* 52, no. 6 (2016): 4762–4769.
8 Jin, Xing, Oleg Wasynczuk, and Gregory M. Shaver. "Computationally Efficient and Flexible Magnetic-Field-Analysis-Based Scaling Strategy for Permanent-Magnet Machines." *IEEE PES* 33, no. 3 (2018): 1222–1232.

Problems

12.1 Consider Fig. 12.2-3. Assume it is desired to produce 400 N · m of torque at $\omega_r = 2000$ rad/s. Calculate V_{qs}^r and V_{ds}^r to achieve this goal.

12.2 For the I_{qs}^r and I_{qs}^r values given in Fig. 12.2-5 that maximize torque at $\omega_r = 360.7$ rad/s, establish V_{qs}^r, V_{ds}^r, and V_s. Verify $V_s \le V_{s,\max}$.

12.3 Repeat Problem 2 for $\omega_r = 541.1$ rad/s.

12.4 Develop a MATLAB or Python script that generates (similar to Figs. 12.2-5 and 12.2-6) plots of I_{qs}^r, I_{qs}^r, I_s, V_{qs}^r, V_{ds}^r, and V_s that minimizes (maximizes negative) torque for the machine parameters given in Section 12.2.

12.5 Derive (12.3-5) and (12.3-6). Hint: start with $v_{qs}^r = r_s i_{qs}^r + \omega_r \left(\lambda_m' + L_d i_{ds}^r\right) + L_q p i_{qs}^r$ and $v_{ds}^r = r_s i_{ds}^r - \omega_r L_q i_{qs}^r + L_d p i_{ds}^r$ and assume $v_{qs}^r = v_{qs}^{r*}$, $v_{ds}^r = v_{ds}^{r*}$.

12.6 In a reluctance machine, $T_e = K i_{qs}^r i_{ds}^r$. Show analytically that to minimize $\sqrt{2} I_s = \sqrt{\left(I_{qs}^r\right)^2 + \left(I_{ds}^r\right)^2}$ for a given value of T_e, the q- and d-axis components of the stator currents should be equal, $i_{qs}^r = i_{ds}^r$.

12.7 For the permanent-magnet machine considered in Section 12.2, the desired torque is 100 N · m. Using MATLAB's fmincon or Python's scipy.optimize.minimize, establish I_{qs}^r and I_{ds}^r that gives the desired torque

while minimizing $\sqrt{2}I_s = \sqrt{\left(I^r_{qs}\right)^2 + \left(I^r_{ds}\right)^2}$. Then, determine the corresponding V^r_{qs} and V^r_{ds}. Assume there are no voltage or current constraints. Sketch the phasor diagram (see Fig. 12.2-9).

12.8 For the operating condition in Problem 2, calculate the electric power in, the mechanical power out, and the efficiency.

12.9 Repeat Problems 4 and 7 for the synchronous reluctance machine described in Section 12.4.

13

Induction Motor Drives

13.1 Introduction

The objective of this chapter is to explore the use of induction machines in variable-speed drive systems. Several strategies will be considered herein. The first, volts-per-hertz control, is designed to accommodate variable-speed commands by using the inverter to apply a voltage of correct magnitude and frequency so as to approximately achieve the commanded speed without the use of speed feedback. The second strategy is constant slip control. In this control, the drive system is designed so as to accept a torque command input—and therefore speed control requires and additional feedback loop. Although this strategy requires the use of a speed sensor, it has been shown to be highly robust with respect to changes in machine parameters and results in high efficiency of both the machine and inverter. One of the disadvantages of this strategy is that in closed-loop speed-control situations, the response can be somewhat sluggish. Another strategy considered is field-oriented control. In this method, nearly instantaneous control of torque can be obtained. A disadvantage of this strategy is that in its direct form, the sensor requirements are significant, and in its indirect form, it is sensitive to parameter measurements unless online parameter estimation or other steps are taken. Another method of controlling torque, called direct torque control (DTC), is also described, and its performance illustrated by computer traces. Finally, slip energy recovery systems, such as those used in modern variable-speed wind turbines, are described.

13.2 Volts-Per-Hertz Control

Perhaps the simplest and least expensive induction motor drive strategy is constant volt-per-hertz control. This is a speed control strategy that is based on two observations. The first of these is that the torque speed characteristic of an induction

Analysis of Electric Machinery and Drive Systems, Fourth Edition.
Paul C. Krause, Oleg Wasynczuk, Scott D. Sudhoff, and Steven D. Pekarek.

Companion website: www.wiley.com/go/krause_aem4e

machine is normally quite steep in the neighborhood of synchronous speed, and so the electrical rotor speed will be near to the electrical frequency. Thus, by controlling the frequency, one can approximately control the speed. The second observation is based on the a-phase voltage equation, which may be expressed

$$v_{as} = r_s i_{as} + p\lambda_{as} \tag{13.2-1}$$

For steady-state conditions at mid- to high speeds wherein the flux linkage term dominates the resistive term in the voltage equation, the magnitude of the applied voltage is related to the magnitude of the stator flux linkage by

$$V_s = \omega_e \Lambda_s \tag{13.2-2}$$

which suggests that in order to maintain constant flux linkage (to avoid saturation), the stator voltage magnitude should be proportional to frequency.

Figure 13.2-1 illustrates one possible implementation of a constant volts-per-hertz drive. Therein, the speed command, denoted by ω_{rm}^*, acts as input to a slew rate limiter (SRL), which acts to reduce transients by limiting the rate of change of the speed command to values between $\alpha_{\min}$ and $\alpha_{\max}$. The output of the SRL is multiplied by $P/2$, where P is the number of poles in order to arrive at the electrical rotor speed command ω_r^* to which the radian electrical frequency ω_e is set. The electrical frequency is then multiplied by the volts-per-hertz ratio V_b/ω_b, where V_b is rated voltage, and ω_b is rated radian frequency in order to form an rms voltage command V_s. The rms voltage command V_s is then multiplied by $\sqrt{2}$ in order to obtain a q-axis voltage command v_{qs}^{e*} (the voltage is arbitrarily placed in the q-axis). The d-axis voltage command is set to zero. In a parallel path, the electrical frequency ω_e is integrated to determine the position of a synchronous reference frame θ_e. The integration to determine θ_e is periodically reset by an integer multiple of 2π in order to keep θ_e bounded. Together, the q- and d-axis voltage commands may then be passed to any one of a number of modulation strategies in order to achieve the commanded voltage as discussed in Chapter 10. The advantages of this control are that it is simple, and that it is relatively inexpensive by virtue of being entirely open loop; speed can be controlled (at least

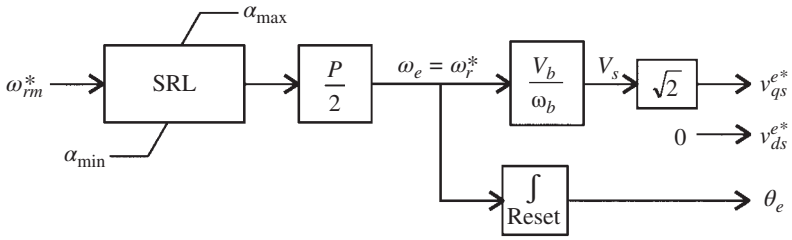

Figure 13.2-1 Elementary volts-per-hertz drive.

to a degree) without feedback. The principal drawback of this type of control is that because it is open loop, some measure of error will occur, particularly at low speeds.

Figure 13.2-2 illustrates the steady-state performance of the voltage-per-hertz drive strategy shown in Figure 13.2-1. In this study, the machine is a 50-hp, four-pole, 1800-rpm, 460-V (line-to-line, rms) with the following parameters: $r_s = 72.5\ \text{m}\Omega$, $L_{ls} = 1.32\ \text{mH}$, $L_M = 30.1\ \text{mH}$, $L'_{lr} = 1.32\ \text{mH}$, $r'_r = 41.3\ \text{m}\Omega$, and the load torque is assumed to be of the form

$$T_L = T_b \left(0.1S(\omega_{rm}) + 0.9 \left(\frac{\omega_{rm}}{\omega_{bm}} \right)^2 \right) \tag{13.2-3}$$

where $S(\omega_{rm})$ is a stiction function that varies from 0 to 1 as ω_{rm} goes from 0 to 0^+. Figure 13.2-2 illustrates the percent error in speed $100\left(\omega^*_{rm} - \omega_{rm}\right)/\omega^*_{rm}$, normalized voltage V_s/V_b, normalized current I_s/I_b, efficiency η, and normalized air-gap flux linkage λ_m/λ_b versus normalized speed command $\omega^*_{rm}/\omega_{bm}$. The base for the air-gap flux linkage is taken to be the no-load air-gap flux linkage that is obtained at rated speed and rated voltage.

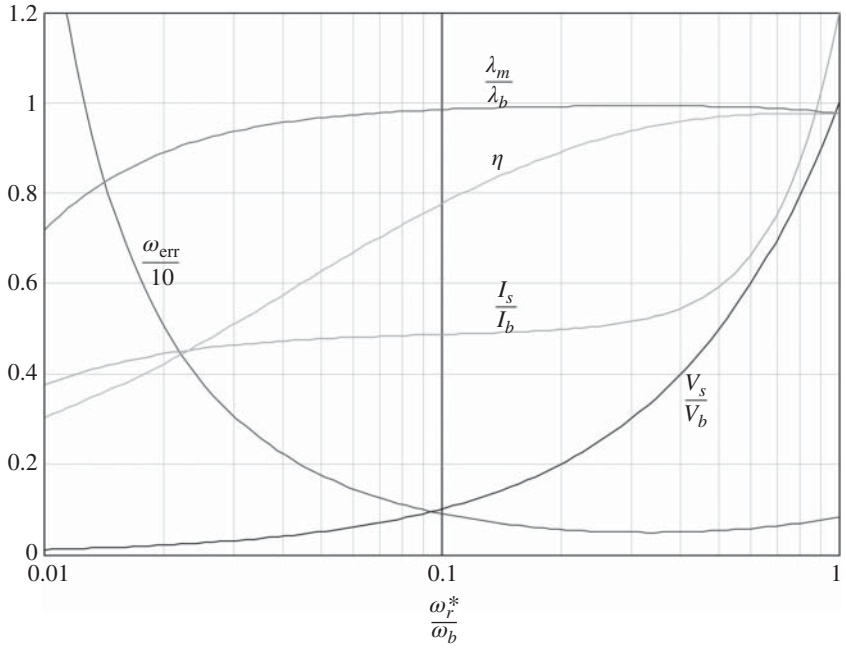

Figure 13.2-2 Performance of elementary volts-per-hertz drive.

As can be seen, the voltage increases linearly with speed command, while the rms current remains approximately constant until about 0.5 pu and then rises to approximately 1.2 pu at a speed command of 1 pu. Also, it is evident that the percent speed error remains less than 1% for speeds from 0.1 to 1 pu; however, the speed error becomes quite large for speeds less than 0.1 pu. The reason for this is the fact that the magnetizing flux drops to zero as the speed command goes to zero due to the fact that the resistive term dominates the flux-linkage term in (13.2-1) at low speeds. As a result, the torque-speed curve loses its steepness about synchronous speed, resulting in larger percentage error between commanded and actual speed.

The low-speed performance of the drive can be improved by increasing the voltage command at low frequencies in such a way as to make up for the resistive drop. One method of doing this is based on the observation that the open-loop speed regulation becomes poorer at low speeds, because the torque-speed curve becomes decreasingly steep as the frequency is lowered if the voltage is varied in accordance with (13.2-2). To prevent this, it is possible to vary the rms voltage in such a way that the slope of the torque-speed curve at synchronous speed becomes independent of the electrical frequency. Taking the derivative of torque with respect to rotor speed in (3.8-20) about synchronous speed for an arbitrary electrical frequency and setting it equal to the same derivative about base electrical frequency yields

$$V_s = V_b \sqrt{\frac{r_{s,est}^2 + \omega_e^2 L_{ss,est}^2}{r_{s,est}^2 + \omega_b^2 L_{ss,est}^2}} \tag{13.2-4}$$

where $r_{s,est}$ and $L_{ss,est}$ are the estimated value of r_s and L_{ss}, respectively. The block diagram of this version of volts-per-hertz control is identical to that shown in Figure 13.2-1, with the exception that (13.2-4) replaces (13.2-2). Several observations are in order. First, it can be readily shown that varying the voltage in accordance with (13.2-4) will yield the same air-gap flux at zero frequency as is seen for no load conditions at rated frequency—thus the air-gap flux does not fall to zero at low frequency as it does when (13.2-2) is used. It is also interesting to observe that (13.2-4) reduces to (13.2-2) at a frequency such that $\omega_e L_{ss,est} \gg r_{s,est}$.

In order to further increase the performance of the drive, one possibility is to utilize the addition of current feedback in determining the electrical frequency command. Although this requires at least one (but more typically two) current sensor(s) that will increase cost, it is often the case that a current sensor(s) will be utilized in any case for overcurrent protection of the drive. In order to derive an expression for the correct feedback, first note that near synchronous speed, the electromagnetic torque may be approximated as

$$T_e = K_{tv}(\omega_e - \omega_r) \tag{13.2-5}$$

where

$$K_{tv} = -\left.\frac{\partial T_e}{\partial \omega_r}\right|_{\omega_r = \omega_e} \tag{13.2-6}$$

If (13.2-4) is used

$$K_{tv} = \frac{3\left(\frac{P}{2}\right) L_{Ms}^2 r_r' V_b^2}{r_r'^2 \left(r_s^2 + \omega_b^2 L_{ss}^2\right)} \tag{13.2-7}$$

regardless of synchronous speed. Next, note that from (3.5-9), torque may be expressed as

$$T_e = \frac{3}{2}\frac{P}{2}\left(\lambda_{ds}^e i_{qs}^e - \lambda_{qs}^e i_{ds}^e\right) \tag{13.2-8}$$

From (3.4-18) and (3.4-19), for steady-state conditions, the stator flux linkage equations may be expressed as

$$\lambda_{ds}^e = \frac{v_{qs}^e - r_s i_{qs}^e}{\omega_e} \tag{13.2-9}$$

and

$$\lambda_{qs}^e = -\frac{v_{ds}^e - r_s i_{ds}^e}{\omega_e} \tag{13.2-10}$$

Approximating v_{qs}^e by its commanded value of v_{qs}^{e*} and v_{ds}^e by its commanded value of zero in (13.2-9) and (13.2-10) and substitution of the results into (13.2-8) yields

$$T_e = \frac{3}{2}\frac{P}{2}\frac{1}{\omega_e}\left(v_{qs}^{e*} i_{qs}^e - 2 r_s I_s^2\right) \tag{13.2-11}$$

where

$$I_s = \frac{1}{\sqrt{2}}\sqrt{i_{qs}^{e2} + i_{ds}^{e2}} \tag{13.2-12}$$

Equating (13.2-7) and (13.2-11) and solving for ω_e yields

$$\omega_e = \frac{\omega_r^* + \sqrt{\omega_r^{*2} + 3P\left(v_{qs}^{e*} i_{qs}^e - 2 r_s I_s^2\right)/K_{tv}}}{2} \tag{13.2-13}$$

In practice, (13.2-13) is implemented as

$$\omega_e = \frac{\omega_r^* + \sqrt{\max\left(0,\ \omega_r^{*2} + \mathrm{X}_{corr}\right)}}{2} \tag{13.2-14}$$

where

$$\mathrm{X}_{corr} = H_{LPF}(s)\chi_{corr} \tag{13.2-15}$$

and where

$$\chi_{corr} = 3P\left(v_{qs}^{e*} i_{qs}^e - 2 r_s I_s^2\right)/K_{tv} \tag{13.2-16}$$

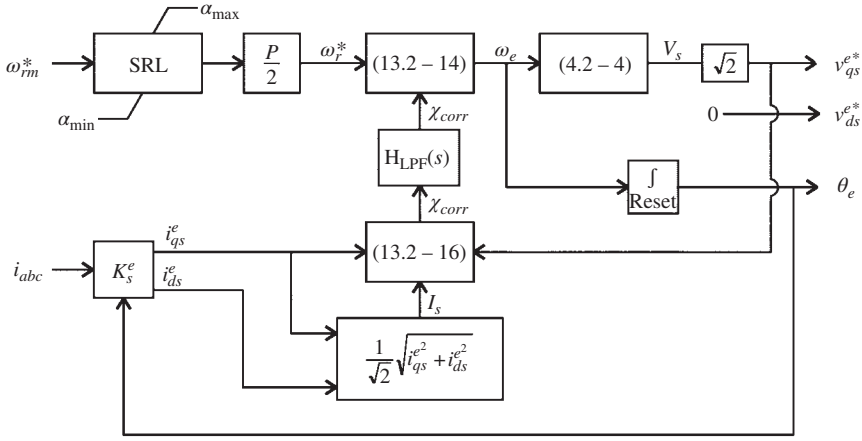

Figure 13.2-3 Compensated volts-per-hertz drive.

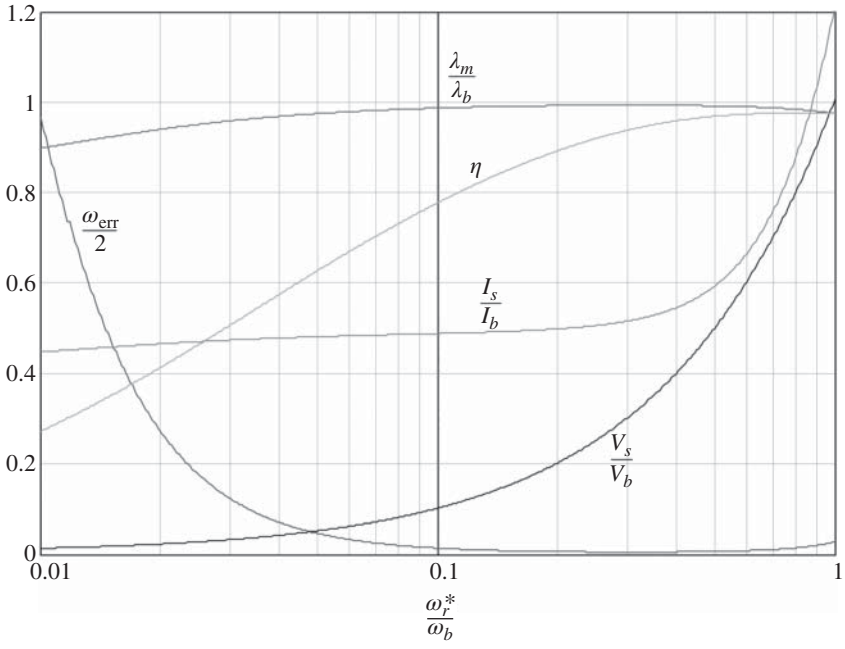

Figure 13.2-4 Performance of compensated volts-per-hertz drive.

In (13.2-15), $H_{LPF}(s)$ represents the transfer function of a low-pass filter, which is required for stability and to remove noise from the measured variables. This filter is often simply a first-order lag filter. The resulting control is depicted in Figure 13.2-3.

Figure 13.2-4 illustrates the steady-state performance of the compensated voltage-per-hertz drive for the same operating conditions as those of the study depicted in Figure 13.2-2. Although in many ways the characteristic shown in Figure 13.2-4 are similar to those of Figure 13.2-2, there are two important differences. First, the air-gap flux does not go to zero at low speed commands. Second, the speed error is dramatically reduced over the entire operating range of drive. In fact, the speed error using this strategy is less than 0.1% for speed commands ranging from 0.1 to 1.0 pu—without the use of a speed sensor.

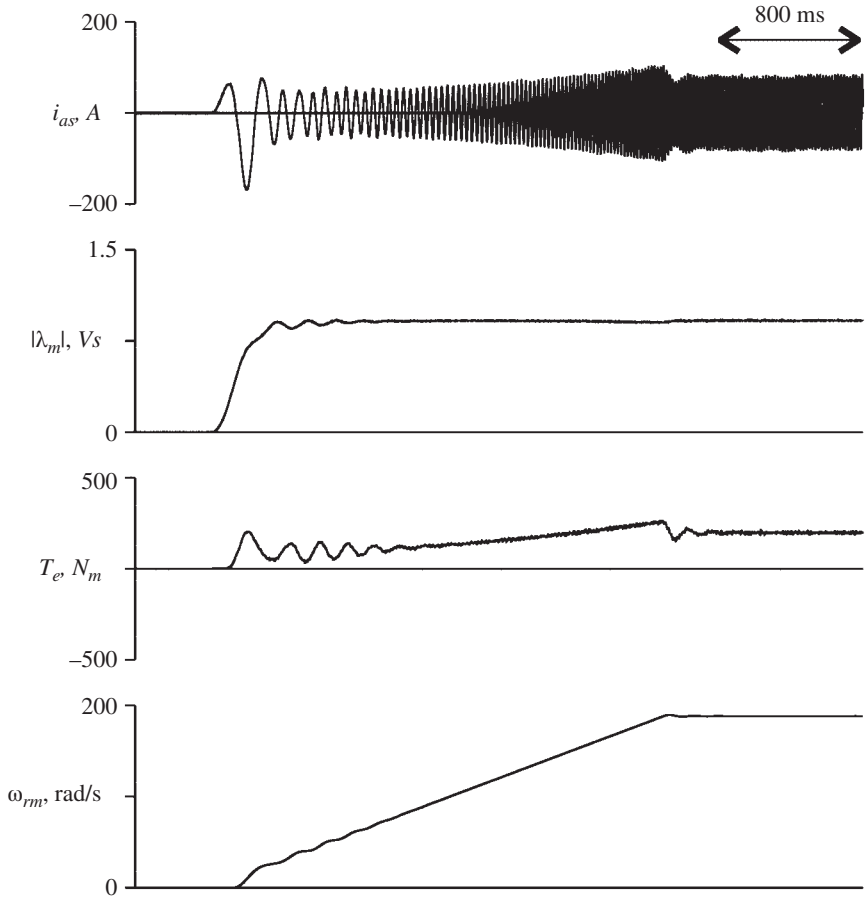

Figure 13.2-5 Start-up performance of compensated volts-per-hertz drive.

In practice, Figure 13.2-4 is over optimistic for two reasons. First, the presence of a large amount of stiction can result in reduced low-speed performance (the machine will simply stall at some point). Second, it is assumed in the development that the desired voltage is applied. At extremely low commanded voltages, semiconductor voltage drops, and the effects of dead time can become important and result in reduced control fidelity. In this case, it is possible to use either closed loop (such as discussed in Section 13.11) or open-loop compensation techniques to help ensure that the desired voltages are actually obtained.

Figure 13.2-5 illustrates the start-up performance of the drive for the same conditions as Figure 13.2-2. In this study, the total mechanical inertia is taken to be 8.2 N m s^2, and the low-pass filter used to calculate X_{corr} was taken to be a first-order lag filter with a 0.1-second time constant. The acceleration limit, $\alpha_{\max}$, was set to 75.4 rad/s^2. Variables depicted in Figure 13.2-5 include the mechanical rotor speed ω_{rm}, the electromagnetic torque T_e, the peak magnitude of the air-gap flux linkage $\lambda_m = \sqrt{\lambda_{qm}^2 + \lambda_{dm}^2}$, and finally the a-phase current i_{as}. Initially, the drive is completely off; approximately 0.6 second into the study, the mechanical rotor speed command is stepped from 0 to 188.5 rad/s. As can be seen, the drive comes to speed in roughly 3 seconds, and the build up in speed is essentially linear (following the output of the slew rate limit). The air-gap flux takes some time to reach rated value; however, after approximately 0.5 second, it is close to its steady state value. The a-phase current is very well behaved during start-up, with the exception of an initial (negative) peak—this was largely the result of the initial dc offset. Although the drive could be brought to rated speed more quickly by increasing the slew rate, this would have required a larger starting current and therefore a larger and more costly inverter. There are several other compensations techniques set forth in the literature [1, 2].

13.3 Constant Slip Current Control

Although the three-phase bridge inverter is fundamentally a voltage source device, by suitable choice of modulation strategy (such as be hysteresis or delta modulation), it is possible to achieve current source based operation. One of the primary disadvantages of this approach is that it requires phase current feedback (and its associated expense); however, at the same time, this offers the advantage that the current is readily limited, making the drive extremely robust, and, as a result, enabling the use of less conservatism when choosing the current ratings of the inverter semiconductors.

One of the simplest strategies for current control operation is to utilize a fixed-slip frequency, defined as

$$\omega_s = \omega_e - \omega_r \tag{13.3-1}$$

By appropriate choice of the radian slip frequency, ω_s, several interesting optimizations of the machine performance can be obtained, including achieving the optimal torque for a given value of stator current (maximum torque per amp), as well as the maximum efficiency [3, 4].

In order to explore these possibilities, it is convenient to express the electromagnetic torque as given by (3.8-17) in terms of slip frequency, which yields

$$T_e = \frac{3\left(\frac{P}{2}\right)\omega_s L_{Ms}^2 I_s^2 r_r'}{\left(r_r'\right)^2 + \left(\omega_s L_{rr}'\right)^2} \tag{13.3-2}$$

From (13.3-2), it is apparent that in order to achieve a desired torque T_e^* utilizing a slip frequency ω_s, the rms value of the fundamental component of the stator current should be set in accordance with

$$I_s = \sqrt{\frac{2\left|T_e^*\right|\left(r'^2_{r,est} + \left(\omega_s L'_{rr,est}\right)^2\right)}{3P|\omega_s|L_{Ms,est}^2 r'_{rr,est}}} \tag{13.3-3}$$

In (13.3-3), the parameter subscripts in (13.3-2) have been augmented with "est" in order to indicate that this relationship will be used in a control system in which the parameter values reflect estimates of the actual values.

As alluded to previously, the development here points toward control in which the slip frequency is held constant at a set value $\omega_{s,set}$. However, before deriving the value of slip frequency to be used, it is important to establish when it is reasonable to use a constant slip frequency. The fundamental limitation that arises in this regard is magnetic saturation. In order to avoid overly saturating the machine, a limit must be placed on the flux linkages. A convenient method of accomplishing this is to limit the rotor flux linkage. From the steady-state equivalent circuit, the a-phase rotor flux linkage may be expressed as

$$\tilde{\lambda}_{ar} = L_{lr}\tilde{I}'_{ar} + L_{Ms}\left(\tilde{I}_{as} + \tilde{I}'_{ar}\right) \tag{13.3-4}$$

From the steady state equivalent circuit it is also clear that

$$\tilde{I}'_{ar} = -\tilde{I}_{as}\frac{j\omega_e L_{Ms}}{j\omega_e L'_{rr} + r'_r/s} \tag{13.3-5}$$

Substitution of (13.3-5) into (13.3-4) yields

$$\tilde{\lambda}'_{ar} = \tilde{I}_{as} L_{Ms}\frac{r'_r}{j\omega_s L'_{rr} + r'_r} \tag{13.3-6}$$

Taking the magnitude of both sides of (13.3-6) yields

$$\lambda_r = I_s L_{Ms}\frac{r'_r}{\sqrt{\omega_s^2 L'^2_{rr} + r'^2_r}} \tag{13.3-7}$$

where λ_r and I_s are the rms value of the fundamental component of the referred a-phase rotor flux linkage and a-phase stator current, respectively. Combining (13.3-7) with (13.3-2) yields

$$T_e = 3\frac{P}{2}\frac{\omega_s \lambda_r^2}{r_r'} \tag{13.3-8}$$

Now, if a constant slip frequency $\omega_{s,set}$ is used, and the rotor flux is limited to $\lambda_{r,\max}$, then the maximum torque that can be achieved in such an operating mode, denoted $T_{e,thresh}$, is

$$T_{e,thresh} = 3\frac{P}{2}\frac{\omega_{s,set}\lambda_{r,\max}^2}{r_{r,est}'} \tag{13.3-9}$$

From (13.3-8), for torque commands in which $|T_e^*| > T_{e,thresh}$, the slip must be varied in accordance with

$$\omega_s = \frac{2T_e^* r_{r,est}'}{3P\lambda_{r,\max}^2} \tag{13.3-10}$$

Figure 13.3-1 illustrates the combination of the ideas into a coherent control algorithm. As can be seen, based on the magnitude of the torque command, the magnitude of the slip frequency ω_s is either set equal to the set point value $\omega_{s,set}$ or to the value arrived at from (13.3-10), and the result is given the sign of T_e^*. The slip frequency ω_s and torque command T_e^* are together used to calculate the rms magnitude of the fundamental component of the applied current I_s, which is scaled by $\sqrt{2}$ in order to arrive at a q-axis current command i_{qs}^{e*}. The d-axis current command i_{ds}^{e*} is set to zero. Of course, the placement of the current command into the q-axis was completely arbitrary; it could have just as well been put in the d-axis or any combination of the two provided the proper magnitude is obtained. In addition to being used to determine I_s, the slip frequency ω_s is added to the electrical rotor speed ω_r in order to arrive at the electrical frequency ω_e, which is in turn integrated in order to yield the position of the synchronous reference frame θ_e.

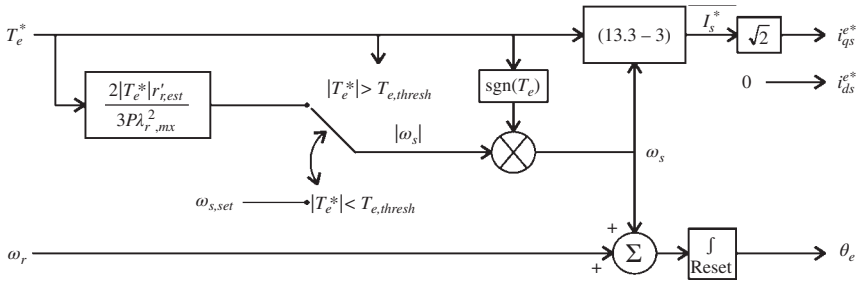

Figure 13.3-1 Constant slip frequency drive.

There are a variety of ways to achieve the commanded q- and d-axis currents as discussed in Chapter 10. Finally, it should also be observed that the control depicted in Figure 13.3-1 is a torque rather than speed control system; speed control is readily achieved through a separate control loop in which the output is a torque command. Using this approach, it is important that the speed control loop is set to be slow relative to the torque controller, which can be shown to have a dynamic response on the order of the rotor time constant.

One remaining question is the selection of the slip frequency set point $\omega_{s,set}$. Herein, two methods of selection are considered; the first will maximize torque for a given stator current and the second will maximize the machine efficiency. In order to maximize torque for a given stator current, note that by setting $\omega_s = \omega_{s,set}$ in (13.3-1), torque is maximized for a given stator current by maximizing the ratio

$$\frac{T_e}{I_s^2} = \frac{3\left(\frac{P}{2}\right)\omega_{s,set}L_{Ms}^2 r_r'}{\left(r_r'\right)^2 + \left(\omega_{s,set}L_r'\right)^2} \tag{13.3-11}$$

Setting the derivative of the right-hand side of (13.3-11) with respect to $\omega_{s,set}$ equal to zero and solving for $\omega_{s,set}$ yields the value of $\omega_{s,set}$, which maximizes the torque for a given stator current. This yields

$$\omega_{s,set} = \frac{r'_{r,est}}{L'_{rr,est}} \tag{13.3-12}$$

In order to obtain an expression for slip frequency that will yield maximum efficiency, it is convenient to begin with an expression for the input power of the machine. With $\widetilde{I}_{as} = I_s$, the input power may be expressed as

$$P_{\text{in}} = 3I_s \text{Re}(\widetilde{V}_{as}) \tag{13.3-13}$$

Using the induction motor equivalent circuit model, it is possible to expand (13.3-13) to

$$P_{\text{in}} = 3r_s I_s^2 + \frac{3I_s^2\omega_e L_{Ms}^2\omega_s r_r'}{r_r'^2 + \left(\omega_s L_{rr}'\right)^2} \tag{13.3-14}$$

Comparison of (13.3-14) to (13.3-2) yields

$$P_{\text{in}} = 3r_s I_s^2 + \frac{2}{P}\omega_e T_e \tag{13.3-15}$$

Noting that $\omega_e = \omega_s + \omega_r$, and that

$$P_{\text{out}} = \frac{2}{P}\omega_r T_e \tag{13.3-16}$$

(13.3-15) may be expressed as

$$P_{\text{in}} - P_{\text{out}} = 3r_s I_s^2 + \frac{2}{P}T_e\omega_s \tag{13.3-17}$$

Substitution of (13.3-2) into (13.3-17) yields an expression for the power losses in terms of torque and slip frequency; in particular

$$P_{\text{loss}} = \frac{2}{P} T_e \left[\frac{r'_r r_s}{\omega_s L_{Ms}^2} + \frac{\omega_s r_s L_{rr}^2}{r'_r L_{Ms}^2} + \omega_s \right] \tag{13.3-18}$$

Setting $T_e = T_e^*$ and $\omega_s = \omega_{s,set}$ in (13.3-18), then minimizing the right-hand side with respect to $\omega_{s,set}$ yields a slip frequency set point of

$$\omega_{s,set} = \frac{r'_{r,est}}{L'_{rr,est}} \frac{1}{\sqrt{\dfrac{L_{Ms,est}^2}{L'^2_{rr,est}} \dfrac{r_{s,est}}{r'_{r,est}} + 1}} \tag{13.3-19}$$

Assuming that $L_{Ms,est} \approx L'_{rr,est}$, and that $r_{s,est} \approx r'_{r,est}$, it is apparent that the slip frequency for maximum efficiency is lower than the slip frequency for maximum torque per amp by a factor of roughly $1/\sqrt{2}$.

The steady-state performance of a constant slip control drive is depicted in Figure 13.3-2, wherein $\omega_{s,set}$ is determined using (13.3-12), and Figure 13.3-3, wherein $\omega_{s,set}$ is determined using (13.3-13). In these studies, the parameters are those of the 50-hp induction motor discussed in Section 13.2, the maximum rotor

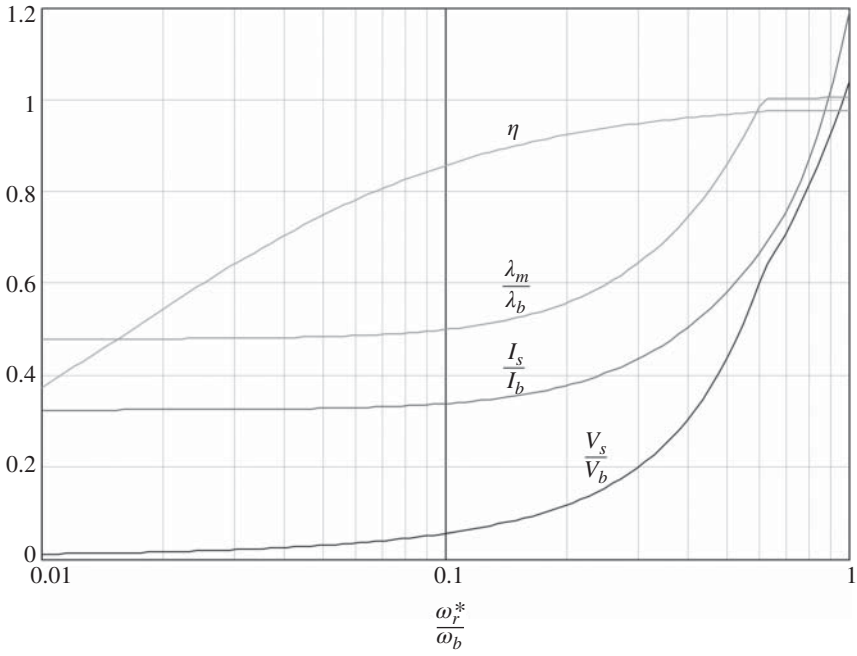

Figure 13.3-2 Performance of constant slip frequency drive (maximum torque-per-amp).

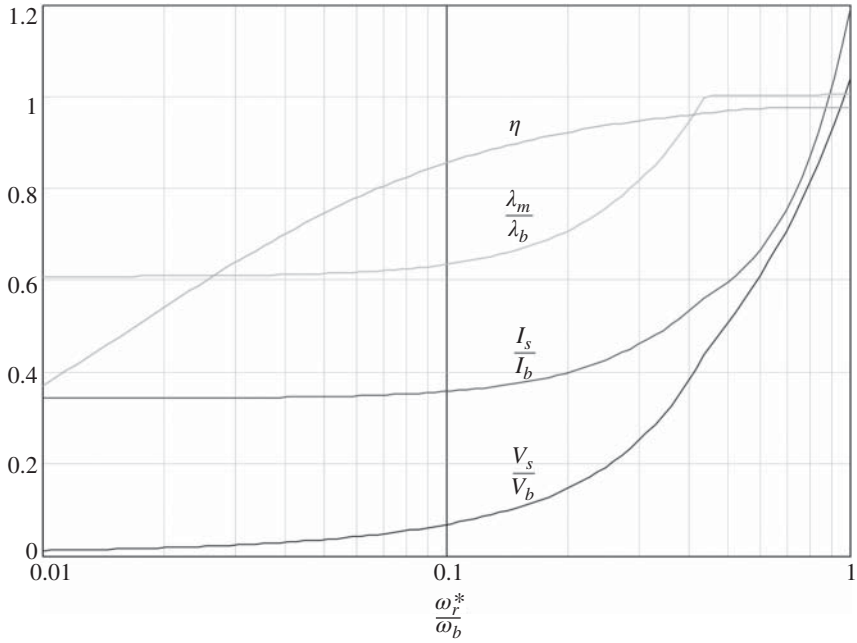

Figure 13.3-3 Performance of constant slip frequency drive (maximum efficiency).

flux allowed is set to be the value obtained for no-load operation at rated speed and rated voltage, and the estimated values of the parameters are assumed to be correct. It is assumed that the speed in this study is equal to the commanded speed (the assumption being the drive is used in the context of a closed-loop speed control since rotor position feedback is present). As can be seen, this drive results in appreciably lower losses for low-speed operation than in the case of the volts-per-hertz drives discussed in the previous section. Because core losses are not included in Figure 13.3-2 and Figure 13.3-3, the fact that these strategies utilize reduced flux levels will further accentuate the difference between constant slip and volts-per-hertz controls. In comparing Figure 13.3-2 with Figure 13.3-3, it is interesting to observe that setting the slip frequency to achieve maximum torque per amp performance yields nearly the same efficiency as setting the slip frequency to minimize losses. Since inverter losses go up with current, this suggest that setting the slip to optimize torque per amp may yield higher overall efficiency than setting the slip to minimize machine losses—particularly in view of the fact that the lower flux level in maximum torque per amp control will reduce core losses relative to maximum efficiency control.

Another question that arises in regard to the control is the effect errors in the estimated value of the machine parameters will have on the effectiveness of the

control. As it turns out, this algorithm is very robust with respect to parameter estimation, as the optimums being sought (maximum torque per amp or maximum efficiency) are broad. An extended discussion of this is set forth in References 3 and 4.

The use of the constant slip control in the context of a speed control system is depicted in Figure 13.3-4. Initially, the system is at zero speed. Approximately 2 seconds into the study, the speed command is stepped to 188.5 rad/s. In this study, the machine and load are identical to those in the study shown in Figure 13.2-4. However, since the constant-slip control is a torque input control, a speed control is necessary for speed regulation. For the study shown in Figure 13.3-4, the torque command is calculated in accordance with the speed control shown in Figure 13.3-5. This is a relatively simple PI control with a limited output, and anti-windup integration that prevents the integrator from integrating the positive (negative) speed error whenever the maximum (minimum) torque limit is invoked.

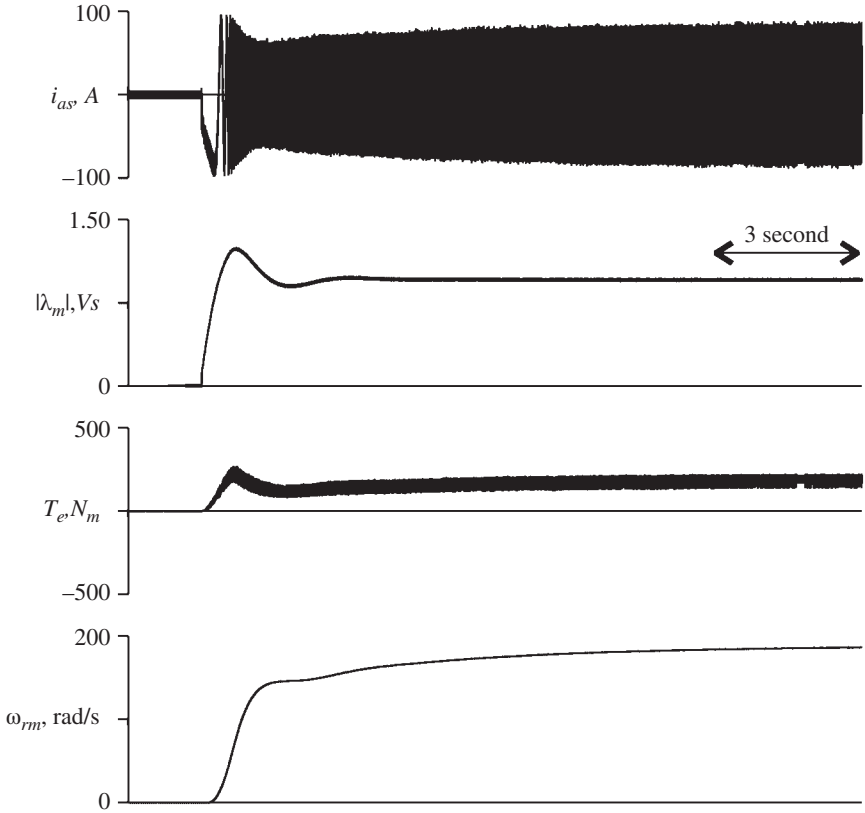

Figure 13.3-4 Start-up performance of constant slip controlled drive.

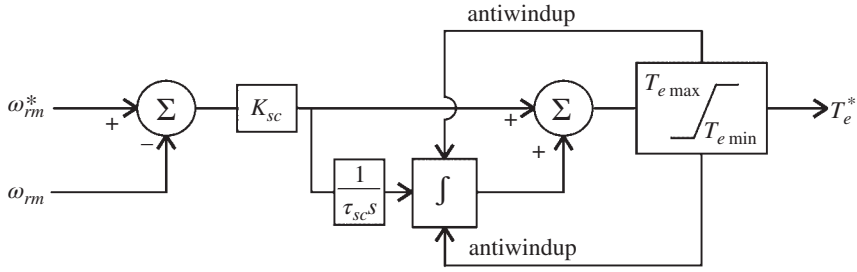

Figure 13.3-5 Speed control.

For the purposes of this study, the maximum and minimum torque commands were taken to 218 N · m (1.1 pu) and 0 N · m, respectively while K_{sc} and τ_{sc} were selected to be 1.64 N · m s/rad and 2 seconds, respectively. It can be shown that if $T_e = T_e^*$, and if the machine were unloaded, this would result in a transfer function between the actual and commanded speeds with two critically damped poles with 1-second time constants. Also used in conjunction with the control system was a synchronous current regulator in order to precisely achieve the current command output of the constant slip control. To this end, the synchronous current regulator depicted in Figure 10.11-1 was used. The time constant of the regulator was set to 16.7 ms.

As can be seen, the start-up performance using the constant slip control is much slower than using the constant volts-per-hertz control; this is largely because of the fact that the speed control needed to be fairly slow in order to accommodate the sluggish torque response. However, one point of interest is that the stator current, by virtue of the tight current regulation, is very well behaved; in fact, the peak value is only slightly above the steady-state value.

13.4 Field-Oriented Control

In many motor drive systems, it is desirable to make the drive act as a torque transducer wherein the electromagnetic torque can nearly instantaneously be made equal to a torque command. In such a system, speed or position control is dramatically simplified because the electrical dynamics of the drive become irrelevant to the speed or position control problem. In the case of induction motor drives, such performance can be achieved using a class of algorithms collectively known as field-oriented control. There are a number of permutations of this control—stator flux oriented, rotor flux oriented, and air-gap flux oriented, and of these types there are direct and indirect methods of implementation. This text will consider the most prevalent types, which are direct rotor flux-oriented control and indirect

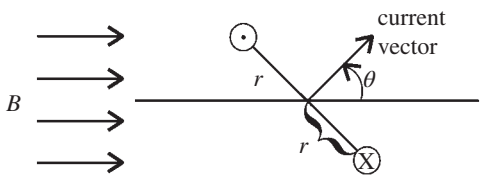

Figure 13.4-1 Torque on a current loop.

rotor flux-oriented control. For discussions of the other types, the reader is referred to texts entirely devoted to field-oriented control such as References 5 and 6.

The basic premise of field-oriented control may be understood by considering the current loop in a uniform flux field shown in Figure 13.4-1. From the Lorentz force equation, it is readily shown that the torque acting on the current loop is given by

$$T_e = -2BiNLr\sin\theta \tag{13.4-1}$$

where B is the flux density, i is the current, N is the number of turns, L is the length of the coil into the page, and r is the radius of the coil. Clearly, the magnitude of the torque is maximized when the current vector (defined perpendicular to the surface of the winding forming the current loop and in the same direction as the flux produced by that loop) is orthogonal to the flux field. The same conclusion is readily applied to an induction machine. Consider Figure 13.4-2. Therein, qd-axis rotor current and flux linkage vectors $i'_{qdr} = \begin{bmatrix} i'_{qr} & i'_{dr} \end{bmatrix}^T$ and $\lambda'_{qdr} = \begin{bmatrix} \lambda'_{qr} & \lambda'_{dr} \end{bmatrix}^T$, respectively, are shown at some instant of time. Repeating (3.5-8)

$$T_e = \frac{3}{2}\frac{P}{2}\left(\lambda'_{qr}i'_{dr} - \lambda'_{dr}i'_{qr}\right) \tag{13.4-2}$$

which may be expressed as

$$T_e = -\frac{3}{2}\frac{P}{2}\left|\lambda'_{qdr}\right|\left|i'_{qdr}\right|\sin\theta \tag{13.4-3}$$

which is analogous to (13.4-1). Again, for a given magnitude of flux linkage, torque is maximized when the flux linkage and current vectors are perpendicular.

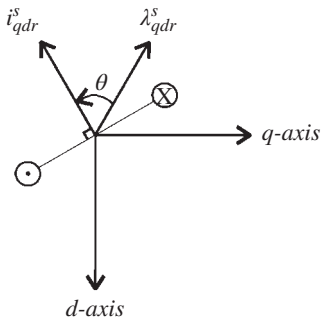

Figure 13.4-2 Torque production in an induction motor.

Thus, it is desirable to keep the rotor flux linkage vector perpendicular to the rotor current vector. As it turns out, this is readily accomplished in practice. In particular, in the steady state, the rotor flux linkage vector and rotor current vector are always perpendicular for all singly fed induction machines. To see this, consider the rotor voltage equations (3.3-15) and (3.3-16). With the rotor circuits short-circuited and using the synchronous reference frame, it can be shown that the rotor currents may be expressed as

$$i_{qr}^{e} = -\frac{1}{r_r'}(\omega_e - \omega_r)\lambda_{dr}^{e} \tag{13.4-4}$$

$$i_{dr}^{e} = \frac{1}{r_r'}(\omega_e - \omega_r)\lambda_{qr}^{e} \tag{13.4-5}$$

The dot product of the rotor flux linkage and rotor current vectors may be expressed as

$$\lambda_{qdr}'^{e} \cdot i_{qdr}'^{e} = \lambda_{qr}'^{e} i_{qr}'^{e} + \lambda_{dr}'^{e} i_{dr}'^{e} \tag{13.4-6}$$

Substitution of (13.4-4) and (13.4-5) into (13.4-6) reveals that this dot product is zero whereupon it may be concluded that the rotor flux and rotor current vectors, as expressed in the synchronous reference frame, are perpendicular. Furthermore, if they are perpendicular in the synchronous reference frame, they are perpendicular in every reference frame. In this sense, in the steady state, every singly excited induction machine operates with an optimal relative orientation of the rotor flux and rotor current vectors. However, the defining characteristic of a field-oriented drive is that this characteristic is maintained during transient conditions as well. It is this feature that results in the high transient performance capabilities of this class of drive.

In both direct and indirect field oriented drives, the method to achieve the condition that the rotor flux and rotor current vectors are always perpendicular is twofold. The first part of the strategy is to ensure that

$$\lambda_{qr}'^{e} = 0 \tag{13.4-7}$$

and the second to is to ensure that

$$i_{dr}'^{e} = 0 \tag{13.4-8}$$

Clearly, if (13.4-7) and (13.4-8) hold during transient conditions, then by (13.4-6), the rotor flux linkage and rotor current vectors are perpendicular during those same conditions. By suitable choice of θ_e on an instantaneous basis, (13.4-7) can always be satisfied by choosing the position of the synchronous reference frame to put all of the rotor flux linkage in the d-axis. Satisfying (13.4-8) can be accomplished by forcing the d-axis stator current to remain constant. To see this, consider the d-axis rotor voltage equation (with zero rotor voltage):

$$0 = r_r' i_{dr}'^{e} + (\omega_e - \omega_r)\lambda_{qr}'^{e} + p\lambda_{dr}'^{e} \tag{13.4-9}$$

By suitable choice of reference frame, (13.4-7) is achieved; therefore λ'^{e}_{qr} can be set to zero in (13.4-9) to yield

$$0 = r'_r i'^{e}_{dr} + p\lambda'^{e}_{dr} \tag{13.4-10}$$

Next, substitution of the d-axis rotor flux linkage equation (3.4-33) into (13.4-10) and rearranging yields

$$pi'^{e}_{dr} = -\frac{r'_r}{L'_{rr}} i'^{e}_{dr} - \frac{L_{Ms}}{L'_{rr}} pi^{e}_{ds} \tag{13.4-11}$$

Equation (13.4-11) can be viewed as a stable first-order differential equation in i'^{e}_{dr} with pi^{e}_{ds} as input. Therefore, if i^{e}_{ds} is held constant, then i'^{e}_{dr} will go to, and stay at, zero, regardless of other transients which may be taking place.

Before proceeding further, it is motivational to explore some of the other implications of (13.4-7) and (13.4-8) being met. First, combining (13.4-8) with (3.4-30) and (3.4-33), respectively, it is clear that

$$\lambda^{e}_{ds} = L_{ss} i^{e}_{ds} \tag{13.4-12}$$

and that

$$\lambda'^{e}_{dr} = L_{Ms} i^{e}_{ds} \tag{13.4-13}$$

Clearly, the d-axis flux levels are set solely by the d-axis stator current. Combining (13.4-2) with (13.4-7), it can be seen that torque may be expressed

$$T_e = -\frac{3}{2}\frac{P}{2} \lambda'^{e}_{dr} i'^{e}_{qr} \tag{13.4-14}$$

Furthermore, from (13.4-7) and (3.4-32), it can be shown that

$$i'^{e}_{qr} = -\frac{L_{Ms}}{L'_{rr}} i^{e}_{qs} \tag{13.4-15}$$

Combining (13.4-14) and (13.4-15)

$$T_e = \frac{3}{2}\frac{P}{2}\frac{L_{Ms}}{L'_{rr}} \lambda'^{e}_{dr} i^{e}_{qs} \tag{13.4-16}$$

Together, (13.4-13) and (13.4-16) suggest the "generic" rotor flux-oriented control depicted in Figure 13.4-3. Therein, variables of the form x^*, $\widehat{x}$, and $\hat{x}$ denote commanded, measured, and estimated, respectively; in the case of parameters, an addition of a ",est" to the subscript indicates the assumed value. As can be seen, a dc source supplies an inverter driving an induction machine. Based on a torque command T^*_e, the assumed values of the parameters, and the estimated value of the d-axis rotor flux $\widehat{\lambda}'^{e*}_{dr}$, (13.4-16) is used to formulate a q-axis stator current command i^{e*}_{qs}. The d-axis stator current command i^{e*}_{ds} is calculated such as to achieve a rotor flux command (which is typically maintained constant or varied only slowly) λ'^{e*}_{dr} based on (13.4-13). The q- and d-axis stator current command

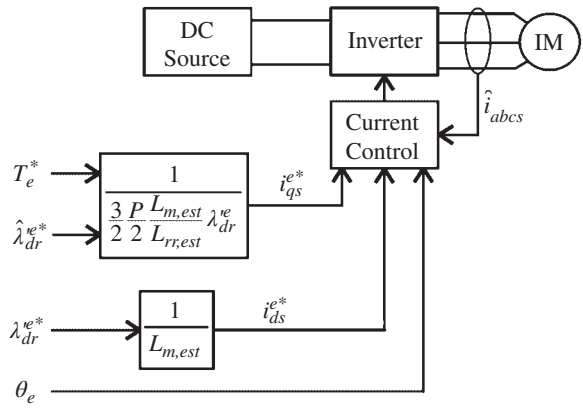

Figure 13.4-3 Generic rotor flux oriented control.

is then achieved using any one of a number of current-source current controls as discussed in Section 10.11. However, this diagram of the rotor flux-oriented field-oriented control is incomplete in two important details—the determination of $\hat{\lambda}_{dr}^{'e*}$ and the determination of θ_e. The difference in direct and indirect field oriented control is in how these two variables are established.

13.5 Direct Field-Oriented Control

In direct field-oriented control, the position of the synchronous reference is based on the value of the q- and d-axis flux linkages in the rotor reference frame. From (2.5-7), upon setting the position of the stationary reference frame to be zero, we have that

$$\begin{bmatrix} \lambda_{qr}^{'e} \\ \lambda_{dr}^{'e} \end{bmatrix} = \begin{bmatrix} \cos\theta_e & -\sin\theta_e \\ \sin\theta_e & \cos\theta_e \end{bmatrix} \begin{bmatrix} \lambda_{qr}^{'s} \\ \lambda_{dr}^{'s} \end{bmatrix} \tag{13.5-1}$$

In order to achieve $\lambda_{qr}^{'e} = 0$, from (13.5-1), it is sufficient to define the position of the synchronous reference frame in accordance with

$$\theta_e = \text{angle}\left(\lambda_{qr}^{'s} - j\lambda_{dr}^{'s}\right) + \frac{\pi}{2} \tag{13.5-2}$$

whereupon it can be shown that

$$\lambda_{dr}^{'e} = \sqrt{\left(\lambda_{qr}^{'s}\right)^2 + \left(\lambda_{dr}^{'s}\right)^2} \tag{13.5-3}$$

The difficulty in this approach is that $\lambda_{qr}^{'s}$ and $\lambda_{dr}^{'s}$ are not directly measurable quantities. However, they can be estimated using direct measurement of the air-gap flux. In this method, hall-effect sensors (or some other means) are placed in the air gap and used to measure the air-gap flux in the q- and d-axis

of the stationary reference frame (since the position of the sensors is fixed in a stationary reference frame). The net effect is that λ^s_{qm} and λ^s_{dm} may be regarded as measurable. In order to establish λ'^s_{qr} and λ'^s_{dr} from λ^s_{qm} and λ^s_{dm}, note that

$$\lambda'^s_{qm} = L_M \left(i^s_{qs} + i'^s_{qr}\right) \tag{13.5-4}$$

Therefore,

$$i'^s_{qr} = \frac{\lambda'^s_{qm} - L_M i^s_{qs}}{L_M} \tag{13.5-5}$$

Recall that the q-axis rotor flux linkages may be expressed as

$$\lambda'^s_{qr} = L_{lr} i'^s_{qr} + L_M \left(i^s_{qs} + i'^s_{qr}\right) \tag{13.5-6}$$

Substitution of (13.5-5) into (13.5-6) yields

$$\lambda'^s_{qr} = \frac{L'_{rr}}{L_M} \lambda^s_{qm} - L'_{lr} i^s_{qs} \tag{13.5-7}$$

Performing an identical derivation for the d-axis yields

$$\lambda'^s_{dr} = \frac{L'_{rr}}{L_M} \lambda^s_{dm} - L'_{lr} i^s_{ds} \tag{13.5-8}$$

This suggests the rotor flux calculator shown in Figure 13.5-1, which calculates both the position of the synchronous reference frame as well as the d-axis flux linkage. This is based directly on (13.5-7), (13.5-8), (13.5-2), and (13.5-3), with the addition of two low-pass filters in order to prevent switching frequency noise from effecting the control (the time constant τ_{rfc} must be set small enough that this transfer function has no effect on the highest frequency fundamental component that will be utilized) and that, as in Figure 13.4-1, a more careful distinction is

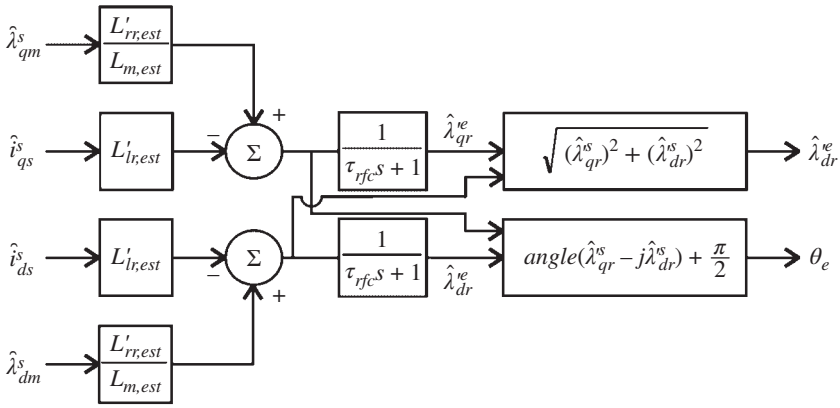

Figure 13.5-1 Rotor flux calculator.

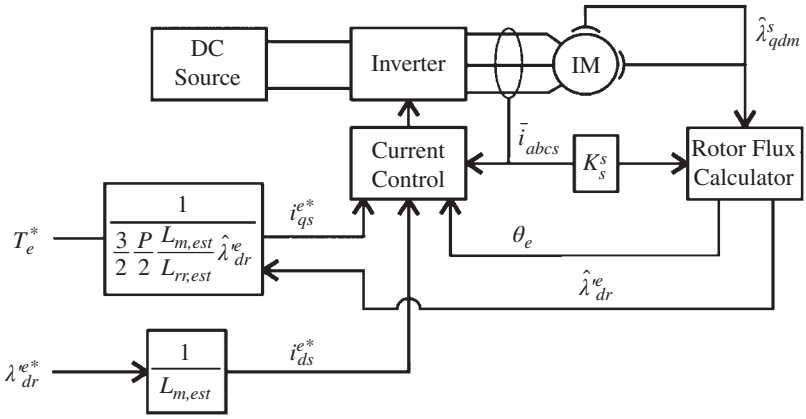

Figure 13.5-2 Direct field-oriented control.

made between measured and estimated values. Figure 13.5-2 depicts the incorporation of the rotor flux calculator into the direct field-oriented control. This will be important in future analysis when the effects of using parameter values in the control algorithms which are not equal to the actual parameters of the machine (which are highly operating-point dependent).

13.6 Robust Direct Field-Oriented Control

One of the problems of the control strategy presented is that it is a function of the parameters of the machine. Because of magnetic nonlinearities and the distributed nature of the machine windings, particularly the rotor windings—the model is not particularly accurate. The machine resistances and inductances are highly operating point dependent. In order to understand the potential sources of error, let us first consider the rotor flux observer. From Figure 13.5-1, recall the rotor flux vector is estimated as

$$\hat{\lambda}'^{e}_{qdr} = \frac{L'_{rr,est}}{L_{Ms,est}}\hat{\lambda}^{s}_{qd,m} - L'_{lr,est}\hat{i}^{s}_{qds} \tag{13.6-1}$$

Assuming that the measured flux and measured current are accurate, (13.6-1) is relatively insensitive to parameter variation. To see this, let us first consider the first term on the right-hand side of (13.6-1). The term is a function of $L_{rr,est}/L_{Ms,est}$. However, note that since the rotor leakage inductance is much less that the magnetizing inductance, this ratio will be close to unity regardless of the actual value of the parameters. Hence, this term will not be a strong function of the parameters of the machine. The second term in (13.6-1) is a strong function of the leakage

inductance. However, the second term as a whole is considerably smaller than the first since the first term represents the air-gap flux and the second has a magnitude equal to the rotor leakage flux. Thus, as a whole, (13.6-1) and the rotor flux estimator are relatively insensitive to the machine parameters.

Another key relationship used in the direct field-oriented control which is a function of the parameters of the machine is the calculation of the q-axis current; in particular

$$i_{qs}^{e*} = \frac{T_e^*}{\frac{3}{2}\frac{P}{2}\frac{L_{Ms,est}}{L_{rr,est}}\hat{\lambda}'^{e*}_{dr}} \tag{13.6-2}$$

Again, since the ratio of $L_{Ms,est}$ to $L_{rr,est}$ is close to unity for the normal range of parameters, this relationship is again relatively insensitive to parameters.

However, this is not the case for the calculation of the d-axis current, which is calculated in accordance with

$$i_{ds}^{e*} = \frac{\lambda_{dr}^{e*}}{L_{Ms,est}} \tag{13.6-3}$$

As can be seen, this relationship is highly sensitive to $L_{Ms,est}$. An error in the d-axis current command will result in an incorrect value of rotor flux linkages. Because the rotor flux linkages can be estimated using the rotor flux estimator shown in Figure 13.5-1, this error can be readily eliminated by introducing a rotor flux feedback loop shown in Figure 13.6-1. The basis of this loop is (13.6-3). However, integral feedback is utilized to force the d-axis rotor flux linkage to be equal to its commanded value. For the purposes of design of this feedback loop, it is convenient to assume that $\lambda_{dr}^{e} = L_{Ms} i_{ds}^{e*}$, and that $\hat{\lambda}'^{e}_{dr} = \lambda'^{e}_{dr}$, whereupon it can be shown that the transfer function between the actual and commanded flux linkages is given by

$$\frac{\lambda'^{e}_{dr}}{\lambda'^{e*}_{dr}} = \frac{\tau_\lambda s + 1}{\tau_\lambda \frac{L_{Ms,est}}{L_{Ms}} s + 1} \tag{13.6-4}$$

From the form of this transfer function, it can be seen that in the steady state, the rotor flux will be equal to the commanded value. Furthermore, note that if

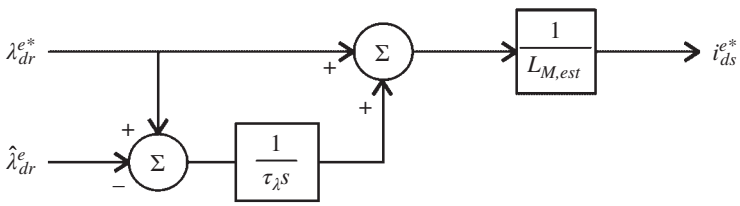

Figure 13.6-1 Flux control loop.

$L_{Ms,est} = L_{Ms}$, the transfer function between the commanded and actual rotor flux is unity. The value of τ_f is chosen so that that $\tau_f 2\pi f_{sw} L_{Ms,\,est}/L_{Ms} > > 1$; as a worst case estimate, $L_{Ms,est} = L_{Ms}$ can be taken to be 0.7 or so in this process.

Although this approach goes a long way in making the direct field-oriented control robust with respect to parameter variations, the design can be made even more robust by adding a torque calculator and feedback loop. From (3.5-9), recall that torque may be expressed as

$$T_e = \frac{3}{2}\frac{P}{2}\left(\lambda^s_{ds} i^s_{qs} - \lambda^s_{qs} i^s_{ds}\right) \tag{13.6-5}$$

Furthermore, the stator flux may be expressed as

$$\lambda^s_{qds} = L_{ls} i^s_{qds} + \lambda^s_{qdm} \tag{13.6-6}$$

Substitution of (13.6-6) into (13.6-5) yields

$$T_e = \frac{3}{2}\frac{P}{2}\left(\lambda^s_{dm} i^s_{qs} - \lambda^s_{qm} i^s_{ds}\right) \tag{13.6-7}$$

which suggests that an estimate for torque can be calculated as

$$\hat{T}_e = \frac{3}{2}\frac{P}{2}\left(\hat{\lambda}^s_{dm}\,\hat{i}^s_{qs} - \hat{\lambda}^s_{qm}\,\hat{i}^s_{ds}\right) \tag{13.6-8}$$

With the torque calculator present, it is possible to introduce a torque feedback loop shown in Figure 13.6-2. For the purposes of analysis of this loop, it is convenient to define

$$K_{t,est} = \frac{3}{2}\frac{P}{2}\frac{L_{Ms,est}}{L'_{rr}}\lambda'^{e*}_{dr} \tag{13.6-9}$$

which will be treated as a constant parameter for the purposes of torque loop design. For the purpose of gaining intuition about the performance of the flux loop, it is convenient to assume that

$$T_e = K_t i^{e*}_{qs} \tag{13.6-10}$$

where

$$K_t = \frac{3}{2}\frac{P}{2}\frac{L_{Ms}}{L'_{rr}}\lambda'^{e}_{dr} \tag{13.6-11}$$

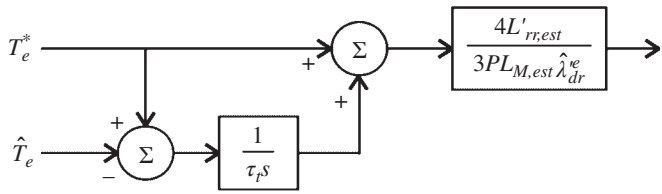

Figure 13.6-2 Torque control loop.

Under these conditions, it is readily shown that transfer function between actual and commanded torque is given by

$$\frac{T_e}{T_e^*} = \frac{\tau_t s + 1}{\tau_t \dfrac{K_{t,est}}{K_t} s + 1} \tag{13.6-12}$$

Upon inspection of (13.6-12), it is clear that at dc, there will be no error between the actual and commanded torque in the steady state (at least if the error in the current and flux sensors is ignored). Further, if K_t and $K_{t,est}$ are equal, the transfer function will be unity, whereupon it would be expected that the actual torque would closely tract the commanded torque even during transients. The time constant τ_t is chosen as small as possible subject to the constraint that $2\pi f_{sw}\tau_t K_{t,est}/K_t \gg 1$ so that switching frequency noise does not enter into the torque command.

Incorporating the rotor and torque feedback loops into the direct field oriented-control yields the robust field-oriented control depicted in Figure 13.6-3. Therein, the use of a flux estimator, torque calculator, and closed-loop torque and flux controls yields a drive that is highly robust with respect to deviations of the parameters from their anticipated values.

The start-up performance of the direct field-oriented control is depicted in Figure 13.6-4. Therein, the machine, load, and speed controls are the same as the study depicted in Figure 13.3-4, with the exception that the parameters of the speed control were changed to $K_{sc} = 16.4$ N·m·s/rad and $\tau_{sc} = 0.2$ second in order to take advantage of the nearly instantaneous torque response characteristic of field-oriented drives. Parameters of the field-oriented controller were: $\tau_{rfc} = 100$ μs, $\tau_\lambda = 50$ ms, and $\tau_t = 50$ ms. The current commands were

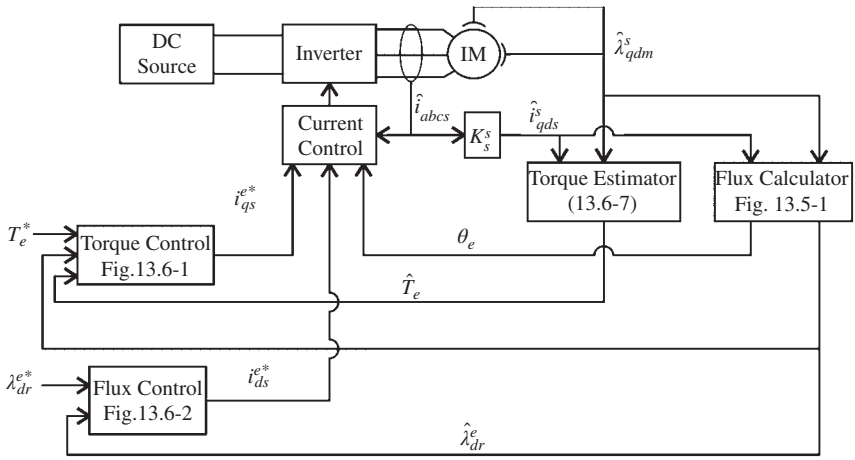

Figure 13.6-3 Robust direct rotor field oriented control.

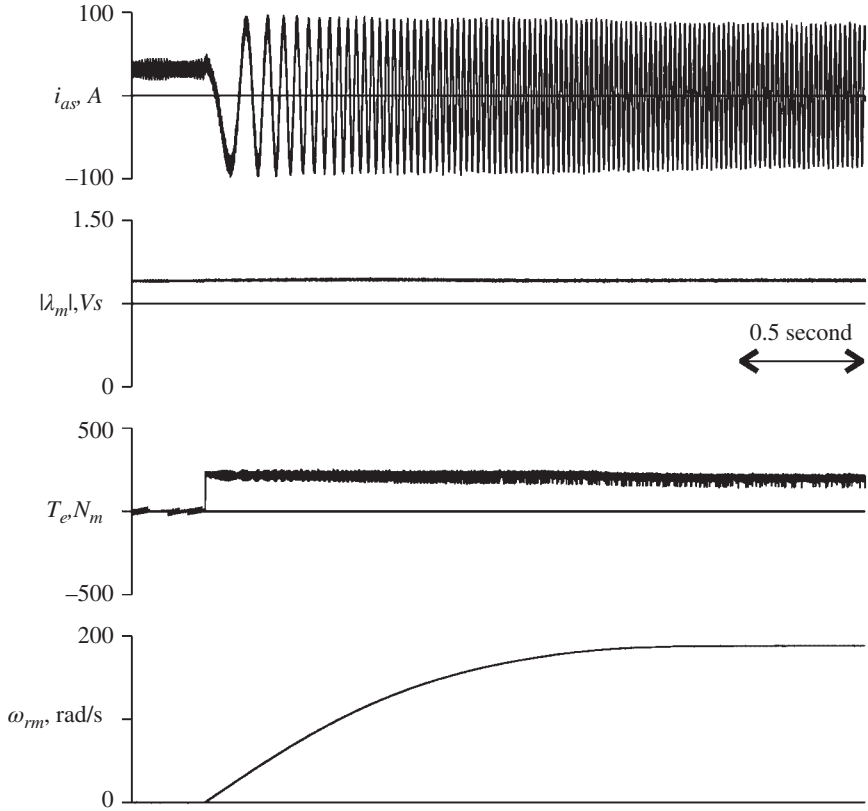

Figure 13.6-4 Start-up performance of robust direct field oriented drive.

achieved using a synchronous current regulator (Fig. 12.11-1) in conjunction with a delta-modulated current control. The synchronous current regulator time constant τ_{scr} and delta modulator switching frequency were set to 16.7 ms and 10 kHz, respectively. Initially, the drive is operating at zero speed, when, approximately 250 ms into the study, the mechanical speed command is stepped from 0 to 188.5 rad/s. The electromagnetic torque steps to the torque limit (which was set to 218 N·m) for approximately 1.5 seconds, after which the torque command begins to decrease as the speed approaches the commanded value. The drive reaches steady-state conditions within 2 seconds, and at the same time, the peak current utilized was only slightly larger than the steady-state value. In this context, it can be seen that although the control is somewhat elaborate, it can be used to achieve a high-degree of dynamic performance with minimal inverter requirements. It is also interesting to observe that the magnitude of the air-gap flux was essentially constant throughout the entire study.

13.7 Indirect Rotor Field-Oriented Control

Although direct field-oriented control can be made fairly robust with respect to variation of machine parameters, the sensing of the air-gap flux linkage (typically) using hall-effect sensors is somewhat problematic (and expensive) in practice. This has led to considerable interest in indirect field-oriented control methods that are more sensitive to knowledge of the machine parameters but do not require direct sensing of the rotor flux linkages.

In order to establish an algorithm for implementing field-oriented control without knowledge of the rotor flux linkages, it is useful to first establish the electrical frequency that is utilized in direct field-oriented control. From the q-axis rotor voltage equation

$$0 = r'_{rr} i'^{e}_{qr} + (\omega_e - \omega_r)\lambda'^{e}_{dr} + p\lambda'^{e}_{qr} \tag{13.7-1}$$

Since $\lambda'^{e}_{qr} = 0$ for the direct field-oriented control, (13.7-1) necessitates

$$\omega_e = \omega_r - r'_r \frac{i'^{e}_{qr}}{\lambda'^{e}_{dr}} \tag{13.7-2}$$

Using (13.4-12) to express i'^{e}_{qr} in terms of i^{e}_{qs}, and (13.4-10) to express λ'^{e}_{dr} in terms of i^{e}_{ds}, (13.7-2) becomes

$$\omega_e = \omega_r + \frac{r'_r}{L'_{rr}} \frac{i^{e}_{qs}}{i^{e}_{de}} \tag{13.7-3}$$

This raises an interesting question. Suppose that instead of establishing θ_e utilizing the rotor flux calculator in Figure 13.5-1, it is instead calculated by integrating ω_e, where ω_e is established by

$$\omega_e = \omega_r + \frac{r'_r}{L'_{rr}} \frac{i^{e*}_{qs}}{i^{e*}_{ds}} \tag{13.7-4}$$

As it turns out, this is sufficient to satisfy the conditions for field-oriented control $\lambda'^{e}_{qr} = 0$ and $i'^{e}_{dr} = 0$ provided that i^{e*}_{ds} is held constant. To show this, first consider the rotor voltage equations

$$0 = r'_r i'^{e}_{qr} + (\omega_e - \omega_r)\lambda'^{e}_{dr} + p\lambda'^{e}_{qr} \tag{13.7-5}$$

$$0 = r'_r i'^{e}_{dr} - (\omega_e - \omega_r)\lambda'^{e}_{qr} + p\lambda'^{e}_{dr} \tag{13.7-6}$$

Substitution of (13.7-4) into (13.7-5) and (13.7-6) yields

$$0 = r'_r i'^{e}_{qr} + \frac{r'_r}{L'_{rr}} \frac{i^{e*}_{qs}}{i^{e*}_{de}} \lambda'^{e}_{dr} + p\lambda'^{e}_{qr} \tag{13.7-7}$$

$$0 = r'_r i'^{e}_{dr} - \frac{r'_r}{L'_{rr}} \frac{i^{e*}_{qs}}{i^{e*}_{de}} \lambda'^{e}_{qr} + p\lambda'^{e}_{dr} \tag{13.7-8}$$

The next step is to utilize the rotor flux linkage equations into (13.4-7) and (13.4-8), which upon making the assumption the stator currents are equal to their commanded values yields

$$0 = r'_r \left[\frac{\lambda'^{e}_{qr} - L_{Ms} i^{e*}_{qs}}{L'_{rr}} \right] i'^{e}_{dr} + \frac{r'_r}{L'_{rr}} \frac{i^{e*}_{qs}}{i^{e*}_{de}} \left[L'_{rr} i'^{e}_{dr} + L_{Ms} i^{e*}_{ds} \right] + p\lambda'^{e}_{qr} \tag{13.7-9}$$

$$0 = r'_r i'^{e}_{dr} - \frac{r'_r}{L'_{rr}} \frac{i^{e*}_{qs}}{i^{e*}_{ds}} \lambda'^{e}_{qr} + p \left[L'_{rr} i'^{e}_{qr} + L_{Ms} i^{e*}_{ds} \right] \tag{13.7-10}$$

Noting that $pi^{e*}_{ds} = 0$ and rearranging (13.4-11) and (13.7-10) yields

$$p\lambda'^{e}_{qr} = -\frac{r'_r}{L'_{rr}} \lambda'^{e}_{qr} - r'_r \frac{i^{e*}_{qs}}{i^{e*}_{ds}} i'^{e}_{dr} \tag{13.7-11}$$

$$pi'^{e}_{dr} = -\frac{r'_r}{L'_{rr}} i'^{e}_{dr} + \frac{r'_r}{\left(L'_{rr}\right)^2} \frac{i^{e*}_{qs}}{i^{e*}_{ds}} \lambda'^{e}_{qr} \tag{13.7-12}$$

Provided that $pi^{e*}_{ds} = 0$, (13.7-11) and (13.7-12) constitute a set of asymptotically stable differential equations with an equilibrium point of $\lambda'^{e}_{qr} = 0$ and $i'^{e}_{dr} = 0$. The conclusion is that λ'^{e}_{qr} and i'^{e}_{dr} will go to and stay at zero, thereby satisfying the conditions for field-oriented control.

Figure 13.7-1 depicts the block diagram of the indirect rotor field-oriented control, which is based on (13.6-2), (13.6-3), and (13.7-3). As can be seen, it is considerably simpler than the direct field-oriented control—though it is much more susceptible to performance degradation as a result of error in estimating the effective machine parameters.

The start-up performance of the indirect field-oriented drive is depicted in Figure 13.7-2. Therein, the parameters of the induction machine, speed control,

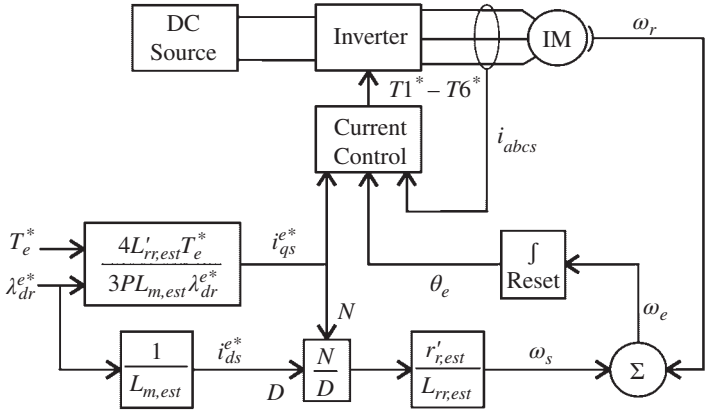

Figure 13.7-1 Indirect rotor field oriented control.

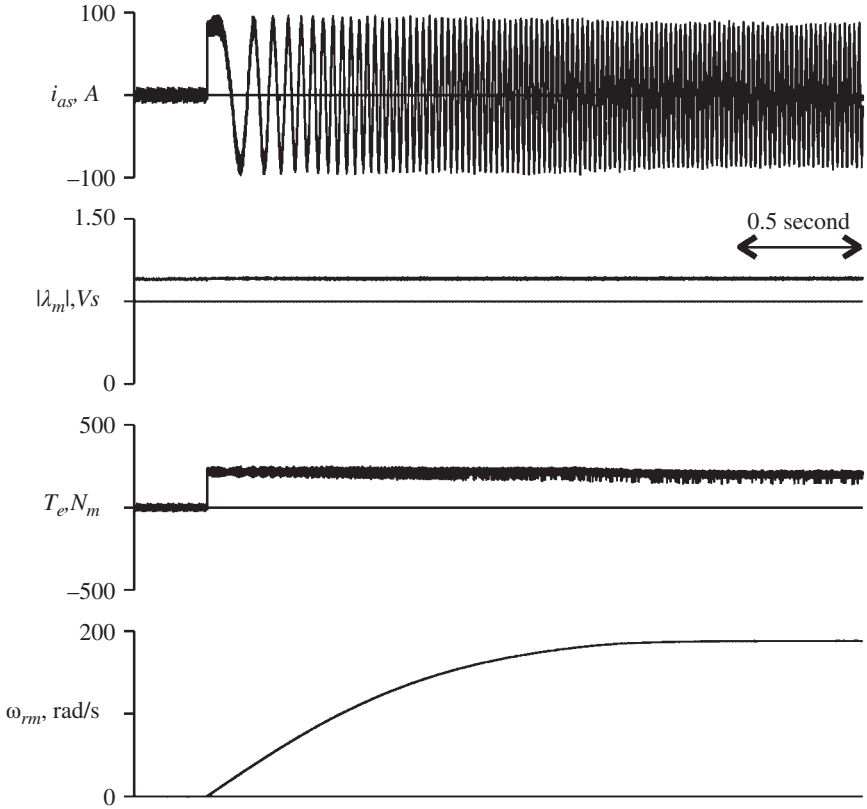

Figure 13.7-2 Start-up performance of indirect field oriented drive.

inverter, and current regulator are all identical to those of the corresponding study shown in Figure 13.6-4. In fact, comparison of Figure 13.6-4. with Figure 13.7-2 reveals that the two controls give identical results. This is largely the result of the fact that the estimated parameters were taken to be the parameter of the machine, and that the machine was assumed to behave in accordance with the machine model described in Chapter 3. However, in reality, the machine parameter can vary significantly. Because of the feedback loops, in the case of the direct field-oriented control parameter, variations will have relatively little effect on performance. In the case of the indirect field oriented drive, significant degradation of the response can result. This is illustrated in Figure 13.7-3, which is identical to Figure 13.7-2, with the exception that an error in the estimated parameters is included in the analysis; in particular $L_{Ms.est} = 1.25L_{Ms}$ and $r'_{r,est} = 0.75r'_r$. As can be seen, although the speed control still achieves the desired speed, the transient performance of the drive is compromised, as can be seen by the variation in

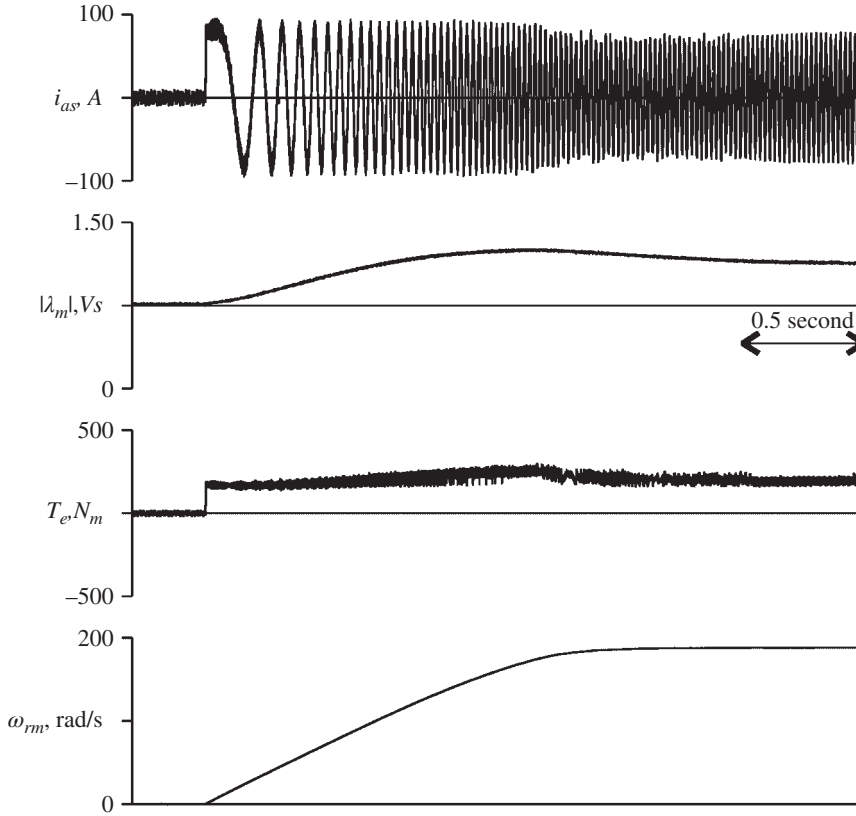

Figure 13.7-3 Start-up performance of indirect field oriented drive with errors in estimated parameter values.

air-gap flux linkages and electromagnetic torque. This degradation is particularly important at low speeds where instability in the speed or position controls can result.

13.8 Direct Torque Control

Another established method of controlling the torque in an induction machine is the method of DTC [6–9]. A block diagram of an induction motor drive using DTC is depicted in Figure 13.8-1, wherein it is assumed that a three-phase induction machine is supplied by a voltage source inverter (Chapter 10). As shown, the DTC includes a block that estimates the stator flux and torque based on measured voltages and currents, and a set of comparators that compare the estimated stator flux

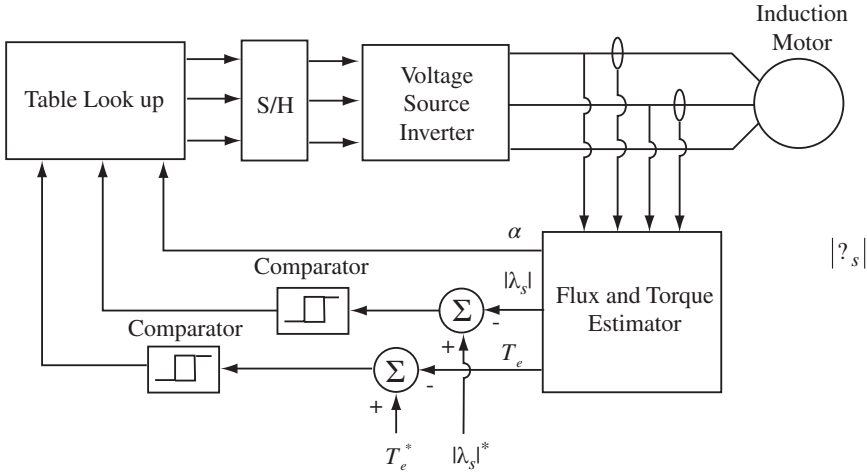

Figure 13.8-1 Direct torque control of an induction motor.

magnitude and electromagnetic torque with their commanded values (denoted with an asterisk), and a table look-up block that supplies the switching signals to the inverter through a sample/hold block that prevents the switching state from changing too fast.

In order to explain the underlying concepts behind DTC, it is helpful to define the stator space flux vector λ_s such that its horizontal component is λ_{qs}^s and vertical component is $-\lambda_{ds}^s$, as shown in Figure 13.8-2a. Likewise, it is convenient to define the inverter output voltage vectors $\mathbf{V}_0$ through $\mathbf{V}_7$, corresponding to each of the inverter switching states, such that the horizontal component is v_{qs}^s and vertical

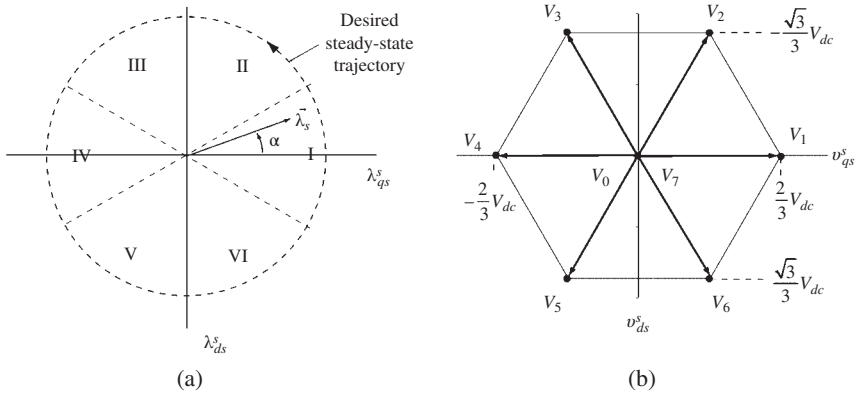

Figure 13.8-2 Stator flux and achievable voltage vectors.

Table 13.8-1 Achievable Voltage Vectors and Corresponding Switching State.

	Switching State		
Voltage Vector	$T_1/\overline{T}_4$	$T_2/\overline{T}_5$	$T_3/\overline{T}_6$
V_0	0	0	0
V_1	1	0	0
V_2	1	1	0
V_3	0	1	0
V_4	0	1	1
V_5	0	0	1
V_6	1	0	1
V_7	1	1	1

component is $-v_{ds}^s$. These voltage vectors as summarized in Table 13.8-1 and plotted in Figure 13.8-2b.

In the steady state at constant torque and rotor speed, the stator flux vector $\boldsymbol{\lambda}_s$ ideally has a constant magnitude and rotates in the counterclockwise direction at an angular velocity of ω_e. The steady-state stator flux trajectory for the desired torque is shown as a dashed line in Figure 13.8-2a. Utilizing the concept of north and south poles discussed in Chapter 2, $\boldsymbol{\lambda}_s$ points in the direction of the net south pole as it enters the inner periphery of the stator. If the north pole attributed to the rotor currents lags (leads) $\boldsymbol{\lambda}_s$, the electromagnetic torque will be positive (negative). In either case, advancing $\boldsymbol{\lambda}_s$ in the counterclockwise direction will increase T_e and delaying $\boldsymbol{\lambda}_s$ will decrease T_e.

At this point, it is possible to explain the underlying concept behind DTC. For this purpose, it is assumed arbitrarily that, at a given instant of time, $\boldsymbol{\lambda}_s$ lies in Sector I (Fig. 13.8-2a) and its magnitude is smaller than the commanded $|\boldsymbol{\lambda}_s|^*$. The control system should then select the inverter switching state that increases the magnitude of $\boldsymbol{\lambda}_s$ and, if T_e is smaller than T_e^*, advances $\boldsymbol{\lambda}_s$ in the counterclockwise direction. From Figure 13.8-2b, voltage vector $\mathbf{V}_2$ should be selected. Using Faraday's law, it can be argued that the subsequent change in $\boldsymbol{\lambda}_s$ will be in the direction of $\mathbf{V}_2$. Specifically, combining the relations $\Delta\lambda_{qs}^s \approx \Delta T v_{qs}^s$ and $\Delta\lambda_{ds}^s \approx \Delta T v_{ds}^s$, where ΔT is the sample/hold interval, into a single vector relation yields the desired result. While the direction of the ensuing change in $\boldsymbol{\lambda}_s$ will be along $\mathbf{V}_2$, the magnitude of the change, $\Delta|\boldsymbol{\lambda}_s|$, will be proportional to ΔT, which should be carefully selected so that $\Delta|\boldsymbol{\lambda}_s|$ is not too large or too small.

Using a similar argument with reference to Figure 13.8-2a,b, if it is necessary to increase flux and decrease torque, voltage vector $\mathbf{V}_6$ should be selected. On the other hand, if λ_s lies outside the circle while still located in Sector I, and the torque is smaller (larger) than its commanded value, it is necessary to decrease the magnitude of λ_s while advancing (delaying) its counterclockwise rotation. Referring again to Figure 13.8-2a,b, voltage vector $\mathbf{V}_3$ ($\mathbf{V}_5$) should be selected. In Reference 9, voltage vector $\mathbf{V}_7$ or $\mathbf{V}_0$ is chosen if $T_e > T_e^*$ irrespective of the magnitude of the stator flux, which results in zero voltages applied to the stator and only a small subsequent change in the stator flux vector (due to the ohmic voltage drop in the stator windings). The preceding switching states are summarized in the column corresponding to Sector I of Table 13.8-2. Therein, ΔT_e and $\Delta|\lambda_s|$ are the desired change in torque and flux, respectively. A similar argument can be applied if λ_s lies in any of the other sectors shown in Figure 13.8-2, resulting in a cyclic permutation of the subscripts as shown in Table 13.8-2.

To illustrate the dynamic performance of an induction motor drive with DTC, it is assumed that the motor described in Section 13.2 is operating at 200 N·m and 1800 rpm, whereupon the torque command is stepped to −200 N·m while holding the commanded stator flux magnitude at its rated value (1.0 V·s) throughout the study. The resulting electromagnetic torque and stator flux magnitude are depicted in Figure 13.8-3 wherein it is assumed that over the time interval shown, the rotor speed does not change. For the given study, the sample/hold rate was set to 4 kHz. As shown, the torque response is very rapid and there is a negligible change in the magnitude of the stator flux. A key advantage of DTC is the fact that the machine parameters are not required to implement the control; however, a disadvantage is the potential for high torque ripple.

Table 13.8-2 Switching Table for Direct Torque Control.

		Sector					
ΔT_e	$\Delta\lvert\lambda_s\rvert$	I	II	III	IV	V	VI
1	1	V_2	V_3	V_4	V_5	V_6	V_1
0	1	V_7	V_0	V_7	V_0	V_7	V_0
−1	1	V_6	V_1	V_2	V_3	V_4	V_5
1	0	V_3	V_4	V_5	V_6	V_1	V_2
0	0	V_0	V_7	V_0	V_7	V_0	V_7
−1	0	V_5	V_6	V_1	V_2	V_3	V_4

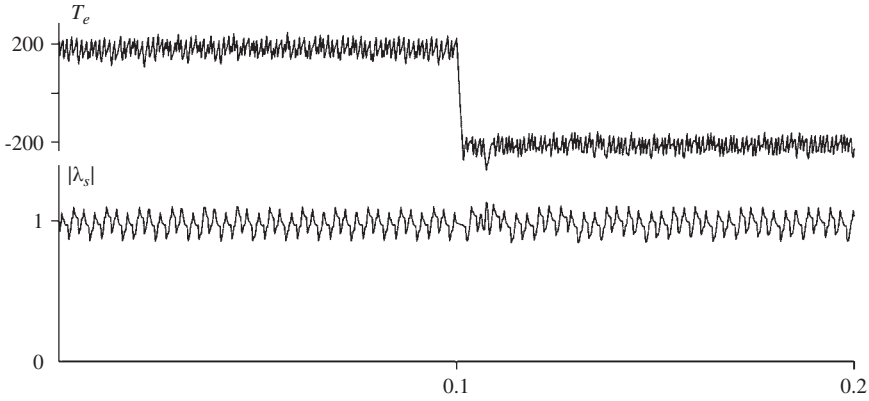

Figure 13.8-3 Step response of an induction motor with DTC.

13.9 Slip Energy Recovery Drives

If an induction machine is supplied by a fixed-frequency fixed-amplitude supply, it exhibits the well-known torque-versus-speed characteristic discussed in Section 3.8. Therein, it was mentioned that increasing the rotor resistance has the benefit of increasing the starting torque and concurrently reducing the reactive power drawn from the source during startup from zero speed. However, once the motor has accelerated to its final steady-state speed, the slip will be larger than with the original rotor resistance thereby increasing losses. With the advent of modern power electronics, it is possible to achieve the benefits of increasing rotor resistance without the associated power losses.

A typical slip energy drive system is depicted in Figure 13.9-1. As shown, the stator is connected to a fixed-frequency, fixed-amplitude source, which also supplies an active bridge rectifier whose dc output is regulated to a fixed value. The dc voltage is then converted to three-phase ac by a six-step inverter using, for example, a sine-triangle or space vector modulator (STM or SVM) as described in Section 10.7. Using this approach, it is possible to control both the amplitude and frequency of the voltages applied to the rotor windings. By doing so appropriately, it is possible to set the electromagnetic torque to any desired value within design limits over a range of rotor speeds. It is also possible to control the net reactive power supplied to or by the electric source. Such an arrangement is commonly used in modern wind turbine generators at the multimegawatt level where the rotor speed at which optimum power extraction occurs varies as a function of the wind speed.

A strategy that can be used to control the electromagnetic torque can be established by considering the steady-state relationships between the rotor and stator

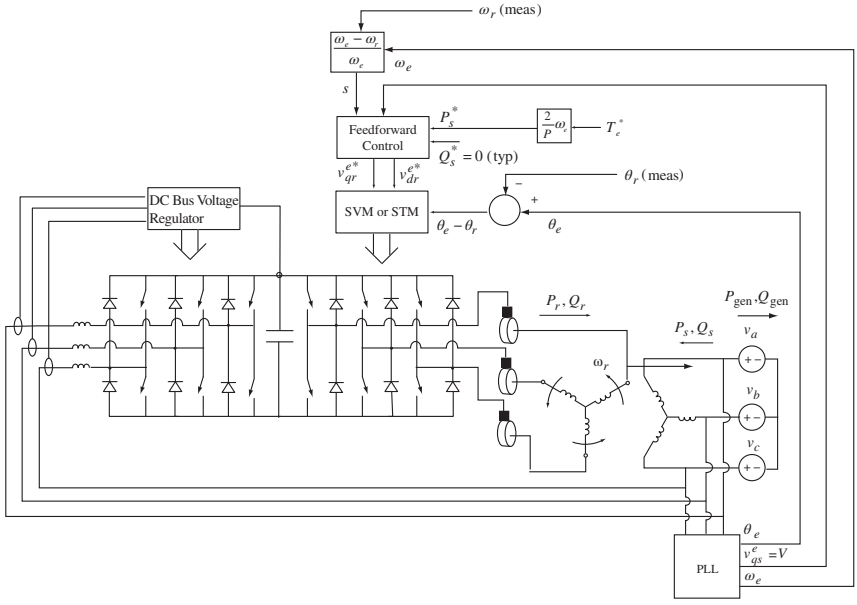

Figure 13.9-1 Circuit/block diagram of a slip energy recovery drive system.

voltage and currents, which are repeated here for convenience. The steady-state real and reactive power supplied to the stator windings may be expressed as

$$P_s = \frac{3}{2}(V_{qs}I_{qs} + V_{ds}I_{ds}) \tag{13.9-1}$$

$$Q_s = \frac{3}{2}(V_{qs}I_{ds} - V_{ds}I_{qs}) \tag{13.9-2}$$

Likewise, the steady-state real and reactive power supplied to the rotor windings may be expressed as

$$P_r = \frac{3}{2}\left(V'_{qr}I'_{qr} + V'_{dr}I'_{dr}\right) \tag{13.9-3}$$

$$Q_r = \frac{3}{2}\left(V'_{qr}I'_{dr} - V'_{dr}I'_{qr}\right) \tag{13.9-4}$$

For analysis purposes, it is convenient to select the synchronous reference frame with its time-zero location set so that $V_{ds}^e = 0$. The steady-state stator voltage equations become

$$V_{qs}^e = r_s I_{qs}^e + \omega_e \Psi_{ds}^e \tag{13.9-5}$$

$$0 = r_s I_{ds}^e - \omega_e \Psi_{qs}^e \tag{13.9-6}$$

where $\Psi = \omega_e \lambda$. In terms of currents, the stator voltage equations become

$$V_{qs}^e = r_s I_{qs}^e + X_{ss} I_{ds}^e + X_M I'^e_{dr} \tag{13.9-7}$$

$$V_{ds}^e = r_s I_{ds}^e - X_{ss} I_{qs}^e - X_M I'^e_{qr} \tag{13.9-8}$$

The rotor voltage equations may be expressed similarly as

$$V'^e_{qr} = r'_r I_{dr}^e + s\left(X_M I_{ds}^e + X'_{rr} I'^e_{dr}\right) \tag{13.9-9}$$

$$V'^e_{dr} = r'_r I_{dr}^e - s\left(X_M I_{qs}^e + X'_{rr} I'^e_{qr}\right) \tag{13.9-10}$$

where $s = (\omega_e - \omega_r)/\omega_e$ is the slip. To establish the voltages that should be applied to the rotor so as to produce the desired value of torque, we start with the established expression for torque

$$T_e = \frac{P}{2}\frac{3}{2}\frac{1}{\omega_e}\left(\Psi_{ds}^e I_{qs}^e - \Psi_{ds}^e I_{qs}^e\right) \tag{13.9-11}$$

If the stator resistance is small, then from (13.9-5) and (13.9-6), $V_{qs}^e \approx \Psi_{ds}^e$ and $V_{ds}^e \approx -\Psi_{qs}^e$, whereupon

$$T_e \approx \frac{P}{2}\frac{3}{2}\frac{1}{\omega_e}\left(V_{qs}^e I_{qs}^e + V_{ds}^e I_{ds}^e\right) \tag{13.9-12}$$

Comparing (13.9-12) with (13.9-1),

$$T_e \approx \frac{P}{2}\frac{1}{\omega_e} P_s \tag{13.9-13}$$

The preceding steady-state relationships suggest the "feedforward" control strategy shown in Figure 13.9-2. Therein, the measured peak stator voltage is established using a phase-locked loop **(**PLL), which also determines the electrical frequency ω_e. Based on the commanded electromagnetic torque and reactive power, the steady-state equations are used to establish, in sequence, the desired stator currents, the desired rotor currents, and finally the commanded rotor voltages, which are supplied to the inverter modulator (SVM or STM). If the calculated rotor currents and voltages are substituted into the expression for rotor power (13.9-3) and the stator losses are small,

$$P_r \approx -sP_s \tag{13.9-14}$$

If the converter losses are small, the net electrical power supplied to the drive system is

$$P_e \approx P_s + P_r \tag{13.9-15}$$

which is positive if the drive system is operating as a motor and negative if it is operating as a generator. The main advantage of a slip energy recovery drive can be seen from (13.9-14) and (13.9-15). If the rotor speeds ω_r over which the drive

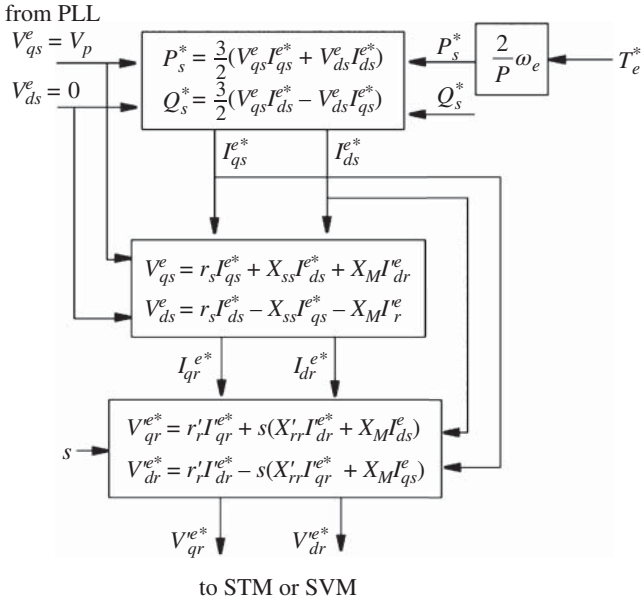

Figure 13.9-2 Feedforward control for a slip energy recovery drive system.

system operates lie in a narrow range about the fixed electrical frequency ω_e, the slip s will be small, and from (13.9-14) and (13.9-15), the power that needs to be supplied to the rotor windings, which determines the power rating of the associated rectifier and inverter, is a small fraction of the net electric power P_e supplied to or by the drive system.

13.10 Conclusions

In this chapter, a variety of induction motor drive schemes have been explored including volts-per-hertz, compensated volts-per-hertz, constant-slip, rotor flux oriented, and DTC. If the rotor speed is expected to vary inside a limited range near synchronous speed, slip energy recovery drive systems are shown to have an advantage. This chapter is intended to be an introduction to these diverse methods of control. For detailed aspects and refinements to the basic approaches described herein, the reader is referred to Reference 9.

References

1 A. Muñoz-García, T. A. Lipo, and D. W. Novotny, "A New Induction Motor *V/f* Control Method Capable of High-Performance Regulation at Low Speeds," *IEEE Trans. Ind. Appl.*, Vol. 34, No. 4, July/August 1998, pp. 813–821.

2 P. P. Waite and G. Pace, "Performance Benefits of Resolving Current in Open-Loop AC Drives," Proceedings of the 5th European Conference on Power Electronics and Applications, September 13–16, 1993, Brighton, UK, pp. 405–409.

3 O. Wasynczuk, S. D. Sudhoff, K. A. Corzine, J. L. Tichenor, P. C. Krause, I. G. Hansen, and L. M. Taylor, "A Maximum Torque per Ampere Control Strategy for Induction Motor Drives," *IEEE Trans. Energy Conversion*, Vol. 13, No. 2, June 1998, pp. 163–169.

4 O. Wasynczuk and S. D. Sudhoff, "Maximum Torque per Ampere Induction Motor Drives—An Alternative to Field-Oriented Control," *SAE Trans., J. Aerosp*., Vol. 107, Section 1, 1998, pp. 85–93.

5 A.M. Trzynadlowski, *The Field Orientation Principle in Control of Induction Motors*, Kluwer Academic Publishers, Boston, 1994.

6 I. Boldea and S. A. Nasar, *Vector Control of AC Drives*, CRC Press, Boca Raton, FL, 1992.

7 I. Takahashi and T. Noguchi, "A New Quick-Response and High-Efficiency Control Strategy of an Induction Motor," *IEEE Trans. Ind. Appl.*, Vol. 22, September/October 1986, pp. 820–827.

8 I. Takahashi and Y. Ohmori, "High-Performance Direct Torque Control of an Induction Motor," *IEEE Trans. Ind. Appl.*, Vol. 25, No. 2, March/April 1989, pp. 257–264.

9 P. Vas, *Sensorless Vector and Direct Torque Control*, Oxford Science Publications, Oxford, 1998.

10 K. Rajashekara, A. Kawamura, and K. Matsuse, *Sensorless Control of AC Motor Drives—Speed and Position Sensorless Operation*, IEEE Press, Piscataway, NJ, 1996 (Selected Reprints).

Problems

13.1 Derive (13.2-4) and (13.2-7).

13.2 Calculate the characteristics shown in Figure 13.2-4 if (a) $r_{s,est} = 0.75r_s$ and (b) $L_{ss,est} = 1.1L_{ss}$.

13.3 Consider the 50-hp induction machine used in the studies in this chapter. Suppose the combined inertia of the machine and load is 2 N·m·s^2. Compute the minimum value of $\alpha_{\max}$ of a slew rate limiter by assuming that there is no load torque and that the rated electrical torque is obtained.

13.4 Using the parameters of the 50-hp induction motor set forth in this chapter, plot the ratio of power loss divided by torque (see 13.3-18) and the corresponding value of the magnitude of the air-gap flux as a function of slip frequency ω_s.

13.5 Repeat the study depicted in Figure 13.3-2 if (a) $r'_{r,est} = 0.75r'_r$ and (b) $r'_{r,est} = 1.25r'_r$.

13.6 Derive the transfer function between commanded and actual speed if the control used in Figure 13.2-5 is used. Assume that the electromagnetic torque is equal to its commanded value, that the load torque is zero, and that the combined inertia of the electric machine and load is J.

13.7 Suppose it is desired that the rms value of the fundamental component of the rotor flux, λ_r, in the constant slip control is to be limited to the value that would be obtained at rated speed, rated frequency, and rated voltage for no-load conditions. Compute the numerical value of λ_r. If maximum torque per amp control is used, at what percentage of base torque does the control change from constant slip to constant flux?

13.8 Using the same criterion as in problem 6, compute λ^{e*}_{dr} for field oriented control.

13.9 At moderate and high speeds, it is possible to measure the applied voltages and currents, and based on this information, form an estimate of λ^s_{qs} and λ^s_{ds}. Draw a block diagram of a control that could achieve this. Given λ^s_{qs} and λ^s_{ds}, devise flux and torque control loops that could be used to add robustness to the indirect field-oriented controller. Why would this method not work at low speeds?

13.10 Derive (13.6-4).

13.11 Derive (13.6-12).

13.12 Derive an indirect field oriented control strategy in which $\lambda'^e_{dr} = 0$ and $i'^e_{qr} = 0$.

14

Permanent-Magnet AC Motor Drives

14.1 Introduction

There are a great variety of permanent-magnet ac motor drive configurations. Generally, these may be described by the block diagram in Figure 14.1-1. Therein, the permanent-magnet ac drive is seen to consist of four main parts, a power converter, a permanent-magnet ac machine (PMAM), sensors, and a control algorithm. The power converter transforms power from the source (such as the local utility or a dc supply bus) to the proper form to drive the PMAM, which, in turn, converts electrical energy to mechanical energy. One of the salient features of the permanent-magnet ac drive is the rotor position sensor (or at least an estimator or observer). Based on the rotor position, and a command signal(s), which may be a torque command, voltage command, speed command, and so on, the control algorithms determine the gate signal to each semiconductor in the power electronic converter.

In this chapter, the converter connected to the machine will be assumed to be a fully controlled three-phase bridge converter, as discussed in Chapter 10. Because we will primarily be considering motor operation, we will refer to this converter as an inverter throughout this chapter.

The structure of the control algorithms determines the type of permanent-magnet ac motor drive, of which there are two main classes, voltage-source-based drives and current-regulated drives. Both voltage-source and current-regulated drives may be used with PMAMs with either sinusoidal or nonsinusoidal back emf waveforms. Machines with sinusoidal back emfs may be controlled so as to achieve nearly constant torque; however, machines with a nonsinusoidal back emf may be less expensive to manufacture. The discussion in this chapter will focus on the machines with sinusoidal back emfs; for information on the nonsinusoidal drives, the reader is referred to References [1–3].

Analysis of Electric Machinery and Drive Systems, Fourth Edition.
Paul C. Krause, Oleg Wasynczuk, Scott D. Sudhoff, and Steven D. Pekarek.

Companion website: www.wiley.com/go/krause_aem4e

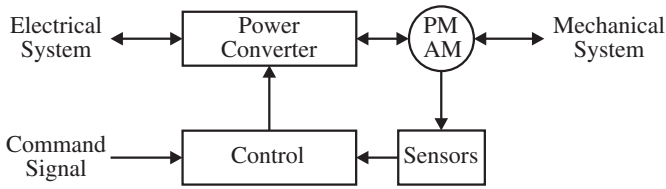

Figure 14.1-1 Permanent-magnet ac motor drive.

In this chapter, a variety of voltage-source and current-regulated drives featuring machines with sinusoidal back emf waveforms will be analyzed. For each drive considered, computer simulations will be used to demonstrate performance. Next, average-value models for each drive are set forth, along with a corresponding linearized model for control synthesis. Using these models, the steady-state, transient, and dynamic performance of each drive configuration considered will be set forth. Design examples will be used to illustrate the performance of the drive in the context of a control system.

14.2 Voltage-Source Inverter Drives

Figure 14.2-1 illustrates a voltage-source-modulated inverter-based permanent-magnet ac motor drive. Here, voltage-source inverter refers to an inverter being controlled by a voltage-source modulation strategy (six-stepped, six-step modulated, sine-triangle modulated, etc.). Power is supplied from the utility through a transformer, which is depicted as an equivalent voltage behind inductance. The transformer output is rectified using a semi-controlled three-phase bridge converter, as discussed in Chapter 9. Since this converter is operated as a rectifier (i.e.,

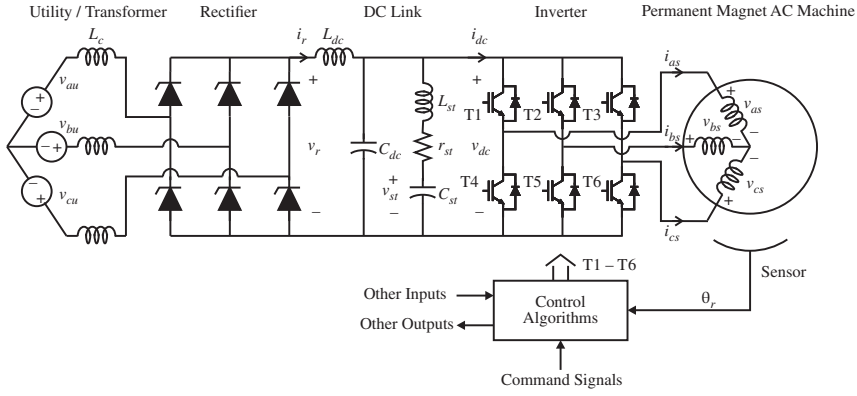

Figure 14.2-1 Permanent-magnet ac motor drive circuit.

converting power from the ac system to the dc system), it will be simply referred to as a rectifier herein. The rectifier output is connected to the dc link filter, which may be simply an LC filter (L_{dc}, C_{dc}), but which may include a stabilizing filter (L_{st}, r_{st}, C_{st}) as well. The filtered rectifier output is used as a dc voltage source for the inverter, which drives the PMAM. This voltage is commonly referred to as the dc link voltage. As can be seen, rotor position is an input to the controller. Based on rotor position and other inputs, the controller determines the switching states of each of the inverter semiconductors. The command signal to the controller may be quite varied depending on the structure of the controls in the system in which the drive will be embedded; it will often be a torque command. Other inputs to the control algorithms may include rotor speed and dc link voltage. Other outputs may include gate signals to the rectifier thyristors if the rectifier is phase-controlled.

Variables of particular interest in Figure 14.2-1 include the utility supply voltage, v_{au}, v_{bu}, and v_{cu}, the utility current into the rectifier i_{au}, i_{bu}, and i_{cu}, the rectifier output voltage, v_r, the rectifier current, i_r, the stabilizing filter current i_{st}, the stabilizing filter capacitor voltage v_{st}, the inverter voltage v_{dc}, the inverter current i_{dc}, the three-phase currents into the machine i_{as}, i_{bs}, and i_{cs}, and the machine line-to-neutral voltages v_{as}, v_{bs}, and v_{cs}.

Even within the context of the basic system shown in Figure 14.2-1, there are many possibilities for control, depending on whether or not the rectifier is phase-controlled and the details of the inverter modulation strategy. Regardless of the control strategy, it is possible to relate the operation of the converter back to the idealized machine analysis set forth in Chapter 4, which will be the starting point for our investigation into voltage-source inverter fed permanent-magnet ac motor drive systems.

14.3 Equivalence of Voltage-Source Inverters to an Idealized Source

Voltage-source inverters are inverters with a voltage-source modulator. In order to make use of our analysis of the PMAM set forth in Chapter 4 when the voltage source is an inverter rather than an ideal source, it is necessary to relate the voltage-source inverter to an ideal source. This relationship is a function of the type of modulation strategy used. In this section, the equivalence of six-stepped, six-step-modulated, sine triangle-modulated, extended-sine triangle-modulated, or space-vector-modulated inverter to an idealized source is established.

The six-stepped inverter-based permanent-magnet ac motor drive is the simplest of all the strategies to be considered in terms of generating the signals required to control the inverter. It is based on the use of relatively inexpensive Hall effect rotor position sensors. For this reason, the six-stepped inverter drive is a relatively low-cost drive. Furthermore, since the frequency of the switching of the

semiconductors corresponds to the frequency of the machine, fast semiconductor switching is not important, and switching losses will be negligible. However, the inverter does produce considerable harmonic content, which will result in increased machine losses.

In the six-stepped inverter, the on/off status of each of the semiconductors is directly tied to electrical rotor position, which is accomplished through the use of the Hall effect sensors. These sensors are configured to have a logical 1 output when they are under a south magnetic pole and a logic 0 when they are under a north magnetic pole of the permanent magnet, and are arranged on the stator of the PMAM as illustrated in Figure 14.3-1, where ϕ_h denotes the position of the Hall effect sensors. The logical output of sensors H1, H2, and H3 are equal to the gate signals for T1, T2, and T3, respectively, so that the gating signals are as indicated in Figure 14.3-2. The gate signals T4, T5, and T6 are the logical complements of T1, T2, and T3, respectively.

Comparing the gating signals shown in Figure 14.3-2 with those illustrated in the generic discussion of six-step operation in Chapter 10 (see Fig.12.3-1), it can be seen that the two sets of waveforms are identical provided the converter angle θ_c is related to rotor position and the Hall effect position by

$$\theta_c = \theta_r + \phi_h \tag{14.3-1}$$

In Section 10.3, expressions for the average-value of the q- and d-axis voltages in the converter reference frame were derived. Taking these expressions as dynamic averages,

$$\hat{v}_{qs}^c = \frac{2}{\pi}\hat{v}_{dc} \tag{14.3-2}$$

$$\hat{v}_{ds}^c = 0 \tag{14.3-3}$$

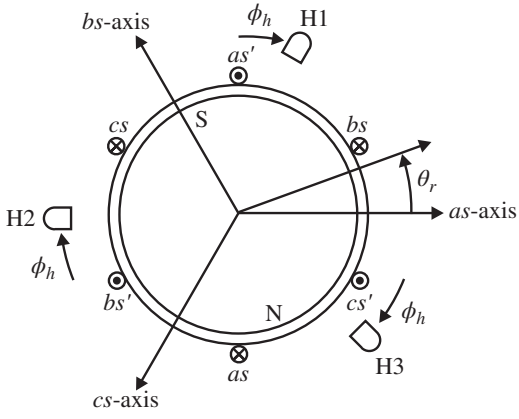

Figure 14.3-1 Electrical diagram of a permanent-magnet ac machine.

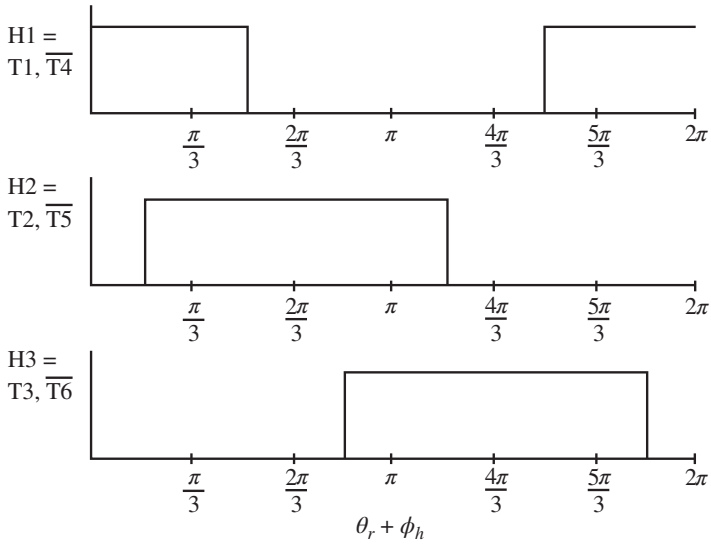

Figure 14.3-2 Semiconductor switching signals.

From (14.3-1), the difference in the angular position between the converter reference frame and rotor reference frame is the Hall effect position ϕ_h. Using this information, the dynamic-average of the stator voltages may be determined in the rotor reference frame using the frame-to-frame transformation ${}^{c}\mathbf{K}_s^r$, which yields

$$\hat{v}_{qs}^r = \frac{2}{\pi}\hat{v}_{dc}\cos\phi_h \tag{14.3-4}$$

$$\hat{v}_{ds}^r = -\frac{2}{\pi}\hat{v}_{dc}\sin\phi_h \tag{14.3-5}$$

From (14.3-4) and (14.3-5), we conclude that at least in terms of the fundamental component, the operation of the PMAM from a six-stepped inverter is identical to a PMAM fed by ideal three-phase variable-frequency voltage source with an rms amplitude of

$$v_s = \frac{1}{\sqrt{2}}\frac{2}{\pi}\hat{v}_{dc} \tag{14.3-6}$$

and a phase advance of

$$\phi_v = \phi_h \tag{14.3-7}$$

Figure 14.3-3 illustrates the steady-state performance of a six-stepped inverter. In this study, the inverter voltage v_{dc} is regulated at 125 V and the mechanical rotor speed is 200 rad/s. The machine parameters are $r_s = 2.98\ \Omega$, $L_q = L_d = 11.4$ mH, $\lambda'_m = 0.156$ Vs, and $P = 4$. There is no phase advance. As can be seen, the nonsinusoidal a-phase voltage results in time-varying q- and d-axis voltages. The effect of

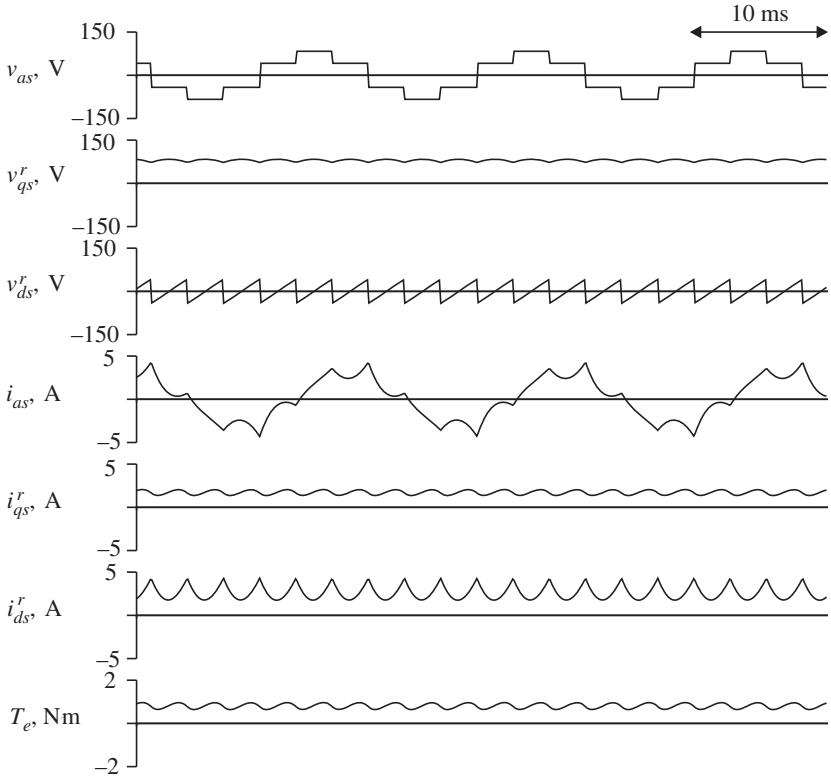

Figure 14.3-3 Steady-state performance of a six-stepped permanent-magnet ac motor drive.

the harmonics is clearly evident in the *a*-phase current waveform, as well as the *q*- and *d*-axis current waveforms. Also apparent are the low-frequency torque harmonics (six times the fundamental frequency) that result. The current harmonics do not contribute to the average torque; therefore, the net effect of the harmonics is to increase machine losses. On the other hand, since the inverter is switching at a relatively low frequency (six times the electrical frequency of the fundamental component of the applied voltage), switching losses are extremely low.

This drive system is easy to implement in hardware; however, at the same time, it is difficult to utilize in a speed control system, since the fundamental component of the applied voltage cannot be adjusted unless a controlled rectifier is used. Although this is certainly possible, and has often been done in the past, it is generally advantageous to control the applied voltages with the inverter rather than rectifier since this minimizes the total number of power electronics devices.

In order to control the amplitude of the fundamental component of the applied voltage, six-step modulation may be used, as is discussed in Section 10.4. In this case, the gate drive signals T1–T6 are modulated in order to control the amplitude of the applied voltage. Recall from Section 10.4 that for six-step modulation, the dynamic-average q- and d-axis voltages are given by

$$\hat{v}_{qs}^{c} = \frac{2}{\pi} d\hat{v}_{dc} \tag{14.3-8}$$

and

$$\hat{v}_{ds}^{c} = 0 \tag{14.3-9}$$

Using (14.3-1) to relate the positions of the converter and rotor reference frames, the frame-to-frame transformation may be used to express the q- and d-axis voltage in the rotor reference frame. In particular,

$$\hat{v}_{qs}^{r} = \frac{2}{\pi} d\hat{v}_{dc} \cos \phi_h \tag{14.3-10}$$

$$\hat{v}_{ds}^{r} = -\frac{2}{\pi} d\hat{v}_{dc} \sin \phi_h \tag{14.3-11}$$

From (14.3-10) and (14.3-11), it is clear that the effective rms amplitude of the applied voltage is

$$v_s = \frac{1}{\sqrt{2}} \frac{2}{\pi} d\hat{v}_{dc} \tag{14.3-12}$$

The phase advance given by (14.3-7) is applicable to the six-step modulated drive in addition to the six-stepped inverter.

Figure 14.3-4 illustrates the performance of a six-step modulated drive. For this study, the parameters are identical to those for the study depicted in Figure 14.3-3, with the exception of the modulation strategy, which is operating with a duty cycle of 0.9 at a frequency of 5 kHz, and the dc rail voltage is 138.9 V, which yields the same fundamental component of the applied voltage as in the previous study. As can be seen, the voltage waveforms posses an envelop similar in shape to that of the six-step case; however, they are rapidly switching within that envelope. Note that the current waveforms are similar to the previous study, although there is additional high-frequency harmonic content.

By utilizing six-step modulation, the amplitude of the applied voltage is readily varied. However, due to the increased switching frequency, the switching losses in the converter are increased. The losses in the machine will be similar to those in the previous study.

Like six-step modulation, sine-triangle modulation may also be used to control the amplitude of the voltage applied to the PMAM. However, in this case, Hall effect sensors are generally not adequate to sense rotor position. Recall from Section 10.5 that phase-leg duty cycles are continuous function of converter angle,

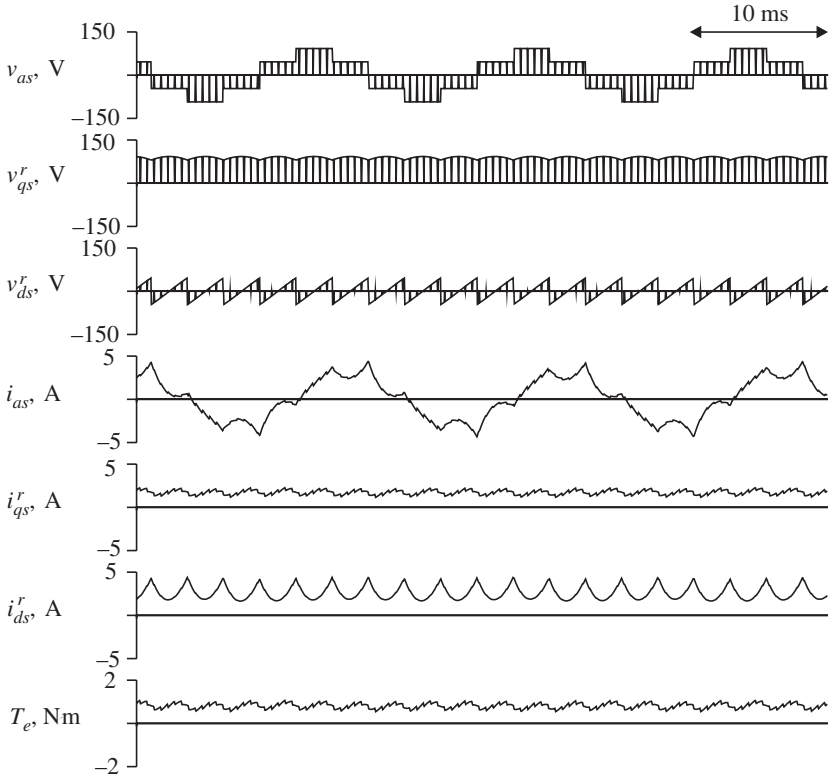

Figure 14.3-4 Steady-state performance of a six-step-modulated permanent-magnet ac motor drive.

which implies that they will be continuous functions of rotor position. For this reason, a resolver or an optical encoder must be used as the rotor position sensor. Although this increases the cost of the drive, and also increases the switching losses of the power electronics devices, the sine-triangle modulated drive does have an advantage in that the low-frequency harmonic content of the machine currents are greatly reduced, thereby reducing machine losses in machines with a sinusoidal back emf and also reducing acoustic noise and torque ripple.

In the case of the sine-triangle modulated inverter, the angular position used to determine the phase-leg duty cycles, that is, the converter angle, is equal to the electric rotor position plus an offset, that is,

$$\theta_c = \theta_r + \phi_v \tag{14.3-13}$$

From Section 10.5,

$$\hat{v}_{qs}^{c} = \begin{cases} \frac{1}{2} d \hat{v}_{dc} & 0 < d \leq 1 \\ \frac{2}{\pi} \hat{v}_{dc} f(d) & d > 1 \end{cases} \tag{14.3-14}$$

$$\hat{v}_{ds}^{c} = 0 \tag{14.3-15}$$

where

$$f(d) = \frac{1}{2}\sqrt{1 - \left(\frac{1}{d}\right)^2} + \frac{1}{4} d \left(\pi - 2 \arccos\left(\frac{1}{d}\right)\right) \quad d > 1 \tag{14.3-16}$$

Using (14.3-13) to compute the angular difference of the locations of the converter and rotor reference frames, the dynamic averages of the q- and d-axis stator voltages may be expressed as

$$\hat{v}_{qs}^{r} = \begin{cases} \frac{1}{2} \hat{v}_{dc} d \cos \phi_v & d \leq 1 \\ \frac{2}{\pi} \hat{v}_{dc} f(d) \cos \phi_v & d > 1 \end{cases} \tag{14.3-17}$$

$$\hat{v}_{ds}^{r} = \begin{cases} -\frac{1}{2} \hat{v}_{dc} d \sin \phi_v & d \leq 1 \\ -\frac{2}{\pi} \hat{v}_{dc} f(d) \sin \phi_v & d > 1 \end{cases} \tag{14.3-18}$$

Figure 14.3-5 illustrates the performance of a sine-triangle modulated inverter drive. The parameters and operating conditions are identical to those in the previous study with a duty cycle is 0.9 and the switching frequency of 5 kHz, with the exception that the dc voltage has been increased to 176.8 V. This yields the same fundamental component of the applied voltage as in the previous two studies. Although on first inspection the voltage waveforms appear similar to the six-step modulated case, the harmonic content of the waveform has been significantly altered. This is particularly evident in the current waveforms which no longer contain significant harmonic content. As a result, the torque waveform is also devoid of low-frequency harmonics. Like six-step modulation, this strategy allows the fundamental component of the applied voltage to be changed. In addition, the phase can be readily changed, and low-frequency current and torque harmonics are eliminated. However, the price for these benefits is that rotor position must be known on a continuous basis, which requires either an optical encoder or resolver, which are considerably more expensive than Hall effect sensors. Several methods of eliminating the need for the encoder or resolver have been set forth in References [4, 5].

In Chapter 10, the next modulation strategy considered was extended sine-triangle modulation. The analysis of this strategy is the same as for

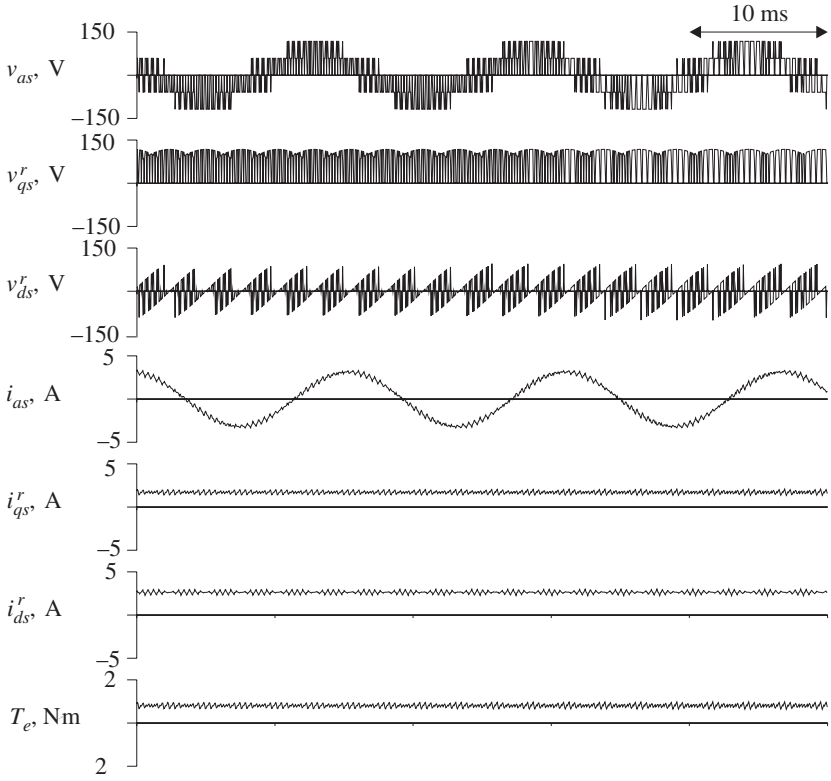

Figure 14.3-5 Steady-state performance of sine-triangle-modulated permanent-magnet ac motor drive.

sine-triangle modulation, with the exception that the amplitude of the duty cycle d may be increased to $2/\sqrt{3}$ before overmodulation occurs. Therefore, we have

$$\hat{v}^r_{qs} = \frac{1}{2} d\hat{v}_{dc} \cos \phi_v \quad 0 \le d \le 2/\sqrt{3} \tag{14.3-19}$$

$$\hat{v}^r_{ds} = -\frac{1}{2} d\hat{v}_{dc} \sin \phi_v \quad 0 \le d \le 2/\sqrt{3} \tag{14.3-20}$$

The final voltage-source modulation strategy considered in Chapter 10 was space-vector modulation. This strategy is designed to control the inverter semiconductors in such a way that the dynamic average of the q- and d-axis output voltages are equal to the q- and d-axis voltage command, provided that the peak commanded line-to-neutral input voltage magnitude is less than $v_{dc}/\sqrt{3}$. If this limit is exceeded, the q- and d-output voltage vector retains its commanded

direction, but its magnitude is limited. Thus, we have that

$$\hat{v}_{qs}^{r} = \begin{cases} v_{qs}^{r*} & v_{spk}^{*} < v_{dc}/\sqrt{3} \\ \dfrac{\hat{v}_{dc}}{\sqrt{3}} \dfrac{v_{qs}^{r*}}{v_{spk}^{*}} & v_{spk}^{*} \geq v_{dc}/\sqrt{3} \end{cases} \tag{14.3-21}$$

$$\hat{v}_{ds}^{r} = \begin{cases} v_{ds}^{r*} & v_{spk}^{*} < v_{dc}/\sqrt{3} \\ \dfrac{\hat{v}_{dc}}{\sqrt{3}} \dfrac{v_{ds}^{r*}}{v_{spk}^{*}} & v_{spk}^{*} \geq v_{dc}/\sqrt{3} \end{cases} \tag{14.3-22}$$

where

$$v_{spk}^{*} = \sqrt{\left(v_{qs}^{r*}\right)^2 + \left(v_{ds}^{r*}\right)^2} \tag{14.3-23}$$

In order to summarize the results of this section, notice that in each case, the dynamic-average q- and d-axis voltages may be expressed as

$$\hat{v}_{qs}^{r} = \hat{v}_{dc} m \cos \phi_v \tag{14.3-24}$$

$$\hat{v}_{ds}^{r} = -\hat{v}_{dc} m \sin \phi_v \tag{14.3-25}$$

where

$$m = \begin{cases} \dfrac{2}{\pi} & \text{six-step operation} \\ \dfrac{2}{\pi} d & \text{six-step modulation } (d \leq 1) \\ \dfrac{1}{2} d & \text{sine-triangle modulation } (d \leq 1) \\ \dfrac{2}{\pi} f(d) & \text{sine-triangle modulation } (1 < d) \\ \dfrac{1}{2} d & \text{extended sine-triangle modulation } (d \leq 2/\sqrt{3}) \\ \dfrac{v_{spk}^{*}}{v_{dc}} & \text{space-vector modulation } (v_{spk}^{*} \leq v_{dc}/\sqrt{3}) \\ \dfrac{1}{\sqrt{3}} & \text{space-vector modulation } (v_{spk}^{*} > v_{dc}/\sqrt{3}) \end{cases} \tag{14.3-26}$$

In the case of space-vector modulation, observe that ϕ_v is defined as

$$\phi_v = \text{angle}\left(v_{qs}^{r*} - j v_{ds}^{r*}\right) \tag{14.3-27}$$

14.4 Average-Value Analysis of Voltage-Source Inverter Drives

The average-value model of a voltage-source inverter drive consist of five parts, (1) the rectifier model, (2) the dc link and stabilizing filter model, (3) the inverter model, and (4) the machine model. From Chapter 9, recall that the dynamic-average rectifier voltage is given by

$$\hat{v}_r = v_{r0}\cos\alpha - r_r\hat{i}_r - l_r p\hat{i}_r \tag{14.4-1}$$

where v_{r0}, r_r, and l_r are given by

$$v_{r0} = \begin{cases} \dfrac{3\sqrt{6}}{\pi}E & \text{three-phase rectifier} \\ \dfrac{2\sqrt{2}}{\pi}E & \text{single-phase rectifier} \end{cases} \tag{14.4-2}$$

$$r_r = \begin{cases} \dfrac{3}{\pi}\omega_{eu}L_c & \text{three-phase rectifier} \\ \dfrac{2}{\pi}\omega_{eu}L_c & \text{single-phase rectifier} \end{cases} \tag{14.4-3}$$

$$l_r = \begin{cases} 2L_c & \text{three-phase rectifier} \\ L_c & \text{single-phase rectifier} \end{cases} \tag{14.4-4}$$

In (14.4-2)–(14.4-4), ω_{eu} is the radian electrical frequency of the source feeding the rectifier, not to be confused with the fundamental frequency being synthesized by the drive, and E is the rms line-to-neutral utility voltage (line-to-line voltage in single-phase applications), and L_c is the commutating inductance. In the typical case wherein a transformer/rectifier is used, E and L_c reflect the utility voltage and transformer leakage impedance referred to the secondary (drive) side of the transformer.

The electrical dynamics of the rectifier current may be expressed as

$$L_{dc}pi_r = v_r - v_{dc} - r_{dc}i_r \tag{14.4-5}$$

Treating the variables in (14.4-5) as dynamic-average values yields

$$L_{dc}p\hat{i}_r = \hat{v}_r - \hat{v}_{dc} - r_{dc}\hat{i}_r \tag{14.4-6}$$

In (14.4-6), the rectifier voltage is given by (14.4-1); however, that expression for the rectifier voltage involves the time derivative of $\hat{i}_r$. Hence, (14.4-1) and (14.4-6) should be combined into a single differential equation. In particular,

$$p\hat{i}_r = \frac{\hat{v}_{r0}\cos\alpha - \hat{v}_{dc} - r_{rl}\hat{i}_r}{L_{rl}} \tag{14.4-7}$$

where

$$r_{rl} = r_r + r_{dc} \tag{14.4-8}$$

$$L_{rl} = L_r + L_{dc} \tag{14.4-9}$$

Finally, using Kirchoff's laws, the dc voltage, stabilizing filter current, and stabilizing filter voltage are governed by

$$p\hat{v}_{dc} = \frac{\hat{i}_r - \hat{i}_{st} - \hat{i}_{dc}}{C_{dc}} \tag{14.4-10}$$

$$p\hat{i}_{st} = \frac{\hat{v}_{dc} - \hat{v}_{st} - r_{st}\hat{i}_{st}}{L_{st}} \tag{14.4-11}$$

and

$$p\hat{v}_{st} = \frac{\hat{i}_{st}}{C_{st}} \tag{14.4-12}$$

respectively. Because the rectifier current must be positive, (14.4-7) is only valid for this condition. If the rectifier current is zero and the derivative given by (14.4-7) is negative, then $p\hat{i}_r$ should be set to zero since the diodes or thyristors will be reverse biased. From (10.3-11), the dc current into the converter may be approximated as

$$\hat{i}_{dc} = \frac{3}{2}\frac{\hat{v}^r_{qs}\hat{i}^r_{qs} + \hat{v}^r_{ds}\hat{i}^r_{ds}}{\hat{v}_{dc}} \tag{14.4-13}$$

Substitution of (14.3-24) and (14.3-25) into (14.4-13) and simplifying yields

$$\hat{i}_{dc} = \frac{3}{2}m\left(\hat{i}^r_{qs}\cos\phi_v - \hat{i}^r_{ds}\sin\phi_v\right) \tag{14.4-14}$$

The next step in developing the average-value model for the voltage-source inverter drive is the incorporation of the electrical dynamics of the machine in average-value form. Taking the dynamic-average of PMAM voltage equations (expressed in terms of currents) and rearranging yields

$$p\hat{i}^r_{qs} = \frac{\hat{v}^r_{qs} - r_s\hat{i}^r_{qs} - \omega_r L_d\hat{i}^r_{ds} - \omega_r\lambda'_m}{L_q} \tag{14.4-15}$$

$$p\hat{i}^r_{ds} = \frac{\hat{v}^r_{ds} - r_s\hat{i}^r_{ds} + \omega_r L_q\hat{i}^r_{ds}}{L_d} \tag{14.4-16}$$

Note that in (14.4-15) and (14.4-16), the electrical rotor speed is not given an average-value designation. Since the rotor speed varies slowly compared with the electrical variables, it can generally be considered a constant as far as the dynamic-averaging procedure is concerned. However, there are instances when this approximation may not be completely accurate—for example, in the case of six-stepped inverter-fed permanent-magnet ac motor drive with an exceptionally

low inertia during the initial part of the start-up transient. Normally, however, the approximation works extremely well in practice.

From Chapter 4, the expression for instantaneous electromagnetic torque is given by

$$T_e = \frac{3}{2}\frac{P}{2}\left(\lambda'_m i^r_{qs} + (L_d - L_q) i^r_{qs} i^r_{ds}\right) \tag{14.4-17}$$

Upon neglecting the correlation between the q-axis current harmonics and the d-axis current harmonics, (14.4-17) may be averaged to yield

$$\hat{T}_e = \frac{3}{2}\frac{P}{2}\left(\lambda'_m \hat{i}^r_{qs} + (L_d - L_q)\hat{i}^r_{qs}\hat{i}^r_{ds}\right) \tag{14.4-18}$$

This approximation (i.e., assuming that the average of the products is equal to the product of the averages) works well in the case of sine-triangle modulation wherein there is relatively little low-frequency harmonic content. However, in the case of the six-step operation or six-step modulation, some error arises from this simplification in salient machines. In the case of nonsalient machines in which the q- and d-axis inductances are equal, (14.4-18) is exact regardless of the modulation scheme.

To complete the average-value model of the drive, it only remains to include the mechanical dynamics. In particular,

$$p\omega_r = \frac{P}{2}\frac{\hat{T}_e - \hat{T}_l}{J} \tag{14.4-19}$$

and, if rotor position is of interest,

$$p\theta_r = \omega_r \tag{14.4-20}$$

Equations (14.4-19) and (14.4-20) complete the average-value model of the voltage-source inverter drive. It is convenient to combine these relationships and express them in matrix-vector form. This yields

$$p\begin{bmatrix} \hat{i}_r \\ \hat{v}_{dc} \\ \hat{i}_{st} \\ \hat{v}_{st} \\ \hat{i}^r_{qs} \\ \hat{i}^r_{ds} \\ \omega_r \end{bmatrix} = \begin{bmatrix} -\frac{r_{rl}}{L_{rl}} & -\frac{1}{L_{rl}} & 0 & 0 & 0 & 0 & 0 \\ \frac{1}{C_{dc}} & 0 & -\frac{1}{C_{dc}} & 0 & 0 & 0 & 0 \\ 0 & \frac{1}{L_{st}} & -\frac{r_{st}}{L_{st}} & -\frac{1}{L_{st}} & 0 & 0 & 0 \\ 0 & 0 & \frac{1}{C_{st}} & 0 & 0 & 0 & 0 \\ 0 & 0 & 0 & 0 & -\frac{r_s}{L_q} & 0 & -\frac{\lambda'_m}{L_q} \\ 0 & 0 & 0 & 0 & 0 & -\frac{r_s}{L_d} & 0 \\ 0 & 0 & 0 & 0 & \frac{3}{2}\left(\frac{P}{2}\right)^2\frac{1}{J}\lambda'_m & 0 & 0 \end{bmatrix} \begin{bmatrix} \hat{i}_r \\ \hat{v}_{dc} \\ \hat{i}_{st} \\ \hat{v}_{st} \\ \hat{i}^r_{qs} \\ \hat{i}^r_{ds} \\ \omega_r \end{bmatrix}$$

$$+\begin{bmatrix} \frac{1}{L_{rl}} v_{r0} \cos\alpha \\ -\frac{3}{2}\frac{m}{C_{dc}}\left(\cos\phi_v \hat{i}^r_{qs} - \sin\phi_v \hat{i}^r_{ds}\right) \\ 0 \\ 0 \\ \frac{1}{L_q}\hat{v}_{dc} m \cos\phi_v - \frac{L_d}{L_q}\omega_r \hat{i}^r_{ds} \\ -\frac{1}{L_d}\hat{v}_{dc} m \sin\phi_v + \frac{L_q}{L_d}\omega_r \hat{i}^r_{qs} \\ \frac{P}{2}\frac{1}{J}\left(\frac{3}{2}\frac{P}{2}(L_d - L_q)\hat{i}^r_{qs}\hat{i}^r_{ds} - \hat{T}_L\right) \end{bmatrix} \tag{14.4-21}$$

14.5 Steady-State Performance of Voltage-Source Inverter Drives

In the previous section, an average-value model of a voltage-source inverter fed PMAC motor drive was set forth. Before using this model to explore the transient behavior of the drive, it is appropriate to first consider the steady-state performance. Throughout this development, variables names will be uppercase, and averages are denoted with an overbar rather than a "∧" since we are considering steady-state quantities. From the work presented in Chapter 10, it is clear that given the modulation strategy and $\overline{V}_{dc}$ the average of the q- and d-axis voltages may be obtained, whereupon the work set forth in Chapter 4 may be used to calculate any quantity of interest. Therefore, the goal of this section will primarily be to establish an expression for $\overline{V}_{dc}$.

The differential equations that govern the dynamic-average value performance of the drive have inputs that are constants in the steady-state; therefore, the solution of these equations is also constant in the steady-state, assuming that a stable solution exists. Therefore, the steady-state solution may be found by setting the derivative terms equal to zero. Thus, for steady-state conditions, the rectifier voltage equation (14.4-7) necessitates that

$$0 = v_{r0}\cos\alpha - \overline{V}_{dc} - r_{rl}\overline{I}_r \tag{14.5-1}$$

Similarly, substitution of (14.4-14) into (14.4-10) and setting the time derivative to zero yields

$$0 = \overline{I}_r - \overline{I}_{st} - \frac{3}{2}m\left(\overline{I}^r_{qs}\cos\phi_v - \overline{I}^r_{ds}\sin\phi_v\right) \tag{14.5-2}$$

Due to the series capacitance in the stabilizing filter, the average of the stabilizing filter current must be equal to zero. Therefore, (14.5-2) reduces to

$$0 = \overline{I}_r - \frac{3}{2}m\left(\overline{I}^r_{qs}\cos\phi_v - \overline{I}^r_{ds}\sin\phi_v\right) \tag{14.5-3}$$

Combining (14.5-3) with (14.5-1) yields

$$\overline{V}_{dc} = v_{r0}\cos\alpha - \frac{3}{2}r_{rl}m\left(\overline{I}^{r}_{qs}\cos\phi_v - \overline{I}^{r}_{ds}\sin\phi_v\right) \tag{14.5-4}$$

The next step in the development is to eliminate the q- and d-axis stator currents from (14.5-4). To this end, setting the time derivatives in (14.4-15) and (14.4-16) to zero and replacing the q- and d-axis voltages with the expressions (14.3-24) and (14.3-25) yields

$$0 = \overline{V}_{dc}m\cos\phi_v - r_s\overline{I}^{r}_{qs} - \omega_r L_d\overline{I}^{r}_{ds} - \omega_r\lambda'_m \tag{14.5-5}$$

$$0 = -\overline{V}_{dc}m\sin\phi_v - r_s\overline{I}^{r}_{ds} + \omega_r L_q\overline{I}^{r}_{qs} \tag{14.5-6}$$

Solving for (14.5-5) and (14.5-6) simultaneously for $\overline{I}^{r}_{qs}$ and $\overline{I}^{r}_{ds}$ in terms of $\overline{V}_{dc}$, m, and ω_r

$$\overline{I}^{r}_{qs} = \frac{r_s\left(\overline{V}_{dc}m\cos\phi_v - \omega_r\lambda'_m\right) + \omega_r L_d\overline{V}_{dc}m\sin\phi_v}{r_s^2 + \omega_r^2 L_d L_q} \tag{14.5-7}$$

$$\overline{I}^{r}_{ds} = \frac{\omega_r L_d\left(\overline{V}_{dc}m\cos\phi_v - \omega_r\lambda'_m\right) - r_s\overline{V}_{dc}m\sin\phi_v}{r_s^2 + \omega_r^2 L_d L_q} \tag{14.5-8}$$

Finally, substitution of (14.5-7) and (14.5-8) into (14.5-4) and solving for $\overline{V}_{dc}$, we have that

$$\overline{V}_{dc} = \frac{\left(r_s^2 + \omega_r^2 L_d L_q\right)v_{r0}\cos\alpha + \frac{3}{2}r_{rl}m\omega_r\lambda'_m(r_s\cos\phi_v - \omega_r L_q\sin\phi_v)}{r_s^2 + \omega_r^2 L_d L_q + \frac{3}{2}m^2 r_{rl}r_s + \frac{3}{4}r_{rl}\omega_r(L_d - L_q)m^2\sin 2\phi_v} \tag{14.5-9}$$

Since (14.4-1) is only valid for rectifier currents greater than zero, it follows that (14.5-9) is only valid when it yields a dc supply voltage such that the rectifier current is positive. In the event that it is not, then the rectifier appears as an open-circuit, and all the diodes or thyristors are reverse biased. In this case, the average dc link current must be equal to zero. Thus, it follows from (14.4-14) that

$$\overline{I}^{r}_{qs}\cos\phi_v - \overline{I}^{r}_{ds}\sin\phi_v = 0 \tag{14.5-10}$$

Substitution of (14.5-7) and (14.5-8) into (14.5-10) yields

$$\overline{V}_{dc}\Big|_{\overline{I}_{dc}=0} = \frac{\omega_r\lambda'_m(r_s\cos\phi - \omega_r L_q\sin\phi_v)}{m\left(r_s + \frac{1}{2}\omega_r(L_d - L_q)\sin 2\phi_v\right)} \tag{14.5-11}$$

Thus, as long as (14.5-9) yields a positive rectifier current, it is a valid expression. In the event that (14.5-9) yields a negative rectifier current, (14.5-11) should be used.

The steady-state performance characteristics of a permanent-magnet ac motor drive are illustrated in Figure 14.5-1. Therein the dc inverter voltage, the peak amplitude of the fundamental component of stator current, defined by

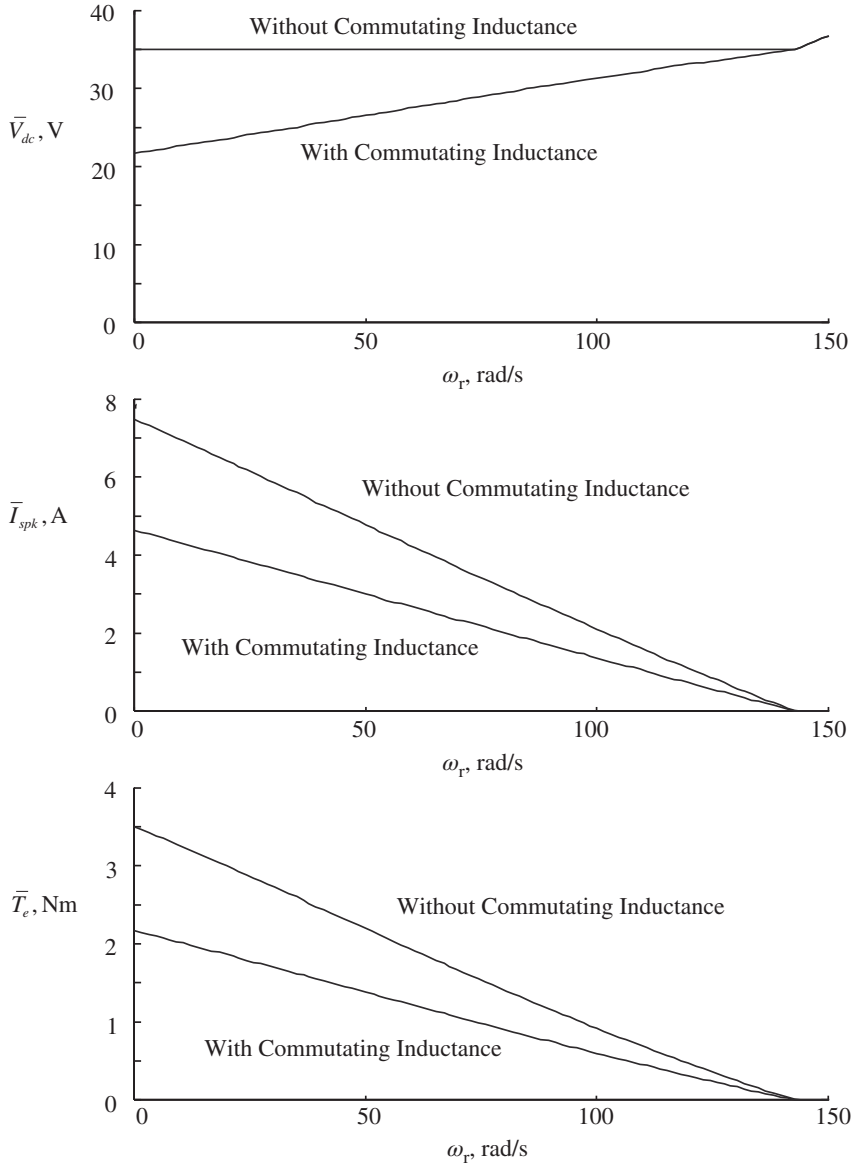

Figure 14.5-1 Steady-state voltage-source inverter-based permanent-magnet ac motor drive characteristics with and without commutating inductance.

$$\bar{I}_{spk} = \sqrt{\bar{I}_{qs}^{r2} + \bar{I}_{ds}^{r2}} \tag{14.5-12}$$

and the average electromagnetic torque are illustrated versus speed for the same parameters that were used in generating Figure 14.3-3. In this case, however, the machine is connected to a transformer rectifier such that $v_{r0} = 35$ V and $r_r = 3.0\ \Omega$. Superimposed on each characteristic is the trace that would be obtained if $\overline{V}_{dc}$ were held constant (i.e., there was no voltage drop due to commutating inductance). As can be seen, the amplitude of the stator current, the electromagnetic torque, and dc voltage are all considerably reduced due to the voltage drop that occurs due to the commutating reactance, although the difference decreases with speed. It is interesting to observe that above 145 rad/s, the dc voltage increases. This is due to the fact that rectified machine voltage is greater than the voltage produced by the rectifier diodes, hence these diodes become reverse biased.

14.6 Transient and Dynamic Performance of Voltage-Source Inverter Drives

In this section, the transient (large disturbance) and dynamic (small disturbance) behavior of voltage-source inverter-based drives is examined. To this end, consider the drive system illustrated in Figure 14.2-1. The parameters for this drive system are $E = 85.5$ V, $\omega_{eu} = 2\pi 60$ rad/s, $L_c = 5$ mH, $L_{dc} = 5$ mH, and $C = 1000\ \mu$F. The rectifier is uncontrolled (diodes are used), and the inverter is sine-triangle modulated. The machine parameters are identical to those of the machine considered in Section 14.6-3, and the load torque is equal to 0.005 N m s/rad times the mechanical rotor speed.

Figure 14.6-1 illustrates the startup performance as the duty cycle is stepped from 0 to 0.9 as calculated by a waveform-level model in which the switching of each semiconductor is taken into account. As can be seen, there is a large inrush of current on startup since initially the impedance of the machine consists solely of the stator resistance, and since initially there is no back emf. This results in a large initial torque so the machine rapidly accelerates. Note that the large inrush current causes a significant drop in the dc voltage. Although the inrush current results in a large initial torque, this is generally an undesirable affect since the initial current is well over the rated current of the machine (3.68 A, peak). In addition, if provision is not made to avoid these overcurrents, then the inverter and rectifier will both have to be sized to insure that the semiconductors are not damaged. Since the cost of the semiconductors is roughly proportional to the voltage rating times the current rating, and since the overcurrent is five times rated current,

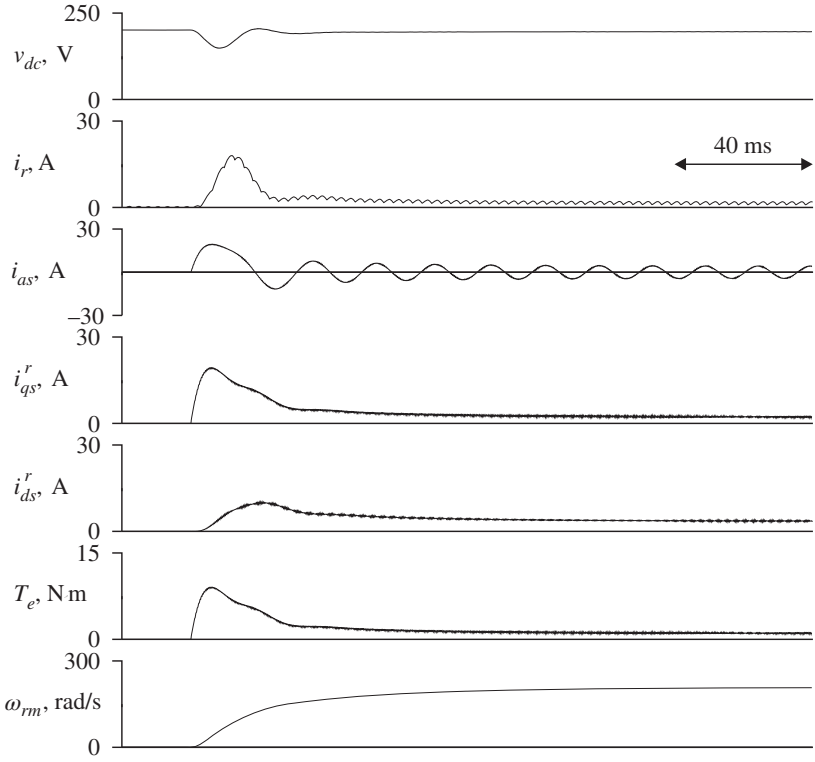

Figure 14.6-1 Start-up performance of a sine-triangle-modulated permanent-magnet ac motor drive as calculated using a waveform-level model.

the cost of the oversizing will be a fivefold increase in the cost of the semiconductors. Fortunately, by suitable control of the duty cycle, the overcurrent can be minimized.

It is interesting to compare the waveform-level portrayal of the drives start-up response to the portrayal predicted by the average-value model (14.4-21), which is illustrated in Figure 14.6-2. Comparing the two figures, it is evident that the average-value model captures the salient features of the start-up with the exception of the harmonics, which were neglected in the averaging procedure. In addition to being considerably easier to code, the computation time using the average-value representation is approximately 120 times faster than the computation time required by a detailed representation in which the switching of all the semiconductors is taken into account, making it an ideal formulation for control system analysis and synthesis.

Since many control algorithms are based on linear control theory, it is convenient to linearize the average-value model. Linearizing (14.4-21) yields

$$p\left[\Delta\hat{i}_r \;\Delta\hat{v}_{dc} \;\Delta\hat{i}_{st} \;\Delta\hat{v}_{st} \;\Delta\hat{i}^r_{qs} \;\Delta\hat{i}^r_{ds} \;\Delta\omega_r\right]^T =$$

$$\begin{bmatrix}
-\frac{r_{rl}}{L_{rl}} & -\frac{1}{L_{rl}} & 0 & 0 & 0 & 0 & 0 \\
\frac{1}{C_{dc}} & 0 & -\frac{1}{C_{dc}} & 0 & -\frac{3}{2}\frac{m_0}{C_{dc}}\cos\phi_{v0} & \frac{3}{2}\frac{m_0}{C_{dc}}\sin\phi_{v0} & 0 \\
0 & \frac{1}{L_{st}} & -\frac{r_{st}}{L_{st}} & -\frac{1}{L_{st}} & 0 & 0 & 0 \\
0 & 0 & \frac{1}{C_{st}} & 0 & 0 & 0 & 0 \\
0 & \frac{m_0}{L_q}\cos\phi_{v0} & 0 & 0 & -\frac{r_s}{L_q} & -\frac{L_d}{L_q}\omega_{r0} & -\frac{L_d}{L_q}\bar{I}^r_{ds0} - \frac{\lambda'_m}{L_q} \\
0 & -\frac{m_0}{L_d}\sin\phi_{v0} & 0 & 0 & +\frac{L_q}{L_d}\omega_{r0} & -\frac{r_s}{L_d} & \frac{L_q}{L_d}\bar{I}^r_{qs0} \\
0 & 0 & 0 & 0 & \frac{3}{2}\left(\frac{P}{2}\right)^2\frac{1}{J} & \frac{3}{2}\left(\frac{P}{2}\right)^2\frac{1}{J} & 0 \\
 & & & & \left(\lambda'_m + (L_d - L_q)\bar{I}^r_{ds0}\right) & (L_d - L_q)\bar{I}^r_{qs0} &
\end{bmatrix}$$

$$\begin{bmatrix} \Delta\hat{i}_r \\ \Delta\hat{v}_{dc} \\ \Delta\hat{i}_{st} \\ \Delta\hat{v}_{st} \\ \Delta\hat{i}^r_{qs} \\ \Delta\hat{i}^r_{ds} \\ \Delta\omega_r \end{bmatrix} +
\begin{bmatrix}
\frac{v_{r0}}{L_{rl}} & \frac{\cos\alpha_0}{L_{rl}} & 0 & 0 & 0 \\
0 & 0 & -\frac{3}{2}\frac{\left(\cos\phi_{v0}\bar{I}^r_{qs0} - \sin\phi_{v0}\bar{I}^r_{ds0}\right)}{C_{dc}} & \frac{3}{2}\frac{m_0\left(\sin\phi_{v0}\bar{I}^r_{qs0} + \cos\phi_{v0}\bar{I}^r_{ds0}\right)}{C_{dc}} & 0 \\
0 & 0 & 0 & 0 & 0 \\
0 & 0 & 0 & 0 & 0 \\
0 & 0 & \frac{\overline{V}_{dc0}}{L_q}\cos\phi_{v0} & -\frac{\overline{V}_{dc0}m_0}{L_q}\sin\phi_{v0} & 0 \\
0 & 0 & -\frac{\overline{V}_{dc0}}{L_q}\sin\phi_{v0} & -\frac{\overline{V}_{dc0}m_0}{L_q}\cos\phi_{v0} & 0 \\
0 & 0 & 0 & 0 & -\frac{P}{2}\frac{1}{J}
\end{bmatrix}$$

$$\begin{bmatrix} \Delta\cos\alpha \\ \Delta v_{ro} \\ \Delta m \\ \Delta\phi_v \\ \Delta T_L \end{bmatrix} \tag{14.6-1}$$

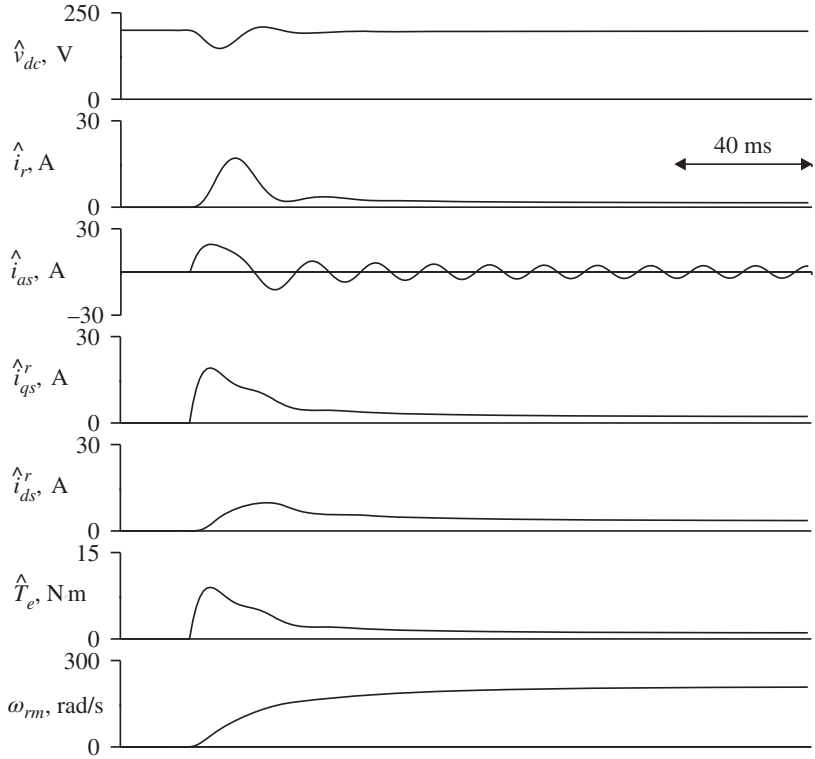

Figure 14.6-2 Start-up performance of a sine-triangle-modulated permanent-magnet ac motor drive as calculated using an average-value model.

In (14.6-1), the addition of a subscript zero designates the initial equilibrium point about which the equations are linearized, and Δ denotes a change in a variable. Thus

$$x = x_0 + \Delta x \tag{14.6-2}$$

where x is any state, input variable, or output variable.

Figure 14.6-3 illustrates the startup response as predicted by the average-value model linearized about the initial operating point. In this figure, (14.6-2) has been used to determine each variable from its initial value and its excursion given by (14.6-1). As can be seen, there are many discrepancies between the prediction of the linearized model and the performance of the drive as illustrated in Figure 14.6-1. In particular, the linearized model does not predict any perturbation to the dc voltage or that there will be any rectifier current. In addition, the linearized model predicts a significantly higher q-axis current than is observed but fails to predict any d-axis current. The linearized model also significantly

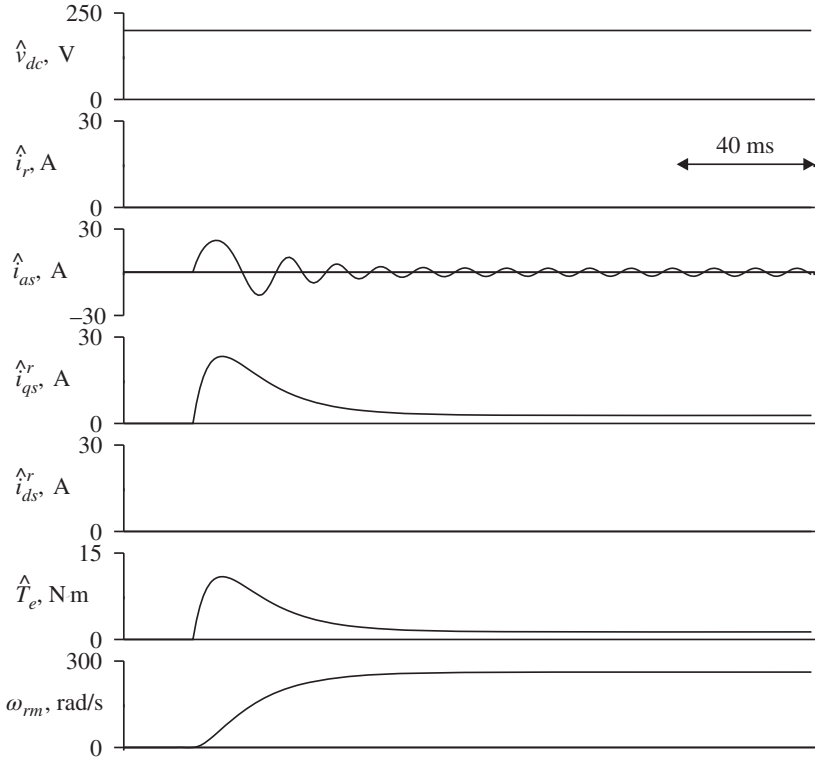

Figure 14.6-3 Start-up performance of a sine-triangle-modulated permanent-magnet ac motor drive as calculated using a linearized model.

overestimates the peak torque and the final speed. Thus, this study illustrates the hazards involved in using the linearized model to predict large disturbance transients.

Although the linearized model cannot be used to predict large-signal transients, it can be used for dynamic analysis such as operating point stability. To illustrate this, Figure 14.6-4 and Figure 14.6-5 depict the performance of the drive as predicted by a waveform-level simulation and the linearized model (determined from the initial operating point) as the duty cycle is changed from 0.9 to 1. In this case, the linearized model accurately portrays the transient.

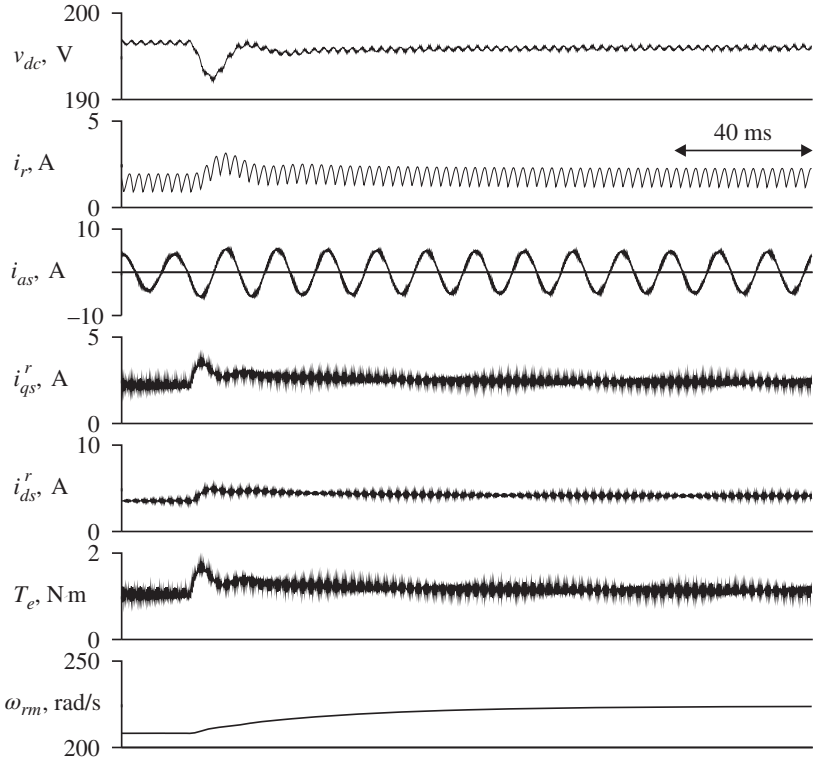

Figure 14.6-4 Response of a sine-triangle-modulated permanent-magnet ac motor drive to a step change in duty cycle as calculated using a waveform-level model.

14.7 Case Study: Voltage-Source Inverter-Based Speed Control

Now that the basic analytical tools to analyze voltage-source inverter based permanent-magnet ac motor motor drives have been set forth, it is appropriate to consider the use of these tools in control system synthesis. To this end, consider a sine-triangle modulated drive with the parameters listed in Table 14.7-1. It is desired to use this drive in order to achieve speed control of an inertial load. Design requirements are: (1) there shall be no steady-state error, and (2) the phase

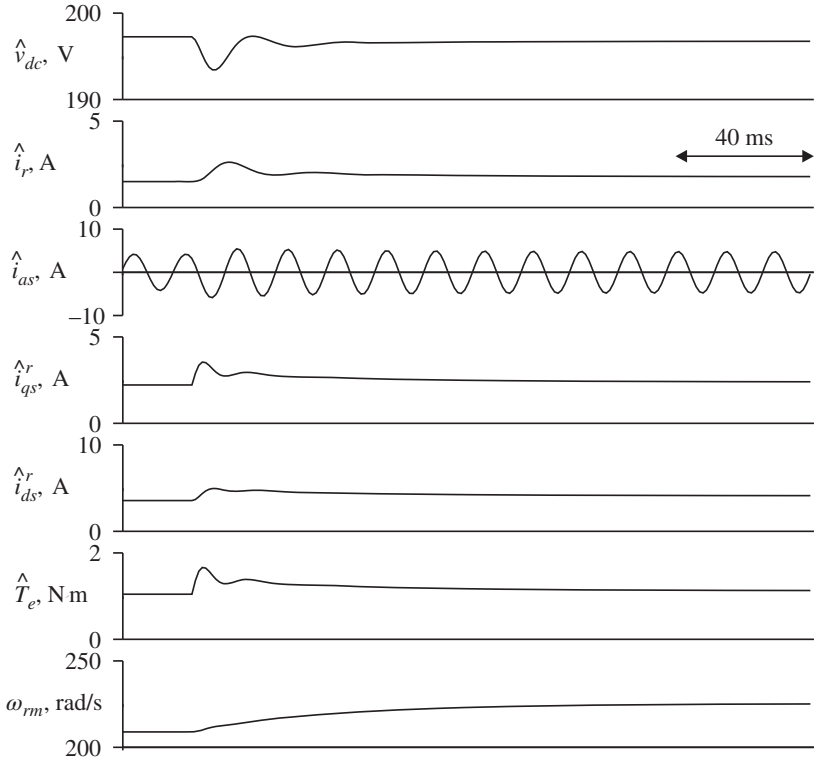

Figure 14.6-5 Response of a sine-triangle-modulated permanent-magnet ac motor drive to a step change in duty cycle as calculated using a linearized model.

Table 14.7-1 Drive System Parameters.

E	85.5 V	C_{dc}	1000 μF	L_d	11.4 mH
ω_{eu}	377 rad/s	J	0.005 N·ms^2	λ'_m	0.156 Vs
L_c	5 mH	r_s	2.98 Ω	P	4
L_{dc}	5 mH	L_q	11.4 mH		

margin will by 60° when the drive is operated at the nominal operating speed of 200 rad/s (mechanical).

The design requirement of no steady-state error necessitates integral feedback. Thus, a proportional plus integral (PI) controller would be appropriate. A block diagram of this control in a system context is illustrated in Figure 14.7-1. In this figure, the *s* represents the time derivative operator in Laplace notation, which is

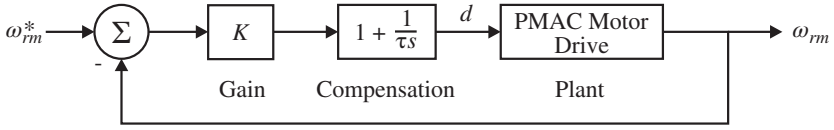

Figure 14.7-1 Speed control system.

typically used for control synthesis. In the time domain, the control law is of the form

$$d = K\left(\omega^*_{rm} - \omega_{rm}\right) + \frac{K}{\tau}\int \left(\omega^*_{rm} - \omega_{rm}\right) dt \tag{14.7-1}$$

For the purpose of design, we will make use of a linearized model of the permanent-magnet ac motor drive, in which the system is linearized about at operating speed of 200 rad/s. The linearized model can either be calculated using (14.6-1), or it can be calculated by automatic linearization of a nonlinear average-value model, a feature common to many simulation languages.

Figure 14.7-2 illustrates the open-loop Bode plot of the permanent-magnet ac motor drive, wherein the output is the mechanical rotor speed and the input is the duty cycle. Since the Bode characteristic is based on a linearized model, strictly speaking, it is only valid about the operating point about which it was linearized (200 rad/s). From Figure 14.7-2, we see that although the gain margin is infinite, the phase margin is only 20°. A phase margin of 30° is often considered to be the minimum acceptable.

The design process begins by selection of τ. The integral feedback will decrease the phase by 90° at frequencies much less than $1/(2\pi\tau)$. Since this will decrease the already small phase margin, it is important to pick τ so that the breakpoint frequency of the compensator is considerably less than the frequency at which the phase of the plant begins to decrease from zero. Selecting the breakpoint frequency of the compensator to be at 0.01 Hz yields τ of 16 seconds.

The Bode characteristic of the compensated plant is depicted in Figure 14.7-3. As can be seen, the phase margin is still 20°. The next step is to select K so as to obtain the desired phase margin, which can be accomplished choosing the gain such that the phase at the gain crossover frequency is −120°. From Figure 14.7-3, it can be seen that the phase of the compensated plant is −120° when the gain of the compensated plant is 12 dB. Thus, choosing $K = 0.25$ (−12 dB) will result in the desired phase margin.

Figure 14.7-4 illustrated the Bode characteristic of the closed-loop plant. As can be seen, the bandwidth of the system is on the order of 100 Hz, and the resonant peak is not overly pronounced. However, the closed-loop frequency response cannot be used as a sole judge of the systems performance since the actual system is nonlinear. For this, the simplest approach is to use a nonlinear average-value

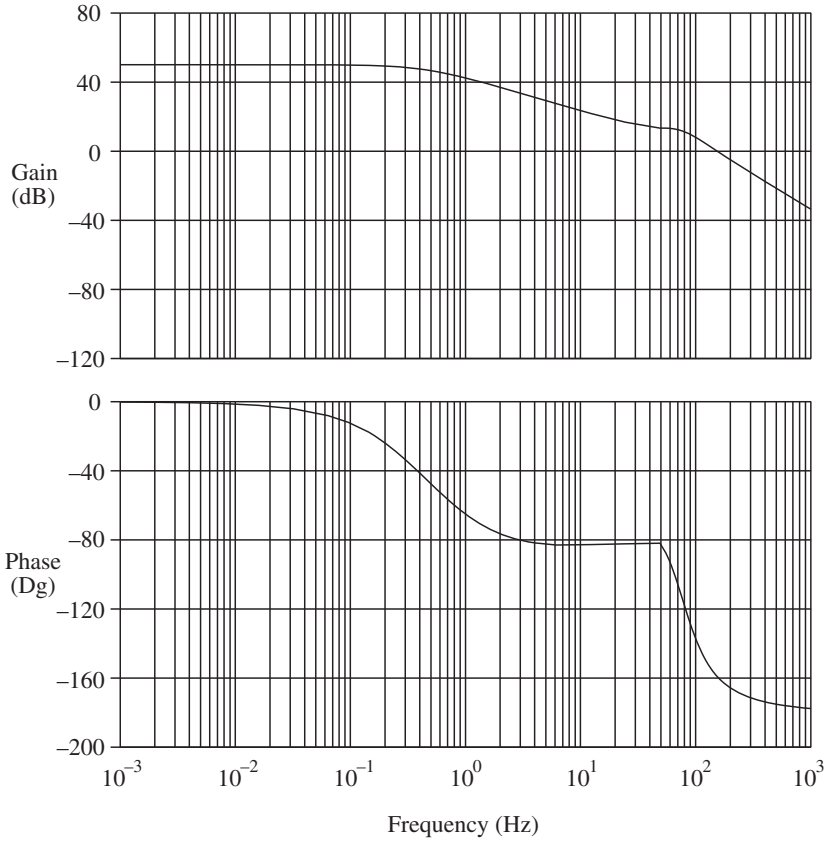

Figure 14.7-2 Frequency response of the open-loop permanent-magnet ac motor drive.

model. Figure 14.7-5 illustrates the system performance during a step change in commanded speed from 0 to 200 rad/s. As can be seen, the transient performance in speed is quite well behaved. Nevertheless, the reader might be surprised by Figure 14.7-5 in several ways. First, it can be seen that the duty cycle, which is normally 0–1, is nearly 50 in the initial part of the study. Thus, the drive will be overmodulated and we can expect the current to exhibit considerable low-frequency harmonics on start-up (these are not apparent in Fig. 14.7-5 since an average-value model was used). Since the applied voltage was effectively much lower than expected, the bandwidth for this large disturbance is not nearly the 100 Hz indicated in Figure 14.7-4. Finally, the rated current for the machine in

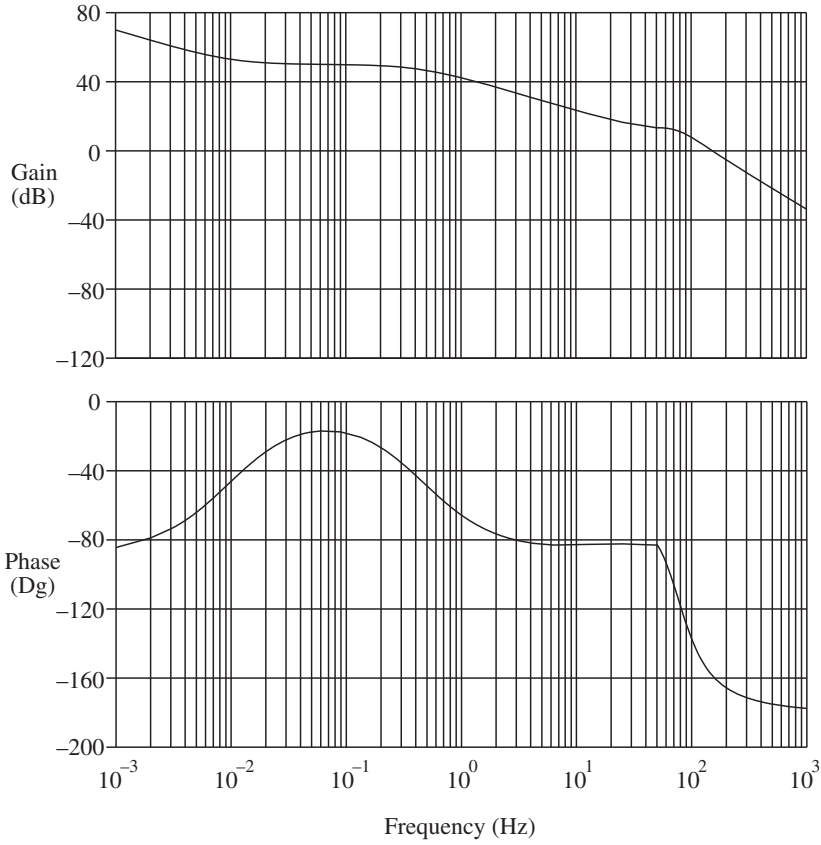

Figure 14.7-3 Frequency response of the compensated permanent-magnet ac motor drive.

question is only 2.6 A, rms. Although the machine could probably withstand the temporary overcurrent, the inverter probably could not, and thus either the bandwidth should be reduced so as to alleviate the overcurrent or the duty cycle should be limited as a function of the current. Finally, close inspection reveals that at the end of the study, the speed is not 200 rad/s, and does not even appear to be rapidly increasing. This is because the bandwidth of the compensation was chosen to be quite low, and as a result, a small error in rotor speed will persist for some time, although it will eventually go to zero. A second design iteration in order to address these issues is left to the reader.

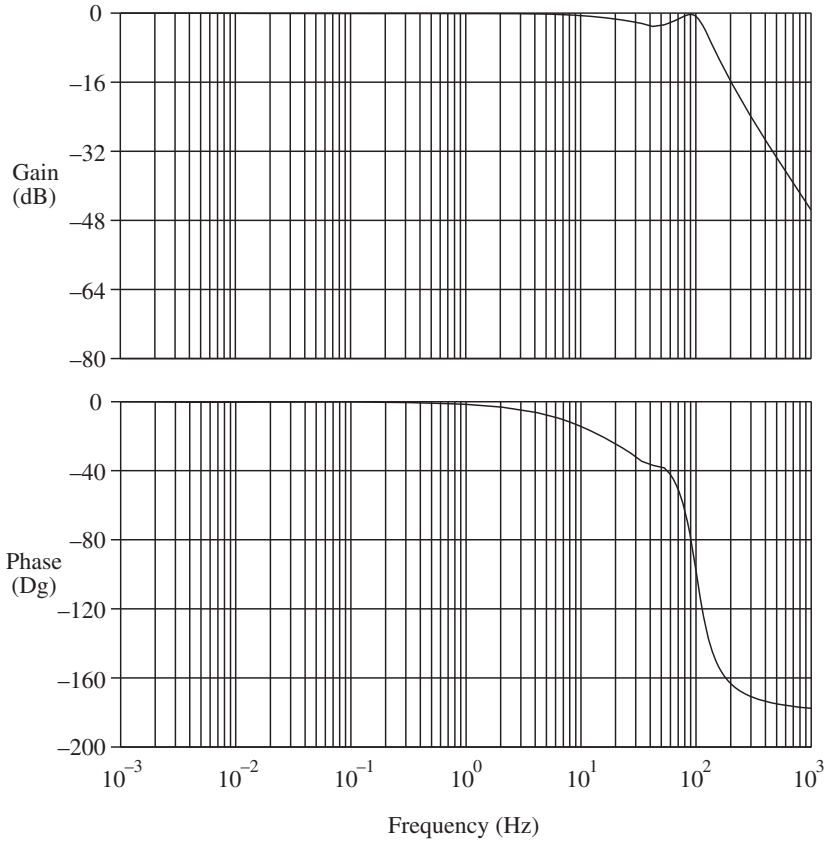

Figure 14.7-4 Frequency response of the closed-loop permanent-magnet ac motor drive.

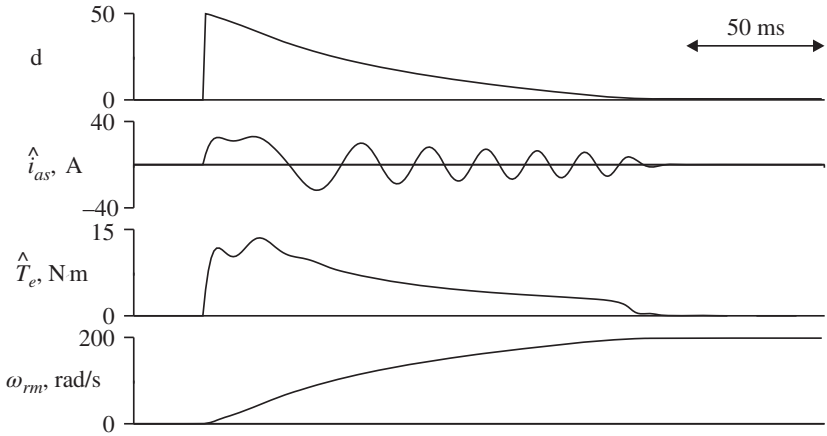

Figure 14.7-5 Start-up response of the closed-loop permanent-magnet ac motor drive.

14.8 Current-Regulated Inverter Drives

Sections 14.1–14.7 explored the performance of drives in which the machine is controlled through suitable regulation of the applied voltages. In the remainder of this chapter, an alternate strategy is considered—control of the machine through the regulation of the stator currents. The hardware configuration for current-regulated inverter drives is identical to that of voltage-source inverter drives, as illustrated in Figure 14.2-1. The only difference is in the way in which the gate signals to the individual semiconductors are established.

Current-regulated inverters have several distinctive features. First, since torque is a function of the machine current, the torque may be controlled with the same bandwidth as to which the stator currents are controlled. In fact, it is often the case that for practical purposes, the torque control is essentially instantaneous. A second feature of current-regulated drives is that they are robust with regard to changes in machine parameters. For example, current-regulated drives are insensitive to parameter variations in the stator leakage inductance or the stator resistance. Current-regulated drives are also robust in regard to faults. In the event of a winding-to-winding short within the machine, the currents are automatically limited, which prevents damage to the inverter. The currents are also automatically limited during start-up.

Figure 14.8-1 illustrates the control of current-regulated drive. Therein, based on the commanded torque T_e^*, electrical rotor speed ω_r, and the inverter voltage v_{dc}, the q- and d-axis current commands i_{qs}^{r*} and i_{ds}^{r*} are formulated. Using the inverse transformation, the corresponding abc variable current command i_{abcs}^* is determined. Finally, based on the abc variable current command and the actual currents, the on and off status of each of the inverter semiconductors (T1–T6) is determined using hysteresis modulation as set forth in Section 10.8. An immediate question that arises is how the q- and d-axis current commands are generated to begin with; this question is addressed in detail in a following section. For the present, it suffices to say that the command is determined in such a way that if the commanded currents are obtained, the commanded torque will also be obtained.

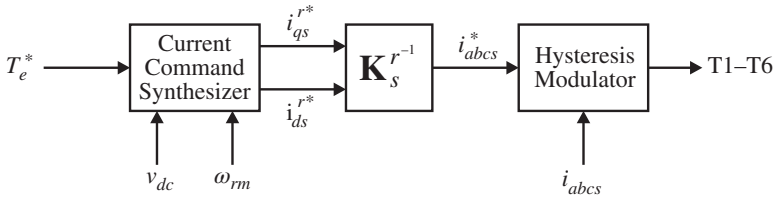

Figure 14.8-1 Hysteresis-modulated current-regulated drive control.

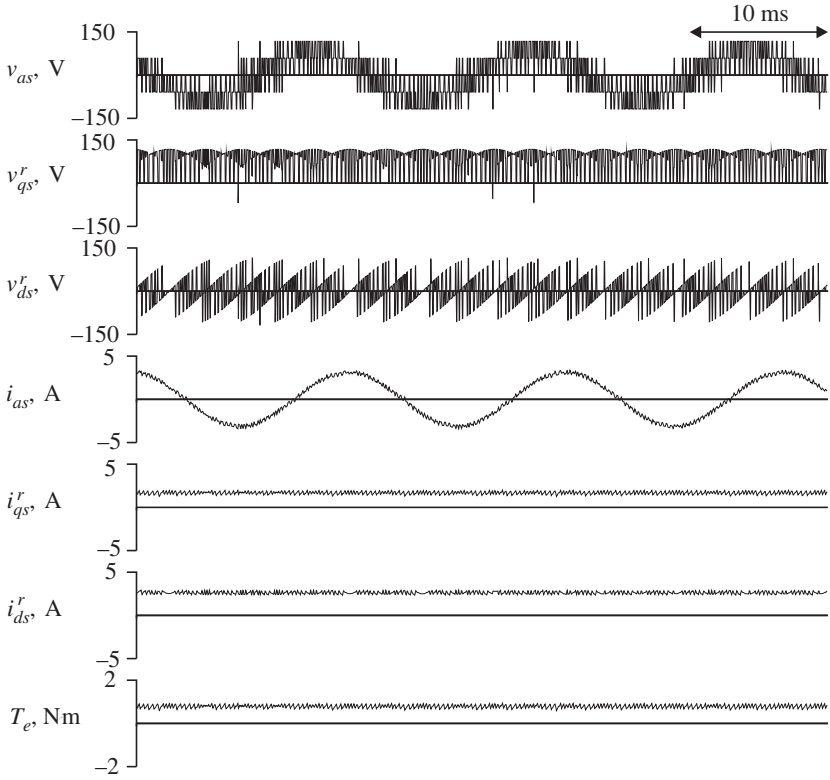

Figure 14.8-2 Steady-state performance of a hysteresis-modulated current-regulated permanent-magnet ac motor drive.

Figure 14.8-2 illustrates the steady-state performance of a hysteresis modulated permanent-magnet ac motor drive. Therein the operating conditions are identical to those portrayed in 14.3-5 except for the modulation strategy. The q- and d-axis current commands are set to 1.73 and 2.64 A, respectively, so that the fundamental component of the commanded current is identical to that in Figure 14.3-5. As can be seen, although the modulation strategies are different, the waveforms produced by the sine-triangle modulation and hysteresis modulation strategies are very similar.

A second method to implement a current-regulated inverter drive is to utilize a current-control loop on a voltage-source inverter drive. This is illustrated in Figure 14.8-3. Therein, the current command synthesizer serves the same function as in Figure 14.8-1. Based on the commanded q- and d-axis currents and the measured q- and d-axis currents (determined by transforming the measured abc variable currents), the q- and d-axis voltage commands (v^{r*}_{qs} and v^{r*}_{ds}) are

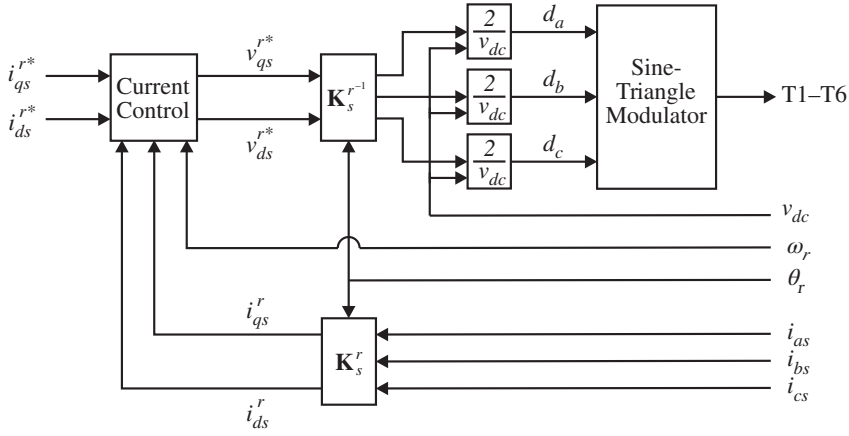

Figure 14.8-3 A sine-triangle-modulator based current regulator.

determined. The q- and d-axis voltage command is then converted to an abc variable voltage command v_{abcs}^{*}, which is scaled in order to determine the instantaneous duty cycles d_a, d_b, and d_c of the sine-triangle modulation strategy. Based on these duty cycles, T1–T6 are determined as described in Section 10.5. There are several methods of developing the current control, such as a synchronous current regulator [6]. An example of the design of a feedback linearization-based controller is considered in Example 14A.

Example 14A Let us consider the design of a current regulator for a nonsalient permanent-magnet ac motor. The goal is to determine the q- and d-axis voltage command so that the actual currents become equal to the commanded currents. Let us attempt to accomplish this goal by specifying the voltage commands as

$$v_{qs}^{r*} = \omega_r \left(L_{ss} i_{ds}^{r} + \lambda_m'\right) + \left(K_p + \frac{K_i}{s}\right)\left(i_{qs}^{r*} - i_{qs}^{r}\right) \tag{14A-1}$$

$$v_{ds}^{r*} = -\omega_r L_{ss} i_{qs}^{r} + \left(K_p + \frac{K_i}{s}\right)\left(i_{ds}^{r*} - i_{ds}^{r}\right) \tag{14A-2}$$

where s denotes the Laplace operator. This control algorithm contains feedback terms that cancel the nonlinearities in the stator voltage equations, feedforward terms that cancel the effect of the back emf, and a PI control loop. Assuming that the actual q- and d-axis voltages are equal to the commanded q- and d-axis voltages, it can be shown that the transfer function between the commanded and actual q-axis currents is given by

$$\frac{i_{qs}^{r}(s)}{i_{qs}^{r*}(s)} = \frac{\dfrac{K_p}{L_{ss}}\left(s + \dfrac{K_i}{K_p}\right)}{s^2 + \dfrac{(r_s + K_p)}{L_{ss}}s + \dfrac{K_i}{L_{ss}}} \tag{14A-3}$$

The transfer function relating the d-axis current to the commanded d-axis current is identical. Assuming the same machine parameters as in the study illustrated in Figure 14.8-2, and selecting pole locations of $s = -200$ and $s = -2000$ (note that the poles may be arbitrarily placed), we have that

$$K_i = 2280\,\Omega/\text{s} \tag{14A-4}$$

$$K_p = 10.7\,\Omega \tag{14A-5}$$

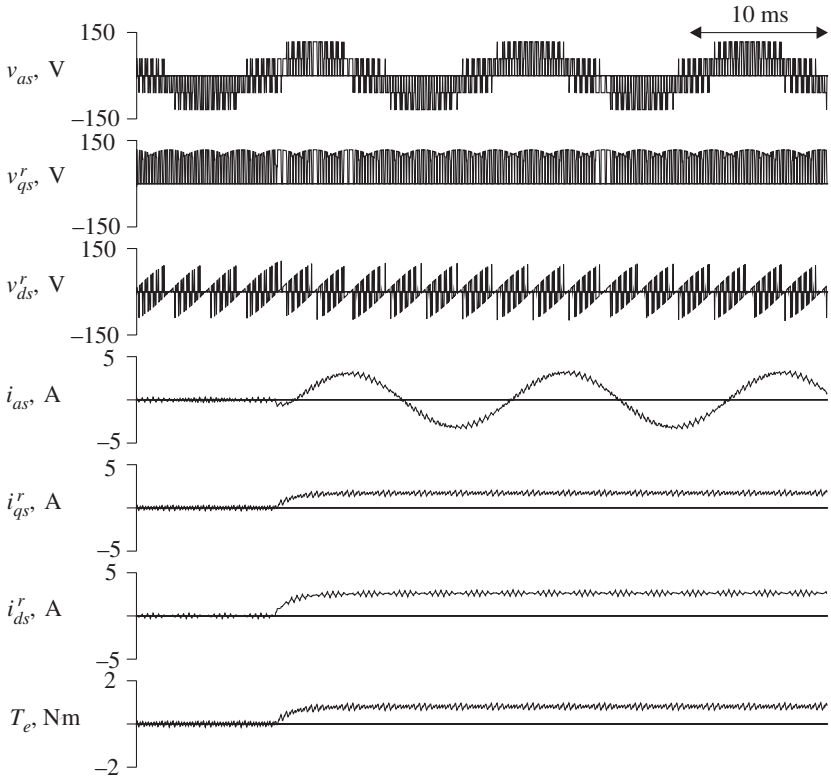

Figure 14A-1 Step response of a feedforward sine-triangle-modulated current-regulated permanent-magnet ac motor drive.

Figure 14A-1 illustrates the response of the permanent-magnet ac drive as the current command is stepped from zero to $i_{qs}^{r*} = 1.73$ A and $i_{ds}^{r*} = 2.64$ A. All operating conditions are as in Figure 14.8-2. As can be seen, the machine performance is extremely well behaved and is dominated by the pole at $s = -200$.

14.9 Voltage Limitations of Current-Regulated Inverter Drives

As alluded to previously, assuming that the current control loop is sufficiently fast, the current-regulated drive can be thought of as an ideal current source. However, there are some limitations on the validity of this approximation. In particular, eventually, the back emf of the machine will rise to the point where the inverter cannot achieve the current command due to the fact that the back emf of the machine becomes too large. Under such conditions, the machine is said to have lost current tracking.

In order to estimate the operating region over which current tracking is obtained, consider the case in which current tracking is obtained, that is

$$\hat{i}_{qs}^{r} = i_{qs}^{r*} \tag{14.9-1}$$

$$\hat{i}_{ds}^{r} = i_{ds}^{r*} \tag{14.9-2}$$

Substitution of (14.9-1) and (14.9-2) into the stator voltage equations and neglecting the stator dynamics

$$\hat{v}_{qs}^{r} = r_s \hat{i}_{qs}^{r} + \omega_r L_d \hat{i}_{ds}^{r} + \omega_r \lambda_m' \tag{14.9-3}$$

$$\hat{v}_{ds}^{r} = r_s \hat{i}_{ds}^{r} - \omega_r L_q \hat{i}_{qs}^{r} \tag{14.9-4}$$

Recall that the rms value of the fundamental component of the applied voltage is given by

$$v_s = \frac{1}{\sqrt{2}} \sqrt{\left(\hat{v}_{qs}^{r}\right)^2 + \left(\hat{v}_{ds}^{r}\right)^2} \tag{14.9-5}$$

Substitution of (14.9-3) and (14.9-4) into (14.9-5) yields

$$v_s = \frac{1}{\sqrt{2}} \sqrt{\left(r_s i_{qs}^{r*} + \omega_r L_d i_{ds}^{r*} + \lambda_m' \omega_r\right)^2 + \left(r_s i_{ds}^{r*} - \omega_r L_q i_{qs}^{r*}\right)^2} \tag{14.9-6}$$

Recall from Section 10.8 that for the hysteresis-controlled current-regulated inverters, the maximum rms value of the fundamental component of the applied voltage that can be obtained without low-frequency harmonics is given by

$$v_s = \frac{1}{\sqrt{6}} \hat{v}_{dc} \tag{14.9-7}$$

If low-frequency harmonics are tolerable, and a synchronous regulator is used, then the maximum RMS value of the fundamental component becomes

$$v_s = \frac{\sqrt{2}}{\pi}\hat{v}_{dc} \tag{14.9-8}$$

In the event that for a given current command and speed (14.9-8) cannot be satisfied, then it is not possible to obtain stator currents equal to the commanded current. If (14.9-8) can be satisfied, but (14.9-7) cannot be satisfied, then it is possible to obtain stator current that have the same fundamental component as the commanded currents provided that integral feedback in the rotor reference frame is present to drive the current error to zero; however, low-frequency harmonics will be present.

Figure 14.9-1 illustrates the effects of loss of current tracking. Initially, operating conditions are identical to those portrayed in Figure 14.8-2. However,

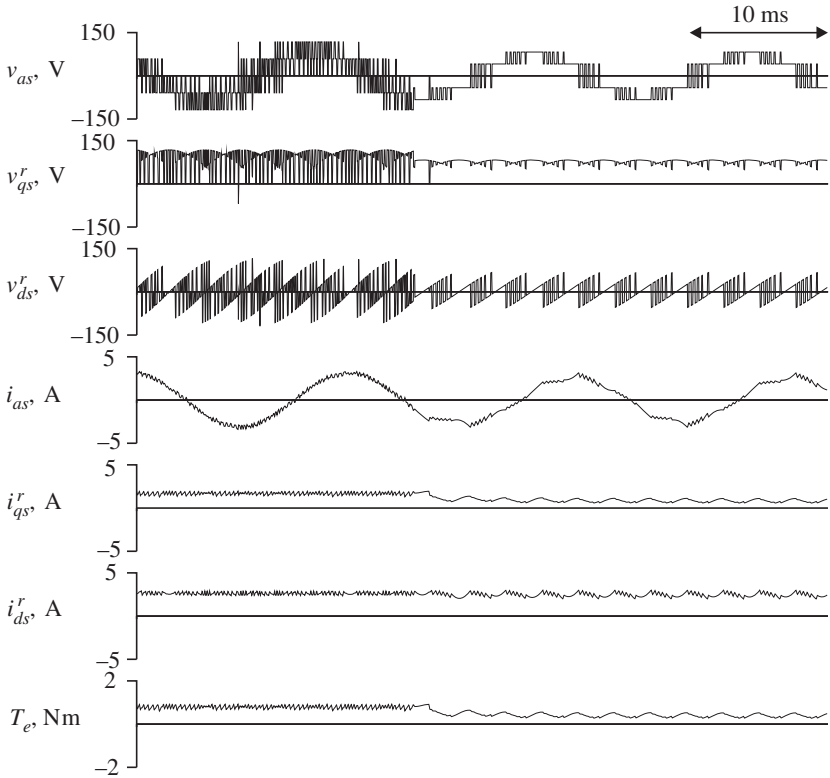

Figure 14.9-1 Response of hysteresis-modulated current-regulated permanent-magnet ac motor drive to step decrease in dc inverter voltage.

approximately 20 ms into the study, the dc inverter voltage is stepped from 177 to 124 V, which results in a loss of current tracking. As can be seen, the switching of the hysteresis modulator is such that some compensation takes place; nevertheless, current tracking is lost. As a result, harmonics appear in the a-phase and q- and d-axis current waveforms, as well as in the electromagnetic torque.

14.10 Current Command Synthesis

It is now appropriate to address the question as to how to determine the current command. Normally, when using a current-regulated inverter, the input to the controller is a torque command. Thus, the problem may be reformulated as the determination of the current command from the torque command. To answer this question, let us first consider a nonsalient machine in which $L_{ss} \triangleq L_q = L_d$. In this case, torque may be expressed as

$$T_e = \frac{3}{2}\frac{P}{2}\lambda'_m i^r_{qs} \tag{14.10-1}$$

Therefore, the commanded q-axis current may be expressed in terms of the commanded torque as

$$i^{r*}_{qs} = \frac{2}{3}\frac{2}{P}\frac{1}{\lambda'_m}T^*_e \tag{14.10-2}$$

Clearly, if the desired torque is to be obtained, then (14.10-2) must be satisfied. The d-axis current does not effect average torque, and so its selection is somewhat arbitrary. Since d-axis current does not affect the electromagnetic torque, but does result in additional stator losses, the d-axis current is often selected to be zero, that is,

$$i^{r*}_{ds} = 0 \tag{14.10-3}$$

This selection of d-axis current minimizes the current amplitude into the machine, thus maximizing torque per amp, and at the same time maximizes the efficiency of the machine by minimizing the stator resistive losses.

Although (14.10-3) has several distinct advantages, there is one reason to command a nonzero d-axis current. To see this, consider (14.9-6) for the nonsalient case:

$$v_s = \frac{1}{\sqrt{2}}\sqrt{\left(r_s i^{r*}_{qs} + \omega_r L_{ss} i^{r*}_{ds} + \lambda'_m \omega_r\right)^2 + \left(r_s i^{r*}_{ds} - \omega_r L_{ss} i^{r*}_{qs}\right)^2} \tag{14.10-4}$$

From (14.10-4), we see that the required inverter voltage goes up with either speed or q-axis current (which is proportional to torque). However, examining the first squared term in (14.10-4), it can be seen that at positive speeds, the required

inverter voltage can be reduced by injecting negative d-axis current. In fact, by solving (14.10-4) for d-axis current in terms of the q-axis current command and speed, we have that

$$i_{ds}^{r*} = \frac{-\lambda'_m L_{ss}\omega_r^2 + \sqrt{2z^2 v_s^2 - \left(r_s\omega_r\lambda'_m + z^2 i_{qs}^{r*}\right)^2}}{z^2} \tag{14.10-5}$$

where

$$z = \sqrt{r_s^2 + \omega_r^2 L_{ss}^2} \tag{14.10-6}$$

Thus, a logical current control strategy is to command zero d-axis current as long as the inverter voltage requirements are not exceeded, and to inject the amount of d-axis current specified by (14.10-5) if they are. Note that there are limitations on d-axis current injection in that (1) (14.10-5) may not have a solution, (2) excessive d-axis current injection may result in demagnetization of the permanent magnet, and (3) excessive d-axis current injection can result in exceeding the current limit of the machine or inverter. In addition, the use of (14.10-5) requires accurate knowledge of the dc inverter voltage (to determine the peak v_s), the rotor speed, and all of the machine parameters. A means of implementing such a control without knowledge of the dc inverter voltage, speed, and machine parameters is set forth in Reference [7].

The process for determining the current command in salient machines, which typically are constructed using buried magnet technology, is somewhat more involved than in the nonsalient case. Let us first consider the problem of computing the q- and d-axis current commands so as to maximize torque-per-amp performance. In the case of the nonsalient machine, from Chapter 4, the expression for electromagnetic torque is given by

$$T_e = \frac{3}{2}\frac{P}{2}\left(\lambda'_m i_{qs}^r + (L_d - L_q) i_{qs}^r i_{ds}^r\right) \tag{14.10-7}$$

Solving (14.10-7) for d-axis current command in terms of the q-axis current command and in terms of the commanded torque yields

$$i_{ds}^{r*} = \frac{4T_e}{3P(L_d - L_q)}\frac{1}{i_{qs}^{r*}} - \frac{\lambda'_m}{L_d - L_q} \tag{14.10-8}$$

In terms of the qd commanded currents, the rms value of the fundamental component of the commanded current is given by

$$i_s = \frac{1}{\sqrt{2}}\sqrt{\left(i_{qs}^{r*}\right)^2 + \left(i_{ds}^{r*}\right)^2} \tag{14.10-9}$$

Substitution of (14.10-8) into (14.10-9) yields an expression for the magnitude of the stator current in terms of the commanded torque and q-axis current. Setting the derivative of the resulting expression with respect to the q-axis current command

equal to zero gives the following transcendental expression for the q-axis current command that maximizes torque per amp:

$$\left(i_{qs}^{r*}\right)^4 + \frac{4T_e\lambda'_m i_{qs}^{r*}}{3P(L_d - L_q)^2} - \left(\frac{4T_e}{3P(L_d - L_q)}\right)^2 = 0 \qquad (14.10\text{-}10)$$

Once the q-axis current command is determined by solving (14.10-10), the d-axis current command may be found by solving (14.10-8). From the form of (14.10-10), it is apparent that the solution of for the q-axis current must be accomplished numerically. For this reason, when implementing this control with a microprocessor, the q- and d-axis current commands are often formulated through a look-up table that has been constructed through offline solution to (14.10-8) and (14.10-10).

Once the q- and d-axis current commands have been formulated, it is necessary to check whether or not the inverter is capable of producing the required voltage. If it is not, it is necessary to recalculate the commanded q- and d-axis currents such that the required inverter voltage does not exceed that obtainable by the converter. This calculation can be conducted by solving (14.9-6) and (14.10-8) simultaneously for the q- and d-axis current command.

Figure 14.10-1 illustrates the graphical interpretation of the selection of the commanded q- and d-axis currents for a machine in which $r = 0.2\ \Omega$, $L_q = 20$ mH,

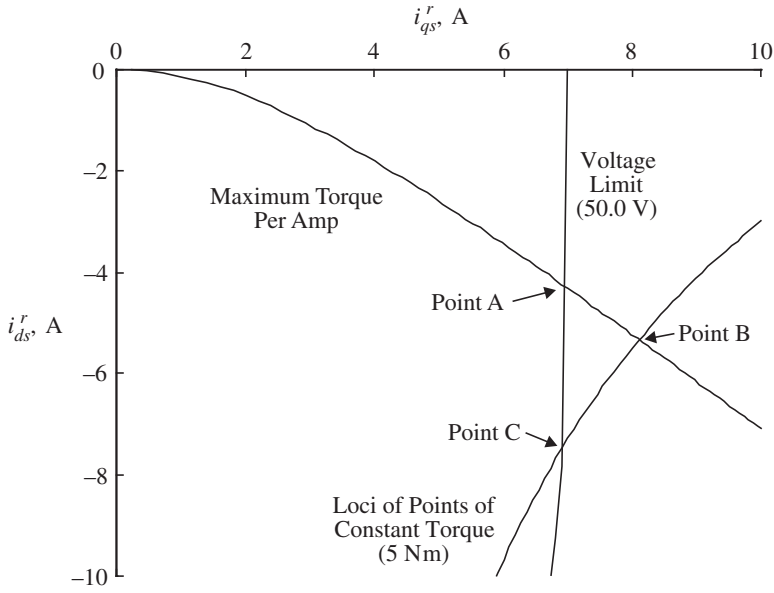

Figure 14.10-1 Selection of q- and d-axis currents.

$L_d = 10$ mH, and $\lambda'_m = 0.07$ Vs. The machine is operating at a speed of 500 rad/s (electrical) and $v_s = 50$ V. Illustrated therein are the trajectory of the maximum torque-per-amp characteristic, the loci of points in the qd plane at which the electromagnetic torque of 5 Nm is obtained, and the loci of points representing the voltage limit imposed by (14.10-4). For a given electromagnetic torque command, the q- and d-axis current command is formulated using the maximum torque-per-amp trajectory, provided this point is inside the voltage limit. However, q- and d-axis currents on this trajectory corresponding to torques greater than that obtainable at Point A cannot be achieved. Suppose a torque of 5 Nm is desired. Point B represents the point on the maximum torque-per-amp trajectory, which has the desired torque. Unfortunately, Point B is well outside of the limit imposed by the available voltage. However, any point on the constant torque locus will satisfy the desired torque. Thus, in this case, the current command is chosen to correspond to Point C.

14.11 Average-Value Modeling of Current-Regulated Inverter Drives

In this section, an average-value model of the current-regulated inverter drive is formulated in much the same way as the average-value model of the voltage-source inverter drive. Since the topology of the rectifier and inverter are the same, it follows that the expressions for the time derivatives of the rectifier current, the dc link voltage, the stabilizing filter current, and the stabilizing filter voltage given by (14.4-7) and (14.4-10)–(14.4-12) are valid. Furthermore, the change in control strategy does not affect the mechanical dynamics, thus (14.4-19) and (14.4-20) may still be used to represent the machine. However, the change in control strategy will change the formulation of the expression for the dc link currents, the stator dynamics, and the expression for electromagnetic torque.

In order to formulate an expression for the dc link current, it is convenient to assume that the actual machine currents are equal to the commanded machine currents, whereupon

$$\hat{i}^r_{qs} = i^{r*}_{qs} \tag{14.11-1}$$

$$\hat{i}^r_{ds} = i^{r*}_{ds} \tag{14.11-2}$$

Of course, this assumption is only valid when the dc link voltage is such that the desired current is actually obtained. An average-value model of a permanent-magnet ac motor drive in which current tracking is not obtained is set forth in Reference [8]. Assuming that the actual currents are equal to the commanded currents, the stator currents are no longer state variables. Neglecting the stator

dynamics, the q- and d-axis voltages may be expressed as

$$\hat{v}_{qs}^{r} = r_s i_{qs}^{r*} + \omega_r L_d i_{ds}^{r*} + \lambda'_m \omega_r \tag{14.11-3}$$

$$\hat{v}_{ds}^{r} = r_s i_{ds}^{r*} - \omega_r L_q i_{qs}^{r*} \tag{14.11-4}$$

The instantaneous power into the machine is given by

$$P = \frac{3}{2}\left[r_s\left(i_{qs}^{r*} + i_{ds}^{r*}\right)^2 + \omega_r(L_d - L_q)i_{qs}^{r*}i_{ds}^{r*} + \omega_r \lambda'_m i_{qs}^{r}\right] \tag{14.11-5}$$

Assuming that no power is lost into the inverter, it follows that the dc link current is given by

$$\hat{i}_{dc} = \frac{P}{\hat{v}_{dc}} \tag{14.11-6}$$

Combining (14.11-5) with (14.11-6) yields

$$\hat{i}_{dc} = \frac{3}{2}\frac{1}{\hat{v}_{dc}}\left[r_s\left(i_{qs}^{r*} + i_{ds}^{r*}\right)^2 + \omega_r(L_d - L_q)i_{qs}^{r*}i_{ds}^{r*} + \omega_r \lambda'_m i_{qs}^{r*}\right] \tag{14.11-7}$$

The other expression affected by the change from a voltage-source inverter to a current-regulated inverter will be the expression for torque. In particular, from (14.4-17) and again assuming that the actual stator currents are equal to the commanded currents

$$T_e = \frac{3}{2}\frac{P}{2}\left(\lambda'_m i_{qs}^{r*} + (L_d - L_q)i_{qs}^{r*}i_{ds}^{r*}\right) \tag{14.11-8}$$

As can be seen from (14.11-8), if it is assumed that the actual currents are equal to the commanded currents, then any desired torque may be instantaneously obtained.

Combining (14.4-7), (14.4-10)–(14.4-12), (14.4-19), (14.11-7), and (14.11-8) yields

$$p\begin{bmatrix} \hat{i}_r \\ \hat{v}_{dc} \\ \hat{i}_{st} \\ \hat{v}_{st} \\ \omega_r \end{bmatrix} = \begin{bmatrix} -\frac{r_{rl}}{L_{rl}} & -\frac{1}{L_{rl}} & 0 & 0 & 0 \\ \frac{1}{C_{dc}} & 0 & -\frac{1}{C_{dc}} & 0 & 0 \\ 0 & \frac{1}{L_{st}} & -\frac{r_{st}}{L_{st}} & -\frac{1}{L_{st}} & 0 \\ 0 & 0 & \frac{1}{C_{st}} & 0 & 0 \\ 0 & 0 & 0 & 0 & 0 \end{bmatrix}\begin{bmatrix} \hat{i}_r \\ \hat{v}_{dc} \\ \hat{i}_{st} \\ \hat{v}_{st} \\ \omega_r \end{bmatrix}$$

$$+\begin{bmatrix} \dfrac{v_{r0}\cos\alpha}{L_{rl}} \\ -\dfrac{1}{C_{dc}}\dfrac{3}{2}\dfrac{1}{\hat{v}_{dc}}\left[r_s\left(i_{qs}^{r*}+i_{ds}^{r*}\right)^2+\omega_r(L_d-L_q)i_{qs}^{r*}i_{ds}^{r*}+\omega_r\lambda_m'i_{qs}^{r*}\right] \\ 0 \\ 0 \\ \dfrac{P}{2}\dfrac{1}{J}\left[\dfrac{3}{2}\dfrac{P}{2}\left(\lambda_m'i_{qs}^{r*}+(L_d-L_q)i_{qs}^{r*}i_{ds}^{r*}\right)-T_L\right] \end{bmatrix} \tag{14.11-9}$$

14.12 Case Study: Current-Regulated Inverter-Based Speed Controller

The control of current-regulated inverter drives is considerably simpler than for their voltage-source-based counterparts, due to the fact that when designing the speed or position control algorithms, the inverter and machine act as a nearly ideal torque transducer (neglecting the stator dynamics of the machine). To illustrate this, let us reconsider the speed control system discussed in Section 14.7. Assuming that a current command synthesizer and current regulator can be designed with sufficiently high bandwidth, the speed control algorithm may be designed by assuming that the drive will produce an electromagnetic torque equal to the desired torque, therefore

$$T_e = T_e^* \tag{14.12-1}$$

In order to ensure that there will be no steady-state error, let us consider a PI control law in accordance with

$$T_e^* = K_p\left(1+\frac{1}{\tau s}\right)\left(\omega_{rm}^*-\omega_{rm}\right) \tag{14.12-2}$$

wherein ω_{rm}^* represents the speed command. Combining (14.12-1), (14.12-2), and the inertial mechanical dynamics of the drive, it can be shown that the resulting transfer function between the actual and commanded rotor speed is given by

$$\frac{\omega_{rm}}{\omega_{rm}^*} = \frac{K(\tau s+1)}{J\tau s^2+K\tau s+K} \tag{14.12-3}$$

Since (14.12-3) is a second-order system and there are two free parameters, the poles of (14.12-3) may be arbitrarily placed. However, some restraint should be exercised since it is important that the current regulator be much faster than the mechanical system if (14.12-1) and hence (14.12-3) are valid. Placing the poles at $s=-5$ and $s=-50$ yields $K=0.257$ N m s/rad and $\tau=0.22$ second. The pole at $s=-5$ will dominate the response.

In order to complete the design, a current command synthesizer (to determine what the current command should be to achieve the desired torque) and a current regulation control strategy need be designed. For this example, let us assume a simple current command synthesizer in which all of the current is injected into the q-axis, and let us use the sine-triangle-modulated voltage-source inverter based current regulator set forth in Example 14A as a current regulator. Recall that the poles of the current regulator are at $s = -200$ and $s = -1000$, which are much faster than those of the mechanical system.

Practically speaking, there are two important refinements that can be made to this control system. First, the q-axis current command generated by the current command synthesizer should be limited to ± 3.68 A in order to limit the current to the rated value of the machine. However, limiting the q-axis current command may cause the integrator in the speed control to wind up. For this reason, the contribution of the $K/(\tau s)$ portion of the speed control (that is the integral portion of the control) should be limited to avoid excessive windup. Herein, the portion of the torque command contributed by the integral term will be limited to 0.861 Nm, which is 50% of the torque, which would be obtained if the q-axis current command is at its maximum value. This value is obtained so that the overshoot for worst-case conditions is limited to an acceptable value (some iteration using time-domain simulations would be used to determine the exact number).

Figure 14.12-1 illustrates the interactions of the various controllers. Based on the speed error, the PI speed control determines a torque command T_e^* (the limit on the integral feedback is not shown). Then the current command synthesizer determines the q-axis current required to obtain the desired torque, subject to the q-axis current limit. In this controller, the d-axis current is set to zero. Based on the commanded q- and d-axis currents, the electrical rotor speed, the actual currents, and the dc supply voltage, the current regulator determines the on or off status of each of the semiconductors in the inverter (T1–T6).

Figure 14.12-2 illustrates the performance of the speed control system. Initially, the system is in the steady state. However, 50 ms into the study, the speed command is stepped from 0 to 200 rad/s. As can be seen, the torque command immediately jumps to the value that corresponds to the maximum q-axis current command. Since the electromagnetic torque is constant, the speed increases linearly with time. As can be seen, the magnitude of the ac current into the rectifier and the dc rectifier current both increase linearly with speed. This is due to the fact that the power going into the machine increases linearly with speed. The increasing rectifier current results in a dc link voltage that decreases linearly with time. Note that the dc link voltage initially undergoes a sudden dip of 5 V since the rectifier was initially under no-load condition, and hence it charged the dc link capacitor to peak rather than the average value of the rectifier voltage. Eventually, the machine reaches the desired speed. At this point, the torque

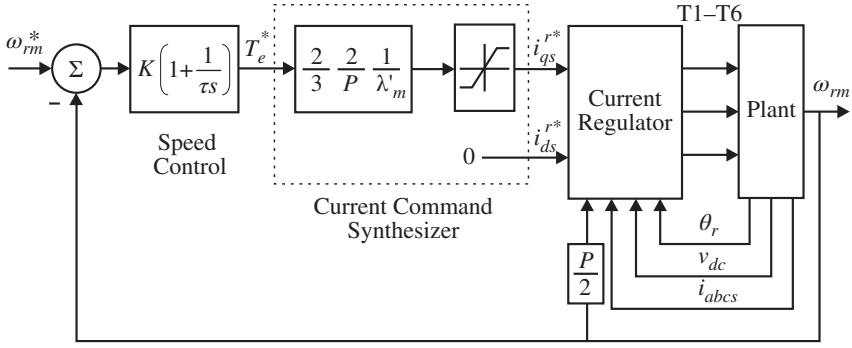

Figure 14.12-1 Current-regulated-inverter based speed control.

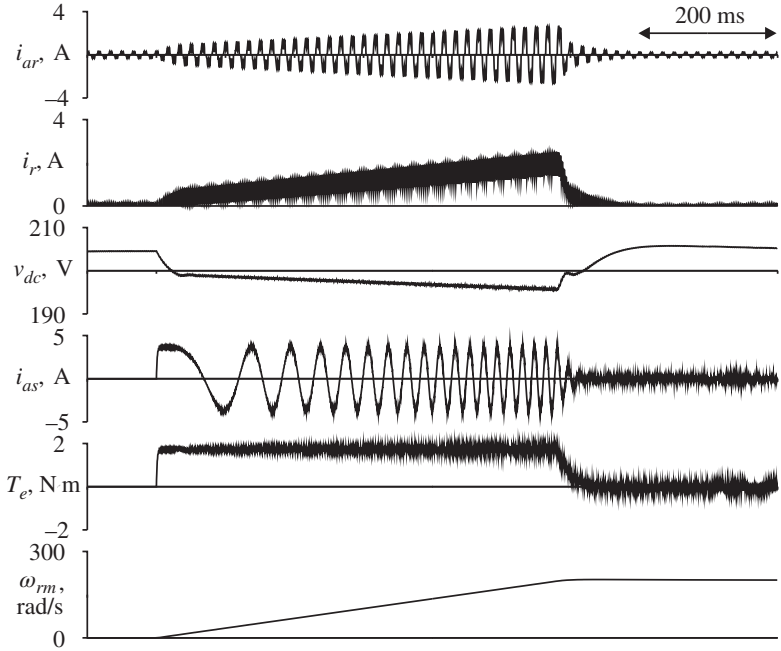

Figure 14.12-2 Start-up response of current-regulated-inverter based speed control system.

command falls off since the load is inertial. As a result, the electromagnetic torque, stator current, and rectifier current all decrease to their original values, and the dc link voltage increases to its original value.

Comparing Figure 14.12-2 with Figure 14.7-5, the reader will observe that the current-regulated inverter based speed control system is considerably more

sluggish than the voltage-source inverter based speed control system. However, this is a result the fact that the machine currents in the current-regulated inverter based system did not exceed the current limits of the machine. In fact, the current-regulated inverter based system brought the machine to speed as fast as possible subject to the limitation of the stator current.

References

1 P. L. Chapman, S. D. Sudhoff, and C. Whitcomb, "Multiple Reference Frame Analysis of Non-Sinusoidal Brushless DC Drives," *IEEE Trans. Energy Conversion*, Vol. 14, No. 3, September 1999, pp. 440–446.

2 P. L. Chapman, S. D. Sudhoff, and C. A. Whitcomb, "Optimal Current Control Strategies for Non-Sinusoidal Permanent-Magnet Synchronous Machine Drives," *IEEE Trans. Energy Conversion*, Vol. 14, No. 3, December 1999, pp. 1043–1050.

3 P. L. Chapman and S. D. Sudhoff, "A Multiple Reference Frame Synchronous Estimator/Regulator," *IEEE Trans. Energy Conversion*, Vol. 15, No. 2, June 2000, pp. 197–202.

4 H. G. Yeo, C. S. Hong, J. Y. Yoo, H. G. Jang, Y. D. Bae, and Y. S. Park, "Sensorless Drive for Interior Permanent Magnet Brushless DC motors," IEEE International Electric Machines and Drives Conference Record, May 18–21, 1997, pp. TD1-3.1-4.3.

5 K. A. Corzine and S. D. Sudhoff, "A Hybrid Observer for High Performance Brushless DC Drives," *IEEE Trans. Energy Conversion*, Vol. 11, No. 2, June 1996, pp. 318–323.

6 T. M. Rowan and R. J. Kerkman, "A New Synchronous Current Regulator and an Analysis of Current-Regulated Inverters," *IEEE Trans. Industry Applications*, Vol. IA-22, No. 4, 1986, pp. 678–690.

7 S. D. Sudhoff, K. A. Corzine, and H. J. Hegner, "A Flux-Weakening Strategy for Current-Regulated Surface-Mounted Permanent-Magnet Machine Drives," *IEEE Trans. Energy Conversion*, Vol. 10, No. 3, September 1995, pp. 431–437.

8 K. A. Corzine, S. D. Sudhoff, and H. J. Hegner, "Analysis of a Current-Regulated Brushless DC Drive," *IEEE Trans. Energy Conversion*, Vol. 10, No. 3, September 1995, pp. 438–445.

Problems

14.1 Consider the permanent-magnet ac motor drive whose characteristics are depicted in Figure 14.5-1. Plot the characteristics if $\phi_v = \text{atan}(\omega_r L_{ss}/r_s)$.

14.2 Consider the drive system whose parameters are given in Table 14.7-1. If $\phi_v = 0$, compute the turns ratio of the transformer with the minimum secondary voltage which would be required if the drive is to supply a 1.72 N·m load at a mechanical rotor speed of 200 rad/s. Assume that the primary of the transformer is connected to a 230 V source (rms, line-to-line) and that the effective series leakage reactance will be 0.05 pu. Further assume that the VA rating of the transformer is 1.5 times the mechanical output power.

14.3 Consider the speed control system considered in Section 14.8. Plot the closed-loop frequency response of the system about a nominal operating speed of 20 rad/s (mechanical).

14.4 Consider the speed-control system considered in Section 14.8. Estimate the bandwidth of the closed-loop plant that could be designed if the current is to be restricted to the rated value of 2.6 A, rms.

14.5 Assuming that the drive discussed in Example 14A is operating at an electrical rotor speed of 200 rad/s, compute the pole locations if the linearizing feedback terms are not used in making up the command voltages.

14.6 Consider a current-regulated buried permanent-magnet ac motor drive in which stator resistances is negligible. Sketch the locus of obtainable q- and d-axis currents in terms of the maximum fundamental component of the applied voltage, the electrical rotor speed, the q- and d-axis inductances, and λ'_m.

14.7 A four-pole permanent-magnet ac motor drive has the following parameters: $r_s = 0.3\,\Omega$, $L_{ss} = 20$ mH, and $\lambda'_m = 0.2$ V·s. The machine is to deliver 10 N·m at a mechanical rotor speed of 200 rad/s. Compute the q- and d-axis current commands such that the power factor is maximized. What is the rms voltage and current applied to the machine, and what is the efficiency?

14.8 Repeat Problem 7, except choose the current command so as to minimize the required dc voltage.

14.9 Repeat Problem 7, except choose the current command so as to minimize the commanded current.

14.10 Compute the locations of Points A, B, and C on Figure 14.10-1.

Appendix A

Abbreviations, Constants, Conversions, and Identities

Term	Abbreviation	Term	Abbreviation
alternating current	AC	megawatt	MW
ampere	A	meter	m
ampere-turn	At	microfarad	μF
coulomb	C	millihenry	mH
direct current	DC	newton	N
electromotive force	emf	newton meter	N · m
foot	ft	oersted	Oe
gauss	G	pound	lb
gram	g	poundal	pdl
henry	H	power factor	pf
hertz	Hz	pulse-width modulation	PWM
horsepower	hp	radian	rad
inch	in	revolution per minute	r/min (rpm)
joule	J	root mean square	rms
kilogram	kg	second	s
kilovar	kvar	voltampere reactive	var
kilovolt	kV	volt	V
kilovoltampere	kVA	voltampere	VA
kilowatt	kW	watt	W
magnetomotive force	mmf	weber	Wb
maxwell	Mx		

Analysis of Electric Machinery and Drive Systems, Fourth Edition.
Paul C. Krause, Oleg Wasynczuk, Scott D. Sudhoff, and Steven D. Pekarek.

Companion website: www.wiley.com/go/krause_aem4e

Constants and Conversion Factors

permeability of free space	$\mu_0 = 4\pi \times 10^{-7}$ Wb/A · m
permittivity of free space	$\varepsilon_0 = 8.854 \times 10^{-12}$ C^2/N · m^2
acceleration of gravity	$g = 9.807$ m/s^2
length	1 m = 3.281 ft = 39.37 in
mass	1 kg = 0.0685 slug = 2.205 lb (mass)
force	1 N = 0.225 lb = 3.6 oz
torque	1 N · m = 0.738 lb · ft
energy	1 J (W · s) = 0.738 lb · ft
power	1 W = 1.341×10^{-3} hp
moment of inertia	1 kg · m^2 = 0.738 slug · ft^2 = 23.7 lb · ft^2
magnetic flux	1 Wb = 10^8 Mx (lines)
magnetic flux density	1 Wb/m^2 = 10,000 G = 64.5 klines/in^2
magnetizing force	1 At/m = 0.0254 At/in = 0.0126 Oe

Trigonometric Identities

(I-1) $e^{j\alpha} = \cos\ \alpha + j \sin\ \alpha$

(I-2) $a\cos x + b\sin x = \sqrt{a^2 + b^2}\ \cos(x + \phi) \quad \phi = \tan^{-1}(-b/a)$

(I-3) $\cos^2 x + \sin^2 x = 1$

(I-4) $\sin 2x = 2 \sin x \cos x$

(I-5) $\cos 2x = \cos^2 x - \sin^2 x = 2\ \cos^2 x - 1 = 1 - 2\ \sin^2 x$

(I-6) $\cos x\ \cos y = \frac{1}{2}\cos(x + y) + \frac{1}{2}\cos(x - y)$

(I-7) $\sin x\ \sin y = \frac{1}{2}\cos(x - y) - \frac{1}{2}\cos(x + y)$

(I-8) $\sin x\ \cos y = \frac{1}{2}\sin(x + y) + \frac{1}{2}\sin(x - y)$

(I-9) $\cos(x \pm y) = \cos x \cos y \mp \sin x \sin y$

(I-10) $\sin(x \pm y) = \sin x \cos y \pm \cos x \sin y$

(I-11) $\cos^2 x + \cos^2\left(x - \frac{2}{3}\pi\right) + \cos^2\left(x + \frac{2}{3}\pi\right) = \frac{3}{2}$

(I-12) $\sin^2 x + \sin^2\left(x - \frac{2}{3}\pi\right) + \sin^2\left(x + \frac{2}{3}\pi\right) = \frac{3}{2}$

(I-13) $\sin x \cos x + \sin\left(x - \frac{2}{3}\pi\right)\cos\left(x - \frac{2}{3}\pi\right) + \sin\left(x + \frac{2}{3}\pi\right)\cos\left(x + \frac{2}{3}\right) = 0$

(I-14) $$\cos x + \cos\left(x - \tfrac{2}{3}\pi\right) + \cos\left(x + \tfrac{2}{3}\pi\right) = 0$$

(I-15) $$\sin x + \sin\left(x - \tfrac{2}{3}\pi\right) + \sin\left(x + \tfrac{2}{3}\pi\right) = 0$$

(I-16) $$\sin x \cos y + \sin\left(x - \tfrac{2}{3}\pi\right)\cos\left(y - \tfrac{2}{3}\pi\right) + \sin\left(x + \tfrac{2}{3}\pi\right)\cos\left(y + \tfrac{2}{3}\pi\right) = \tfrac{3}{2}\sin(x - y)$$

(I-17) $$\sin x \sin y + \sin\left(x - \tfrac{2}{3}\pi\right)\sin\left(y - \tfrac{2}{3}\pi\right) + \sin\left(x + \tfrac{2}{3}\pi\right)\sin\left(y + \tfrac{2}{3}\pi\right) = \tfrac{3}{2}\cos(x - y)$$

(I-18) $$\cos x \sin y + \cos\left(x - \tfrac{2}{3}\pi\right)\sin\left(y - \tfrac{2}{3}\pi\right) + \cos\left(x + \tfrac{2}{3}\pi\right)\sin\left(y + \tfrac{2}{3}\pi\right) = \tfrac{3}{2}\sin(x - y)$$

(I-19) $$\cos x \cos y + \cos\left(x - \tfrac{2}{3}\pi\right)\cos\left(y - \tfrac{2}{3}\pi\right) + \cos\left(x + \tfrac{2}{3}\pi\right)\cos\left(y + \tfrac{2}{3}\pi\right) = -\tfrac{3}{2}\cos(x - y)$$

(I-20) $$\sin x \cos y + \sin\left(x + \tfrac{2}{3}\pi\right)\cos\left(y - \tfrac{2}{3}\pi\right) + \sin\left(x - \tfrac{2}{3}\pi\right)\cos\left(y + \tfrac{2}{3}\pi\right) = \tfrac{3}{2}\sin(x + y)$$

(I-21) $$\sin x \sin y + \sin\left(x + \tfrac{2}{3}\pi\right)\sin\left(y - \tfrac{2}{3}\pi\right) + \sin\left(x - \tfrac{2}{3}\pi\right)\sin\left(y + \tfrac{2}{3}\pi\right) = -\tfrac{3}{2}\cos(x + y)$$

(I-22) $$\cos x \sin y + \cos\left(x + \tfrac{2}{3}\pi\right)\sin\left(y - \tfrac{2}{3}\pi\right) + \cos\left(x - \tfrac{2}{3}\pi\right)\sin\left(y + \tfrac{2}{3}\pi\right) = \tfrac{3}{2}\sin(x + y)$$

(I-23) $$\cos x \cos y + \cos\left(x + \tfrac{2}{3}\pi\right)\cos\left(y - \tfrac{2}{3}\pi\right) + \cos\left(x - \tfrac{2}{3}\pi\right)\cos\left(y + \tfrac{2}{3}\pi\right) = \tfrac{3}{2}\cos(x + y)$$

Appendix B

Phasors and Phasor Diagrams

The concept of the phasor is quite convenient in the analysis of balanced steady-state operation of AC electromechanical devices. Therefore, it is important to be familiar with phasor theory. For this purpose, let a steady-state sinusoidal variable be expressed as

$$F_a = \sqrt{2}F\cos\theta_{ef} \tag{B-1}$$

where capital letters are used to denote steady-state quantities and F is the rms value of the sinusoidal variation. In the text, the subscript s or r is added to denote variables associated with the stator or rotor, respectively. In (B-1),

$$\theta_{ef} = \int_0^t \omega_e(\xi)\, d\xi + \theta_{ef}(0) \tag{B-2}$$

where ω_e is the electrical angular velocity and ξ is a dummy variable of integration. For steady-state conditions, (B-2) may be written as

$$\theta_{ef} = \omega_e t + \theta_{ef}(0) \tag{B-3}$$

Substituting (B-3) into (B-1) yields

$$F_a = \sqrt{2}F\cos\left[\omega_e t + \theta_{ef}(0)\right] \tag{B-4}$$

We know that

$$e^{j\alpha} = \cos\alpha + j\sin\alpha \tag{B-5}$$

Thus, (B-4) may also be written as

$$F_a = \mathrm{Re}\left[\sqrt{2}Fe^{j[\omega_e t+\theta_{ef}(0)]}\right] \tag{B-6}$$

where Re is shorthand for the "real part of." Equations (B-4) and (B-6) are identical. We can rewrite (B-6) as

$$F_a = \mathrm{Re}\left[\sqrt{2}Fe^{j\theta_{ef}(0)}e^{j\omega_e t}\right] \tag{B-7}$$

Analysis of Electric Machinery and Drive Systems, Fourth Edition.
Paul C. Krause, Oleg Wasynczuk, Scott D. Sudhoff, and Steven D. Pekarek.

Companion website: www.wiley.com/go/krause_aem4e

By definition, the phasor representing F_a is

$$\widetilde{F}_a = Fe^{j\theta_{ef}(0)} \tag{B-8}$$

which is a complex number. Equation (B-7) may now be written as

$$F_a = \text{Re}\left[\sqrt{2}\widetilde{F}_a e^{j\omega_e t}\right] \tag{B-9}$$

A shorthand notation for (B-8) is

$$\widetilde{F}_a = F\underline{/\theta_{ef}(0)} \tag{B-10}$$

Equation (B-10) is commonly referred to as the *polar form* of the phasor. The *cartesian form* is

$$\widetilde{F}_a = F\cos\ \theta_{ef}(0) + jF\sin\theta_{ef}(0) \tag{B-11}$$

When using phasors to calculate steady-state voltages and currents, we think of the phasors as being stationary at $t = 0$. On the other hand, a phasor is related to the instantaneous value of the sinusoidal quantity it represents. Let us take a moment to consider this aspect of the phasor and, thereby, give some physical meaning to it. We know that

$$e^{j\omega_e t} = \cos\omega_e t + j\sin\omega_e t \tag{B-12}$$

is a constant-amplitude line of unity length rotating counterclockwise at an angular velocity of ω_e. Now,

$$\begin{aligned}\sqrt{2}\widetilde{F}_{as}e^{j\omega_e t} &= \sqrt{2}Fe^{j\theta_{ef}(0)}e^{j\omega_e t}\\ &= \sqrt{2}Fe^{j[\omega_e t+\theta_{ef}(0)]}\\ &= \sqrt{2}F\{\cos[\omega_e t + \theta_{ef}(0)] + j\sin[\omega_e t + \theta_{ef}(0)]\}\end{aligned} \tag{B-13}$$

is a constant-amplitude line $\sqrt{2}F$ in length rotating counterclockwise at an angular velocity of ω_e with a time zero displacement from the positive real axis of $\theta_{ef}(0)$. The instantaneous value of F_a is the real part of (B-13). In other words, the real projection of the phasor $\widetilde{F}_a$ is the instantaneous value of $(1/\sqrt{2})F_a$ at time zero. As time progresses, $\widetilde{F}_a$ rotates at ω_e in the counterclockwise direction, and its real projection, in accordance with (B-9), is the instantaneous value of $(1/\sqrt{2})F_a$. Thus, for

$$F_a = \sqrt{2}F\cos\omega_e t \tag{B-14}$$

the phasor representing F_a is

$$\widetilde{F}_a = Fe^{j0} = F\underline{/0°} = F + j0 \tag{B-15}$$

For

$$F_a = \sqrt{2}F\cos\left(\omega_e t + \frac{1}{6}\pi\right) \tag{B-16}$$

the phasor is

$$\widetilde{F}_a = Fe^{j\pi/6} = F\underline{/30°} = F(0.866 + j0.5) \tag{B-17}$$

Finally, for

$$F_a = \sqrt{2}F \sin \omega_e t \tag{B-18}$$

the phasor is

$$\widetilde{F}_a = Fe^{-j\pi/2} = F\underline{/-90°} = 0 - jF \tag{B-19}$$

Although there are several ways to arrive at (B-19) from (B-18), Is it helpful to ask yourself where must the rotating phasor be positioned at time zero so that, when it rotates counterclockwise at ω_e, its real projection is $(1/\sqrt{2})F \sin \omega_e t$? Is it clear that a phasor of amplitude F positioned at $\frac{1}{2}\pi$ would represent $-\sqrt{2}F \sin \omega_e t$?

It is often instructive to be able to construct a phasor diagram. For example, let us consider a voltage equation of the form

$$\widetilde{V} = (r + jX)\widetilde{I} + \widetilde{E} \tag{B-20}$$

where r is the resistance and X is the reactance. In most cases, we will deal with an inductive reactance; however, in a series LC circuit,

$$X = X_L + X_C = \omega_e L + \frac{-1}{\omega_e C} \tag{B-21}$$

where L is the inductance and C is the capacitance. The inductive reactance is X_L and X_C is the capacitive reactance. Let us assume that $\widetilde{V}$ and $\widetilde{I}$ are known and that we are to calculate $\widetilde{E}$. The phasor diagram may be used as a rough check on these calculations. Let us construct this phasor diagram by assuming that X is equal to X_L (or $|X_L| > |X_C|$) and $\widetilde{V}$ and $\widetilde{I}$ are known as shown in Figure B-1. Solving (B-20) for $\widetilde{E}$ yields

$$\widetilde{E} = \widetilde{V} - (r + jX)\widetilde{I} \tag{B-22}$$

To perform this graphically, start at the origin in Fig. B-1 and walk to the terminus of $\widetilde{V}$. Now, we want to subtract $r\widetilde{I}$. To achieve the proper orientation to do this, stand at the terminus of $\widetilde{V}$, turn, and look in the $\widetilde{I}$ direction which is at the angle ϕ. But we must subtract $r\widetilde{I}$; hence, $-\widetilde{I}$ is 180° from $\widetilde{I}$, so do an about face and now we are headed in the $-\widetilde{I}$ direction which is $\phi - 180°$. Start walking in the direction of $-\widetilde{I}$ for the distance $r|\widetilde{I}|$ and then stop. While still facing in the $-\widetilde{I}$ direction, let us consider the next term. We must subtract $jX\widetilde{I}$, so let us face in the direction of $-jX\widetilde{I}$. We are still looking in the $-\widetilde{I}$ direction, so we need only to j ourselves. Thus, we must rotate 90° in the counterclockwise direction, whereupon we are standing at the end of $\widetilde{V} - r\widetilde{I}$ looking in the direction of $\phi - 180° + 90°$. Start walking in this direction for the distance of $X|\widetilde{I}|$, whereupon we are at the terminus of $\widetilde{V} - r\widetilde{I} - jX\widetilde{I}$. According to (B-22), $\widetilde{E}$ is the phasor drawn from the origin of

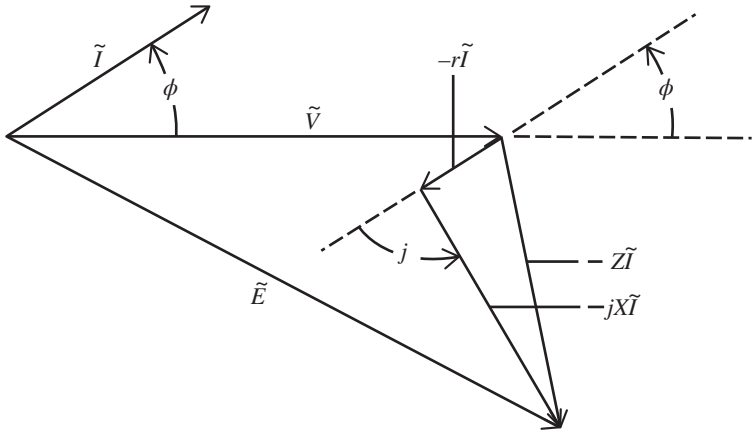

Figure B-1 Phasor diagram for (B-22).

the phasor diagram to where we are. Note that in Fig. B-1 $-Z\tilde{I}$ is $-(r + jX)\tilde{I}$, where Z is the impedance.

The average steady-state power may be calculated by using phasors,

$$P = |\tilde{V}||\tilde{I}| \cos \phi_{\text{pf}} \tag{B-23}$$

where the power is in watts and the so-called power factor angle is defined as

$$\phi_{\text{pf}} = \theta_{ev}(0) - \theta_{ei}(0) \tag{B-24}$$

Here, $\tilde{V}$ and $\tilde{I}$ are phasors with the positive direction of $\tilde{I}$ taken in the direction of the voltage drop and $\theta_{ev}(0)$ and $\theta_{ei}(0)$ are the phase angles of $\tilde{V}$ and $\tilde{I}$, respectively.

The reactive power is defined as

$$Q = |\tilde{V}||\tilde{I}| \sin \phi_{\text{pf}} \tag{B-25}$$

The units of Q are in var (voltampere reactive). An inductance is said to absorb reactive power and thus, by definition, Q is positive for an inductor and negative for a capacitor. Actually, Q is a measure of the exchange of energy stored in the electric (capacitor) and magnetic (inductance) fields; however, there is no average power interchanged between these energy storage devices.

Index

Analysis of Electric Machinery and Drive Systems, Fourth Edition.
Paul C. Krause, Oleg Wasynczuk, Scott D. Sudhoff, and Steven D. Pekarek.

Companion website: www.wiley.com/go/krause_aem4e

b

c

d

f

g

h

i

k

l

m

S

t

WILEY END USER LICENSE AGREEMENT

Go to www.wiley.com/go/eula to access Wiley’s ebook EULA.